Mines and Minerals Division

Ontario Geological Survey
Miscellaneous Paper 130

Geoscience Research Grant Program
Summary of Research
1985-1986

edited by
V.G. Milne

1986

Ontario
Ministry of
Northern Development
and Mines

©1986 Government of Ontario
Printed in Ontario, Canada

ISSN 0704-2752 (Series)
ISBN 0225-5316 (Sub-series)

Publications of the Ontario Geological Survey, Ministry of Northern Development and Mines, are available from the following sources. Orders for publications should be accompanied by cheque or money order payable to the *Treasurer of Ontario*.

Reports, maps, and price lists (personal shopping or mail order):

Public Information Centre, Ministry of Natural Resources
Room 1640, Whitney Block, Queen's Park
Toronto, Ontario M7A 1W3

Reports and accompanying maps only (personal shopping):

Ontario Government Bookstore
Main Floor, 880 Bay Street
Toronto, Ontario M7A 1N8

Reports and accompanying maps (mail order or telephone orders):

Publications Services Section, Ministry of Government Services
5th Floor, 880 Bay Street
Toronto, Ontario M7A 1N8
Telephone (local calls) 965-6015
Toll-free long distance 1-800-268-7540
Toll-free from Area Code 807 0-ZENITH-67200

Every possible effort is made to ensure the accuracy of the information contained in this report, but the Ministry of Northern Development and Mines does not assume any liability for errors that may occur. Source references are included in the report and users may wish to verify critical information.

Parts of this publication may be quoted if credit is given. It is recommended that reference be made in the following form:

Donaldson, J.A., Michel, F.A., Rust, B.R., Smyk, M., Watkinson, D.H., and Wilson, B.
1986: Sedimentary Rocks and Strata-Bound Mineralization in the Cobalt Region; Grant 173, p.4-15 *in* Geoscience Research Grant Program, Summary of Research, 1985-1986, edited by V.G. Milne, Ontario Geological Survey, Miscellaneous Paper 130, 235p.

If you wish to reproduce any of the text, tables, or illustrations in this report, please write for permission to the Director, Ontario Geological Survey, Ministry of Northern Development and Mines, 11th floor, 77 Grenville Street, Toronto, Ontario, M7A 1W4.

Scientific Editor: M.L.T. Stuart

2000-86-Maracle Press

CONTENTS

Introductory Remarks, *V.G. Milne* 2

Grant 173 Sedimentary Rocks and Strata-Bound Mineralization in the Cobalt Region, *J.A. Donaldson, F.A. Michel, B.R. Rust, M. Smyk, D.H. Watkinson, and B. Wilson* 4

Grant 189 The Sedimentology and Stratigraphy of the Bar River Formation (Huronian Supergroup) at Bay Finn, Lake Huron, *B.R. Rust and M.J. Shields* 16

Grant 192 Geochemical Exploration for Gold, *Ian Nichol and Gene S. Shelp* 24

Grant 193 The Geological Setting and Genesis of the Cameron Lake Gold Deposit, *D.R. Melling and D.H. Watkinson* 27

Grant 205 Clay Mineralogy of Two Selected Carbonate Reservoirs in Southwestern Ontario, *P.L. Churcher and M.B. Dusseault* 36

Grant 216 The Depositional Environment for the Black Shales of the Upper Devonian Long Rapids Formation, Northern Ontario, *R.K. Bezys and M.J. Risk* 39

Grant 221 Implications of Chemical Trends within the Chloritoid-Altered Volcanic Rocks of the Wawa Belt, *M.B. Lockwood and J.M. Franklin* 54

Grant 225 Genesis of Pegmatites in the Quetico Gneiss Belt of Northwestern Ontario—Granitoids, "Barren" Pegmatites, and Metasediments, with Additional Data on Rare-Element Pegmatites, from the Georgia Lake Pegmatite Field, *S.A. Kissin, B. Zayachkivsky, and L.A. Branscombe* 65

Grant 227 Relationship Between Gold Deposits and the Tectonic Framework of the Abitibi Greenstone Belt in the Kirkland Lake-Larder Lake Area, *D.J. Toogood and C.J. Hodgson* 79

Grant 230 Petrologic, Chemical, Isotopic, and Ecomonic Potential Studies of the Nipissing Diabase, *P.C. Lightfoot, D. Conrod, A.J. Naldrett, and N.M. Evensen* 87

Grant 233 The Dating of Ontario's Gold Deposits, *A. Masliwec, D. McMaster, and D. York* 107

Grant 236 Au-Quartz Vein and Intrusion-Hosted Cu-Au-Ag-Mo Mineralization, Hollinger-McIntyre Mines, Timmins, Ontario: Geological Characteristics, Structural Examination, Igneous and Hydrothermal Alteration Geochemistry, and Light Stable Isotope (Hydrogen and Oxygen) Geochemistry, *P.C. Wood, D.R. Burrows, and E.T.C. Spooner* 115

Grant 242 Structural Studies in the Beardmore-Geraldton Belt, Northern Ontario, *Howard R. Williams* 138

Grant 249 Geochemical Studies of Formation Waters from Paleozoic Strata, Southwestern Ontario, *P. Dollar, S.K. Frape, R.H. McNutt, P. Fritz, and R.W. Macqueen* 147

Grant 254 Exploration for Buried Aggregates by Remote Sensing Techniques: An Assessment, *H. George, M.B. Dusseault, and A.B. Kesik* 155

Grant 256 Cyanide in Gold Deposits, *H.P. Schwarcz* 161

Grant 259 Development of Analytical Methods for Trace Lanthanides, *A.D. Westland and C. Kantipuly* 165

Grant 260 Magnetotelluric Mapping of the Destor-Porcupine Fault, *J.D. Redman, S.K. Zhao, and D.W. Strangway* 170

Grant 262 Lithological Features and Economic Significance of Reduced Carbonaceous Rocks in Gold Deposits, *Graham C. Wilson and John C. Rucklidge* 177

Grant 265 Metal Uptake by Microorganisms: Retardation of Toxic Heavy Metal Dispersion From Tailing Environments, Elliot Lake, Timmins, and Sudbury, *H. Mann, F.G. Ferris, T.J. Beveridge, W.S. Fyfe, R. Humphrey, and K. Tazaki* 190

Grant 266 Carbonate Till on the Canadian Shield: Economic and Environmental Implications in the Hemlo Area, Ontario, *Stephen R. Hicock* 210

Grant 269 Compositional Characteristics of Pyrite in Barren and Gold Mineralized Veins, *N.D. MacRae and H.W. Nesbitt* 218

Grant 271 Petrographic and Chemical Properties Affecting Calcining of High Purity Carbonates, *Peter P. Hudec* 225

Conversion Factors for Measurements in Ontario Geological Survey Publications

If the reader wishes to convert imperial units to SI (metric) units or SI units to imperial units the following multipliers should be used:

CONVERSION FROM SI TO IMPERIAL			**CONVERSION FROM IMPERIAL TO SI**		
SI Unit	*Multiplied by*	*Gives*	*Imperial Unit*	*Multiplied by*	*Gives*
			LENGTH		
1 mm	0.039 37	inches	1 inch	**25.4**	mm
1 cm	0.393 70	inches	1 inch	**2.54**	cm
1 m	3.280 84	feet	1 foot	**0.304 8**	m
1 m	0.049 709 7	chains	1 chain	20.116 8	m
1 km	0.621 371	miles (statute)	1 mile (statute)	**1.609 344**	km
			AREA		
1 cm^2	0.155 0	square inches	1 square inch	**6.451 6**	cm^2
1 m^2	10.763 9	square feet	1 square foot	**0.092 903 04**	m^2
1 km^2	0.386 10	square miles	1 square mile	2.589 988	km^2
1 ha	2.471 054	acres	1 acre	0.404 685 6	ha
			VOLUME		
1 cm^3	0.061 02	cubic inches	1 cubic inch	**16.387 064**	cm^3
1 m^3	35.314 7	cubic feet	1 cubic foot	0.028 316 85	m^3
1 m^3	1.308 0	cubic yards	1 cubic yard	0.764 555	m^3
			CAPACITY		
1 L	1.759 755	pints	1 pint	0.568 261	L
1 L	0.879 877	quarts	1 quart	1.136 522	L
1 L	0.219 969	gallons	1 gallon	**4.546 090**	L
			MASS		
1 g	0.035 273 96	ounces (avdp)	1 ounce (avdp)	28.349 523	g
1 g	0.032 150 75	ounces (troy)	1 ounce (troy)	**31.103 476 8**	g
1 kg	2.204 62	pounds (avdp)	1 pound (avdp)	**0.453 592 37**	kg
1 kg	0.001 102 3	tons (short)	1 ton (short)	**907.184 74**	kg
1 t	1.102 311	tons (short)	1 ton (short)	**0.907 184 74**	t
1 kg	0.000 984 21	tons (long)	1 ton (long)	**1016.046 908 8**	kg
1 t	0.984 206 5	tons (long)	1 ton (long)	**1.016 046 908 8**	t
			CONCENTRATION		
1 g/t	0.029 166 6	ounce (troy)/ ton (short)	1 ounce (troy)/ ton (short)	34.285 714 2	g/t
1 g/t	0.583 333 33	pennyweights/ ton (short)	1 pennyweight/ ton (short)	1.714 285 7	g/t

OTHER USEFUL CONVERSION FACTORS

1 ounce (troy)/ton (short)	20.0	pennyweights/ton (short)
1 pennyweight/ton (short)	0.05	ounce (troy)/ton (short)

NOTE—Conversion factors which are in bold type are exact. The conversion factors have been taken from or have been derived from factors given in the Metric Practice Guide for the Canadian Mining and Metallurgical Industries published by The Mining Association of Canada in cooperation with the Coal Association of Canada.

Geoscience Research Grant Program
Summary of Research 1985-1986

---

edited by
V.G. Milne

Director, Ontario Geological Survey

Introductory Remarks

The Ontario Geoscience Research Grants Program was initiated in 1978 to encourage geoscience research at Ontario universities. By supporting mission-oriented geological projects, a program of research was established which would complement the work of the Ontario Geological Survey through its mandate:

> To stimulate exploration for, and facilitate sound planning in, all matters related to, mineral and other earth resources by providing an inventory and analysis of the geology and mineral deposits of Ontario.

The program supports applied studies of up to three years duration towards: mineral deposit characterization involving studies of specific occurrences or groups of occurrences within Ontario; petrology, rock geochemistry, structural geology, stratigraphy, and geochronology studies; field and laboratory studies leading to the development of new geophysical or geochemical concepts and techniques; engineering and environmental geology studies; and methods for improving automated or manual processing, and facilitating the interpretation of geoscience data.

In order to receive funding, applications must be forwarded to the Ontario Geological Survey prior to November 15. Project proposals are subject to review by a committee which reports to the Director of the Ontario Geological Survey. This committee advises the Minister of Northern Development and Mines concerning geoscience research priorities at Ontario universities and of the scientific merit and relevance of proposals submitted to the Ontario Geoscience Research Grants Program. The committee consists of four representatives of the mineral industry, three representatives of the university community, and four representatives of the Survey. Members of the 1985-86 committee include:

Dr. D.J. Misener, Chairman; Paterson, Grant, and Watson Limited
Dr. W. Coker; Kidd Creek Mines Limited
Dr. J.A. Donaldson; Carleton University
Dr. V.K. Gupta; Ontario Geological Survey
Dr. R. Hodder; University of Western Ontario
Dr. C.J. Hodgson; Queen's University
E.V. Sado; Ontario Geological Survey
Dr. J. Springer; Ontario Geological Survey
Dr. H. Seigel; Scintrex Limited
J. Stewart; Selco Division-BP Resources Canada Limited
J. Wood; Ontario Geological Survey

Successful grant recipients are expected to submit reports for publication in the annual *Summary of Research* and participate in an annual OGS Geoscience Research Seminar held annually in December.

Publication in other scientific journals is encouraged and a final report summarizing the research will be released as an Ontario Geological Survey Open File Report. Open File Reports concerning the Ontario Geoscience Research Grant Program are released from time to time and are available at the Mines Library, 77 Grenville Street, Toronto, or at Ministry of Northern Development and Mines regional offices. The following research projects partially or wholly funded by this program during 1985-86 will be released as Open File Reports (only principal applicant's name listed):

Grant 149: Structural Signature and Tectonic History of Deformed Gold-Bearing Rocks in Northwestern Ontario; W.M. Schwerdtner, University of Toronto.

Grant 168: Petrogenesis of Mineralized Horizons in Uchi Lake Greenstones; N.M. Evensen, University of Toronto.

Grant 173: Sedimentary Rocks and Stratabound Mineralization; J.A. Donaldson, Carleton University.

Grant 187: Sedimentology of the Cambro-Ordovician Sandstones of Eastern Ontario; R.W. Dalrymple, Queen's University.

Grant 189: Sedimentology of the Bar River Formation, Huronian Supergroup, Ontario; B.R. Rust, University of Ottawa.

Grant 192: Geochemical Exploration for Gold; Ian Nichol, Queen's University.

Grant 193: The Geological Setting and Genesis of the Cameron Lake Gold Deposit; D.H. Watkinson, Carleton University.

Grant 205: Clay Mineralogy of Two Selected Carbonate Reservoirs in Southwestern Ontario, M.B. Dusseault, University of Waterloo.

Grant 221: Chloritoid in Altered Volcanic Rocks; J.M. Moore, Carleton University.

Grant 256: Cyanide in Gold Deposits; H.P. Schwarcz, McMaster University.

Grant 259: Development of Analytical Methods for Trace Lanthanides; A. Westland, University of Ottawa.

Grant 260: Magnetotelluric Mapping of the Porcupine-Destor Fault; D.W. Strangway, University of Toronto.

Grant 269: Compositional Characteristics of Pyrite in Barren and Gold Mineralized Veins; N.D. MacRae, University of Western Ontario.

Grant 271: Effect of Grain Size on Calcining Properties of Carbonates; P.P. Hudec, University of Windsor.

During 1985-86. 26 projects were funded under the program. Of these. 15 were renewal projects:

University	Value of Grants	No. of Grants
Brock	$ 17 208	1
Carleton	42 105**	3
Lakehead	10 440	1
McMaster	46 022	2
Ottawa	16 865	2
Queen's	62 809++	3
Toronto	172 369+	7
Waterloo	64 769*	3
Western	54 626	3
Windsor	12 787	1
TOTAL	500 000	26

*A grant of $23 900 to the University of Waterloo involved staff from McMaster University.

**A grant of $21 319 to Carleton University involved staff of the University of Ottawa.

+Two grants to the University of Toronto are not reported. They will be published in the 1986-87 Summary of Research.

++A grant of $1195 to Queen's University was reported in full in the 1984-85 Summary of Research.

The undersigned would like to thank Dr. D.J. Misener, who acted as Committee Chairman, and the rest of the Review Committee Members who gave freely of their time. The efforts of the researchers are acknowledged. Mr. R.B. Watson, who served as Grants Administrator and Secretary to the Committee, and Mrs. M.L.T. Stuart, who acted as scientific editor for this publication, deserve thanks.

V.G. Milne
Director
Ontario Geological Survey

Grant 173 Sedimentary Rocks and Strata–Bound Mineralization in the Cobalt Region

J.A. Donaldson[1], F.A. Michel[1], B.R. Rust[2], M. Smyk[1], D.H. Watkinson[1], and B. Wilson[1]

[1]Ottawa-Carleton Centre for Geoscience Studies, Department of Geology, Carleton University, Ottawa

[2]Ottawa-Carleton Centre for Geoscience Studies, Department of Geology, University of Ottawa, Ottawa

ABSTRACT

Immature turbiditic interflow sedimentary strata in Archean basement of the Cobalt area are generally best exposed above volcanic flow units, where some are in juxtaposition with exhalative chert and massive sulphides. Sphalerite is abundant in the exhalative deposits, and iron sulphides predominate in syngenetic nodules and interlayers within associated pelagic black shales. Epigenetic sulphides (±sulpharsenides) are abundant in veinlets that branch from the syngenetic sulphide layers, and in pervasive sulphide replacements that are accompanied by extensive chloritization, carbonatization, and silicification.

Isotopic and mineralogical studies of sulphides have been carried out on samples of both Archean and Huronian sedimentary rocks in close proximity to silver-bearing veins. At one study locality (Little Silver Vein), the sulphide mineralogy is complex and zoned within 6 m of the vein; the sulphide minerals beyond 6 m of the vein consist almost entirely of pyrite and minor chalcopyrite. Near the vein, the pyrite is predominantly euhedral, whereas farther than 6 m from the vein the pyrite is subhedral to anhedral. Although some sulphide-rich clasts in the Cobalt area may be detrital, most sulphides in the Huronian strata probably originated from fluids circulating through the sediments.

Preliminary sulphur-isotope analyses of the sulphides show a decrease in $\delta^{34}S$ values with increasing distance from the Little Silver Vein. This trend is opposite to that observed for syngenetic sulphides in Archean volcanic rocks adjacent to veins in the Beaver-Temiskaming Mine. These data are interpreted to represent the derivation of sulphur (and metals) through reaction of Archean sulphides with Proterozoic formational waters, the extensive interaction of metal-enriched fluids with the Proterozoic strata, and the ultimate precipitation of Ag, Bi, Co, Ni, and As in veins related to joint patterns after solidification of the Nipissing Diabase.

INTRODUCTION

Previously reported studies in the Cobalt area supported by Ontario Geoscience Research Fund (OGRF) Grant 173 have focused primarily on the sedimentology and mineralization of the Gowganda Formation (Donaldson *et al.* 1984, 1985; Mustard 1985; Rainbird 1985). This report provides a preliminary evaluation of: (1) sulphide-rich units within the Archean basement rocks, and (2) the utility of isotopic and mineralogical data for the development of genetic models for silver-bearing veins in the Cobalt area.

THE ARCHEAN BASEMENT AT COBALT

Although an association has long been noted between silver veins and interflow sedimentary rocks of the Archean basement (Knight 1924), few detailed maps or stratigraphic studies of Archean volcanic and sedimentary rocks of the Cobalt area have been published. In an attempt to remedy this, detailed mapping of Archean inliers was begun in 1985 by Smyk (M.Sc. Thesis study, Carleton University) with the following goals in mind:

1. To describe and classify interflow sedimentary rocks and their contained sulphide (and sulpharsenide) minerals.
2. To attempt to use the interflow units to delineate stratigraphy, and to assess the structural deformation of the volcano-sedimentary strata.

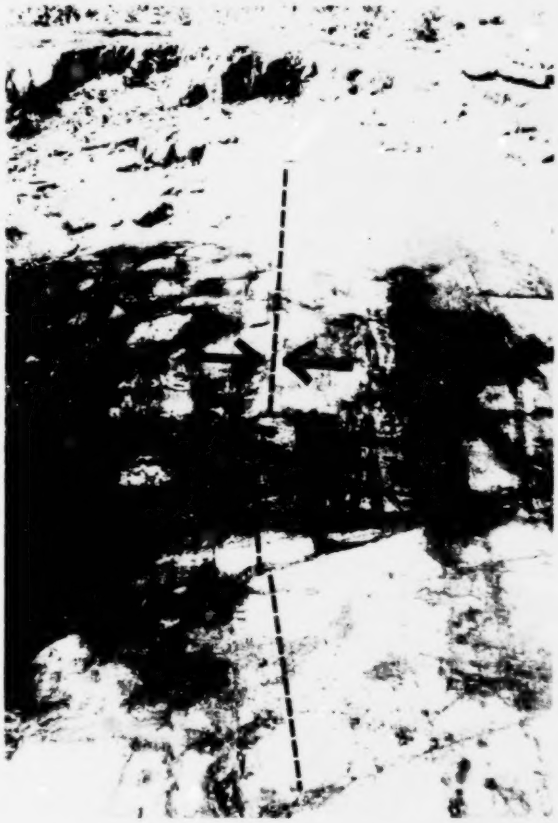

Photo 173.1. *Isoclinal fold in interflow sedimentary rocks. Nipissing Hill (south) RL 404 Property. Fold axis is offset by minor faults. Handle of hammer in background indicates the fold axis.*

3. To attempt to correlate observed distinctive structures, mineralogy, and alteration products of possible genetic significance with respect to the Archean rocks, especially the interflow sedimentary units, that contain Ag-Bi-Co-Ni-As veins.

GEOLOGY OF THE INTERFLOW SEDIMENTARY ROCKS

The Archean geology of the Cobalt area has been summarized by Jambor (1971). Volcanic rocks of the Archean basement have been studied by Patterson (1979) and Dillon-Leitch (1980).

Most sedimentary rocks occur as thin units intercalated with massive and pillowed volcanic rocks. Despite their relative paucity in many areas, the sedimentary strata commonly display lateral continuity over distances of several hundred metres. The interflow sedimentary rocks locally compose up to 20% of the Archean volcano-sedimentary successions, as exemplified by the Nipissing Hill (south) RL 404 Property (Figure 173.1; MacRobbie 1986; Smyk and MacRobbie 1986). Sedimentary accumulations up to 300 m thick occur near the northern end of Sasaginaga Lake, around Clear Lake, and on the southwest end of Cross Lake.

The Archean sedimentary and volcanic strata have been extensively folded and faulted; most units now have steeply dipping to vertical attitudes. The rocks have undergone lower greenschist regional metamorphism, and have been altered as a result of emplacement of both the Nipissing Diabase and numerous narrow silver-bearing veins. Narrow zones of flattening and/or shearing, characterized by boudinage and imposed strain fabrics, occur in the volcanic rocks, especially near intercalated sedimentary units. Evidence of tectonic deformation is even more apparent in the associated sedimentary rocks. Foliation, where developed, is commonly steeply dipping, parallel to bedding, and defines axial planar folds. Isoclinal folds (Photo 173.1) that may be sheath folds (cf. Cobbold and Quinquis 1979), low-

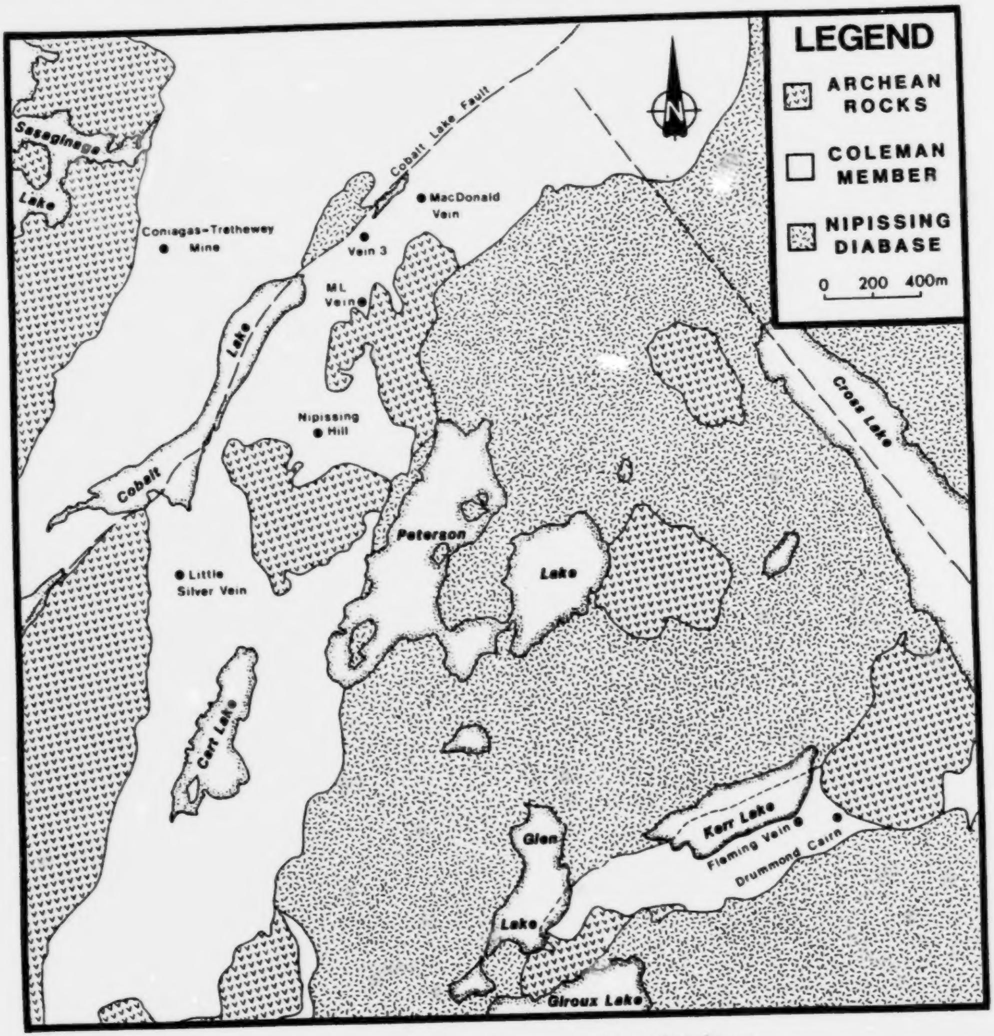
LEGEND
ARCHEAN ROCKS
COLEMAN MEMBER
NIPISSING DIABASE
0 200 400m
N
Sasaginaga Lake
Cobalt Lake Fault
MacDonald Vein
Coniagas-Trethewey Mine
Vein 3
ML Vein
Lake
Nipissing Hill
Cobalt
Little Silver Vein
Cart Lake
Peterson
Lake
Cross Lake
Kerr Lake
Fleming Vein
Drummond Cairn
Glen
Lake
Giroux Lake

Figure 173.1. Location map of sites studied during the present investigations.

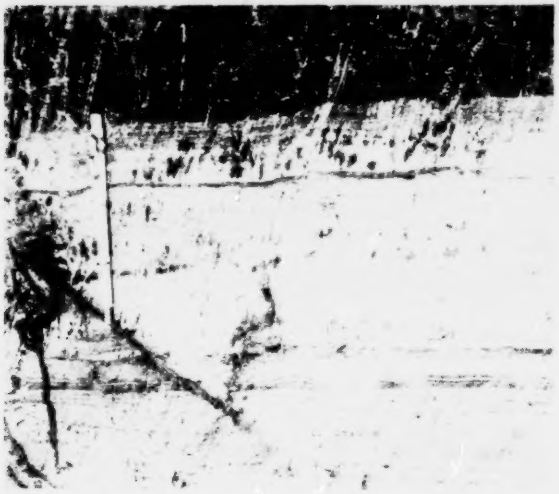

Photo 173.2. *Distal turbidites displaying load casting, flame structures and graded bedding. Nipissing Hill (south) RL 404 Property.*

Photo 173.3. *Graded paraconglomerate. Note clast angularity and sulphide replacement of chloritized clasts and matrix. Nipissing Hill (south) RL 404 Property. Markings are in centimetres.*

angle faults, and décollement zones have developed, presumably as a result of bulk simple shear during regional folding. This has resulted in reversals in younging directions and in juxtaposition of different rock types within individual interflow units. Fault and joint sets at high angles to bedding are ascribed to a late tectonic event that deformed both the Nipissing Diabase and the Huronian sedimentary rocks.

Most of the interflow sedimentary rocks are interpreted to be deep-water turbidites with minor pelagic interbeds, characteristic of the resedimented facies association (Turner and Walker 1973). Interbedded chert also is common, but in part may be a product of silicification. Constituent facies include wacke with interbedded argillite, paraconglomerate and sedimentary breccia, banded iron formation, and black shale.

Turbidites, which comprise the bulk of the interflow units, typically are well bedded, locally graded, and display primary sedimentary structures such as load casts, flame structures, and rip-up clasts (Photo 173.2). Most individual beds are thin, ranging from 1 to 30 cm. Full A to E Bouma sequences up to 1 m thick are common.

The framework grains are feldspar, quartz, and minor lithic fragments. Framework and matrix constituents have been partially to completely replaced by chlorite and sericite. Detrital sulphide and oxide grains are rare. Reworking of tuffaceous source beds is the likely origin for many of the turbidites.

Matrix-supported conglomerates, a minor but significant component of the resedimented association, are intercalated with wackes and shales, and have limited lateral continuity. The clasts range from granules to small cobbles, and generally are subangular to subrounded. Most of the clasts are either sedimentary or altered volcanic fragments. Well developed graded bedding (Photo 173.3) suggests that the clasts were supported above the bed by a turbulent flow during transport (cf. Walker 1984). Associated ungraded matrix-supported beds may be attributed to mass movement (debris flows).

Sedimentary breccias, abundant within the turbidite sequences, are characterized by angular rip-up clasts of argillite and chert in coarse-grained, massive wacke beds. The clasts generally are confined to the lower parts of these beds, but some occur up to 50 cm from the scoured basal surface. Tabular clasts commonly display flow alignment or imbrication. Scattered angular black chert fragments which contain sphalerite occur at a uniform stratigraphic level within a bed of coarse wacke between a pillowed volcanic flow and an overlying unit of finer grained clastic sedimentary rocks (Photo 173.4).

Banded iron formation occurs in the Silver Hill, Fisher-Eplett, and Cross Lake Silver Mines properties. Samples from these localities illustrate three distinct types of oxide facies iron formation. The Silver Hill iron formation consists of subhedral to anhedral magnetite grains disseminated throughout a fine-grained, poorly bedded quartz siltstone that contains minor chlorite. Reticulate fractures may represent dewatering and/or syneresis. Banded siltstone-magnetite iron formation and chert (jasper)-magnetite iron formation occur in the Fisher-Eplett and Cross Lake localities, respectively. These iron formations are characterized

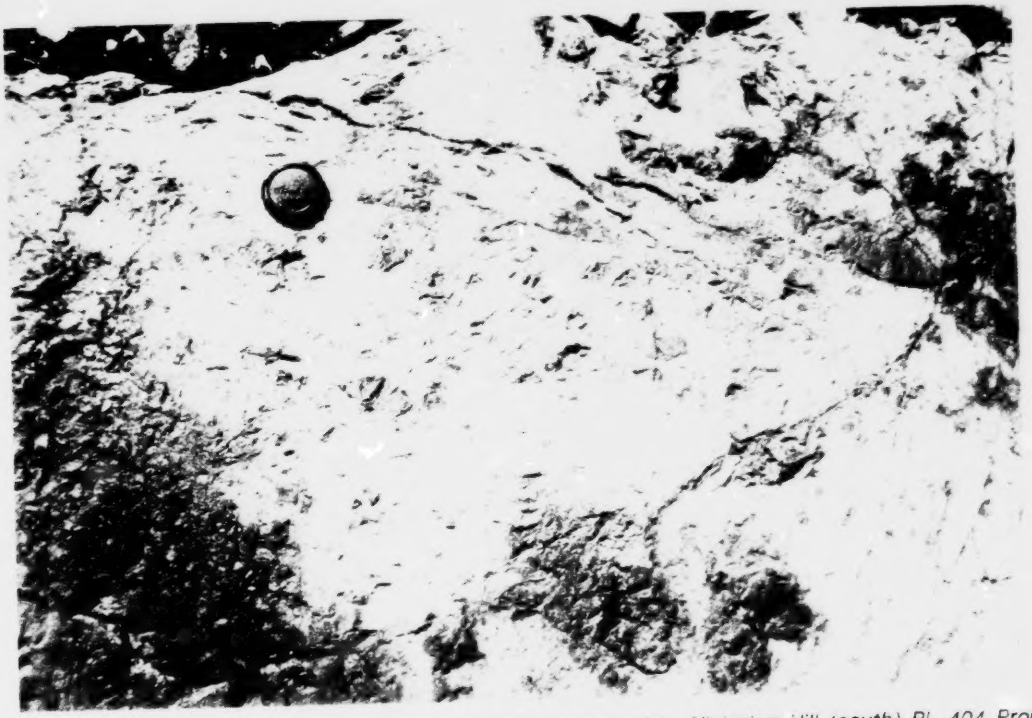

Photo 173.4. *Angular black chert fragments in greywacke matrix. Nipissing Hill (south) RL 404 Property. Diameter of lens cap is 5 cm.*

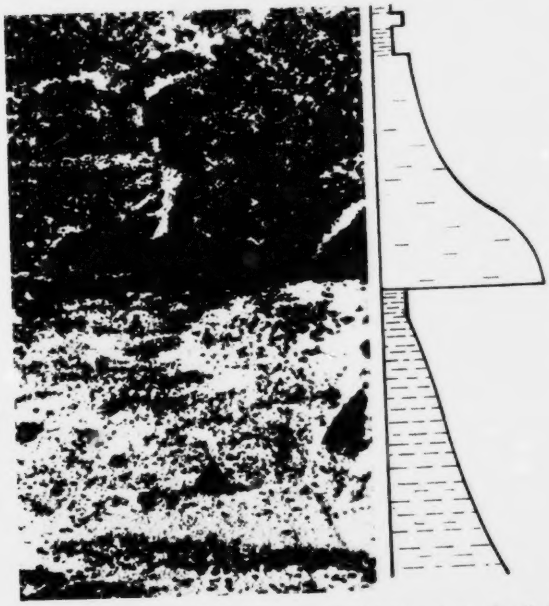

Photo 173.5. *Graded magnetite-siltstone bed in banded iron formation, Fisher-Eplett Property. Magnetite is concentrated in upper part of the siltstone bed. Beds are approximately 4 mm thick.*

by thin (less than 2 cm) interlayers of magnetite and siltstone or chert with millimetre-scale microbanding. Graded siltstone-magnetite beds, parallel laminations and magnetite-rich upper portions to the beds (Photo 173.5) suggest that these rocks are fine-grained deep-water distal turbidites with a chemical-rainout interturbidite component (cf. Barrett and Fralick 1985).

Black shales and local occurrences of graphitic schist and slate probably represent pelagic sedimentation. Intercalation of these rocks with the turbidites is common; truncation of the fine-grained units, possibly due to scouring, has produced numerous lateral discontinuities in the shale units. Bedding is indistinct, except where silty or sandy interbeds are present. The most notable feature of these shales is extensive syngenetic nodules, lenses, and layers of pyrite, marcasite, and pyrrhotite.

Thinly bedded to massive, grey to black chert occurs throughout the turbidite successions. The black varieties in places are indistinguishable from siliceous argillites. Some units, previously mapped as chert, actually are fine-grained clastic sedimentary rocks and/or silicified equivalents.

The predominance of rocks belonging to the resedimented (turbidite) facies association (wacke, paraconglomerate, and minor intercalated banded iron formation) is indicative of the displacement of sediment from shallow into deep water on a submarine fan. The preservation of abundant primary sedimentary structures and the abundance of intercalated pelagic black shales also reflect deposition below

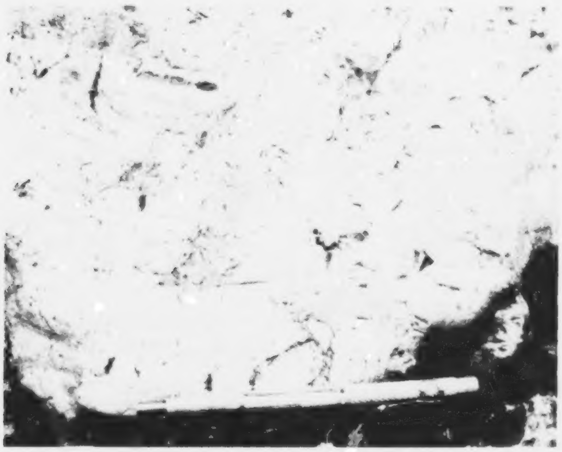

Photo 173.6. *Mud infilling synsedimentary fracture in turbidite (immediately above 15 cm pencil), Nipissing Hill (south) RL 404 Property.*

wave base. Definitive features suggestive of provenance, paleocurrent directions, and basin morphology unfortunately are lacking. However, features indicative of syndepositional deformation, such as slumps, convolute bedding, sedimentary breccias, synsedimentary faults, and sandstone dikes (Photo 173.6) suggest that the depositional environment was tectonically active, perhaps due to contemporaneous volcanic processes. Spatial association of the interflow sedimentary and volcanic rocks, as well as the abundance of volcaniclastic and epiclastic components, support a predominantly volcanic provenance for the sediments.

SULPHIDE MINERALIZATION

Sulphide mineralization in Archean volcanic and interflow sedimentary rocks in the Cobalt area has been described most recently by Patterson (1979). Subsequent studies by Goodz (1985) and Goodz *et al.* (in press) have stressed the spatial association of silver veins to base-metal occurrences in the basement rocks. The present study further assesses syngenetic and epigenetic sulphides (±sulpharsenides) in the interflow sedimentary rocks, and to a lesser extent in the volcanic rocks, in an effort to identify distinct mineralization events and processes.

Syngenetic sulphides in volcanic rocks are well documented (Dillon-Leitch 1980; MacQueen 1985; MacRobbie 1986). Pyrrhotite and pyrite, with minor chalcopyrite, galena, sphalerite, and marcasite, occur as disseminated grains in pillowed and massive flows. The sulphides commonly are concentrated in pillow selvages, interpillow spaces, hyaloclastites, and in breccias of flow or pyroclastic origin (Photo 173.7). Volcanogenic massive sulphides are observed as thin and discontinuous lenses at the top of the flow sequences, and typically are underlain by a sulphide stockwork.

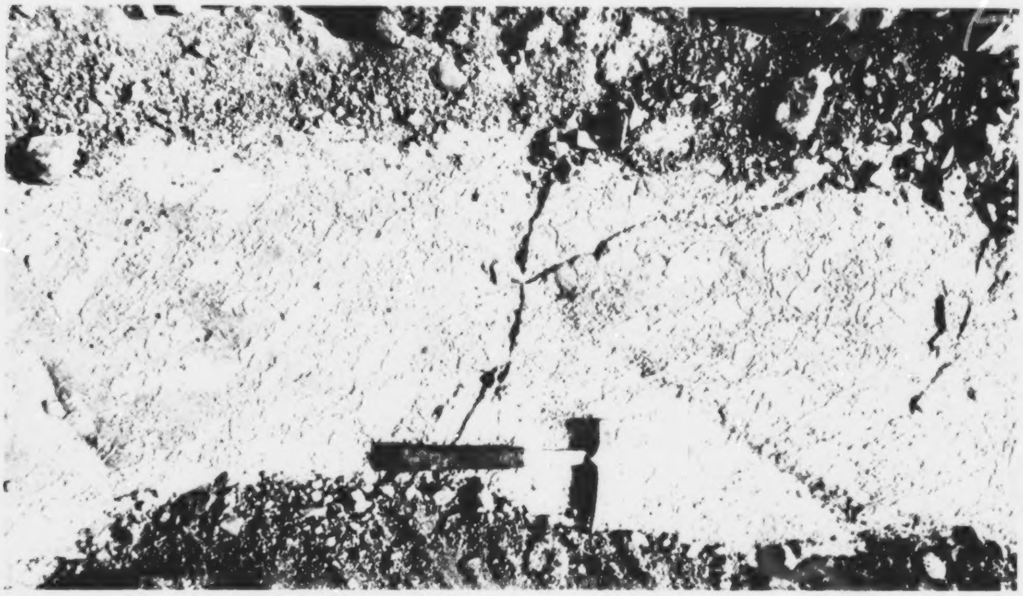

Photo 173.7. *Phreatic breccia in volcanic flow, Nipissing Hill (south) RL 404 Property. Angular silicified volcanic clasts are in massive pyrite matrix.*

Two broad types of syngenetic sulphides have been identified in the interflow sedimentary rocks:

1. Volcanogenic (exhalative) sulphides in chert and siliceous argillite.
2. Iron sulphides of probable diagenetic origin in pelagic black shales.

An exhalative origin has been ascribed to examples of the first type (Petruk 1971a), which commonly consists of sphalerite-rich sulphide layers and lenses

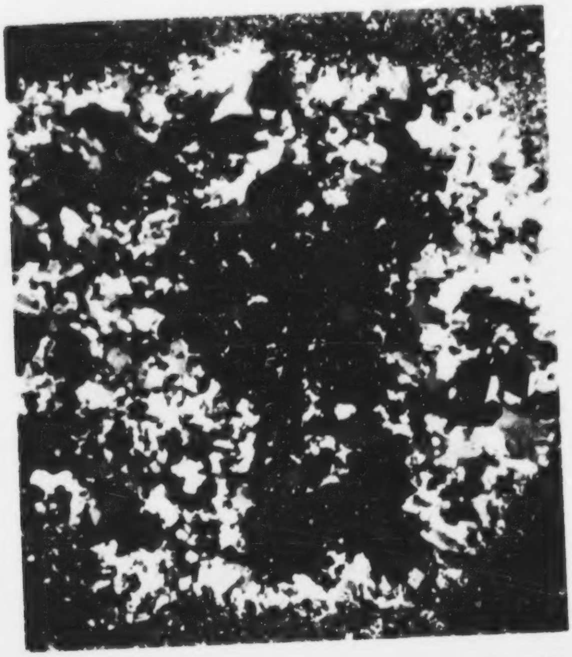

Photo 173.8. *Photomicrograph in transmitted light of pyrite - quartz nodule in black shale. Nipissing Hill (south) RL 404 Property. Field of view is 8 mm wide.*

Photo 173.9. *Aggregate of pyrite nodules and lenticular sulphide masses, Windsor - Cobalt Property.*

intercalated with cherts and siliceous argillites. Chlorite and quartz are intimately associated with these sulphides.

The primary sulphides in the black shales comprise pyrite, pyrrhotite, and marcasite. Although a diagenetic origin is favoured, the iron and sulphur may have had a volcanogenic source. This type is characterized by a marked absence of sphalerite and other base-metal sulphides. Pyrite and pyrrhotite ± marcasite occur as disseminated grains and in lenses and thin layers. Less commonly, grains of pyrite (± marcasite ± pyrrhotite) form small (1 to 3 mm) nodules with quartz (Photo 173.8) or larger (up to 20 mm) concretionary nodules with a radial and/or concentric internal geometry. These nodules are either isolated or form large coalescing aggregates (Photo 173.9). Primary pyrite and marcasite commonly are replaced by pyrrhotite, chalcopyrite, galena, and sphalerite. Drusy chlorite commonly mantles the sulphides. Quartz-filled pressure shadows have developed on some strained nodules.

Epigenetic sulphides in both volcanic and sedimentary rocks are due to the mobilization of syngenetic basement sulphides and to the introduction of sulphides associated with later Ag-Bi-Co-Ni-As hydrothermal solutions. Mobilization of pre-existing sulphides has been considered to be essential in the development of silver-vein hydrothermal systems (Goodz 1985; Goodz *et al.*, in press; Watkinson, in press). As a result, a detailed study of mobilized sulphides has been undertaken to evaluate vein-basement paragenetic relationships.

Mobilized sulphide mineralization has been distinguished from vein sulphides and sulphides in brecciated wall rocks adjacent to veins by Goodz (1985) and Goodz *et al.* (in press). Features suggestive of mobilization can be observed in all rocks with pre-existing sulphides, and in those proximal to mineralized zones. Sphalerite-galena-chalcopyrite-pyrite veinlets extend obliquely from stratiform iron-sulphide layers in the interflow sedimentary rocks, especially argillite (Photo 173.10). Narrow, possible shear zones that contain massive chalcopyrite, galena, and sphalerite in close association with chlorite and quartz, may represent similar processes on a larger scale. Some of these zones contain cobaltite and other sulpharsenide minerals. More notable, however, is the evidence of pervasive sulphides in the clastic sedimentary rocks. Sphalerite and chalcopyrite, the predominant introduced sulphides, compose up to 20% of the altered rock. These minerals occur in small veinlets or, more commonly, as extensive replacements of both matrix and framework constituents and primary sulphides (Photo 173.3). Mineralization has been accompanied by chloritization, carbonatization, and silicification, all of which have served to obscure or destroy primary textures and structures.

Limited chemical analyses of sulphides in zones of presumed mobilization have revealed that the sulphides have distinct chemical and isotopic characteristics. Sulphur isotope data obtained by Wilson (discussed below) for veinlets branching from stratiform sulphide layers show relatively high δ^{34}S values, comparable to those obtained from the associated stratiform sulphides and to those considered to be background levels in basement sulphides (Goodz 1985; Goodz *et al.*, in press). Electron microprobe analyses of coexisting sphalerite and chlorite in interflow sedimentary rocks have revealed that both minerals have slightly lower Fe contents in comparison to pairs from stratiform sulphides in argillite. Significant variations in composition do exist, however, and thus the suggested trends may be applicable only for distinguishing distinct types on a local scale.

Photo 173.10. *Sphalerite-galena-chalcopyrite-pyrite veinlets branching from stratiform pyrrhotite-pyrite bands in siliceous argillite, Nipissing Hill (south) RL 404 Property.*

DISCUSSION

Doyle and Dass (1971) proposed that ore and gangue elements in native silver veins were derived principally from sulphide-rich interflow sedimentary rocks, and to a lesser extent from the volcanic rocks. Petruk (1971a) suggested that interflow units may have served as loci for fracturing and subsequent ore deposition, and thus may have structurally influenced the vein development. Subsequent workers have studied the geochemical and structural relationships that exist between silver veins and Archean host rocks in an attempt to better understand the genetic processes, and to delineate favourable areas for silver exploration. The present study has revealed features in Archean rocks which may have directly influenced the development of silver veins, and which can aid in the recognition of vein-related processes.

A working hypothesis, summarized by Watkinson (in press), suggests that sulphide units in the Archean basement near silver veins were the source of metals, sulphur, and other non-metals in the veins. According to this hypothesis, these elements were concentrated in Proterozoic formational fluids which migrated from the sedimentary strata of the overlying Gowganda Formation into permeable zones in the basement, particularly along the sulphide-rich interflow sedimentary units and shear zones. Intrusion of the Nipissing Diabase locally heated these fluids and increased both the metal solubility and hydrostatic pressure. When fracturing occurred, the metal-rich fluids escaped into fractures, resulting in rapid precipitation of the vein minerals as they underwent phase separation or boiling (Strong 1985).

Since this model relies heavily on spatial, structural, and geochemical relationships of the silver veins to interflow sedimentary rocks, careful description of the latter in terms of petrology, structure, mineralogy, and alteration is imperative. Although petrologic studies have identified a variety of interflow sedimentary facies and have aided in developing a sedimentological model, additional work is required to determine the possible petrologic and/or geochemical affinities between specific rock types and silver vein mineralization. Similarly, detailed mapping of Proterozoic and Archean rocks is essential to develop a stratigraphic and structural framework which will enable the tracing of narrow interflow sedimentary units beneath Proterozoic cover rocks, and the recognition of sites of fluid migration and vein deposition. Preliminary studies have shown that the Archean rocks have had a complex history of mineralization and alteration which, when elucidated, will greatly assist in resolving the relationship between basement sulphides and Ag-Bi-Co-Ni-As veins.

SUMMARY

Archean interflow sedimentary rocks in the Cobalt area can be assigned to a predominantly immature turbidite facies (wacke, paraconglomerate, iron formation, and derived breccias). Chert and pelagic black shale constitute a lesser but significant part of the sedimentary rocks. Although some interflow units are laterally continuous, abrupt facies changes due to turbidite scouring, synsedimentary deformation, folding and faulting may significantly impede lithologic correlation and the construction of representative stratigraphic sections. The Archean sedimentary units generally are best exposed above massive to pillowed volcanic flow units, and some are in juxtaposition with lenses of exhalative chert and massive sulphides.

Syngenetic sulphides occur in interflow sedimentary rocks as banded to nodular iron-sulphides in pelagic black shales, and as sphalerite-dominant exhalative sulphides associated with chert and siliceous argillite. Epigenetic sulphide mineralization has been well developed in all rock types in the form of mobilized sulphides (±sulpharsenides) in veinlets that branch from syngenetic sulphide layers, and in pervasive sulphide replacements that are accompanied by extensive chloritization, carbonatization, and silicification.

The close spatial association of silver veins and sulphide-rich interflow sedimentary rocks is suggestive of a genetic relationship. Petrographic study has revealed a complex mineralization and alteration history. Additional study is needed to identify the common paragenetic features, and to establish the causative factors of sulphide, sulpharsenide, and Ag-Bi-Co-Ni-As mineralization.

SULPHUR ISOTOPES

Sulphur-isotope ratios have been determined for sulphide minerals from eight sites in addition to those described by Donaldson *et al.* (1984) and Goodz *et al.* (in press) (Figure 173.1). Most samples come from the Coleman Member of the Gowganda Formation, although some Archean rocks were sampled as well. Most of the sample sites are surface exposures near abandoned mines where host-rock samples were taken at specific distances from the veins. Areas sampled include: Little Silver Vein, MacDonald Vein, Vein Three, Fleming Vein, Drummond Cairn, Nipissing Hill, Coniagas-Trethewey Mine, and the northern extension of Vein 65. Data from these sites will be presented in the final report for Grant 173 and by Wilson (in preparation). The Little Silver Vein area is described here in terms of sulphur-isotope variations; preliminary descriptions of these sulphides were presented by Donaldson *et al.* (1985).

Thinly laminated siltstones at Little Silver Vein contain about 0.5% blastic sulphide minerals with a grain size less than 2 mm. Sulphide mineralogy within 6 m of the vein-cut is dominated by pyrrhotite, chalcopyrite, and gersdorffite. Blastic pyrite predominates at distances farther from the vein. Sulphur-isotope ratios of these minerals with respect to distance from Little Silver Vein are presented in Figure 173.2. Pyrrhotite appears to be a pseudomorph after euhedral pyrite (Photos 173.11 and 173.12), and probably resulted from interaction with a fluid of low sulphur fugacity capable of altering pyrite to pyrrhotite and generating pyrrhotite with isotopically heavier sulphur; such fluids are typical of the vein-related fluids that precipitated silver in the Cobalt camp (Goodz *et al.*, in press). Goodz *et al.* (in press) suggested that the ore-forming fluids derived sulphur from a reaction in the Archean basement rocks where pyrite altered to pyrrhotite and released sulphur with a $\delta^{34}S$ value of +5.0 to +11.0 ‰. Sulphur-isotope ratios of the pyrrhotite and chalcopyrite are much higher than those presumed to be representative of background $\delta^{34}S$ values in pyrite (Figure 173.2), and are compatible with the higher isotopic ratios characteristic of vein sulphides (Petruk 1971b; Donaldson *et al.* 1984).

The presence of a Co-Ni-As-bearing mineral (tentatively identified as gersdorffite) in siltstone immediately adjacent to the Little Silver Vein also suggests interaction with a vein-related fluid capable of carrying and precipitating these elements. Pyrite adjacent to this zone contains up to several percent chalcopyrite as inclusions, and has higher $\delta^{34}S$ values than pyrite several metres farther from the vein. This suggests that laterally migrating, vein-related fluids reacted with pyrite and altered its isotopic signature, without causing mineralogic change.

Arenites and orthoconglomerates occur stratigraphically above the siltstones at Little Silver Vein. At distances greater than 6 m from the vein-cut wall, sulphide minerals in the arenites are minor to absent. Closer to the vein, a wide variety of sulphide minerals occur in close association with chlorite. The sulphide minerals are chalcopyrite, arsenopyrite, ger-

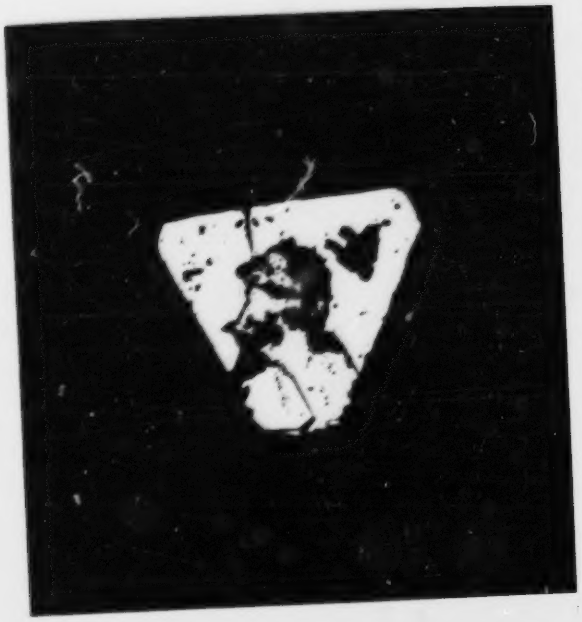

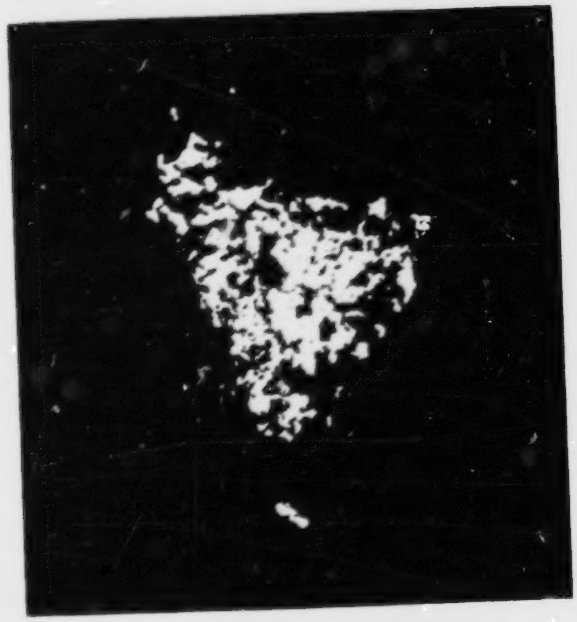

Photo 173.11. *Photomicrograph in reflected-light, showing sulphide minerals in laminated siltstone, Little Silver Vein*

a) Euhedral pyrite with a core of chalcopyrite. Diameter of grain is 0.2 mm.

b) Pyrrhotite pseudomorph, after euhedral pyrite. Diameter of grain is 0.8 mm.

sdorffite, boulangerite, acanthite, galena, silver-rich tetrahedrite, pyrrhotite and pyrite. The presence of Ag, Co, Ni, Sb, and As-bearing minerals, and their high sulphur-isotope ratios (Table 173.1), suggest that these sulphide minerals also were deposited from vein-related fluids.

Sulphide minerals in the orthoconglomerate adjacent to the arenite-orthoconglomerate contact are similar to those in the arenite, but the sulphide minerals are less abundant with increasing distance from this contact, and consist mainly of pyrite with lesser chalcopyrite. The sulphides are isotopically heavier near the vein, and lighter farther away (Table 173.1), indicating that vein-related fluids interacted with the sulphides near the vein, and altered their sulphur-isotope composition.

Sulphide minerals within the siltstones have higher than background $\delta^{34}S$ values as much as 10 m from the vein contact, but in the arenite and the conglomerate this distance is about 6 m. This probably is due to differential permeabilities of the wall rocks. The siltstones are characterized by fine laminations and are fractured to a much greater degree than the arenites and orthoconglomerates (Donaldson *et al.* 1984). This probably permitted the vein-related fluids to migrate farther in the siltstones than in the arenites and conglomerates, thus affecting a wider area on either side of the vein.

In summary, sulphide minerals are more abundant nearest the silver-bearing vein at Little Silver Vein, and consist of a wide variety of species that contain a wide variety of elements, whereas, farther away, the sulphides generally are less abundant or absent, and consist mainly of pyrite with subordinate chalcopyrite. Sulphur-isotope ratios are highest in the multi-element sulphides nearest the vein, and are lowest in the pyrite distant from the vein. The vein-related fluids are inferred to have migrated through the rocks at a rate determined by local permeability, which in turn controlled the distance from the vein within which the fluids were able to interact. As these fluids permeated the wall rocks, they deposited isotopically heavier-than-background sulphide minerals, some of which contain elements characteristic of the vein, and/or altered the isotopic signature of any pre-existing sulphide minerals.

ACKNOWLEDGMENTS

We express thanks to B.O. Dressler, A.C. Colvine, and John Wood (Geologists, Ontario Geological Survey, Toronto), for their helpful advice during preliminary planning of this project. Leo Owsiacki (Resident Geologist, Ontario Geological Survey, Cobalt), together with his staff, provided invaluable advice and access to their library and laboratory facilities. Paul MacRobbie provided cheerful assistance during the 1985 field season.

The effort, time, and accessibility to the Beaver-Temiskaming and Langis Mines provided by Agnico-Eagle Mines Limited, Cobalt, is greatly appreciated. Special thanks are extended to Douglas Robinson and David Marek, the mine geologists for these mines. Field work was supported in part by Natural Sciences and Engineering Research Council (NSERC)

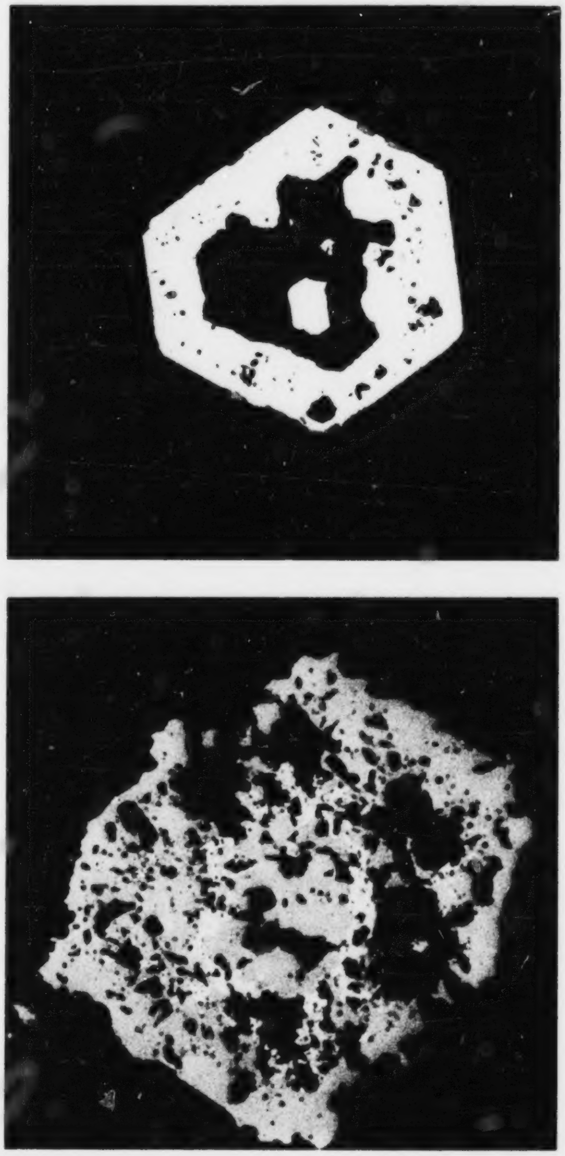

Photo 173.12. *Photomicrograph in reflected-light, showing sulphide minerals in laminated siltstone, Little Silver Vein.*

a) Euhedral pyrite showing a hexagonal outline. Core is composed of silt-sized detritus. Diameter of grain is 0.3 mm.

b) Pyrrhotite pseudomorph after euhedral pyrite. The vermiform zone of slightly higher reflectance within the pyrrhotite is gersdorffite.

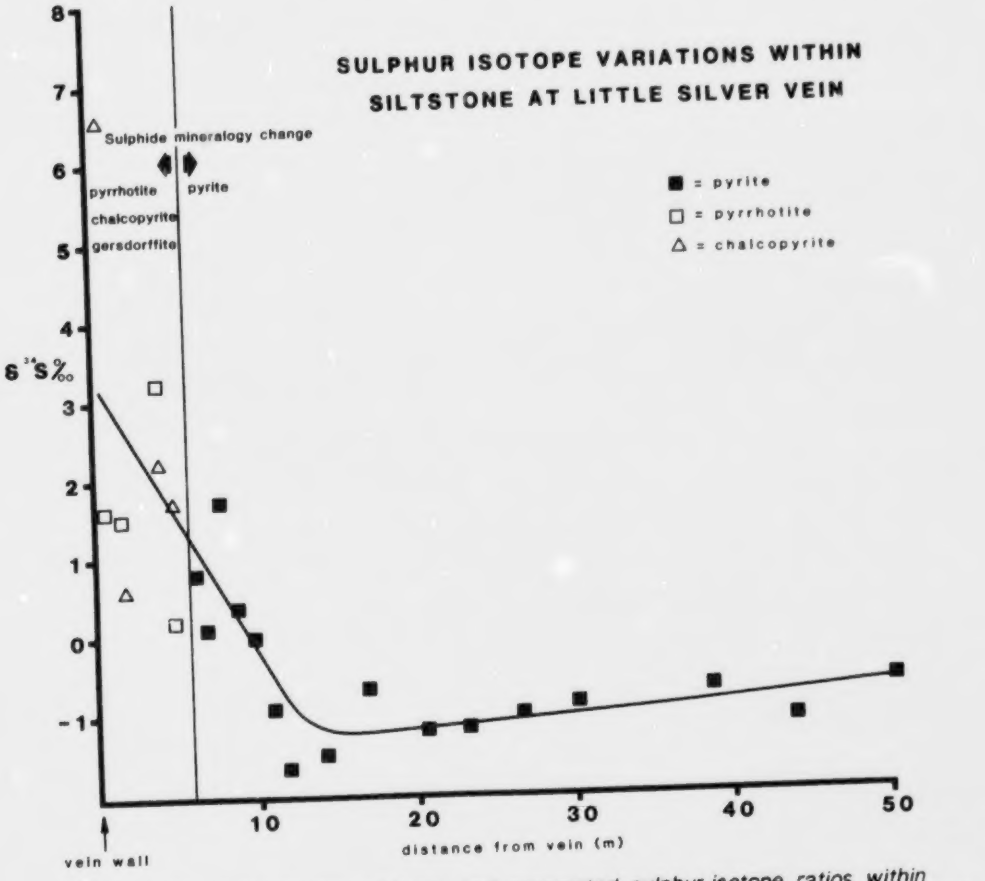

Figure 173.2. Sulphide assemblages and associated sulphur-isotope ratios within laminated siltstone at Little Silver Vein, displayed with respect to distance from the vein

Grants A5536 (J.A. Donaldson), A2646 (F.A. Michel), and A7874 (D.H. Watkinson).

The advice of, and banter with, students and colleagues engaged in ancillary projects previously reported was of extreme value in preparing this report. In this regard, we wish to particularly mention: P. Mustard, R. Rainbird, L. Aspler, G. Burbidge, and M. Goodz.

REFERENCES

Barrett, T.J., and Fralick, P.W.
1985: Sediment Redeposition in Archean Iron Formation: Examples from the Beardmore–Geraldton Greenstone Belt, Ontario; Journal of Sedimentary Petrology, Volume 55, Number 2, p.205-212.

Boyle, R.W., and Dass, A.S.
1971: The Origin of the Native Silver Veins at Cobalt, Ontario; p.414-417 *in* The Silver–Arsenide Deposits of the Cobalt–Gowganda Region, Ontario, edited by L.G. Berry, Canadian Mineralogist, Volume 11, Part 1.

Cobbold, P.R., and Quinquis, H.
1979: Development of Sheath Folds in Shear Regimes; Journal of Structural Geology, Volume 2, Number 1-2, p.119-126.

Dillon-Leitch, H.
1980: Alteration and Mineralization in Archean Volcanic Rocks of the Cobalt Area, p.191-194 *in* Summary of Field Work, 1980, by the Ontario Geological Survey, edited by V.G. Milne, O.L. White, R.B. Barlow, J.A. Robertson, and A.C. Colvine, Ontario Geological Survey, Miscellaneous Paper 96.

Donaldson, J.A., Goodz, M.D., Michel, F.A., Mustard, P.S., Rainbird, R.H., Rust, B.R., Watkinson, D.H., and Wilson, B.
1984: Sedimentary Rocks and Strata-Bound Mineralization in the Cobalt Region; Grant 173, p.198-210 *in* Geoscience Research Grant Program, Summary of Research 1983-1984, edited by V.G. Milne, Ontario Geological Survey, Miscellaneous Paper 121, 252p.

TABLE 173.1. SULPHUR ISOTOPE COMPOSITION OF SAMPLES FROM WALLROCK, LITTLE SILVER VEIN.

Sample Number	Type	Distance from Vein (m)	Rock Type	$\delta^{34}S$ (‰CT)
LSV-33	cp	3.7	arenite	1.0
LSV-38	cp	4.1	arenite	0.9
LSV-39	cp	4.6	arenite	1.3
LSV-47	cp 20% py 60% ars 20%	1.4	arenite	0.8
LSV-51	cp	5.7	arenite	0.9
LSV-59	py 75% cp 15% ars 10%	0.9	arenite	1.6
LSV-60	cp	4.5	arenite	1.1
LSV-63	cp	5.1	arenite	0.8
LSV-64	cp	5.3	arenite	1.1
LSV-42	ars	5.3	siltstone	4.6
LSV-43	ars	4.5	siltstone	4.5
LSV-44	ars 90% cp 10%	3.0	siltstone	3.9
LSV-30	py	4.0	conglomerate	1.2
LSV-32	cp	4.5	conglomerate	1.0
LSV-35	po	1.2	conglomerate	1.1
	cp			2.6
	gal			-0.9
LSV-36	ars 90% cp 10%	1.8	conglomerate	3.6
LSV-56	py	6.8	conglomerate	-0.5
LSV-57	cp+py	16.8	conglomerate	-1.1

Donaldson, J.A., Michel, F.A., Mustard, P.S., Rainbird, R.H., Rust, B.R., Watkinson, D.H., and Wilson, B.
1985: Sedimentary Rocks and Strata-Bound Mineralization in the Cobalt Region; Grant 173, p.87-100 *in* Geoscience Research Grant Program, Summary of Research 1984-1985, edited by V.G. Milne, Ontario Geological Survey, Miscellaneous Paper 127, 246p.

Goodz, M.D.
1985: Geology and Isotope Geochemistry of the Beaver–Timiskaming Silver Mine, Cobalt, Ontario; Unpublished M.Sc. Thesis, Carleton University, Ottawa, Ontario, 246p.

Goodz, M.D., Watkinson, D.H., Smejkal, V., and Pertold, Z.
In Press: Sulphur Isotope Geochemistry of Silver–Sulpharsenide Vein Mineralization, Cobalt, Ontario; Canadian Journal of Earth Sciences.

Jambor, J.L.
1971: General Geology; p.12-33 *in* The Silver–Arsenide Deposits of the Cobalt–Gowganda Region, Ontario, edited by L.G. Berry, Canadian Mineralogist, Volume 11, Part 1.

Knight, C.W.
1924: Geology of the Mine Workings of Cobalt and South Lorrain Silver Areas; Ontario Department of Mines, Annual Report for 1922, Volume 31, Part 2, p.1-238.

MacQueen, J.K.
1985: Sulphide Mineralogy and Chemistry in Archean Rocks Near Silver Veins, Cobalt, Ontario; Unpublished B.Sc. Thesis, Carleton University, Ottawa, Ontario, 57p.

MacRobbie, P.A.
1986: Archean Volcanic Rocks and Associated Base-Metal Sulphides, Nipissing Hill (South) Area, Cobalt, Ontario; Unpublished B.Sc. Thesis, Carleton University, Ottawa, Ontario, 52p.

Mustard, P.J.
1985: Sedimentology of the Lower Gowganda Formation Coleman Member (Early Proterozoic) at Cobalt, Ontario; Unpublished M.Sc. Thesis, Carleton University, Ottawa, Ontario, 143p.

Patterson, G.C.
1979: Metallogenetic Relationships of Base-Metal Occurrences in the Cobalt Area; p.222-229 *in* Summary of Field Work, 1979, by the Ontario Geological Survey, edited by V.G. Milne, O.L. White, R.B. Barlow, and C.R. Kustra, Ontario Geological Survey, Miscellaneous Paper 90, 245p.

Petruk, W.
1971a: General Characteristics of the Deposits; p.76-107 *in* The Silver–Arsenide Deposits of the Cobalt–Gowganda Region, Ontario, edited by L.G. Berry, Canadian Mineralogist, Volume 11, Part 1.

1971b: Sulphur Isotope Abundance Ratios for the Sulphides in the Cobalt-Gowganda Ores; p.391-395 *in* The Silver-Arsenide Deposists of the Cobalt-Gowganda Region Ontario, edited by L.G. Berry, Canadian Mineralogist, Volume 11, Part 1.

Rainbird, R.H.
1985: Sedimentology of the Firstbrook Member of the Gowganda Formation in the Eastern Cobalt Basin, Ontario: Unpublished M.Sc. Thesis, Carleton University, Ottawa, Ontario, 157p.

Smyk, M.C., and MacRobbie, P.A.
1986: A Preliminary Investigation of Archean Interflow Sedimentary Rocks, Cobalt Silver Area, Ontario, 22nd Western Inter-University Geological Conference Program with Abstracts, Saskatoon, Saskatchewan, January 23-25, 1986.

Strong, D.F.
1985: Genesis of Ag-Co-Ni Arsenide Vein Deposits Like those of the Cobalt District of Ontario; Silver '85 Symposium, Geological Association of Canada, Cordilleran Section, Vancouver, British Columbia, March 27-28, 1985, Program, p.13-16.

Turner, C.C., and Walker, R.G.
1973: Sedimentology, Stratigraphy, and Crustal Evolution of the Archean Greenstone Belt near Sioux Lookout, Ontario; Canadian Journal of Earth Sciences, Volume 10, p.817-845.

Walker, R.G.
1984: Turbidites and Associated Coarse Clastic Deposits; p.171-188 *in* Facies Models, edited by R.G. Walker, Geological Association of Canada.

Watkinson, D.H.
In Press: Mobilization of Archean Elements Into Proterozoic Veins: an Example from Cobalt, Canada; Metallogenesis of the Precambrian, Geological Survey of Czechoslovakia.

Wilson, B.
In Preparation: A Sulphur Isotope and Structural Study of the Silver-Vein Host-Rocks at Cobalt, Ontario; M.Sc. Thesis, Carleton University, Ontario.

Grant 189 The Sedimentology and Stratigraphy of the Bar River Formation (Huronian Supergroup) at Bay Finn, Lake Huron

B.R. Rust and M.J. Shields

Department of Geology, University of Ottawa and Ottawa-Carleton Centre for Geoscience Studies, Ottawa

ABSTRACT

The thickest exposed section of the Bar River Formation is at Bay Finn, where about 1 km of strata is present. The conformable contact with the Gordon Lake Formation shows gradual upward coarsening over a 30 m interval.

The lower 80 m of the Bar River Formation is composed of horizontally stratified to massive quartzites. Above this level, cross-strata are common in sets less than 30 cm thick, mainly planar/tangential, with minor troughs. Bi-directional orientation is a persistent feature: wave and current-formed ripples are also present. This suite of sedimentary structures and the maturity of the quartzites suggest deposition in a shallow marine environment. In the context of the conformable Lorrain-Gordon Lake-Bar River succession, the Bar River is interpreted as a shoaling shelf or barrier deposit, separated from the coastal/alluvial plain of the Lorrain by the inner shelf/lagoonal Gordon Lake Formation.

X-ray diffraction of Bar River argillites shows illite/sericite to be the dominant clay mineral. Major element analyses yield chemical alteration indices varying from 70 to 80, which indicate intense weathering of the source area, consistent with the mature composition of the quartzites. Thinning- and fining-upward sequences from quartzite to minor argillite predominate over thickening-upward sequences. The former are attributed to lateral migration of tidal inlet channels or to general subsidence, the latter to seaward progradation of the barrier system. The absence of eolian cross-strata suggests domination by wave and current reworking, mainly within tidal limits. Horizontally stratified lower Bar River quartzites are attributed to washover progradation into the lagoon.

The barrier, postulated for the Bar River Formation, restricted circulation in the Gordon Lake lagoons. The resulting reduced environment caused precipitation of stratiform metalliferous deposits near the Lorrain-Gordon Lake boundary.

INTRODUCTION

The Bar River Formation is mainly composed of quartzose sandstone or quartzite, and occurs at the top of the Cobalt, the uppermost group of the Huronian Supergroup. The Cobalt Group is composed of four conformable formations which are, in ascending order, the Gowganda, Lorrain, Gordon Lake, and Bar River Formations (Card 1978).

Exposures of the Bar River Formation are known from five main areas within the Huronian outcrop belt (Figure 189.1). Preliminary work was done in 1984 on the Flack Lake and Bay Finn areas (Wright and Rust 1985). Field work in 1985 concentrated on the Bay Finn area (Figure 189.2) because it contains the thickest section of the Bar River Formation, and ex-

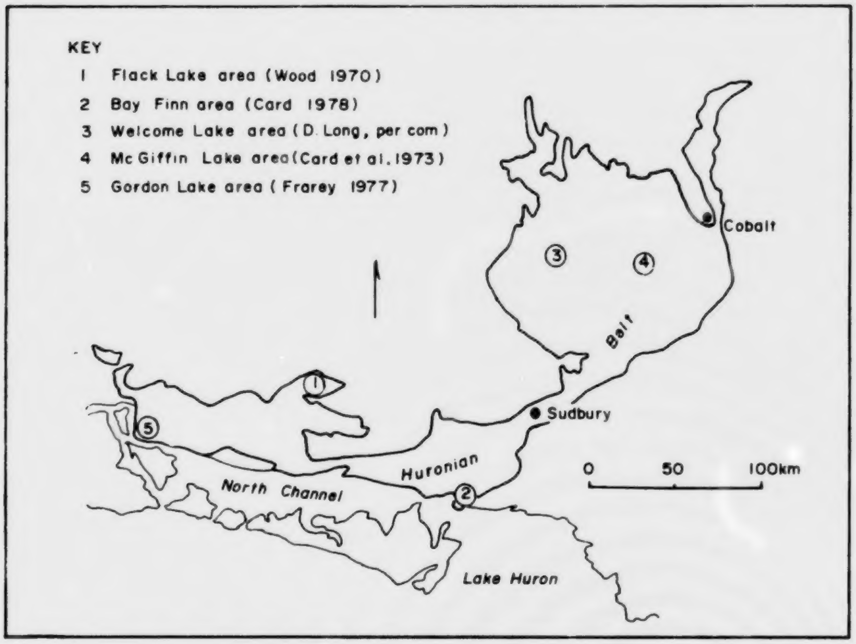
KEY
1 Flack Lake area (Wood 1970)
2 Bay Finn area (Card 1978)
3 Welcome Lake area (D. Long, per com)
4 McGiffin Lake area (Card et al. 1973)
5 Gordon Lake area (Frarey 1977)
Cobalt
③
④
Belt
①
Sudbury
⑤
Huronian
②
North Channel
Lake Huron
0
50
100km

Figure 189.1. *Outcrop areas of Bar River Formation within Huronian belt.*

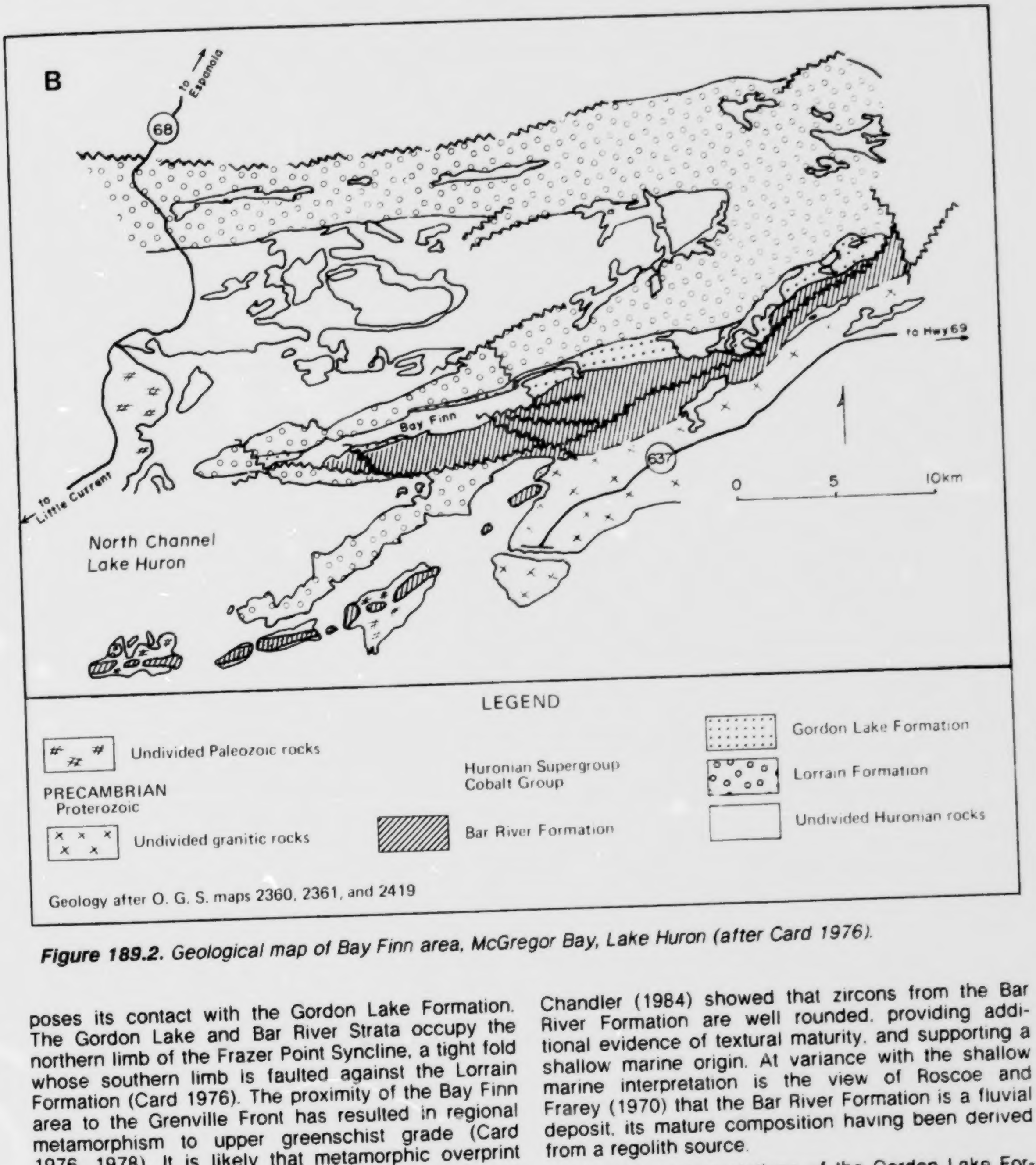
B
68
to Espanola
to Hwy69
Bay Finn
637
to Little Current
North Channel
Lake Huron
0
5
10km
LEGEND
Undivided Paleozoic rocks
PRECAMBRIAN
Proterozoic
Undivided granitic rocks
Huronian Supergroup
Cobalt Group
Bar River Formation
Gordon Lake Formation
Lorrain Formation
Undivided Huronian rocks
Geology after O. G. S. maps 2360, 2361, and 2419

Figure 189.2. *Geological map of Bay Finn area, McGregor Bay, Lake Huron (after Card 1976).*

poses its contact with the Gordon Lake Formation. The Gordon Lake and Bar River Strata occupy the northern limb of the Frazer Point Syncline, a tight fold whose southern limb is faulted against the Lorrain Formation (Card 1976). The proximity of the Bay Finn area to the Grenville Front has resulted in regional metamorphism to upper greenschist grade (Card 1976, 1978). It is likely that metamorphic overprint has obscured some of the sedimentary features, so that massive strata in the Bay Finn area may not have been originally structureless.

Pettijohn (1970) interpreted the Bar River Formation as a shallow marine deposit on the basis of textural and compositional maturity. On the same basis, plus polymodal paleocurrents, Card (1978) concluded that the Bar River environment was a nearshore, coastal shelf, subject to repetitive transgressions and regressions. Based on observations in the Flack Lake area, Wood (1973) attributed the Bar River to deposition on a beach subject to eolian influence. Chandler (1984) showed that zircons from the Bar River Formation are well rounded, providing additional evidence of textural maturity, and supporting a shallow marine origin. At variance with the shallow marine interpretation is the view of Roscoe and Frarey (1970) that the Bar River Formation is a fluvial deposit, its mature composition having been derived from a regolith source.

Previous interpretations of the Gordon Lake Formation have also varied, although all workers have agreed on a marine origin. Wood (1973), Card (1976), and Frarey (1977) identified desiccation cracks in fine-grained units in the Flack Lake, McGregor Bay, and Sault Ste. Marie areas respectively, concluding that deposition was on tidal or supratidal flats. However, Card (1978) reinterpreted the desiccation cracks as syneresis cracks, a view supported by Chandler (1984, 1986). In addition, Card (1978) attributed graded units and other features of the Gordon Lake succession to turbidity currents, and postulated

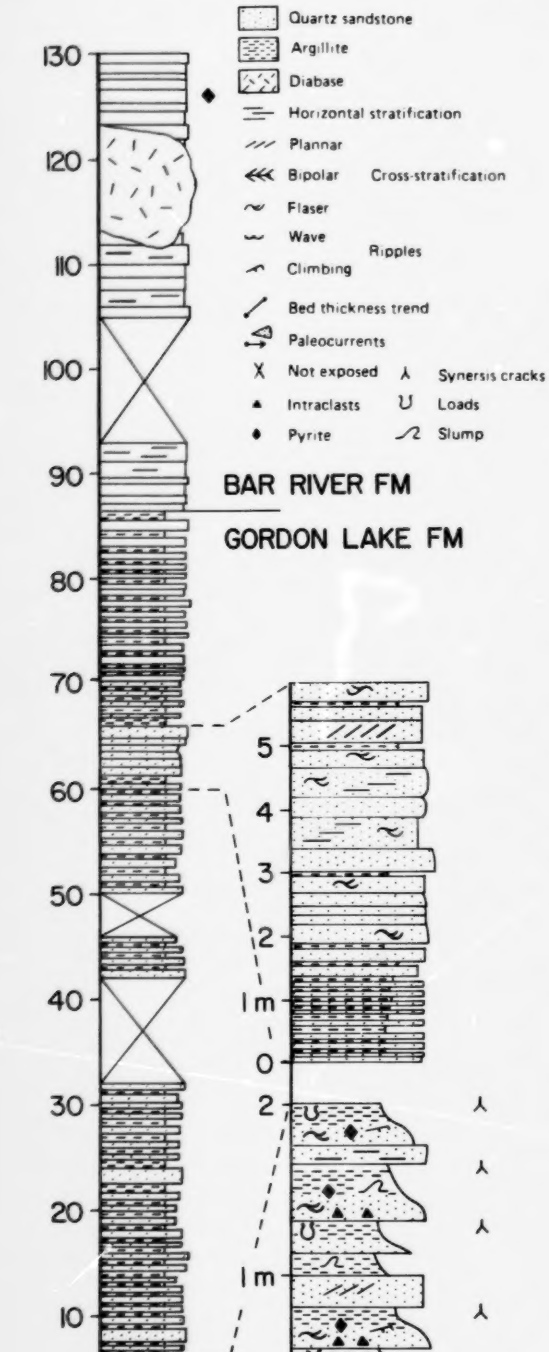

Figure 189.3. Composite section of upper part of Gordon Lake Formation and lower part of Bar River Formation, scuth shore of Bay Finn.

deposition below wave base. Chandler (1984, 1986) reinterpreted the graded units as storm deposits, and assigned the greater part of the Gordon Lake Formation to deposition on a storm-dominated marine shelf. Chandler (1985, 1986) attributed gypsum- and anhydrite-bearing units at the base of the Bar River Formation, previously recognized by Wood (1973), to deposition on tidal flats in hot, relatively dry conditions.

THE GORDON LAKE–BAR RIVER TRANSITION

Figure 189.3 shows a composite section of the transition from the upper Gordon Lake to the lower Bar River Formation compiled from sections measured along several traverses south of Bay Finn. The expanded section from 4 to 6 m shows typical Gordon Lake strata, essentially identical to those illustrated by Chandler (1984, Figure 27.3B) from the Flack Lake area. Identification of hummocky cross-stratification in several graded sandstone layers provides confirmation of Chandler's (1984) hypothesis of an origin as storm-generated units (Duke 1985; Dott and Bourgeois 1982). The identification of syneresis as opposed to desiccation cracks was not always possible because of the rarity of bedding-plane exposures at Bay Finn. However, the cross-sectional views of these structures are identical to syneresis cracks seen also on bedding-planes in the Flack Lake section of the Gordon Lake Formation.

The upper part of the Gordon Lake Formation shows gradual transition to the Bar River over a 30 m interval. Nevertheless, the formational boundary as described by Card (1976, 1978) can be recognized without difficulty at the level where interbedded quartzite/argillite pairs are replaced consistently by quartzite units that lack argillite, or are separated by thin argillite partings (87 m, Figure 189.3). This change in sedimentary style is anticipated by a coarsening-upward sequence between 60 and 66 m, which also shows upward increase in bed thickness. Another feature indicative of the onset of Bar River depositional conditions is that these quartzite units lack the upward grading typical of the Gordon Lake. Instead, they are "blocky" with sharp tops as well as bases.

The Gordon Lake-Bar River succession is interpreted as a shoaling-upward sequence, in which sand was no longer worked only during storms, but was subject to more continuous wave and current reworking. Hence, fine sediment was winnowed from the depositional system, to be deposited elsewhere in quiet, deeper water.

THE BAR RIVER FORMATION

Figure 189.4 is a composite section of the Bar River Formation compiled from several traverses across the northern limb of the Frazer Point Syncline (Card 1976, Map 1317). The synclinal axis could not be located precisely, due to scattered outcrop and the presence of several parasitic folds. Hence, the measured section was discontinued at 975 m although the full thickness of the Bar River probably exceeds 1000 m at this locality.

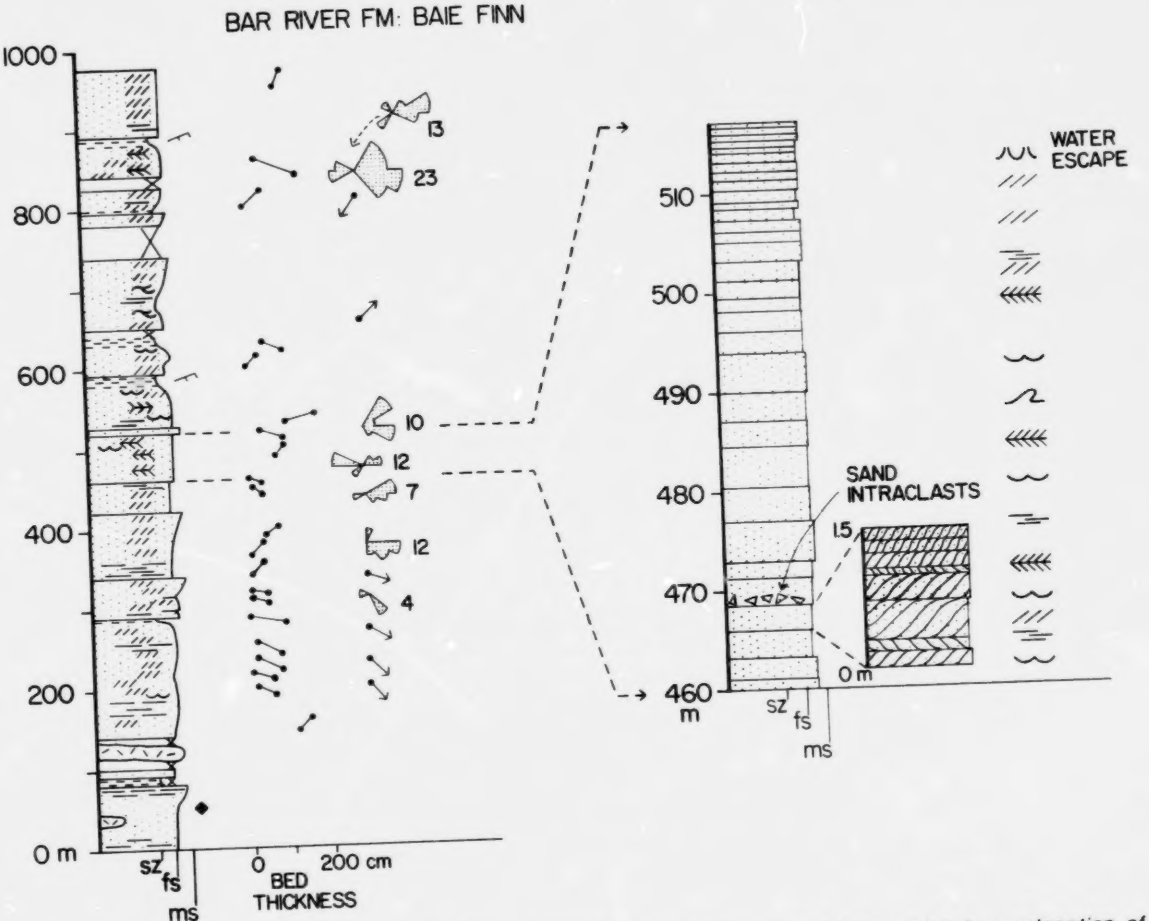

Figure 189.4. Composite section of Bar River Formation at Bay Finn. See Figure 189.3 for explanation of symbols.

STRATIGRAPHY AND SEDIMENTOLOGY

The lower 80 m of Bar River strata are characterized by horizontally stratified or massive quartzite units, with minor cross-strata. The breccia described by Wright (1985) was found to contain fragments of the amphibolitic intrusions that cut the Bar River Formation. It does not appear to be a stratiform unit, and most probably is a tectonic breccia.

From 80 to 575 m the section is dominated by cross-stratified quartzite in sets up to 30 cm thick (Figure 189.4). There are two minor units of argillite, but this part of the section essentially lacks argillite interbeds. The cross-strata are predominantly planar/tangential, but minor troughed sets are also present. Horizontally-stratified quartzite and wave rippled bedding planes are abundant. Soft-sediment deformation features in the form of slumps and water escape features are present but rare. They represent penecontemporaneous adjustment to depositional slopes (mainly crossbed foresets), or to superimposed load or adjustment to external shock such as breaking waves (Dalrymple 1979).

Stratigraphically adjacent cross-stratal sets with opposed dip directions ("herring-bone" sets) are a significant, but not abundant, feature of this part of the succession. The bi-directional nature of paleocurrents suggested by the herring-bone sets is borne out by the paleocurrent data (Figure 189.4), which show a principal eastward trend, with a minor westward and other trends. The distribution can be described as bimodal to polymodal.

The upper part of the Bar River Formation at Bay Finn (575 to 975 m, Figure 189.4) is characterized by quartzites similar to those between 80 and 575 m, but differs in the presence of several argillite units up to 20 m thick. Four of these units are exposed, but gaps in exposure probably conceal additional argillite units. They contain quartzitic lenses with current-formed ripple cross-lamination, but are commonly too highly sheared to distinguish internal structures. Paleocurrents derived from the quartzites are similar to those observed at lower stratigraphic levels: bimodal east-west, with strongest mode directed eastward. As before, the bi-directional nature of the

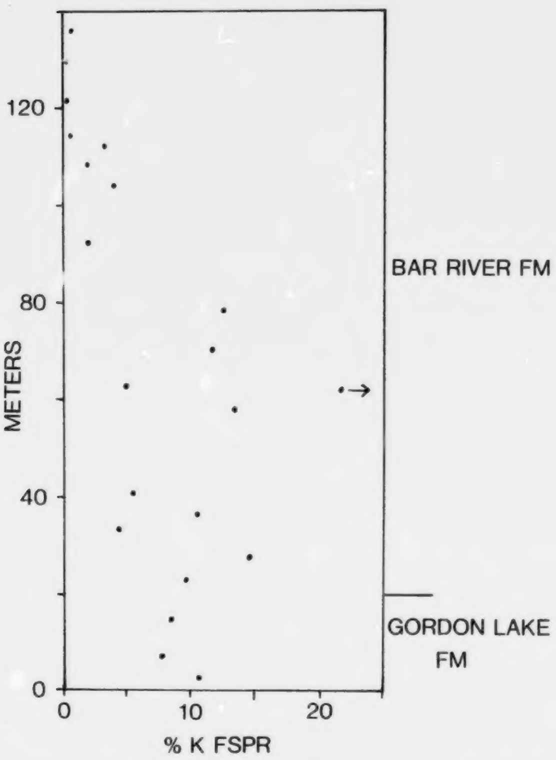

Figure 189.5. *Potassium feldspar content of quartzites from upper Gordon Lake and lower Bar River Formations, Bay Finn.*

paleocurrent distribution is corroborated by several herring-bone sets of cross-strata.

The upper part of the Bar River Formation is characterized by a number of fining-upward sequences on the scale of several tens of metres. Several, but not all, of these sequences terminate upwards in argillite units and are accompanied by upward-thinning trends of stratal thickness within the quartzites. Elsewhere within the Bar River succession, upward-thinning and upward-thickening trends have been distinguished (Figure 189.4), but metamorphic overprint has obliterated grain size trends. In these cases, the appropriate grain size trends are probably present, but have not been proven. On this basis, fining-upward trends predominate for the formation as a whole, with subsidiary coarsening-upward trends.

MINERALOGICAL AND CHEMICAL TRENDS

Hand specimens and thin sections from the upper Gordon Lake and Bar River Formations were stained for potassium feldspar. The results (Figure 189.5) show that feldspar content of the lower Bar River quartzites is similar (5% to 15%) to that of the upper Gordon Lake quartzites. The feldspar content of Bar River quartzites decreases upward to essentially zero at about 100 m above the Gordon Lake/Bar River contact, and remains at that level throughout the rest of the stratigraphic section. Another aspect of feldspar content is the fact that feldspar grains are notably smaller and more angular than quartz grains in the same rock. This observation implies a different source and/or transport history, because the feldspars would have been eliminated if they had been subjected to the same amount of abrasion as the larger, rounded quartz grains.

The upward decrease in feldspar content within the Bar River Formation is paralleled by a similar decrease in the amount of matrix. X-ray diffraction showed that this matrix is sericite, probably formed by metamorphism of illite. The lower Bar River quartzites have similar matrix content to quartzites in the upper Gordon Lake Formation, but matrix content decreases to nearly zero upward within the Bar River. It is probable that the illite (now sericitic) matrix of the upper Gordon Lake and lower Bar River Formations was derived from attrition and chemical decay of detrital feldspars.

Major element distributions in argillites of the Bar River Formation were determined by X-ray fluorescence analysis. The results were expressed in terms of the Chemical Index of Alteration (CIA):

$$\mathrm{CIA} = \frac{\mathrm{Al_2O_3}}{\mathrm{Al_2O_3 + CaO + Na_2O + K_2O}} \times 100$$

(Nesbitt and Young 1982).

The results (Figure 189.6) show that values of CIA for the Bar River lie between 70 and 80, which agree with data given by Nesbitt and Young (1982). The results suggest a high degree of weathering in the source area and during transport to the depositional area of the Bar River Formation. The trend within the measured section is for a slight but consistent upward increase in the CIA. This is compatible with the petrographic data showing upward decrease in content of feldspar and sericitic matrix, implying increasingly thorough weathering in the source area.

Figure 189.6 also shows the CIA data for the Bar River Formation in relation to data for other formations of the Cobalt Group (Nesbitt and Young 1982). The values fit on a smooth curve, which is consistent with the conformable nature of the Cobalt Group formations. Lowest CIA values correspond to the Gowganda Formation, interpreted as a glaciogenic deposit, for which source weathering would have been minimal. Thereafter, CIA values increase through the Gordon Lake and Bar River Formations, corresponding to increasing intensity of source weathering as the climate warmed progressively.

DISCUSSION: PALEOGEOGRAPHY OF THE BAR RIVER FORMATION IN RELATION TO UNDERLYING FORMATIONS

The data given above are consistent with earlier interpretations of the Bar River as a shallow marine deposit. Notably, this study has demonstrated bi-directional paleocurrents as a consistent feature of the formation. Although reversing paleocurrents have been documented within fluvial deposits in Australia (Alam *et al.* 1985), they occur in distinctive low-gradient rivers with abundant overbank mud. Bi-directional paleocurrents combined with a texturally and

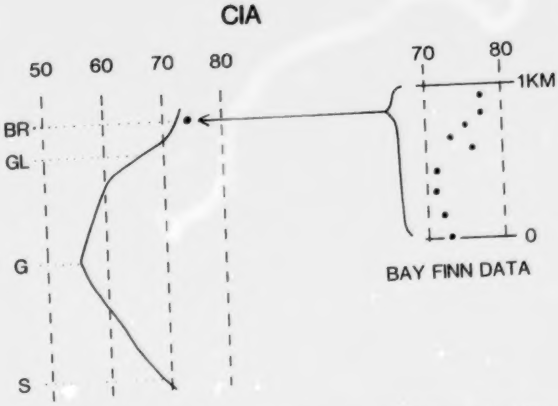

Figure 189.6. *Variation of Chemical Index of Alteration for formations of the Cobalt Group. Data from Nesbitt and Young (1982), plus results from this study for the Bar River Formation. BR: Bar River Formation, GL: Gordon Lake Formation, G: Gowganda Formation, S: Serpent Formation.*

compositionally mature succession provide excellent evidence of a shallow marine origin.

Chandler (1986) has attributed the Gordon Lake Formation to deposition on a storm-dominated marine shelf. His conclusion is based on well documented storm cycles, which succeeded the tidal flat deposits of the basal Gordon Lake Formation. The latter conclusion is based on the presence of evaporitic strata and evidence for intermittent subaerial exposure (Wood 1973; Chandler 1986).

There is general consensus that the Lorrain Formation was deposited on a broad alluvial plain, based on its textural and compositional immaturity and unidirectional paleocurrent distribution (Frarey 1977; Wood 1973; Lowey 1985; Chandler 1986). In general, the paleocurrents indicate an approximately southward sloping paleoslope. Some authors have argued that the uppermost unit of the Lorrain Formation is a coastal deposit (Hadley 1968; Card 1976) because it is more quartzose than lower parts of the formation. However, Chandler (1984, Figure 27.4a, 27.4b) showed that the upper Lorrain quartzites contain angular zircons and are locally feldspathic (Chandler 1986).

The application of Walther's Law (Middleton 1973) to the upper three formations of the Cobalt Group suggests the following. The Bar River Formation represents a shoaling barrier, separated from the alluvial/coastal plain of the Lorrain Formation by a deeper water, lagoonal environment in which the Gordon Lake Formation accumulated. Analogy with modern environments is helpful, but the scale of equivalent modern environments is small compared with that of the Cobalt Group. Thus the Bar River Formation can be compared with barrier systems on the east coast of North America (Reinson 1984; Galloway and Hobday 1983; Leatherman 1985) and elsewhere. However, the Bar River Formation contains up to 1 km of similar strata, extends over a considerable part of the Huronian outcrop belt, and (at least for the Bay Finn area) does not show evidence for emergence. We, therefore, see it as an extensive shoal system on a very broad shelf, rather than a discrete series of barrier bars and islands. Like modern barriers, the Bar River shoals were probably attached to the coast in places, so that they could receive direct coarse clastic input from the alluvial/coastal plain system of the Lorrain Formation. This implies that the Lorrain and Bar River Formations may, in places, be in stratigraphic continuity. If so, the strata equivalent to the Bar River would not be recognized because they are so similar to those of the upper Lorrain Formation.

The lower Bar River strata, which are dominated by horizontally stratified quartzites, probably accumulated as washover deposits into the Gordon Lake lagoon system (Leatherman 1985). The thickness and extent of the Gordon Lake Formation suggest that it, like the Bar River, was much more extensive than modern lagoons. It probably represents a broad inner shelf in which sedimentation was generally quiet, interrupted only by occasional storms.

The main succession of the Bar River Formation is characterized predominantly by upward-fining, upward-thinning sequences (Figure 189.4) and minor upward-thickening (probably coarsening) sequences. The upward-fining sequences could be due to lateral migration of tidal inlets (Galloway and Hobday 1983, Figure 6.12; Moslow and Tye 1985), although most fining-upward sequences seem rather thick for this explanation. The alternative is a response to rising sea level as the shelf sediments were influenced by general subsidence (Young 1983). Coarsening-upward (or rather, thickening-upward) sequences in the Bar River Formation are attributed to progradation of the shoal system across the shelf. There is no evidence within existing strata that the shelf anywhere deepened to a continental slope.

Paleocurrents in the Bar River Formation can best be understood if the southward paleoslope inferred for the Lorrain Formation (Wood 1973; Lowey 1985; Chandler 1986) is presumed to have prevailed into Bar River times. This is reasonable in view of the epeirogenic tectonic setting for the Cobalt Group (Young 1983). On this basis, the predominantly eastward trend of Bar River paleocurrents at Bay Finn represents longshore transport of sand driven by prevailing wind-driven and perhaps tidal currents. The minor westward trend represents reversal of these currents, and minor northward/southward trends probably relate to tidal flow across the barrier. As already discussed, the similarity between lower Bar River and upper Lorrain feldspathic quartzites suggest that Bar River sands came from the Lorrain alluvial plain. The distinctive grain size and roundness difference between quartz and potassium feldspar in lower Bar River quartzites can be explained by differing transport histories. The well rounded larger quartz grains are thought to have been transported a considerable distance by longshore currents, whereas the smaller, angular feldspars came more directly from the coastal plain to the offshore shoal.

The paleogeography discussed above is relevant to the presence of strata-bound copper deposits at the Lorrain-Gordon Lake boundary (Pearson 1979; Chandler 1986). According to our paleogeographic model, the sands of the Bar River Formation acted as a partial barrier to circulation of oxidized open-shelf waters into the inner shelf or lagoonal environment represented by the Gordon Lake Formation. The waters of the lagoon were a favourable habitat for the simple organisms that existed at that time. This, together with restricted circulation, lead to the development of a reducing, and locally anoxic environment.

Oxidizing ground water from the alluvial/coastal plain leached copper and other metals from feldspars and rock fragments in the Lorrain Formation sediments. Judging from the evaporitic nature of the lower Gordon Lake Formation (Wood 1973; Chandler 1986), the climate was warm and favourable to intense leaching. On reaching the reducing environment of the Gordon Lake sediments, the dissolved metals were precipitated as strata-bound sulphides.

ACKNOWLEDGMENTS

We would like to thank Fred Chandler (GSC, Ottawa) for discussion and the Geological Survey of Canada for logistic help. Thanks are also due to Natalie Morisset for drafting and Julie Hayes for typing.

REFERENCES

Alam, M.M., Crook, K.A.W., and Taylor, G.
1985: Fluvial Herring-Bone Cross-Stratification in a Modern Tributary Mouth Bar, Coonamble, New South Wales, Australia; Sedimentology, Volume 32, p.235-244.

Card, K.D.
1976: Geology of the McGregor Bay-Bay of Islands Area, Districts of Sudbury and Manitoulin; Ontario Division of Mines, Geoscience Report 138, 63p.
1978: Geology of the Sudbury-Manitoulin Area, Districts of Sudbury and Manitoulin; Ontario Geological Survey Report 166, 238p.

Chandler, F.W.
1984: Sedimentary Setting of an Early Proterozoic Copper Occurrence in the Cobalt Group, Ontario, A Preliminary Assessment; p.185-192 *in* Current Research, Part A, Geological Survey of Canada, Paper 84-1A.
1985: Geology of the Early Aphebian Copper and Gold-bearing Gordon Lake Formation Ontario, Canada (Abstract); Symposium on Precambrian Exogenetic Processes, International Correlation Project 160.
1986: Sedimentology and Paleoclimatology of the Huronian (Early Aphebian) Lorrain and Gordon Lake Formations and Their Bearing on Models for Sedimentary Copper Mineralization; p.121-132 *in* Geological Survey of Canada Paper 86-1A.

Dalrymple, R.W.
1979: Wave-induced Liquefaction: a Modern Example from the Bay of Fundy; Sedimentology, Volume 26, p.835-844.

Dott, R.H., and Bourgeois, J.
1982: Hummocky Stratification: Significance of its Variable Bedding Sequences; Bulletin of Geological Society of America, Volume 93, p.663-680.

Duke, W.L.
1985: Hummocky Cross-Stratification, Tropical Hurricanes, and Intense Winter Storms; Sedimentology, Volume 32, p.167-194.

Frarey, M.J.
1977: Geology of the Huronian Belt between Sault Ste. Marie and Blind River, Ontario; Geological Survey of Canada, Memoir 383, 87p.

Galloway, W.E., and Hobday, D.K.
1983: Terrigenous Clastic Depositional Systems; Springer-Verlag, New York, 423p.

Hadley, D.G.
1968: Sedimentology of the Huronian Lorrain Formation, Ontario and Quebec, Canada; Unpublished Ph.D. Thesis, Johns Hopkins University, Baltimore, 301p.

Leatherman, S.P.
1985: Geomorphic and Stratigraphic Analysis of Fire Island, New York; Marine Geology, Volume 63, p.173-195.

Lowey, G.W.
1985: Stratigraphy and Sedimentology of the Lorrain Formation, Huronian Supergroup (Aphebian), between Sault Ste. Marie and Elliot Lake, Ontario, and Implications for Stratiform Gold Mineralization; Geological Survey of Canada, Open File 1154.

Middleton, G.V.
1973: Johannes Walther's Law of the Correlation of Facies; Bulletin of Geological Society of America, Volume 84, p.979-988.

Moslow, T.F., and Tye, R.S.
1985: Recognition and Characterization of Holocene Tidal Inlet Sequences; Marine Geology, Volume 63, p.129-151.

Nesbitt, H.W., and Young, G.M.
1982: Early Proterozoic Climates and Plate Motion Inferred from Major Element Chemistry of Lutites; Nature, Volume 299, p.715-717.

Pearson, W.N.
1979: Copper Metallogeny, North Shore Region of Lake Huron, Ontario; p.289-304 *in* Geological Survey of Canada Paper 79-1A.

Pettijohn, F.J.
1970: The Canadian Shield—A Status Report, 1970; p.239-255 *in* Symposium on Basins and Geosynclines in the Canadian Shield, edited by A.J. Baer, Geological Survey of Canada, Paper 70-40.

Reinson, G.E.
1984: Barrier-Island and Associated Strand-Plain Systems; p.119-140 *in* Facies Models, Second Edition, edited by R.G. Walker.

Roscoe, S.M., and Frarey, M.J.
1970: Comments on: The Canadian Shield—A Status Report, 1970, by F.J. Pettijohn; p.255-262 *in* Symposium on Basins and Geosynclines in the Canadian Shield, edited by A.J. Baer, Geological Survey of Canada, Paper 70-40.

Wood, J.
1973: Stratigraphy and Depositional Environments of Upper Huronian Rocks of the Rawhide Lake-Flack Lake area, Ontario; p.73-95 *in* Huronian Stratigraphy and Sedimentation, edited by G.M. Young, Geological Association of Canada, Special Paper 12.

Wright, D.J.
1985: Preliminary Report on the Stratigraphy and Sedimentology of the Huronian Bar River Formation, Ontario; p.111-116 *in* Geological Survey of Canada Paper 85-1B.

Wright D.J., and Rust, B.R.
1985: Preliminary Report on the Stratigraphy and Sedimentology of the Bar River Formation; Ontario Geological Survey, Miscellaneous Paper 127, p.119-123.

Young, G.M.
1983: Tectono-Sedimentary History of Early Proterozoic Rocks of the Northern Great Lakes Region; Geological Society of America, Memoir 160, p.15-32.

Grant 192 Geochemical Exploration for Gold

Ian Nichol[1] **and Gene S. Shelp**[2]

[1]Department of Geological Sciences, Queen's University, Kingston

[2]Overburden Drilling Management Limited, Nepean

ABSTRACT

The investigation has been concerned with an examination of the nature of gold distribution in glacial till associated with a number of gold deposits. The objective of the study was to assess the reliability of currently adopted procedures and hopefully identify ways by which exploration reliability may be increased. A number of problems have been identified relating to sample representivity, sample processing, and interpretation that, providing they are overcome, promise to add materially to the effectiveness of exploration applied to the search for gold deposits.

INTRODUCTION

The background to the investigation lies in the fact that gold deposits of the Canadian Shield have a wide variety of characteristics relevant to the search for further deposits. These include occurrence in a range of host rocks, structural settings, varying mineralogy, with gold occurring alternatively in pyrite, free gold, or as tellurides, and wide variations in the grain size of the gold. Superimposed on this diversity of characteristics of the gold deposits, and mineralization themselves, exploration is further complicated by wide diversities in the nature of associated glacial overburden. It is to be expected that the geochemical response due to gold mineralization in glacial overburden will vary according to features both of the primary deposits and surface overburden. Effective exploration should as far as possible be capable of detecting as wide a range of deposit types in different environments as possible.

One of the most common geochemical exploration procedures adopted in areas of glacial overburden involves the sampling of glacial till, although the sampling of specific soil horizons and humus is also employed in certain cases. Depending upon the depth of the glacial overburden, till samples may be obtained by surface sampling, trenching, or deep overburden sampling employing various drilling techniques. Treatment of the sample may involve the direct analysis of a certain size fraction of the till. Frequently, a heavy mineral concentrate is obtained from the sample by tabling and heavy liquid separation. Documented case histories indicate the contribution of these methods in the discovery of several important gold deposits (Gray 1983; Averill and Zimmerman 1986; Sauerbrei *et al.*, in press; and Thomson *et al.*, in press) or alternatively, their ability to identify known deposits (Closs and Sado 1979; Bird and Coker, in press).

As indicated previously, the objective of the current investigation was to examine the nature of gold dispersion associated with a variety of gold deposits and thereby assess the effectiveness of commonly adopted methodology. On the basis of the results, it was hoped to identify ways by which exploration effectiveness may be increased.

This report presents a review of results obtained, earlier results having been described previously in Nichol and Shelp (1985) and Shelp and Nichol (in press).

RESULTS AND CONCLUSIONS

Work undertaken has been based on a relatively small number of samples, but the consistency of the results allows some confidence in the conclusions that can be drawn.

1. Till samples collected by reverse circulation drilling are deficient in fine grain sized material relative to the grain size of the material being sampled.
2. Till samples contain from 20% to 50% of silt- and clay-sized material.
3. Heavy mineral concentrates are biased towards recovering the -500 +63 μm fractions and include only an insignificant proportion of silt- and clay-sized material.
4. The non-magnetic heavy mineral concentrates show a marked enhancement of gold content relative to the light mineral fraction.
5. The extent to which gold particles are preferentially enriched in the heavy mineral concentrate tends to decrease with decreasing particle size (Wang and Poling 1983).
6. In certain instances, significant concentrations of gold remain in the light mineral fractions.
7. The proportion of total gold content concentrated in the heavy mineral fraction varies in the range 4% to 15% and, therefore, does not give a reliable measure of the total contained gold in the sample.
8. The majority of gold in heavy mineral concentrates occurs in the -125 μm fraction where there is a marked reduction in the recovery efficiency of the gravity table with decreasing grain size and variation in shape.
9. Inter-laboratory comparisons display marked variations in the concentration of gold in the heavy mineral concentrates, the weight of the heavy mineral concentrates, and thus the absolute content of gold recovered in the heavy mineral concentrates. Comparisons of the grain size distribution of gold in heavy mineral concentrates indicates, in some cases, marked variation between laboratories. A heavy mineral concentrating procedure, involving a closed system of wet panning and heavy liquid separation, indicates that significant proportions of the total gold in a sample occur in the intermediate heavy mineral fraction (S.G. >2.9 <3.3) and a major proportion in the light mineral fraction, suggesting varying degrees of liberation of the gold. Whilst recognizing the existence of these inter-laboratory variations, their significance in terms of exploration is not known, but nevertheless they indicate the

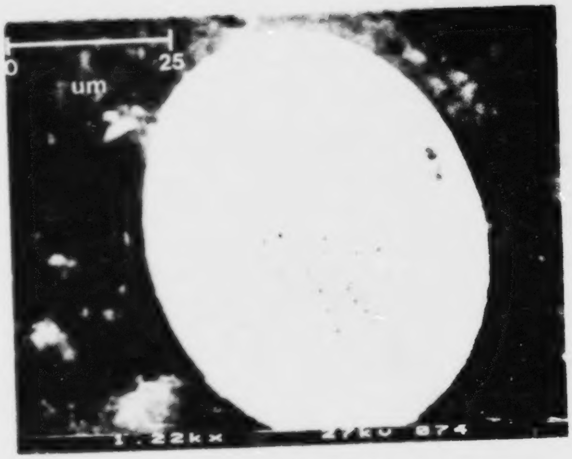

Photo 192.1. Spherical grain of gold.

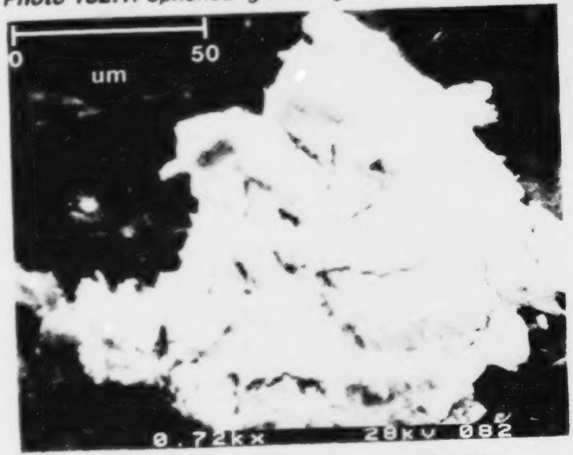

Photo 192.2. Fractured irregular grain of gold.

importance of taking into account the sample preparation procedure adopted in interpreting data. In order to try to identify the cause of these variations in gold contents, the mineralogical composition of the concentrates was examined. Binocular microscope examination of individual size fractions revealed the existence of gold spheres and irregularly shaped particles in certain fractions. These were mounted on graphite discs and then examined by scanning electron microscope. Spheres of up to 150 μm in diameter (Photo 192.1) and irregularly fractured gold grains (Photo 192.2) were noted. Semi-quantitative spot analyses of the surface of a number of these gold grains indicated compositions varying from almost 100% Au or 100% Ag to mixed compositions of 50% Au, 27% Ag, 12% Cu, and 5% Zn. Considerable interest has risen from the description of gold spherules in till that contain varying amounts of Au, Ag, and Cu and are considered to have formed by chemical precipitation (DiLabio *et al.* 1985). However, the association of gold spherules with fractured grains whose texture suggests deposition from a melt raises doubts as to their origin. Further investigation is necessary to try to identify their origin.

10. Notwithstanding the indicated potential limitations of gold exploration, based on heavy mineral concentrate analyses using commonly adopted procedures, heavy mineral concentrates can provide unique information on the type of source mineralization and distance of transport, based on a consideration of the mineralogy of the heavy mineral concentrate and shape of the gold grains.
11. Anomalous gold contents occur in the silt- and clay-sized fraction of tills associated with both the Owl Creek and Hemlo Deposits, which indicates these deposits can be identified on the basis of the direct analysis of the fine grain sized fraction of till.
12. The distribution of gold in hydraulically equivalent fractions of the -63 μm portion of the sample varies with deposit type, indicating variations in the size and/or shape of the gold grains within the silt- and clay-sized fraction.
13. Comparison of gold dispersion in the nonmagnetic heavy mineral fraction and the -63 μm fraction of tills associated with the Owl Creek Deposit shows very comparable dispersion trains.
14. The analyses of the silt- and clay-sized fraction, however, is also suited to the detection of fine-grained gold deposits that are not amenable to detection on the basis of heavy mineral concentrate analyses, and thus, offers the opportunity for greater effectiveness of gold exploration.
15. Analyses of silt- and clay-sized fractions reduce the sample representativity problems associated with analyzing coarser fractions, and inherent in basing exploration solely on the analysis of the heavy mineral concentrate.
16. In regards to variations in the character of sought after gold deposits, particularly the particle size of the gold grains, it may be concluded that exploration reliability can be increased by analyzing both the silt- and clay-sized fractions and the heavy mineral concentrate.
17. In recognizing indications of potential weaknesses of currently adopted procedures, it is fully recognized that conventional procedures have played a key role in the discovery of a number of important deposits. However, it is considered that by the adoption of various modifications in exploration methodology the overall effectiveness of exploration directed to the search for gold deposits may be improved.

FUTURE WORK

As described above, work to date has identified some areas in which the reliability of exploration methodology may be improved, and continuing work under the terms of a broader-based investigation is being directed towards this end. Aspects being considered include:

1. Substantiating the validity of the results by analyzing more samples from more deposit types and with varying spatial relationship to mineralization but, despite the small number of samples analyzed, the consistency of the results bears testimony to their reliability.
2. Investigating the mineralogical mode of occurrence of gold in silt-sized fractions, i.e. whether it is of mechanical or hydromorphic origin.
3. Examining the representativity of samples collected by a variety of drilling systems, and ways of improving the representativity of samples collected from different systems. This involves the examination of the use of a floculating agent to recover fine-grained suspended matter normally lost from the collection bucket used in reverse circulation drilling.
4. Examining ways of improving the reliability that can be attached to gold analyses of heavy mineral concentrates, with respect to their relation to mineralization.
5. Identifying an exploration methodology that will improve the overall effectiveness of geochemical exploration applied to gold exploration.

ACKNOWLEDGMENTS

Additional assistance for this investigation was provided by C.F. Minerals Limited, Cominco Limited, Esso Minerals Canada, INCO Limited, Kidd Creek Mines Limited, Noranda Explorations Limited, Nuclear Activation Services Limited, Overburden Drilling Management Limited, Placer Devlopment Limited, Teck Explorations Limited, and X-Ray Assay Laboratories Limited. Without this generous cooperation and assistance the investigation would not have been possible.

REFERENCES

Averill, S.A., and Zimmerman, J.R.
1986: The Riddle Resolved. The Discovery of the Partridge Gold Zone Using Sonic Drilling in Glacial Overburden at Waddy Lake, Saskatchewan; Canadian Geological Journal of the Canadian Institute of Mining, Volume 1, Number 1, p.14-20.

Bird, D.J., and Coker, W.B.
In Press: Quaternary Stratigraphy and Geochemistry at the Owl Creek Gold Mine, Timmins, Ontario; *in* Geochemical Exploration 1985, edited by R.G. Garrett, Journal of Geochemical Exploration.

Closs, L.G., and Sado, E.V.
1979: Geochemical Drift Prospecting Studies Near Gold Mineralization Beardmore-Geraldton Area, Northwest Ontario, Canada: p.459-477 *in* Geochemical Exploration 1978, edited by J.R. Watterson, and P.K. Theobald, Association of Exploration Geochemists, Special Volume 7.

DiLabio, R.N.W., Newsome, J.W., and McIvor, D.F.
1985: Gold Spheres in Surficial Sediments: Episodes, Volume 8, Number 1, March, p.39.

Gray, R.S.
1983: Overburden Drilling as a Tool for Gold Exploration; Canadian Institute of Mining and Metallurgy, Annual Meeting, Winnipeg, April 1983, Unpublished Paper.

Nichol, Ian, and Shelp, G.S.
1985: Geochemical Exploration for Gold; Grant 192, p.124-135 *in* Geoscience Research Grant Program, Summary of Research 1984-1985, edited by V.G. Milne, Ontario Geological Survey, Miscellaneous Paper 127, 246p.

Sauerbrei, J.A., Pattison, E.F., and Averill, S.A.
In Press: Till Sampling in the Casa Berardi Area, Quebec: A Case History in Orientation and Discovery; Journal of Geochemical Exploration.

Shelp, G.S., and Nichol, Ian
In Press: Distribution and Dispersion of Gold in Glacial Till Associated with Gold Mineralization in the Canadian Shield; *in* Geochemical Exploration 1985, edited by R.G. Garrett, Journal of Geochemical Exploration.

Thomson, I., Burns, J.S., and Faulkner, F.H.
In Press: Gold Exploration in Deep Glaciated Overburden: Experiences from the Belore Case History; Journal of Geochemical Exploration.

Wang, W., and Poling, G.W.
1983: Methods for Recovering Fine Placer Gold; Canadian Institute of Mining and Metallurgy Bulletin, Volume 76, Number 860, p.47-56.

Grant 193 The Geological Setting and Genesis of the Cameron Lake Gold Deposit

D.R. Melling and D.H. Watkinson

Ottawa-Carleton Centre for Geoscience Studies, Carleton University, Ottawa

ABSTRACT

Based on field mapping, petrographic studies, and lithogeochemistry, the volcanic rocks in the Cameron-Rowan Lakes area can be subdivided into two distinct volcanic successions. The lower Rowan Lake Volcanics consist of tholeiitic pillowed basalts. These rocks are overlain by the Cameron Lake Volcanics, a mixed succession of tholeiitic massive and pillowed basalts, and intermediate to felsic volcaniclastic rocks.

Many of the gold occurrences in the Cameron-Rowan Lakes area are confined to the mixed Cameron Lake Volcanics. Most of these, including the Cameron Lake gold deposit, are situated within shear zones localized near gabbroic-volcanic rock contacts. The contrasting competency between mafic flows, intermediate to felsic volcaniclastic rocks, and intrusive rocks of the Cameron Lake Volcanics could have localized strain forming shear zones into which gold-bearing fluids gained access. The potential of successfully identifying economic gold concentrations seems greatest within such mixed volcanic successions in the Cameron-Rowan Lakes area and elsewhere in the Wabigoon Subprovince.

INTRODUCTION

The Cameron-Rowan Lakes area is located in the Kenora Mining District of northwestern Ontario, about 80 km southeast of Kenora (Figure 193.1). Although the area has yielded no significant precious metal production to date, gold occurrences and prospects have been discovered and sporadically worked since the 1800s. The recognition of a major gold zone at Cameron Lake in 1983 by Nuinsco Resources Limited initiated a "gold rush" in an area which continues to sustain exploration activity unequalled in the recent history of the Kenora District (The Northern Miner 1983a, 1983b). Proven reserves at Cameron Lake presently total 1 625 202 short tons grading 0.16 ounce Au per ton, including 1 006 704 short tons grading 0.20 ounce Au per ton (Archibald 1985). Complete and colourful histories of mining in the Kenora-Fort Frances region and exploration in the vicinity of Cameron Lake are given by Beard and Garratt (1976) and Hunter (1985).

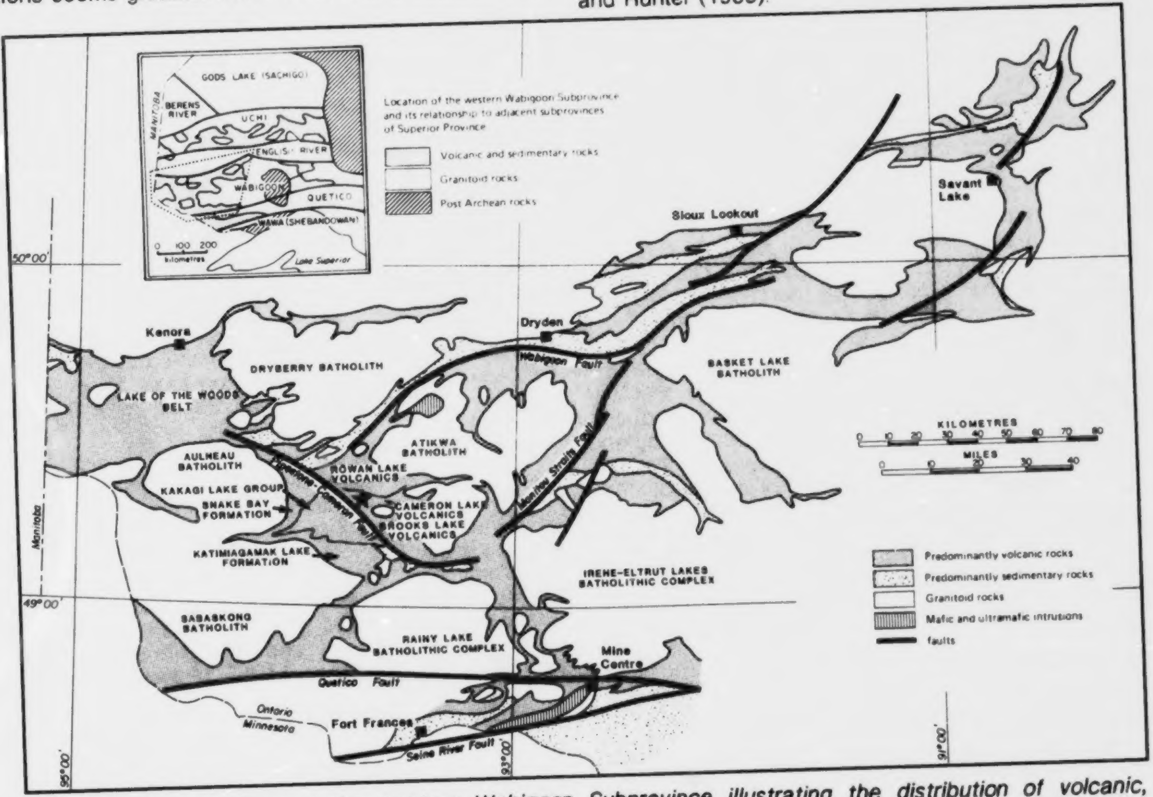
GODS LAKE (SACHIGO)
MANITOBA
BERENS RIVER
UCHI
ENGLISH RIVER
WABIGOON
QUETICO
WAWA (SHEBANDOWAN)
0 100 200
kilometres
Lake Superior
Location of the western Wabigoon Subprovince and its relationship to adjacent subprovinces of Superior Province
Volcanic and sedimentary rocks
Granitoid rocks
Post Archean rocks
50°00'
49°00'
95°00'
93°00'
91°00'
Sioux Lookout
Savant Lake
Kenora
Dryden
Wabigoon Fault
DRYBERRY BATHOLITH
BASKET LAKE BATHOLITH
LAKE OF THE WOODS BELT
AULNEAU BATHOLITH
KAKAGI LAKE GROUP
SNAKE BAY FORMATION
KATIMIAGAMAK LAKE FORMATION
ATIKWA BATHOLITH
ROWAN LAKE VOLCANICS
CAMERON LAKE VOLCANICS
BROOKS LAKE VOLCANICS
Pipestone-Cameron Fault
Manitou Straits Fault
IRENE-ELTRUT LAKES BATHOLITHIC COMPLEX
SABASKONG BATHOLITH
RAINY LAKE BATHOLITHIC COMPLEX
Mine Centre
Quetico Fault
Ontario
Minnesota
Fort Frances
Seine River Fault
Manitoba
KILOMETRES
0 10 20 30 40 50 60 70 80
MILES
0 10 20 30 40
Predominantly volcanic rocks
Predominantly sedimentary rocks
Granitoid rocks
Mafic and ultramafic intrusions
faults

Figure 193.1. *Geology of the western Wabigoon Subprovince illustrating the distribution of volcanic, sedimentary, and granitoid rocks (modified after Blackburn et al. 1985). The Cameron Lake gold deposit is indicated by a star.*

The purpose of this two-year study has been to document the geology of the Cameron Lake gold deposit. Emphasis has been placed on three aspects of the deposit: geologic setting, structure, and alteration. Previous work (Melling *et al.* 1985; Melling and Watkinson 1985; Melling *et al.*, in press) has focused primarily on the structure and alteration at the Cameron Lake deposit. This contribution provides more complete documentation of the geology of the Cameron-Rowan Lakes area.

REGIONAL SETTING

The Cameron-Rowan Lakes area lies at the western extremity of the Archean, Savant Lake-Crow Lake metavolcanic-metasedimentary belt (Trowell *et al.* 1980) in the Wabigoon Subprovince of the Canadian Shield (Figure 193.1). It occurs within a region of greenstones bounded on all sides by granitoid batholiths (Dryberry, Atikwa, Aulneau, and Sabaskong). The region is divided geologically by the southeast-striking, northeast-dipping Pipestone-Cameron Fault, a major zone of deformation and displacement similar in its characteristics to the Larder Lake-Kirkland Lake, Destor-Porcupine, and the Cadillac-Malartic Lake Breaks recognized in other Canadian Archean gold camps.

Southwest of the Pipestone-Cameron Fault is a north- to east-facing, volcanic complex centred on Kakagi Lake (Schwerdtner *et al.* 1979), which is underlain by thick (>5 km) accumulations of mafic volcanic flows and sills of the correlative Snake Bay and Katimiagamak Lake Volcanics (Figures 193.1 and 193.2). These rocks are unconformably overlain by an equally thick succession of intermediate to felsic pyroclastics and metasediments of the Kakagi Lake Group, which are intruded by differentiated mafic to ultramafic sills (Blackburn *et al.* 1985). The entire complex is bounded to the west by the Aulneau Batholith and to the south by the Sabaskong Batholith (Figure 193.1). Davis and Edwards (1986) have shown that the evolution of this volcanic-plutonic complex occurred during a time interval of 32 Ma and that the emplacement of early phases of the Sabaskong Batholith was coeval with the oldest volcanism. In addition, they have suggested that deformation of the volcanic successions occurred during late diapiric remobilization of the Sabaskong and Aulneau Batholiths, and that the younger Stephen Lake Stock may have intruded into a zone of dilatancy developed during flexural slip folding, marking the end of regional ductile deformation.

Northeast of the Pipestone-Cameron Fault lies the Cameron-Rowan Lakes area which contains the Cameron Lake gold deposit (Figures 193.1 and 193.2). The structural geology of the area is dominated by the Shingwak Lake Anticline (Figure 193.2) (Kaye 1973). The rocks exposed in the core of this anticline comprise a thick, south- to west-facing, subaqueous mafic flow succession (Rowan Lake Volcanics). These rocks are overlain by a mixed succession of subaqueous pillowed and massive mafic flows, and intermediate to felsic pyroclastics and volcaniclastics (Cameron Lake Volcanics) (Figure 193.2). Gabbroic sills were emplaced at all levels in the succession before folding. Felsic porphyry sills and dikes intrude all of the earlier strata. The volcanic rocks were intruded by the granitic Nolan Lake Stock to the south. All rocks have been metamorphosed to greenschist facies assemblages.

South of the Cameron Lake Volcanics lies the thick mafic flow succession of the Brooks Lake Volcanics (Blackburn *et al.* 1985). These rocks are tentatively interpreted to overlie the Cameron Lake Volcanics.

GEOLOGY OF THE CAMERON–ROWAN LAKES AREA

Studies by Trowell *et al.* (1980) and Blackburn *et al.* (1985) have shown that broad regional correlations can be made between several volcanic complexes within the Savant Lake-Crow Lake metavolcanic-metasedimentary belt (Figure 193.1). Their correlations, based on similarities in superposition of strata, the continuity and projection of marker units, and geological similarities of the various complexes, have shown that the volcanic stratigraphy commonly comprises lower mafic tholeiitic successions overlain by mixed mafic to felsic, tholeiitic to calc-alkaline successions, which in some areas are overlain by a second thick, mafic, tholeiitic succession.

Several workers (Blackburn and Janes 1983; Blackburn and Hailstone 1983) have noted that gold occurrences in the Cameron-Rowan Lakes area are, to a large extent, confined to the Cameron Lake Volcanics (Figure 193.2). An integral part of this study has been to assess this apparent stratigraphic control on the distribution of gold prospects and occurrences in the Cameron-Rowan Lakes area. In addition, our observations and data have allowed us to compare and contrast this area with other volcanic successions in the Savant Lake-Crow Lake Belt, as modeled by Trowell *et al.* (1980) and Blackburn *et al.* (1985).

STRUCTURE

Key structural elements of the Cameron-Rowan Lakes area include: the Pipestone-Cameron Fault, the Shingwak Lake Anticline, the Cameron Lake Shear Zone (CLSZ), and the Monte Cristo Shear Zone (MCSZ) (Figure 193.2).

The Pipestone-Cameron Fault bounds the Cameron-Rowan Lakes area to the southwest (Figure 193.2). It consists of strongly foliated chlorite-sericite schists which are locally carbonatized. The fault has been defined over 100 km of strike length. The sense of displacement remains contentious (Melling *et al.* 1985); however, major offset is suggested by the juxtaposition of the two different volcanic complexes previously discussed, and the transposition of lithologies into the plane of the fault on a regional scale (Figure 193.2). Correlation of rock types across the fault, although suspected, has not been possible (Trowell *et al.* 1980).

Kaye (1973) recognized the Shingwak Lake Anticline and determined the trace of its axial surface. Data obtained during this study has permitted further refinement of its geometry. Graded beds and well formed pillows in the hinge zone of the anticline indicate that the fold faces west-southwest. On the

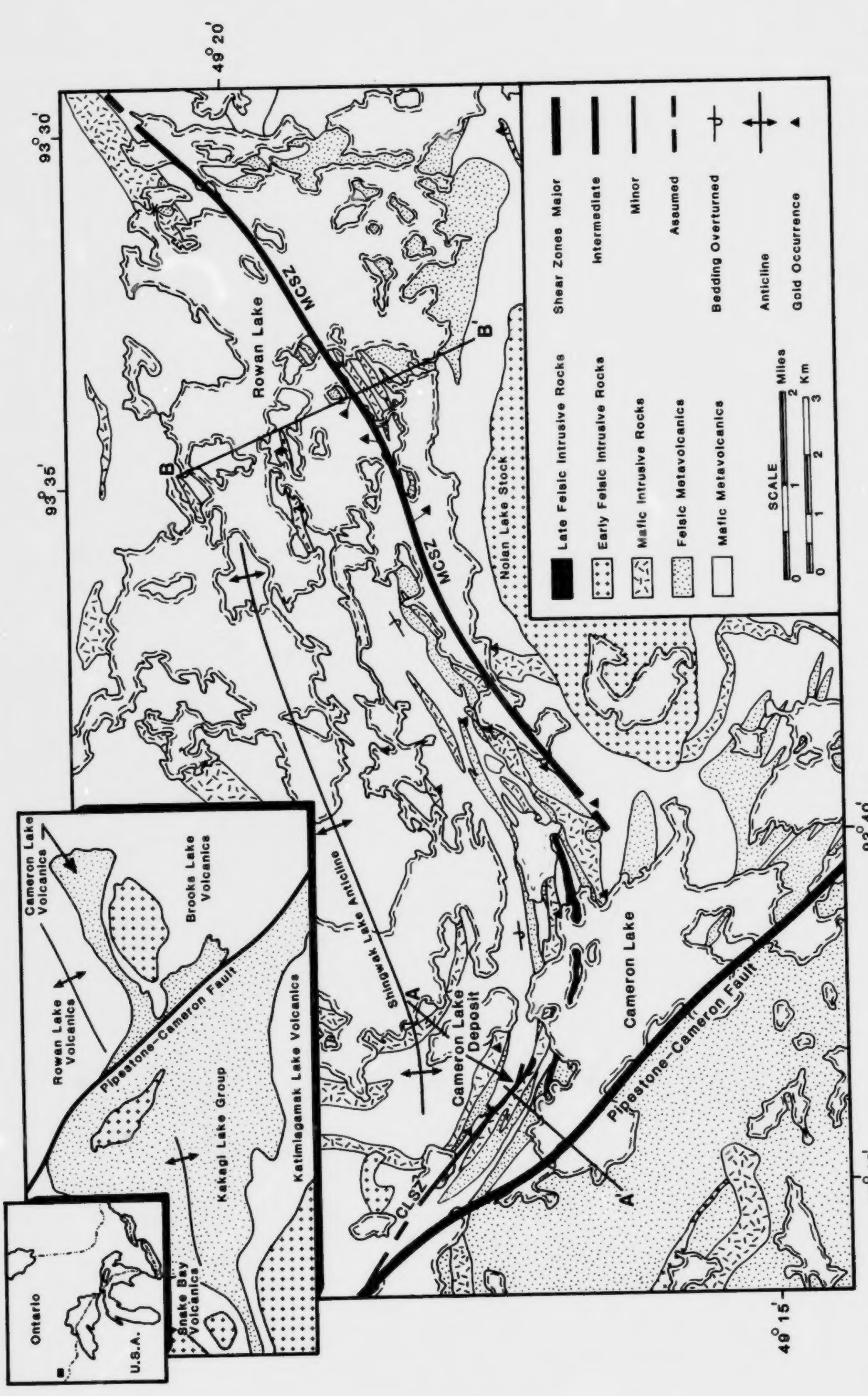
93°30'
49°20'
93°35'
93°40'
93°45'
49°15'
Rowan Lake
MCSZ
MCSZ
B
B'
A
A'
Nolan Lake Stock
Shingwak Lake Anticline
Cameron Lake Deposit
Cameron Lake
Pipestone–Cameron Fault
CLSZ
Late Felsic Intrusive Rocks
Early Felsic Intrusive Rocks
Mafic Intrusive Rocks
Felsic Metavolcanics
Mafic Metavolcanics
Shear Zones Major
Intermediate
Minor
Assumed
Bedding Overturned
Anticline
Gold Occurrence
SCALE
Miles
Km
0
1
2
0
1
2
3
Ontario
U.S.A.
Snake Bay Volcanics
Kakagi Lake Group
Katimiagamak Lake Volcanics
Rowan Lake Volcanics
Cameron Lake Volcanics
Brooks Lake Volcanics
Pipestone–Cameron Fault

Figure 193.2. Geology of the Cameron-Rowan Lakes area and positions of stratigraphic sections (modified after Blackburn and Janes 1983; Kaye 1973; and incorporating new data). Cross-sections A-A' and B-B' are shown in Figure 193.3. CLSZ = Cameron Lake Shear Zone. MCSZ = Monte Cristo Shear Zone.

south limb of the fold, overturned and north-dipping bedding measurements were obtained primarily from volcaniclastic rocks. In the hinge zone on Shingwak Lake, mafic pillowed flows predominate and bedding measurements are not easily obtained. A method of determining bedding direction and structural facing, outlined by Sawyer *et al.* (1983), was adopted, in which the orientations of pillow shelves were measured. From these data, both the axial plane (288°/80°N) and plunge (70°E/072°) of the fold were determined. This geometry defines an asymmetric, synformal anticline with a south-southeast vergence.

Kaye (1973) inferred the presence of a synclinal keel localized through Sullivan Bay in southeastern Rowan Lake (Figure 193.2) that has not been confirmed by this study. Top determinations as far south as the Nolan Lake Stock consistently indicate a steeply north dipping, overturned succession facing south.

The Cameron Lake Shear Zone (315°/65°N) has been extensively examined in the vicinity of the Cameron Lake Deposit (Figure 193.2) (Melling *et al.* 1985; Melling *et al.*, in press; Melling 1986). It is a brittle-ductile shear zone up to 60 m wide and over 3000 m in strike length which exhibits evidence of dextral strike-slip shear.

The regionally significant Monte Cristo Shear Zone (240°/80°N) occurs in south-central Rowan Lake (Figure 193.2) and has been studied by Wade (1985). Wade (1985) showed that the displacement on the Monte Cristo Shear Zone has a significant dip-slip component, with the south side having moved up relative to the north. He also noted the presence of sinistral-sense folds of the shear foliation whose hinge-line orientations are similar to those of measured stretching lineations. In addition, Wade (1985) recognized a brittle fault of unresolved sense along the south boundary of the Monte Cristo Shear Zone.

STRATIGRAPHY

In order to assess the apparent stratigraphic control on gold mineralization in the Cameron-Rowan Lakes area, two stratigraphic sections were compiled (Figure 193.3). The sections were drawn south from the axial surface trace of the Shingwak Lake Anticline, one through Cameron Lake, and one through Rowan Lake (Figure 193.2).

The oldest rocks exposed are the Rowan Lake Volcanics which occur at the base of both sections and have minimum thicknesses of about 3 km (Figure 193.3). The rocks consist of aphanitic to fine-grained, subaqueous, mafic, pillowed flows and minor massive flows. The best exposures occur on islands and along the shores of Shingwak Lake where the pillows are well formed and locally display shelf structures. Amygdules comprising up to 20% of the pillowed flows are infilled by chlorite and carbonate. The rocks are weakly foliated, most prominently within pillow selvages. This foliation is interpreted as being axial planar to the Shingwak Lake Anticline. In north-central Rowan Lake, the pillows are irregular in shape and top determinations are not easily obtained.

The overlying Cameron Lake Volcanics consist of approximately equal proportions of mafic volcanic flows and interbedded intermediate to felsic volcaniclastic rocks. The mafic volcanic rocks comprise units of both massive and pillowed flows (Photo 193.1g). Amygdules locally comprise up to 30% of the flows (Photo 193.1e). Massive flow units are more common in the Cameron Lake Volcanics than in the underlying Rowan Lake Volcanics (Figure 193.3). Minor pillow breccia (Photo 193.1d) and mafic tuff are also present.

The intermediate to felsic volcaniclastic rocks comprise units of both monolithic and heterolithic lapilli-tuff which commonly contain abundant plagioclase phenocrysts. The lapilli-tuff units are variable in composition, texture, and grain size. In south-central Rowan Lake, a distinctive unit of tuff-breccia was interpreted by Kaye (1973) as occurring in a proximal vent facies environment. This interpretation is consistent with the occurrence of thicker volcaniclastic units in the Rowan Lake section. The finer grain sizes observed in the Cameron Lake section may represent a distal facies (Figure 193.3 and Photos 193.1f and 193.1g).

The contact between the lower Rowan Lake Volcanics and the overlying Cameron Lake Volcanics is defined by the first appearance of intermediate to felsic volcaniclastic rocks (Figures 193.2 and 193.3). In drill core from the Cameron Lake Deposit from the Cameron Lake section (Figure 193.3), this unit consists of well bedded pyroclastic rocks (Photo 193.1a) and interbedded, laminated, carbonaceous mudstones and epiclastic rocks. Disrupted bedding and rip-up clasts (Photo 193.1b) within the epiclastic beds suggests either shallow-water conditions above storm wave base or reworking due to gravity flows. Local thickening of this unit along strike may reflect deposition on an irregular erosional surface which would suggest a hiatus in volcanism coincident with the transition in volcanism.

Numerous mafic sills were intruded into both the Cameron Lake and Rowan Lake Volcanic successions prior to folding. They are, in general, thicker and more abundant in the Cameron Lake section (Figure 193.3). This is compatible with Kaye's (1973) proposed relationship of these rocks to mafic-ultramafic rocks to the north. Minor felsic sills and markedly discordant dikes are also present.

The most significant gold occurrences within the Cameron-Rowan Lakes area (including the Cameron Lake Deposit) are located within the Cameron Lake Volcanics (Figures 193.2 and 193.3). Most of these are situated within high strain zones localized at or near gabbroic-volcanic rock contacts. Two distinct gold-bearing high strain zones have been recognized within the Cameron Lake Volcanics (Melling 1986). These are the Cameron Lake and Monte Cristo Shear Zones which occur within Cameron Lake and Rowan Lake, respectively (Figures 193.2 and 193.3). These two shear zones contain the most significant gold prospects discovered to date and remain the principal exploration targets. Despite the presence of these two shear zones, no major displacements have been recognized and stratigraphic correlations can be made within the Cameron-Rowan Lakes area (Figure 193.3).

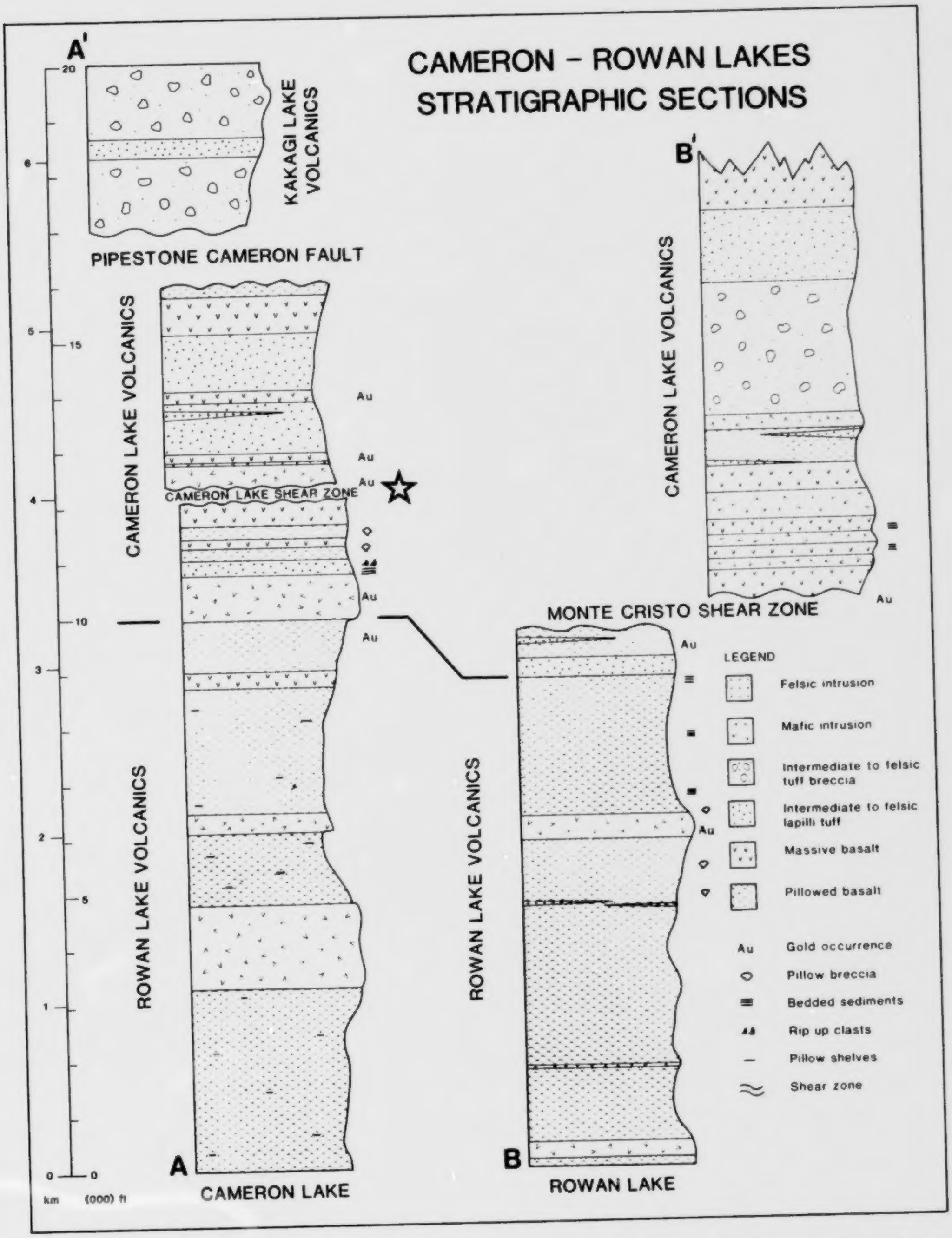
CAMERON - ROWAN LAKES
STRATIGRAPHIC SECTIONS
A'
B'
KAKAGI LAKE VOLCANICS
PIPESTONE CAMERON FAULT
CAMERON LAKE VOLCANICS
CAMERON LAKE SHEAR ZONE
ROWAN LAKE VOLCANICS
MONTE CRISTO SHEAR ZONE
Au
A
B
CAMERON LAKE
ROWAN LAKE
km
(000) ft
0
1
2
3
4
5
6
5
10
15
20
LEGEND
Felsic intrusion
Mafic intrusion
Intermediate to felsic tuff breccia
Intermediate to felsic lapilli tuff
Massive basalt
Pillowed basalt
Au Gold occurrence
Pillow breccia
Bedded sediments
Rip up clasts
Pillow shelves
Shear zone

Figure 193.3. *Stratigraphic sections from the Cameron-Rowan Lakes area. Thicknesses of units are those exposed on surface uncorrected for dip. The Cameron Lake Deposit is indicated by a star.*

CHEMICAL COMPOSITION OF THE VOLCANIC ROCKS

A lithogeochemical sampling program was undertaken in the Cameron-Rowan Lakes area for several reasons:

1. To characterize the bulk composition of the least altered volcanic rocks in the area in order to compare them with their altered equivalents that are associated with gold occurrences.
2. To support our field-based stratigraphic compilation and further define the geological setting of the area.

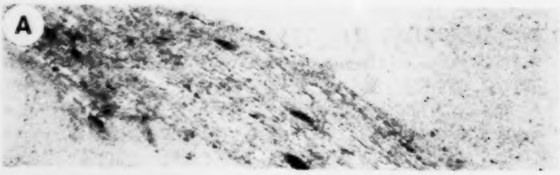

Photo 193.1a. Polished core sample of heterolithic, felsic lapilli-ash tuff interbedded with fine-grained ash tuffs. This unit represents the first occurrence of intermediate to felsic volcanic rocks, defining the base of the Cameron Lake Volcanics. Sample NC-71-44.

Photo 193.1b. Polished core sample of epiclastic rock containing volcanic fragments and rip-up clasts of fine-grained, carbonaceous mudstone from the same unit as 4A. Sample NC-77-55.

Photo 193.1c. Polished core sample of weakly amygdaloidal, aphanitic pillowed basalt with chloritic selvages. Sample NC-36-435.

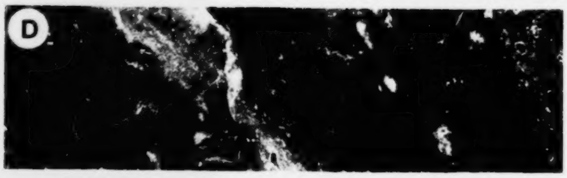

Photo 193.1d. Polished core sample of aphanitic, amygdaloidal, framework-supported pillow breccia. Amygdules are infilled with quartz and chlorite. Note the stronger foliation than that in 4C. Sample NC-48-215.

Photo 193.1e. Polished core sample of aphanitic amygdaloidal basalt with quartz-calcite-chlorite amygdules, commonly rimmed by epidote. Sample NC-28-234.

Photo 193.1f. Polished core sample of massive, monolithologic, intermediate crystal-ash tuff, a possible distal facies of 4G. Sample NCX-7-250.

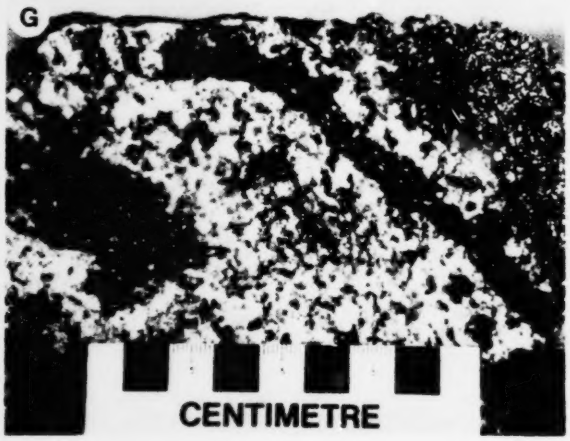

Photo 193.1g. Rock slab showing massive, monolithologic, intermediate lapilli-crystal-ash tuff, a possible vent-proximal facies equivalent of 4F, from a small island in north-central Cameron Lake.

3. To facilitate comparison of this area with the general model for the organization of supracrustal rocks in the Savant Lake-Crow Lake metavolcanic-metasedimentary belt (Trowell *et al.* 1980; Blackburn *et al.* 1985).

The geochemical data used here are tabulated and discussed by Melling (1986). Some of the analyses presented in Figure 193.4 were provided by C.E. Blackburn (Resident Geologist, Ontario Ministry of Northern Development and Mines, Kenora).

Sample grouping into the Rowan Lake Volcanics is based on the criteria previously outlined. To facilitate comparison of our data with those of Blackburn *et al.* (1985), similar volcanic rock classification schemes have been adopted.

The Rowan Lake Volcanics may be classified as subalkaline, (Figure 193.4a) tholeiitic basalts. Well developed chemical evolutionary trends are not indicated by either the Jensen (1976) diagram (Figure 193.4b) or the Irvine and Baragar (1971) AFM plot (Figure 193.4c). In general, these rocks are less Fe-rich than the Katimiagamak and Snake Bay Volcanics located to the west across the Pipestone-Cameron Fault.

The Cameron Lake Volcanics are geochemically variable. Volcanic rock compositions range from subalkaline basalts (Figure 193.4c) to rhyolites and a well developed calc-alkaline trend is shown on both the Jensen diagram (Figure 193.4b) and the AFM plot (Figure 193.4c). These trends are similar to those of the Kakagi Lake Group which overlie the Katimiagamak and Snake Bay Volcanics to the west.

DISCUSSION

Based on mapping and geochemical criteria, the metavolcanic rocks in the Cameron-Rowan Lakes area can be divided into a lower mafic succession and an overlying mixed, mafic to felsic succession. The Rowan Lake Volcanics (lower mafic succession), consisting of about a 3 km thickness of tholeiitic pillowed basalt with minor interbedded massive flows, represent the oldest rocks in the area. The overlying Cameron Lake Volcanics (mixed mafic to felsic succession) consist of tholeiitic flows and calc-alkaline volcaniclastic rocks.

The transition between these two volcanic successions is defined by the first appearance of intermediate to felsic volcanic rocks. North of the Cameron Lake deposit, this intermediate to felsic unit consists of interbedded pyroclastic rocks, thin-bedded sedimentary rocks, and epiclastic rocks. The irregular thickness of this unit, the presence of laminated sedimentary rocks and rip-up clasts, coupled with overlying, locally amygdule-rich basaltic rocks and more abundant mafic massive flows, suggest both a hiatus in volcanism between the two successions and possible shallow-water conditions during the deposition of the Cameron Lake Volcanics. This could be due to either the regression of Archean seas or the emergence of local volcanic edifices. This is compatible with the occurrence of coarse volcaniclastic deposits in south-central Rowan Lake which have been interpreted as a proximal vent facies. Based on regional, vertical gradiometer survey data, Blackburn and Hailstone (1983) inferred the presence of an unconformity at the base of the Cameron Lake Volcanics.

Most of the gold occurrences in the Cameron-Rowan Lakes area occur in the Cameron Lake Volcanics near the transition from the lower tholeiitic Rowan Lake Volcanics (Blackburn and Janes 1983; Blackburn and Hailstone 1983). However, this stratigraphic control does not imply primary, syngenetic gold enrichment as suggested by Blackburn and Janes (1983). Most of the gold occurrences in the Cameron-Rowan Lakes area are in zones of high strain, localized near lithologic contacts. The contrasting competency between mafic flows, intermediate to felsic volcaniclastic rocks, and intrusive rocks, of the Cameron Lake Volcanics, could have localized shear zones. Gold-bearing fluids move along zones of greatest permeability in response to temperature and pressure gradients. The high frequency of gold occurrences within the Cameron Lake Volcanics is due to the presence of these shear zones and therefore represents a structural rather than stratigraphic control.

These interpretations have broad implications in terms of exploration elsewhere in greenstone terrains. Firstly, the stratigraphy of the Cameron-Rowan Lakes area is not unique; similarly organized volcanic successions are recognized throughout the western Wabigoon Subprovince. Secondly, the distribution of gold occurrences within other volcanic successions is commonly asymmetrically related to upper mixed successions. Consequently, the potential of successfully identifying economic gold concentrations seems greatest within these mixed volcanic successions, which, because of competency contrasts between different lithologies, have better developed "ground-preparation" characteristics during deformation.

ACKNOWLEDGMENTS

The authors wish to express their gratitude to the staff of Nuinsco Resources Limited for providing unrestricted access to data on their properties in the Cameron-Rowan Lakes area. Appreciation is also extended to Bigstone Minerals Limited, Calaveras Explorations Limited, Canolan Resources Limited, Gold Fields Canadian Mining Limited, INCO Limited, Silver Lake Resources Incorporated, and Tantalus Resources Limited, for providing access to the data they have obtained while conducting exploration in the Cameron-Rowan Lakes area.

C.E. Blackburn (Resident Geologist, Ontario Ministry of Northern Development and Mines, Kenora) is also gratefully acknowledged for his encouragement, discussions, and providing the data upon which the preliminary stratigraphic subdivisions in the Cameron-Rowan Lakes area were made. M. Bucke, A.D. Hunter, P.L. Jones, M.P.H. Wade, and R. Westendorp, provided assistance in the field and contributed to our understanding of the area through numerous discussions.

The study of gold metallogeny in the Cameron-Rowan Lakes area was part of an M.Sc. thesis completed by D.R. Melling at Carleton University under the supervision of D.H. Watkinson, L.B. Chorlton, and K.H. Poulsen. The authors express their gratitude to

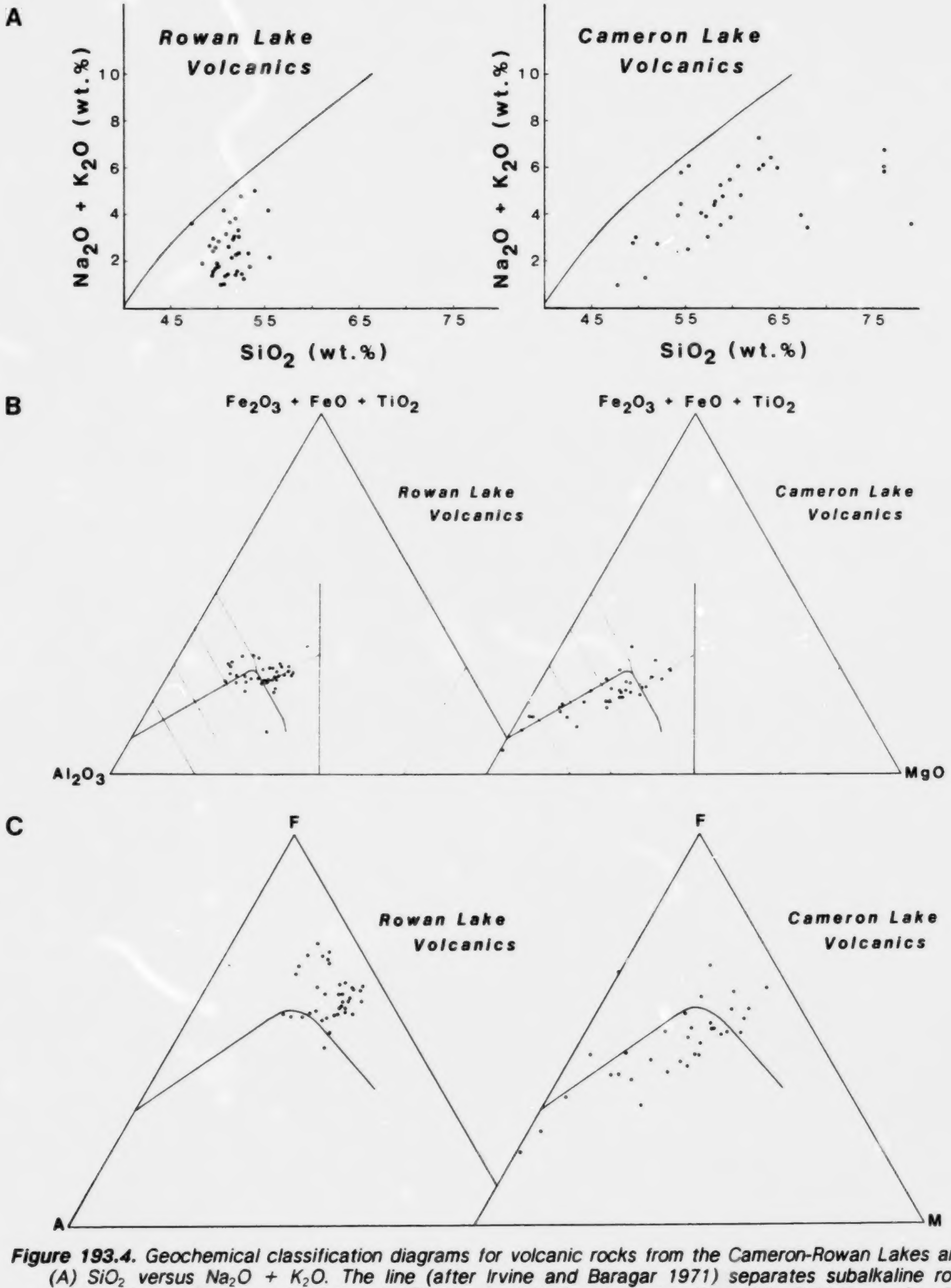

Figure 193.4. *Geochemical classification diagrams for volcanic rocks from the Cameron-Rowan Lakes area. (A) SiO_2 versus $Na_2O + K_2O$. The line (after Irvine and Baragar 1971) separates subalkaline rocks (below) from alkaline rocks (above). (B) Jensen (1976) cation plot. Komatiitic field is on the right, tholeiitic field in the upper left, high magnesian tholeiitic field slightly left of centre, and the calc-alkaline field lower left. (C) AFM diagram ($A = Na_2O + K_2O$, F = total iron as FeO, and M = MgO). The line (after Irvine and Baragar 1971) separates tholeiitic rocks (above) from calc-alkaline rocks (below).*

K.H. Poulsen and L.B. Chorlton for their direction in the field and numerous fruitful discussions. G.W. Johns (Geologist, Ontario Geological Survey, Toronto) reviewed this manuscript and significantly improved its clarity.

REFERENCES

Archibald, G.F.
1985: Summary Report on 1985 Diamond Drilling Program, Cameron Lake Gold Zone; Unpublished Company Report, Nuinsco Resources Limited, 7p.

Beard, R.C., and Garratt, G.L.
1976: Gold Deposits of the Kenora-Fort Frances Area, Districts of Kenora and Rainy River; Ontario Division of Mines, Mineral Deposits Circular 16, 46p. Accompanied by Chart A, scale 1:253 440 or 1 inch to 4 miles.

Blackburn, C.E., and Hailstone, M.R.
1983: The Geological Environment of Gold Mineralization, Cameron-Rowan Lakes, Northwestern Ontario; Paper Presented at the Geoscience Research Seminar, December 6-7, 1983, Toronto, Ontario, 13p.

Blackburn, C.E., and Janes, D.A.
1983: Gold Deposits in Northwestern Ontario; p.194-210 *in* The Geology of Gold in Ontario, edited by A.C. Colvine, Ontario Geological Survey, Miscellaneous Paper 110, 278p.

Blackburn, C.E., Bond, W.D., Breaks, F.W., Davis, D.W., Edwards, G.R., Poulsen, K.H., Trowell, N.F., and Wood, J.
1985: Evolution of Archean Volcanic-Sedimentary Sequences of the Western Wabigoon Subprovince and Its Margins: A Review; Geological Association of Canada, Special Paper 28, p.89-116.

Davis, D.W., and Edwards, G.R.
1986: Crustal Evolution of Archean Rocks in the Kakagi Lake Area, Wabigoon Subprovince, Ontario, As Interpreted From High-Precision U-Pb Geochronology; Canadian Journal of Earth Sciences, Volume 23, p.182-192.

Hunter, A.D.
1985: Cameron Lake: Another Reason to Re-evaluate Old Showing; Canadian Mining Journal, April, p.45-48.

Irvine, T.N., and Baragar, W.R.A.
1971: A Guide to the Chemical Classification of Common Volcanic Rocks; Canadian Journal of Earth Sciences, Volume 8, p.523-548.

Jensen, L.S.
1976: A New Cation Plot for Classifying Subalkalic Volcanic Rocks; Ontario Division of Mines, Miscellaneous Paper 66, 22p.

Kaye, L.
1973: Rowan Lake Area, District of Kenora; Ontario Division of Mines, Preliminary Map P.831, Geological Series, scale 1 inch to 1/4 mile.

Melling, D.R.
1986: The Geological Setting, Structure, and Alteration Associated with Gold-Pyrite Mineralization at Cameron Lake, Wabigoon Subprovince, Northwestern Ontario; Unpublished M.Sc. Thesis, Carleton University, Ottawa, Ontario, 112p.

Melling, D.R., and Watkinson, D.H.
1985: The Cameron Lake Gold Deposit: Introductory Discussion and Field Guide; p.1-11 *in* Field Trip Guide Book, Thirty-First Annual Institute on Lake Superior Geology, Kenora, edited by G. Beakhouse, 186p.

Melling, D.R., Watkinson, D.H., Poulsen, K.H., Chorlton, L.B., and Hunter, A.D.
In Press: The Cameron Lake Gold Deposit, Northwestern Ontario: Geological Setting, Structure, and Alteration; *in* Gold '86, Proceedings of the International Symposium, Toronto.

Sawyer, E.W., Barnes, S., and Bucke, M.J.
1983: Pillow Shelves: Determination of Bedding Direction and Structural Facing Direction from Shelves in Deformed Pillow Lavas; Canadian Journal of Earth Sciences, Volume 20, p.1483-1487.

Schwerdtner, W.M., Stone, D., Osadetz, K., Morgan, J., and and Stott, G.M.
1979: Granitoid Complexes and the Archean Tectonic Record in the Southern Part of Northwestern Ontario; Canadian Journal of Earth Sciences, Volume 16, p.1965-1977.

The Northern Miner
1983a: Cameron Lake Gold Rush Builds Momentum; The Northern Miner, Volume 69, Number 16, p.1, 16.
1983b: Cameron Lake Find Spurs Kenora District; The Northern Miner, Volume 69, Number 33, p.B12-B13.

Trowell, N.F., Blackburn, C.E., and Edwards, G.R.
1980: Preliminary Synthesis of the Savant Lake-Crow Lake Metavolcanic-Metasedimentary Belt, Northwestern Ontario, and Its Bearing Upon Mineral Exploration; Ontario Geological Survey, Miscellaneous Paper 89, 30p. Accompanied by Chart A.

Wade, M.P.H.
1985: A Kinematic Study of the Monte Cristo Shear Zone, Northwestern Ontario; Unpublished B.Sc. Thesis, Carleton University, Ottawa, Ontario, 59p.

Grant 205 Clay Mineralogy of Two Selected Carbonate Reservoirs in Southwestern Ontario

P.L. Churcher and M.B. Dusseault

Department of Earth Sciences, University of Waterloo, Waterloo

ABSTRACT

In the second year of the project, detailed X-ray diffraction and scanning electron microscopy/KEVEX EDS work was conducted to determine the type, relative amount, and location of clay minerals found in the two Silurian carbonate reservoirs being studied. In addition to this, a preliminary study was conducted on two samples from the Middle Ordovician Hillman Pool, also located in southwestern Ontario.

Findings confirm the presence of a monomineralic assemblage of illite, which appears to be detritial in origin. In the majority of the samples studied, illite was found to comprise less than one weight percent, and was rarely seen situated in the pore space. It is, therefore, considered unlikely that it would present any problems in terms of oil recovery efficiency.

The samples taken from the Middle Ordovician Trenton-Black River Groups show a significant amount of fines present in the pore space which may represent a problem during oil production in this reservoir. Further work is required to delineate these fines.

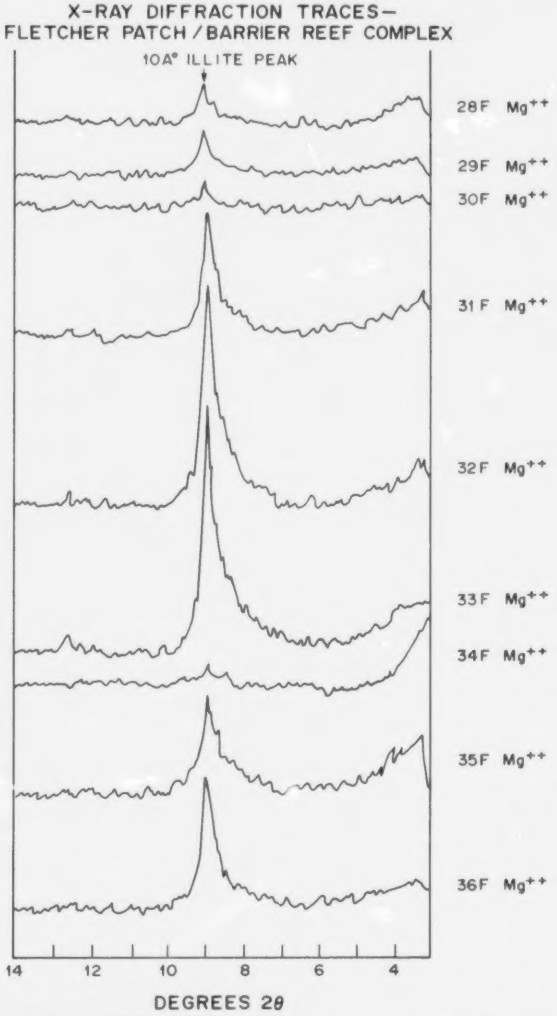

Figure 205.1. Representative X-ray diffraction traces from the Fletcher Patch/Barrier Reef Complex showing 10 angstrom illite peak.

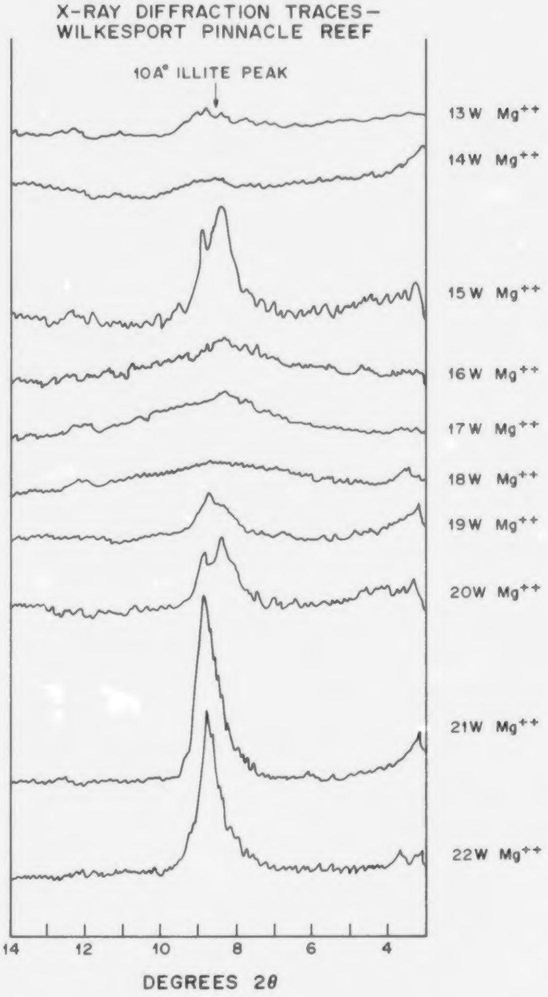

Figure 205.2. Representative X-ray diffraction traces from the Wilkesport Pinnacle Reef showing 10 angstrom illite peak.

INTRODUCTION

In 1984, a study was begun to define the clay mineralogy of two Silurian carbonate reservoirs in southwestern Ontario. The two reservoirs studied were the Fletcher Patch Barrier Reef Complex and the Wilkesport Pinnacle Reef. The objectives of the study were to qualitatively define the type, relative amount, and location of any clay minerals present within the two reservoirs and to determine if these clays would present any significant problems during various stages of oil recovery. Clay minerals have been shown to reduce oil recovery efficiency dramatically (Hutcheon and Oldershaw 1985).

During the first year of the study, detailed geological work was conducted on the core from both reservoirs. The cores were geologically logged and facies were determined as an aid to implementing a sampling scheme. A preliminary set of samples were studied using a scanning electron microscope/KEVEX EDS analyzer and an X-ray diffractometer. The results indicated a monomineralic assemblage of detrital illite to be present in both reservoirs. Details of this work may be found in Churcher and Dusseault (1985).

During the second year of the project, a more comprehensive scanning electron microscope/KEVEX and X-ray diffraction study was conducted on samples from each facies. The findings of this work are discussed in this report.

RESULTS AND DISCUSSION

The work done in the last year of this study confirmed the presence of a monomineralic assemblage of detrital illite (Figures 205.1, 205.2, and 205.3). The illite delineated in the two resevoirs appears to be scattered throughout the matrix/cement and rarely occurs as a pore-fill constituent. Concentrations of illite were noted in stylolites, vadose silt seams, and in the green shale at the top of the Guelph Formation.

In general, the illite appears to be more abundant in the lagoonal facies than it is in the reefal facies of both reservoirs. This may indicate an influx of terrigenous material, which may have contributed to the demise of the reefal community. The lack of neogenetic clay minerals in the free pore space shows clearly that very little clay was trapped in the reefal porosity during the formation of the reef, and that no diagenetic conditions have existed which could have given rise to clay neoformation in the reefs studied.

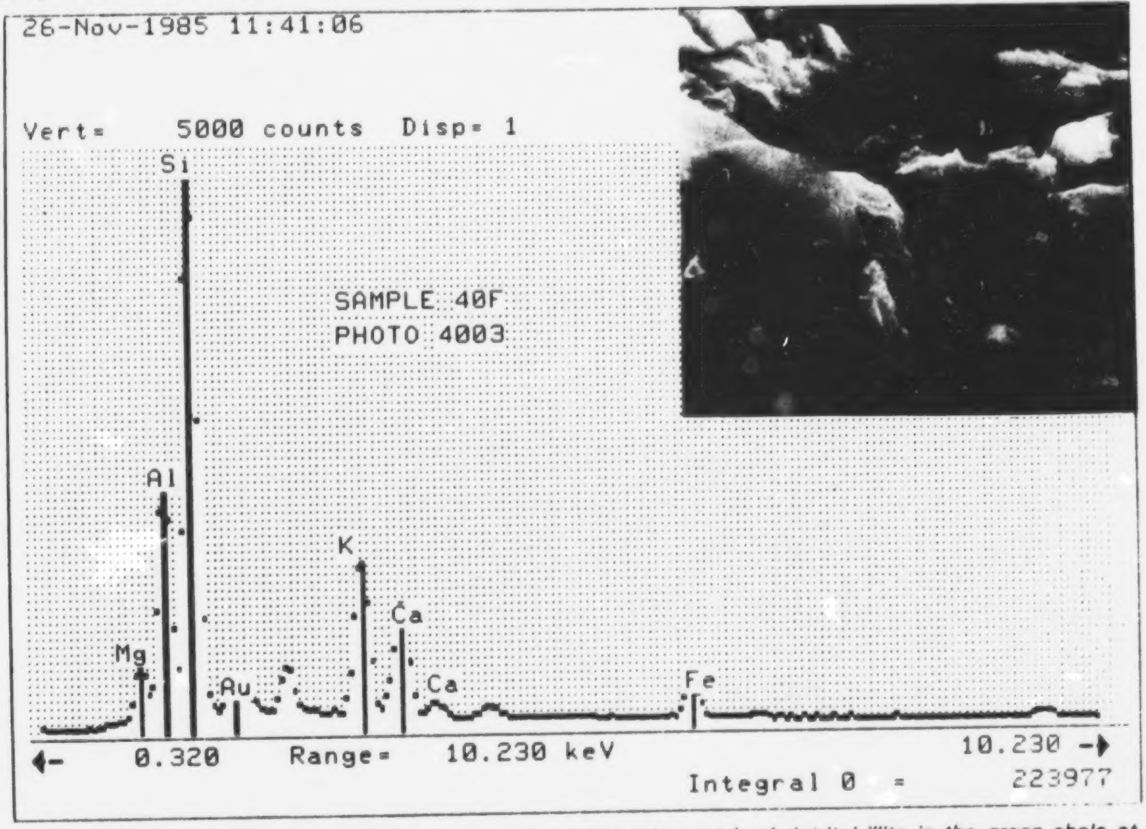

Figure 205.3. Typical scanning electron microscope photomicrograph of detrital illite in the green shale at the top of the Guelph Formation. Accompanying KEVEX EDS trace confirms the presence of illite by the peak ratios between Al, Si and K.

The majority of the samples contained less than one weight percent illite. This, coupled with location (matrix as opposed to open pore space), limits the probability of formation damage due to fines migration during enhanced or conventional oil recovery. It is unlikely that foreign fluids introduced into these reservoirs would have any significant undesirable effect on reservoir performance due to this small amount of illite. Most nonthermal enhanced oil recovery (EOR) colloidal structures contain high molecular weight polymers which adsorb onto mineral surfaces and the large surface areas of clays adsorb great quantities of these expensive chemicals. The lack of free clay means few losses by this mechanism.

The preliminary scanning electron microscope/ KEVEX EDS study conducted on the two samples from the Hillman Pool indicated abundant fines (unspecified mineralogy) to be present in the pore space of this carbonate reservoir. The potential for formation damage due to fines migration and/or swelling *in situ* is much higher than for the other two reservoirs studied. Further work is required to delineate clay speciation (Figure 205.4).

CONCLUSIONS

A monomineralic clay mineral assemblage, consisting of detrital illite, was defined in all facies of both reservoirs. This was found scattered throughout the matrix/cement and was only rarely noted in the pore space in any sample. The illite was observed to be concentrated in stylolites, vadose silt seams, and in the green shale at the top of the Guelph Formation.

The amount of illite present in the samples varies from one facies to the next. In general, the facies of the lagoonal environments of both reefs contain the most clays. Those facies associated with the reef growth were found to be relatively clay free.

The amount and location of the illite negate the possibility of a fines migration problem existing in either of the Silurian reservoirs. The fines noted in the Middle Ordovician Hillman reservoir do represent a significant fines migration/swelling problem.

REFERENCES

Churcher, P.L., and Dusseault, M.B.
1985: Clay Mineralogy of Two Selected Carbonate Reservoirs in Southwestern Ontario; p.157-164 *in* Geoscience Research Grant Program, Summary of Research 1984-1985, edited by V.G. Milne, Ontario Geological Survey, Miscellaneous Paper 127, 246p.

Hutcheon, I., and Oldershaw, A.
1985: The Effect of Hydrothermal Reactions on the Petrophysical Properties of Carbonate Rocks; Bulletin of Canadian Petroleum Geology, Volume 33, p.359-377.

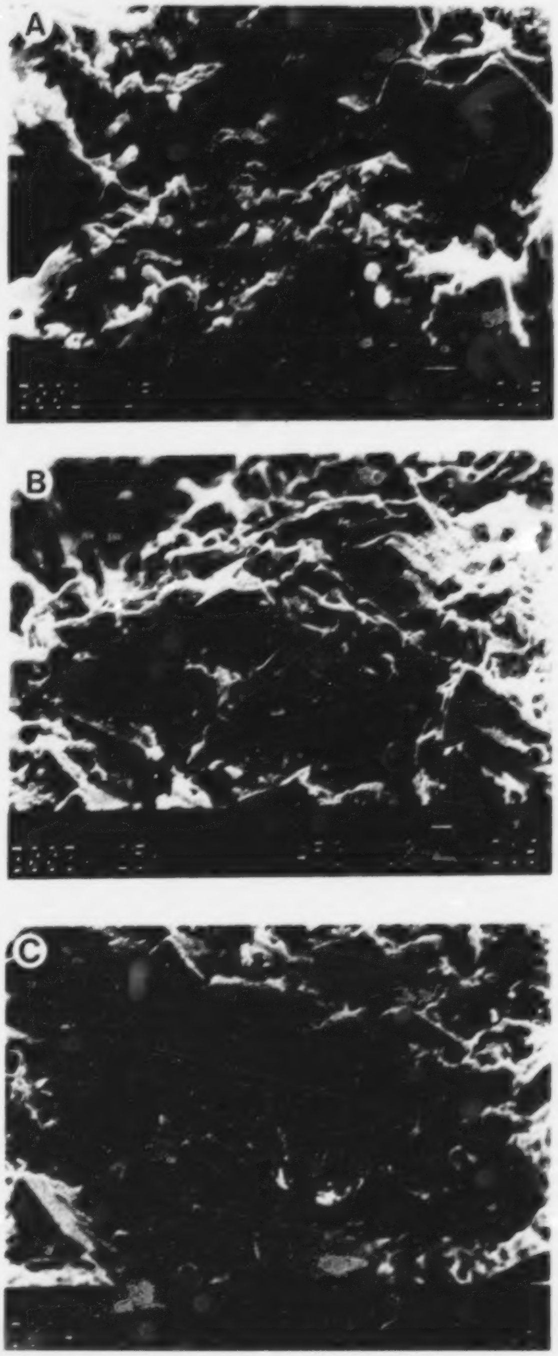

Figure 205.4. *Scanning electron photomicrographs showing abundant fines (unspecified mineralogy) in the pore space of the dolomitized reservoir, Hillman Pool, Gull River Formation, Black River Group.*

Grant 216 The Depositional Environment for the Black Shales of the Upper Devonian Long Rapids Formation, Northern Ontario

R.K. Bezys[1] **and M.J. Risk**[2]

[1]Engineering and Terrain Geology Section, Ontario Geological Survey, Toronto

[2]Department of Geology, McMaster University, Hamilton

ABSTRACT

The Upper Devonian Long Rapids Formation in northern Ontario was deposited in a warm, tropical environment which experienced periodic fluctuations in oxygen content of the water column. These environmental changes are reflected in the type of sediments deposited and in the fossil record preserved. Mean values of total organic carbon for the black shales are 2.05% and 4.25% (respectively, for outcrop and core samples) and values reach as high as 10.13%. Stable carbon isotope analyses (δ^{13}C) indicate a terrestrial source for the organic matter, although the fossil evidence indicates a marine setting for these shales. A possible explanation may be isotopic fractionation due to diagenetic alteration.

The black shales were deposited under anoxic water conditions, and other sedimentary components, such as green-grey mudstones and carbonates, were deposited under oxygenated water conditions. The deposition of these units can best be explained with a model using a stratified water column, where a pycnocline separates anoxic and oxic waters. Periodic movements of this pycnocline to the sediment-water interface, or the disappearance of it altogether, would determine the type of sediment deposited. Movement of the pycnocline may be due to surface

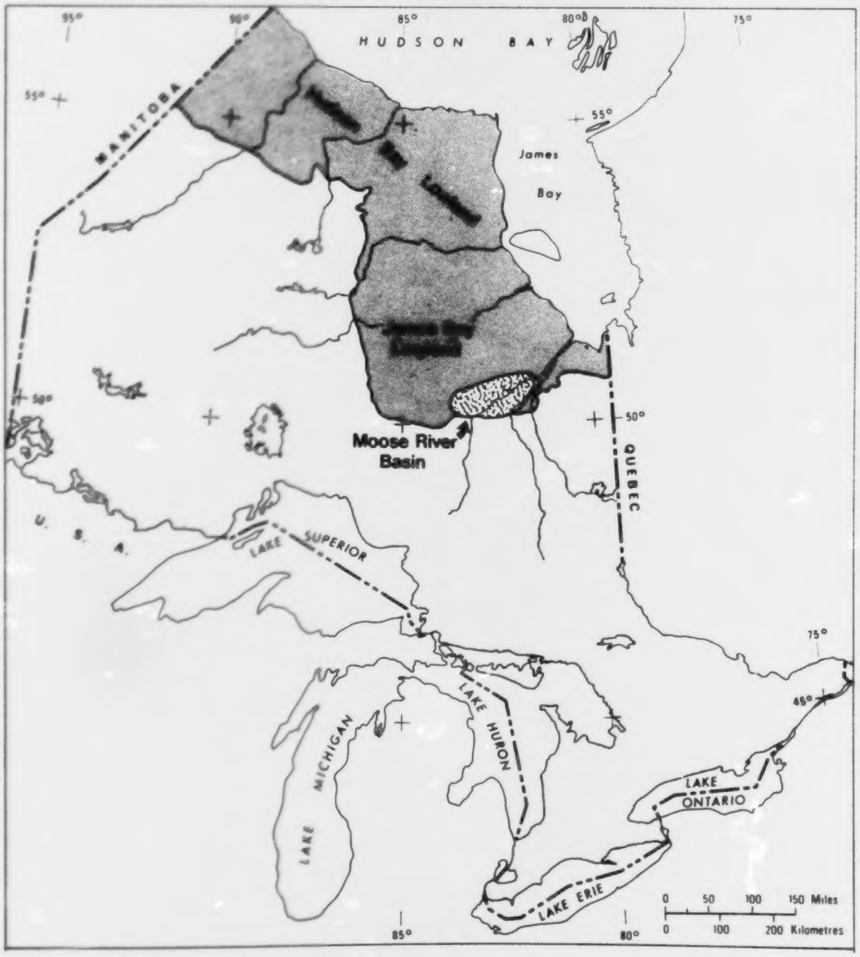

Figure 216.1. Location of the Long Rapids Formation in the Moose River Basin. From Telford and Verma (1982 ; Figure 1.1, p.3).

plankton blooms, tectonic readjustments along the craton's marginal edge, or climatic variance.

INTRODUCTION

The Upper Devonian Long Rapids Formation, located in the Moose River Basin (Figure 216.1), consists of interbedded brownish black shales, greenish grey shales and mudstones, and carbonate beds or nodules. The formation is the youngest Paleozoic unit in the Moose River Basin and crops out along river banks on the eastern side of the basin. The subsurface area of the Long Rapids is estimated to be 5400 km^2 and its maximum thickness is approximately 80 m (Figure 216.2).

The black shales of the Long Rapids have largely been ignored or overlooked in northern Ontario, until the worldwide energy shortage drew attention to them as a possible shale oil resource. This project is a study of the depositional environment for the Moose River Basin during the Upper Devonian, and encompasses sedimentological, stratigraphic, ichnological, and geochemical observations. This study is part of a larger program that also includes the economic potential of the rocks (as shale oil) in the Moose River Basin by the authors and the Ontario Geological Survey. The preliminary report (Bezys and Risk 1985) on the project presented evidence for a marine setting which experienced periodic water stratification that in turn induced anoxia. The present paper suggests further evidence supporting this earlier hypothesis.

LONG RAPIDS FORMATION STRATIGRAPHY

The study area lies in the James Bay Lowlands, a region of extensive wetlands and difficult accessibility. The formation crops out along river banks and is intersected in subcrop via drilling. Outcrops are sparse and only one section, on the bank of the

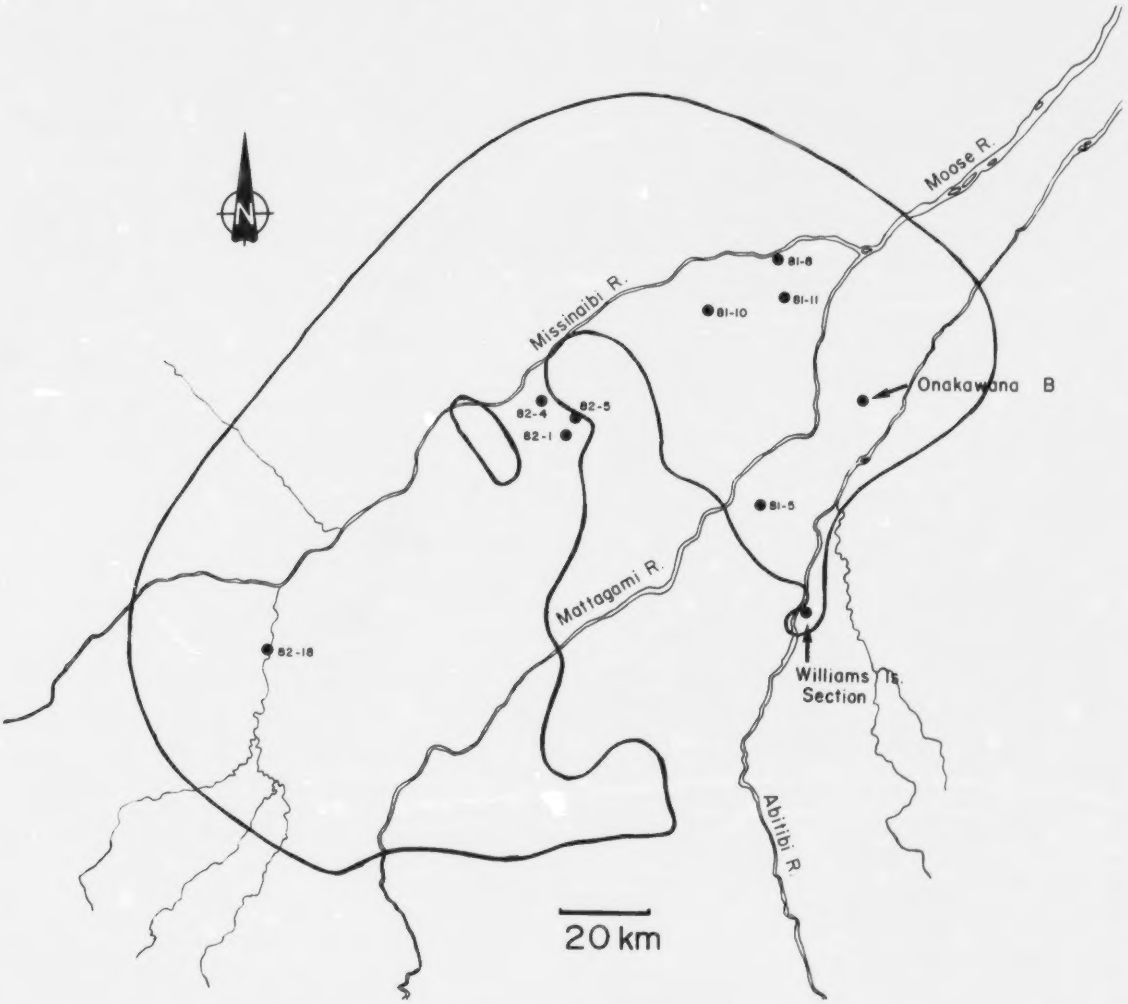

Figure 216.2. Subsurface area map of the Long Rapids Formation and the drillholes studied.

Abitibi River, can be confidently placed on a disconformable contact with Middle Devonian rocks. Other sections do exist, but they contain no reliable marker beds or contacts for correlation. Core data is available, but incomplete since Devonian strata were not the targets in many drillhole surveys in the basin. Geophysical data is also sparse.

The Moose River Basin lies to the southwest of James Bay and encompasses an area of approximately 100 000 km^2. A positive basement high, the Grand Rapids High, runs roughly northwest to southeast through the middle of the basin and can be shown on the Long Rapids subsurface map (Figure 216.2). Dyer and Crozier (1933) subdivided the Long Rapids into three members, and their convention is still used today:

UPPER MEMBER: Interbedded green-grey mudstones and grey shales (approximatley 20 m).

MIDDLE MEMBER: Black-grey shale with thin bands of green-grey mudstones (approximatley 30 m).

LOWER MEMBER: Green-grey claystones and mudstones with bands of dark black and abundant, hard carbonate horizons (approximatley 37 m).

The formation is unconformably overlain by Cretaceous sediments, which in the field are frequently indistinguishable from the underlying Devonian sediments. Identification of Cretaceous or Devonian strata can only be accomplished with palynology. A total of nine drillholes and one outcrop section comprise the extent of data collection. The holes logged in this study include: Onex 82-1, 82-4, 82-5, 82-18; OEC 81-5, 81-8, 81-10, 81-11; and Onakawana "B", and are located in Figure 216.2. Holes that contained minor amounts of Upper Devonian sediments as core, but possessed a geological drill log, were also investigated. Samples were collected from the Williams Island section and from the holes that were logged. Due to the sparseness of drillholes that extended into the Long Rapids Formation, as mentioned previously, regional correlation is difficult. The formation contains no distinct marker beds that are correlative and lower and upper contacts do not always exist.

WILLIAMS ISLAND SECTION

The section is located on the southeast bank of the Abitibi River next to Williams Island. The beds dip slightly (2° to 5°) to the southeast. Gentle folding of the strata is also observed and may have been caused by glaciation or by the section's proximity to the Williams Island Structural Dome. Due to the slight dip of the sediments, the section was mapped in increments, starting at the base to the north and proceeding southward. A thickness of approximately 60 m was measured (Figure 216.3).

The lower contact of the Long Rapids Formation to the Williams Island Formation (Middle Devonian) is sharp, but very weathered. The underlying Middle Devonian limestone unit is quite brecciated and may be karstic. The unit is overlain by 3 to 4 m of Upper Devonian greenish grey mudstones. It is within this bed that the most abundant fossils are found, including crinoid ossicles, rugose corals, and brachiopods. Nearly all brachiopods found here were whole specimens and weathered out of the unit easily due to the unit's clayey nature.

The next 30 m contained interbedded greenish grey mudstones, grey-black shales, and carbonate beds. This constitutes the Lower Member of the formation and contains the most abundant occurrence of carbonate beds. Carbonate bed thicknesses vary from 1 cm to about 30 cm, and may sometimes occur as concretions or nodules instead of beds. It is within one of these carbonate beds, 10.5 m from the base, that the stratigraphically important goniatite zone occurs. Within this 5 cm thick bed, other fossils such as brachiopods, orthoconic nautiloids, gastropods, and crinoids also occur, and many are fragmented, such as the goniatites. It is also within this Lower Member that abundant minor rhythmic sedimentary units occur. The contacts between each cycle consist of a black shale, green-grey mudstone/shale, and a carbonate bed, and are usually sharp and only rarely gradational.

The next 30 m consists of grey-black shales with some interbedded greenish grey mudstones, and are referred to as the Middle Member. No carbonate beds or concretions occur within this member. Black shale beds occur in the greatest abundance here, and are up to 2.6 m thick. Body fossils are very rare, and trace fossils common. Traces occur where there is a transition from a black shale to a green-grey mudstone. Most lower contacts of greenish grey mudstones are sharp, whereas tops are sometimes gradational. The highest total organic carbon (TOC) values occur within this member, though the lowermost black shale bed in the Lower Member (6 m thick) also contains high TOC values.

ONAKAWANA "B" DRILLHOLE

This hole, drilled in March 1985 by the Ontario Geological Survey, was a re-drill of the original 1929 Onakawana "A" hole (Dyer and Crozier 1933). Both holes penetrated the entire sedimentary sequence in the Moose River Basin to the Precambrian basement. The core from the first hole has since disappeared and the Onakawana "B" hole therefore represents the only complete cored drillhole through the Moose River Basin (refer to Sanderson and Telford (1985) for further information). Approximately 80 m of Upper Devonian strata were cored (Figure 216.4), and are roughly equivalent to the 87 m Dyer and Crozier logged in 1933.

The upper and lower contacts for the Long Rapids Formation were placed at depths of 76.70 m and 156.20 m, respectively, for the Onakawana "B" hole. The upper contact is gradational and is distinguished by the presence of Cretaceous coal chips from the Mattagami Formation. The lithology at this contact is a greenish grey mudstone, and does not change across the contact. Therefore, to determine the exact location of the contact, J. Legault (Professor, University of Waterloo, Waterloo, personal communication, 1985) ran a palynological analysis on a sample from this upper contact, at 76.75 m, and reported that the majority of the microfossils found were Devonian, with two poorly preserved Cretaceous specimens. This could be a Cretaceous sample with reworked Devonian fossils, but the large number of

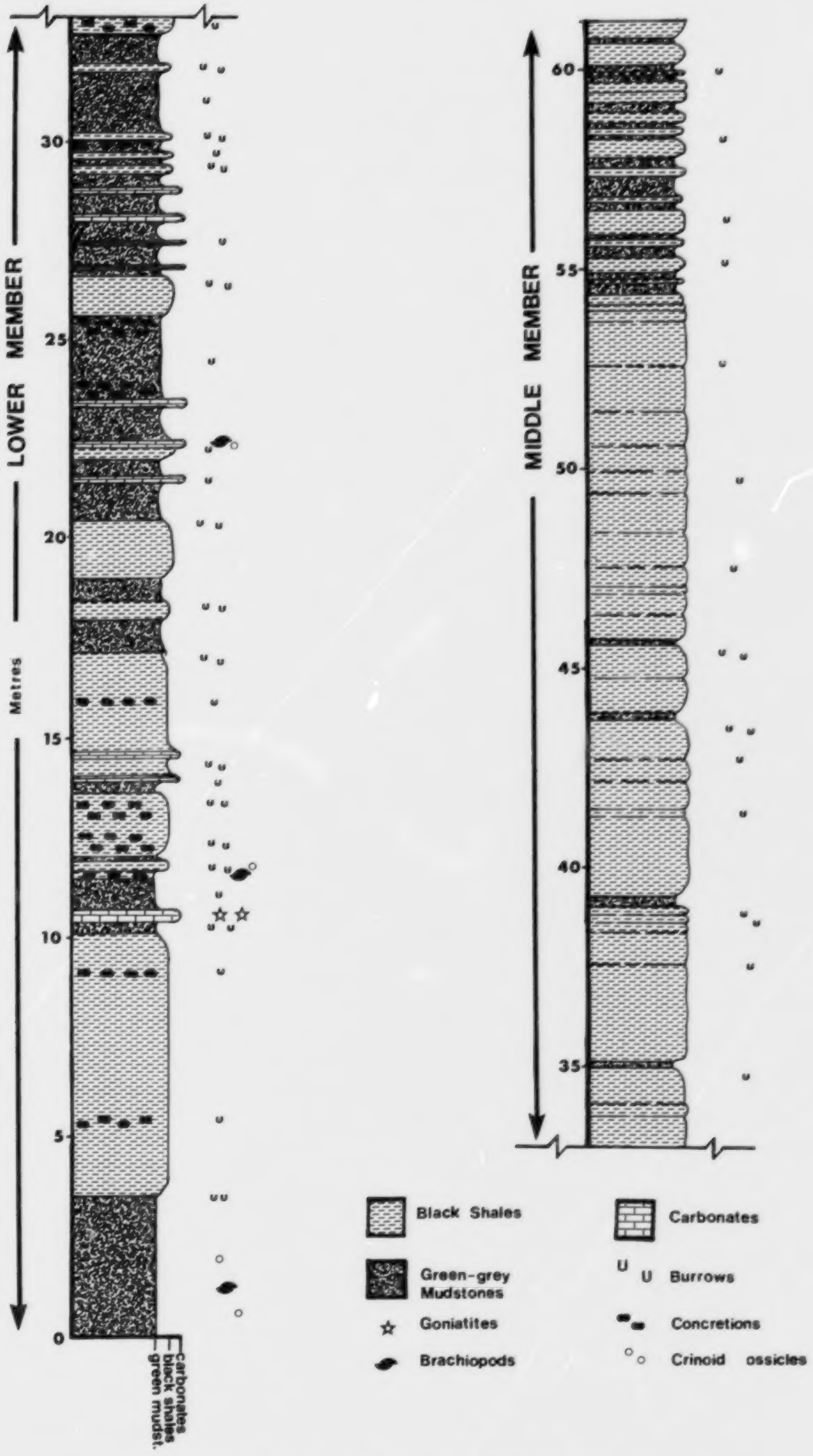
LOWER MEMBER
MIDDLE MEMBER
Metres
0
5
10
15
20
25
30
35
40
45
50
55
60
carbonates
black shales
green mudst.
Black Shales
Carbonates
Green-grey Mudstones
Burrows
Goniatites
Concretions
Brachiopods
Crinoid ossicles

Figure 216.3. The Williams Island outcrop section.

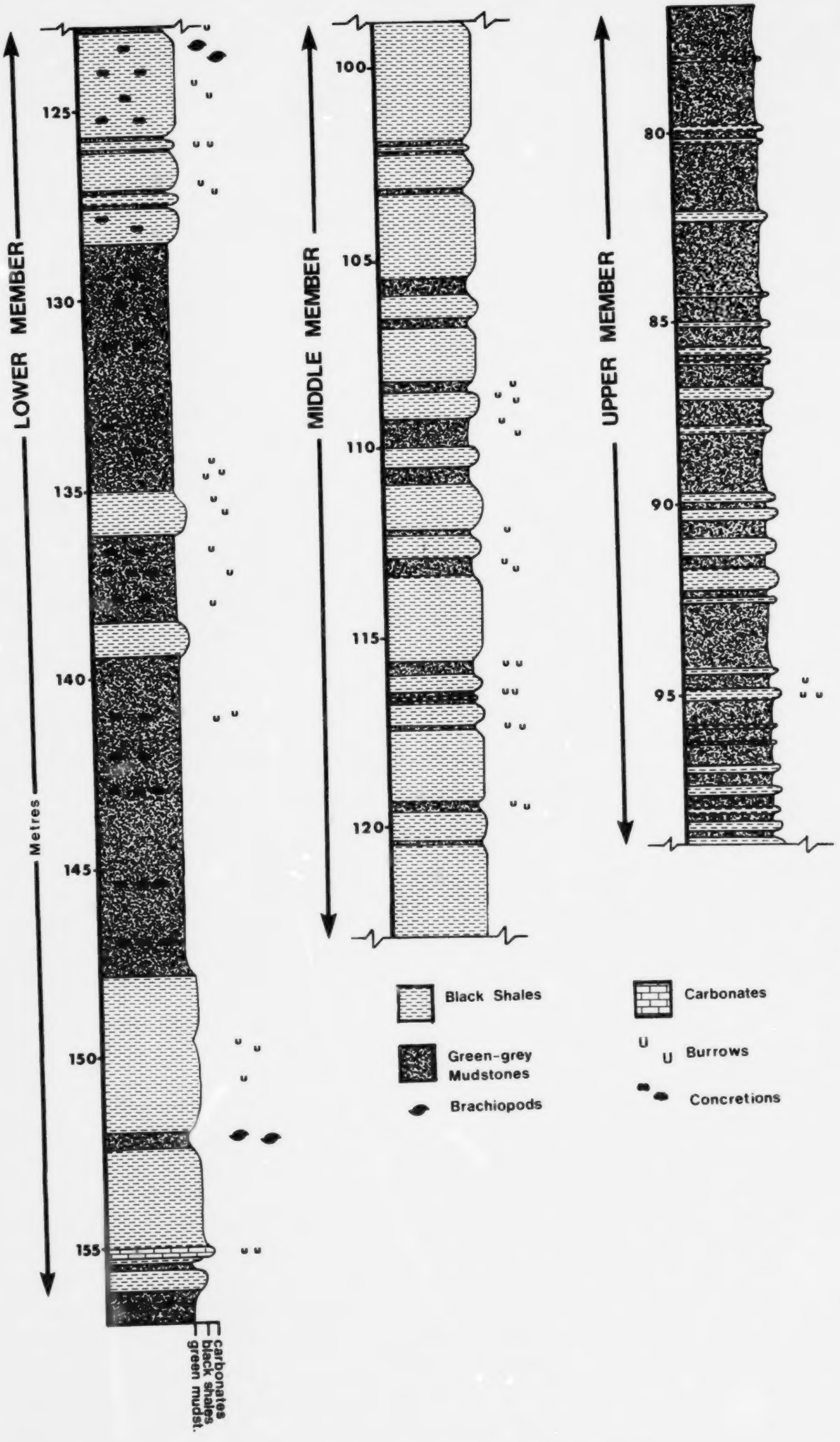
LOWER MEMBER
Metres
125
130
135
140
145
150
155
carbonates
black shales
green mudst.
MIDDLE MEMBER
100
105
110
115
120
UPPER MEMBER
80
85
90
95
Black Shales
Green-grey Mudstones
Brachiopods
Carbonates
Burrows
Concretions

Figure 216.4. The Onakawana "B" drillhole.

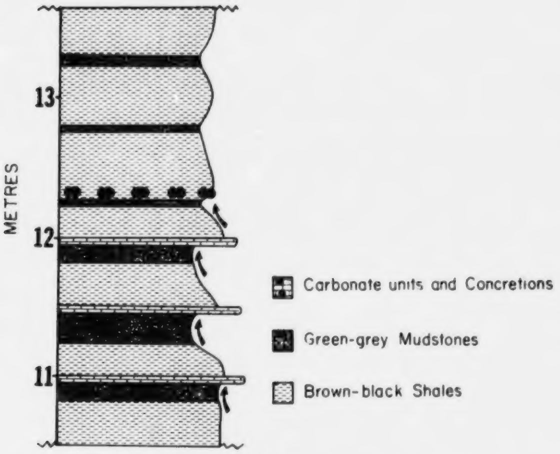

Figure 216.5. *A rhythmic sedimentary unit from the Williams Island section.*

Devonian versus the rarity of Cretaceous forms and their state of preservation suggest a Devonian sample with Cretaceous as a contaminant.

The lower contact of the Long Rapids Formation is placed at 156.20 m. Beyond this depth, all black shales encountered are thinly bedded, occurring with abundant green-grey mudstones and carbonate beds. This is the upper portion of the Williams Island Formation.

The three members within the hole are indicated on Figure 216.5. The Upper Member is 22 m thick, the Middle Member 24 m, and the Lower Member is 33 m thick. These three members fit Dyer and Crozier's (1933) description of the Onakawana "A" hole. The contacts between the members in the "B" hole were chosen arbitrarily. The changes between the carbonate beds, the black shales, the green-grey mudstones, and their abundances signify a member change.

The TOC values for the shales within the Onakawana "B" hole are high (compared to outcrop averages), but samples were selectively chosen to consist mainly of black shales. TOC values range from 0.42% to 5.72%. The highest values occur in the lowermost black shale beds in the Lower Member. Drillhole TOC values from these beds are 4.39% and 5.69%, which correlate well with TOC percentages from the outcrop samples from these same beds: 6.77%, 4.74%, 6.27%, 6.12%, and 6.23%. High TOC values (up to 6%) also occur in the Lower Member within black shale units. The TOC values for the outcrop Middle Member correlate somewhat with equivalent samples from drillhole TOC's (Table 216.1).

SEDIMENTOLOGY

In outcrop, the Long Rapids shales are very fissile and in some places are cut by long, near-vertical joints, up to 1 m in length. In core, the shales are massive, very indurated, and fracture subconchoidally. The dark colour of the black shales is caused by organic matter, but intensity of colouration is not necessarily controlled by percentage of organic matter. The colour difference may be due to the refractory or labile nature of the organic matter itself (Goldhaber 1978). This is evident in the Long Rapids shales, where the darkest specimens do not necessarily produce the highest TOC values.

TABLE 216.1. CORRELATION BETWEEN THE OUTCROP AND DRILLHOLE SECTIONS OF SIMILAR SHALE BEDS IN THE MIDDLE MEMBER AND THEIR CORRESPONDING TOC VALUES.

	Outcrop Samples			Onak. "B" Samples	
Number	**m**	**TOC (%)**	**Number**	**m**	**TOC (%)**
28-8-a	27.98	4.72	72	122.01	5.28
25-10-a	28.30	5.16	73	119.03	5.25
25-10-c	29.31	6.57	74	118.32	5.50
25-14-b	30.65	3.43			
25-14-c	30.77	1.49		n = 3	
25-14-d	30.95	3.33		x = 5.34	
25-16-a	31.48	3.82		s = 0.14	
25-18-a	31.96	5.61			
25-20-a	32.29	3.23			
25-20-b	32.64	4.19			
25-22-a	33.16	6.22			
25-24-a	33.55	4.99			
25-28-a	34.10	4.69			
25-30-a	34.16	4.36			
25-31-a	34.34	6.56			
25-34-a	34.52	5.14			
25-36-a	35.06	8.04			
	n = 17				
	x = 4.80				
	s = 1.55				

Other constituents within the shales include quartz, clay minerals, iron sulphides, and carbonates (mainly calcite). The overall grain size is very fine, and mineral identification in thin sections is often impossible. Laminations in the shales, leading to fissility, are due to quartz-rich, clay-rich, and organic-rich layers less than 1 mm in thickness. When studied with a scanning electron microscope, the lighter coloured lithologies (greenish grey) are similar in grain size and mineralogy to the darker shales, but lack the organic matter.

Only the Lower Member contains abundant carbonate beds and concretions. Calcite is the dominant carbonate mineral, though dolomite crystals sometimes occur in large carbonate concretions found at the outcrop locality. Most carbonate beds can be classified as biomicrites, based on the presence of fossiliferous material, pellets, and micrite (Folk's classification, Folk 1962). Sparry calcite occurs infilling void spaces, fossils, and burrows. Many carbonate units cap green-grey shale or mudstone beds and may, in turn, be sharply overlain by a black shale bed (a rhythmic sedimentary unit; Figure 216.5). (This terminology follows Houses' (1983) classification for large and small scale rhythms in the Upper Devonian Rhinestreet Shale in New York). The sequence may then repeat itself. The thickness of the individual units and the overall sedimentary rhythm may vary considerably, from a few centimetres to several metres. Occasionally, mottled grey or beige concretions occur within black or green units.

PALEONTOLOGY

Various fossil fragments have been found within green-grey mudstone or carbonate beds and include goniatites, brachiopods, corals, crinoids, orthoconic nautiloids, and molluscs. The goniatites (*Maniticoceras sinuosum*) occur within one distinct carbonate bed with a conodont (*Ancyognathus triangularis*) date of Frasnian. Abundant, well preserved brachiopods occur in the lower portion of the Lower Member and some 30 species have been identified:

Ambocoelia sp.
Calvinaria cf. *variabilis athabascensis*
Costatrypa americana (Stainbrook)
Cyrtina sp.
Desquamatia (Seratrypa) cf. *snyderensis* (Greger)
Douvillina arcuata (Hall)
Ladogioides pax
Leiorhynchus cf. *quadracostatum*
Productella sp.
Pseudoatrypa cf. *devoniana* (Webster)
Rhipidomella sp.
Schizsophoria iowensis (Hall)
Tecnocyrtina cf. *missouriensis*
Tylothyris sp.
?Warrenella

(Telford 1985; P. Copper, Professor, Laurentian University, Sudbury, personal communication, 1986)

Sizes for most of the brachiopods, except the large atrypids, are relatively dwarfed and are well below the norm for the genera (at least 50% below on average). These represent benthic fauna that are predominantly sedentary, except for *Schizsophoria*, *Cyrtina*, and *Tylothyris*. P. Copper (Professor, Laurentian University, Sudbury, personal communication, 1986) suggests that this indicates muddy conditions with few holdfast opportunities, probably deeper or sheltered quiet waters. Coupled with dwarfism, this implies poor circulation and oxygen deficient conditions.

Abundant conodonts have also been extracted from carbonate beds and observed on black shale bedding planes. Telford (1985) reports that at least six of the standard Upper Devonian conodont zones are represented by Long Rapids conodont species. The zones range from the earliest Frasnian Lower *asymmetricus* zone, to the middle Famennian Lower *rhomboidea* zone. Along black shale bedding planes, whole *Lingula* shells and fragments can be found. In thin sections and scanning electron microscope (SEM) photographs, the algal spore case, *Tasmanites*, can be identified. Rare plant remains, *Callixylon*, can also be preserved. Thin sections from carbonate beds reveal biomicrites with abundant pellets and fossiliferous material, commonly recrystallized to sparry and blocky calcite, within a micritic matrix. Types of fossils that can be identified include shelly material with well preserved growth lamellae, gastropod sections, pelleted material, and ammonoid fragments.

TRACE FOSSILS

Trace fossils in the Long Rapids Formation occur where there is a colour change between shales or mudstones (such as that from a black shale to a green-grey mudstone). Burrowing is present in all three members, but is most abundant in the Middle Member. Recognizable burrows occur within black shale units, directly below green-grey shales or mudstone beds.

Most of the cut slabs from the carbonate horizons are quite mottled and probably so bioturbated that no distinct burrows can be seen. Weathered, planar views of some of these horizons reveal burrows; thus bioturbation is suspected throughout. The smaller sized concretions (average size: 3 cm by 6 cm) contain spaghetti-like burrows oriented at various angles. It is possible that these burrows are the nucleus about which these concretions started to grow. In core and outcrop, all trace fossils were found in association with green-grey shales/mudstones, carbonate beds, and concretions. Trace fossils were found in black shales only when they were overlain by green beds. When found in black shales, the burrows possessed a green-grey sediment infill (usually similar to the overlying green beds) and some extended as far as 20 cm down into black shale beds.

So far, the trace fossils found include: *Alcyonidiopsis*, *Chondrites*, *?Cylindrichnus*, *Planolites*, *?Skolithos*, *Teichichnus*, *Terebellina*, *Zoophycos*, and *Ichnogenus "A"*. All are of normal size, with *Chondrites* and *Planolites* being the most abundant. These traces were studied in outcrop and cores, in thin sections, and with a scanning electron microscope.

The presence of trace fossils in green beds, or directly beneath them within black shales, implies that oxygen was available at the sediment-water interface, even if in lower than normal quantities. The majority of black shales (ancient or recent) are deposited under anoxic water conditions, thus the supply of oxygen must have been intermittent. This is reflected in the type of trace fossils found. Most of the forms found represent infaunal or epifaunal deposit-feeding traces produced by soft-bodied organisms, such as *Chondrites, Planolites*, and *Zoophycos*. This indicates that the organisms were using the sediment medium only for food, and not as a domicile (as a suspension feeder would, such as *Skolithos*). This implies that oxygen was the major restricting factor for the presence or absence of the organisms.

GEOCHEMISTRY

TOTAL ORGANIC CARBON (TOC)

A measure of a shale's potential for production of shale oil is the percentage of organic matter, preferably aliphatic, that is present. In total, 205 samples were analyzed on a LECO carbon determinator; 125 of these from outcrops and 80 from cores. Mean TOC values for the outcrop and core samples, respectively, were 2.05% (range: 0.02% to 6.77%) and 4.25% (range: 0.26% to 10.13%) (Table 216.2). These data represent samples from all lithology types, excluding carbonate beds. The higher mean values for the core samples may be due to two reasons: 1) only black shale horizons were sampled, whereas the outcrop samples came from either black shale or green-grey mudstone horizons; 2) all the outcrop samples are exposed to weathering, and thus may be depleted in organic matter content.

The amount of organic matter preserved in a sediment depends on its rate of accumulation, and the rate of sedimentation of sediments other than organic matter. Under oxic water conditions, there is a positive correlation between sedimentation rates and organic carbon content in recent sediments. The organic carbon content of modern marine sediments in oxic environments ranges from 0.3% to 4.0% (Demaison and Moore 1980). In modern anoxic sediments, this relationship does not apply, and the range is wider and higher (1% to 20%), regardless of sedimentation rates.

Significant amounts of shale oil may be extracted from the Long Rapids shales. The lower limit of organic matter required for economic recovery is generally set at 5%. The temperature of pyrolysis for shale retorting is never greater than 500° to 600°C, and the energy required to raise the temperature of the sample to 500°C is about 250 calories per gram of rock (Macauley 1984). This is based on the heat value of organic matter at approximately 10 000 calories per gram of rock, which would put the minimum organic content at 2.5%. The Long Rapids shales, therefore, may have future potential as a shale oil resource, depending on mining and transportation costs and future technological advances.

STABLE CARBON ISOTOPE COMPOSITION

Carbon possesses two stable isotopes, ^{12}C and ^{13}C, with a ratio (12°C/13°C) of about 99.1 (Fuex 1977). Differences in this ratio may be used to elucidate chemical processes that have occurred in the geologic record. For the Long Rapids shales, analyses were completed to determine the type of organic matter present in the shales. Marine (sapropelic) organic matter contains hydrogen-rich aliphatic compounds that are a likely source of petroleum, or will yield greater volumes of shale oil upon pyrolysis. See Bezys and Risk (1985) for a further discussion on stable carbon isotopes.

The δ^{13}C values for the organic carbon from the Long Rapids Formation samples range from -25.29‰ to -30.46‰ with a mean of -29.59‰ (Table 216.3). Coaly plant samples (vitrinite) had values of -22.90‰ and -22.67‰. These shale values are depleted in ^{13}C when compared to organic matter in modern marine sediments. An average value of -21.0‰ was recorded for modern marine sediments in Atlantic Ocean sediments (with surface water temperatures at about 25°C) by Sackett *et al.* (1965).

Isotopic values for the Long Rapids shales indicate a terrestrial source for the organic matter, yet, paleoecological evidence suggests a marine setting for the basin with an equatorial climate. These signatures may not represent terrestrial input, but rather marine organic matter that has undergone biogenic or non-biogenic alterations. Hailer *et al.* (1983) obtained similar carbon isotope results on the Upper Devonian New Albany shale. The formation consists of black shale horizons with interbedded green mudstone beds. Carbon isotope values for 137 samples ranged from -24.5‰ to -31.0‰, with a median of -29.35‰. These shales are also paleoecologically interpreted to be marine, and yet, have depleted isotope values. Quiescent, warm, and productive conditions are thought to have existed in the Illinois Basin where the shales were deposited, and such conditions would not have caused extreme photosynthetic fractionations that would result in large ^{13}C depletions.

The most probable explanation is diagenetic alteration of the carbon isotope abundances. Non-biological alteration could arise from thermal degradation of heavier ^{12}C compounds, such as proteins and carbohydrates. The remaining residue would then be enriched with more refractory ^{12}C-rich lipids. Biologically, anaerobic bacteria may alter the isotopic value by consuming proteins and carbohydrates in the sediments and leaving behind the lipids that are relatively resistant to biological destruction. Also, recycling of any sediment already depleted in ^{13}C could produce these similar results. For the New Albany Shale, Hailer *et al.* (1983) predict that the most likely cause of the observed depletion in ^{13}C is diagenetic alteration.

For the Long Rapids shales, it is probable that the carbon isotope values attained represent marine organic matter, and that isotopic fractionation has occurred to alter the original values. This fractionation may have conceivably been caused by either biologic or non-biologic alterations. The determination of which pathway is beyond the scope of this study. The stable isotope results are complemented by ^{13}C

TABLE 216.2. TOTAL ORGANIC CARBON VALUES (OUTCROP SAMPLES).

Sample Number	Elevation from Base of Section (metres)	Total Organic Carbon (%)
9a	4.26	6.77
9b	4.76	4.74
9c	5.26	6.27
9d	5.76	6.12
9e	6.26	6.23
10-1-a	6.41	5.61
10-2-a	6.90	1.80
10-2-bx	6.94	2.08
10-2-c	6.98	2.15
10-4-b	7.71	0.85
10-4-c	8.12	1.04
11-1-a	8.27	3.77
11-3-a	8.50	2.83
11-3-b	8.61	2.27
11-4-a	8.70	0.53
11-5-ax	8.86	0.78
11-6-a	8.91	0.17
11-8-a	8.99	3.76
11-8-b	9.15	1.46
11-8-cx	9.13	1.99
11-8-d	9.20	1.86
11-9-a	9.29	0.39
12-1-a	9.54	3.76
12-2-a	9.74	0.89
12-3-a	9.81	0.44
12-5-a	9.95	4.10
12-5-b	10.01	4.43
12-6-a	10.12	0.46
12-8-a	10.29	1.28
12-8-b	10.38	3.01
12-9-a	10.56	0.55
13-1-a	10.89	2.38
13-1-b	10.97	3.29
13-2-b	11.13	0.21
14-1-a	11.25	3.74
14-1-b	11.40	2.29
14-1-c	11.51	4.39
14-3-a	11.86	3.58
14-3-b	12.11	2.38
14-4-a	12.19	0.46
14-5-a	12.34	5.27
14-6-a	12.49	1.78
15-1-a	12.81	1.41
15-2-a	13.04	0.55
15-3-a	13.56	1.93
16-3-a	15.45	3.01
16-4-a	16.35	0.47
17-1-a	16.59	0.05
17-2-a	16.65	0.16
17-3-a	16.72	0.02
17-4-a	16.81	0.16
17-5-a	17.00	0.05
17-6-a	17.38	0.86
17-7-a	17.81	0.30
17-8-a	18.05	0.59
17-9-a	18.16	0.13
17-10-a	18.22	0.04
17-11/12-a	18.32	0.04
17-13-a	18.42	0.06
17-14-a	18.48	0.03
17-15-a	19.00	0.04
17-16-a	19.55	0.48
17-17-a	19.80	0.06
17-17-b	19.89	0.20
17-18-a	19.98	0.50
17-19-a	20.06	0.05
17-20-a	20.13	0.81
17-21-a	20.19	0.06
17-22-a	20.35	0.41
17-23-a	20.44	0.04
17-24-a	20.47	0.37
17-25-a	20.55	0.08
17-26-a	20.76	0.81
17-26-b	21.19	0.79
17-27-a	21.30	0.09
17-28-a	21.42	0.21
17-29-a	21.54	0.64
18-1-a	22.05	6.12
18-1-b	22.54	5.16
18-2-a	22.75	0.58
18-4-a	23.06	0.91
18-5-a	23.14	2.07
18-6-a	23.32	0.36
18-8-a	23.84	0.23
19-1-a	24.29	0.75
19-2-a	24.42	1.08
19-3-a	24.72	0.66
19-4-a	25.00	1.66
19-5-a	25.18	1.33
25-1-a	25.46	0.62
25-1-b	26.66	0.35
25-1-c	27.19	0.06
25-2-a	27.32	0.06
25-3-a	27.48	0.55
25-4-a	27.63	4.82
25-5-a	27.71	0.69
25-6-a	27.78	5.11
25-7-a	27.86	0.62
25-8-a	27.98	4.72
25-9-a	28.09	4.94
25-10-a	28.30	5.16
25-10-b	29.00	3.82
25-10-c	29.30	6.57
25-11-a	29.62	0.19
25-13-a	30.15	4.70
25-14-b	30.65	3.43
25-14-c	30.77	1.49

TABLE 216.2. cont'd.

Sample Number	Elevation from Base of Section (metres)	Total Organic Carbon (%)
25-14-d	30.95	3.33
25-16-a	31.48	3.82
25-17-a	31.90	0.08
25-18-a	31.96	5.61
25-20-a	32.29	3.23
25-20-b	32.64	4.19
25-21-a	32.76	0.94
25-22-a	33.16	6.22
25-23-a	33.51	1.10
25-24-a	33.55	4.99
25-25-a	33.59	0.94
25-27-a	34.06	0.33
25-28-a	34.10	4.69
25-29-a	34.14	1.79
25-30-a	34.16	4.36
25-31-a	34.34	6.56
25-32-a	34.43	2.84
25-34-a	34.52	5.14
25-36-a	35.06	8.04

n = 125

x = 2.10%

TOTAL ORGANIC CARBON VALUES (DRILLHOLE SAMPLES)

Sample Number	Drillhole Number	Depth (m)	Total Organic Carbon (%)
OX 1	Onex 82-4	95.73	2.30
OX 2	Onex 82-4	97.03	3.09
OX 3	Onex 82-4	98.83	4.84
OX 4	Onex 82-4	113.13	1.44
OX 5	Onex 82-4	114.63	3.88
OX 6	Onex 82-4	127.63	4.31
OX 7	Onex 82-4	131.33	2.93
OX 8	Onex 82-4	135.10	1.56
OX 9	Onex 82-5	106.93	4.46
OX 10	Onex 82-5	108.03	4.65
OX 11	Onex 82-5	112.71	2.90
OX 12	Onex 82-5	116.01	1.45
OX 13	Onex 82-5	117.40	4.87
OX 14	Onex 82-5	118.61	5.08
OX 15	Onex 82-5	120.61	4.02
OX 16	Onex 82-5	122.20	4.62
OX 17	Onex 82-5	124.92	0.26
OX 18	Onex 82-5	130.60	2.34
OX 19	Onex 82-5	132.61	7.46
OX 20	Onex 82-5	133.30	3.45
OX 21	Onex 82-5	133.61	5.75
OX 22	Onex 82-18	112.80	4.19
OX 23	Onex 82-18	114.20	5.06
OX 24	Onex 82-18	114.62	2.21
OX 25	Onex 82-18	116.41	3.98
OX 26	Onex 82-18	110.91	3.73
OX 27	Onex 82-18	109.91	3.91
OX 28	Onex 82-18	106.32	3.83
OX 29	Onex 82-18	103.02	5.10
OX 30	Onex 82-1	78.52	10.13
OX 31	Onex 82-1	76.31	6.46
OX 33	Oec 81-5	116.10	3.76
OX 34	Oec 81-5	114.01	6.17
OX 35	Oec 81-5	112.70	7.35
OX 36	Oec 81-5	111.30	4.05
OX 37	Oec 81-5	110.23	8.21
OX 38	Oec 81-5	107.53	5.60
OX 39	Oec 81-5	104.80	5.44
OX 40	Oec 81-5	103.00	7.51
OX 41	Oec 81-5	99.89	5.92
OX 42	Oec 81-5	97.47	3.63
OX 43	Oec 81-5	94.73	4.71
OX 44	Oec 81-5	92.41	4.77
OX 45	Oec 81-8	63.05	2.11
OX 46	Oec 81-8	59.16	4.70
OX 47	Oec 81-8	58.30	3.32
OX 48	Oec 81-8	54.50	3.31
OX 49	Oec 81-8	52.78	4.51
OX 50	Oec 81-8	48.75	3.82
OX 51	Oec 81-10	97.41	2.79
OX 52	Oec 81-10	90.96	3.09
OX 54	Oec 81-11	106.85	4.43
OX 55	Oec 81-11	105.82	3.47
OX 56	Oec 81-11	105.03	5.40
OX 57	Oec 81-11	100.26	3.44
OX 58	Oec 81-11	99.24	3.04
OX 59	Oec 81-11	97.22	2.40
OX 60	Oec 81-11	93.54	4.61
OX 61	Oec 81-11	91.14	4.64
OX 62	Oec 81-11	85.94	2.91
OX 63	Onak B	150.80	4.39
OX 64	Onak B	148.19	5.69
OX 65	Onak B	137.42	3.51
OX 66	Onak B	134.31	3.45
OX 67	Onak B	127.66	3.96
OX 68	Onak B	126.66	4.33
OX 69	Onak B	125.68	4.81
OX 70	Onak B	124.38	5.72
OX 71	Onak B	123.93	5.28
OX 72	Onak B	122.01	5.28
OX 73	Onak B	119.03	5.25
OX 74	Onak B	118.32	5.50
OX 75	Onak B	114.35	3.39
OX 76	Onak B	111.66	2.83
OX 77	Onak B	106.89	4.80
OX 78	Onak B	104.74	1.89
OX 79	Onak B	102.20	4.48
OX 80	Onak B	102.12	4.99
OX 81	Onak B	100.67	4.72
OX 82	Onak B	92.29	0.42

n = 80

x = 4.23%

TABLE 216.3. STABLE CARBON ISOTOPE VALUES

Drillhole Samples			Outcrop Samples		
Number	$\delta^{13}C$	**TOC(%)**	**Number**	$\delta^{13}C$	**TOC(%)**
OX-3	-29.99	4.84	10-2-b	-30.00	-
9c	-29.78	6.27	10-2-bx	-29.85	2.10
12-5-a	-30.29	4.10	11-5-a	-29.60	-
OX-14	-30.29	5.08	11-5-ax	-29.62	0.79
OX-23	-27.95	5.06	11-8-c	-30.32	2.02
OX-31	-30.05	6.46	12-2-a	-29.73	0.90
OX-37	-29.45	8.21	12-5-a	-30.36	4.12
OX-50	-30.09	3.82	12-9-a	-29.33	0.56
OX-52	-30.15	3.09	19-1-a	-25.29	0.76
OX-59	-29.76	2.40			
OX-64	-30.46	5.69	coaly fragment		-22.90
OX-73	-29.49	5.25	coaly fragment		-22.67
OX-74	-29.15	5.50			

$n = 22$

$x = -29.59$

$s = 1.10$

NMR (nuclear magnetic resonance) data that give results correlative with other marine oil shales (Miknis *et al.* 1979).

CHEMICAL INDEX OF MATURITY

The chemical index of maturity is a measure of weathering. By comparing profiles of shales, information can be obtained on provenance, mechanical mixing of components, and diagenetic processes. Weathering profiles are produced when compositional changes occur in a rock, and by determining the exent to which weathering has proceeded; this can be illustrated on ternary diagrams. The end members include: K_2O (felsic end member), $CaO + Na_2O$ (basic end member), and Al_2O_3 (aluminum end member). The weathering trends for various igneous rocks can thus be illustrated. Felsic rocks have weathering trends towards the K_2O end member, mafic towards the $CaO + Na_2O$ end member and intermediate rocks trend between mafic and felsic trends (Hoy 1980).

The major clay minerals in shale include kaolinite, illite, montmorillonite, chlorite, and quartz (Shaw and Weaver 1965). Mineralogical and chemical changes occur within shales with increasing maturity, and are similar to weathering profiles. Information may be gained on: a) possible source area or provenance; b) processes which occur during diagenesis; c) trends which indicate mechanical mixing of various components which constitute the sediment (Nesbitt, *in* Hoy 1980). This study concentrated on determining the provenance of the Long Rapids shales.

Sediments within the Moose River Basin are principally thought to have a source off the Precambrian Shield (or possibly the Old Red Sandstone continent). These sediments would then be subsequently reworked within the basin to form younger units. Since the southern boundary of the Moose River Basin abuts sharply onto the Shield, a prediction of the probable source rock can be made. An Ontario Geological Survey map (Map 2393) shows the Precambrian Shield at the basin's southern end to be granodiorites and granites. By using Nesbitt's method (*in* Hoy 1980) for determining the chemical index of maturity (CI), a probable provenance rock can be determined. The CI can be determined as follows:

$$CI = \frac{1 - (\%Al_2O_3)}{100} \qquad (1)$$

or

$$CI = \frac{CaO_{sil} + Na_2O + K_2O}{CaO_{sil} + Na_2O + K_2O + Al_2O_3} \qquad (2)$$

Values for the CI lie within the range 0.0 to 0.5 and represent the following maturities:

0.5	0.35	0.15	0.0
immature	mature	supermature	

Once plotted on a ternary diagram, a weathering trend can be determined (from Figure 216.6). Any shifts of the points above or below the weathering trend represents a diagenetic trend and/or mixing of the two weathering trends. This can be represented better pictorially in Figure 216.7a. Diagenetic trends can also indicate continental or marine environmental diagenesis (Figure 216.7b).

A total of 20 core samples were analyzed for major element composition. The CI values range from 0.21 to 0.35 with a mean of 0.26 ±0.04 (Table 216.4). This places the Long Rapids shale samples in the mature zone. The average values for selected igneous rocks and the Long Rapids shales are also plotted on Figure 216.6. From the ternary diagram, the shales exhibit a weathering trend indicative of a granitic gneiss as the source rock. This correlates well with the predicted source rocks of granites and granodiorites, and thus verifies the probable prov-

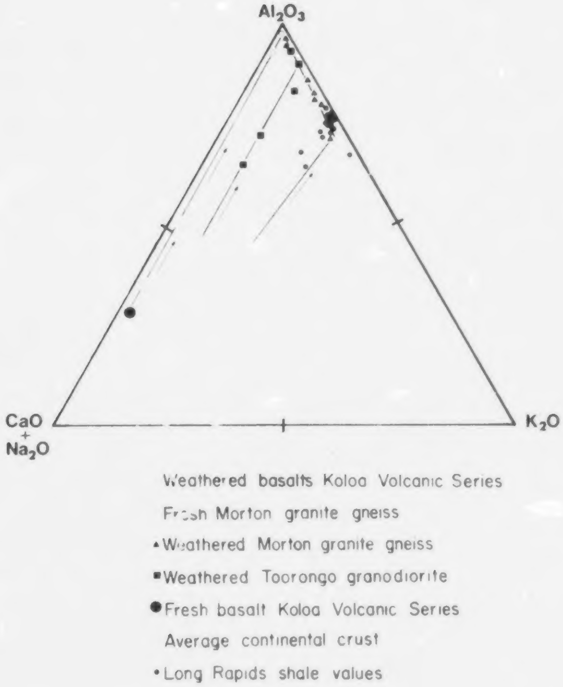

Figure 216.6. A ternary diagram of the plots of various igneous rocks and Long Rapids shale data. From Hoy (1980), Figure 5, p.28.

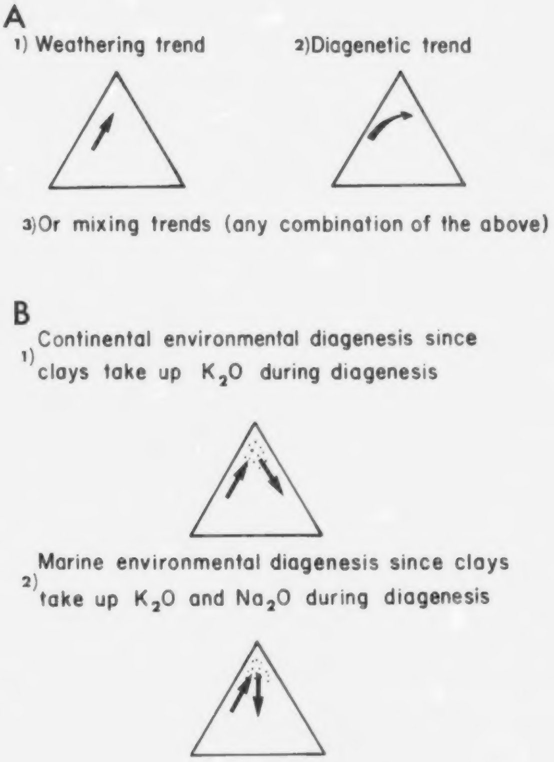
A
1) Weathering trend
2)Diagenetic trend
3)Or mixing trends (any combination of the above)
B
1) Continental environmental diagenesis since clays take up K_2O during diagenesis
2) Marine environmental diagenesis since clays take up K_2O and Na_2O during diagenesis

Figure 216.7. Weathering trends under various conditions for the chemical index of maturity.

enance area as the Precambrian Shield to the south. The Long Rapids shale data show no diagenetic or mixing trends.

SUMMARY AND CONCLUSIONS

The organic richness of the Long Rapids black shales imply reducing conditions in the water column, and that conditions were ideal for the production and preservation of the organic matter. The type of organic matter is probably composed mainly of aliphatic compounds and thus has the potential of producing petroleum (or shale oil). The black shales were deposited under anoxic water conditions and the other sedimentary components, such as the greenish grey mudstones, shales, and carbonates, were deposited under oxygenated water conditions. These shales contain some fossils and are lean in organic matter. They may be interbedded with black shales on a large or small scale (metres or centimetres) and interpreting their origin is difficult.

The greenish grey mudstone and shale lithology occur as two types. The mudstone type is unlaminated, homogeneous, and appears mottled by bioturbation. The second type, greenish grey shale, is laminated and may contain very fine dark laminae. These may represent distal turbidity currents traveling downslope off the marginal basin, probably from the southeast. The provenance studies (chemical index of maturity) done on the Long Rapids shales also confirm this direction.

The origin of the unlaminated greenish grey mudstones is less clear, but they may have formed in three ways. Firstly, laminated sediments may have been deposited as described above, with the turbidity currents bringing in oxygenated waters and colonizing organisms. As long as oxygen was present (even in restricted amounts) bioturbation could occur. This is evident in the trace fossil record, where most of the traces present represent an oxygen-minimum ichnofacies. The sediment produced by the activities of these burrowers would be a mottled, greenish grey mudstone.

The two other methods are related to the vertical migration of a pycnocline. As the pycnocline migrates up or down the basin slope, either 1) oxygenation of the previous anoxic sediments will occur or 2) greenish grey sediments will be deposited. Bioturbation will then occur in these sediments. Russel (1985) explains the presence of greenish grey mudstones in the Upper Devonian Kettle Point black shales (in southern Ontario) due to pycnocline fluctuations in a stratified water column. He stresses that the absolute depth of the basin is not important, but the relative depth of the pycnocline to the sediment-water interface is. Similar mechanisms probably occurred during the Long Rapids deposition.

The paleogeographic position of Laurasia placed the Moose River Basin (an intracratonic basin) in proximity to the equator (Figure 216.8). The Acadian

TABLE 216.4. CHEMICAL INDEX OF MATURITY VALUES.

Sample Number	Drillhole Number	Depth (m)	Chemical Index of Maturity
4	Onex 82-4	113.10	0.28
7	Onex 82-4	131.30	0.24
10	Onex 82-5	108.00	0.22
14	Onex 82-5	118.60	0.24
22	Onex 82-18	112.80	0.24
24	Onex 82-18	114.60	0.22
29	Onex 82-18	103.00	0.21
30	Onex 82-1	78.50	0.25
31	Onex 82-1	76.30	0.26
37	OEC 81-5	110.23	0.27
39	OEC 81-5	104.80	0.24
45	OEC 81-8	63.05	0.35
49	OEC 81-8	52.78	0.32
58	OEC 81-11	99.24	0.25
62	OEC 81-11	85.94	0.33
65	Onak B	137.42	0.25
67	Onak B	127.66	0.28
72	Onak B	122.01	0.27
75	Onak B	114.35	0.24
81	Onak B	100.67	0.21

$x = 0.26$
$n = 20$

Mountains along the continent's eastern edge acted as an orographic barrier to the prevailing trade winds. A starved basin was produced to the leeward side of the mountains, but the trade winds did not cross the equator. This allowed for erosion and clastic deposition on the leeward side of the mountains as the Catskill Delta.

Due to the proximity of the equator, the climate was probably very hot and humid. Large amounts of marine organic matter were produced. Carbonate beds were formed when the oxygen content in the water column increased. The cyclicity of the units was probably caused by the development of a stratified water column and a pycnocline. Position of the pycnocline to the sediment-water interface would predict the type of unit that would be deposited, either a black shale, green-grey mudstone, or a carbonate bed. Frequent movements of the pycnocline can possibly be explained by: tectonic readjustments along the craton's marginal edge during the Upper Devonian; planktonic blooms in the surface waters; or climatic changes.

ACKNOWLEDGMENTS

Appreciation and thanks go out to Peter Telford (Geologist, Ontario Geological Survey, Toronto), Martin Knyfe (Technician, McMaster University, Hamilton) and the helicopter pilot, Bill Denomme.

REFERENCES

Bezys, R.K., and Risk, M.J.
1985: Sedimentology of the Long Rapids Formation, Preliminary Results: Grant 216, p.165-174 *in* Geoscience Research Grant Program, Summary of Research 1984-1985, Ontario Geological Survey, Miscellaneous Paper 127, 246p.

Demaison, G.J., and Moore, G.T.
1980: Anoxic Environment and Oil Source Bed Genesis; American Association of Petroleum Geologists Bulletin, Volume 64, p.1179-1209.

Dyer, W.S., and Crozier, A.R.
1933: Lignite and Refractory Clay Deposits of the Onakawana Lignite Field; Ontario Department of Mines, Annual Report for 1933, Volume 42, Part 3, p.46-78.

Ettensohn, F.R., and Barron, L.S.
1981: Depositional Model for the Devonian–Mississippian Black Shales of North America: A Paleoclimatic and Paleogeographic Approach; Morgantown Energy Technological Center, Morgantown, West Virginia, Document 12040-2, 80p.

Folk, R.L.
1962: Petrography and Origin of the Silurian Rochester and McKenzie Shales, Morgan County, West Virginia; Journal of Sedimentary Petrology, Volume 32, p.539-578.

Fuex, A.N.
1977: The Use of Stable Carbon Isotopes in Hydrocarbon Exploration; Journal of Geochemical Exploration, Volume 7, p.155-188.

Goldhaber, M.
1978: Euxinic Facies; *in* The Encyclopedia of Sedimentology, edited by R.W. Fairbridge and J. Burgeois, Dowden, Hutchinson, and Ross, 901p.

Hailer, J.G., Leininger, R.K., and Hayes, J.M.
1983: Marine versus Terrestrial Sources and other Influences on the Carbon Isotopic Composition of the Organic Matter in the New Albany Shale; 1983 Eastern Oil Shale Symposium (list of papers), p.207-213.

Heckel, P.H., and Witzke, B.J.
1979: Devonian World Paleogeography Determined from Distribution of Carbonates and Related Lithic, Paleoclimatic Indicators; p.99-123 *in* The Devonian System, edited by M.R. House, C.T. Scrutton, and M.G. Basset, Paleontology, Special Paper Number 23, p.99-123.

House, M.R.
1983: Devonian Eustatic Events; Proceedings of the Ussher Society, Volume 5, p.396-405.

Hoy, D.
1980: A Study of the Chemistry of Shales with Emphasis on Shales from the Road River Formation, Yukon Territory; Unpublished M.Sc. Thesis, The University of Western Ontario, 97p.

Macauley, G.
1984: Geology of the Oil Shale Deposits of Canada; Geological Survey of Canada Paper 81-25, 65p.

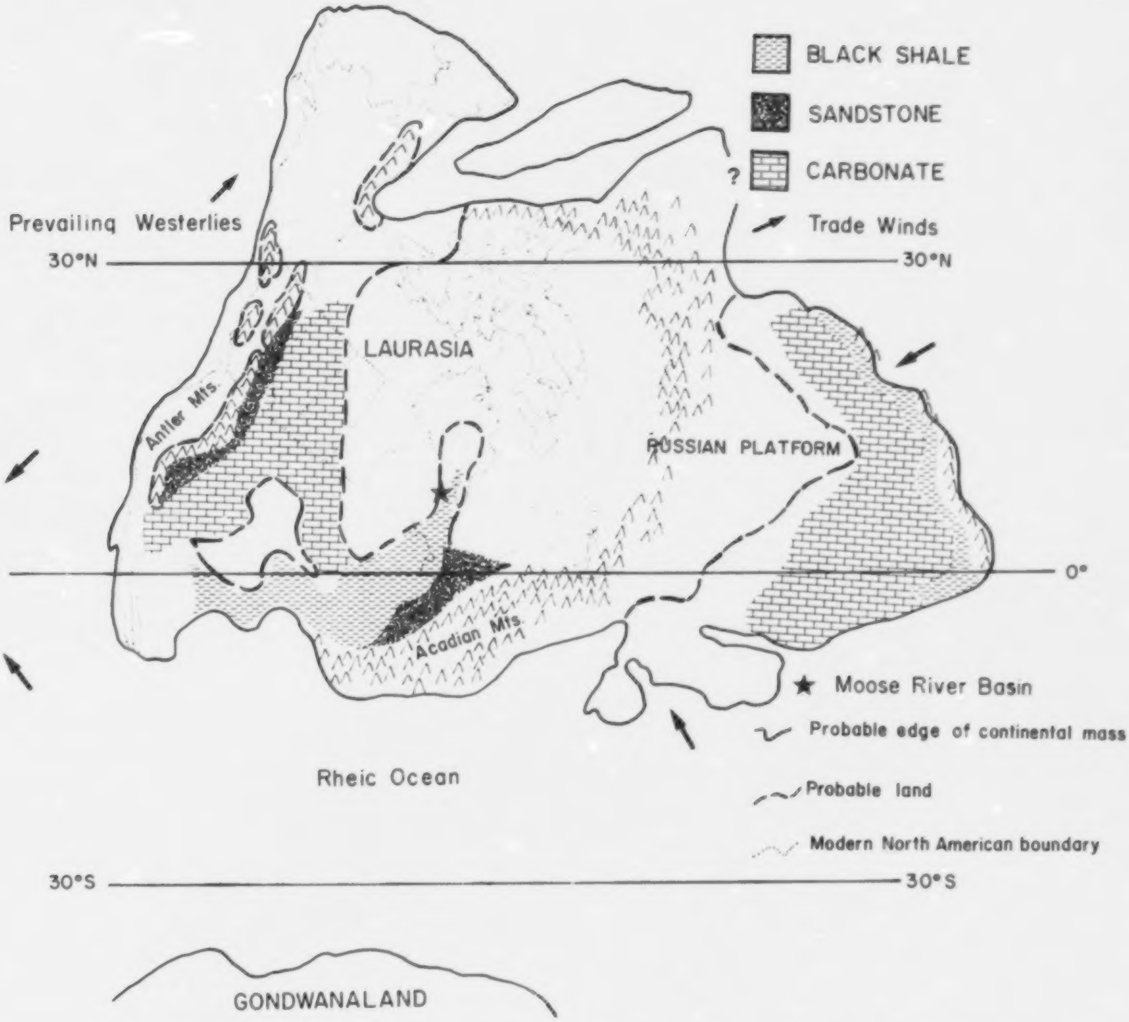
BLACK SHALE
SANDSTONE
CARBONATE
Trade Winds
?
Prevailing Westerlies
30°N
30°N
LAURASIA
Antler Mts.
RUSSIAN PLATFORM
0°
0°
Acadian Mts.
Moose River Basin
Probable edge of continental mass
Probable land
Modern North American boundary
Rheic Ocean
30°S
30°S
GONDWANALAND

Figure 216.8. *Possible reconstruction of the North American continent in the Upper Devonian. From Ettensohn and Barron (1981), Figure 81, p.348. and Heckel and Witzke (1979), Figure 3. p.105.*

Miknis, F.P., Maciel, G.E., and Bartuska, V.J.
1979: Cross Polarization Magic-Angle Spinning ^{13}C NMR Spectra of Oil Shales; Organic Geochemistry, Volume 1, p.169-176.

Russel, D.L.
1985: Depositional Analysis of a Black Shale by Using Gamma-Ray Stratigraphy: The Upper Devonian Kettle Point Formation of Ontario; Bulletin of Canadian Society of Petroleum Geologists, Volume 33, p.236-253.

Sackett, W.M., Eckelmann, W.R., Bender, M.L., and Be, A.W.
1965: Temperature Dependence of Carbon Isotope Composition in Marine Plankton and Sediments; Science, Volume 148, p.235-237.

Sanderson, J.W., and Telford, P.G.
1985: The Onakawana B Drillhole, District of Cochrane; p.165-166, *in* Summary of Fieldwork and Other Activities 1985, Ontario Geological Survey, edited by J. Wood, Owen L. White, R.B. Barlow, and A.C. Colvine, Miscellaneous Paper 126, 351p.

Shaw, D.B., and Weaver, C.E.
1965: The Mineralogical Composition of Shales; Journal of Sedimentary Petrography, Volume 35, p.213-222.

Telford, P.G., and Verma, H.M.
1982: Mesozoic Geology and Mineral Potential of the Moose River Basin; Ontario Geological Survey, Study 21, 193p.

Telford, P.G.
1985: Biostratigraphy of the Long Rapids Formation (Upper Devonian), Moose River Basin, Ontario; *in* Programme with Abstracts, Canadian Paleontology and Biostratigraphy Seminar, Quebec City, September 28-29, 1985.

Grant 221 Implications of Chemical Trends within the Chloritoid–Altered Volcanic Rocks of the Wawa Belt

M.B. Lockwood[1] **and J.M. Franklin**[2]

[1]Ottawa-Carleton Centre for Geoscience Studies, Ottawa

[2]Geological Survey of Canada, Ottawa

ABSTRACT

Volcanic rocks associated with three iron deposits and one base-metal occurrence are variably altered. With progressive alteration, chloritoid increases in abundance in both felsic and mafic rocks. Chemical analyses and mass balance studies indicate that Al_2O_3, TiO_2, and Zr were immobile. Iron, Mn, and CO_2 were added to all altered rocks, but the former two elements were added separately from the lattermost. Na_2O is depleted in all rocks. Sulphur and base metals are not enriched in the alteration zones associated with the iron deposits. An initial high temperature hydrothermal fluid probably underwent phase separation at low hydrostatic confining pressures (due to shallow water), generating a CO_2- and S-rich vapour which separated from the residual metalliferous fluid and migrated up through the volcanic rocks to form carbonate alteration. The more dense and cooled residual fluid subsequently passed through the same rocks, enriching them in iron, and was then expelled onto the seafloor to form the iron deposits.

Although the loss of Na_2O and, more locally, CaO generated a peraluminous composition, the bulk composition of the altered rocks was insufficiently depleted in these elements to have enabled the formation of chloritoid. As CaO and eventually MgO were consumed from the primary silicate minerals to form carbonates during the early stages of alteration, the remaining silicate component became exceptionally peraluminous, thus enabling the formation of chloritoid during regional metamorphism.

INTRODUCTION

Chloritoid, generally considered to be a constituent of iron-rich aluminous pelitic schists, has also been recognized as an alteration product associated with various types of ore deposits including Algoma-type iron formation (Morton and Nebel 1984), base-metal massive sulphide deposits (Franklin *et al.* 1975; Osterberg 1985), and structurally controlled vein copper-gold deposits (Eckstrand 1963). The purpose of this study is to determine if the occurrence of chloritoid in volcanic rocks is even indirectly genetically related to hydrothermal activity and base-metal deposition, and thus can serve as a possible exploration guide. To achieve this, we have determined the mineral assemblages in areas of chloritoid alteration and have established the chemical changes that have occurred in these altered areas. In order to assess the possible relationship between the physical nature of the volcanic rocks and alteration assemblages, paleo-environmental indicators within the volcanic rocks were also described (Lockwood *et al.* 1985).

To obtain a thorough understanding of the factors governing the distribution and occurrence of chloritoid alteration, four areas in the Wawa Belt (Figure 221.1), representing a variety of geological settings, were mapped and sampled during the 1984 field season (Lockwood *et al.* 1985). They are:

1. The Rand #2 Deposit—a sulphide-facies iron formation.
2. The "C" Deposit—a deformed sulphide facies iron formation
3. The Josephine Deposit—an oxide-carbonate iron formation.
4. The Kozak Lake Showing—a Pb-Zn-Ag occurrence with no associated iron formation.

During the past year, petrographic studies, including microprobe analyses of the various alteration minerals, were complemented by mass balance comparisons and correlation analyses on major and minor element chemical data.

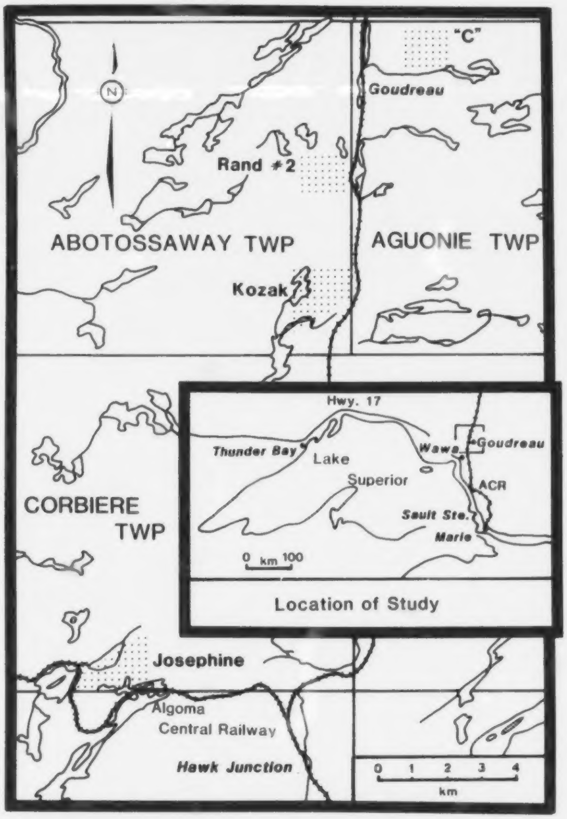

Figure 221.1. *Location of the four study areas.*

SUMMARY OF STRATIGRAPHIC AND VOLCANOLOGICAL CHARACTERISTICS

The Rand #2, the "C", and the Josephine Properties contain, in ascending order (Figure 221.2), a sequence of mafic flow rocks felsic pyroclastic rocks, and iron formation. The Kozak Property is underlain entirely by felsic pyroclastic and massive flow rocks. The Kozak and Josephine Properties are entirely in strata of the first cycle. The Rand #2 and "C" Properties span parts of the boundary between the first and second volcanic "cycles" of the Wawa Belt as defined by Goodwin (1962) and Sage (1981); the boundary between these cycles is marked by the iron formation, present on both properties.

A summary of the volcanological characteristics of the four study areas has been given by Lockwood *et al.* (1985). They have interpreted the environments of deposition for the four areas to be shallow subaqueous to subaerial. This interpretation is endorsed by textures such as very vesiculated pillows, pipe vesicles along flow bottoms, and fiamme, noted at the Rand #2 and the Josephine Properties. Parallel and contorted flow-banded rocks adjacent to relatively coarse breccias on the Kozak Property may indicate that these rocks formed as an exogeneous dome, supporting the interpretation of a subaerial depositional environment for other strata in the study areas.

SUMMARY OF ALTERATION CHARACTERISTICS

Alteration types have been defined by specific mineral assemblages and the percentages of key minerals as a fraction of the total modal volume (Lockwood *et al.* 1985). Minerals and their abundances were defined by petrographic and X-ray diffraction studies. Gradational changes in mineral abundances exist between the alteration types. The majority of the rocks in the Wawa Belt have been metamorphosed to lower to middle greenschist facies assemblages (Goodwin 1962), with higher grade assemblages present near the contact with intrusions. Alteration "intensity" is determined by the abundance of minerals that are either atypical constituents or excessively abundant compared with regionally metamorphosed but unaltered protoliths. For example, chloritoid and carbonate (>5%) are unusual minerals in regionally metamorphosed basalt or rhyolite; sericite or chlorite in excess of 10% in felsic volcanic rocks are also anomalously abundant. For purposes of preliminary classification of alteration types, we assume that the anomalous abundances of minerals or atypical mineral species are the metamorphosed products of primary alteration assemblages.

Listed by increasing alteration intensity, the alteration types are:

For the felsic rocks:

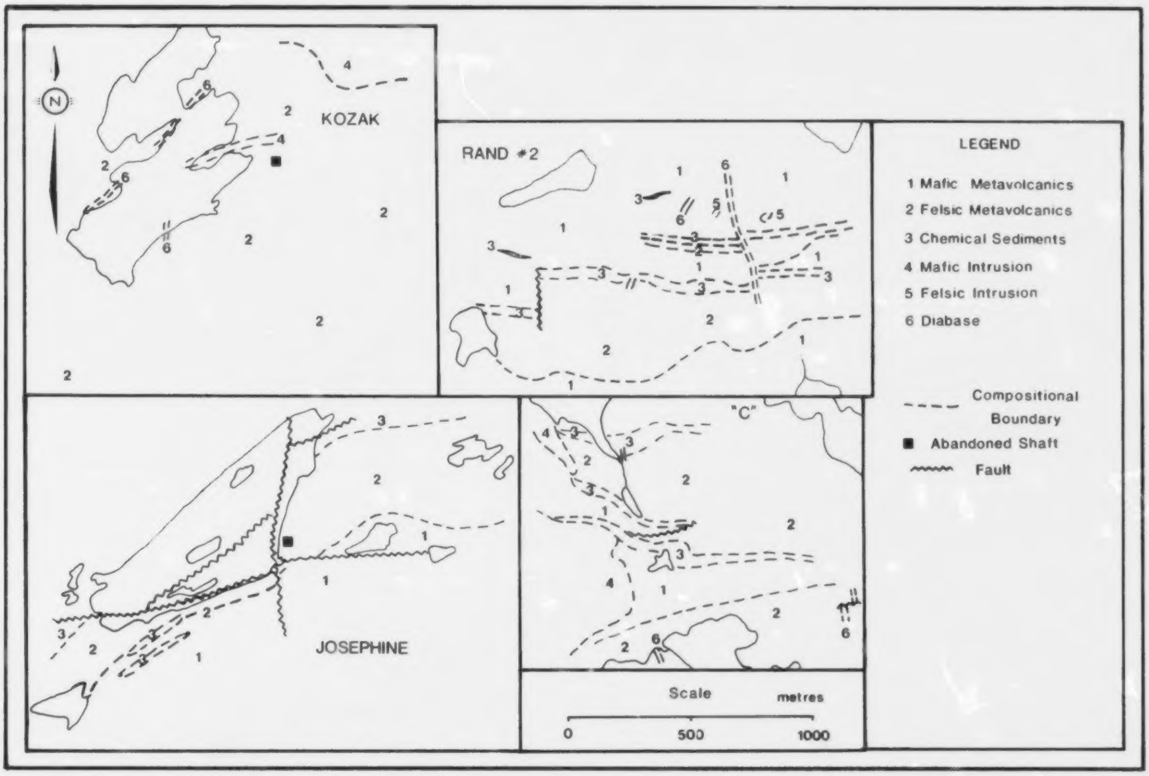

Figure 221.2. Simplified geologic maps of the study areas.

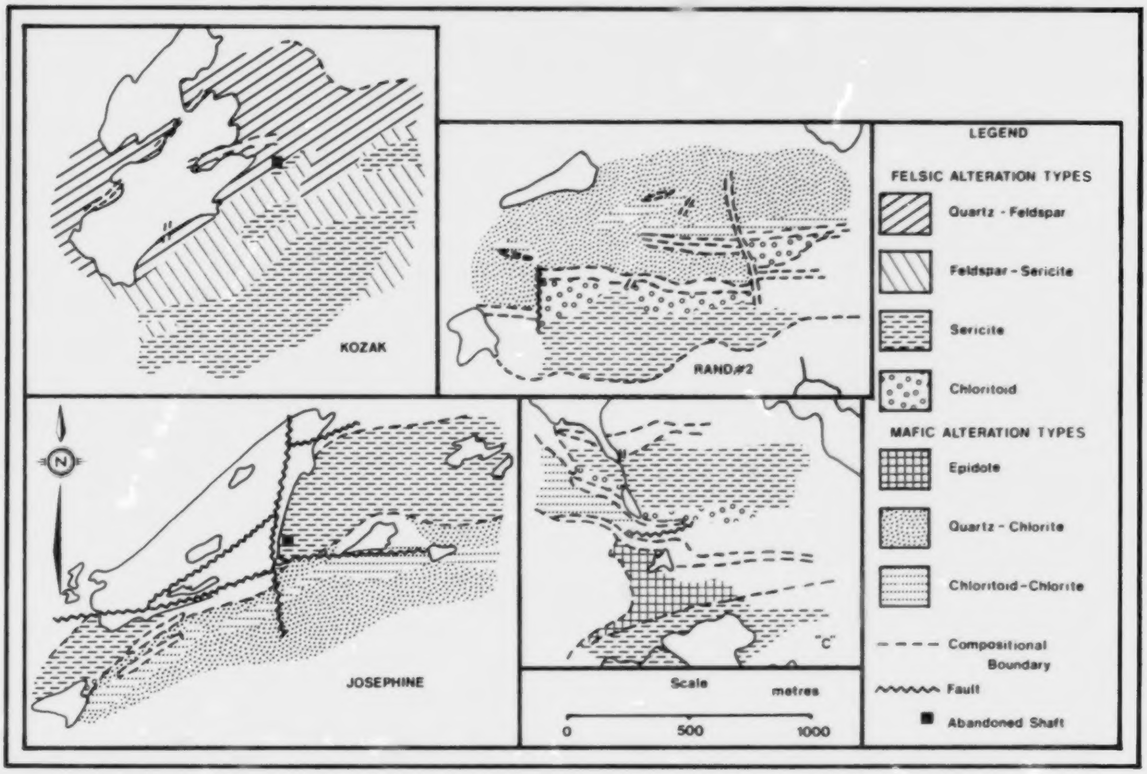

Figure 221.3. *Simplified distribution of alteration types in the study areas.*

1. Least Altered: a) Sericite-feldspar-carbonate: Quartz (30% to 45%), Feldspar (20% to 40%), Sericite (5% to 15%), Carbonate (10% to 25%), Chlorite (<1% to 2%), b) Sericite-feldspar-chlorite: Quartz (30% to 50%), Feldspar (10% to 30%), Sericite (10% to 25%), Carbonate (2% to 25%), Chlorite (2% to 10%)
2. Sericite-chloritoid: Quartz (25% to 75%), Sericite (5% to 50%), Feldspar (10% to 30%), Carbonate (1% to 40%), Chlorite (2% to 15%), Chloritoid (0% to 10%), Stilpnomelane (<1% to 3%)
3. Chloritoid-sericite: Quartz (20% to 60%), Sericite (1% to 40%), Feldspar (0 to 15%?), Carbonate (3% to 30%), Chlorite (0% to 20%), Chloritoid (10% to 50%)
4. Chlorite-garnet: Quartz (35% to 50%), Sericite (5% to 7%), Chlorite (10% to 35%), Carbonate (5% to 20%), Chloritoid (<1% to 3%), Garnet (3% to 5%)

Mineral assemblages for the mafic rocks are:

1. Epidote-chlorite: Quartz (5% to 10%), Chlorite (30% to 45%), Feldspar (10% to 50%), Carbonate (15% to 20%), Epidote (3% to 7%), (Amphibole (0% to 15%))
2. Chlorite-chloritoid: Quartz (10% to 50%), Chlorite (5% to 50%), Feldspar (0% to 15%?), Sericite (1% to 15%), Carbonate (5% to 50%), Chloritoid (0% to 5%), Stilpnomelane (0% to 3%)
3. Chloritoid-Chlorite: Quartz (25% to 60%), Chlorite (0% to 35%), Sericite (1% to 20%), Carbonate (0% to 65%), Chloritoid (10% to 65%)

Lockwood *et al.* (1985) found that the distribution of alteration types is conformable to semi-conformable with the stratigraphic units in the study areas (Figure 221.3). The chloritoid-bearing assemblages are the most easily mapped, and can occupy zones of up to several kilometres in strike length and as wide as 300 m (Sage 1981). No well defined footwall pipe-structures are evident, in contrast to the footwall to the Helen Mine iron formation (Morton and Nebel 1984). On the Rand #2, the "C", and the Josephine Properties, chloritoid-chlorite type alteration envelops beds of iron formation; chloritoid is accompanied by carbonate mineral contents of greater than 25%. Carbonate is distributed at least 7 m below and 5 m above the iron formation beds.

Chloritoid type alteration zones also occur adjacent to the sulphide veins on the Kozak Property. Carbonate, generally siderite and ankerite, is pervasive within these zones, consistent with all chloritoid-altered rocks of the Wawa Belt (Sage 1981).

The most widespread alteration is the sericite-type in the felsic rocks and the epidote-chlorite type in the mafic rocks, both generally surrounding chloritoid-bearing rocks (Lockwood *et al.* 1985). Rocks of the chlorite-garnet type are the most restricted in areal extent in the felsic rocks. At the "C" Property, immediately underlying iron formation, veins

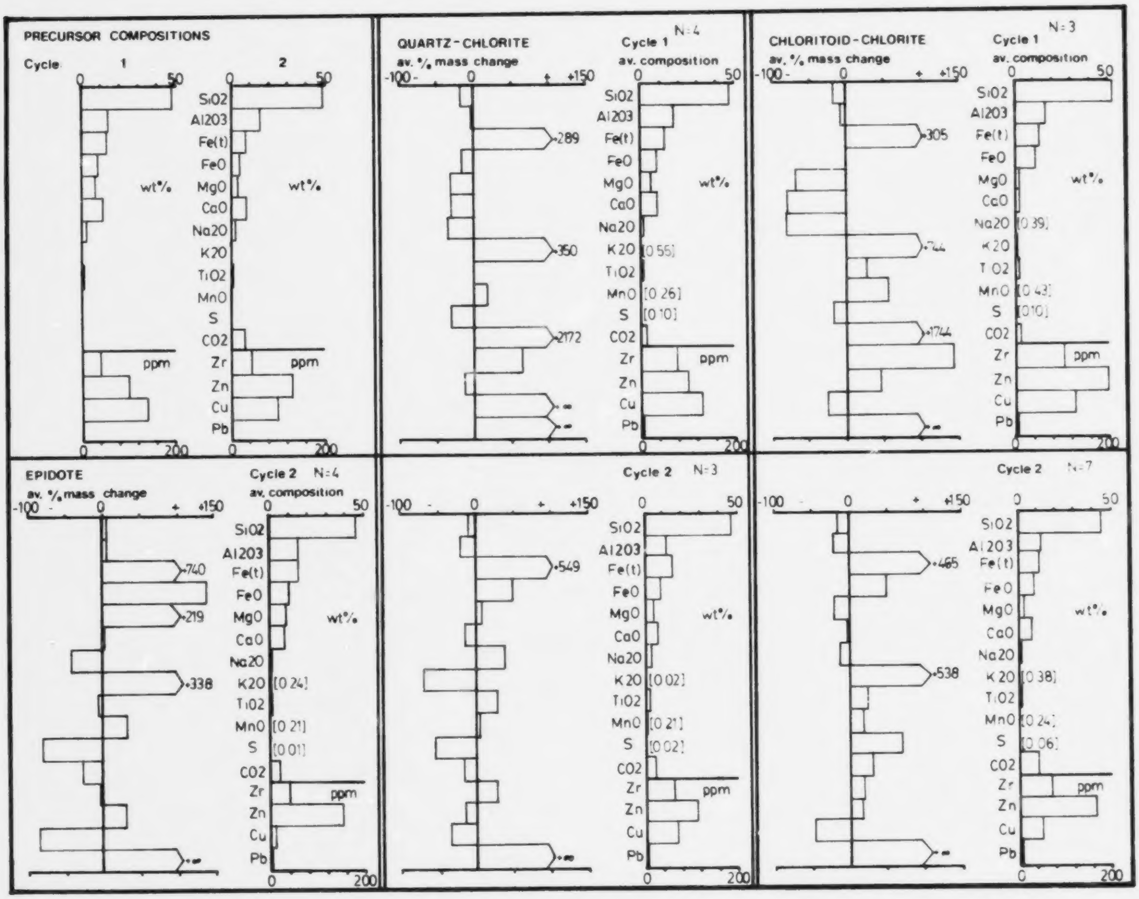

Figure 221.4. *Average mass balance comparison histograms for the alteration types in the mafic rocks.*

of chlorite-garnet alteration cut chloritoid-type alteration zones.

Primary permeability probably has been an important factor in determining the intensity of alteration within both the mafic and felsic rocks. Both sericite and chloritoid are most abundant within pillow selvages and hydro-fractures in the mafic rocks (Lockwood *et al.* 1985) as well as within numerous minor fractures within the felsic rocks. Anastomosing networks of sericitic veins have been noted within the Josephine and Kozak felsic rocks (Lockwood *et al.* 1985). Sericite is also disseminated throughout the felsic rocks, giving them a yellow-green appearance on the weathered surface. Sericite has pseudomorphically replaced pumiceous clasts within felsic footwall rocks of the Rand #2 and the Josephine Properties.

CHEMICAL TRENDS OF THE ALTERATION TYPES

Mass balance calculations, using the isocon method of Grant (in press) were undertaken for analyses of major and a few minor elements (Tables 221.1, 221.2, 221.3, and 221.4) to determine the principal gains or losses accompanying alteration (Figures 221.4 and 221.5). Correlation coefficients were also calculated from these data to determine possible covariant additions or losses.

Chemical analyses of the least altered rocks reveal an unusually high carbonate content, and atypically high iron contents, in comparison with "typical" Archean volcanic rocks of similar types (Goodwin 1977), indicating that some chemical modification has affected very broad areas around the iron formations and base-metal occurrences examined in this study. "Least altered" samples used for mass balance comparisons, therefore, had to be derived from unaltered areas in the first and second volcanic cycles. Analyses of the latter samples were provided by R.P. Sage (Geologist, Ontario Geological Survey, Toronto).

CHEMICAL TRENDS IN THE MAFIC ROCKS

The chemical compositions of the mafic rocks are less variable than those of the felsic rocks. However, because chemical analyses of the mafic rocks are representative of two cycles, each with three alteration types, populations for the mafic suites are smaller and, therefore, less statistically significant than those of the felsic rocks, which occur only in

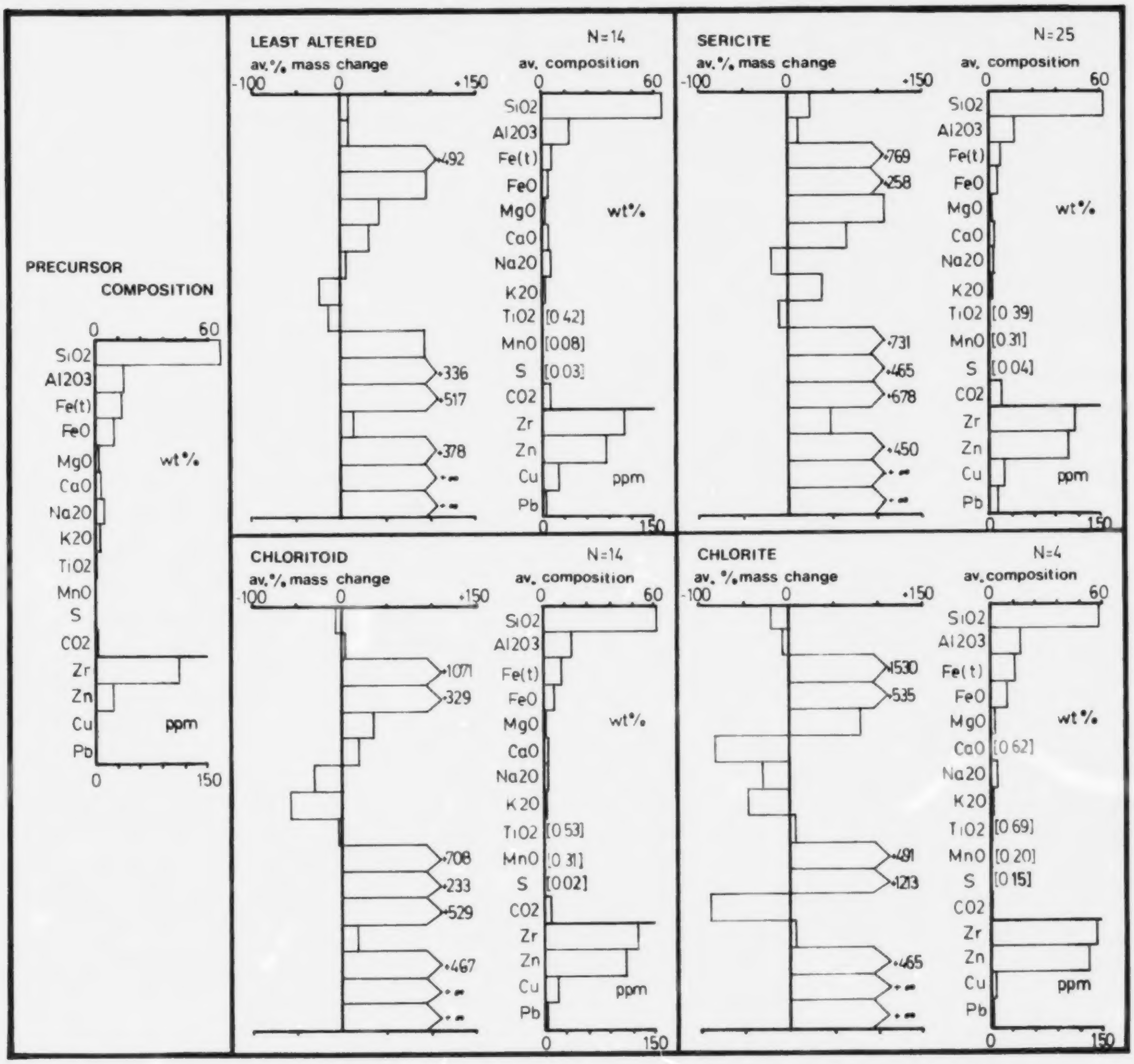

Figure 221.5. Average mass balance comparison histograms for the alteration types in the felsic rocks.

the lower cycle. TiO_2 and Al_2O_3 are considered to be immobile for mass balance comparisons, in part because of their "historical" immobility (Parry and Hutchinson 1981; Costa *et al.* 1983; Morton and Nebel 1984) and in part because in virtually all of the comparisons done in this study (using the method of Grant, in press), these elements remained colinear along a line of constant volume. TiO_2 and Al_2O_3 are distinctly positively correlated in both chlorite-chloritoid and chloritoid-chlorite alteration types. Zr, also considered to be immobile (Floyd and Winchester 1975; Hallberg 1975), is also strongly covariant with Al_2O_3 and TiO_2 (Table 221.1). Costa *et al.* (1983) have noted that to have proportional and covarying additions and depletions of elements like Ti, Al, and Zr, would require a very contrived petrogenetic explanation. The covariance of these three elements may, therefore, be due to their complementary "dilution" by addition (or loss) of other components during alteration.

Mass balance comparisons (Figure 221.4) show that there has been considerable enrichment in total iron [$Fe_{(t)}$], largely as FeO, relative to the unaltered precursor. The average MgO content decreases with increasing intensity of alteration in both first and second cycle mafic rocks. No correlation exists between MgO and iron. This may reflect the decrease in the abundances of Mg-chlorite and dolomite, and the increase of Fe-chlorite and ferrodolomite and siderite observed in the more highly altered rocks. K_2O is negatively correlated with Na_2O and CaO, possibly reflecting the incremental decomposition of feldspar, releasing the latter two elements to solution, with concomitant replacement of plagioclase by sericite. Mass balance comparisons further indicate that Na_2O and CaO have been removed from the mafic rocks in

TABLE 221.1. MAFIC ALTERATION TYPES.

+ve correlation

	SiO_2	Al_2O_3	Fe(t)	FeO	MgO	CaO	Na_2O	K_2O	TiO_2	MnO	S	CO_2	Zr	Zn	Cu
SiO_2	-	B							B				B		
Al_2O_3		-						A B	A B	A b			A B		
Fe(t)			-	B			a								B
FeO				-											B
MgO	B	B			-	A					a	B			
CaO	B	a B		A	b	-	B								
Na_2O		A B		b			-								
K_2O						A B	A B	-	A B	A b			A B		b
TiO_2				b	A	A B	B		-	A			A B		
MnO	A			b		a b	A b			-			A		b
S			A	a							-				B
CO_2	B	B		B	a				B			-			
Zr					b	a B	B					B	-		
Zn									a	A			A	-	
Cu	A						A					a			-

-ve correlation

lowercase >/= 0.55 <0.70 A = Quartz-Chlorite Type

uppercase >/= 0.70 </= 1.00 B = Chloritoid-Chlorite Type

TABLE 221.2. FELSIC ALTERATION TYPES.

+ve correlation

	SiO_2	Al_2O_3	Fe(t)	FeO	MgO	CaO	Na_2O	K_2O	TiO_2	MnO	S	CO_2	Zr	Zn	Cu	Pb
SiO_2	-															
Al_2O_3		-	C						C d E				C E			
Fe(t)	d E		-	D E	d e					D E	e	D				
FeO	d E	E		-	D E					D E	e	e		E		
MgO	c d E	E			-	c e				E	e	c E			c	
CaO	d	e				-						c d e			c e	
Na_2O							-							c		
K_2O								-		c	c					c
TiO_2					e	e			-				c E			
MnO	D E	e								-	C E	d e				C
S	e	e									-					C
CO_2	c D e	d E							E			-			e	
Zr					e					e		E	-			
Zn														-		d
Cu															-	
Pb																-

-ve correlation

lowercase >/= 0.55 <0.70 C = Least Altered Type

uppercase >/= 0.70 </= 1.00 D = Sericite Type

E = Chloritoid Type

TABLE 221.3. TYPICAL CHEMICAL ANALYSES OF FELSIC ROCKS.

Altn Fc Sample No.	Lst Atd K1D-40	Sct CA-32	Chtd CA-37A	Cht CA-37C
	wt. %			
SiO_2	65.86	64.93	61.88	64.67
Al_2O_3	14.36	15.27	16.70	15.15
Fe_2O_3	0.85	0.93	10.41	1.18
FeO	3.04	4.19	6.98	8.51
MgO	1.45	2.17	0.99	1.55
CaO	2.78	2.49	0.42	0.46
Na_2O	2.64	3.96	2.62	3.58
K_2O	1.68	1.34	2.17	1.07
TiO_2	0.41	0.56	0.69	0.57
MnO	0.06	0.06	0.18	0.15
S	0.02	0.03	0.02	0.10
CO_2	5.16	2.93	0.12	0.10
	ppm			
Zr	96	126	142	126
Zn	73	73	77	135
Cu	24	3	5	3
Pb	5	3	5	1
	wt. %			
Total	98.31	98.31	98.31	98.31

Altn Fc = Alteration Type
Lst Atd = Least Altered
Sct = Sericite-Chloritoid
Chtd = Chloritoid-Sericite
Cht = Chlorite-Garnet

most of the alteration types, especially those of the first cycle. Both are negatively correlated with Al_2O_3.

CO_2 is abundant in all alteration types and particularly in rocks of the first cycle. It is especially abundant in the chloritoid-chlorite alteration in both cycles. CaO is positively correlated with CO_2 in the chloritoid-chlorite type; as CaO has not been added to the rocks, this correlation probably reflects an increasing carbonatization of the mafic rocks of this alteration type. Therefore, the partial pressure of CO_2 must have been higher in the areas which eventually contained the chloritoid-chlorite assemblage.

Sulphur contents of all of the mafic rocks are very low, in comparison with rocks of similar alteration assemblages near Sturgeon Lake or the Onaman River areas, Ontario (Franklin *et al.* 1975; Osterberg 1985). Sulphur content is not correlated with other elements, except Cu in the chloritoid-chlorite alteration type.

CHEMICAL TRENDS IN THE FELSIC ROCKS

Again Al_2O_3 and TiO_2 were considered to be immobile in the mass balance calculations for the reasons cited previously. Good positive correlation exists between Al_2O_3 and TiO_2 for all felsic-hosted types of alteration (Table 221.2). Both elements are also positively correlated with Zr.

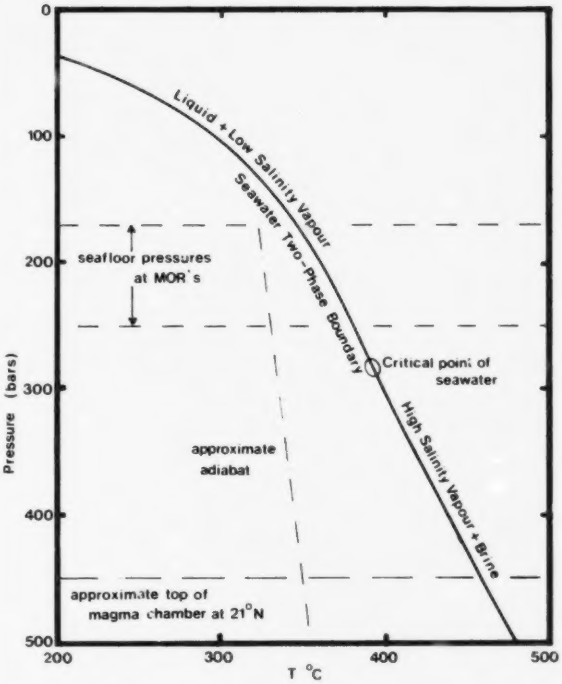

Figure 221.6. *Diagram illustrating the relationship of the two-phase boundary of seawater with temperature and pressure (after Bischoff and Rosenbauer 1984; Franklin 1986). Hydrothermal fluids from the Wawa area probably became heated to temperatures of less than 385°C and rose adiabatically until they intersected the two-phase boundary. As boiling and fluid ascent continued, temperature of the residual fluid decreased along this boundary line, until the fluid reached the seafloor.*

FeO concentrations range from 2% in the low levels of alteration to 16% in the chloritoid-sericite and chlorite-garnet alteration types. Mass balance comparisons show that even the least altered rocks have had a major addition of $[Fe_{(t)}]$, primarily as FeO (Figure 221.5). The greatest iron enrichment occurs in the most altered rocks, reflecting the abundant ferruginous carbonate, chloritoid, chlorite, and iron oxide observed petrographically. Mass balance comparisons indicate that MgO contents are generally enriched, but no correlation exists between MgO and iron. MgO, however, does correlate well with CaO, corresponding to the abundance of dolomite, present in all types of alteration. MnO concentrations correlate well with $[Fe_{(t)}]$ and FeO, and mass balance comparisons reveal that it has been enriched within the felsic rocks in all types of alteration.

CaO is erratically distributed, as in the mafic rocks. Mass balance comparisons indicate that CaO concentrations have been weakly to moderately enriched in all but the chlorite-garnet alteration type, a trend also shared by CO_2. CO_2 contents correlate with those of CaO, MgO, and MnO, reflecting dolomite abundance in all alteration types. Weak correlation also exists between iron and CO_2 in the sericite-chloritoid and chloritoid-sericite alteration zones reflecting the formation of ferruginous dolomite and siderite. The correlation between CO_2 and the other constituents of the carbonate alteration minerals probably reflects the addition of only CO_2 to the rocks to metasomatically form carbonate, as CaO, and the other constituents of these minerals (except iron) are not added in significant amounts.

Mass balance data also indicates that Na_2O was relatively immobile within the least altered rocks, but is progressively more depleted in the most altered rocks, reflecting progressive destruction of primary feldspar. K_2O is generally depleted in the altered rocks, except for those of the sericite type. Unlike the distribution of alkali elements within the mafic rocks, no correlation exists between any of these elements in the felsic rocks.

Sulphur contents are very low, although slightly enriched in all the felsic rocks relative to the unaltered equivalents. The greatest S enrichment occurs within the chlorite-garnet alteration. No correlation appears to exist with Cu, Zn, or Fe, but S is weakly correlated with Pb.

The base-metal contents are generally low. Cu contents do not correlate with those of Pb and Zn. Copper is less abundant than in the average Superior Province rhyolite or dacite (Goodwin 1977). Pb is enriched relative to the other felsic rocks encountered in this study, particularly in the sericite alteration zones of the Kozak Property.

IMPLICATIONS OF CHEMICAL TRENDS

The following generalizations may be drawn from the above data:

1. In both the felsic and mafic rocks, Al_2O_3, TiO_2, and Zr were immobile during the alteration process.
2. Iron, manganese, and CO_2 were consistently added to both felsic and mafic rocks. Fe and Mn are not correlated with CO_2 contents, possibly indicating separate emplacement of the latter. K_2O was also added to many alteration types, but in relatively small amounts compared to iron and CO_2.
3. CaO is consistently depleted in the mafic rocks, added to the less intensely altered felsic rocks, but depleted in the chloritized felsic strata.
4. Na_2O is depleted in all types of alteration in both rock types.
5. MgO was added to all altered rocks in the felsic suite, but probably was only redistributed in the mafic rocks.

Of special note is that the alteration types in both felsic and mafic rocks are not particularly enriched in sulphur or base metals. Only the Kozak Occurrence has significant base-metal enrichment. These latter veins are not particularly deformed, and Sage (Geologist, Ontario Geological Survey, Toronto, personal communication, 1986) suggested that they may have formed epigenetically. Lead isotope data ($^{206}Pb/^{204}Pb$ = 13.208, $^{207}Pb/^{204}204Pb$ = 14.402, $^{208}Pb/^{204}204Pb$ = 33.083) are consistent with compositions for Superior Province massive sulphide deposits (Franklin and Thorpe 1982) and give a model age of 2724 Ma., (Abitibi model, Ralph Thorpe, Research Scientist, Geological Survey of Canada, Ottawa, personal communication, 1986) close to the age of the enclosing strata (cycle 1, 2743 Ma.; cycle 2, 2717 Ma.; Turek *et al.* 1984). This indicates that primary lead enrichment in the Kozak area probably occurred contemporaneously with volcanism. The possibility of remobilization of this lead, as well as other sulphide minerals, into veins during later metamorphic or tectonic events remains unresolved.

The lack of sulphur in the other alteration zones indicates that either the hydrothermal fluid contained no reduced sulphur, or that such sulphur could not precipitate due to extreme oxidizing conditions. The latter seems unlikely, because at the Rand #2 deposit, as well as elsewhere in the Wawa district, pyrite is abundant (Goodwin *et al.* 1985). Most of this pyrite was formed through organic reduction of seawater sulphate (Goodwin *et al.* 1985), and although the Wawa iron formations are locally very sulphur-rich, direct formation of sulphides from hydrothermal fluids seems to have been ineffective.

Thus, although iron has accumulated abundantly in both the altered volcanic rocks and the iron deposits, it seems to have been concentrated separately from either the CO_2 or sulphur. The exceptional abundance of iron formation in this district, together with the presence of a subjacent ferruginous alteration pipe at the Helen Mine (Morton and Nebel 1984) indicate a probable hydrothermal source for these deposits. Other aspects of alteration, such as the enrichment of MgO in felsic footwall strata, the abundance of sericite in all alteration types, and the loss of Na_2O in the most intensely altered rocks, are all typical of high-temperature "pipe-type" alteration associated with volcanic-associated massive sulphide deposits (Franklin, in press).

The gains and losses observed in association with the altered rocks are similar to those described by Osterberg (1985) and Morton and Nebel (1984) in geologically similar environments. Large amounts of iron and CO_2 must have been added from a hydrothermal source, but their lack of mutual correlation may indicate somewhat independent emplacement of these elements, either at different times or from separate sources. The other gains and losses in the altered rocks (MgO, CaO, Na_2O) are similar to those observed in many areas of moderate to high temperature submarine hydrothermal activity. MgO was typically added in the uppermost parts of a focused discharge zone, probably due to rapid heating of cold seawater by the hydrothermal fluids (Franklin, in press). CaO and Na_2O were usually lost in the discharge region, provided that the water/rock ratio in the reaction environment was high (>25) (Mottl 1983), and that the hydrothermal fluid was modified seawater; these conditions are normal for a focused discharge area. In the present study areas, the alteration patterns are quite unconstrained and well focused discharge does not seem to have prevailed. However, the observed changes in chemical composition are indicative of the passage of large volumes of warm, modified seawater through the footwall sequences to the iron formations.

Two fluids, one of which was CO_2-rich, the other iron-rich, and neither particularly rich in reduced sulphur, could have been produced by separating an initial high temperature fluid, typical of that for hydrothermal systems proposed for massive sulphide deposits, into two phases. Boiling could have induced complete vapour phase separation from a hydrothermal fluid, effectively segregating CO_2 and H_2S from heated (and chemically modified) seawater (Nesbitt 1984; Drummond and Ohmoto 1985; Franklin, in press). The very low density of the vapour would have allowed rapid separation of CO_2 and H_2S from the liquid phase. This separated vapour could have swiftly moved up into the overlying rocks, especially under shallow subaqueous conditions (Delaney and Cosens 1982). CO_2 probably reacted with feldspar to produce carbonate, but H_2S in the absence of dissolved metal cations would have exited into the overlying hydrosphere, where it would be available for incorporation into biota, and to the atmosphere. Goodwin *et al.* (1985) have pointed out that most of the sulphide in the Wawa area is of organic, rather than hydrothermal origin, consistent with the model proposed here.

The boiling temperature of seawater is constrained only by the pressure (i.e. water depth) and follows the 2-phase boundary curve (Figure 221.6) defined by Bischoff and Rosenbauer (1984). Once boiling of the ascending liquid commences, it ceases to rise adiabatically. Instead, as 2-phase separation occurs, the temperature of the boiling liquid decreases along the boundary curve. LaTour *et al.* (1980) have found that the isotopically-derived temperature of hydrothermal fluids taken from chloritoid-altered second cycle mafic pillowed flows is 200°C. The strata sampled by LaTour *et al.* (1980) are the stratigraphically highest part of the volcanic accumulation that existed at the time of alteration. Fluids contained within these rocks would have reacted at the lowest hydrostatic pressure within the hydrothermal system. If the Wawa hydrothermal fluids were undergoing boiling, then 200°C would have been a minimum temperature. The amount of vapour phase separation that would have taken place in order to enable the hydrothermal fluid to reach such a low temperature would have been considerable; all of the CO_2 and H_2S would have been removed from the fluid, thus preventing the formation of sulphide minerals during cooling at the seafloor.

Initial low temperatures of the Wawa hydrothermal fluids have been attributed by Goodwin *et al.* (1985) and Morton and Nebel (1984) to be an alternate explanation of the deficiency of base-metal concentrations. Franklin (in press), on the basis of experimental work by Seyfried and Janecky (1983), suggested that at temperatures under 385°C at low water/rock ratios, hydrothermal fluids would not be sufficiently acidic to leach significant quantities of metal from the rocks. Abundant epidote-chlorite alteration observed by Calvert (1983), well within the footwall of the Josephine Property, is indicative that relatively low water/rock ratios, between 2 and 35 (Mottl 1983), predominated during the development of the hydrothermal system. This assemblage may also indicate that the hydrothermal fluid did attain moderately high temperatures in its "reservoir" zone (Mottl 1983; MacGeehan and McLean 1980) and thus the low temperatures extant at and near the paleo-

TABLE 221.4. TYPICAL CHEMICAL ANALYSES OF MAFIC ROCKS.

Cycle **Altn Tp** **Sample No.**	**1** **Qtz-Cht** **W7-504**	**1** **Chtd-Cht** **W6-259B**	**2** **Ep** **CC-3**	**2** **Cht-Ctd** **R-86A**	**2** **Chtd-Cht** **R-117AN**
		wt. %			
SiO_2	46.96	50.35	48.02	47.78	45.13
Al_2O_3	15.97	17.50	14.77	12.85	12.77
Fe_2O_3	2.82	1.79	4.24	3.98	1.53
FeO	7.00	13.47	6.97	10.01	9.82
MgO	6.41	3.22	9.92	4.72	4.02
CaO	10.02	1.44	8.24	7.18	8.28
Na_2O	1.86	0.20	1.41	3.31	1.55
K_2O	0.03	1.06	0.02	0	0.45
TiO_2	1.29	2.29	0.69	1.29	1.32
MnO	0.25	0.56	0.17	0.20	0.28
S	0.16	0.12	0.01	0.04	0.03
CO_2	3.23	3.55	1.19	5.72	12.40
		ppm			
Zr	74	114	36	67	61
Zn	102	203	135	113	219
Cu	116	240	5	88	28
Pb	4	6	1	6	8
		wt. %			
Total	96.00	95.65	95.65	97.08	97.58

Altn Tp = Alteration Type
Ep = Epidote-Chlorite
Cht-Ctd = Chlorite-Chloritoid
Chtd-Cht = Chloritoid-Chlorite

seafloor may have formed due to the phase separation scheme as suggested above rather than due to insufficient initial heating of the hydrothermal fluid.

IMPLICATIONS FOR FORMATION OF CHLORITOID

Chloritoid is best known to occur in meta-pelites that are typically rich in Fe relative to Mg, and similarly very deficient in K, Na, and Ca (Winkler 1976). The per-aluminous nature of the volcanic rocks in this study is partially achieved by their loss of Na_2O and CaO to alteration. As discussed above, they are also enriched in iron. However, if the resultant compositions are compared with the field of chloritoid stability presented by Hoschek (1967), many of the bulk compositions lie outside this field, and chlorite or biotite, rather than chloritoid, is the expected ferromagnesian phase. Carbonate has apparently played a significant role in enabling chloritoid to form. As indicated by the mineralogic and mass balance studies, with progressive alteration, more CaO, and at most intense alteration stages, MgO and eventually FeO were consumed by the formation of carbonate. This progressive consumption occurred in a regime of increasing pCO_2. As MgO and CaO were entirely used in the carbonate, they became unavailable for formation of chlorite or biotite. The loss of Na_2O provided considerable alumina which eventually combined with excess iron to form chloritoid. Thus syndepositional carbonatization of the volcanic rocks was a critical process enabling the formation of chloritoid during regional metamorphism.

CONCLUSIONS

The following tentative conclusions have been made resulting from the work to date:

1. Alteration of the volcanic rocks associated with the iron deposits and Kozak base-metal occurrence in the Goudreau district involved addition of CO_2, Fe, and Mn. Ti, Al, and Zr were immobile during alteration; CaO and Na_2O were variably lost.
2. Carbonatization took place separately, and possible earlier than iron addition.
3. The CO_2-rich phase separated from the parent hydrothermal fluid due to sub-seafloor boiling: CO_2, probably along with H_2S formed a rapidly-rising vapour phase that moved upwards in an unfocused manner, reacting with the volcanic rocks in the immediate sub-seafloor to produce carbonate. H_2S and probably some CO_2 were expelled to the seawater or atmosphere. Very efficient phase separation took place due to the very low hydrostatic pressure, a consequence of the shallow submarine to subaerial depositional environment prevalent throughout much of the Wawa area during the time of deposition of the iron formations.
4. The phase separation effectively cooled the residual ferruginous fluid; relatively low-temperature fluids were sufficiently dense that they rose slowly through the volcanic strata (c.f. those responsible for massive sulphide formation). Consequently, slow, rather unfocused discharge prevailed during the period of deposition of the iron formations.
5. Base metals probably were discharged in the absence of reduced sulphur, and lost to seawater. At Kozak, sufficient sulphur was retained in the metalliferous fluid to enable local zinc and lead deposition. This deposition may have occurred during the early stages of boiling of the hydrothermal fluid.
6. Chloritoid formation was dependent primarily on early intensive carbonatization of the volcanic strata, which "consumed" the ferromagnesian components. Its presence in volcanic rocks signifies the development of a major, probably metalliferous hydrothermal system, but the preservation of the base metals in economic quantities was dependent on sufficient hydrostatic pressure (i.e. water depth) to prevent the loss of H_2S during phase separation. In the Wawa area, water depths were too shallow to prevent this loss.

ACKNOWLEDGMENTS

The author would like to thank Ron Hartree (University of Ottawa, Ottawa) for his help in XRF analysis. Thanks are also due to Dan Marshall and Dave Kingston (Carleton University, Ottawa) for their time and assistance with computer programs. Discussions with Ron Sage (Geologist, Ontario Geological Survey, Toronto) and Howard Poulsen (Geological Survey of Canada, Ottawa) have been valuable.

REFERENCES

Bischoff, J.L., and Rosenbauer, R.J.
1984: The Critical Point and Two-Phase Boundary of Seawater, 200 to 500 Degrees Celsius; Earth and Planetary Science Letters, Volume 68, p.172-180.

Calvert, H.T.
1983: Petrography and Geochemistry of an Archean Volcanic Sequence of the Josephine Area, Wawa, Ontario; Unpublished B.Sc. Thesis, Brock University, 69p.

Costa, U.R., Barnett, R.L., and Kerrich, R.
1983: The Mattagami Lake Mine Archean Zn-Cu Sulfide Deposit, Quebec: Hydrothermal Coprecipitation of Talc and Sulfides in a Sea-Floor Brine Pool—Evidence from Geochemistry, $^{16}O/^{18}O$, and Mineral Chemistry; Economic Geology, Volume 78, p.1144-1203.

Delaney, J.R., and Cosens, B.A.
1982: Boiling and Metal Deposition in Submarine Hydrothermal Systems; Marine Technology Society Journal, Volume 16, p.62-66.

Drummond, S.E., and Ohmoto, H.
1985: Chemical Evolution and Mineral Deposition in Boiling Hydrothermal Systems; Economic Geology, Volume 80, p.126-147.

Eckstrand, O.R.
1963: Crystal Chemistry of Chlorite; Unpublished Ph.D. Thesis, Harvard University, 128p.

Floyd, P.A., and Winchester, J.A.
1975: Magma Type and Tectonic Setting Discrimination Using Immobile Elements: Earth and Planetary Science Letters, Volume 27, p.211-218.

Franklin, J.M.
In Press: Volcanic Associated Massive Sulphide Deposits—An Update: Irish Association of Economic Geologists, Special Volume, 46p.

Franklin, J.M., Kasarda, J., and Poulsen, K.H.
1975: Petrology and Chemistry of the Alteration Zone of the Mattabi Massive Sulphide Deposit: Economic Geology, Volume 20, p.63-79.

Franklin, J.M., and Thorpe, R.I.
1982: Comparative Metallogeny of the Superior, Slave and Churchill Provinces: p.3-90 *in* H.S. Robinson Memorial Volume, Precambrian Sulphide Deposits, edited by R.W. Hutchinson, C.D. Spence, and J.M. Franklin, Geological Association of Canada, Special Paper 25, 791p.

Goodwin, A.M.
1962: Structure, Stratigraphy, and Origin of Iron Formations, Michipicoten Area, Algoma District, Ontario, Canada: Geological Society of America Bulletin, Volume 73, p.561-586.
1977: Archean Volcanism in Superior Province, Canadian Shield: p.205-242 *in* Volcanic Regimes in Canada, edited by W.R.A. Baragar, L.C. Coleman, and J.M. Hall, Geological Association of Canada, Special Paper 16, 476p.

Goodwin, A.M., Thode, H.G., Chou, C.-L., and Karkhansis, S.N.
1985: Chemostratigraphy and Origin of the Late Archean Siderite–Pyrite-Rich Helen Iron Formation, Michipicoten Belt, Canada, Canadian Journal of Earth Sciences, Volume 22, p.72-84.

Grant, J.A.
In Press: The Isocon Diagram–A Simple Solution to Gresens's Equation for Metasomatic Alteration: Economic Geology, 17p.

Hallberg, J.A.
1975: A Geochemical Aid to Igneous Rock Type Identification in Deeply Weathered Terrain: Journal of Geochemical Exploration, Volume 20, p.1-8.

Hoschek, G.
1967: Untersuchungen zum Stabilitätsbereich von Chloritoid und Staurolith: Contributions to Mineralogy and Petrology, Volume 14, p.126-162.

LaTour, T.E., Kerrich, R.W., Hodder, R.W., and Barnett, R.L.
1980: Chloritoid Stability in Very Iron-Rich Altered Pillow Lavas: Contributions to Mineralogy and Petrology, Volume 74, p.165-173.

Lockwood, M.L., Franklin, J.M., and Moore, J.M.,
1985: The Significance and Genesis of Chloritoid Alteration in Volcanic Rocks of the Michipicoten Belt, Ontario: Brant 221, p.175-185 *in* Geoscience Research Grant Program, Summary of Research 1984-1985, edited by V.G. Milne, Ontario Geological Survey, Miscellaneous Paper 127, 246p.

MacGeehan, P.J., and MacLean, W.H.
1980: An Archean Sub Seafloor Geothermal System, "Calc-alkali" Trends and Massive Sulphide Genesis: Nature, Volume 286, Number 5775, p.767-771.

Morton, R.L., and Nebel, M.L.
1984: Hydrothermal Alteration of Felsic Volcanic Rocks at the Helen Siderite Deposit, Wawa, Ontario: Economic Geology, Volume 79, p.1319-1333.

Mottl, M.J.
1983: Metabasalts, Axial Hot Springs, and the Structure of Hydrothermal Systems at Mid–Ocean Ridges: Geological Society of America Bulletin, Volume 94, p.161-180.

Nesbitt, H.W.
1984: Calculation of the Solubility of CO_2 in NaCl-Rich Hydrothermal Solutions Using Regular Solution Equations: Chemical Geology, Volume 43, p.319-330.

Osterberg, S.A.
1985: Stratigraphy and Hydrothermal Alteration of Archean Volcanic Rocks of the Headway-Coulee Massive Sulfide Prospect, Northern Onaman Area, Northwestern Ontario: Unpublished M.Sc. Thesis, University of Minnesota, 114p.

Parry, S., and Hutchinson, R.W.
1981: Origin of a Complex Alteration Assemblage, Four Corners Cu-Zn Prospect, Quebec, Canada: Economic Geology, Volume 76, p.1186-1201.

Sage, R.P.
1981: Josephine Area, District of Algoma: p.41-44 *in* Summary of Field Work, 1981, by the Ontario Geological Survey, edited by J. Wood, Owen L. White, R.B. Barlow, and A.C. Colvine, Ontario Geological Survey Miscellaneous Paper 100, 253p.

Seyfried, W.E., Jr., and Janeckey, D.R.
1983: Experimental Basalt-Solution Interactions: Implications for the Origin of Ridge Crest Hydrothermal Fluids; Fourth International Symposium on Water-Rock Interactions, Extended Abstracts, Misasa, Japan, p.433-436.

Turek, A., Smith, P.E., and Van Schmus, W.R.
1984: U-Pb Zircon Ages and the Evolution of the Michipicoten Plutonic-Volcanic Terrane of the Superior Province, Ontario: Canadian Journal of Earth Sciences, Volume 21, Number 4, p.457-464.

Winkler, H.J.F.
1976: Petrogenesis of Metamorphic Rocks, Fourth Edition: Springer-Verlag, New York, 334p.

Grant 225 Genesis of Pegmatites in the Quetico Gneiss Belt of Northwestern Ontario—Granitoids, "Barren" Pegmatites, and Metasediments, with Additional Data on Rare–Element Pegmatites, from the Georgia Lake Pegmatite Field

S.A. Kissin[1], **B. Zayachkivsky**[2], **and L.A. Branscombe**[1]

[1]Department of Geology, Lakehead University, Thunder Bay

[2]Precambrian Section, Ontario Geological Survey, Toronto

ABSTRACT

Additional studies of two-mica leucogranites from the Georgia Lake Pegmatite Field confirm that satellite plutons (MNW stock, Barbara Lake stock) are more highly fractionated that the main mass of the Glacier Lake pluton, which itself shows increasing fractionation in border zones. Rare earth element (REE) studies confirm a link between metasediments of the Georgia Lake area and two-mica leucogranites (S-type) presumed to be derived by partial anatexis of similar parental rocks. The Barbara Lake stock appears to be the source of pegmatitic fluids, which are seen in increasingly fractionated "barren" pegmatites eastward to the Southern Group rare-element pegmatites. Although the Central Group rare-element pegmatites appear to be derived from the Barbara Lake stock as well, no clear fractionation trend in "barren" pegmatites east of the Central Group is discernible. Only minor occurrences of beryl-bearing pegmatite were found east of the Southern Group, and only one minor occurrence was found east of the Central Group. A number of additional occurrences of Ta-Nb-Sn oxide minerals were discovered in the rare-element pegmatites, suggesting some economic potential for these minerals.

INTRODUCTION

In the previous year's report (Kissin and Zayachkivsky 1985), the geochemistry and mineralogy of rare-element pegmatites of the Georgia Lake Pegmatite Field were discussed, together with the characteristics of possible parental granitoid rocks of the area. The Georgia Lake Pegmatite Field is located southeast of Lake Nipigon within the Quetico Subprovince of the Archean Superior Province. The area lies immediately east of Highway 11, about midway between the towns of Nipigon and Beardmore.

This report deals with the extensively developed "barren" pegmatites of the area and their relationships to rare-element pegmatites and parental granitoids of the area. F.W. Breaks (Geologist, Ontario Geological Survey, Toronto, personal communication, 1983) suggested, based on limited observation and on theories of pegmatite zonation, that a zone of beryl-bearing pegmatites might be present nearer to the parental granitoids than the rare-element pegmatites. Potential beryl-bearing zones were explored in the field, as well as a number of rare-element pegmatites not studied in the course of the previous year's work. The two-mica leucogranites of the Glacier Lake pluton, MNW stock and Barbara Lake stock were shown to be likely parental to most rare-element pegmatites of the area. As little is known about the internal features of the Glacier Lake pluton, its geology and geochemistry were studied in greater detail.

METHODOLOGY

In general, analytical methods employed were the same as those described by Kissin and Zayachkivsky (1985). In the present study, analyses for trace amounts of Li, Sn, and Pb were carried out at Lakehead University by atomic absorption (AA) spectrophotometry. Analyses of Ta-Nb-Sn oxide minerals were carried out using a natural microlite standard for Na, Ca, Ta, and Nb, pure element or oxide standards for Sn and Fe, and natural willemite for Mn on the electron microprobe at the University of Toronto. Peak overlaps were corrected by appropriate measurements on standards. Most components of beryls were also determined on the electron microprobe using synthetic glass standards. Cs_2O was determined by Geoscience Laboratories of the Ontario Geological Survey by means of AA.

Radiochemical neutron activation analyses (RNAA) for rare earth elements (REE) and certain other trace components were carried out using procedures developed at Lakehead University. REE abundances are displayed in log normalized plots relative to the Leedey chondrite (Masuda 1975; Masuda *et al.* 1973).

GRANITOIDS

INTRODUCTION

As discussed in the previous year's report (Kissin and Zayachkivsky 1985) and in greater detail by Zayachkivsky (1985), granitoids of the Georgia Lake area can be subdivided into three petrographically and geochemically distinct groups: (1) two-mica leucogranites, (2) the Kilgour Lake Group, and (3) tonalitic dikes. Geochemical data suggested that the two-mica leucogranites were the most likely parental granitoids to rare-element pegmatites. As well, the MNW stock and Barbara Lake stock are geochemically very similar to the batholithic-sized Glacier Lake pluton and are perhaps satellite bodies to it (Figure 225.1). For these reasons, it was though to be important to further study the Glacier Lake pluton in particular.

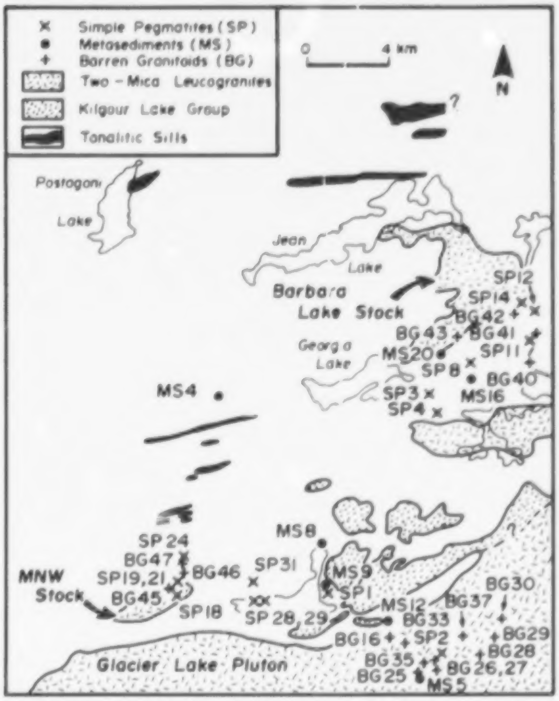

Figure 225.1. Sample locations for granitoid (BG) and metasediment (MS) specimens analyzed in Table 225.1. "Barren" pegmatite (SP) locations are also shown. Locations for BG21 and BG39 lie south of the map area near the centre of the Glacier Lake pluton. Granitoid bodies (simplified after Pye 1965) are also shown.

FIELD RELATIONS

Pye (1965) concluded on the basis of field relations that the granitoid rocks of the Georgia Lake area exhibited intrusive relationships with respect to the metasedimentary rocks of the area. These relationships are fairly obvious in the tonalitic dikes, and stock-like bodies of the Kilgour Lake Group and various satellite plutons of the Glacier Lake pluton (MNW stock and Barbara Lake stock). The Glacier Lake pluton is clearly of batholithic dimensions, extending south to Lake Superior, west at least as far as Highway 11, and for an unknown distance farther west and east to the limits of the map area. Pye (1965) noted that a zone bounding the intrusion contained a number of thin, granite dikes striking parallel to the contact of the pluton. Sampling of metasediments from this zone revealed only a moderate increase in their metamorphic grade, as described later.

The granites within about 1 km of the contact generally display a lineation of micas and feldspar phenocrysts parallel to the contact. The granites are generally fine-grained within this border zone, and as demonstrated by Kissin and Zayachkivsky (1985) they are more highly fractionated than the main mass of the pluton. Apparently due to compositional differences related to this fractionation, garnetiferous granites occur here as well.

Within the main mass of the pluton, the granites are unfoliated, but zones of the pluton are pegmatitic, with pods of coarser granite lying within finer grained to even aplitic material. Magmatic textures are evident throughout the main mass, even adjacent to metasedimentary inliers, which are discussed in a later section.

GEOCHEMISTRY

Selected specimens of two-mica leucogranites were analyzed for major components and trace elements, as located in Figure 225.1. A limited number of these were analyzed for additional trace elements by instrumental neutron activation analysis (INAA), as shown in Table 225.1. An attempt was made to discern trends in geochemistry based upon the petrography of the granites (i.e. porphyritic, fine-grained, pegmatitic, biotite-bearing, or garnetiferous), but only the garnetiferous granite (BG42) of the Barbara Lake stock displayed a clear relationship to geochemistry. This specimen had the highest peraluminous index ($Al_2O_3/(Na_2O+K_2O+CaO)$ = A/CNK moles) of any of the specimens analyzed, and showed very high fractionation in terms of other chemical ratios.

All of the analyses are broadly similar in that all are peraluminous (A/CNK 1.12) and are obviously true granites based on their high SiO_2, Al_2O_3 and alkali contents. Differences, however, are apparent on an examination of trace element content.

High Li and Rb, and depletion in Sr, Ba, and Zr, leading to high K/Ba, Ba/Sr, and Rb/Sr, and low K/Rb, Ba/Rb, and Mg/(Lix10) ratios are considered by Goad and Černý (1981) and Trueman and Černý (1982) to reflect increasingly fractionated magmas parental to rare-element pegmatites. The data in Table 225.1 reflect these trends to a greater or lesser extent. Li contents are low in general; however, the Barbara Lake stock is generally enriched compared to the Glacier Lake pluton. This Li-enrichment cannot be attributed to metasomatic contamination as no spodumene-bearing pegmatites occur within or near the Barbara Lake stock. Rb is similarly enriched in the Barbara Lake stock and MNW stock, while Sr is depleted. Ba and Zr abundances do not yield any clear-cut trends.

Examination of trace element abundance ratios reveals no clear trends in K/Ba and Ba/Sr ratios, due to the variability in Ba abundances noted. However, the other abundance ratios, mentioned above, sharply separate the main body of the Glacier Lake pluton from its satellites, the MNW and Barbara Lake stocks. The K/Rb ratios are >150 in the Glacier Lake pluton, while they are invariably <150, with many <100, in the satellite plutons. The Rb/Sr ratios are variable, but mostly <2 in the Glacier Lake pluton, and always >2 in the satellite plutons, while Ba/Rb is variable, ranging to high values in the Glacier Lake pluton, but <2 and lower in the satellite plutons. These ratios indicate that the satellite plutons are more fractionated than the main mass of the Glacier Lake pluton.

Within the Glacier Lake pluton, trends reported by Kissin and Zayachkivsky (1985) on the basis of rather limited data are supported by the more extensive analyses given here. BG16, BG33, and BG33A from border zones of the pluton have the lowest

TABLE 225.1. ANALYSES OF TWO-MICA LEUCOGRANITES FROM THE GEORGIA LAKE AREA.

	Glacier Lake Pluton									
			pg			bg	bg		fg	peg
	BG16	BG21	BG25	BG26	BG27	BG28	BG29	BG30	BG33	BG33A
SiO_2(%)	76.82	74.48	75.17	73.60	75.72	74.11	75.27	74.82	74.36	76.03
TiO_2	0.65	0.11	0.16	0.14	0.11	0.13	0.06	0.15	0.18	0.08
Al_2O_3	13.12	14.15	14.42	15.43	13.65	14.83	13.53	14.56	14.72	15.00
Fe_2O_3	0.62	1.43	1.36	0.78	1.24	1.04	1.05	1.68	0.62	0.83
FeO	0.02	0.00	0.26	0.14	0.00	0.00	0.00	0.00	0.00	0.02
CaO	0.35	0.24	1.36	0.53	0.53	0.30	0.25	0.55	0.70	0.44
MnO	0.02	0.00	0.00	0.01	0.00	0.01	0.00	0.00	0.01	0.00
MgO	0.21	0.37	0.44	0.19	0.19	0.28	0.43	0.36	0.30	0.18
Na_2O	3.42	3.32	3.80	2.99	2.36	3.14	3.05	1.88	3.12	2.36
K_2O	3.90	5.23	2.34	5.34	5.33	5.58	5.42	5.22	5.12	4.08
P_2O_5	0.15	0.17	0.09	0.17	0.15	0.17	0.11	0.20	0.18	0.16
CO_2	0.15	0.00	0.07	0.15	0.15	0.11	0.26	0.07	0.04	0.18
H_2O	0.54	0.45	0.45	0.45	0.45	0.54	0.54	0.45	0.36	0.45
Total	99.98	99.95	99.92	99.91	99.89	100.23	99.96	99.93	99.71	99.81
Li(ppm)	0	0	0	0	0	0	4	0	0	0
Rb	286	238	95	180	174	190	217	196	253	191
Sr	72	151	152	111	142	122	117	113	117	86
Ba	≤18	280	≤18	348	291	≤18	54	340	≤18	162
Pb	27	45	64	45	27	45	27	36	36	27
Zr	95	158	112	134	113	111	67	126	157	62
Cs				2.8	3.5			3.8		3.3
Hf				3.1	2.9			0.28		2.6
Sc				2.5	1.6			1.3		2.3
Ta				2.2	4.6			6.1		3.1
Co				35	83			117		51
Th				18	15			19		3.0
K/Rb	113	315	205	246	254	244	207	221	168	177
K/Ba	-	155	-	127	152	-	833	128	-	209
Ba/Rb	-	2.02	-	1.93	1.67	-	0.249	1.74	-	0.848
Ba/Sr	-	1.85	-	3.14	2.05	-	0.462	3.01	-	1.88
Rb/Sr	3.97	0.913	0.625	1.62	1.23		1.86	1.74		2.22
Mg/(Lix10)	-	-	-	-	-	-	65		-	-
A/CNK	1.25	1.22	1.28	1.32	1.29	1.26	1.19	1.49	1.23	1.65
FeO/Fe_2O_3	0.03	-	0.19	0.18	-	-	-	-	-	0.02

Cr sought but not detected in INAA analyses
pg = porphyritic granite, bg = biotite granite, fg = fine-grained leucogranite, peg = pegmatitic granite.

K/Rb ratios and generally higher Rb/Sr ratios than most other samples from the interior of the pluton. BG21 and BG39 from well within the pluton, and south of the map area of Figure 225.1 have higher K/Rb and lower Rb/Sr ratios than most other samples. Thus, the marginal zones of the Glacier Lake pluton are more highly fractionated than more central zones, and, indeed, more fractionated than some specimens from the satellite plutons.

METASEDIMENTS

PETROGRAPHY

The metasedimentary rocks of the Georgia Lake area have all been metamorphosed to low to moderate metamorphic grades. The rocks are strongly foliated schists to gneisses; however, all are relatively fine grained. Porphyroblastic textures are only locally developed, especially in the central portion of the map, where porphyroblasts of almandine and cordierite are developed. Primary bedding is obscure in most places, and although bedding can occasionally be observed, in at least one location inversion of bedding due to polyphase deformation was noted. The rocks are dominantly of pelitic affinity, although psammitic beds and amphibolite units occur locally.

Metamorphic assemblages observed in this section are characteristic of upper greenschist to lower most amphibolite facies. All assemblages were formed above the biotite isograd, as indicated by its ubiquitous presence. Primary chlorite is indicative of greenschist facies in many sections. A transition to amphibolite facies is manifested by the absence of primary chlorite and increasing abundance of almandine garnet. Highest grade assemblages contain:

chlorite-biotite-quartz±almandine

with variations, apparently reflecting compositional differences:

TABLE 225.1 (cont'd). ANALYSES OF TWO-MICA LEUCOGRANITES FROM THE GEORGIA LAKE AREA.

	Glacier Lake Pluton			Barbara Lake Stock				MNW Stock		
	peg	fg				gar				fg
	BG35	BG37	BG39	BG40	BG41	BG42	BG43	BG45	BG46	BG47
SiO_2(%)	73.01	74.56	72.29	75.58	75.45	73.17	74.13	75.22	75.31	74.72
TiO_2	0.11	0.10	0.25	0.15	0.16	0.05	0.13	0.22	0.19	0.09
Al_2O_3	15.82	15.74	15.21	14.20	14.27	14.06	15.51	14.83	14.87	15.07
Fe_2O_3	0.80	0.55	1.70	1.44	0.63	6.59	1.19	1.35	1.21	0.97
FeO	0.10	0.42	0.54	0.00	0.42	0.00	0.10	0.00	0.00	0.00
CaO	0.12	0.15	0.12	0.43	0.10	0.11	0.66	0.36	0.45	0.13
MnO	0.00	0.00	0.00	0.04	0.02	0.12	0.03	0.01	0.01	0.00
MgO	0.20	0.00	0.45	0.29	0.36	0.05	0.27	0.43	0.32	0.03
Na_2O	3.62	3.30	2.51	2.94	3.17	4.51	2.89	2.44	2.01	3.93
K_2O	4.75	4.14	5.75	4.08	4.74	0.85	4.35	3.57	4.70	3.28
P_2O_5	0.19	0.12	0.19	0.08	0.17	0.24	0.10	0.37	0.31	0.28
CO_2	0.26	0.07	0.07	0.00	0.18	0.04	0.15	0.07	0.11	0.33
H_2O	0.90	0.63	0.63	0.81	0.54	0.36	0.36	1.08	0.45	0.63
Total	99.88	99.80	99.82	99.94	99.89	100.12	99.87	99.95	99.93	99.46
Li(ppm)	0	0	0	4	4	9	167	13	0	0
Rb	121	176	169	281	267	198	346	372	329	397
Sr	350	79	124	119	123	36	112	79	94	40
Ba	616	298	331	498	416	33	348	298	112	31
Pb	36	27	18	27	27	5	27	9	27	9
Zr	59	109	207	151	156	86	122	509	147	70
Cs		3.9		6.2		5.2	33.2	28.3		12.1
Hf		2.1		2.4		2.4	0	0		0.56
Sc		2.7		2.4		0.65	1.5	2.8		1.5
Ta		2.6		3.6		6.5	4.7	8.4		17.8
Co		46		42		39	46	30		107
Th		12		30		6.8	14	21		1.8
K/Rb	326	187	283	121	147	35.6	104	79.7	119	68.6
K/Ba	64.0	111	144	68.0	94.6	213	104	100	348	878
Ba/Rb	5.09	1.69	1.95	1.77	1.56	0.167	1.01	0.801	0.340	0.0781
Ba/Sr	1.76	3.77	2.67	4.19	3.38	0.917	3.11	3.77	1.19	0.775
Rb/Sr	0.346	2.23	1.36	2.36	2.17	5.50	3.09	4.71	3.50	9.93
Mg/(Lix10)	-	-	-	44	54	3.4	1.0	20	-	-
A/CNK	1.40	1.51	1.44	1.42	1.36	1.65	1.46	1.74	1.61	1.47
FeO/Fe_2O_3	0.13	0.79	0.32	-	0.67	-	0.08	-	-	-

Cr sought but not detected in INAA analyses.
pg = porphyritic granite, bg = biotite granite, fg = fine-grained leucogranite, peg = pegmatitic granite.

biotite-quartz-almandine-hercynite±orthoclase
quartz-almandine-albite-almandine-actinolite
chlorite-quartz-albite-biotite

A garnet isograd is probably mapable in some areas, as closely situated sampling localities often show an abrupt appearance of almandine. Field sampling suggests that proximity to intrusions such as the MNW stock and the Barbara Lake stock may be spatially related to the garnet isograd. However, sampling at close intervals in relation to the contact of the Glacier Lake pluton revealed no clear increase in metamorphic grade with proximity to this batholith-sized body.

The transition to lowermost amphibolite facies is manifested by the typical assemblages:

muscovite-biotite-quartz-staurolite
biotite-muscovite-albite-cordierite-quartz±orthoclase

There is some indication that metasediments bordering the Kilgour Lake group intrusions and the Barbara Lake stock have developed higher grade assemblages; however in other areas, notably the northern and central portions of the map area, no relationship to plutons exposed at the surface is evident.

Pye's (1965) map shows numerous, elongated inliers of metasedimentary rock in the southeastern part of the Glacier Lake pluton. These were examined and found to be much smaller than indicated on the map. The inliers have sharp contacts with the granite, and in some cases contacts are perpendicular to the foliation in the metasediments. Metamorphic assemblages within inliers are typically:

quartz-albite-biotite
quartz-muscovite-albite-orthoclase
biotite-quartz-orthoclase

TABLE 225.2. ANALYSES OF METASEDIMENTS FROM THE GEORGIA LAKE AREA.

	MS1	MS2	MS3	MS4	MS5	MS7	MS8	MS9	MS12	MS16	MS20
SIO_2(%)	54.06	57.41	53.68	68.25	63.22	58.78	63.23	62.64	58.08	64.51	61.01
TIO_2	0.63	0.72	0.82	0.67	0.71	0.76	0.63	0.66	0.77	0.78	0.66
AL_2O_3	13.37	16.28	19.74	17.02	15.44	17.61	16.36	18.30	17.95	19.77	17.04
*FE_2O_3	11.77	7.14	9.74	1.81	7.14	8.12	7.16	8.05	8.89	1.09	8.65
CaO	5.25	4.35	2.49	1.38	2.65	1.90	2.57	1.47	2.25	1.61	1.32
MnO	0.11	0.10	0.10	0.06	0.11	0.02	0.12	0.07	0.11	0.14	0.07
MgO	6.17	5.45	3.82	3.09	3.08	3.55	2.63	2.75	3.25	2.87	3.20
Na_2O	3.27	2.62	4.69	2.32	3.37	2.15	1.37	3.83	3.83	2.74	3.45
K_2O	2.62	3.65	3.19	2.98	2.84	2.55	2.20	0.11	3.19	3.65	2.11
P_2O_5	0.22	0.25	0.18	0.13	0.14	0.14	0.12	0.13	0.13	0.36	0.16
CO_2	0.62	0.15	0.11	0.18	0.07	0.26	0.11	0.15	0.15	0.11	0.22
H_2O	2.34	1.89	1.62	1.62	1.26	1.89	1.26	2.61	1.62	1.89	2.07
Total	100.43	100.01	100.18	99.53	100.03	99.87	100.01	99.76	100.18	99.51	99.94
Rb(ppm)	90	112	110	91	187	90	82	117	89	553	96
Sr	599	373	444	245	254	280	392	278	350	247	349
Ba	1000	1266	869	506	297	340	458	1319	1024	437	391
Zr	120	173	132	196	138	148	141	177	152	130	148
Pb	119	27	36	27	18	18	27	36	36	9	18
Li	4	117	88	28	26	23	2	70	58	431	91

*Total iron as Fe_2O_3.

lacking indications of even the garnet zone and clearly of greenschist facies. Based on the foregoing characteristics, it is believed that metasedimentary inliers in the Glacier Lake pluton are roof pendants stoped into the magma chamber at the time of its emplacement.

GEOCHEMISTRY

Aside from REE and trace element data obtained by RNAA and presented in a later section, whole-rock and limited trace element analyses were performed on the metasedimentary rocks of the Georgia Lake area (Table 225.2). A striking feature of these analyses is the relatively high concentrations of Li in the metasediments. In fact, the metasediments are generally rich in Sr, Ba, Zr, and Pb as compared to the granitoids of Table 225.1, with only Rb being somewhat lower in most cases. The major elemental components of the metasediments are low in SiO_2 in comparison with the granitoids, but markedly higher in TiO_2, total Fe, CaO, and MgO. Within the metasediment analyses, the only pattern to emerge is that MS4 and MS16, from the northern part of the map area (Figure 225.1), are enriched in SiO_2 and deficient in total Fe as compared to samples from farther south. This difference may be a manifestation of the increasingly psammitic nature of the metasediments, as opposed to the pelitic ones that predominate to the south.

"BARREN" PEGMATITES

INTRODUCTION

"Barren" pegmatites, i.e. mineralogically simple pegmatites without Li-bearing minerals, occur sporadically throughout the Georgia Lake Pegmatite Field but are particularly abundant in the vicinity of Barbara Lake and the region north of the contact of the Glacier Lake pluton near the MNW stock and Cosgrave Lake. The "barren" pegmatites are dikes of a maximum few metres thickness consisting of perthitic microcline, quartz, and muscovite, with traces of other minerals such as beryl and tourmaline. According to theories of pegmatite zoning (e.g. Trueman and Černý 1982), as one nears the parental granite, rare-element pegmatites should pass from Be-, Ta-, Li-, Cs-rich to Be-, Nb-Ta-, Li-rich, to Be-, Nb-Ta-rich to beryl-bearing to barren pegmatites. Thus, the Central Group rare element pegmatites at the west end should pass into a zone of beryl-bearing and then barren pegmatites as one passes easterly toward the Barbara Lake stock. The situation with respect to the Southern Group pegmatites is less clear, as rare-element pegmatites occur within a possible parental granite, the MNW stock. Mineralogical zonation as outlined above should also be paralleled by trace element zonation, e.g. increasing K/Rb ratio in microcline toward the parental granite (Trueman and Černý 1982). These trends were compared to the actual trends observed in the occurrence of beryl and geochemistry of microcline and mica in "barren" pegmatites in the Georgia Lake Pegmatite Field.

GEOCHEMISTRY

Beryl

Zones of beryl-bearing pegmatites were sought with rather disappointing results. Beryl was found only within the MNW and Swanson pegmatites and in a few "barren" pegmatites in the vicinity of Cosgrave Lake. The only other beryl occurrence was a single locality at Barbara Lake (Figure 225.2). At all localities, beryl, although sometimes present in crystals several centimetres long, was always a very minor constituent of the pegmatite. Partial analyses of beryls from some of these localities (Table 225.3) reveal marked differences between beryls from the MNW pegmatite and those from "barren" pegmatites near Cosgrave Lake. The compositions of beryls from "barren" pegmatites are essentially identical, are low in Na_2O, and lack Cs_2O, but contain a small amount of FeO. The beryls from the MNW pegmatites are zoned with respect to SiO_2 and Cs_2O from core to rim and contain considerable Cs_2O and Na_2O in relation to the beryls from the "barren" pegmatites.

Microcline

Perthic microclines from "barren" pegmatites were analyzed for selected trace elements (Table 225.4). K_2O was assumed to be near the ideal amount for microcline at 16.00 weight percent for purposes of calculation of the K/Rb ratio. The K/Rb ratio in microcline has been shown to be an indicator of the degree of fractionation in pegmatites (Goad and Černý 1981), with lowest values indicating the highest degree of fractionation. It is apparent from Table 225.4 that high Cs and low Ba and Sr are correlated with low K/Rb, while Zr generally shows little variation.

In noting the locations of these "barren" pegmatites in Figure 225.1, SP2, occurring within the Glacier Lake pluton, is among the least fractionated in terms of K/Br ratio and has the highest Ba and Sr contents of any of the microclines analyzed. Although SP2 may be related to other "barren" pegmatites in the vicinity of Cosgrave Lake and the MNW stock, it may also be representative of pegmatitic phases internal to the Glacier Lake pluton. On the other hand, a fairly regular trend of decreasing fractionation from west to east is apparent in "barren" pegmatites proximal to the Southern Group rare-element pegmatites, i.e. the MNW, Swanson, and newly discovered SP18. Microclines from SP18 yield approximately the same K/Br ratios as microclines from nearby "barren" pegmatites, as well as similar values for Cs, Sr, and Ba, suggesting that these "barren" pegmatites may deserve further investigation for rare-element mineralization.

In the vicinity of Barbara Lake, perthitic microclines in "barren" pegmatite show no clear trend in increasing fractionation in a westerly direction toward the Central Group rare-element pegmatites west of Georgia Lake. As well, only one minor beryl occurrence was noted. This result is a little surprising in that the rare-element pegmatites west of Georgia, as reported by Kissin and Zayachkivsky (1985) display a strong trend of increasing fractionation in a westerly direction. The genetic link between this group of "barren" pegmatites and the Central Group pegmatites is thus not particularly strong.

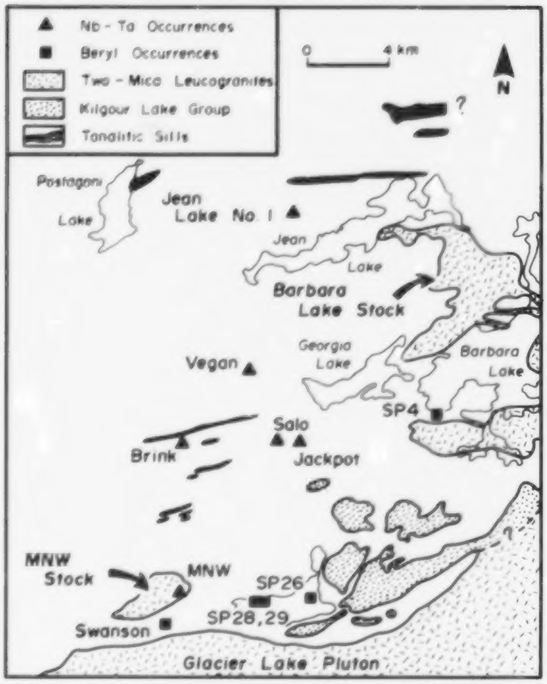

Figure 225.2. Occurrences of beryl and Ta-Nb-Sn oxide minerals in rare-element (named) and "barren" (SP) pegmatites. The Swanson and MNW pegmatites contain both beryl and Ta-Nb-Sn oxide minerals.

TABLE 225.3. PARTIAL CHEMICAL ANALYSES OF BERYLS FROM THE GEORGIA LAKE PEGMATITE FIELD.

wt.%	MNW Core	MNW Wall	SP28 1	SP28 2	SP29 1	SP29 2
SiO_2	59.97	63.77	66.80	65.53	66.62	67.42
Al_2O_3	16.86	18.03	18.02	18.08	18.35	18.60
FeO*	0.00	0.00	0.40	0.37	0.43	0.37
MnO	0.00	0.00	0.00	0.00	0.00	0.00
CaO	0.00	0.00	0.00	0.00	0.00	0.00
MgO	0.73	0.75	0.82	0.53	0.62	0.53
Na_2O	1.48	1.38	0.49	0.45	0.55	0.45
Cs_2O**	1.06	6.79	-	-	-	-

*Total iron as FeO.
**Determined by AA; all other components by electron microprobe analysis.
A dash denotes not detected.

TABLE 225.4. COMPOSITIONAL CHARACTERISTICS OF PERTHITIC MICROCLINE FROM "BARREN" PEGMATITES.

wt.%	SP1	SP2	SP3	SP4	SP8	SP11	SP12	SP14	SP18C	SP18D	SP19	SP21	SP24	SP28	SP29	SP31
K_2O	16.00 assumed for all samples															
ppm																
Rb	593	258	764	704	1572	1046	756	976	1510	1362	1542	1535	2177	270	206	1222
Cs	32	7	17	17	35	41	18	21	98	204	274	172	65	28	20	52
Sr	82	117	62	73	48	60	51	50	64	62	58	67	58	99	103	58
Ba	190	196	94	177	108	≤7	91	108	≤7	≤7	≤7	≤7	≤7	≤7	≤7	≤7
Zr	63	59	62	58	63	64	60	62	67	66	69	69	69	105	112	68
K/Rb	224	515	179	189	84.5	127	176	136	88.0	97.5	86.1	86.5	61.0	492	645	109

Rb and Cs determined by INAA: other elements by XRF.

TABLE 225.5. TRACE ELEMENTS IN PEGMATITIC MUSCOVITE.

ppm	SP3	SP19	SP26	SP31	Swanson
Rb	2046	2095	1188	1787	2593
Cs	72	260	25	85	70
Ta	43	91	15	23	72
Co	10.4	0.59	16.6	0.41	1.2
Sc	2.2	5.5	10.9	0.8	4.5
Ba	-	-	-	-	-
Hf	0.28	0.82	0.31	4.1	1.1
Th	-	-	-	-	7

A dash denotes not detected at ≤100 ppm Ba and ≤1 ppm Th.
All elements determined by INAA.

Muscovite

Muscovites separated from "barren" pegmatites SP3, SP19, and SP31 (Figure 225.1) and SP26 and the Swanson rare-element pegmatite (Figure 225.2) were analyzed by INAA (Table 225.5). As in the case of perthitic microclines, muscovites in the Swanson rare-element pegmatite and the "barren" pegmatites SP19, SP31, and SP26 display increasing fractionation from east to west as seen in nearly uniformly increasing Rb, Cs, Ta, and possibly Th, and decreasing Co, Sc, and Hf. SP3, from the vicinity of Barbara Lake, which appears to be moderately highly fractionated, however, does not seem to be following the same trend with respect to abundances of all elements.

ADDITIONAL DATA ON RARE-ELEMENT PEGMATITES

INTRODUCTION

On the basis of geochemical characteristics and, to a lesser extent petrographic features, the rare-element pegmatites have been subdivided into three groups (Kissin and Zayachkivsky 1985): (1) the Northern Group, lying east of Postagoni Lake; (2) the Central Group, lying west of Georgia Lake; and (3) the Southern Group, in and around the MNW stock. Further field and laboratory investigations were carried out on rare-element pegmatites not examined in the previous year's work. Additional pegmatites investigated include the Swanson of the Southern Group, the Vegan, Jackpot, Newkirk, and a re-examination of the Salo of the Central Group and the Jean Lake No. 1, included by us in the Northern Group, but differentiated from that group by Milne (1962). As well, a previously unreported rare-element pegmatite dike was discovered within the MNW stock, about 200 m west of the MNW pegmatite (Figure 225.2). Except for the latter, designated SP18, all of the newly investigated or reinvestigated pegmatite are unzoned dikes composed of perthitic microcline, quartz, muscovite, xenocrystic spodumene, and various accessory minerals such as tourmaline and Ta-Nb-Sn oxide minerals. SP18 is crudely zoned with a quartz core containing pods of lithiophilite. The dike is, however, poorly expressed, and extensive stripping will be required for more detailed study of this body.

Ta, Nb, AND Sn MINERALIZATION

Analyses of Ta, Nb, and Sn oxide minerals found in the current year's work are presented in Table 225.6. The majority of the minerals found are of the columbite-tantalite group and are low in Sn. Cassiterite in the apparent absence of columbite-tantalite mineralization was found in the Salo pegmatite, however. An early-formed phase in the Jean Lake No. 1 pegmatite is a Ca-Nb oxide, probably the rare mineral vigezzite or fersmanite.

Taken together with data on columbite-tantalite series minerals from the MNW, Brink, and Southwest pegmatites (Kissin and Zayachkivsky 1985), it is possible to consider fractionation trends within the mineral series by calculating the atomic ratios Mn/(Mg+Fe) and Ta/(Ta+Nb). As demonstrated by Černý *et al.* (1985, 1986), a plot of such ratios obtained from minerals from individual pegmatites or pegmatite fields will often yield distinctive fractionation trends. The "normal" trend is from low to high Mn/(Mn+Fe) and Ta/(Ta+Nb). The data from the Georgia Lake Pegmatite Field (Figure 225.3) do not display many clearly developed trends. The Swanson, and intermediate and core zones of the MNW of the Southern Group pegmatites seem to lie on a linear, "normal" trend. The core to rim zoning of the light and dark phases of the Brink, the Vegan, and the Salo pegmatites also define a roughly linear, "normal" trend. This trend is in agreement with the trend of increasing fractionation as seen in the geochemistry of the silicate minerals of the pegmatites, as discussed previously in this report and by Kissin and Zayachkivsky (1985). The Jean Lake No. 1 pegmatite lies on the same trend, although the fractionation from a Ca-Nb oxide core to a manganocolumbite rim represents quite a different process than that observed in the other minerals. The Jean Lake No. 1 is a member of group 2 as defined by Milne (1962); however, the present work does little to clarify its relationship to the Central Group pegmatites. The Jackpot pegmatite is apparently a result of a "reverse" fractionation trend, yielding ferrotantalite. As the Jackpot is included in the Central Group, a branching fractionation path must be responsible for the compositions observed.

TABLE 225.6. MICROPROBE ANALYSES OF Ta-Nb-Sn OXIDE MINERALS FROM THE GEORGIA LAKE RARE-ELEMENT PEGMATITES.

wt.%	1	2	3	4	5	6	7	8	9	10	11	12	13	14
Ta_2O_5	12.06	23.50	25.77	24.61	25.83	15.96	24.43	21.69	20.23	82.24	81.96	80.90	3.25	2.89
Nb_2O_5	67.29	59.05	56.32	56.23	56.93	65.73	58.07	60.36	58.86	0.80	0.67	0.85	1.15	0.85
TiO_2	0.34	n.d.	n.d.	0.29	0.29	0.00	0.00	0.38	0.43	0.00	0.26	0.00	n.d.	n.d.
SnO_2	n.d.	n.d.	n.d.	n.d.	n.d.	n.d.	n.d.	n.d.	n.d.	n.d.	n.d	0.70	93.80	92.20
FeO*	17.23	10.95	10.85	10.97	10.53	11.72	11.50	4.07	2.62	12.92	13.17	13.07	0.87	0.91
MnO	3.44	7.98	7.92	6.91	7.49	7.69	7.14	10.72	4.78	1.17	0.94	0.97	0.00	0.00
CaO	0.00	0.00	0.27	0.00	0.26	0.00	0.00	3.76	10.13	0.00	0.00	0.00	n.d	n.d.
Na_2O	0.00	0.00	0.00	0.62	0.00	0.00	0.00	0.00	0.00	0.00	0.00	0.00	n.d	n.d
Total	100.36	101.48	101.13	99.62	101.32	101.10	101.15	100.97	97.05	97.13	97.00	96.50	99.07	96.85

Notes:

1. Swanson-ferrocolumbite
2. Vegan (lath, center) - ferrocolumbite
3. Vegan (lath rim) - ferrocolumbite
4. Vegan (narrow lath, center) - ferrocolumbite
5. Vegan (narrow lath, rim) - ferrocolumbite
6. Vegan (large lath, centre) - ferrocolumbite
7. Vegan (large lath, rim) - ferrocolumbite
8. Jean Lake No. 1 - manganocolumbite
9. Jean Lake No. 1 (grey area) vigezzite or fersmanite(?)
10. Jackpot (grain 1, area A) - ferrotantalite
11. Jackpot (grain 1, area B) - ferrotantalite
12. Jackpot (grain 1, area E) - ferrotantalite
13. Salo - cassiterite
14. Salo - cassiterite

n.d. = not determined

* total iron as FeO.

TABLE 225.7. COMPOSITIONAL CHARACTERISTICS OF PERTHITIC MICROCLINE FROM RARE-ELEMENT PEGMATITES.

wt.%	1	2	3	4
K_2O	16.00 assumed for all samples			
ppm				
Rb	1652	5004	780	4467
Cs	36	326	15	145
Sr	60	77	47	92
Ba	≤7	95	≤7	542
Zr	68	83	179	77
K/Rb	80.4	26.5	170	29.7

1 - Swanson
2 - Jackpot
3 - Newkirk
4 - Jean Lake No. 1

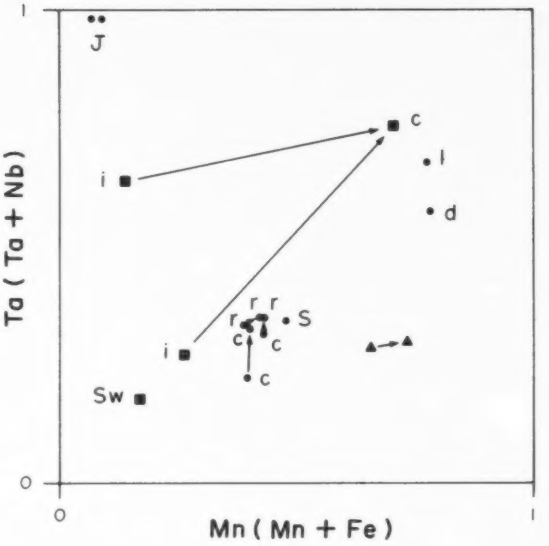

Figure 225.3. *Atomic ratios Ta/(Ta+Nb) vs. Mn/(Mn+Fe) for Ta-Nb oxide minerals from the Georgia Lake Pegmatite Field. Data from Table 225.6 and Kissin and Zayachkivsky (1985, Table 225.8). Triangles = Northern Group pegmatites (Jean Lake No. 1 with arrows showing trend from Ca-Nb oxide cores to Mn-Nb rims); circles = Central Group pegmatites (c=core, r=rim of Vegan; S=Salo; l=light BSE image, d=dark BSE image of Brink; J=Jackpot) and squares = Southern Group pegmatites (i=intermediate zone, c=core zone of MNW; Sw=Swanson).*

MICROCLINE

Perthitic microclines from rare-element pegmatites (Figure 225.2) were analyzed by INAA for selected trace elements, and the results are tabulated in Table 225.7. The Jackpot and Newkirk (not shown in Figure 225.2, but located approximately 1 km southeast of the Vegan pegmatite) of the Central Group present an interesting contrast in fractionation trends. On the one hand, the Jackpot is a near perfect fit to the trend in the Central Group demonstrated by Kissin and Zayachkivsky (1985), while the Newkirk emerges as the least fractionated of all the pegmatites in the group and is anomalous in all respects to trace element fractionation trends within the group.

The Swanson is less fractionated than the core and intermediate zones of the MNW pegmatite, its neighbour in the Southern Group, but more highly fractionated than nearby "barren" pegmatites including SP18 (Table 225.4). This finding is consistent with the general impression that the Swanson (unzoned, simple mineralogy) is less evolved than the MNW, but still a rare-element pegmatite.

Finally, the Jean Lake No. 1, although the only one of the Northern Group to bear Ta-Nb oxide mineralization, does seem to belong to that group on the basis of the geochemistry of its perthitic microcline. The combining of Milne's (1962) groups 3 and 4 pegmatites into one Northern Group by Kissin and Zayachkivsky (1985) does, then, seem to be further justified.

RARE EARTH ELEMENT ANALYSES

Granitoids, whose petrographic and other geochemical characteristics were described in detail in the previous year's report (Kissin and Zayachkivsky 1985), and a number of metasediments were selected for RNAA analysis for REE and selected trace elements from localities indicated in Figure 225.4. The results of these analyses are presented in Table 225.8.

The chondrite-normalized REE plot for metasediments (Figure 225.5) yields a very tight grouping with enrichment in light REE. Europium anomalies are either absent or of negligible magnitude, with a rather flat, heavy REE trend. Although Rb and Zr were not determined, other trace elements are similar to those of the two-mica leucogranites, especially in a marked enrichment in Ta.

The Kilgour Lake I-type granitoids (Kissin and Zayachkivsky 1985) display similar trends and Σ 7REE as the metasediments (Figure 225.6), however, other trace element values differ significantly. Ba is markedly enriched and Ta depleted, although Sc values are similar. It is also significant to note that one of the tonalitic sills, BG23, plots with the Kilgour Lake Group granitoids. Its trace element content is also similar to that of the Kilgour Lake Group. Although other samples of the tonalitic sills (Figure 225.7) are markedly depleted with respect to Σ 7REE, the plots are of similar form. The foregoing suggests a genetic link between the Kilgour Lake Group and the tonalitic sills, not previously apparent. Fractionation of Kilgour Lake granitoids could, then, give rise to the tonalitic sills, although in the case of extreme REE depletion in Figure 225.7, it might be expected to give rise to a negative Eu anomaly.

The two-mica leucogranites (Figure 225.8) generally exhibit marked negative Eu anomalies and moderately heavy REE depletion. While samples from the Barbara Lake stock and MNW stock are generally

TABLE 225.8. REE AND TRACE ELEMENT IN GRANITOIDS FROM THE GEORGIA LAKE AREA. (All concentrations in ppm)

	Two-Mica Leucogranites									
	Glacier Lake Pluton			Barbara Lake Stock		MNW Stock			Tonalites	
Sample	BG17	BG19	BG24	BG22	BG1	BG4	BG5	BG23	BG2*	BG3
La	25.8	4.48	26.2	36.8	45.1	20.8	40.2	26.6	3.90	1.55
Ce	47.5	10.6	52.7	42.9	66.5	44.1	58.0	47.7	-	2.29
Nd	19.5	2.92	20.5	17.3	27.5	19.5	29.9	19.9	-	1.49
Sm	1.0	4.6	3.0	3.9	3.9	3.3	5.1	3.8	4.5	0.26
Eu	0.40	0.080	0.30	0.33	0.39	0.22	0.27	0.79	-	0.081
Tb	0.27	0.14	0.27	0.39	0.52	0.31	0.34	0.20	-	0.029
Yb	0.18	0.25	0.33	0.94	1.3	0.63	0.55	0.43	-	0.089
7REE	94.65	23.07	103.30	102.56	145.21	88.86	134.36	99.42	-	5.79
Ba	357	79.7	335	517	573	341	370	745	405	408
Rb	168	351	332	303	357	377	377	900	357	85
Sc	3.4	2.0	1.6	2.6	2.8	2.3	2.8	4.6	2.6	1.2
Ta	1.0	2.5	2.6	1.6	3.2	1.9	3.0	0.22	0.19	0.093
Th	19	4.4	16	24	18	17	18	4.9	0.80	0.21
Hf	2.5	1.0	2.8	3.7	4.5	3.4	4.1	3.0	3.3	1.3
Zr	81	40	99	138	145	139	138	116	8	6

*Values from INAA only due to loss of sample during analysis.

TABLE 225.8 (Cont.) REE AND TRACE ELEMENTS IN GRANITOIDS FROM THE GEORGIA LAKE AREA.

	Kilgour Lake Group						Metasediments			
							Northern Group		Southern Group	
Sample	BG6	BG7	BG10	BG11	BG14	BG15	MS1	MS21	MS4	MS22
La	42.6	32.2	62.0	47.4	17.2	25.6	22.0	21.6	36.9	23.8
Ce	74.4	64.1	117	130	33.7	55.6	49.7	39.1	68.9	42.9
Nd	37.2	29.4	57.8	73.5	15.4	23.0	20.0	18.2	33.3	17.3
Sm	5.1	4.5	6.9	12	2.7	4.7	3.3	4.0	3.0	5.3
Eu	1.2	1.1	2.1	3.5	0.60	1.0	1.0	0.90	1.2	0.96
Tb	0.35	0.28	0.72	1.0	0.08	0.19	0.31	0.30	0.45	0.36
Yb	0.48	0.44	1.5	2.2	0.30	0.54	1.3	1.4	1.9	1.6
7REE	161.33	132.02	248.02	269.6	69.98	110.63	97.61	85.50	145.65	92.22
Ba	928	991	1494	2363	1203	863	1130	361	821	463
Rb	106	103	160	97	101	122	-	-	-	-
Sc	4.4	4.8	5.9	18	4.2	4.1	17	16	15	17
Ta	0.31	0.23	0.60	0.39	0.27	0.41	2.0	4.2	1.7	2.2
Th	6.8	4.9	11	8.1	6.5	6.7	6.5	7.1	11	6.9
Hf	3.8	3.5	5.1	5.9	3.2	2.7	3.3	3.2	4.1	3.3
Zr	152	152	218	219	110	133	-	-	-	-

similar in REE and trace element abundances, marked differences are present among the Glacier Lake pluton samples. BG19 is depleted in REE and all trace elements except Rb and Sc, while BG17 lacks a Eu anomaly and is depleted in Ta and Rb with respect to the other two-mica leucogranites. These differences seem to reflect the internal evolution of the Glacier Lake pluton, with BG17 considerably less fractionated than BG19, which is from the margin of the pluton.

As discussed by Kissin and Zayachkivsky (1985), the two-mica leucogranites are S-type granitoids, i.e. derived by anatexsis of sedimentary rocks. Although field relationships preclude derivation of the two-mica leucogranites at the crustal level, where they are presently exposed, it is not unlikely that the metasediments of the Georgia Lake area are at least similar to the ones giving rise to the two-mica leucogranites through the process of anatexis. Before discussing this point further, the close similarity between REE distributions in the metasediments (Figure 225.5) and the Kilgour Lake I-type granitoids (Figure 225.6) does not indicate a genetic link between the two because gross dissimilarities in trace element abundances make such a link highly unlikely.

The fractionation of REE between melt and residue has been reviewed by Hanson (1978), and his conclusions may be applied to a hypothetical derivation of the two-mica leucogranites from a source similar to the metasediments of the Georgia Lake

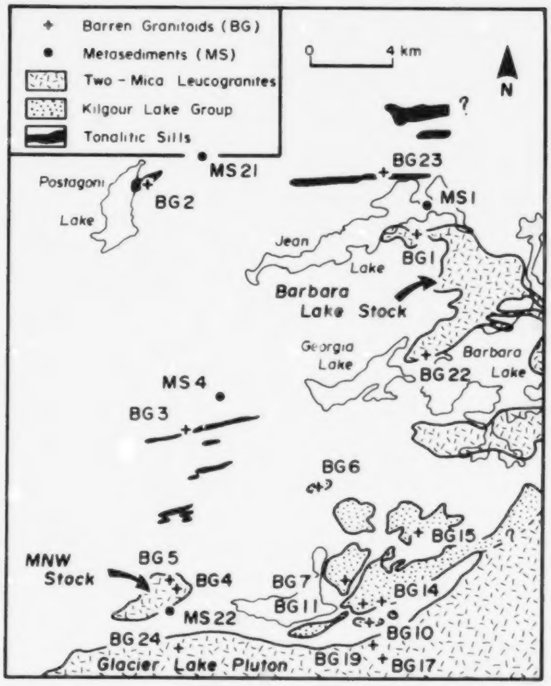
Barren Granitoids (BG)
Metasediments (MS)
Two - Mica Leucogranites
Kilgour Lake Group
Tonalitic Sills
0
4 km
N
?
MS 21
BG23
Postagoni Lake
BG2
MS I
Jean Lake
BG I
Barbara Lake Stock
Georgia Lake
Barbara Lake
BG 22
MS 4
BG 3
BG 6
BG 15
MNW Stock
BG 5
BG 4
BG 7
BG 14
BG I I
MS 22
BG 10
BG 24
Glacier Lake Pluton
BG 19
BG 17

Figure 225.4 *Sample localities for granitoids (BG) and metasediments (MS) selected for RNAA analysis.*

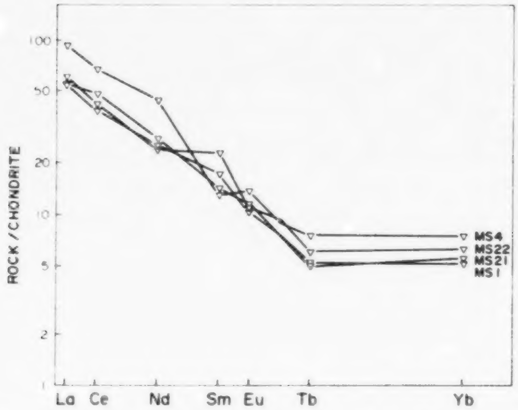

Figure 225.5 *Chondrite-normalized log-normal REE plot for metasediments from the Georgia Lake area.*

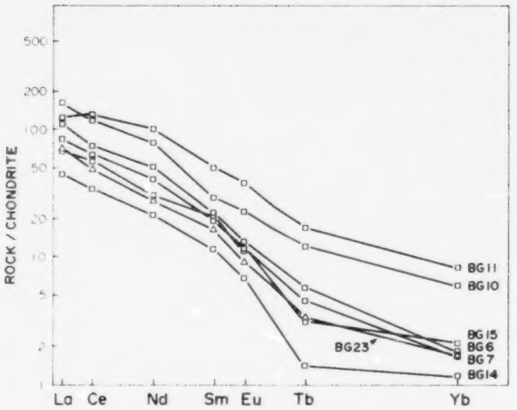

Figure 225.6 *Chondrite-normalized log-normal REE plot for Kilgour Lake Group granitoids. Triangles are for BG23 of the tonalitic sills.*

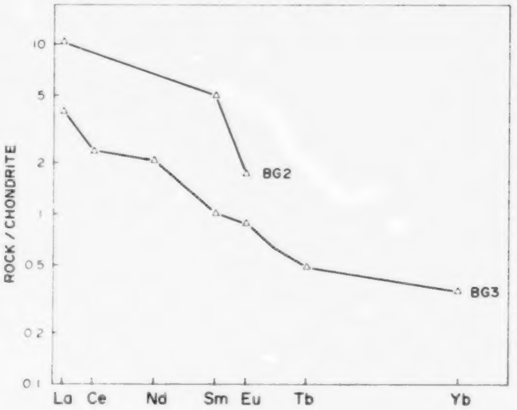

Figure 225.7 *Chondrite-normalized log-normal REE plot for tonalitic sills (data incomplete for BG2).*

area. If partial melting of metasediments has occurred to the extent of 10% to 50%, leaving a residue of quartz + garnet + plagioclase + biotite + amphibolite ± pyroxene ± orthoclase, Hanson showed that REE in the melt would be somewhat enriched in light REE, somewhat depleted in heavy REE, and would exhibit a small, negative Eu anomaly in presumed partial melts parental to the two-mica leucogranites. This partial melting scenario is consistent with the patterns in REE chondrite-normalized log-normal plots for the metasediments (Figure 225.5) and two-mica leucogranites (Figure 225.8). The presumed residuum is also consistent with the depletion in total iron, MgO, and CaO in the two-mica leucogranites (Table 225.1) as compared with the metasediments (Table 225.2).

CONCLUSIONS

On the basis of the past year's work we have reached the following conclusions:

1. More extensive sampling and analysis of the two-mica leucogranites of the Georgia Lake area reveal that the satellite plutons (MNW stock and Barbara Lake stock) are generally more highly fractionated than the main mass of the Glacier Lake pluton. Border zones of the Glacier Lake pluton are much more highly fractionated than the interior, and the fractionation in these zones rivals that of the satellite plutons. The satellite plutons, particularly the Barbara Lake stock, ap-

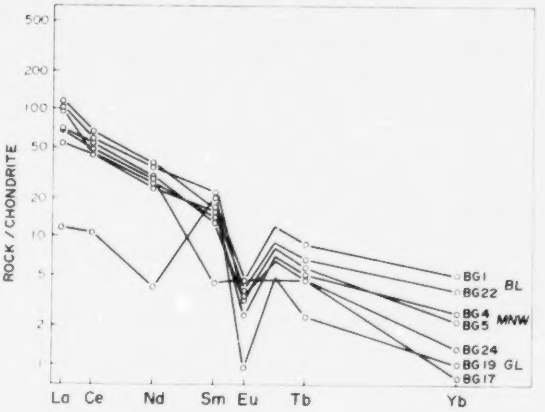

Figure 225.8 *Chrondrite-normalized log-normal REE plot for two-mica leucogranites from the Georgia Lake area (GL=Glacier Lake pluton, BL=Barbara Lake stock, MNW-MNW stock).*

pear to be the most likely sources for the highly fractionated rare-element pegmatites.

2. Metasedimentary rocks of the area are of relatively low-grade (upper greenschist to lowermost amphibolite facies) and show only weak increases, at most, in metamorphic grade with increasing proximity to the plutons of the area. Metasedimentary inliers in the Glacier Lake pluton are of similar low grade and have sharp, angular contacts with the granitoids. They are here interpreted as roof pendants. Field relationships and petrographic considerations thus appear to preclude an origin for the granitoids and pegmatites by the melting of *in situ* parental rocks.
3. "Barren" pegmatites of the Georgia Lake Pegmatite Field contain only minor, scattered occurrences of beryl, particularly in the vicinity of the MNW pegmatite. Geochemical zonation, as evidenced by trace element concentrations in muscovite and microcline separates, indicates a trend of decreasing fractionation eastward from the Southern Group (MNW, Swanson) rare-element pegmatites. A source for pegmatitic fluids in the vicinity of the Barbara Lake stock is thus suggested. No clear fractionation trends were discernible in "barren" pegmatites occurring east of the Central Group rare-element pegmatites.
4. Additional occurrences of Ta-Nb-Sn oxide minerals were discovered in rare-element pegmatites of both the Southern and Central Group, suggesting that there is additional potential for these minerals in the area.
5. REE studies support the hypothesis that sedimentary parental rocks similar to the metasediments of the Georgia Lake area yielded the two-mica leucogranites by the process of partial anatexis.

ACKNOWLEDGMENTS

Assistance in laboratory work at Lakehead University was provided by M. Artist-Downey, T.J. Griffith, K. Pringnitz, R. Churchman, D.L. Archibald, and T.C. McCuaig. C.M. Cermignani assisted with electron microprobe analyses at the University of Toronto. Analyses for selected elements were conducted by the Geoscience Laboratories of the Ontario Geological Survey through the support of G.C. Patterson, Thunder Bay District Geologist. Typing was done by W.C. Bons, and drafting was done by S.T. Spivak.

REFERENCES

Černý, P., Meinzer, R.E., and Anderson, A.J.
1985: Extreme Fractionation in Rare-Element Granitic Pegmatites: Selected Examples of Data and Mechanisms; Canadian Mineralogist, Volume 23, p.381-421.

Černý, P., Goad B.E., Hawthorne, F.C., and Chapman, R.
1986: Fractionation Trends of the Nb- and Ta-bearing Oxide Minerals in the Greer Lake Pegmatitic Granite and its Pegmatite Aureole, Southeastern Manitoba; American Mineralogist, Volume 71, p.501-517.

Goad, B.E., and Černý, P.
1981: Peraluminous Pegmatitic Granites and the Pegmatite Aureoles in the Winnipeg River District, Southeastern Manitoba; Canadian Mineralogist, Volume 38, p.26-43.

Hanson, G.N.
1978: The Application of Trace Elements to the Petrogenesis of Igneous Rocks of Granitic Composition; Earth and Planetary Science Letters, Volume 38, p.26-43.

Kissin, S.A., and Zayachkivsky, B.
1985: Genesis of Pegmatites in the Quetico Gneiss Belt of Northwestern Ontario—Rare-Element Pegmatites and Associated Granitoids of the Georgia Lake Pegmatite Field, Grant 225, p.186-199 *in* Geoscience Research Grant Program, Summary of Research 1984-1985, edited by V.G. Milne, Ontario Geological Survey, Miscellaneous Paper 127, 246p.

Masuda, A.
1975: Abundances of Monisotopic REE, Consistent with the Leedey Chondrite Values; Geochemical Journal, Volume 9, p.183-184.

Masuda, A., Nakamura, N., and Tanaka, T.
1973: Fine Structure of Mutually Normalized Rare Earth Patterns of Chondrites; Geochimica et Cosmochimica Acta, Volume 27, p.239-248.

Milne, V.G.
1962: The Petrography and Alteration of Some Spodumene Pegmatites near Beardmore, Ontario; Unpublished Ph.D. Thesis, University of Toronto, 242p.

Pye, E.G.
1965: Georgia Lake Area; Ontario Department of Mines, Geological Report 31, 113p.

Trueman, D.L., and Černý, P.
1982: Exploration for Rare-Element Granitic Pegmatites; p.463-493 *in* Granitic Pegmatites in Science and Industry, edited by P. Černý, Mineralogical Association of Canada, Short Course Handbook, Volume 8, 555p.

Zayachkivsky, B.
1985: Granitoids and Rare-Element Pegmatites of the Georgia Lake Area, Northwestern Ontario; Unpublished M.Sc. Thesis, Lakehead University, 234p.

Grant 227 Relationship Between Gold Deposits and the Tectonic Framework of the Abitibi Greenstone Belt in the Kirkland Lake–Larder Lake Area

D.J. Toogood and C.J. Hodgson

Department of Geological Sciences, Queen's University, Kingston

INTRODUCTION

The Archean (2.7 Ga) Abitibi Subprovince in Ontario is underlain by predominantly mafic volcanic assemblages and associated intrusions of tholeiitic, komatiitic, and calc-alkalic affinity (Jensen and Langford 1985). Intercalated with these rocks are significant felsic and komatiitic ultramafic successions and locally important sedimentary units. This study is concerned with the southern part of the area, in the vicinity of the Kirkland Lake and Larder Lake mining camps.

Trending east-west across the study area is a narrow, sinuous belt, approximately 60 km long and up to 5 km wide, of steeply dipping clastic sedimentary rocks, pyroclastic units, and trachyte flows (collectively referred to as the Timiskaming Group). Although the Timiskaming is reportedly in an unconformable relationship with the somewhat older mafic volcanic assemblages along its northern contact (Thompson 1946; Kimberly *et al.* 1985), those exposures of the contact seen by the authors are all faulted. A major shear zone, the Kirkland-Larder Lakes Break which is probably the westward extension of a similar feature in Quebec referred to as the Cadillac Fault, coincides over much of its length with the southern contact of the Timiskaming Group.

Stocks, plugs, and dikes of generally syenite composition intrude all the above assemblages.

There are two nationally important gold camps in the region with a total of three current producers. The Kirkland Lake camp is centred in Teck Township and contains the Lakeshore and Macassa Mines. The mineralization is associated with the Kirkland Lake Main Break, a fracture system cutting syenites and fluviatile sediments within the Timiskaming. The Larder Lake camp encompasses three townships: from east to west they are, McGarry, McVittie, and Gauthier. Most of the former producers, and the one extant producer, the Kerr Addison Mine, are related to the Kirkland-Larder Lakes Break.

The objective of the study, now the subject of two field seasons' investigation, is to document the spatial and genetic relationship existing between the main structural features and the gold deposits in this part of the Abitibi Greenstone Belt. Work so far has indicated that fracture systems and deformation zones have exercised the dominant control on the location of gold deposits.

LITHOSTRUCTURAL DOMAINS

As a result of studies in 1985, it has become evident that the region is divisible into a series of domains, each of which has a distinctive lithological association and/or structural imprint. Eight domains have been outlined, but further refinement can be expected with more detailed mapping. Some domains are large and irregularly shaped, while others are narrow zones of highly deformed rocks which separate the larger domains. The narrow zones with anomalously high deformation may conveniently be referred to as high-strain domains or deformation zones. It does not appear feasible as yet to make unequivocal stratigraphic or structural correlations across the deformation zones. Virtually all of the significant gold deposits occur within, or close to, the borders of the high strain domains.

The domains are illustrated in Figure 227.1 and are described briefly in the following paragraphs.

DOMAIN 1

In the extreme southwestern part of the area is an approximately 1 km wide deformation zone in direct contact with the Round Lake Batholith. The zone contains a variety of altered and strongly foliated rocks previously referred to as the Pacaud Tuffs (Ridler 1970). The foliation in the zone is a transposition foliation. It is coplanar with an extensive marginal envelope of gneissic banding and cataclastic foliation in the batholith (Lafleur and Hogarth 1981) suggesting that the deformation zone developed contemporaneously with the emplacement of the intrusion.

DOMAIN 2

To the northeast of domain 1 is a succession of mafic to ultramafic volcanic rocks belonging to the Wabewawa and Catharine Groups and felsic rocks of the Skead Volcanic Group which strike northwest and face uniformly away from the Round Lake Batholith. No folds or penetrative foliations were seen in this sequence. The contact with domain 1 is sharp and a shadow magnetic map of the area (Photo 227.1) clearly shows the northwest-trending stratigraphic units of domain 2 terminated at the boundary with domain 1.

DOMAIN 3

Separating domains 2 and 4 is a deformation zone, so far identified only on the basis of reconnaissance investigations. The domain trends southeast from the vicinity of the Adams Mine in the Boston Iron Formation to the Cathroy Larder Mine at the border of Catharine and McElroy Townships. The deformation zone occurs to the south of, and parallels, a prominent serpentinized peridotite and approximately demarcates the boundary between the Skead and Larder Lake Groups as shown by Jensen and Langford (1985). A strong transposition foliation is present in the zone together with sporadically developed alteration products. To the northwest, domain 3 merges with domain 5 near the Adams Mine.

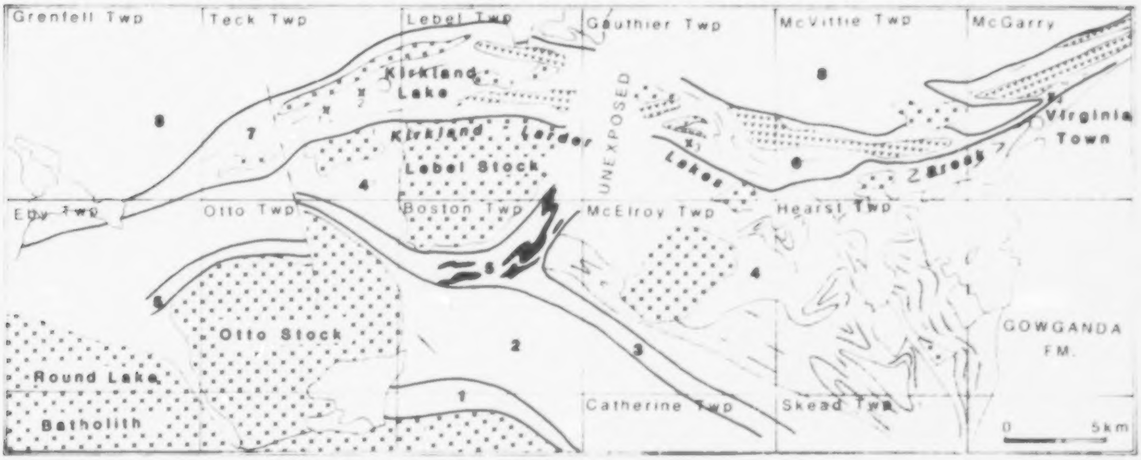
Grenfell Twp
Teck Twp
Lebel Twp
Gauthier Twp
McVittie Twp
McGarry
Kirkland Lake
8
7
Kirkland Larder Lakes Break
Lebel Stock
4
UNEXPOSED
X1
6
Virginia Town
Eby Twp
Otto Twp
Boston Twp
McElroy Twp
Hearst Twp
5
4
Otto Stock
2
3
1
Round Lake Batholith
Catherine Twp
Skead Twp
GOWGANDA FM.
0
5km

Figure 227.1. Lithostratigraphic domains in the Kirkland-Larder Lakes area: syenite and granite intrusions - cross pattern; trachytes in the Timiskaming - v pattern: sedimentary rocks (pre-Timiskaming?) south of the Kirkland-Larder Lakes Break - dot pattern; Boston Iron Formation - solid; X1 - Macassa Mine; X2 - Lakeshore Mine; X3 - McBean Mine; X4 - Kerr Addison Mine.

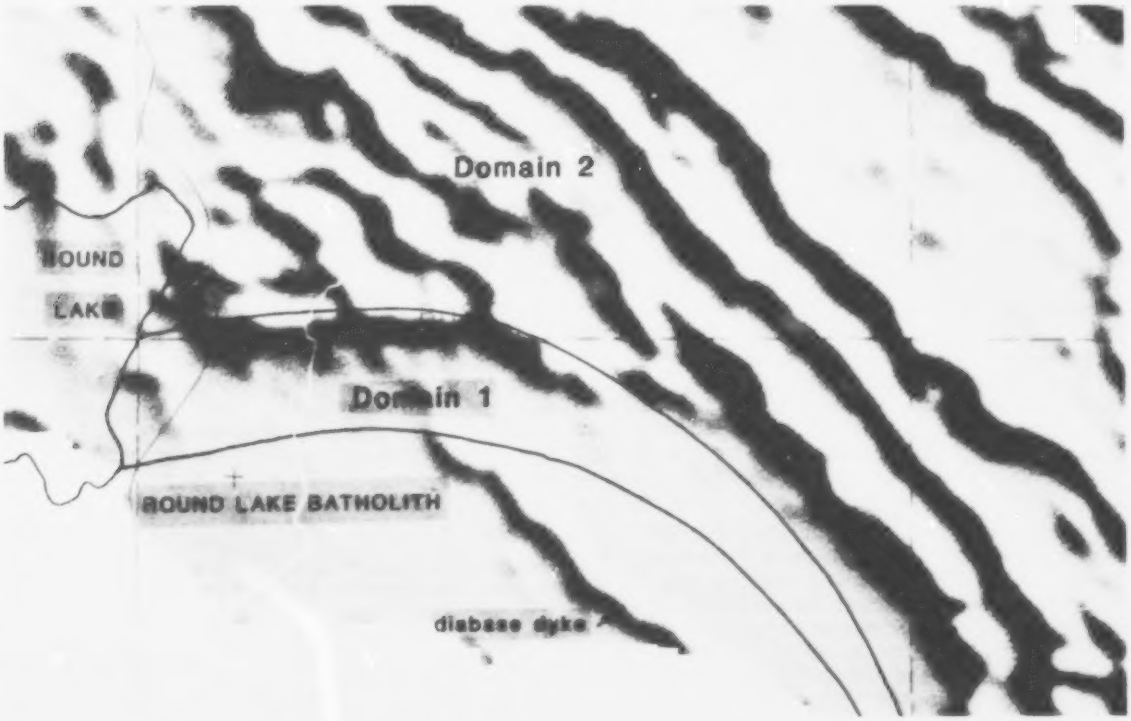
Domain 2
ROUND LAKE
Domain 1
ROUND LAKE BATHOLITH
diabase dyke

Photo 227.1. Enhanced shadow magnetic map showing the relationship between domains 1 and 2. Township boundaries 10 km apart.

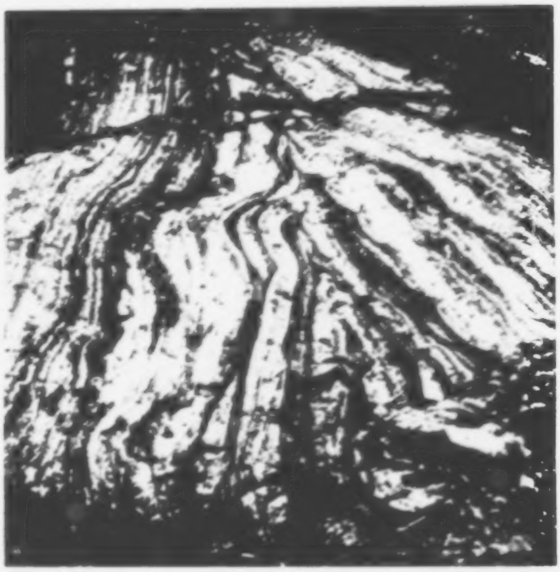

Photo 227.2. *Isoclinally folded Boston Iron Formation, Adams Mine. Hammer in foreground. Boston Township.*

DOMAIN 4

Where not overlain by Proterozoic cover rocks, domain 4 is bounded by deformation zones on all sides: domain 3 to the south; domain 5 to the west; and the Kirkland-Larder Lakes Break to the north, defining the contact with domain 6. Lithologically, the domain is characterized by mafic and ultramafic lavas with minor rhyolites and intercalated sediments which together constitute the Larder Lake Group, as defined by Jensen and Langford (1985). The clastic sedimentary rocks south of the Break have been the subject of some dispute. Thompson (1949) and Kalliokoski (1968) both pointed out the dissimilarities in clast composition between conglomerates north and south of the Break, and more recent detailed work (Hyde 1978) has confirmed a difference in provenance. Jensen and Langford (1985) have subsequently emphasized the total absence of komatiitic clasts in the north, whereas conglomerates immediately south of the Break contain abundant komatiite pebbles, often with spinifex texture. Considering the difference in the clast composition of the sedimentary assemblages between the two areas, we tentatively accept Jensen and Langford's (1985) view that the Timiskaming north of the Break should be distinguished as a separate lithostratigraphic unit, from those assemblages of sedimentary rocks to the south of the Break.

Unique to this domain are complex, large-scale fold patterns produced by the interference of a northwest-trending fold set and a north-northeast-trending fold set. This pattern is illustrated schematically by contacts and form lines in Figure 227.1. Outcrop-scale refolded folds confirm the geometry shown on the map. Both fold sets have steep to vertical plunges and have associated axial plane foliation.

The area to the west of the Lebel Stock is tentatively included as part of this domain, on the basis of reported similarity in volcanic stratigrapny.

DOMAIN 5

A 2 km wide deformation zone is present to the southeast of the Lebel Stock and it continues westwards, curving around the southern contact of the stock. The curvilinear nature of the deformation zone reflects the control exercised on the development of the structural pattern by the presence of large, rigid, intrusive bodies. The domain contains a wide variety of rock types, some of which are so highly strained and altered as to make recognition of the protolith difficult. Felsic units have been mapped as part of the Skead volcanic Group while mafic and ultramafic units, now represented by chlorite and talc-chlorite schists, have been placed in the Larder Lake Group (MERQ-OGS 1983). In addition, an isoclinally folded banded iron formation, the Boston Iron Formation, shows a strong spatial association with the domain (Photo 227.2).

A steeply dipping foliation is present which parallels the deformation zone boundaries and changes strike accordingly. The planar fabric is mainly a transposition foliation (Photo 227.3) but becomes mylonitic in some localities (Photo 227.4). In general, the folded Boston Iron Formation does not show a foliation, although thinly bedded horizons have been transposed. Domains 5 and 3 merge near the Adams Mine and two foliation directions can be seen in the same outcrop. However, no overprinting relationships were determined. The area where domains 5 and 6 would be expected to come into contact is obscured by glacio-fluvial deposits.

DOMAINS 6 AND 7—THE TIMISKAMING GROUP

The Timiskaming belt, as defined by Jensen and Langford (1985), separates domains 4 and 8 which have distinctly different lithological associations and structural styles. Because there are marked facies changes and equally significant variations in the degree of deformation between the eastern and western sections of the belt, a subdivision of the Timiskaming into two domains is warranted. The exact boundary between the domains has not been finalized but will eventually be placed somewhere in Lebel Township with domain 6 to the east incorporating Gauthier, McVittie, and McGarry Townships, and domain 7 to the west incorporating Teck and Grenfell Townships.

DOMAIN 6

Greywackes with subordinate argillite and conglomerate are the most abundant sediments in domain 6. Sandstone-argillite Bouma Sequences, graded bedding, and sole markings are commonly encountered features which help define a predominantly resedimented facies (Hyde 1978). Intercalated with these units are thick, laterally continuous trachyte flows. The width of the Timiskaming, of Jensen and Langford (1985), varies from about 3 km in Gauthier Township, to possibly zero in central McGarry Town-

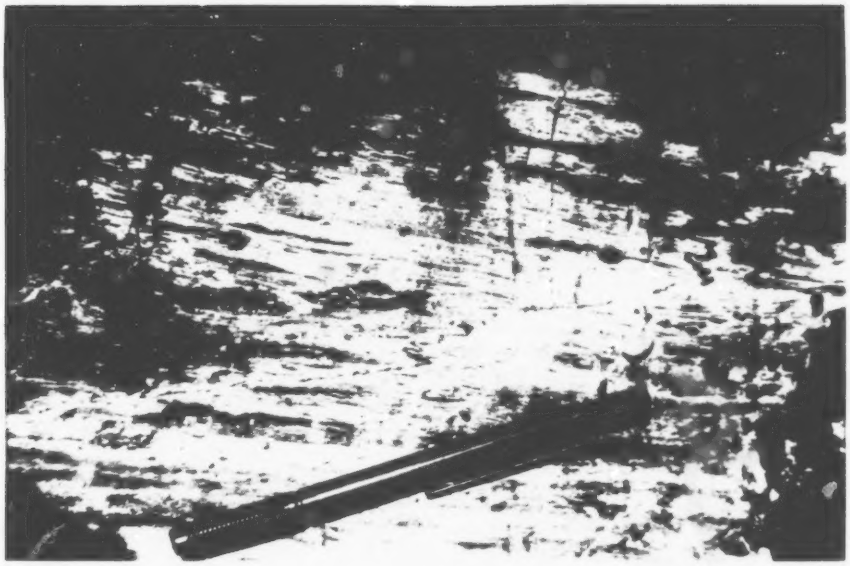

Photo 227.3. *Transposition foliation, domain 5, Boston Township.*

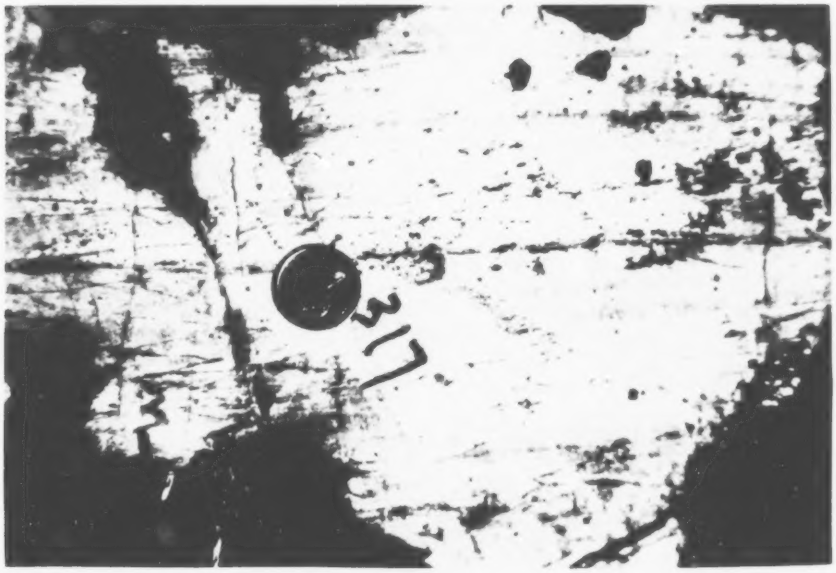

Photo 227.4. *Mylonite, domain 5, Otto Township.*

ship. With some exceptions, the beds dip and face south at moderate to steep angles.

Domain 6 is a deformation zone. The sedimentary rocks, in particular, are strongly foliated and lineated. The zone appears to be related to the highly strained, extensively altered schistose rocks along the Kirkland-Larder Lakes Break, which forms the southern boundary of domain 6. Although the Break is the most continuous and important zone of highly strained rocks, other discrete zones with comparable high strains occur in domain 6, especially along the trachyte contacts, and splays off the Break at points where it changes direction. Well developed in these zones are two planar fabrics intersecting at angles of usually 30° or less which were both previously given the designation S since age relationships could not be determined (Toogood and Hodgson 1985). Reinvestigation of many outcrops has now indicated that these fabrics appear to be shear-related S-C foliation patterns combining a shear-parallel C surface and a flattening S surface (Berthe *et al.* 1979). If this interpretation of the fabrics is correct, their geometric

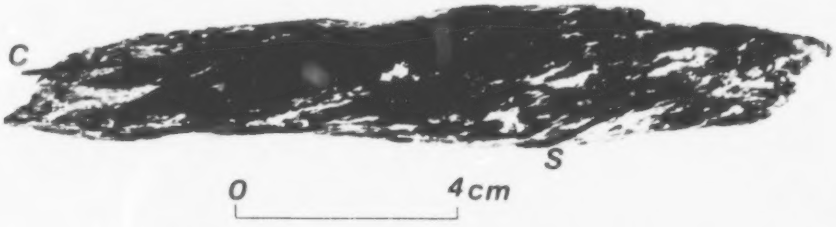

Photo 227.5a. *Shear-related S-C foliations in the Kirkland-Larder Lakes Break. McBean Mine, Gauthier Township.*

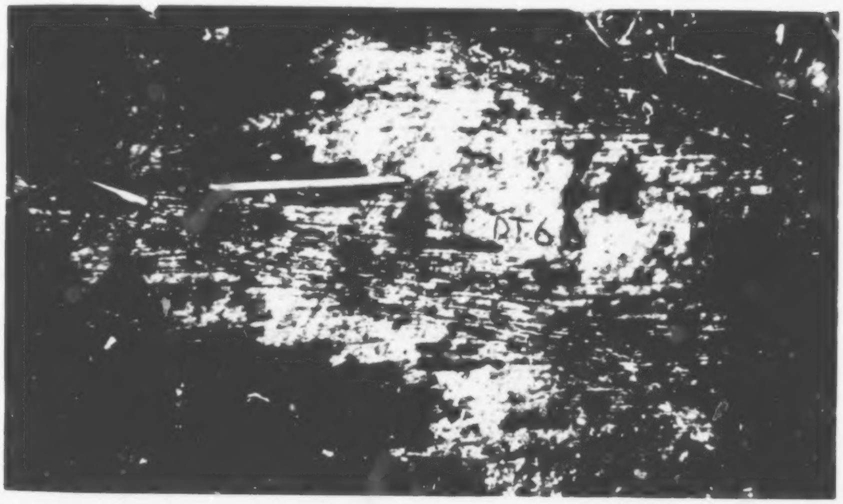

Photo 227.5b. *Dextral displacement in shear zones in the Kirkland-Larder Lakes Break nea the Kerr Addison Mine, McGarry Township.*

relationship would indicate dextral strike slip movement in the Kirkland-Larder Lakes Break. The combination of fabrics has been observed at the Upper Canada Mine, the McBean Mine, the Omega Mine, and in the carbonate ore at the Kerr Addison Mine (Photos 227.5a and 227.5b). Similar fabrics, resulting in the development of lensoid "fish" (Hanmer 1986) were observed by the authors in the Cadillac Fault across the provincial border near Rouyn (Photo 227.6). The shear-related foliations change orientation as the Break changes strike. On the scale of the Abitibi Subprovince, the strike of the Break is east-west, but in Gauthier Township it has a 120° trend, and, in parts of McGarry and McVittie Townships, the strike is 060°.

Overprinting these earlier fabrics, is a subvertical foliation, which maintains a constant northeast orientation regardless of changes in strike of the Break. This foliation can occur in the form of a flattening surface, a pressure solution cleavage, or a crenulation cleavage (sometimes associated with folds). While the earlier fabrics are confined to narrow zones, the younger overprint is pervasively developed throughout the Timiskaming and forms the regional foliation. It is tentatively suggested that the foliation might be related to subsequent expansion in width of the shear zone with progressive dextral displacement.

Work during the first field season, and previous work by Thompson (1943) and Downes (1979), established that the Kirkland-Larder Lakes Break in this domain forms a boundary across which there is a marked change in lineation plunge direction. It was also reported (Toogood and Hodgson 1985) that extension lineations and intersection lineations are parallel along the Break, which posed a question of kinematic interpretation. Further study in the area indicates that the northeast-trending fabric, south of the Kirkland Lake Break, is a domain 4 foliation predating the development of the shear zone; the steep south and southwesterly plunging lineation in this area is an extension lineation which is present only within this domain. Within, and north of, the Break, there is a separate, steeply northeasterly plunging intersection lineation related to the S-C fabric pattern.

Collectively, these observations confirm the identity of the Kirkland-Larder Lakes Break as an impor-

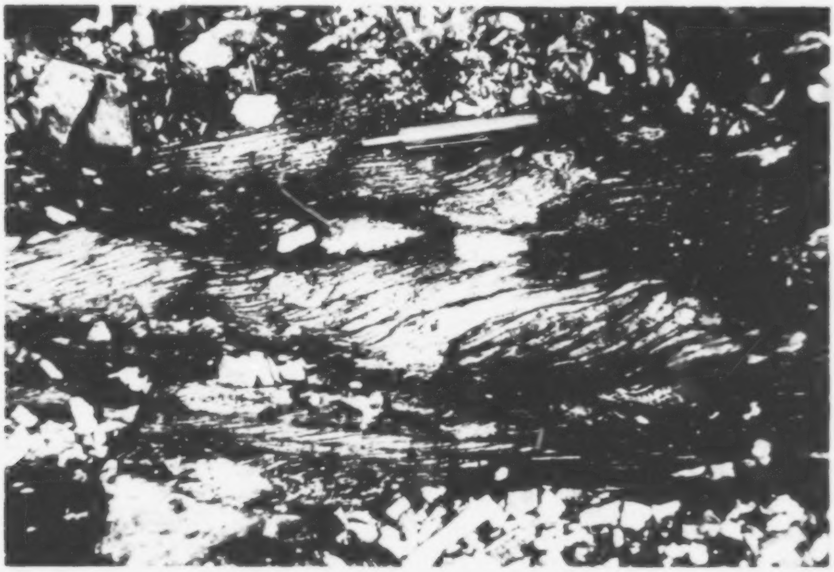

Photo 227.6. *Shear-related S-C foliations in the Cadillac-Larder Fault, Rouyn, Quebec. Compare with Hanmer (1986), Photo 227.5b.*

tant crustal break across which there is both a stratigraphic and structural discordance.

DOMAIN 7

The Timiskaming in Teck and Grenfell Townships is composed almost entirely of fluviatile conglomerates with minor argillites and various pyroclastic deposits. The resedimented facies that is dominant in domain 6 is practically absent.

Deformation in this domain is far less strongly developed than farther east. Where two, and sometimes three, foliations are common in a single domain 6 outcrop, the western Timiskaming rarely shows more than one, and there are areas where foliations are entirely absent. The single foliation trends northeast and is probably the same northeast-trending regional foliation seen in domain 6. No S-C foliations were seen along the Kirkland-Larder Lakes Break in this area, although this may be due to poorer outcrop.

Foliation distribution allows the subdivision of domain 7 into three zones which appear to be bounded by fracture systems (Figure 227.2). The most northerly of the three zones is limited to the south, by the Kirkland Lake Main Break, and contains either a very weakly spaced cleavage or a flattening surface in the conglomerates which is typically seen as a slight flattening of the mafic clasts only. The central zone contains no pervasive foliations, and its southern limit is at the Amalgamated Kirkland-Blanche River Fault and the Murdock Creek fault systems. The southern zone is the most strongly foliated and the northeast-trending fabric is pervasively developed.

The Kirkland Lake Main Break trends about 065° and is less than 1 m wide where seen on the surface by the authors. It is a brittle-ductile fault zone with both shear generated foliations and fractures. In central Teck Township, zones of an *en echelon* quartz-filled fractures trending 100° are associated with the Main Break and may represent a Riedel shear set.

It is interesting to note that, while the major gold deposits in domain 6 are related to the Kirkland-Larder Lakes Break, and those in domain 7 are related to the Kirkland Lake Main Break, they both share the same association with a structural discontinuity which separates blocks with different structural histories. It is also noteworthy that in domain 6 there are no present- or past-producing mines in the central undeformed zone, while both the foliated zones host gold deposits.

To the south of the Kirkland-Larder Lakes Break, domain 4 foliations trend parallel to the contact of the Lebel Stock and an unnamed syenite stock to the east. The margins of both intrusions also have a contact-parallel foliation except where the stocks are cut by the Break, in which case the intrusives are fractured, veined, and carbonatized. Clasts of foliated syenites typical of the stock marginal zones were found in conglomerates in Teck Township. These relationships suggest that the stocks predate the movement within the Break, and may have been a source area for the Timiskaming Group.

DOMAIN 8

North of the Timiskaming is an extensive, unsubdivided domain, containing a monotonous sequence of mafic volcanic rocks belonging to the Kinojevis Group, and less abundant felsic volcanics of the Blake River Group. No foliations are pervasively developed in this domain, which has not been studied in detail. Folds with shallow plunges and axial traces striking approximately east-west are shown on government maps (MERQ-OGS 1983), but none were re-

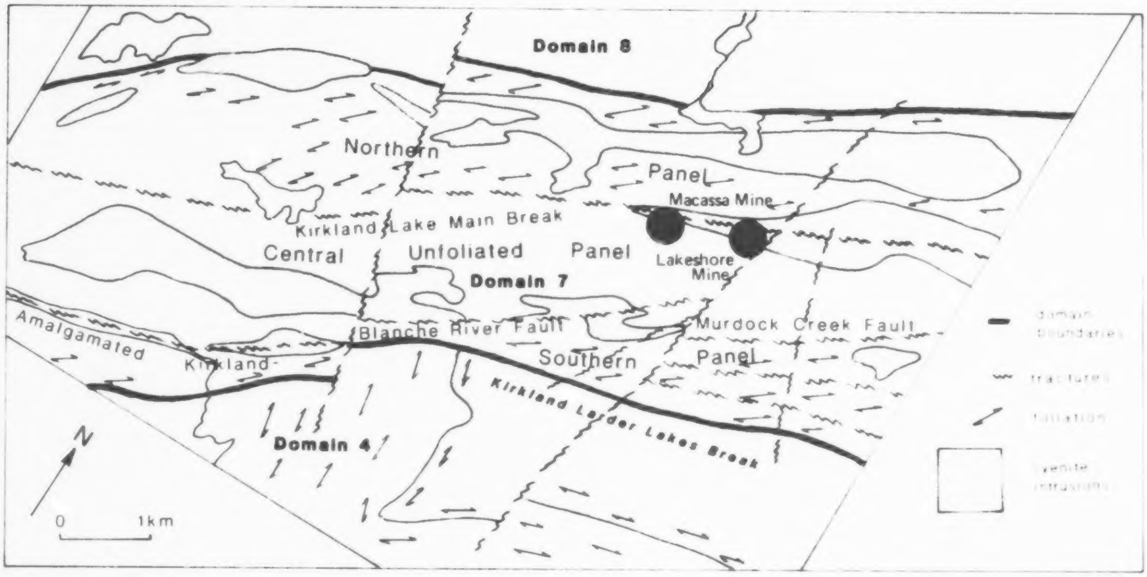
Domain 8
Northern
Panel
Macassa Mine
Kirkland Lake Main Break
Central
Unfoliated
Panel
Lakeshore Mine
Domain 7
Amalgamated
Kirkland
Blanche River Fault
Southern
Panel
Murdock Creek Fault
Kirkland Larder Lakes Break
Domain 4
N
0
1km
domain boundaries
fractures
foliation
syenite intrusions

Figure 227.2. Foliation and fracture patterns in domain 7 (Timiskaming Group) and adjacent part of domain 4, Teck Township.

corded in the areas examined by the authors. In McGarry Township, fold-like patterns are visible on the township geological map (Thompson 1943) defined by lithological units in the Kinojevis Group (Spectacle Lake Anticline) and the contact of the Timiskaming with domain 8 (Beaver Lake Syncline). The significance of these structures remains to be determined.

CONCLUSIONS

The area is composed of a number of relatively weakly deformed lithostructural domains, separated by linear high strain zones. The best gold deposits occur in or near the high strain zones. Structural and stratigraphic correlations cannot, as yet, be confidently made across most domain boundaries.

REFERENCES

Berthe, D., Choukroune, P., and Jegouzo, P.
1979: Orthogenesis, Mylonite, and Non-Coaxial Deformation of Granites: The Example of the South Armorican Shear Zone; Journal of Structural Geology, Volume 1, p.31-42.

Downes, M.S.
1979: Kirkland Lake Area, Stratigraphic Mapping, District of Timiskaming; Ontario Geological Survey, Miscellaneous Paper 90, p.121-125.

Hanmer, Simon
1986: Asymmetrical Pull-Aparts and Foliation Fish as Kinematic Indicators; Journal of Structural Geology, Volume 8, p.111-122.

Hyde, R.S.
1978: Sedimentology, Volcanology, Stratigraphy, and Tectonic Setting of the Archean Timiskaming Group, Abitibi Greenstone Belt, Northeastern Ontario, Canada; Unpublished Ph.D. Thesis, McMaster University, 422p.

Jensen, L.S., and Langford, F.F.
1985: Geology and Petrogenesis of the Archean Abitibi Belt in the Kirkland Lake Area, Ontario; Ontario Geological Survey, Miscellaneous Paper 123, 130p.

Kalliokoski, J.
1968: Structural Features and Some Metallogenic Patterns in the Southern Part of the Superior Province, Canada; Canadian Journal of Earth Sciences, Volume 5, p.1118-1208.

Kimberly, M.M., Jensen, L., Grandstaff, D.E., and Foster, R.F.
1985: Archean Paleosol: Weathered Kinojevis Basalt Beneath Fluvial Timiskaming Sandstone (Abstract); Geological Society of America, Annual General Meeting.

LaFleur, J., and Hogarth, D.D.
1981: Geology of the Round Lake Batholith, Kirkland Lake Area, Ontario; Geological Survey of Canada, Paper 81-1A, p.91-94.

MERQ-OGS
1983: Lithostratigraphic Map of the Abitibi Subprovince, Ontario Geological Survey/Ministere de l'Energie et des Ressources, Quebec; catalogued as "Map 2484" in Ontario and "DV83-16" in Quebec, scale 1:500 000.

Ridler, R.H.
1970: Relationship of Mineralization to Volcanic Stratigraphy in the Kirkland-Larder Lakes Area, Ontario; Geological Association of Canada, Proceedings, Volume 21, p.33-42.

Thompson, J.E.
1943: Geology of the McGarry and McVittie Townships; Ontario Department of Mines, Annual Report for 1941, Volume 50, Part 7, 99p.
1946: The Keewatin-Timiskaming Unconformity in the Kirkland Lake District; Royal Society of Canada, Transactions, Volume 40, Section 4, p.113-124.
1949: Geology of Hearst and McFadden Townships; Ontario Department of Mines, Annual Report for 1947, Volume 56, Part 8, p.1-34.

Toogood, D.J., and Hodgson, C.J.
1985: A Structural Investigation Between the Kirkland and Larder Lakes Gold Camps; Ontario Geological Survey, Miscellaneous Paper 119, p.200-204.

Grant 230 Petrologic, Chemical, Isotopic, and Economic Potential Studies of the Nipissing Diabase

P.C. Lightfoot, D. Conrod, A.J. Naldrett, and N.M. Evensen

Department of Geology, University of Toronto, Toronto

ABSTRACT

The Nipissing Diabase comprises a suite of tholeiitic rocks and associated differentiates that extends from Cobalt to Sault Ste. Marie, Ontario, in the form of undulating sills, cone sheets, and dikes. It, therefore, represents a major igneous event around 2150±50 Ma (Rb-Sr date, Fairbairn *et al.* 1969; Van Schmus 1965) which most likely represents the intrusive portion of an eroded Continental Flood Basalt (CFB), where magmas rose as dikes which cut the underlying Archean granitoid rocks, and spread out laterally in the Huronian metasediments.

Mafic intrusions associated with flood basalt volcanism and rifting environments often contain significant concentrations of magmatic sulphides rich in Ni-Cu-Co and platinum group elements (PGE); examples include the Triassic-aged intrusion hosting the Noril'sk Deposit which feeds the Siberian flood basalts, and the Duluth Complex, Minnesota, which feeds the Keweenawan basalt, where incorporation of external sulphur caused sulphide segregation in the magmas and concentration of Ni-Cu and PGE's. Sudbury is an example where incorporation of external silica may have caused sulphide segregation.

The Nipissing Diabase is spatially associated with different types and styles of mineralization across its extent. Progress is being made using trace elements to determine whether crustal contamination has played a role in the petrogenesis of the rocks and associated mineralization.

INTRODUCTION

This report summarizes work completed in three occurrences of Nipissing Diabase in the study area shown in Figure 230.1. The Bruce Mines and Basswood Lake Intrusions were chosen from the western sector, the Bonanza Lake Intrusion from the centre, and the Portage Bay and Cross Lake Intrusions from the east of the study area. Intrusions in the eastern sector of the study area generally contain associated Ni and Co arsenides, Ag veins, and Cu in carbonate veins. Intrusions in the centre of the study area have associated PGE in some Ni-sulphides (e.g. Rathbun Lake). The Basswood Lake and Bruce Mines Intrusions have associated Cu-sulphide-rich carbonate veins. The areas were chosen to represent the entire spectrum of Nipissing rocks from east to west and to include those associated with different types and styles of mineralization (Card and Pattison 1973).

The possibility that contamination of mafic magmas by silica-rich crustal material may have triggered sulphide segregation at Sudbury has been suggested

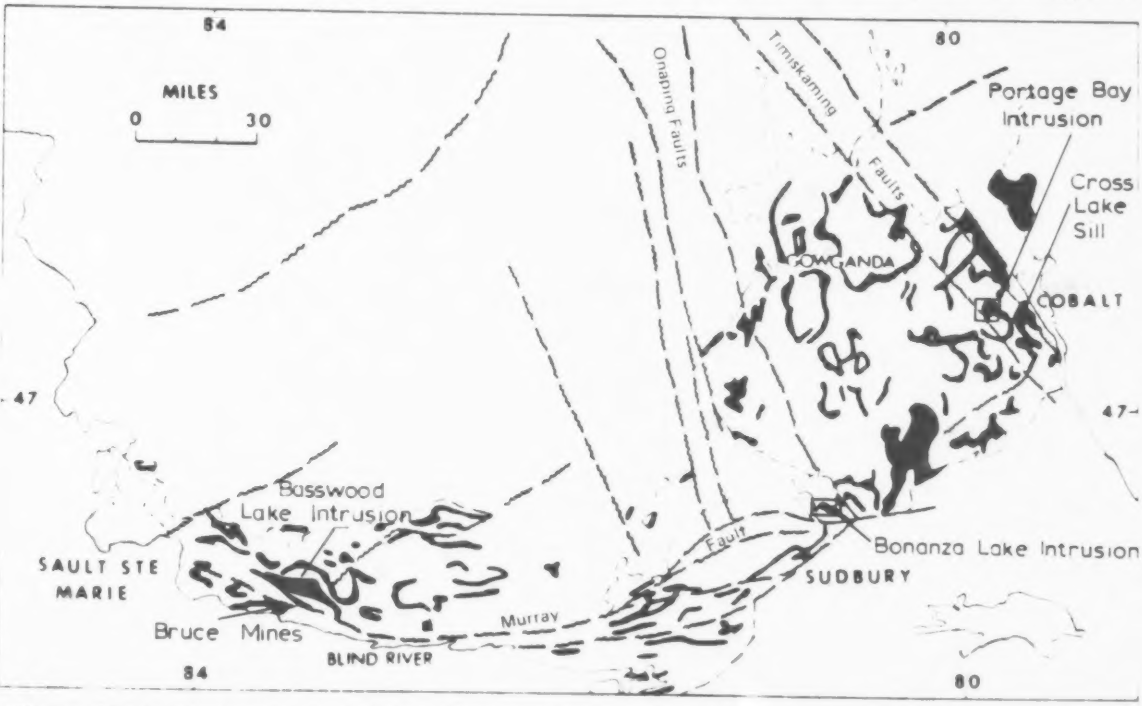

Figure 230.1. Distribution of Nipissing Diabase Intrusions throughout Ontario (modified from Card and Pattison 1973).

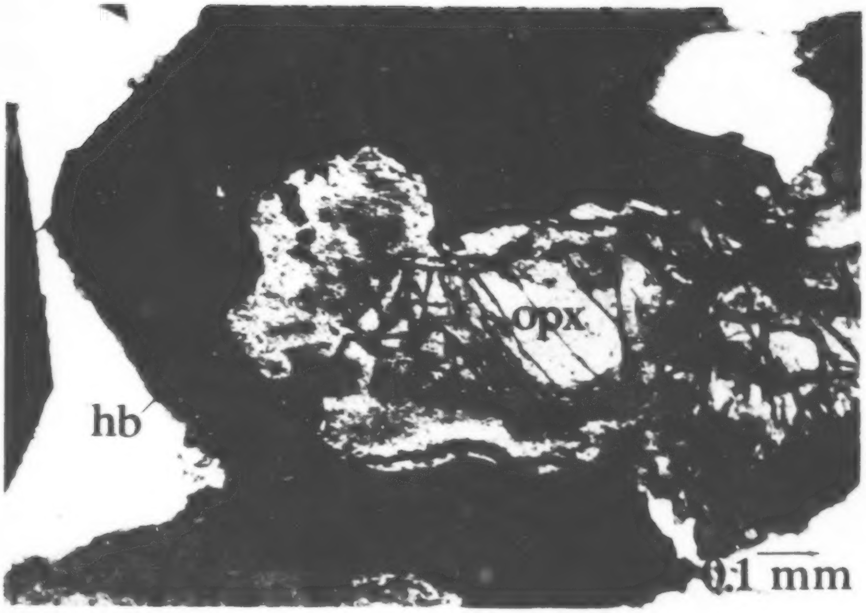

***Photo 230.1a.** The replacement of orthopyroxene by hornblende in the granodioritic-gabbro transition phase of the Bonanza Lake Intrusion (length of photo = 1.38 mm).*

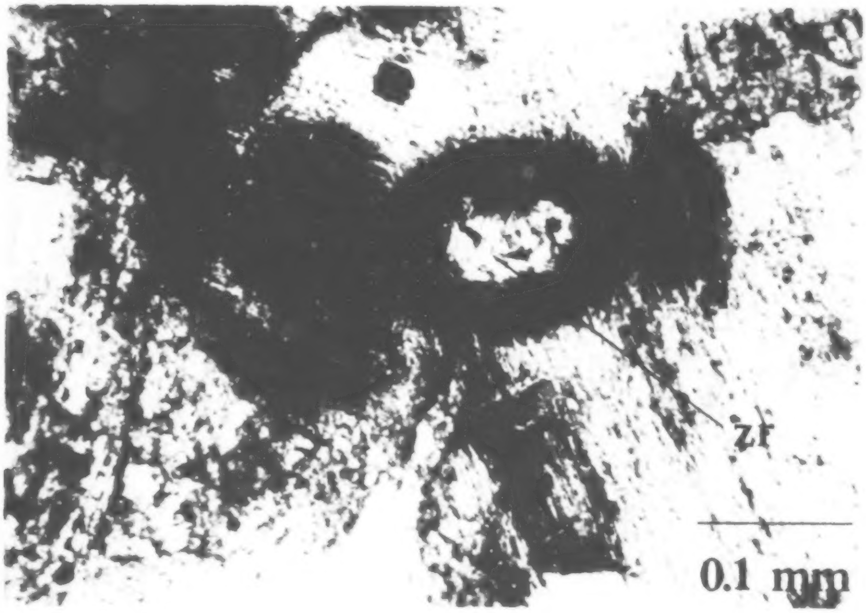

***Photo 230.1b.** Euhedral zircon in the basal quartz diabase of the Cross Lake Intrusion (length of photo = 0.55 mm).*

by Rao *et al.* (1985). The geochemical fingerprints of contaminated basalts are often recognizable on the basis of the ratios of Large Ion Lithophile (LIL) elements (Rb, K, Th) to High Field Strength (HFS) elements (e.g. Zr, Y, Ta, Hf). This study uses mineralogical data and whole-rock geochemical data to investigate the potential that these intrusions represent important hosts for magmatic Ni-sulphides.

GEOLOGY, PETROLOGY, AND MINERALOGY

Mapping and petrographic studies undertaken during this investigation indicate that the thick, sill-like intrusions (such as Cross Lake Sill, Bonanza Lake, Basswood Lake, and Bruce Mines Intrusions) are characterized by: basal and capping quartz-diabase in which plagioclase, inverted pigeonite, and augite grow in a diabasic texture; a thick gabbro-norite zone in the lower to central regions of the sill in which hypersthene replaces the inverted pigeonite; a varied texture diabase above the hypersthene zone, containing pods of pegmatitic gabbro within the quartz diabase; and in some intrusions, the presence of granodioritic and granitic differentiates (not developed in the Cross Lake Sill section). Dike-like intrusions (e.g. the Portage Bay Intrusion) appear to be enriched in the more differentiated pegmatitic gabbros and granodioritic phases, and lack the hypersthene zone of the sills. Olivine was observed only in intrusions of the eastern sector within the basal quartz diabase and the hypersthene zone. The diabasic texture is best developed in the quartz-diabase zones.

Petrographically, the transition from gabbro-norite into the granodioritic differentiates can be observed by the replacement of pyroxene by hornblende, and an increase in the proportion of potassic feldspar (Photo 230.1a). The presence of small amounts of euhedral zircon in the diabase, as well as in the differentiated rocks of the intrusions, suggests that early zircon may have crystallized in the melt (Photo 230.1b).

MINERAL CHEMISTRY

Mineral chemical studies have been somewhat limited due to their dependence on the presence of unaltered crystals. The microprobe analyses of orthopyroxene, plagioclase, and olivine from samples of the Nipissing rocks from the central and eastern sectors of the study area, show trends compatible with the trends in trace element compositional variation.

Anorthite content of the generally normally zoned plagioclase varies from about 70 to 90 for both the Bonanza Lake and Cross Lake Intrusions (Figures 230.2a, and 230.2b). Both intrusions show an increase in An content within plagioclase away from the lower contact and into the hypersthene-bearing gabbro. The An content of plagioclase decreases from the upper hypersthene zone towards the top of the intrusions.

The apparent reverse differentiation trend from the base toward the centre of the intrusions is also reflected in the Fo content of the olivine within the Cross Lake Sill (Figure 230.3), and in the Mg-number of the orthopyroxene crystals along a north-south traverse through the Bonanza Lake Intrusion (Figure 230.4a). Little to no cryptic variation occurs in the cores of orthopyroxene crystals along a second north-south traverse of the Bonanza Lake Intrusion. However, the rims of the orthopyroxenes show an increase in the Mg-number away from the lower contact towards the centre of the intrusions (Figure 230.4b). No apparent cryptic variation for the given sampling interval was observed in the Mg-number of orthopyroxene from the Cross Lake Sill (Figure 230.4c).

The reverse differentiation trend from the base of the intrusions towards the centres is in no way unique, and has been documented in many other intrusions including: Finn *et al.* (1982) for the Wanapitei Intrusion of the Nipissing magmatic event, and by Lightfoot *et al.* (1984) for the Waterfall Gorge section of the Insizwa Complex in the Karoo of South Africa.

The mineral chemistry data may suggest that the Nipissing magma did not enter its present location as one simple single pulse followed by fractionation during cooling. The next phase of the project will attempt to couple these observations with variations in whole-rock compositional data to evaluate whether or not multiple intrusions of variably fractionated and/or mixed magmas may be responsible for the variations through the sills. For the present, this problem is tackled on a more general level by investigating the role of fractional crystallization and mixing in terms of the trace element data.

GEOCHEMICAL STUDIES

Geochemical data for representative samples of diabase were chosen from three regions of the study area (Figures 230.5 to 230.8). Major- and trace-element data were determined by conventional X-ray fluorescence spectroscopy (XRF) techniques (Lightfoot 1985; Potts *et al.* 1984, 1985). Rare earth elements (REE) and other trace elements were determined by Instrumental Neutron Activation Analysis (INAA) using the SLOWPOKE reactor and counting facilities at the University of Toronto.

Geochemical studies focus on four major themes:

1. An evaluation of the geochemical variations across the thickness of each sill or dike, and between different sills and dikes from throughout the study area.
2. The characteristic fingerprints exhibited by the diabases relative to other Continental Flood Basalts (CFB).
3. The relative amounts of fractional crystallization and cumulus enrichment exhibited by the rocks.
4. The composition of the phase extract responsible for the compositional variations within the sills.

Each of the intrusions investigated shows a wide range of major- and trace-element compositional variation (Figures 230.5 to 230.7). The Basswood Lake, Bonanza Lake, and Cross Lake Intrusions show a depletion in the incompatible elements (Zr, Y, Nb, and Rb) away from the lower contact (chill and basal quartz diabase) into the overlying hypersthene diabase. Above this level, there is an enrichment in the incompatible elements from the hypersthene diabase into the upper quartz diabase and overlying granophyres (not developed at Cross Lake Sill). The Portage Bay Intrusion shows an enrichment in incompatible elements from the western and eastern contacts towards the centre of the intrusion. Interestingly, these variations compare well with the variations in mineral chemistry documented above (Figure 230.8).

These geochemical observations are also consistent with earlier field, petrographic, and mineralogical studies which suggest that the Basswood Lake, Bonanza Lake, and Cross Lake Intrusions have a sill-like morphology, while the portion of the Portage Bay Intrusion that was sampled appears to be a dike.

The petrogenesis of these rocks is now examined with reference to Figure 230.9 which shows the variation in Mid-Ocean Ridge Basalt (MORB)-normal-

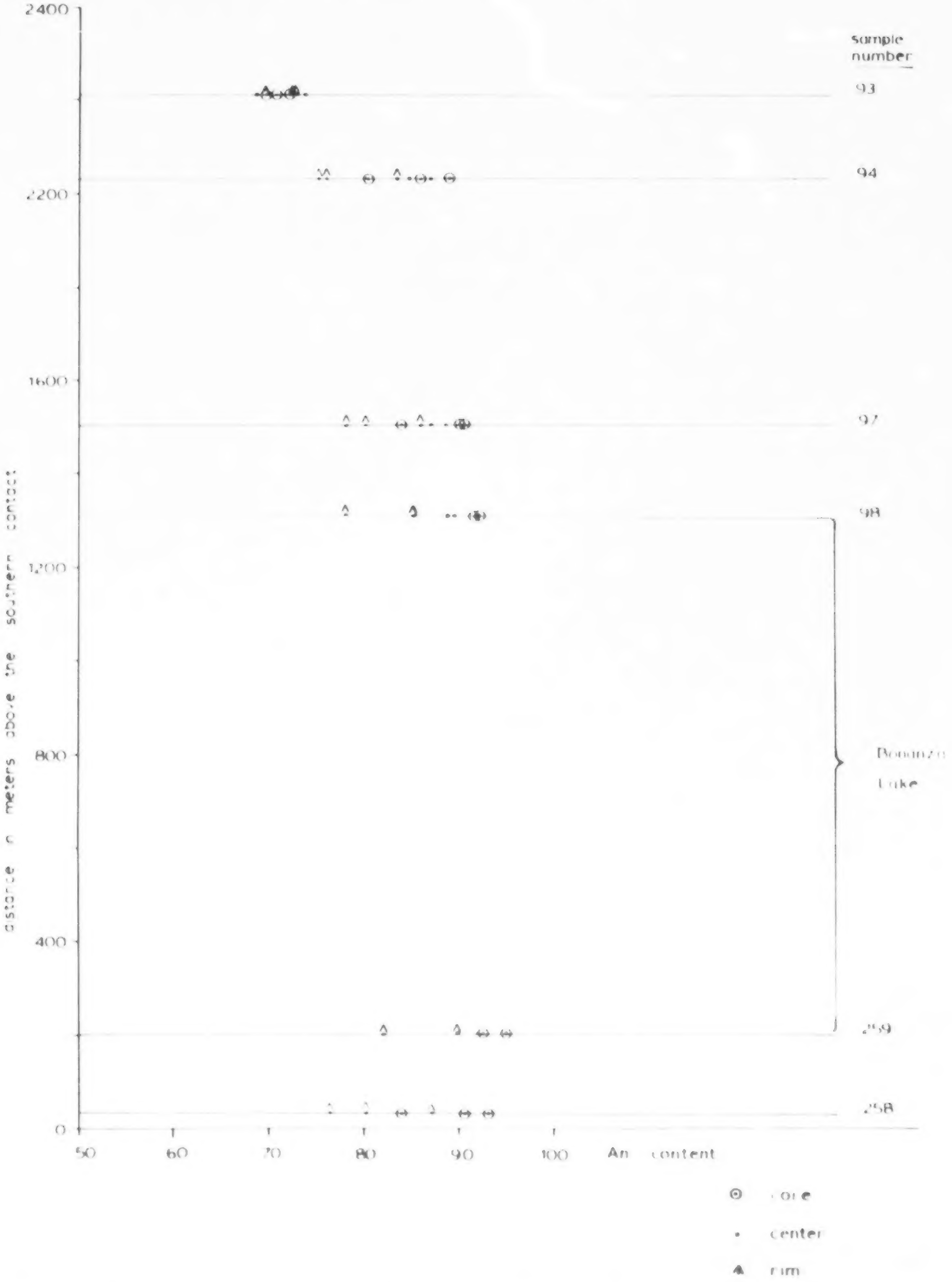

Figure 230.2a. Variation in anorthite content across the Cross Lake Sill

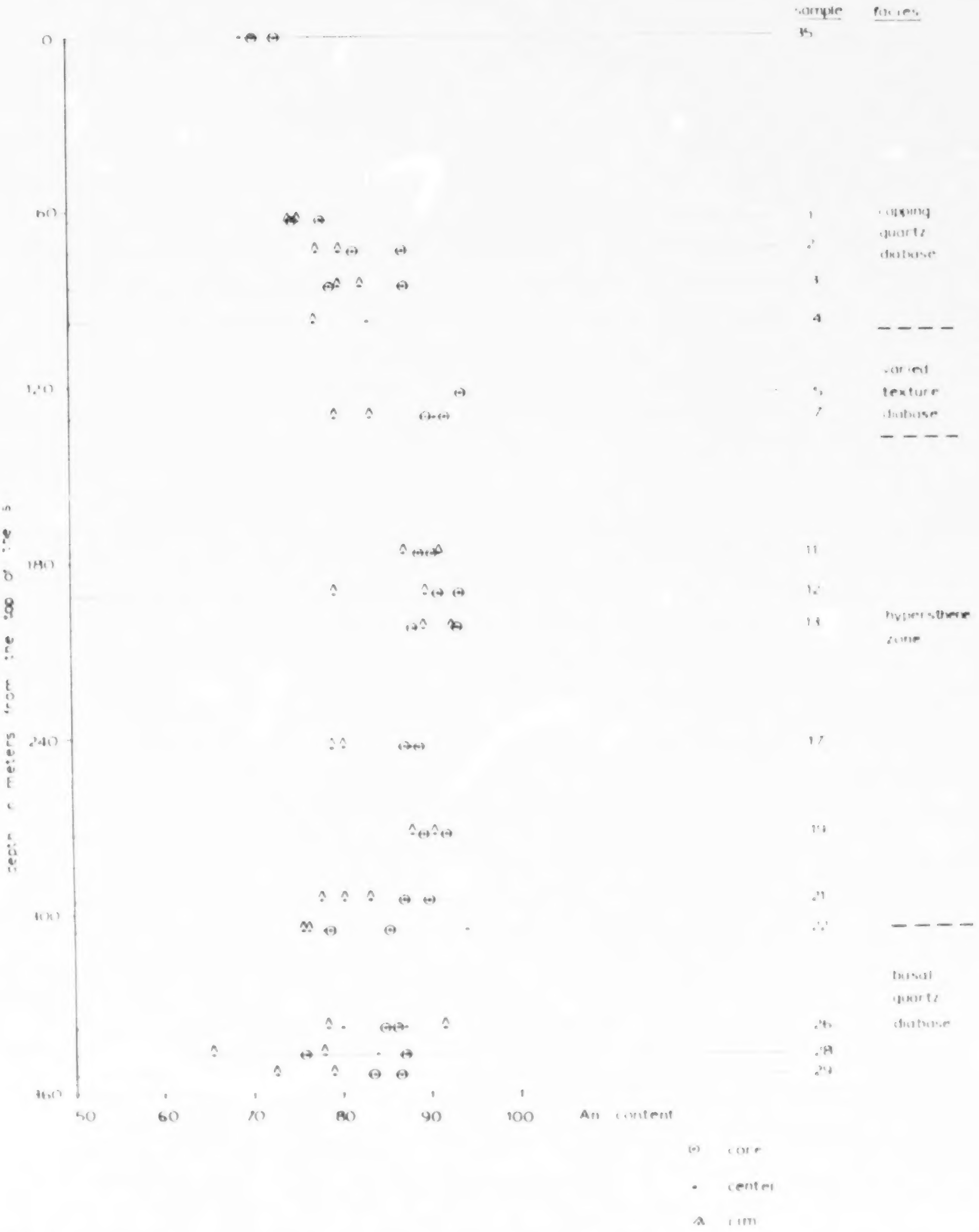

Figure 230.2b. Variation in anorthite contents across the Bonanza Lake Intrusion

ized trace element concentrations (Pearce 1983) for averages of representative samples of mafic and evolved diabase and granophyre from the western sector of the study area (Basswood Lake and Bruce Mines, Table 230.1). The data for the average Nipissing samples cover the entire spectrum of com-

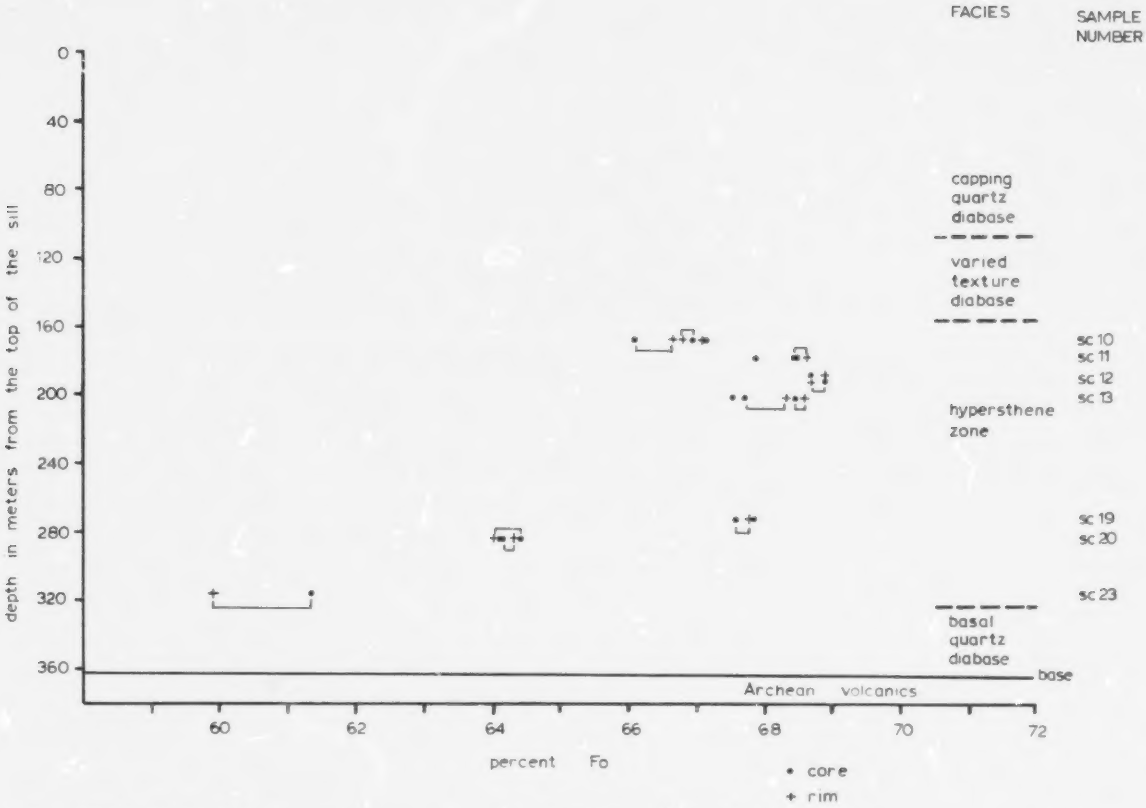

Figure 230.3. Variation in forsterite content of olivine across the Cross Lake Intrusion.

positional variation in all intrusions, and show a remarkably coherent sense of trace element enrichment through the intrusions, with very little evidence to suggest that the trace elements were excessively mobile under low grade metamorphism and alteration conditions, or strongly contaminated with crustal material to variable extents.

Also shown in Figure 230.9 are representative averages for CFB derived directly from an enriched mantle source (Mahabaleshwar basalts of the Deccan Province; Lightfoot 1985) and mantle-derived basalts which have been contaminated with upper crust (Bushe basalt of the Deccan Province; Lightfoot 1985). There is a remarkable correspondence between the Nipissing spidergrams and that of the contaminated Deccan basalt, while there is little evidence for an enriched mantle signature in these rocks of the type recorded in the Mahabaleshwar basalts. Also shown in Figure 230.9 are chondrite-normalized REE profiles for representative samples included in the average data, together with representative samples from the central and eastern sectors of the study area, which detail the basal reversal in compositional variation. The samples all show a strong overall REE enrichment, but a strong LREE/HREE enrichment from the diabases into the granophyres. The basal reversal in incompatible element enrichment is also shown by the REEs. In both the case of the spidergram and REE plots, the Portage Bay chilled margin is enriched in all incompatible elements relative to the more mafic diabases of the intrusion.

In order to investigate more fully the range and source of the wide spectrum of compositional variation, La is used as an index of the state of enrichment of the rocks in highly incompatible elements. Variations in composition are discussed relative to this element. Variation diagrams are plotted in Figures 230.10 to 230.13; in each case, samples from different intrusions are distinguished. The rationale for using La lies in the highly incompatible nature of this element, and the 1:1 enrichment which La exhibits relative to Ta (which, conventional wisdom would suggest to be highly incompatible; Pearce 1983). Distribution coefficients are given in Table 230.1. The plots of Ta and Ce versus La produce a single tight linear trend for all intrusions, anchored at the trace element-depleted extreme by more pyroxene-rich diabases, and at the enriched extreme by granophyres. The representative averages plotted in the spidergram together with the composition of the Portage Bay chilled margin are shown. Also shown are 1:1 vectors which assume that these elements are all equally incompatible ($K_d=0$) in phases involved in fractional crystallization, and that the representative mafic end members, presented in Table 230.1, are

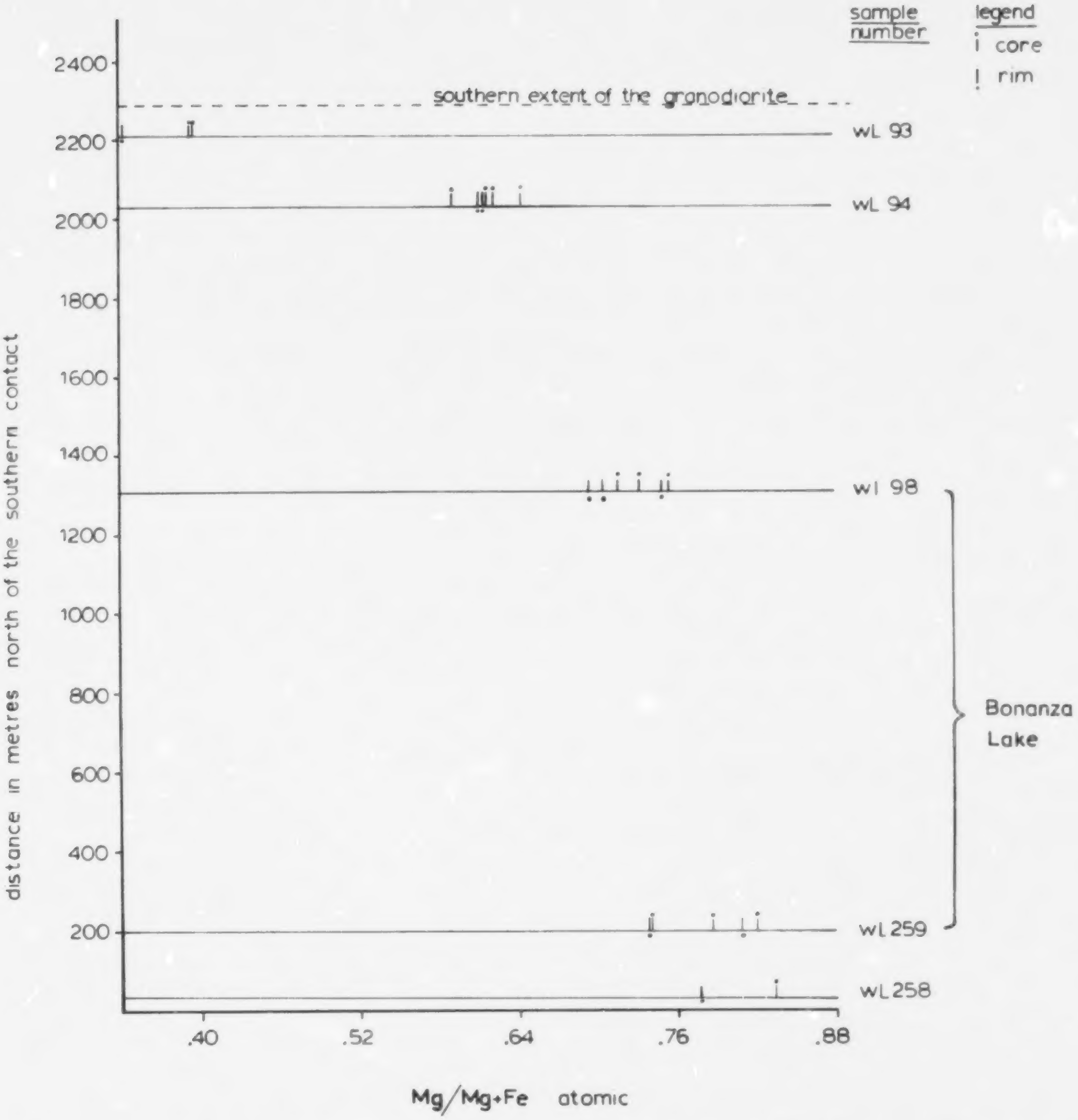

Figure 230.4a. Variation in Mg-number of orthopyroxene across the Bonanza Lake Intrusion (traverse C-D).

suitable anchors for the vectors. Significantly, the 1:1 vector passes through the data in plots of Ta and Ce versus La (Ta has a larger analytical uncertainty, one sigma is shown as a line propagated from the chilled margin sample in Figure 230.10) and close to this line in the plot of Th versus La (where the granophyres show slight Th-enrichment). Furthermore, it can be observed that irrespective of the parental liquid composition chosen, as long as it falls on the array, the 1:1 vector will always pass through all the observed data. This suggests that the liquid composition lies somewhere on the array between the depleted and enriched extreme, or on an extension of the array towards depleted compositions. The fact that the Ta versus La data define a trend which could be produced by ideal Rayleigh fractional crystallization, suggests that the La/Ta ratio is constant, and that any crustal contamination or mixing fingerprint was introduced before fractional crystallization to maintain this constant ratio, assuming that Ta is not introduced in equal proportions to La during contamination.

The variations in Sr, Ni, and Cr versus La are shown in Figures 230.11 and 230.12. The Ni plot is quite tight while that for Cr is a little more scattered. The Sr plot is very scattered, but the Bruce Mines and Basswood Lake Intrusions provide samples which

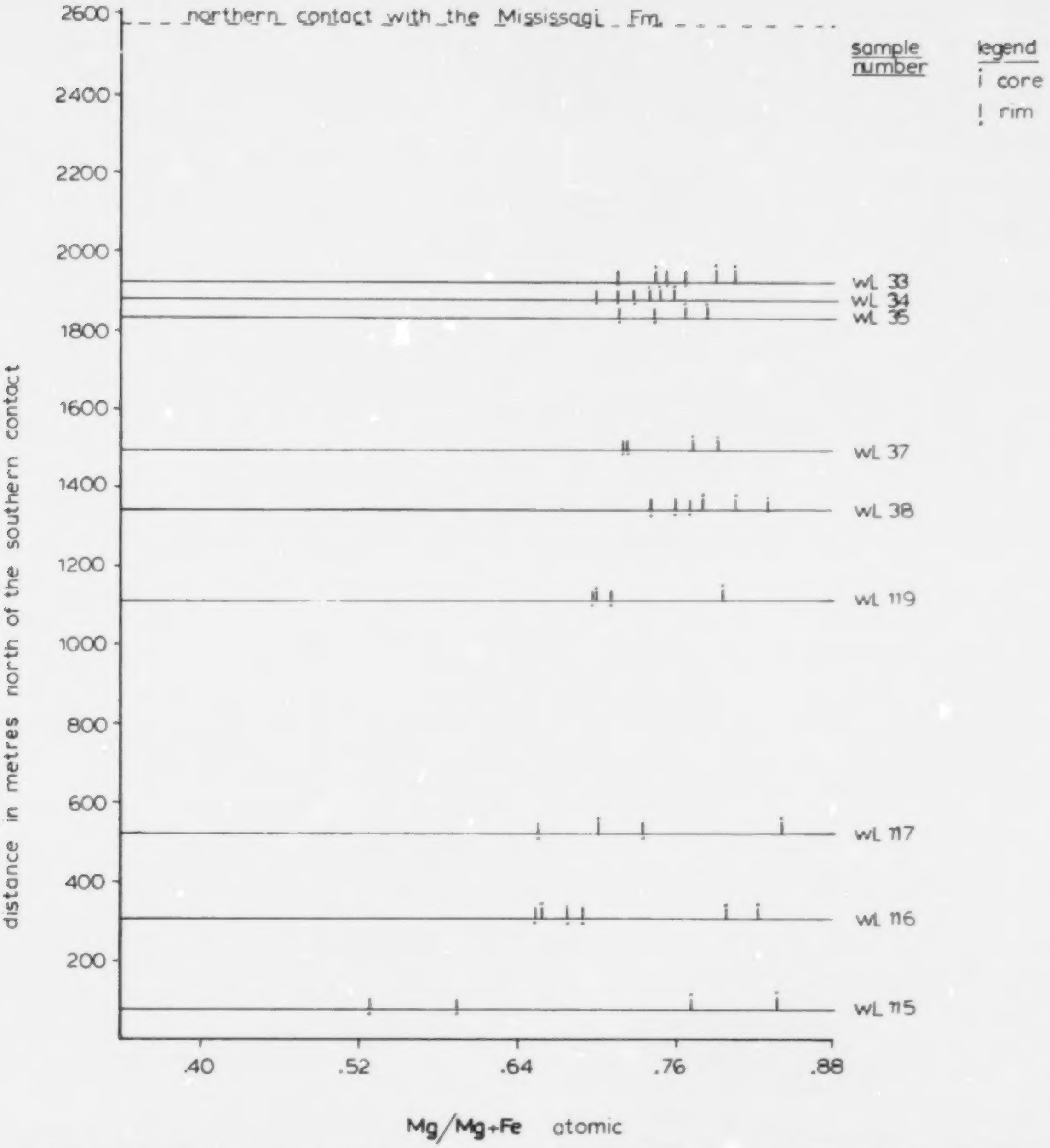

Figure 230.4b. *Variation in Mg-number of orthopyroxene across the Bonanza Lake Intrusion (traverse A-B).*

define tighter trends of Sr versus La than the other rocks (Figure 230.11).

The variations in incompatible and compatible trace element behaviour are modeled in terms of two end-members (Table 230.1). This initial approach is suggested by the wider range of Zr/La in the diabases compared to the granophyres (*see* below).

Assuming a starting liquid which has the composition of the Portage Bay chilled margin, the Sr-La trend of the diabases can be modeled in terms of about 66% overall fractional crystallization of a phase extract containing 40% plagioclase. The Cr data is an index of the amount of pyroxene fractionation, and is consistent with 50% pyroxene in the phase extract. These figures are supported by Sc and V (not shown), which furthermore suggest that equal proportions of clinopyroxene and orthopyroxene contributed to the phase extract (Table 230.1). The Ni and Co data, when considered in relation to these amounts of pyroxene fractionation, would not be in-

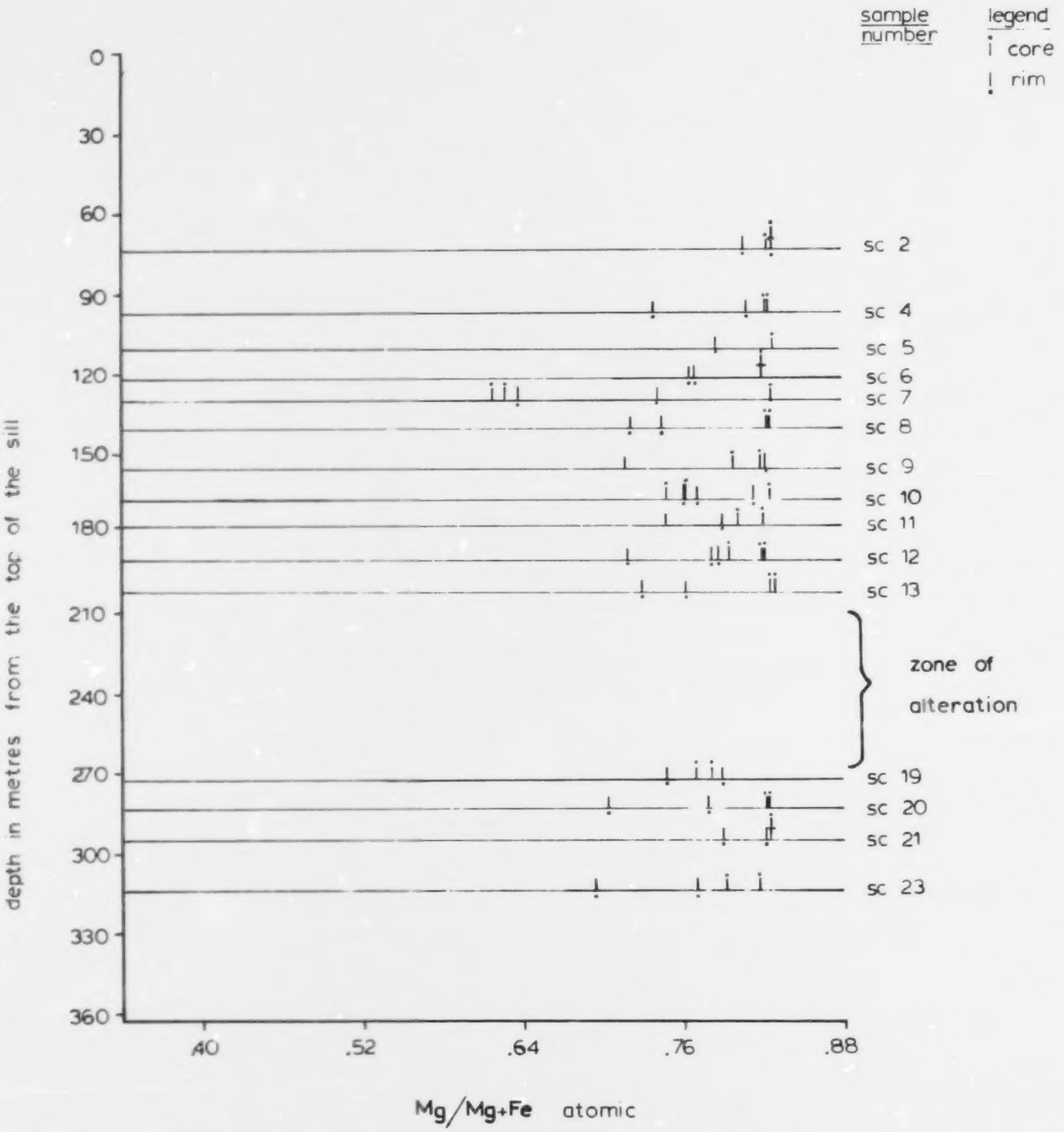

Figure 230.4c. Variation in Mg-number of orthopyroxene across the Cross Lake Sill.

consistent with a small amount of olivine fractionation (about 4% of the phase extract).

Within the granophyres, the La data are consistent with 28% fractional crystallization encompassing the mafic and evolved averages. The Sr data suggest that 60% plagioclase entered the phase extract, while the Cr, V, Sc, Co, and Ni data suggest that 35% clinopyroxene, approximately 1% Fe-Ti-V oxide, and some amphibole were in the phase extract (Table 230.1).

The effects of cumulus enrichment are hard to distinguish from fractional crystallization on the basis of this approach, as the cumulus effects of pyroxene and plagioclase would have identical effects on plots of incompatible elements versus La. The wide range in Ni/Sr in the pyroxene-rich diabases compared to the rest of the rocks may suggest that the trace element contents of these rocks have been more substantially influenced by cumulates than the other rocks.

Figure 230.13 shows Zr and Y versus La. These elements are generally all regarded as incompatible

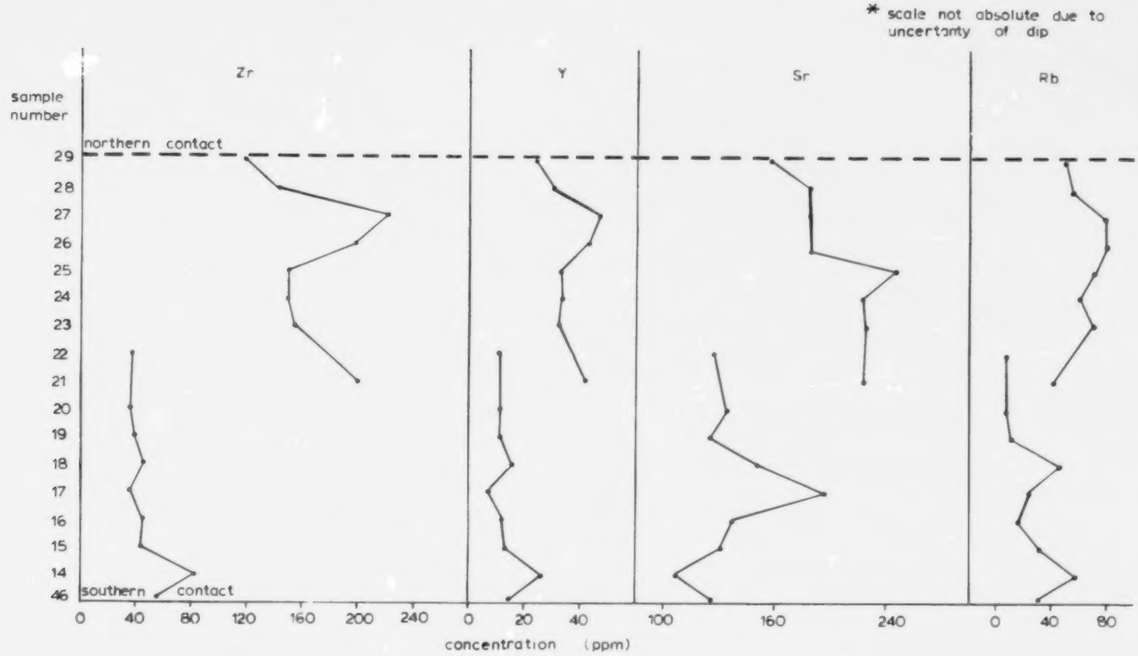

Figure 230.5. *Variation in selected trace element concentrations in the Highway 129 section of the Basswood Lake Intrusion (relative positions of samples are not stratigraphically controlled).*

in basaltic melts (Pearce and Norry 1979), but these data suggest that this is not the case, assuming that La is behaving as an ideal incompatible element. The elements Y, Yb, Zr, Hr, and Sm are enriched in variable amounts in the mafic diabases relative to the evolved diabases. In contrast, there is a consistent 1:1 enrichment in these elements relative to La in the granophyres. The fact that the trends of falling Zr/La, etc., are continuous is illustrated in Figure 230.14 where Zr/La and Y/La are plotted against La. Table 230.1 shows the values of the predicted bulk distribution coefficients for Zr, Y, Sm, Yb, and Hf. The Y and Yb data fall on a 1:1 trend (Figure 230.14b) which precludes garnet fractionation at high pressure as a cause of the variation (given the distribution coefficients of Y and Yb into garnet as 2 and 30, respectively). There is limited evidence from the observed mineralogical compositions of the rocks for an important component of primary amphibole fractionation (a point supported by the Cr data which are explained best by pyroxene fractionation). Furthermore, clinopyroxene fractionation (25% in the phase extract) cannot explain the high bulk distribution coefficients of Zr, Hr, and Sm (although clinopyroxene can take in a limited amount of Y and Yb). These data appear to suggest that the break in fractionation at about 15 ppm La suggested by the Sr, Cr, and Ni data may not be unrealistic.

Partial melting may be ruled out as a source of the variation in Zr/La and Y/La on the grounds that the most mafic diabases, found close to the base of the intrusion, have highest Zr/La and Y/La. Very large degrees of partial melting would produce liquids with high Zr/La and Y/La (as all the clinopyroxene in the mantle would enter the melt), while lower degrees of partial melting (with residual clinopyroxene) would be required to fractionate Zr and Y from La to produce magmas with lower Zr/La and Y/La. In effect, the first magmas to be introduced into the magma chamber would have to result from greater degrees of partial melting of the mantle than subsequent magmas, and this is clearly unreasonable.

The possibility that a minor phase has fractionated Zr, Hf, Y, Yb, and Sm from La remains a possibility. The only phase which would meet these criteria would be zircon. When combined with the influence of clinopyroxene, this phase may account for the high bulk distribution coefficients for these elements. While this solution must only be considered as tentative, the combination of zircon and pyroxene fractionation may explain the range of Zr/La and Y/La. Alternative explanations are presently under investigation, which may explain the shift in Zr/La, Y/La, etc., by mixing between two magmas with different Zr/La, Y/La, etc. or AFC (Assimilation Fractional Crystallization, DePaolo 1981). Nd-isotopic compositional data are being determined for representative samples from the curved trend on the Zr/La versus La array (Figure 230.14b).

Thus, a preliminary look at the trace element data reveals evidence for considerable variations in trace element concentrations within each intrusion. The compositional variations exhibited by different intrusions are largely similar in magnitude and absolute concentration (with the exception of Ni, Cr, and Sr). Fractional crystallization and cumulus enrichment have undoubtedly played a key role in the

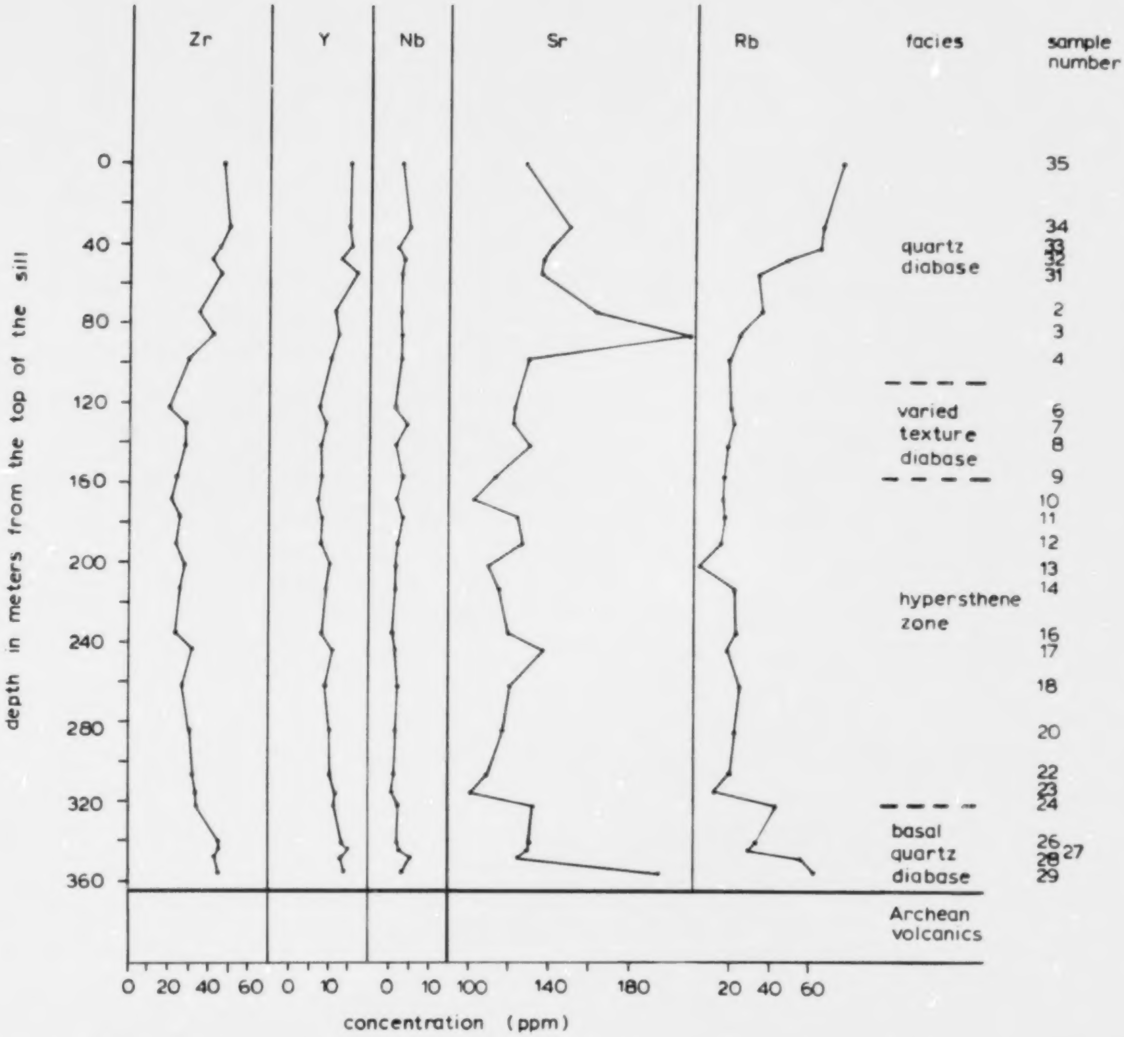

***Figure 230.6.** Variation in selected trace element concentrations across the Cross Lake Sill.*

petrogenesis of these rocks. However, there is evidence from the incompatible element ratios to suggest that important contamination or mixing processes were overprinted by as much as 60% low pressure fractional crystallization of pyroxene, plagioclase, and olivine.

ECONOMIC POTENTIAL

One of the major interests in the sills of the Nipissing Diabase is that of the potential for magmatic sulphides. The possibility of sulphide segregation from the Nipissing Diabase was investigated in the Cross Lake Sill, using the Ni and forsterite (Fo) contents of olivine as an index of the likelihood that the magma had segregated an immiscible sulphide (Naldrett *et al.* 1984). The observation that the magmas contain olivines with essentially normal to high Ni-Fo contents suggests that this particular intrusion may not have fractionated sulphide. While this is not particularly encouraging for Cu-Ni sulphides, it does mean that PGE may have remained quite high, to become enriched in the fractionating magma, and be available for any late-stage sulphide-forming processes.

It has been suggested that contamination of magma by siliceous country rocks has caused sulphide to segregate at Sudbury (Irvine 1975; Rao *et al.* 1985). The trace element data appear to suggest that there is limited evidence for variable amounts of contamination, either within or between the different Nipissing intrusions. This conclusion must be viewed as tentative, and awaits more detailed studies of the Rb/Sr and Sm/Nd isotope systematics which are highly sensitive (when combined with trace element studies) to contamination processes (Lightfoot 1985). Some insight into the end-members involved in possible mixing mechanisms will be further investigated using inter-element ratio and Nd-isotope data.

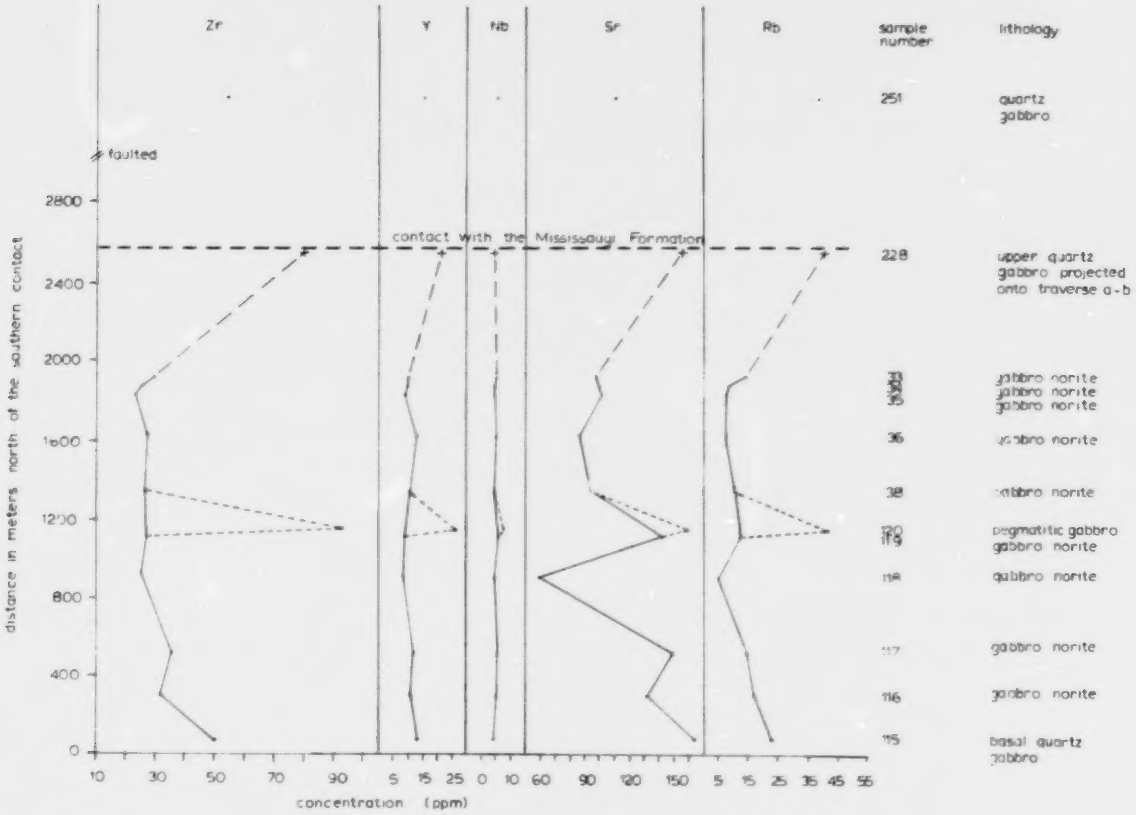

Figure 230.7a. *Variation in selected trace element concentrations across the Bonanza Lake Intrusion (traverse A-B).*

The fact that the Wanapitei Intrusion documented by Finn *et al.* (1982) has revealed Au in the gabbro-norite, and Ag, Au, Pt, and Pd from shear zones within the gabbro-norite, suggests that concentrations of magmatic sulphides may exist. It remains to be seen whether the high Cu, Ni, and PGE values reported from the central region of the study area are related to significantly different trace element ratio and isotopic characteristics, compared to diabases from the west of the region (associated with Cu-rich mineralization), and the east of the region (associated with Ag-rich mineralization).

CONCLUSIONS AND FUTURE PLANS

The intrusions investigated in this study show many remarkable similarities in structure, petrography, mineralogy, and geochemical variations throughout rocks collected as far as 500 km distant from each other. These variations are not inconsistent with a strong fractional crystallization imprint. This appears to be superimposed on a trace element signature which is very similar to contaminated basalts from the Deccan. Furthermore, the range in Zr/La in the diabases suggests that the fractionation process was superimposed on a compositional spectrum produced by mixing or contamination.

Future studies will concentrate on:

1. More detailed investigations of the geochemical variations within each intrusion to evaluate the roles of fractional crystallization, AFC, and mixing of magmas.
2. Evaluation of Sr and Nd isotope evidence for contamination and/or mixing processes, and the relationship of inter-element ratio data for the incompatible elements to isotope data.
3. Determination of accurate U/Pb zircon age dates for the Nipissing Diabase, and correlation of these ages with evidence from paleomagnetic work by Buchan and Card (1985) which suggests that there may have been at least two stages of Nipissing magmatism.
4. Correlations between the styles of mineralization and the trace element and isotope geochemistries will be investigated.

ACKNOWLEDGMENTS

We are grateful to Ron Hancock (SLOWPOKE Reactor Facility, University of Toronto, Toronto) for allowing us to use the SLOWPOKE reactor and counting facilities for neutron activation work. Both Phil Potts and John Watson (Department of Earth Sciences, Open University, United Kingdom) are thanked for assis-

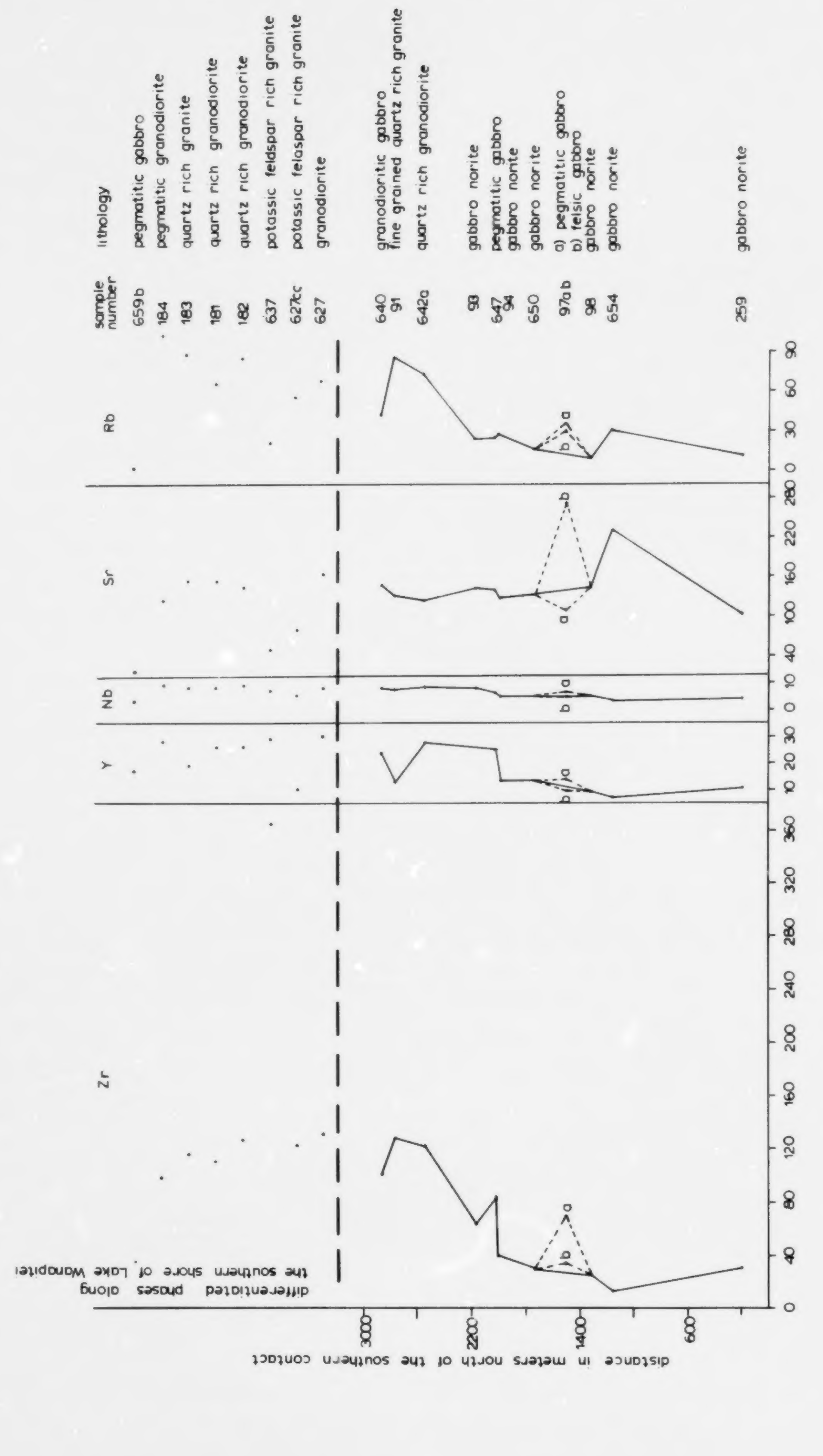

Figure 230.7b. Variation in selected trace element concentrations across the Bonanza Lake Intrusion (traverse C-D).

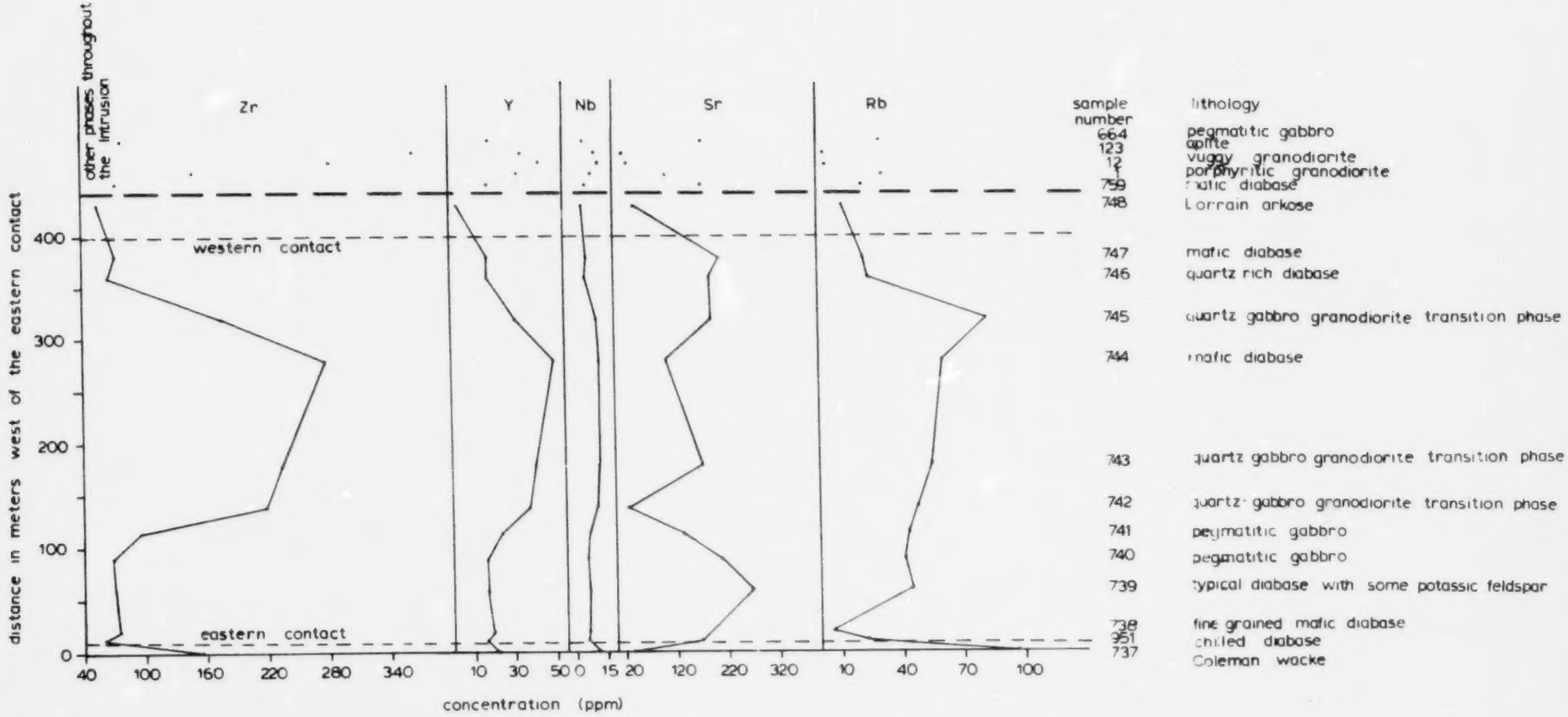

Figure 230.8. Variation in selected trace element concentrations in the Portage Bay Intrusion (traverse A-B).

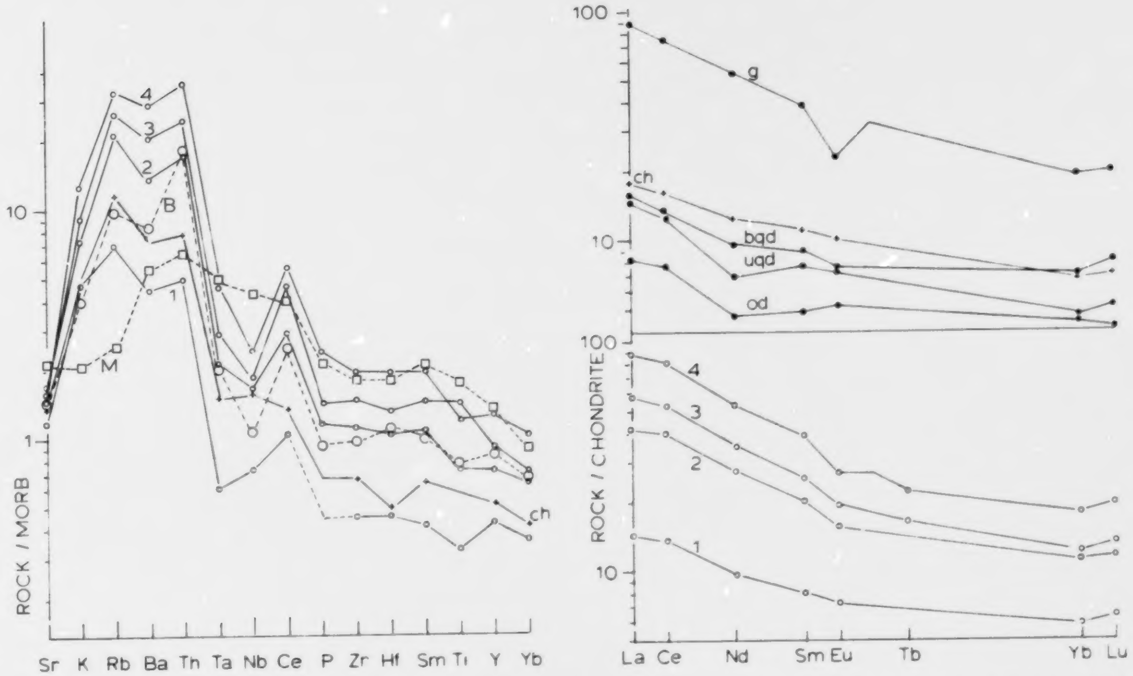

Figure 230.9. MORB-normalized trace element data for average mafic and evolved diabases and granophyres from the western sector of the study area. Also shown are the compositions of the Portage Bay chill and the compositions of basalts from the Deccan CFB (Lightfoot 1985). REE plots show chondrite-normalized concentrations in representative samples of diabase and granophyre. 1 = mafic diabase, 2 = evolved diabase, 3 = mafic granophyre, 4 = evolved granophyre. ch = chill, B = Bushe basalt (Deccan), M = Mahabaleshwar basalt (Deccan). bqd = basal quartz diabase, od = olivine diabase, uqd = upper quartz diabase, g = granophyre (all from eastern sector).

tance with ED-XRF. Discussions with Chris Hawkesworth (Department of Earth Sciences, Open University, United Kingdom) on general aspects of CFB magmatism are acknowledged.

REFERENCES

Buchan, K.L., and Card, K.D.
1985: Preliminary Comparison of Petrographic and Paleomagnetic Characteristics of Nipissing Diabase Intrusions in Northeastern Ontario; Geological Survey of Canada, Current Research, Paper 85-1A, p.131-141.

Card, K.D., and Pattison, E.F.
1973: Nipissing Diabase of the Southern Province, Ontario; Geological Association of Canada, Special Paper 12, p.7-30.

DePaolo, D.J.
1981: Trace Element Effects of Combined Wallrock Assimilation and Fractional Crystallization; Earth and Planetary Science Letters, Volume 53, p.189-202.

Dressler, B.O.
1980: Geology of the Wanapitei Lake Area, District of Sudbury; Ontario Geological Survey, Open File Report 5287.

Fairbairn, H.W., Hurley, P.M., Card, K.D., Knight, C.J.
1969: Correlation of Radiometric Ages of Nipissing Diabase and Huronian Metasediments with Proterozoic Orogenic Events in Ontario; Canadian Journal of Earth Sciences, Volume 6, p.489-497.

Finn, G.C., Edgar, A.D., and Rowell, W.F.
1982: Petrology, Geochemistry, and Economic Potential of the Nipissing Diabase; Ontario Geological Survey, Miscellaneous Paper 103, p.43-57.

Henderson, P.
1983: Inorganic Geochemistry; Pergamon Press, 353p.
1984: Rare Earth Element Geochemistry, 2 volumes.

Irvine, T.N.
1975: Primary Precipitation of Concentrated Deposits of Magmatic Ores; Geological Survey of Canada, Paper 75-1B, p.73-79.

Irving, A.J.
1978: A Review of Experimental Studies on Crystal/Liquid Trace Element Partitioning; Geochimica et Cosmochimica Acta, Volume 42, p.743-770.

Lightfoot, P.C.
1985: Isotopic and Trace Element Geochemistry of the South Deccan Lavas, India; Unpublished Ph.D. Thesis, Open University, 589p.

TABLE 230.1. END-MEMBER COMPOSITIONS USED TO MODEL FRACTIONAL CRYSTALLIZATION TRENDS FOR THE DIABASES AND GRANOPHYRES.

Element	Portage Bay Chill	Evolved Diabase	Cal. Bulk Kd	Distribution Coefficients						
				Plag.	Ol.	Cpx.	Opx.	Amph.	Gt.	Zr.
Diabase Trend:										
La	5.6	12.8	-	z	z	z	z	z	z	z
Ce	13.4	29.2	0.05	z	z	z	z	z	z	z
Ta	0.16	0.41	0	z	z	z	z	z	z	z
Th	1.56	3.50	0.02	z	z	z	z	z	z	z
Ba	120	271	0.01	z	z	z	z	z	z	z
Zr	60	101	0.37	z	z	z	z	z	0.3	high
Y	15.7	21.6	0.61	z	z	z	z	z	2	30
Sm	2.2	3.6	0.40	z	z	z	z	z	0.9	4
Yb	1.42	2.14	0.50	z	z	z	z	z	30	290
Hf	1.2	2.5	0.11	z	z	z	z	z	0.6	high
Sr	166	204	0.75	1.9	z	z	z	z	z	z
Ni	110	61	1.72	z	14	2.6	2	z	z	z
Sc	38.1	40.3	0.93	z	z	2.7	0.5	z	z	z
Cr	350	86	2.71	z	z	2	9	z	z	z
V	240	263	0.89	z	z	1.3	1.9	z	z	z
Co	45	53	0.80	z	3.8	1	1.5	z	z	z

Legend:
Portage Bay Chill values used in all cases except Ta, Ni, Sc, Cr, V, and Co, for which values were chosen at 5.6 ppm La on the data trend.
z - values are assumed to be approximately zero.
Data sources are. Henderson (1984), Irving (1979), Pearce and Norry (1979).

Phase extract:

Plagioclase	40%
Olivine	4%
Clinopyroxene	25%
Orthopyroxene	25%

Element	Average mafic granophyre	Average evolved granophyre	Calculated bulk Kd
Granophyre Trend:			
La	18.0	25.0	-
Ce	42.1	56.8	0.09
Ta	0.52	0.83	0
Th	4.9	7.1	0
Ba	408	580	0
Zr	132	177	0.11
Y	27.6	38.0	0.03
Sm	4.9	6.6	0.09
Yb	2.41	3.53	0
Hf	3.2	4.7	0
Sr	200	192	1.12
Ni	54	19	4.2
Sc	38.4	38.0	1.0
Cr	82	88	0.8
V	338	157	3.3
Co	46	47	0.9

Phase extract:

Plagioclase	60%
Clinopyroxene	35%

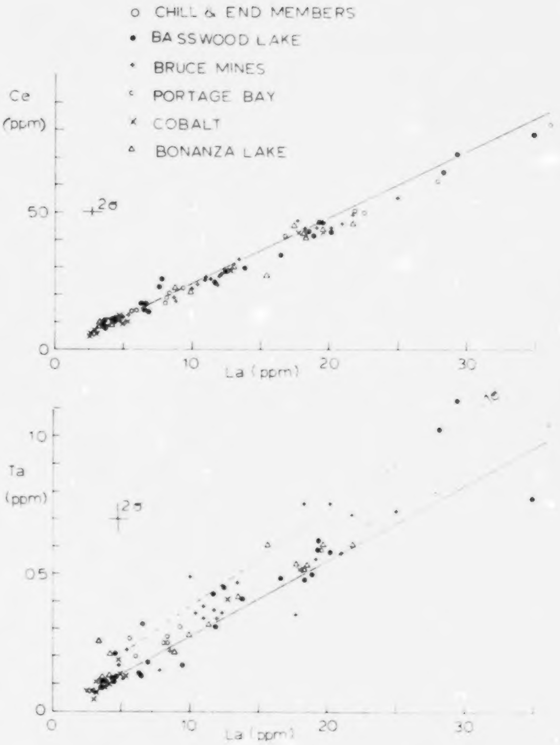

Figure 230.10. *Variation in Ce and Ta versus La. Line is 1:1 ideal Rayleigh fractionation, assuming $K_d=0$ (one-sigma errors on Ta content of chill are propagated). Two-sigma errors based on UTB1 multiple analyses.*

Lightfoot, P.C., Naldrett, A.J., and Hawkesworth, C.J.
1984: The Geology and Geochemistry of the Waterfall Gorge Section of the Insizwa Complex with Particular Reference to the Origin of the Nickel Sulphide Deposits; Economic Geology, Volume 79, p.1857-1879.

Naldrett, A.J., Duke, J.M., Lightfoot, P.C., and Thompson, J.F.H.
1984: Quantitative Modelling of the Segregation of Magmatic Sulphides: An Exploration Guide: Canadian Institute of Mining and Metallurgical Bulletin, Volume 77, Number 864, p.46-56.

Pearce, J.A.
1983: Role of the Sub-Continental Lithosphere in Magma Genesis at Active Continental Magins; *in* SHIVA, Continental Basalts and Mantle Xenoliths, edited by C.J. Hawkesworth and M.J. Norry.

Pearce, J.A., and Norry, M.J.
1979: Petrogenetic Implications of Ti, Zr, Y, and Nb, Variation in Volcanic Rocks; Contributions Mineralogy and Petrology, Volume 69, p.33-47.

Potts, P.J., Webb, P.C., and Watson, J.S.
1984: Energy Dispersive X-ray Fluorescence Analyses of Silicate Rocks for Major and Trace Elements; X-ray Spectrometry, Volume 13, Number 1, p.2.
1985: Energy Dispersive X-ray Fluorescence Analyses of Silicate Rocks: Comparison with Wavelength Dispersive Performance; Analyst, Volume 10.

Rao, B.V., Naldrett, A.J., and Evensen, N.M.
1985: Crustal Contamination of the Sublayer, Sudbury Igneous Complex, and its Relevance to the Genesis of Ni-Cu Sulphides [Abstract]: Magmatic Sulphide Field Conference IV, The Canadian Mineralogist, Volume 23, Part 2, p.329-330.

Van Schmus, W.R.
1965: The Geochronology of the Blind River-Bruce Mines Area, Ontario, Canada: Journal of Geology, Volume 73, p.755-780.

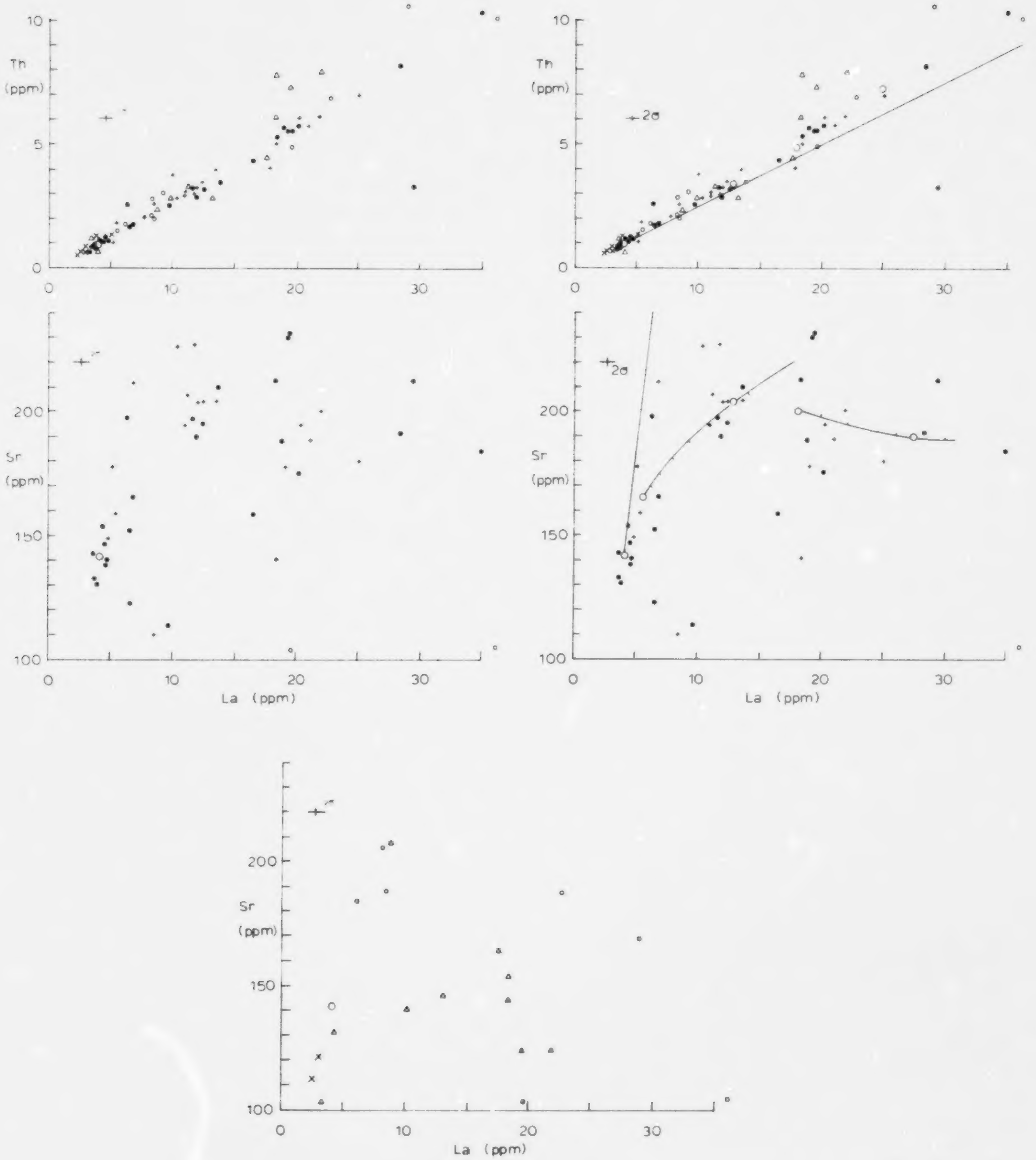

Figure 230.11. Variation in Th and Sr versus La. Explanation of symbols is given in Figure 230.10. Large circles are representative end members. Lines show effects of Rayleigh fractionation (see Table 230.1).

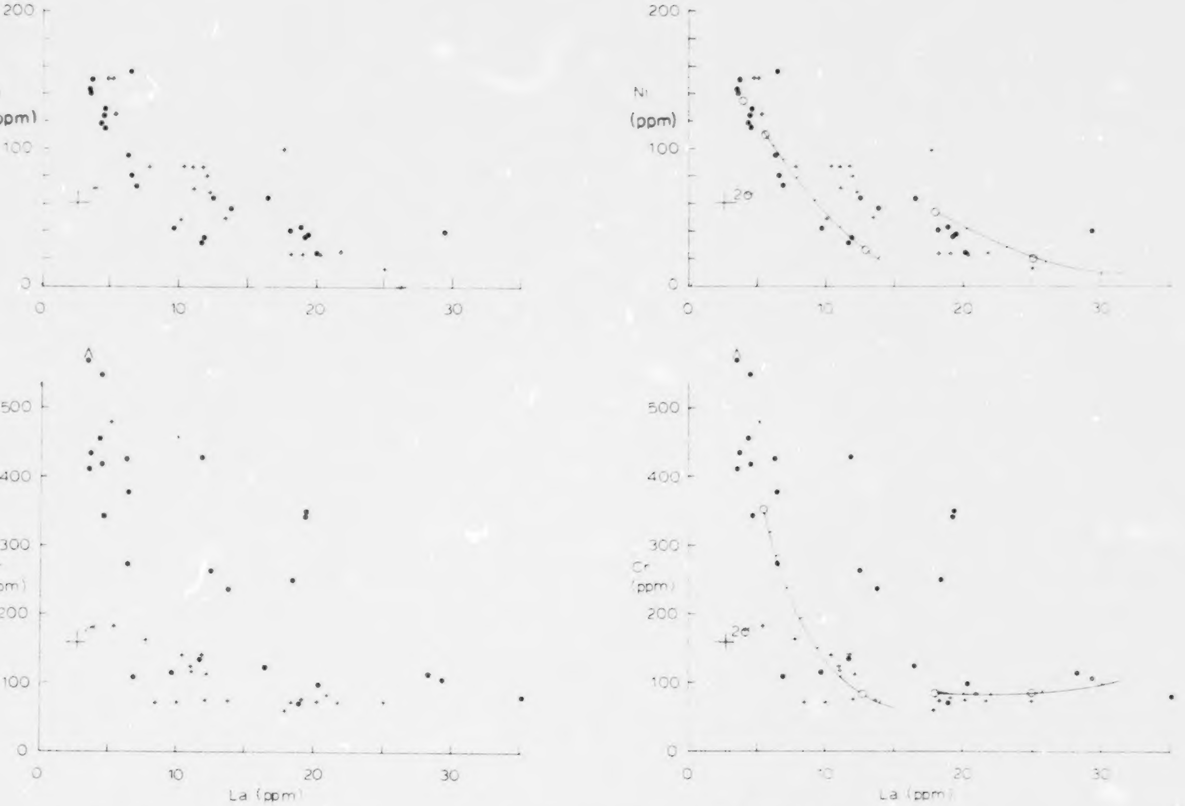

Figure 230.12. Variation in Ni and Cr versus La. See Figures 230.10 and 230.11 for explanation.

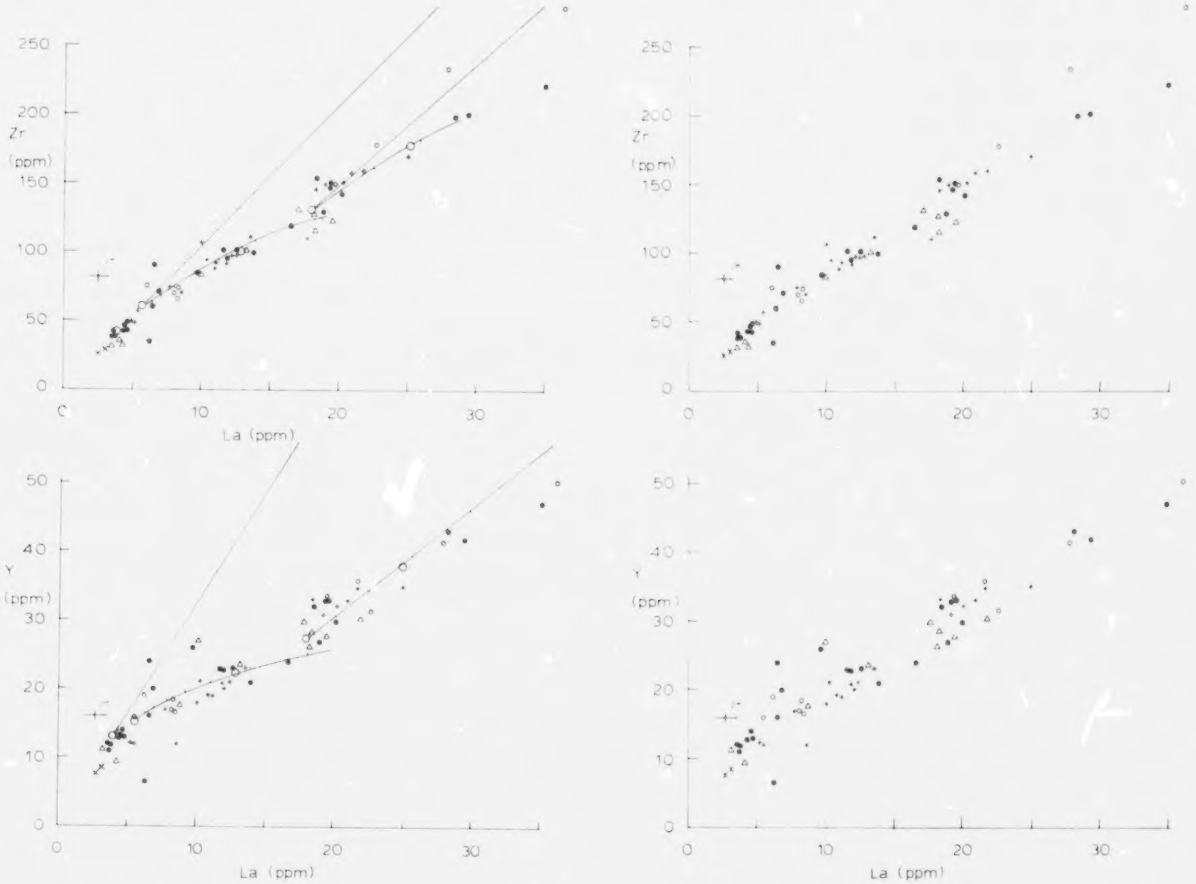

Figure 230.13. Plot of Zr and Y versus La. See Figure 230.10 for explanation of symbols.

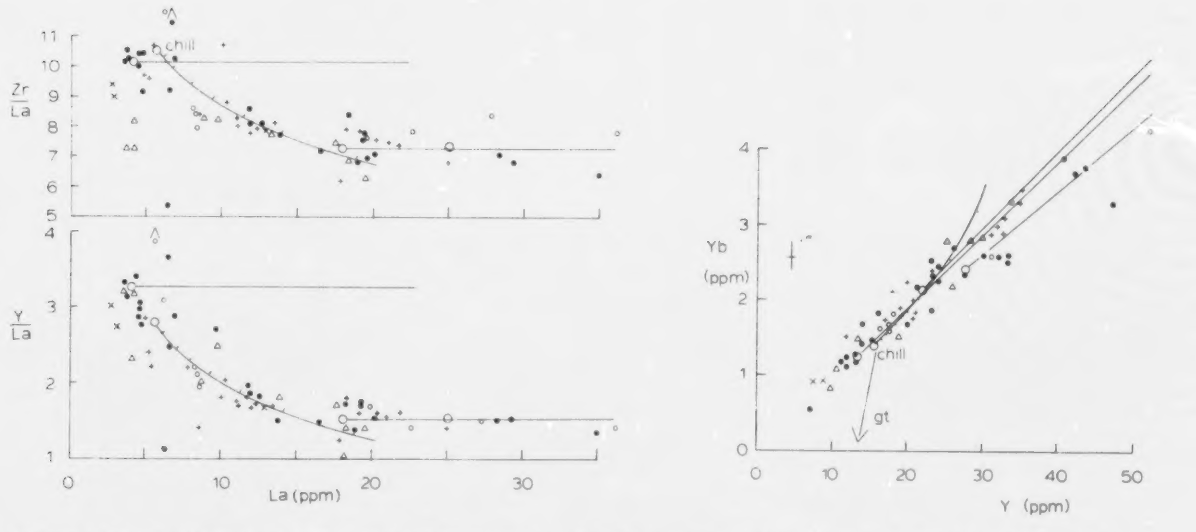

Figure 230.14. (a) Plot of Zr/La and Y/La versus La. Symbols are explained in Figure 230.10. (b) Plot of Yb versus Y. Explanation of symbols is in Figure 230.10.

Grant 233 The Dating of Ontario's Gold Deposits

A. Masliwec, D. McMaster, and D. York

Geophysics Division, Department of Physics, University of Toronto, Toronto

ABSTRACT

Attempts have been made to set limits to the ages of gold formation in the Timmins, Hemlo, and Red Lake areas of Ontario. In the first two regions, lower limits have been set to the age(s) of gold formation by the ^{40}Ar/^{39}Ar dating of green mica (fuchsite) associated with the gold. When the data for the Timmins camp are combined with U-Pb dates on zircons (performed by S. Marmont, Geologist, Ontario Geological Survey, Toronto), we find that the age of the Dome Mine gold lies between 2633±6 million years (Ma) and 2685±3 Ma Hollinger Mine gold is over 2617±8 Ma old and presumably younger than 2685±3 Ma. The Hemlo gold is over 2671±5 Ma old. In the Red Lake region, ^{40}Ar/^{39}Ar dating of the contact aureole of the Trout Lake Batholith, which may have had a genetic connection with the gold, shows very rapid cooling of the area ≅2670 Ma ago. Mica samples from three producing mines, however, show the effects of argon loss during a significantly later event which produced very localized disturbance.

INTRODUCTION

The purpose of the project is to apply the ^{40}Ar/^{39}Ar method of dating to minerals associated with some of Ontario's gold deposits (e.g. Timmins camp, Hemlo, and Red Lake) so that reliable estimates can be made of the time(s) of gold formation. At the onset of this project, these times were only imprecisely known. While U-Pb dating of zircons is beginning to produce an accurate volcano-stratigraphic framework for the evolution of the gold-bearing greenstone belts, it remains extremely difficult to position the gold-forming events within this time-matrix.

Initially, an approach has been developed in the Timmins camp which has, in the first two years of the project, shown clear signs of being extremely useful in the dating of gold deposits. A number of the producing deposits are located in porphyries. The crystallization ages of these are being measured by S. Marmont (Geologist, Ontario Geological Survey, Toronto) by U-Pb dating of zircons. The gold is, therefore, younger than the associated zircon age. The gold is, however, apparently associated with a green mica alteration product and is considered to be syn- or pre-mica. We are, therefore, ^{40}Ar/^{39}Ar-dating the green mica to get a minimum age of gold formation. In the following pages, the green mica will be shown to be a very suitable mineral for ^{40}Ar/^{39}Ar work. It has enabled us to bracket the age of formation of the Dome Mine deposit at between 2633±6 Ma from the micas and 2685±3 Ma from the zircons. Similarly, Hollinger has been bracketed between 2617±8 Ma and 2685±3 Ma.

The method has been extended to Hemlo whose fuchsite, we find, has experienced a more tranquil post-crystallization history than that of Dome and Hollinger. The Hemlo gold is seen to be older than 2671±5 Ma from the ^{40}Ar/^{39}Ar work. If the associated porphyries at Hemlo are the same age as those in the Timmins camp (2685±3 Ma), then the Hemlo deposit will be the most precisely dated Archean gold deposit known. The Hemlo zircons are currently being dated by F. Corfu at the Geochronology Laboratory, Royal Ontario Museum, Toronto.

In the Red Lake area, gold formation, hydrothermal alteration and activity on deformation zones are all intimately related to batholith intrusion and resulting metamorphism. We are collaborating with A.J. Andrews (Geologist, Ontario Geological Survey, Toronto) and co-workers to try to outline the thermal history of the contact zone of the Trout Lake Batholith and to position the time of hydrothermal activity and gold formation within this history.

Hornblende and mica from the contact zone yield beautiful plateaus with ages of about 2675 Ma and 2665 Ma respectively. At this time, cooling evidently was rapid and the subsequent history was tranquil. However, micas from the nearby Cochenour, Campbell, and A.W. White Mines, while retaining evidence of a pre-2630 Ma existence, have been seriously disturbed after this, perhaps reflecting late activity in the gold-associated deformation zones.

The thrust of the next year's work will be to extend the Red Lake study. The results so-far obtained show that intriguing variations in thermal history can be seen. The initial spectra indicate that this region is well suited to ^{40}Ar/^{39}Ar dating.

EXPERIMENTATION

Mineral separates with over 99% purity were obtained and taken in milligram quantities for age analysis. All samples were irradiated in the McMaster University reactor along with the Zartmann hornblende standard, 3 gr (Zartmann 1964, Hall *et al.* 1984). Cadmium shielding was used to reduce radiation hazard. The irradiated samples were then step-heated in an ultra-high vacuum system (Berger and York 1981). Heating steps of 45 minutes were used, and the purified gas fractions released in each step were subsequently isotopically analyzed on an MS10 mass spectrometer.

One green mica (from Hollinger Mine) was dated with the continuous laser system (York *et al.* 1981) by C.M. Hall (*see* Figure 233.7). This step-analysis was performed on a single grain (1.0 x 0.5 x 0.5 mm) and the gas fractions were analyzed with the MS 1200 mass spectrometer.

SAMPLES

At Dome and Hollinger Mines, samples of both vein and host rock were taken.

Dome Mine

Fuchsite samples were obtained from the 1200-foot level from a quartz ankerite vein. The associated host rock sampled is the Preston Porphyry.

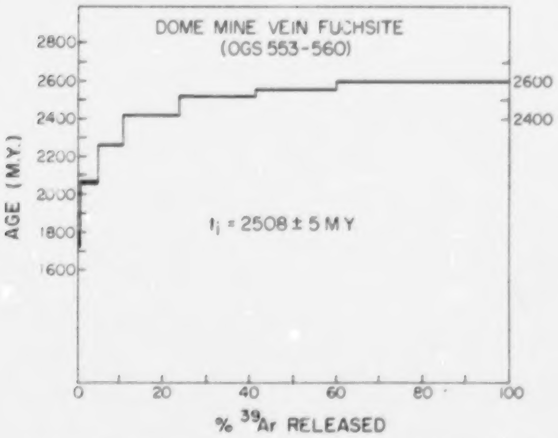

***Figure 233.1.** First exploratory run on fuchsite from Dome vein. ti = integrated age.*

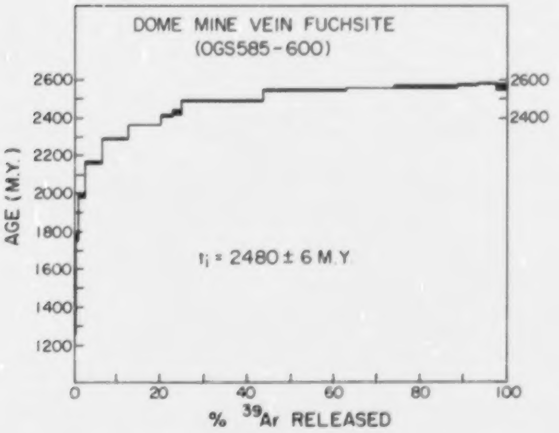

***Figure 233.2.** Age spectrum of fuchsite from Dome vein.*

Hollinger Mine

Green mica was collected from the number 400 pit from a siliceous carbonate, pyrite-rich vein. Fuchsite was also obtained from the associated host rock Millerton porphyry.

Hemlo Deposit

Fuchsite was separated from a sample of the quartz, muscovite schist host rock in William's Trench on the main ore zone.

In the Red Lake region, the samples dated were taken from the contact aureole of the Trout Lake Batholith, and from the Cochenour, Campbell, and A.W. White Mines.

Contact Aureole

Hornblende was extracted from an amphibolite grade basalt located about 20 m from the granite contact. Biotite was collected from a greenschist grade basalt about 5 km from the contact.

Cochenour Mine

A muscovite-sericite mixture was prepared from a highly altered felsic dike closely related to the ore.

Campbell Mine

A muscovite-sericite mixture was prepared from a highly altered felsic volcanic.

A.W. White Mine

Hydrothermal biotite was collected from highly altered rock from the ore stope.

AGE ANALYSES

Dome Mine

Two vein fuchsites and two micas from the hosting porphyry were analyzed (Figures 233.1 to 233.4). The first analysis (Figure 233.1) was of an exploratory nature carried out to map out the argon evolution characteristics of fuchsite. Only eight steps were taken in the analysis. The three subsequent analyses were much more detailed and each included sixteen steps. Significant argon loss is revealed by all age spectra.

Hollinger Mine

Sixteen-step analyses were done on this green mica (Figures 233.5 and 233.6). In addition, because it was suspected that there may have been significant between-grain age variations, a seventeen-step laser run was performed on a single grain (Figure 233.7). In fact, this analysis did yield the highest single step-age (2617±8 Ma) seen in Hollinger samples. All the age spectra exhibit the effects of argon loss.

Hemlo

As a preliminary examination prior to a more detailed series of measurements in future, a fourteen-step

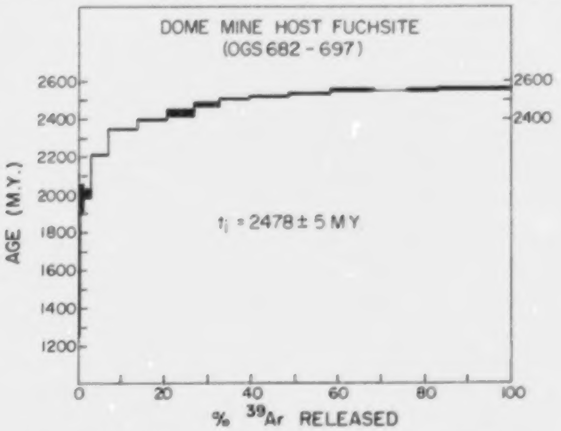

***Figure 233.3.** Age spectrum of fuchsite from Dome host porphyry.*

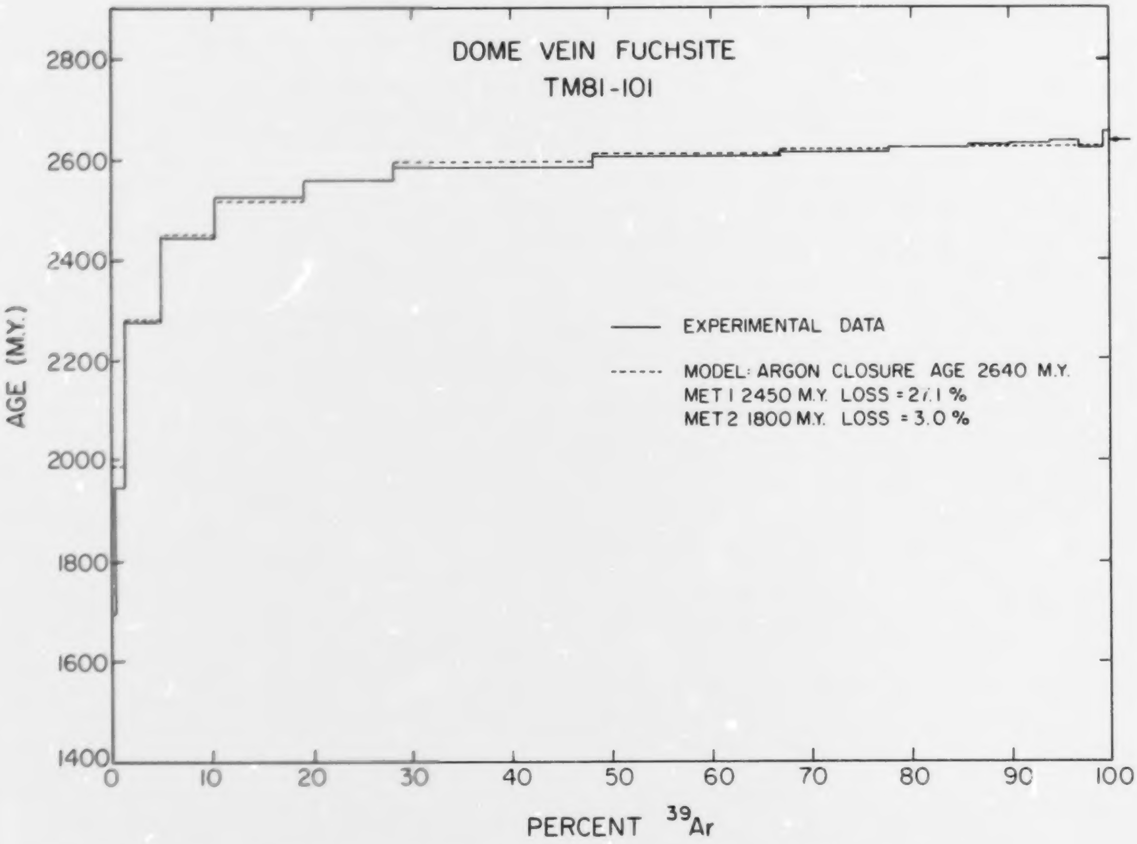

Figure 233.4. *Age spectrum of fuchsite from Dome vein porphyry. Two-pulse spectrum also shown.*

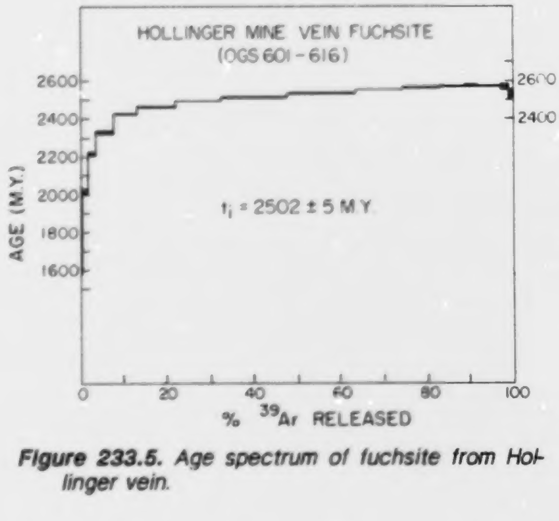

Figure 233.5. *Age spectrum of fuchsite from Hollinger vein.*

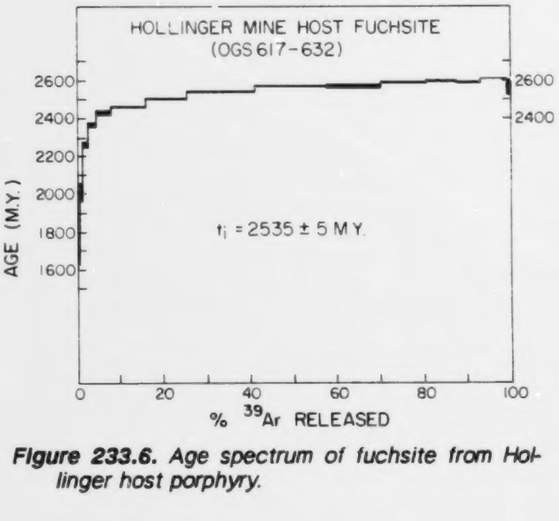

Figure 233.6. *Age spectrum of fuchsite from Hollinger host porphyry.*

analysis was carried out on mica from the Hemlo host. The remarkably flat plateau found is shown in Figure 233.8.

Trout Lake Aureole

Seventeen-step and fifteen-step analyses were performed on the hornblende and biotite samples respectively. The extensive flat plateaus found, similar to that for the Hemlo fuchsite, are shown in Figures 233.9 and 233.10.

Red Lake Mine

Sixteen-step and fifteen-step analyses were carried out on muscovite-sericite mixtures from the Cochenour and Campbell Mines, respectively. Both yielded argon-loss spectra (Figures 233.11 and 233.12) reminiscent of those derived from the Dome and Hollinger samples. A sixteen-step analysis of biotite from the A.W. White Mine produced a unique spectrum (Figure 233.13) which is interpreted below.

DISCUSSION

Dome Fuchsites (Figures 233.1 to 233.4)

All four spectra, whether from vein or host exhibit the same characteristic shape, displaying an essentially monotonic increase in age with temperature of argon release. There has clearly been argon loss from each of the samples, but obviously the highest (precisely measured) ages of the high temperatures represent *minimum* estimates of the age of the mica.

The age spectrum of the Dome mica with the highest reliable high temperature age is shown in Figure 233.4. This minimum age for the mica is 2633±6 Ma. But the hosting Preston porphyry has been zircon-dated (S. Marmont, Geologist, Ontario Geological Survey, Toronto) at 2685±3 Ma, so that age of the Dome Mine gold lies between 2633±6 Ma and 2685±3 Ma. The uncertainty in the age of the gold is, therefore, about ±25 Ma, or about ±1%. To the best of the authors' knowledge, such a precise date on an Archean gold deposit has not been published.

The overall shape of the Dome age spectra cannot be explained by a single episode of argon loss. The simplest model which gives a good fit to the experimental data involves two episodes of argon loss. All the observed age spectra require a significant perturbation at about 2400 Ma ago (Figure 233.4) followed by a much milder disturbance at about 1800 Ma ago.

There is little evidence of a significant igneous or metamorphic event in this area 2400 Ma ago, and we speculate that the event is connected with movement(s) on the fault system associated with the gold in this region.

Hollinger Fuchsites (Figures 233.5 to 233.7)

All three age spectra resemble those from Dome (and must reflect very similar thermal histories) and we adopt the same interpretation. In this case, the highest high-temperature age is the value of 2617±8 Ma obtained in the laser run on one grain of Hollinger host mica (analyst: C.M. Hall). While the zircons from the hosting Millerton porphyry have not yet been U-Pb dated, several other porphyries, such as the Preston, in the area are about 2685 Ma old. The Hollinger deposit is, therefore, older than 2617±8 Ma and is very probably younger than about 2685, meaning that the uncertainty in its age is likely about ±35 Ma, or less than ±1.5%.

As was the case with Dome, the Hollinger age spectra are consistent with a significant perturbation at about 2400 Ma ago.

If the age spectra in Figures 233.1 to 233.7 are examined, it can be seen that there are small but definitely detectable differences among all the fuchsites. This suggests that there have either been slight differences in thermal history on a geographically small scale, or that the different micas have slightly different blocking temperatures (there may have been a combination of both factors involved). Regardless of the exact explanation, these results suggest that small, real-age differences can be detected experimentally. This strongly suggests that it would be possible to obtain even older lower bounds on the ages of the Dome and Hollinger deposits by further analyses.

Hemlo Fuchsite

As may be seen in Figure 233.8, the age spectrum contrasts sharply with those from Dome and Hollinger. The spectrum is almost completely flat with an indication of only slight argon loss. If this result is characteristic of the whole deposit, then Hemlo has experienced a far more tranquil history than that of Dome and Hollinger. Seventy-five percent of the released argon defines a plateau age of 2658±5 Ma. The ages in the final 18% of argon release climb in two steps through 2665±5 Ma to 2671±5 Ma. Evidently, the Hemlo mica is older than this latter age. Since the gold at Hemlo appears to be older than the green mica, then 2671±5 Ma is a minimum age for this deposit.

Unfortunately, at the time of writing, U-Pb dating of the associated zircons, which should give a maximum age for the deposit, had not been completed. However, the setting of the Hemlo deposit is quite similar to that of Dome and Hollinger. If, as seems likely (S. Marmont, personal communication, 1985), the Hemlo porphyry is the same age as the porphyries in the Dome-Hollinger region, then the Hemlo gold will have been bracketed to between 2671±5 and 2685±3 Ma. There seems to be a great probability that, because of its relatively peaceful post-crystallization history, the Hemlo deposit will be dated with a precision limited only by the uncertainties in the uranium and potassium isotope half-lives.

Age Studies in Red Lake Region

In the Red Lake greenstone belt, gold formation, hydrothermal alteration, and activity on deformation zones are all intimately related to batholith intrusion and resulting metamorphism. In an attempt to unravel this complex sequence of events, a collaborative study is being carried out with A.J. Andrews (and his co-workers) of Ontario Geological Survey, Toronto. The $^{40}Ar/^{39}Ar$ data are being integrated with the detailed Ontario Geological Survey study of the area.

Initial studies are focused on the contact aureole of the Trout Lake Batholith and on the Cochenour, Campbell, and A.W. White Mines. The intent is to discover the thermal history of the contact zone and to position the time of hydrothermal activity and gold formation within this history.

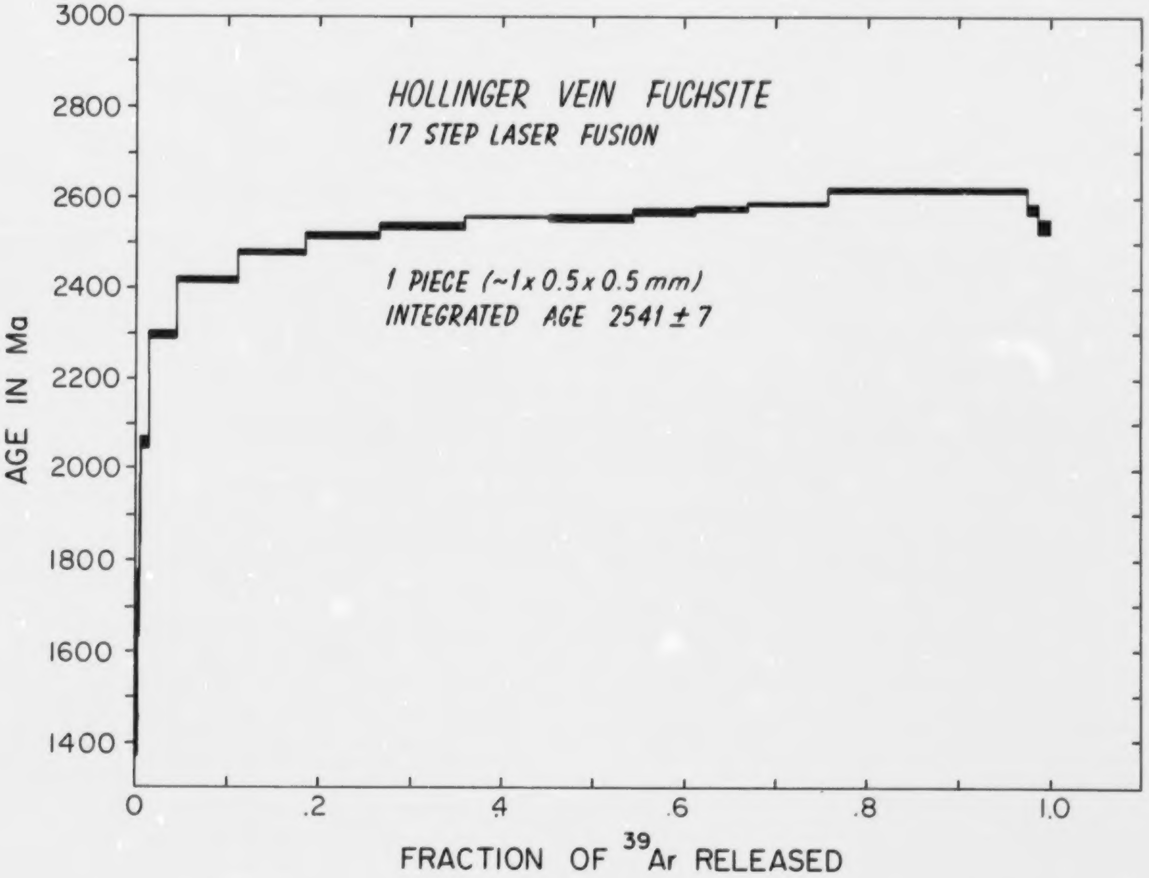

Figure 233.7. *Age spectrum of Hollinger vein fuchsite—single grain.*

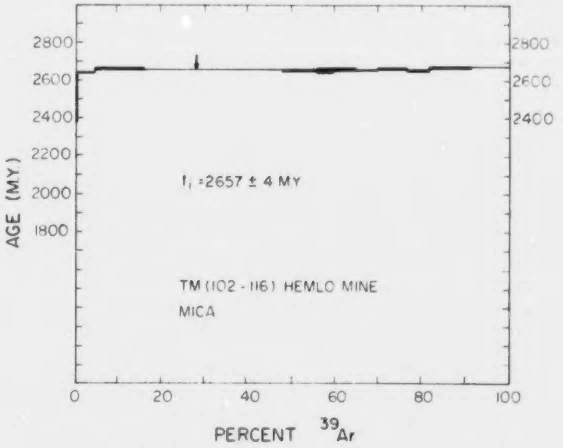

Figure 233.8. *Age spectrum of fuchsite from Hemlo.*

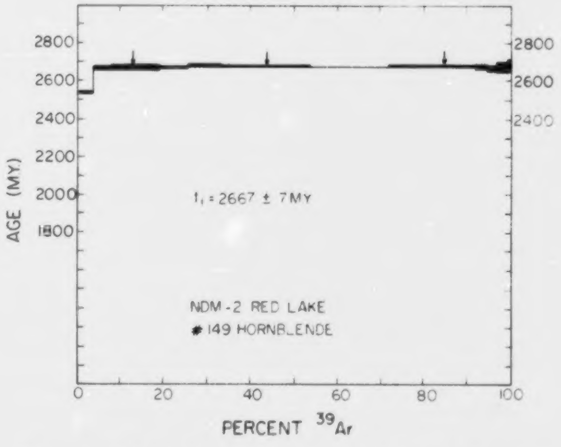

Figure 233.9. *Age spectrum of hornblende from Trout Lake Batholith aureole.*

Contact Aureole Samples

Detailed age spectra have been derived from one hornblende and one mica (Figures 233.9 and 233.10).

The hornblende was extracted from an amphibolite grade basalt located about 20 m from the granite contact. As may be seen in Figure 233.9, over the vast majority of its argon release, the hornblende

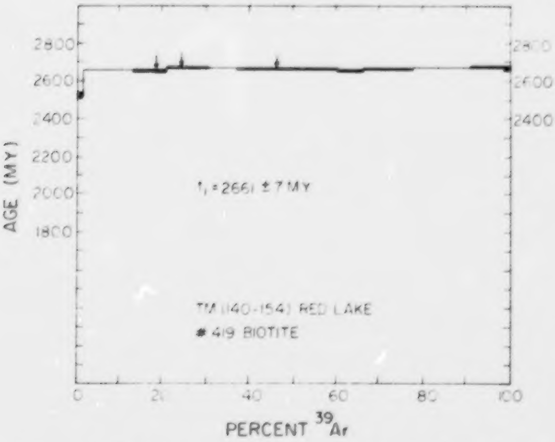

Figure 233.10. Age spectrum of biotite from Trout Lake Batholith aureole.

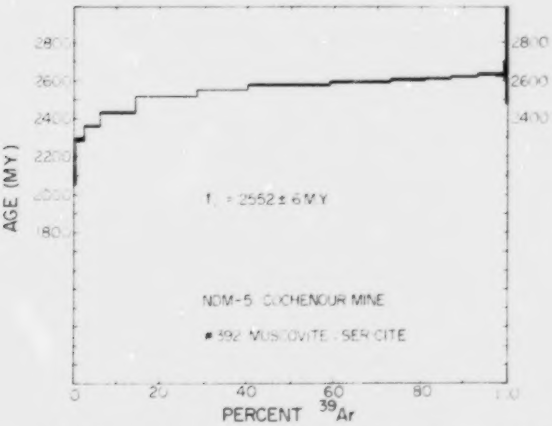

Figure 233.11. Age spectrum of muscovite-sericite from Cochenour Mine.

exhibits a remarkable plateau with an age of about 2675 Ma. The sharp climb in age at low temperatures indicates that the ambient temperature fell quickly (at this time) through the hornblende argon blocking temperature.

The biotite was extracted from a greenschist grade basalt about 5 km from the contact. Once again, a remarkable plateau is seen in the argon age spectrum (Figure 233.10). Evidently only the most minute amount of argon has been lost from this sample after it became a closed system about 2665 Ma ago. Furthermore, the rapid rise in age at low temperatures indicates that the ambient temperature fell swiftly through the argon blocking temperature of the mica.

Thus, the hornblende and biotite age spectra results both point to relatively rapid cooling at two different points in the contact aureole. Furthermore, the undisturbed nature of the biotite plateau indicates a very peaceful history at that immediate locale post 2665 Ma ago.

Cochenour, Campbell, and A.W. White Mine Micas

In contrast with the evidently tranquil histories just seen in the contact aureole samples, all three micas from the mines have obviously undergone significant perturbation long after crystallization.

Cochenour and Campbell Muscovite-Sericite Mixtures

The Cochenour minerals were extracted from a highly altered felsic dike closely related to the ore. The Campbell micas were taken from a highly altered felsic volcanic.

The age spectra for these two different mines (Figures 233.11 and 233.12) are indistinguishable over the whole range of argon release. The agreement is remarkable testimony to essentially **identical** thermal-mechanical histories of the two mines during the past 2650 Ma.

The most striking feature of these two identical spectra is their similarity in shape to the families of spectra found for the Dome and Hollinger fuchsites. Just as we concluded the Dome gold was over 2633±6 Ma, so we can deduce here, from the high-temperature asymptotes of the age spectra for Cochenour and Campbell, that their gold is over 2629±6 Ma in age. Since the Red Lake gold is younger than the Dome Stock, which has been U-Pb dated at 2718±1 Ma (Corfu and Wallace 1986), the Cochenour and Campbell gold deposits are both between about 2630 and 2720 Ma in age.

Preliminary numerical modeling of the muscovite-sericite age spectra is consistent with these two deposits having been perturbed about 2400 Ma ago in harmony with the conclusions we reached earlier about Dome and Hollinger. Since there is no evidence of a significant magmatic or metamorphic event at this time in the region (e.g. the contact aureole mica suffered no significant disturbance at 2400 Ma ago), we conclude, as we did for Dome and Hollinger, that the perturbation was connected with activity along fault (deformation) zones.

It is curious that two very widely separated regions (Red Lake and Timmins) show apparent fault activity at about 2400 Ma ago. Recently, M. Lopez-Martinez of this laboratory has found $^{40}Ar/^{39}Ar$ evidence that a surge of uplift along the Kapuskasing Zone may have occurred at this time. It is interesting to speculate that the associated crustal warping on either side of the Zone may have reactivated formerly quiescent deformation zones in the Timmins and Red Lake districts.

A.W. White Biotite

This hydrothermal mineral is taken from highly altered rock from the ore stope. The age spectrum (Figure 233.13) is slightly more complex than the other two Red Lake spectra. The age climbs quickly at low temperature, but then sags slightly before going into a monotonic rise. The low temperature behaviour is difficult to interpret, but it seems again reasonable to regard the precise high temperature age as a minimum. In this case, we conclude that the biotite is over 2634±4 Ma in age. Thus the lower limit

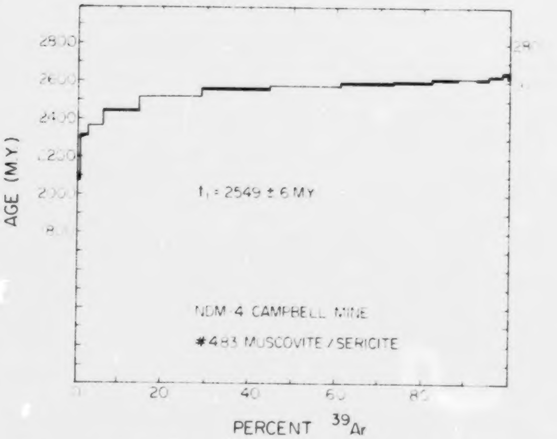

Figure 233.12. *Age spectrum of muscovite-sericite from Campbell Mine.*

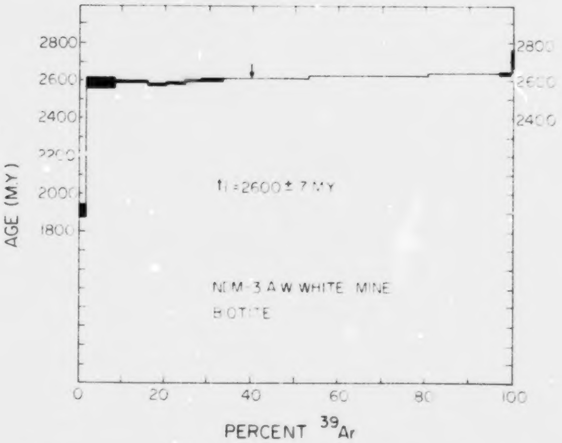

Figure 233.13. *Age spectrum of biotite from A.W. White Mine.*

for the age of the White gold is essentially the same as that just found for Cochenour and Campbell.

SUMMARY

The following conclusions may be drawn from the research so far completed.

1. The results on Dome and Hollinger samples show that the strategy of dating some gold deposits via the combination of analyzing green micas and zircons is effective.
2. The highest reliable high-temperature age found for the Dome fuchsites is 2633±6 Ma. The hosting Preston porphyry U-Pb zircon age (S. Marmont, Geologist, Ontario Geological Survey, Toronto) is 2685±3 Ma. Therefore, the Dome gold mineralization occurred sometime between these two dates. The uncertainty of this age is therefore only about ±25 Ma.
3. The Hollinger green micas are over 2617±8 Ma old. If, as we have argued above, the hosting porphyry age is 2685±3 Ma, then the age of the Hollinger gold lies between these two dates.
4. Detailed mathematical modeling of a Dome mica age spectrum shows the latter is consistent with the following history: (a) the mica became a closed system for argon retention 2640 Ma ago; and (b) the system remained closed except for two, sharp, disturbing pulses which produced argon losses of about 27% and 3% at approximately 2450 Ma and 1800 Ma ago, respectively.
5. The general flatness of the Hemlo mica age spectrum strongly suggests an extremely quiet history for this sample during the past 2660 Ma. The final steps indicate that the Hemlo gold is over 2671±5 Ma old. Because of this apparently tranquil history, Hemlo offers the prospect of becoming easily the most precisely dated Archean gold deposit known.
6. In the Red Lake region, a significant beginning has been made in unraveling the complex series of events surrounding the emplacement of the Trout Lake Batholith and gold formation. The remarkable flatness and the sharp rise at low temperatures seen in the contact aureole hornblende and mica age spectra both testify to rapid cooling. The hornblende became a closed system at ≅550°C about 2675 Ma ago. The mica followed suit at about ≅300°C 10 Ma later.
7. The flatness of the biotite plateau indicates a very peaceful history after 2665 Ma ago at the collection site.
8. In complete contrast with this undisturbed history seen in the contact aureole specimens, the muscovite-sericite mixtures from the Cochenour and Campbell Mines show argon-loss age spectra which are very similar to those derived from the Dome and Hollinger specimens.
9. Since the perturbations affecting the Red Lake Mine samples evidently did not extend to the contact aureole material, we speculate that these disturbances were probably due to reactivation of the narrow deformation zones in which the mines are located.
10. The Cochenour and Campbell mica age spectra are identical within experimental error, demonstrating that these mines have experienced essentially identical thermal histories.
11. The oldest precisely measured high-temperature age measured for the Cochenour and Campbell mica mixtures is 2629±6 Ma. If the micas are associated with gold formation, as suggested by A.J. Andrews (Geologist, Ontario Geological Survey, Toronto, personal communication, 1985), then the gold mineralization here occurred prior to 2629±6 Ma ago, but more recently than the 2718±1 Ma age of the Dome Stock (Corfu and Wallace 1986).
12. The highest, precise high-temperature age of the A.W. White biotite is 2634±4 Ma. If the White gold formation is related to that of the biotite (A.J. Andrews, personal communication, 1985), then the age of the ore lies between 2634±4 Ma and the 2718±1 Ma age of the Dome Stock.

ACKNOWLEDGMENTS

The project is significantly supported by Natural Sciences and Engineering Research Council (NSERC) grants. We are indebted to S. Marmont and A.J. Andrews (Geologists, Ontario Geological Survey, Toronto) for the provision of samples. P. Kuybida (Technician, University of Toronto, Toronto) performed mineral separations, and he and W. John Kenyon (Technician, University of Toronto, Toronto) assisted with sample fusions and mass spectrometry. C.M. Hall (Research Associate, University of Toronto, Toronto) performed a laser step analysis.

REFERENCES

Berger, G.W., and York, D.
1981: Geothermometry from $^{40}Ar/^{39}Ar$ Dating Experiments; Geochimica et Cosmochimica Acta, Volume 45, p.795-811.

Corfu, F., and Wallace, H.
1986: U-Pb Ages for Magmatism in the Red Lake Belt, Northwestern Ontario; Canadian Journal of Earth Sciences, Volume 23, p.27-42.

Hall, C.M., Walter, R.C., Westgate, J.A., and York, D.
1984: Geochronology, Stratigraphy, and Geochemistry of Cindery Tuff in Pliocene Hominid-Bearing Sediments of the Middle Awash, Ethiopia; Nature, Volume 308, p.26-31.

York, D., Hall, C.M., Yanase, Y., Hanes, J.A., and Kenyon, W.J.
1981: $^{40}Ar/^{39}Ar$ Dating of Terrestrial Minerals with a Continuous Laser; Geophysical Research Letters, Volume 8, p.1136-1138.

Zartmann, R.E.
1964: A Geochronologic Study of the Lone Grove Pluton from the Llano Uplift, Texas; Journal of Petrology, Volume 5, p.359-409.

Grant 236 Au–Quartz Vein and Intrusion–Hosted Cu–Au–Ag–Mo Mineralization, Hollinger–McIntyre Mines, Timmins, Ontario: Geological Characteristics, Structural Examination, Igneous and Hydrothermal Alteration Geochemistry, and Light Stable Isotope (Hydrogen and Oxygen) Geochemistry

P.C. Wood, D.R. Burrows, and E.T.C. Spooner

Department of Geology, University of Toronto, Toronto

ABSTRACT

The Hollinger-McIntyre Au-quartz vein system occurs within a series of flows which dip and young to the south. The flows have been intruded by a number of lensoidal quartz-feldspar porphyry stocks that also dip to the south and pitch approximately to the east. Several albitite dikes that are post-porphyry but pre-ore in age, also occur within the mine area. Both the deformed metavolcanics and porphyries exhibit a well developed prolate fabric of the same magnitude which indicates that the porphyries were intruded before the development of fabric.

Main stage vein attitudes are extremely variable, but do show a principal concentration which does not correspond to the attitude of the principal foliation, and no concentrations which could reasonably correspond to extension normal to σ_3 or to Riedel shears in a shear zone. In fact, the veins appear to have been developed in one event as no crosscutting relationships have been observed. The concentration of vein attitudes is interpreted to be a result of hydraulic fracturing and oriented normal to σ_3. An important point relevant to continued mineral exploration in the Timmins area is that the Hollinger-McIntyre mineralization developed within, but crosscuts, a high-strain shear zone.

The least altered porphyries are characterized by an intermediate SiO_2 content (66.8±2.1%; 1σ), a relatively high Na_2O content (5.29% to 5.71%), and a relatively low K_2O content (1.67% to 1.92%). On a QAP ternary diagram, they plot in the quartz-monzodiorite and granodiorite fields. Albitite dikes are very altered as indicated by high CO_2 contents. However, they appear to be markedly different, less fractionated compositions than the porphyries, as indicated by high TiO_2, Fe (as Fe_2O_3), MgO, CaO, and particularly Cr, Ni, and V contents. SiO_2 contents, even on a completely CO_2 free basis, are only 53.9% and 54.8%.

Hydrothermal alteration of porphyry is characterized by gains in K, Fe, S, and CO_2 (latter variable) and losses in Na and Mg. Alteration pyrite did not develop just by sulphidation of wall-rock, as it appears that some Fe was also provided by the fluid.

Hollinger fluid $\delta^{18}O$ values of +4.7±0.5‰ (1σ; n=24) derived from carbonates, quartz, and scheelite measurements are closely comparable with estimates for the Mink Lake Au- and W-enriched MoS_2 fluid (+6.0±1.9‰; n=19) which is provably of magmatic origin. Similarly, six out of nine direct fluid inclusion H_2O δD measurements (-57±12‰; 1σ) also lie within the general magmatic range (-85‰ to -50‰) of Taylor (1979) and, therefore, add further evidence in support of a magmatic origin for the Hollinger-McIntyre Au-quartz vein ore fluids.

INTRODUCTION

The objectives of this report are:

1. To provide documentation of characteristics of the main Au mineralization in the form of surface pit maps, an underground stope map, and photographs. These illustrations are all in *addition* to those in Wood *et al.*, in press) and Burrows and Spooner (in press).
2. To examine aspects of the structural geology of the local area which are relevant to controls on the spatial location of mineralization, and to the relative timing of events.
3. To discuss the major and trace element geochemistry of the igneous intrusions (porphyries and albitites).
4. To describe the basic geochemistry of hydrothermal alteration as it affects strained porphyries.
5. To estimate and discuss the hydrogen and oxygen isotope geochemistry of the main-stage Au ore fluid.

GEOLOGICAL CHARACTERISTICS

The Hollinger-McIntyre Au-quartz vein system is located within a folded series of volcanic flows (Figure 236.1 and Table 236.1). These rocks range in composition from iron to magnesium tholeiites (Pyke 1982), exhibit a well developed fabric due to folding and shearing, and have undergone hydrothermal alteration. These flows have been intruded by a number of lensoidal porphyry stocks that dip to the south and pitch approximately to the east (Figure 236.1). Several albitite dikes that are post-porphyry, but pre-ore in age, also occur in the mine area but do not outcrop at surface.

The Central Formation, intruded by the Pearl Lake and Millerton porphyries, hosts the bulk of the main ore zone mineralization. It is composed of a series of massive, pillowed and brecciated flows. The Northern and Vipond Formations also host mineralization, but to a much lesser extent (Figure 236.1 and Table 236.1).

The up-plunge extension of the Hollinger central ore zone has been, and is currently being, mined by a number of small, fairly high grade open pits. These

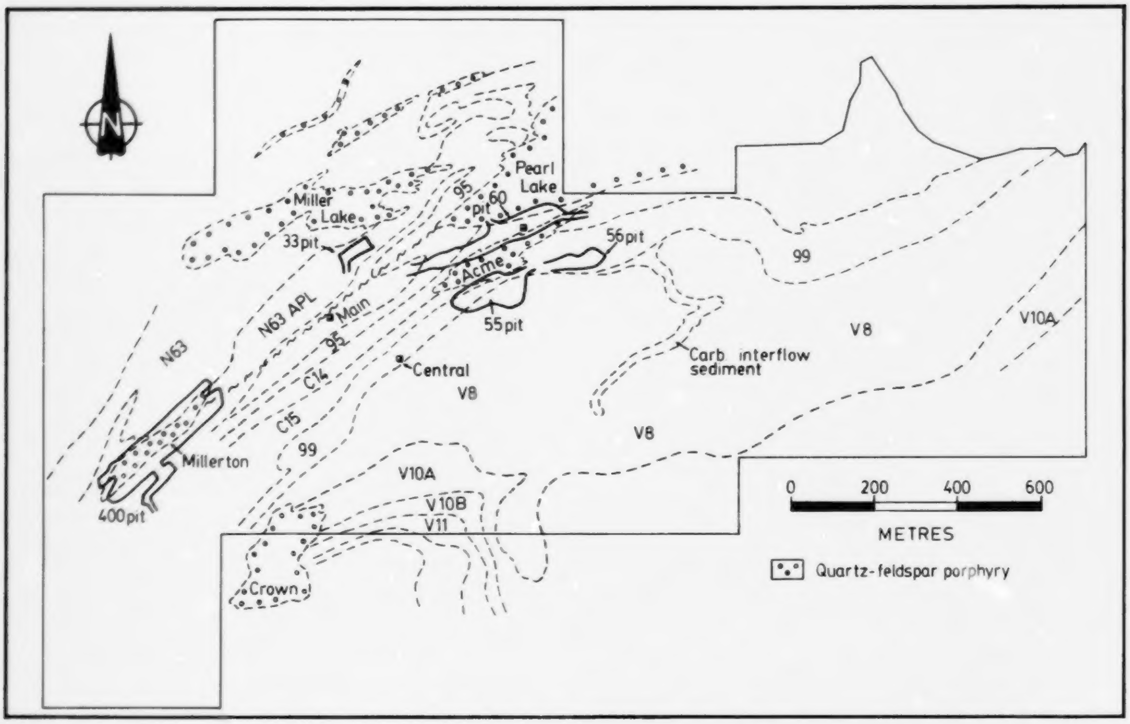
N
Pearl Lake
Miller Lake
33pit
95 pit
60
56pit
Acme
55pit
N63 APL
Main
95
C14
C15
99
Central
V8
N63
Millerton
400pit
V10A
V10B
V11
Crown
Carb interflow sediment
99
V8
V8
V10A
0
200
400
600
METRES
Quartz-feldspar porphyry

Figure 236.1. Geological map of the Hollinger Property showing the distribution of strained porphyritic intrusions, lithological relationships, and pit locations. Both 1 and 92 Pits, located to the west and southwest of Central Shaft respectively, and a few other minor surface workings have not been included in order to simplify the diagram.

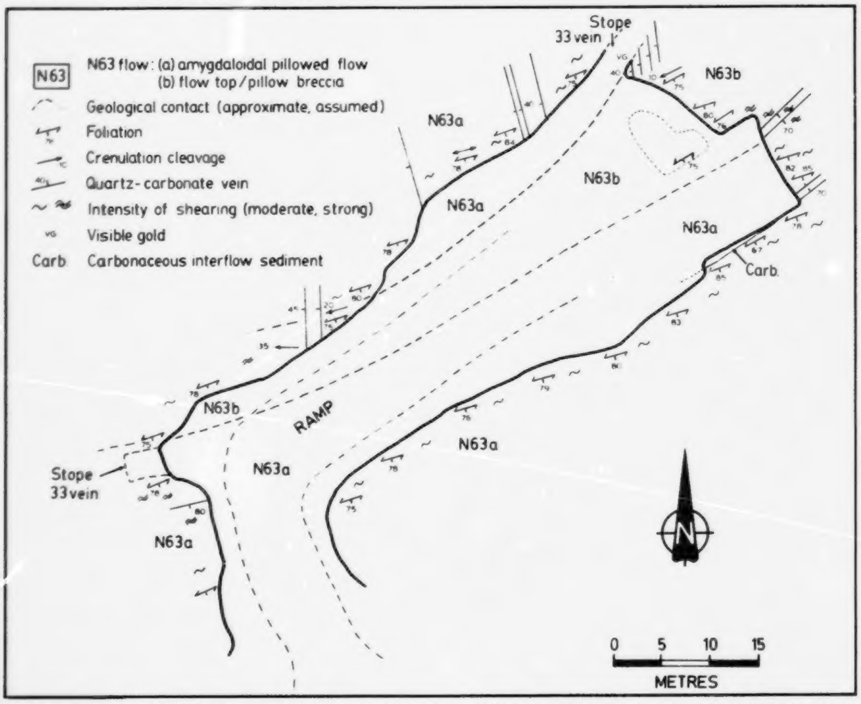
N63
N63 flow: (a) amygdaloidal pillowed flow
(b) flow top/pillow breccia
Geological contact (approximate, assumed)
Foliation
Crenulation cleavage
Quartz-carbonate vein
Intensity of shearing (moderate, strong)
VG
Visible gold
Carb
Carbonaceous interflow sediment
Stope 33 vein
N63b
N63a
N63b
N63a
N63a
Carb
N63b
RAMP
N63a
N63a
Stope 33vein
N63a
N
0
5
10
15
METRES

Figure 236.2. Detailed geological map of 33 Pit in the Hollinger Property showing lithological relationships, structure and vein distribution.

TABLE 236.1. LITHOLOGIES PRESENT IN THE HOLLINGER-McINTYRE AREA (MODIFIED AFTER FERGUSON 1968).

Matachewan		
	Quartz diabase dikes	
Algoman		
	(Mineralization)	
	Albitite dikes	
	Quartz-feldspar porphyry	
Keewatin		
Tisdale Group		
Vipond formation (subgroup)		
	V11 flow	-pillowed tholeiite
	V10B flow	-brecciated variolitic pillow lava ("chicken feed")
	V10A flow	-massive to finely brecciated tholeiite overlain by carbonaceous interflow sediments
	V9	-carbonaceous interflow sediments
	V8 flow	-variolitic pillow lava
	V7	-carbonaceous interflow sediments
	99 flow	-massive unpillowed tholeiite
Central formation (subgroup)		
	C16 flow	-massive unpillowed tholeiite overlain by carbonaceous interflow sediments
	C15 flow	-amygdaloidal pillow lava (APL)
	C14 flow	-amygdaloidal pillow lava (APL) and uniform textured tholeiite
	55 flow	-brecciated tholeiite overlain by interflow sediments
	95 flow	-pillowed tholeiite in places showing brecciated variolitic texture
Northern formation (subgroup)		
	N63 flow	-amygdaloidal pillow lava (APL) overlain in some localities by carbonaceous interflow sediments
	N63 flow	-uniform textured dacite

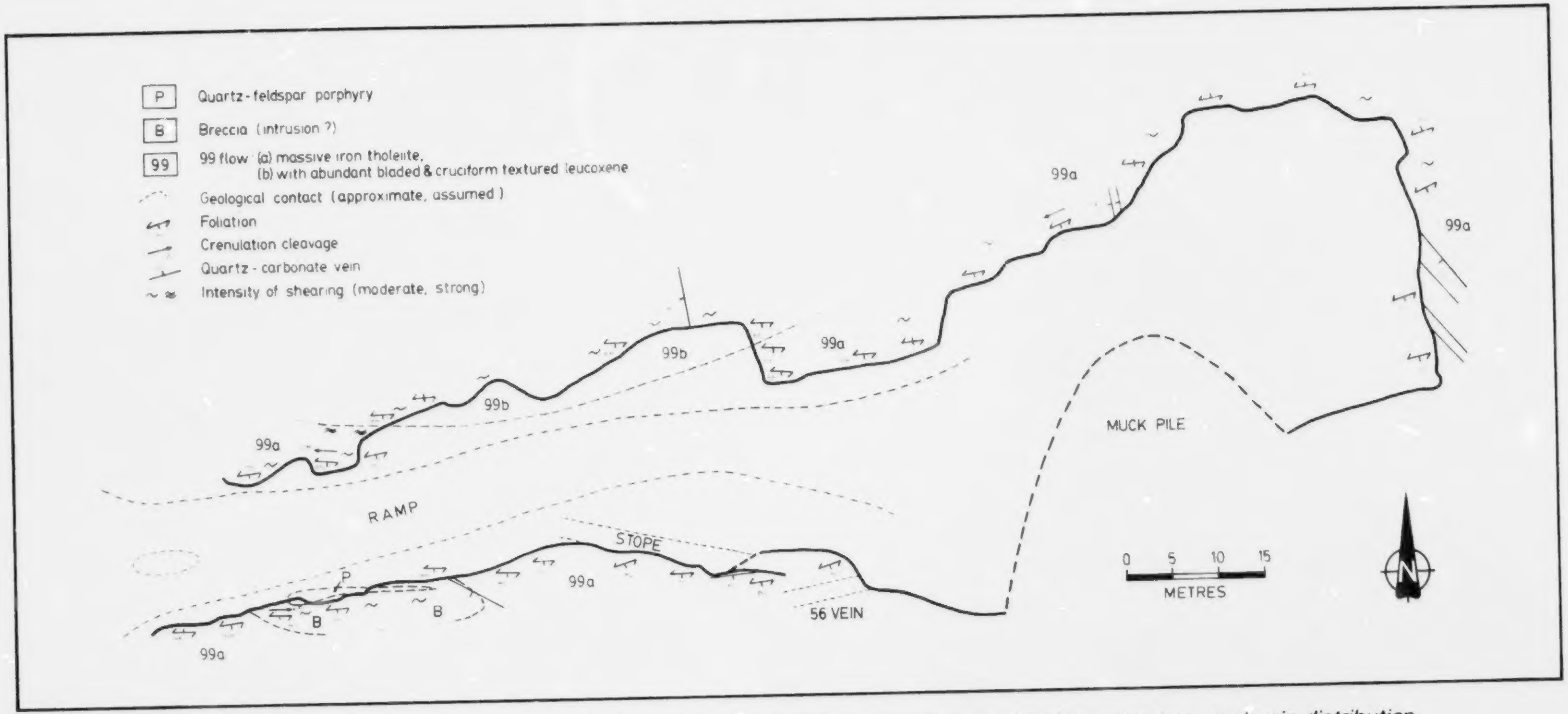
P Quartz-feldspar porphyry
B Breccia (intrusion ?)
99 99 flow (a) massive iron tholeiite,
(b) with abundant bladed & cruciform textured leucoxene
Geological contact (approximate, assumed)
Foliation
Crenulation cleavage
Quartz-carbonate vein
Intensity of shearing (moderate, strong)
99a
99b
99a
99b
99a
99a
99a
RAMP
STOPE
P
B
B
99a
99a
56 VEIN
MUCK PILE
0 5 10 15
METRES
N

Figure 236.3. *Detailed geological map of 56 Pit in the Hollinger Property showing lithological relationships, structure, and vein distribution.*

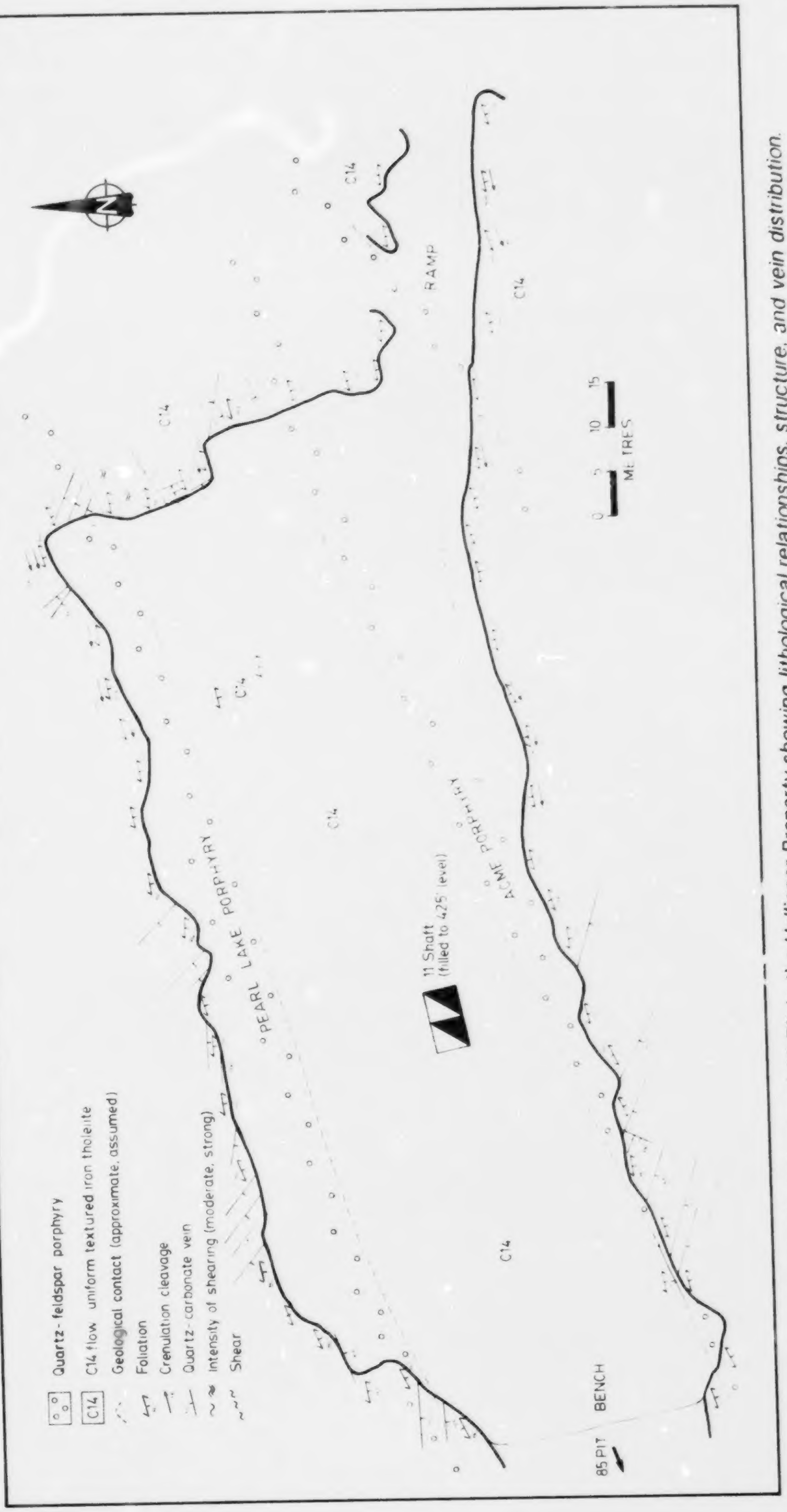
Quartz - feldspar porphyry
C14 flow uniform textured iron tholeiite
Geological contact (approximate, assumed)
Foliation
Crenulation cleavage
Quartz - carbonate vein
Intensity of shearing (moderate, strong)
Shear
N
C14
PEARL LAKE PORPHYRY
ACME PORPHYRY
11 Shaft (filled to 425' level)
RAMP
BENCH
85 PIT
0
5
10
15
METRES

Figure 236.4. Detailed geological map of 60 Pit in the Hollinger Property showing lithological relationships, structure, and vein distribution.

provide an excellent opportunity to examine the lithological and structural controls on mineralization in detail. Thus four pits (33, 55, 56, and 60), which occur at various locations within the stratigraphy and mineralization, were mapped and sampled in detail (Figures 236.1 to 236.4). The 55 Pit has been described by Wood *et al.* (in press).

33 PIT

This small pit, developed to recover ore left behind under the old Hollinger mill foundations, is located within the N63 flow of the Northern Subgroup which contains the oldest rocks in the mine stratigraphy (Table 236.1 and Figure 236.2). They are composed of amygdaloidal pillowed flows. The upper portion of the flows exhibits breccias, which in some areas are cemented with dark carbonaceous interflow material. Mineralization is associated with a series of small, sometimes parallel to subparallel quartz-carbonate veins where coarse gold commonly occurs along vein footwalls. Sphalerite forms a common vein accessory and is often associated with the gold. This gold-sphalerite association has also been recorded in the Pamour #1 Mine, particularly in high-grade sections (Price and Bray 1948). Veins are generally oriented oblique to fabric, though some earlier fabric parallel veins were observed (Figure 236.2). Veins often exhibit well developed pyrite-rich alteration selvages where, in some cases, wall-rock breccia fragments have been almost completely replaced. These zones are often ore grade material and gold is intimately associated with the alteration pyrite (Spooner *et al.* 1985).

56 PIT

This pit is situated to the southeast of the Acme Porphyry and located entirely within the 99 flow. This unit is located at the top of the Vipond Subgroup and forms an important marker horizon because of its lateral continuity and close relationship to the very distinctive, overlying variolitic pillowed flow (V8) (Jones 1948). The flow is a medium-grained, generally massive iron tholeiite (Pyke 1982) that contains leucoxene. On the northern face of the pit, the leucoxene is particularly well developed as euhedral, bladed to cruciform-textured grains, which impart a "spinifex-like" texture to the rock. Small porphyry pods with associated intrusion breccias intrude the flow on the southwest face (Figure 236.3). Mineralization is associated with quartz-carbonate veins which are oriented oblique to foliation and have well developed bleached, pyrite-rich alteration halos.

60 PIT

This large pit forms the eastern portion of a large pit complex (80, 85, and 60) developed to recover the central ore zone from surface down to about the 200-foot level. The 60 Pit mines the 11 shaft pillar and is situated between the Pearl Lake Porphyry to the north and the Acme Porphyry to the south (Figure 236.4). The thin volcanic screen which occurs between the two porphyries forms part of the C14 flow of the Central Subgroup. This unit is a fairly massive basalt with a fine, amygdaloidal, pillowed phase, and is the host to the bulk of the mineralization. Both porphyries are highly deformed as seen by buckling, kink banding, and shearing, while the veins are, in comparison, relatively undeformed. Mineralization is associated with quartz-carbonate veins of various orientations, but which are again generally oblique to fabric.

STYLE OF MINERALIZATION

Quartz veins consist of two main types: (i) early quartz-tourmaline-calcite veins (≤50 cm) generally parallel to the fabric occurring dominantly in volcanics close to the porphyries or in the porphyries themselves (Photo 236.1a); and (ii) "main stage" quartz-ankerite-pyrite veins. The former type is observed to be crosscut by the main stage veins. The quartz-tourmaline set lack pyritized bleached margins and are generally barren of Au. They were, however, mined where extensively reveined. A possible exception is in the "Main Flat-Vein system" in the southeastern part of Hollinger. These flat veins and intervening shear-controlled verticals are high grade, and yet tourmaline is distinctively present. Much of the Au is free, however, and the quartz strongly recrystallized and fractured, suggesting that this too may represent a later mineralizing event.

A significant contribution of last year's (1985) mapping underground in McIntyre was the observation of quartz-tourmaline veins cutting albitite dikes (Photo 236.1b) (discussed below). This relationship was suspected (e.g. Langford 1938) but not documented until now. These veins (Photo 236.1c) show a typical orientation approximately parallel to the fabric (and in this case dike margin), but in detail, small spurs extend off the main vein discordant to the weak fabric (Photo 236.1d)

As discussed in Spooner *et al.* (1985), it is possible to divide the main-stage veins into three types: (i) tabular continuous veins (Photo 236.2a), some of which branch, pinch, and swell (Photos 236.2b and 236.2c). This type is often localized at interflow horizons (e.g. #5 and #92 veins, Photos 236.2d and 236.2e). Considerable brecciation and inclusion of wall-rock material takes place as a result of multiple injection; (ii) tabular "vein zones" with a series of irregular, but approximately parallel, stringers (Photos 236.2f and 236.2g); and (iii) *en echelon* quartz stringers in shear-generated fractures. The spectacular appearance of this mineralization style is illustrated in Figure 236.5 , a large-scale, detailed stope map. During 1983, this stope, with an average grade of 3.4 to 6.9 grams Au per tonne, made a significant contribution to the underground production at Hollinger. These veins are typical of zones within the Millerton and other porphyries, and result from brittle fracture and dilation within small shear zones with development of sigmoidal veins, and occasionally a central "principal vein" (Photo 236.2h).

A detailed description of the vein mineralogy is given in Wood *et al.* (in press). The bleached, pyritized, vein selvage hosts 95% of the gold (e.g. Photo 236.2i).

A complete vertical and lateral examination of the Hollinger central ore zone was quite difficult due to limited accessibility and safety reasons. Thus, a problem encountered in describing the Hollinger min-

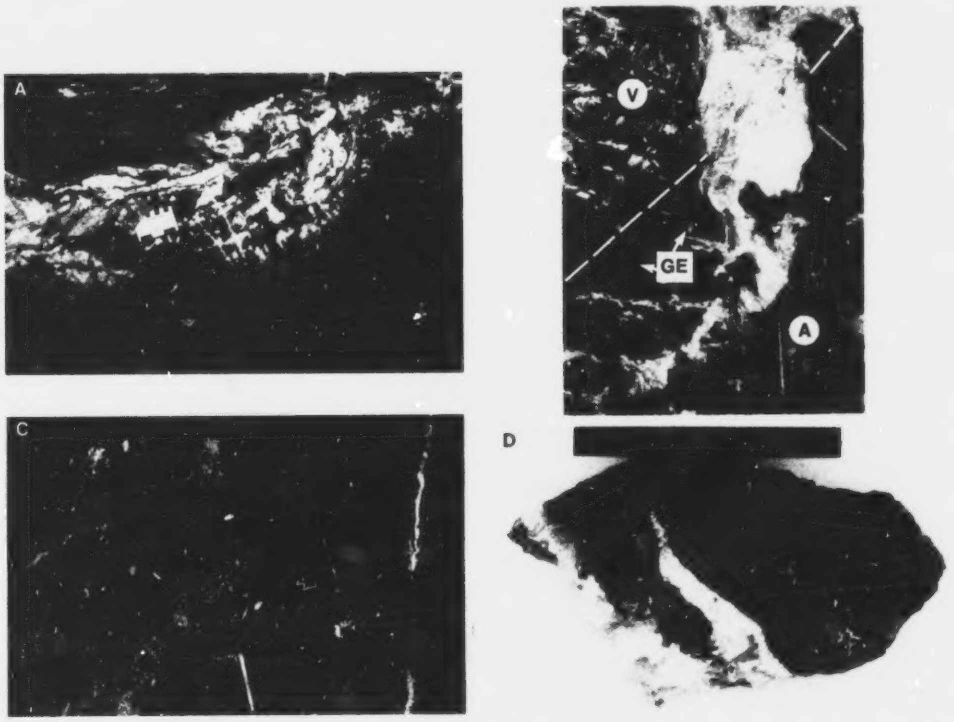

Photo 236.1. *(a) Early fabric-parallel quartz-tourmaline-carbonate vein with later quartz-filled extensional fractures, Hollinger Mine, 2750-foot level.*

(b) Quartz-carbonate-sulphide-tourmaline vein crosscutting albitite dike. Contact between albitite (A) and volcanics (V) is indicated by a dashed line. Note small elliptical "goose eggs" (GE).

(c) Quartz-carbonate-tourmaline vein within albitite dike and oriented parallel to contact, McIntyre Mine, 2500-foot level south of 11 shaft.

(d) Detail of quartz-carbonate-tourmaline vein in albitite with small spur extending from the main vein which is discordant to the weak fabric. Note bleaching of wall-rock proximal to vein. Location as in (c).

eralization was in determining whether our observations were representative of the system as a whole. Figure 236.6 shows drawings of composite photographs taken by L.C. Graton, H.E. McInstry, and others during a detailed examination of Hollinger in 1932. They represent typical vein structures at recorded locations and show the same distinctive vein shapes as we were able to observe.

STRUCTURAL EXAMINATION

STEREOGRAMS

Fabrics

Stereograms in Figure 236.7 illustrate the relationships between fabrics, vein geometries, lithological contacts, and lineations. Figure 236.7a shows that 66% of foliation poles (n=302, total) are relatively tightly concentrated in a zone corresponding to a planar fabric striking 046° to 086° and dipping 55° to 80° to the southeast. This foliation contains a strong prolate linear fabric plunging 45°to 65° to the east-southeast (064° to 110°), and affects both metavolcanics and porphyritic intrusions (Pearl Lake, Millerton, etc). As can be seen in Photo 236.3, the lineation defines an approximately 5:1:1 strain ellipsoid in *both* lithologies. Hence, since the porphyries show approximately the same amount of strain as the metavolcanics, they were intruded essentially completely *before* development of this L-S fabric. The latter fabric is equivalent to the "later" N65°E/73°S fabric recorded by Griffis (1962, 1978). The stereogram also shows a less prominent foliation which dips steeply (approximately 60° to 85°) to the north, as opposed to the southeast, and which has a similar strike (052° to 126°) to the main foliation. This fabric is more often observed in the northern parts of the McIntyre and Coniaurum Properties at depth, and also in peripheral areas such as in the Northern and Crown Porphyries in Hollinger. It may represent an earlier foliation preserved in areas outside the "central zone" of intense fabric development. It could also relate to the minor Northern Anticline (Ferguson *et al.* 1968), the existence of which is indicated by the presence of Vipond Subgroup Fe-tholeiites to the north of Gillies Lake, since the foliation has been occasionally observed to be axial planar to small north-verging folds on the 3625-foot level in McIntyre.

Late strain of the metavolcanics and strained porphyries occurs as a weak crenulation cleavage plunging at approximately 10° towards 090° to 100° in the plane of the main fabric, and, more rarely, in

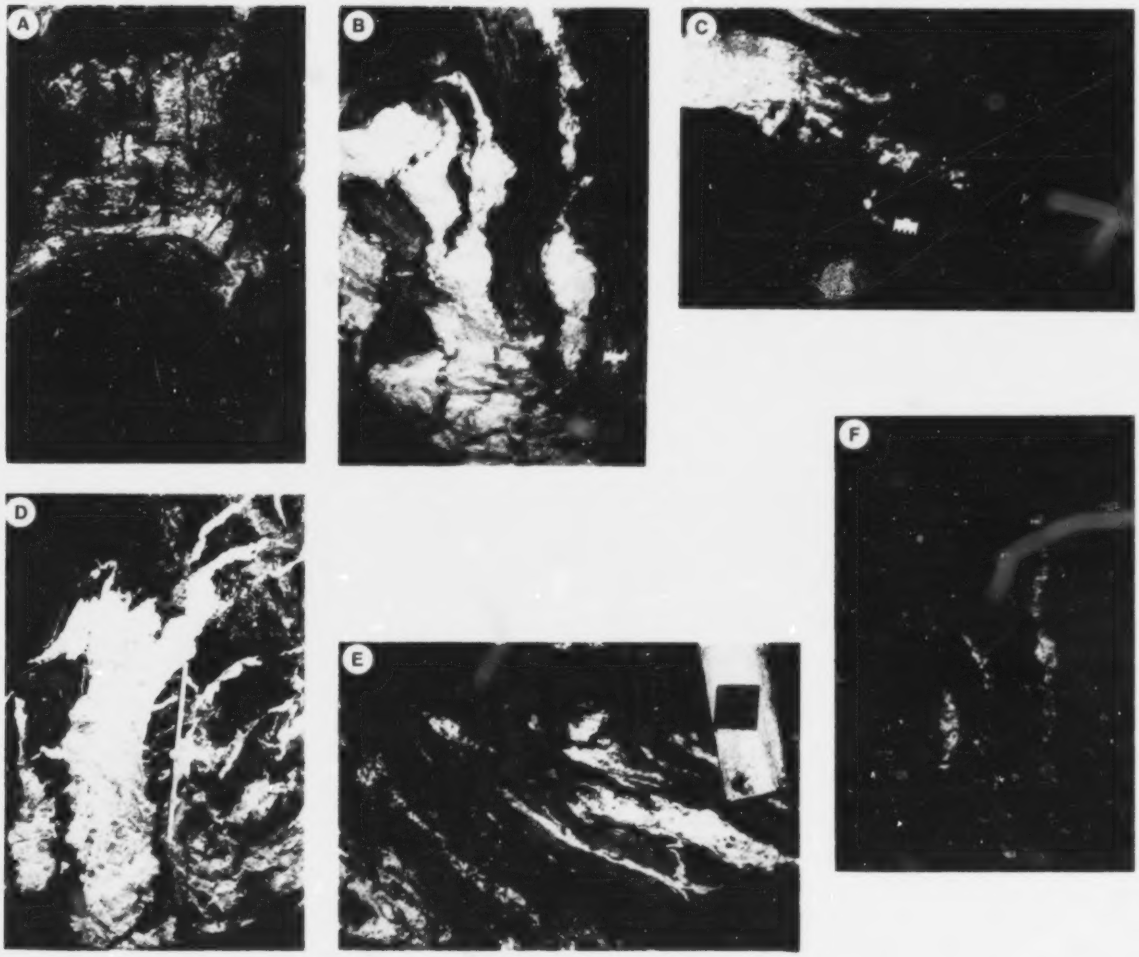

Photo 236.2 Photographs of vein structures from the Hollinger-McIntyre system.

(a) Large, tabular, continuous vein with numerous ribboned wall-rock inclusions, Hollinger Mine, 1400-foot level.
(b) Veins with irregular terminations, some of which pinch and swell, Hollinger Mine, 15-08-01 stope east end, 1550-foot level.
(c) Termination of larger vein branching into irregular feathers, Hollinger Mine, 15NH-W7, 1550-foot level.
(d) Irregular vein with small branching marginal spurs. McIntyre Mine, #5 vein, 1600-foot level.
(e) Deformed quartz-carbonate stringers and pods developed in ductile carbonaceous interflow sediments (92 vein). Hollinger Mine, 1250-foot level.
(f) Series of small, irregular, but approximately parallel stringers. Hollinger Mine, 55 vein E10, 1250-foot level.

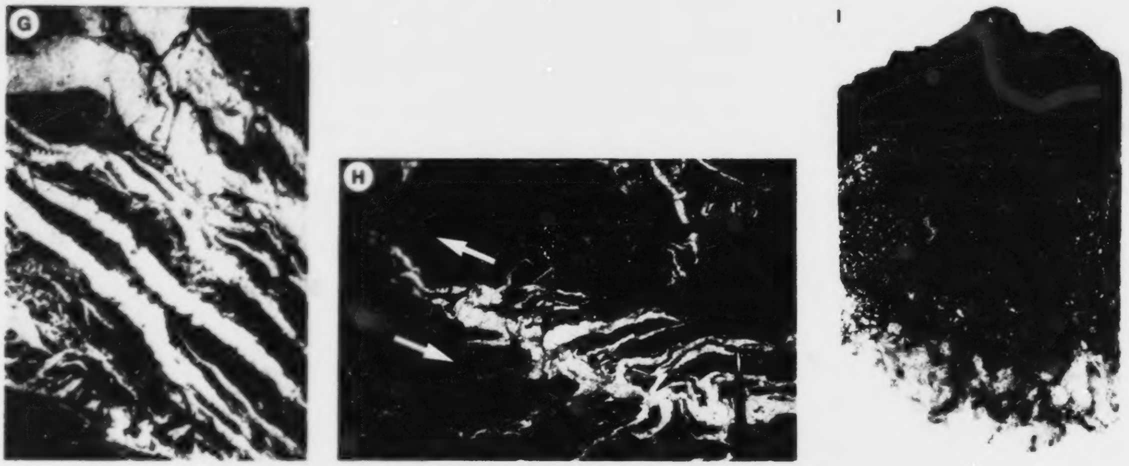

Photo 236.2 *Photographs of vein structures from the Hollinger-McIntyre system.*

- *(g) Subparallel veins forming a composite zone with a small set of shear-generated fractures in the lower left corner. Hollinger Mine, 18-83-01 stope, 1850-foot level.*
- *(h) Well developed sigmoidal shear veins with central "principal vein". Note sinistral sense of shearing. Hollinger Mine, 18-83-01 stope, 1850-foot level.*
- *(i) Bleached and pyritized alteration selvage developed proximal to a quartz-carbonate vein in mafic volcanic flow. At Hollinger ~95% of the gold produced is intimately associated with pyrite within the altered wall-rock.*

small buckles in highly foliated Acme and Pearl Lake Porphyries.

Vein Geometries

The very variable attitudes of measured Au-quartz veins and vein segments are shown in the stereogram in Figure 236.7b (147 poles). The bulk dip south to southwest at intermediate angles. However, there are also north, northeast, and northwest-dipping veins, and a significant number of relatively shallow-dipping veins. It can be seen quite clearly that the main concentration of vein attitudes does *not* correspond to the attitude of the principal foliation (Figure 236.7a)—an observation which is consistent with the fact that veins clearly crosscut the foliation (Spooner *et al.* 1985; Wood *et al.*, in press). However, several vein poles do occupy the same general region as the main fabric and as the measured porphyry contacts shown in Figure 236.7c, suggesting some local control. Likewise, several vein poles correspond to the attitude of south-dipping interflow horizons—an observation consistent with the occurrence of several major veins in McIntyre at carbonaceous interflow positions (e.g. #5, #7, and #25). It may also be noted that the vein poles do not show any particular concentrations relative to the attitude of the fabric lineation which might be interpreted as Riedel shears (e.g. Hugon and Schwerdtner 1985). Hence, it appears to be unlikely that the stress system which produced the L-S fabric probably in a shear zone (see below) was still in existence at the time of main stage Au-quartz vein mineralization.

The main stage Au-quartz veins in Hollinger-McIntyre show significant evidence of having been produced by hydraulic fracturing (Spooner *et al.* 1985). If $\sigma_1 \neq \sigma_2 \neq \sigma_3$, hydraulic fractures open normal to σ_3 (e.g. Haimson 1981). On the other hand, if $\sigma_1 \equiv \sigma_2 \equiv \sigma_3$, then hydraulic fractures are randomly oriented in a perfectly isotropic medium, or affected by anisotropy in an inhomogeneous medium (Haimson 1981). Hence, a possible interpretation of the vein geometry data is that: (i) the concentration of poles dipping south at intermediate angles reflects the orientation of original σ_3; (ii) the differences between σ_1, σ_2, and σ_3 were not large so that veins were actually opened up in variable orientations: and (iii) there was local control by lithological and strong pre-existing structural anisotropopy (e.g. interflow horizons in McIntyre).

Lineations

Lineations measured from stretched varioles (V8) and feldspar phenocrysts (porphyries) (Photo 236.3) are given in Figure 236.7d. They concentrate in a zone which plunges at 30° to 70° towards 080° to 100° (approximately to the east). This is similar to the regional plunge in the area which causes the porphyries to recede eastward on a line striking 084° (plunging at 40° to 60°) with increasing depth.

Finally, it may be noted that although the overall plunge of the Hollinger central ore zone is similar to the plunge of the porphyries and the L-S fabric, the internal vein geometries show no such relationship. Interpretation of this observation, which is consistent with observed timing relationships, is that the strained porphyries and the fabric acted in a gross sense as a control on dilatancy, but that the orientations of the individual veins which make up the ore zone were controlled by more immediate local factors.

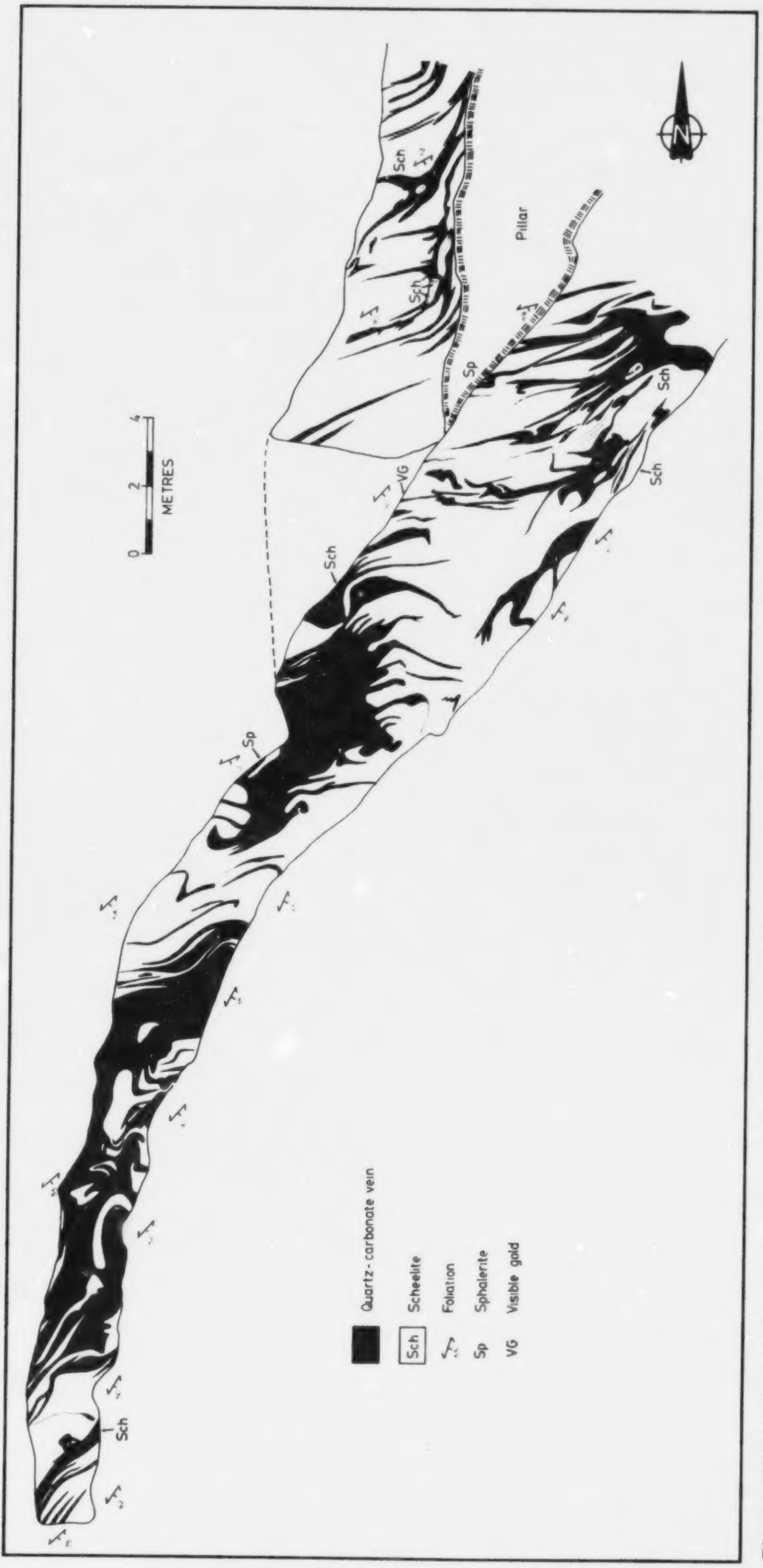
Quartz-carbonate vein
Sch Scheelite
Foliation
Sp Sphalerite
VG Visible gold
0 2 4
METRES
Sch
Sp
VG
Pillar
N

Figure 236.5. Detailed geological map of 15-08-01 stope (west end), 1550-foot level, Hollinger Mine, located entirely within the Millerton Porphyry, showing the complex nature of the veining and scheelite distribution.

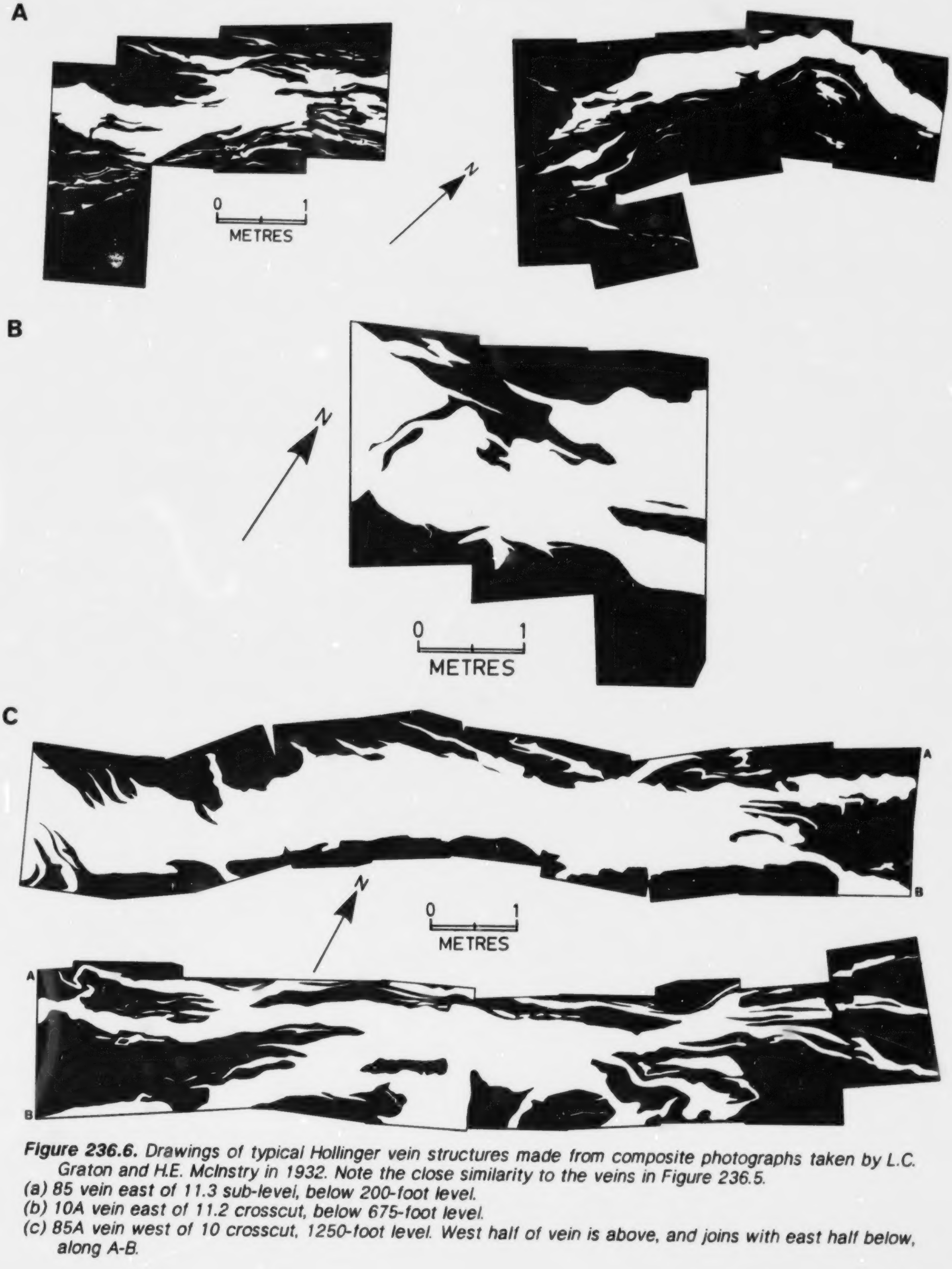

Figure 236.6. Drawings of typical Hollinger vein structures made from composite photographs taken by L.C. Graton and H.E. McInstry in 1932. Note the close similarity to the veins in Figure 236.5.
(a) 85 vein east of 11.3 sub-level, below 200-foot level.
(b) 10A vein east of 11.2 crosscut, below 675-foot level.
(c) 85A vein west of 10 crosscut, 1250-foot level. West half of vein is above, and joins with east half below, along A-B.

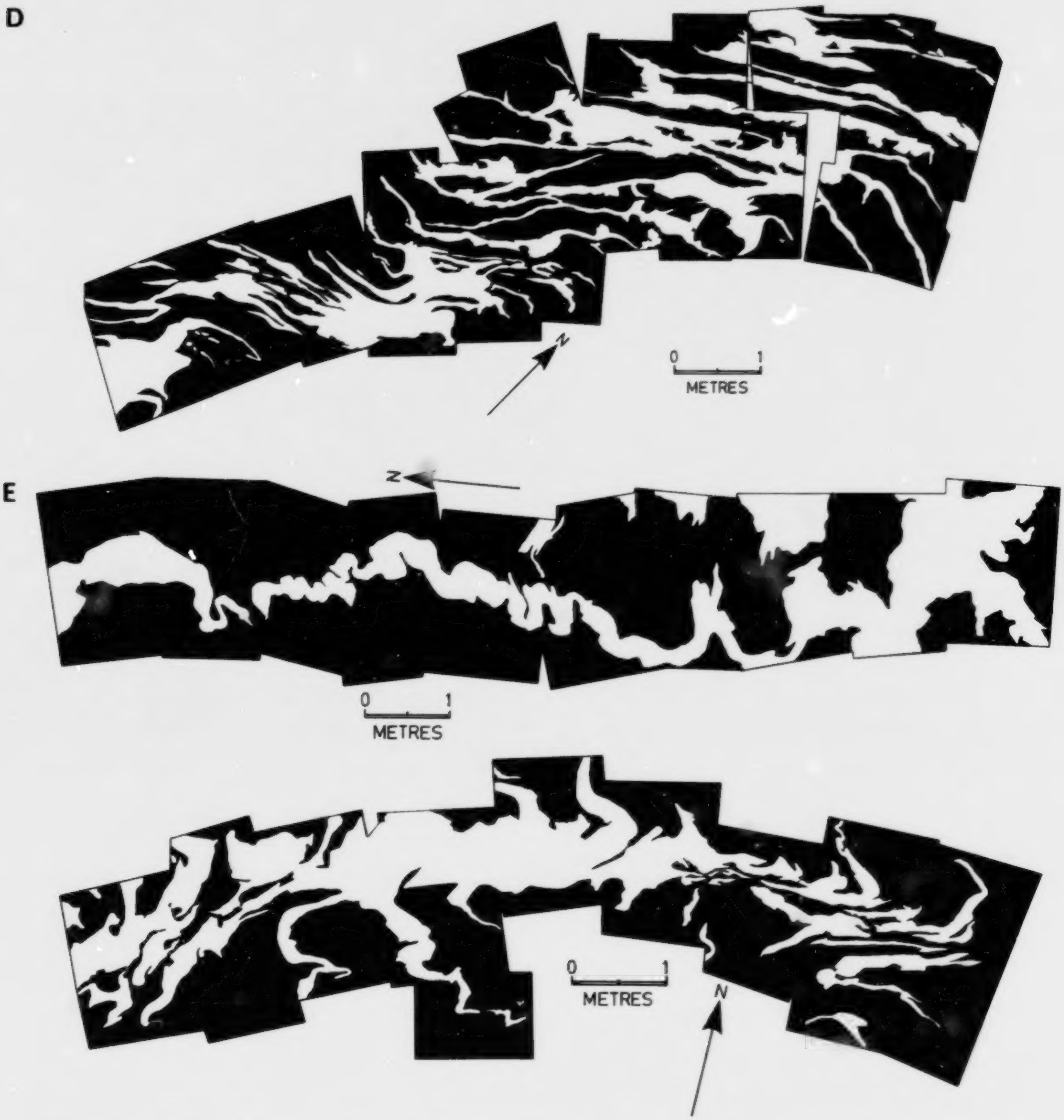

Figure 236.6. Drawings of typical Hollinger vein structures made from composite photographs taken by L.C. Graton and H.E. McInstry in 1932. Note the close similarity to the veins in Figure 236.5.

(d) 95 vein east of 15 crosscut, 2750-foot level.

(e) 97 vein south heading west of 13 crosscut, below 425-foot level (top), and 55 vein east of 15 crosscut, 3650-foot level (bottom).

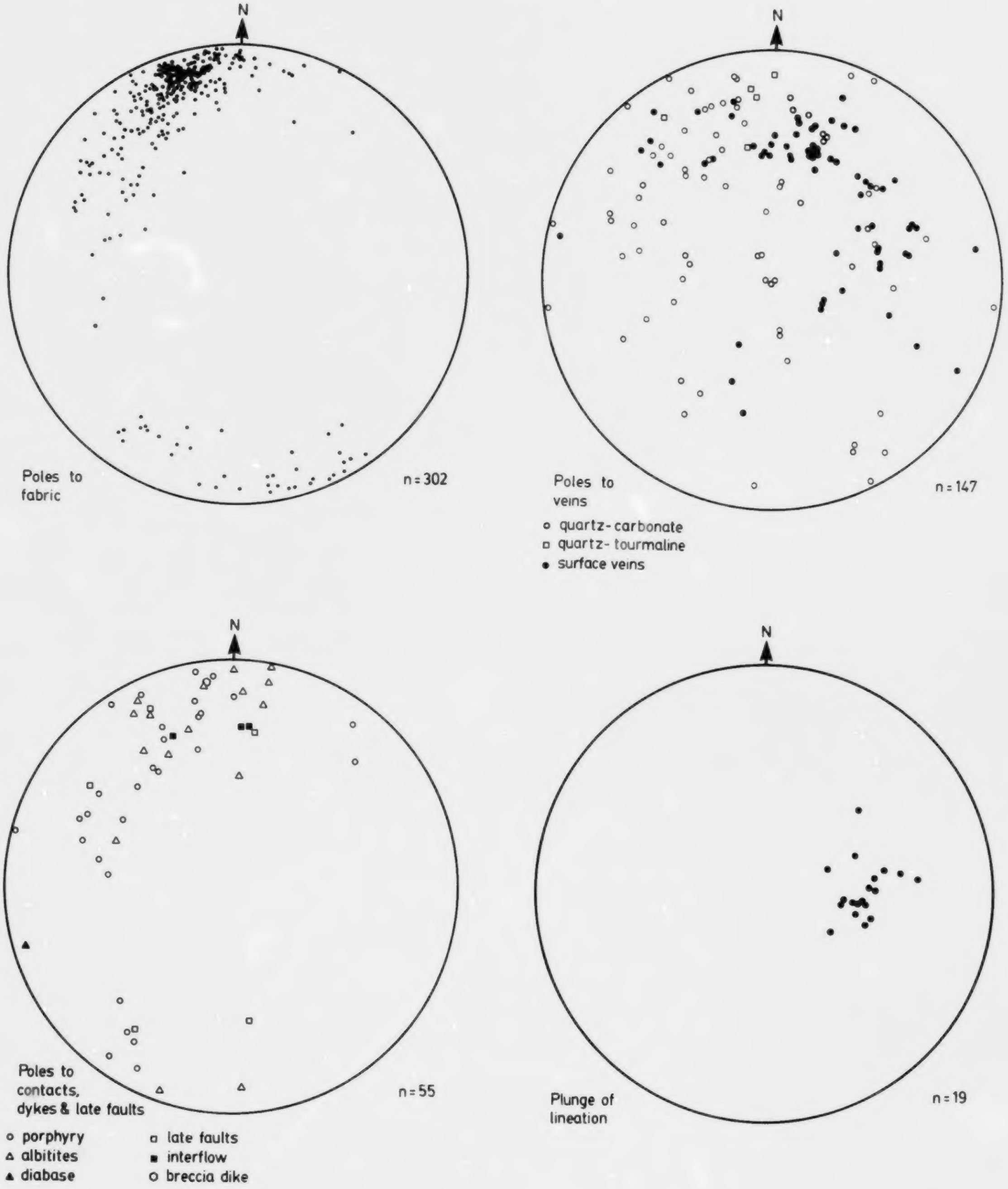

Figure 236.7. *Stereograms (lower hemispheres) of (a) fabrics, (b) vein geometries, (c) lithological contacts, dikes, and late faults, and (d) lineations from the Hollinger-McIntyre area.*

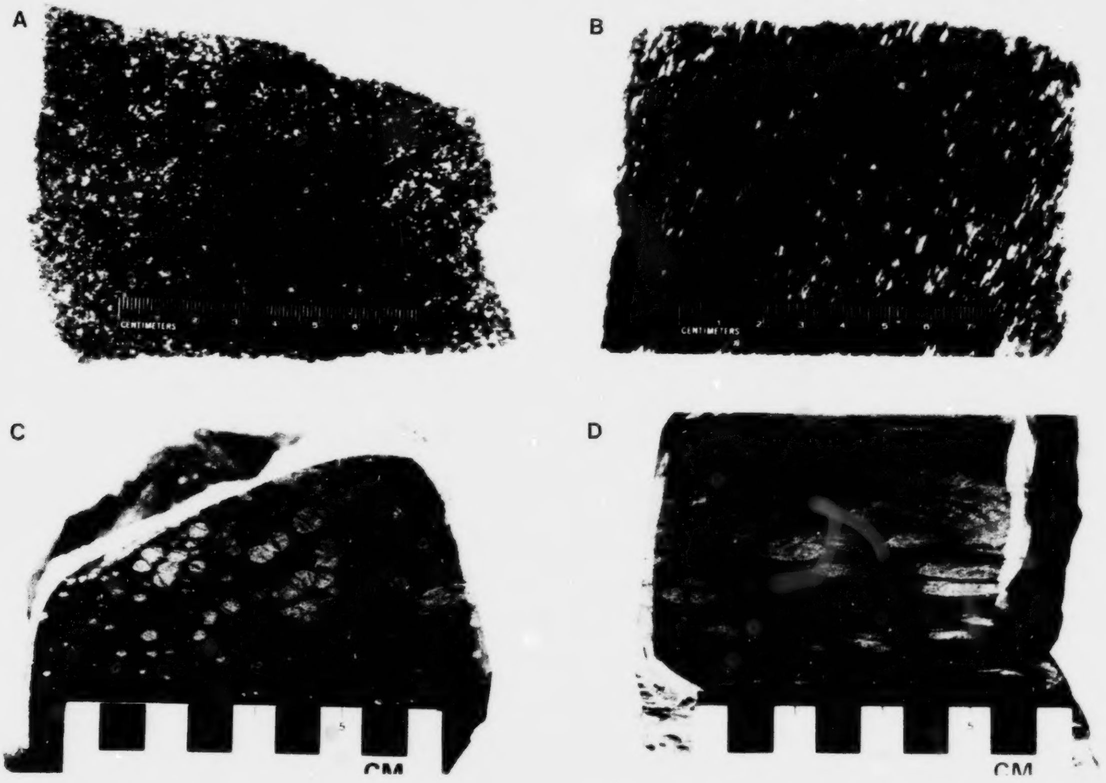

Photo 236.3. *(a) and (b) Millerton Porphyry sample sliced perpendicular and parallel (respectively) to lineation of stretched feldspar grains. (c) and (d) Variolitic pillowed basalt (V8) sliced perpendicular and parallel (respectively) to lineation of stretched varioles.*
Note that both samples display a well developed prolate stretching lineation which defines a strain ellipsoid of up to ∼5:1:1.

Lithological Contacts

Figure 236.7c shows the attitudes of various lithological contacts and late faults. Porphyry contact poles occupy the same general region as poles to the main foliation, suggesting an original sub-parallelism between the two, enhanced by transposition during strain. Albitite dike poles also occupy the same general region. Observationally, the albitite dikes are markedly less deformed than the strained porphyries and metavolcanics which they cut. They show no plunge, and intruded as steeply dipping sheets.

One measured pole for a diabase dike is consistent with 340° to 345° strikes for diabase dikes in the Timmins area. Diabase dikes cut mineralization and indicate that a radical change in stress field and type of magmatic activity occurred by 2633±93 (1σ) Ma (Rb-Sr date from Gates and Hurley 1973).

HIGH STRAIN ZONES

The presence of belts of shearing with steep dips, which cut metavolcanics, metasediments, and porphyries, was recognized by such early workers in the Timmins area as Cook and Johnstone (1929), Skavlem (1933), and Furse (1953). Au mineralization was regarded as being spatially associated with such high strain zones; an interesting observation in the light of recent work which has shown that the only structural signature common to Au mineralization in northwestern Ontario is intense shearing (e.g. Poulsen 1983; Hugon and Schwerdtner 1984, 1985; Stott and Wallace 1984). Three main northeast-trending high strain zones were recognized in the Timmins area: the northern Pearl Lake zone, the central Vipond zone, and the southern Dome-Dome Lake zone. The northern zone runs from Moneta through Hollinger, McIntyre, and Coniaurum for approximately 2700 m, and is up to 700 m wide at surface. At depth in McIntyre, the northern and central (Vipond) high strain zones merge. As long ago as 1929, Cook and Johnstone noted that veins are not parallel to foliation (046° to 086°/55° to 80°S), but cut across at shallow angles (average vein attitude = 050° with steep north or south dips). An important observation was that where veins run out of high strain zones they feather and die. These observations of a possible relationship between mineralization and high strain zones require detailed evaluation since they could be *very relevant to continued mineral exploration in the Timmins area.*

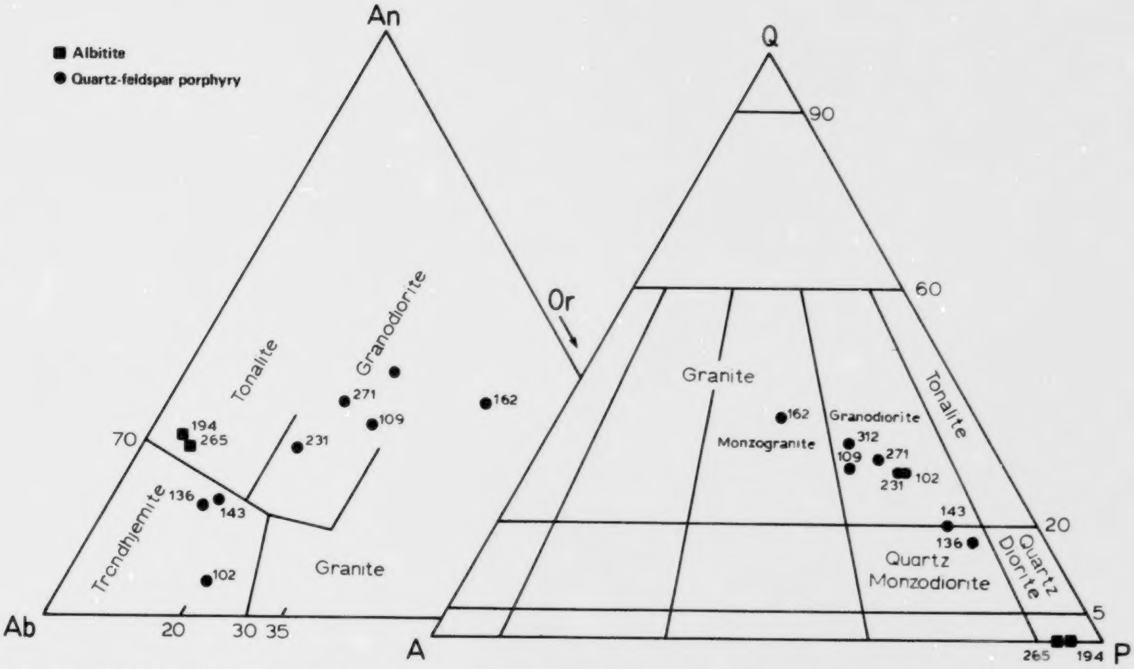

Figure 236.8. Major element data for porphyries and albitites plotted on QAP and 3-feldspar triangular diagrams (after Barker 1979).

STRUCTURAL ORE CONTROLS

Mineralization appears to have been controlled principally by a combination of: (i) a high strain zone up to 700 m wide, containing a steeply plunging lineation (Photo 236.3) and, at present, indications are that the geometry of the fabric relative to the zone is consistent with normal movement, as the fabric flattens out slightly on the northern side; (ii) the locations of the strained porphyritic intrusions which acted as plunging structural "pillars" controlling the location of the Hollinger central ore zone; (iii) lithological contacts such as the dilated carbonaceous interflow horizons in McIntyre; and (iv) favourable lithologies such as the permeable Central Subgroup breccias in the Hollinger central ore zone. Vein type largely reflects lithology. In massive lithologies such as Fe-tholeiite flows (e.g. 99 flow), strained porphyries, and albitite dikes, mineralization occurs as quartz-filled brittle fractures with mineralized alteration envelopes and increased free gold, whereas in breccia/fragmental units, mineralization tends to be dispersed as highly pyritized wall-rock.

MAJOR AND TRACE ELEMENT GEOCHEMISTRY OF IGNEOUS INTRUSIONS

Major and trace element geochemical data for eight samples of porphyritic intrusions (Pearl Lake, Millerton, Miller Lake, Northern, and Crown), and two albitite dikes from the Hollinger-McIntyre Mine area, are given in Table 236.2. The major element data are plotted on a standard QAP diagram and on a 3-feldspar triangular diagram (Barker 1979) in Figure 236.8.

STRAINED PORPHYRIES

Petrography

Despite the fact that the samples were chosen to be least altered, they show ubiquitous evidence of alteration in thin section. For example, the Miller Lake and Northern Porphyry samples, which were collected from relatively unstrained material, show carbonate alteration of plagioclase phenocrysts, and relatively high CO_2 contents of 3.56% and 3.72%. The Crown Porphyry sample shows less carbonate alteration and only 0.82% CO_2. However, it shows moderate sericitization associated with recrystallization and brittle deformation, and a slightly higher K_2O content (2.22%) than the Miller Lake and Northern strained porphyry samples (1.86% and 1.61%). The Pearl Lake Porphyry samples are all altered to some degree, containing 4.30% to 5.23% CO_2. Original plagioclase feldspar phenocrysts are replaced by carbonate clumps, and the matrix consists of quartz, oligoclase, secondary carbonate, secondary muscovite, and rutile pseudomorphs of original hornblende with original inclusions of apatite, rutile, and zircon. The Millerton samples, which are the most altered, contain 6.33% to 6.52% CO_2 consisting of relict quartz phenocrysts in a fine sericite-carbonate matrix with only rare carbonate pseudomorphs of plagioclase feldspar phenocrysts.

Major Element Geochemistry

Recalculating the SiO_2 contents of the strained porphyry samples to only 0.4% CO_2 (e.g. Mink Lake) gives an intermediate value of 66.8±2.1% (1σ; n=8) and a total range from 60.4% (#162) to 68.5%

TABLE 236.2. MAJOR AND TRACE ELEMENT GEOCHEMICAL DATA FOR 8 SAMPLES OF PORPHYRITIC INTRUSIONS (PEARL LAKE, MILLERTON, MILLER LAKE, NORTHERN, AND CROWN) AND 2 ALBITITES FROM THE HOLLINGER-McINTYRE MINE AREA.

	Pearl Lake			Millerton		Miller L.	Northern	Crown	Albitites	
	162	271	231	109	312	143	136	102	265	194
SiO_2	57.5	63.3	61.1	62.4	61.4	64.5	63.4	68.2	49.0	47.7
TiO_2	0.43	0.34	0.38	0.27	0.33	0.33	0.37	0.37	0.56	0.55
Al_2O_3	17.9	15.5	15.8	14.2	14.6	15.4	15.7	17.2	11.8	11.6
Fe_2O_3	6.10	3.43	5.30	4.08	3.64	2.93	3.07	2.33	6.78	6.61
MnO	0.09	0.12	0.12	0.18	0.11	0.09	0.08	0.02	0.15	0.14
MgO	2.18	1.37	2.01	1.91	2.58	1.67	1.55	0.88	7.46	7.42
CaO	3.35	4.54	3.40	4.35	4.56	3.19	3.48	0.92	7.49	7.98
Na_2O	0.81	2.52	3.09	2.39	1.62	5.12	5.52	5.32	3.65	3.55
K_2O	3.37	2.57	2.12	3.04	2.72	1.86	1.61	2.22	0.58	0.41
P_2O_5	0.15	0.15	0.16	0.10	0.15	0.15	0.16	0.16	0.26	0.26
H_2O^+	2.3	1.8	1.7	0.9	1.7	1.1	1.1	1.5	2.2	2.0
H_2O^-	0.1	0.1	0.1	0.1	0.1	0.1	0.1	0.1	0.1	0.1
CO_2	5.23	4.30	4.70	6.33	6.52	3.56	3.72	0.82	10.7	11.5
S	0.51	0.03	0.71	0.27	0.11	0.29	0.13	0.01	0.01	0.07
Cl	less than 50 ppm in all cases									
Total	100.02	100.07	100.69	99.80	100.14	100.29	99.99	100.05	100.74	99.89
Cr	77	62	61	n.d.	51	n.d.	49	63	600	601
Ni	23	24	20	n.d.	59	n.d.	16	14	135	128
V	90	64	71	n.d.	59	n.d.	69	75	169	174
Rb	71	60	47	59	71	40	31	44	20	10
Sr	150	145	142	128	91	198	258	168	253	571
Zr	128	116	120	98	109	120	131	132	132	151
Y	9	8	9	8	9	9	9	7	13	14
Nb	4	5	5	3	4	4	4	4	12	11

n.d. = not determined

Analysts: X-Ray Assay Laboratories Ltd., Toronto, and D.R.B. All major elements determined by standard X-ray fluorescence techniques with a detector limit of 0.010%. CO_2 and H_2O determined by wet chemistry with detection limits of 0.010% and 0.1% respectively. Trace element analyses determined by standard X-ray fluorescence techniques by D.R.B. at the University of Toronto, Department of Geology with an estimated uncertainty of ±1 ppm.

(#102). The intrusions are otherwise characterized by: a relatively high Na_2O content of 5.29% to 5.71% (recalculated from data for numbers 143, 136, and 102); a relatively low K_2O content of 1.67% to 1.92% (recalculated from numbers 143 and 136, since number 102 is sericitized); and a Fe content, as Fe_2O_3, of 2.34% to 3.18% (recalculated from numbers 143, 136, and 102). On a QAP diagram (Streckeisen 1973) the three least modified samples (numbers 143, 136, and 102) plot in the quartz monzodiorite and granodiorite fields. On the 3-feldspar diagram (Barker 1979) these three samples actually plot in the trondhjemite field (Figure 236.8). According to Streckeisen's (1973) strict definition, however, these rocks are not trondhjemites since they do not plot in the tonalite field on a QAP diagram (a trondhjemite is defined as a tonalite with a normative colour index <10). Nevertheless, Barker (1979) states that K_2O contents should be ≅2.5 weight percent, and typically <2.0 weight percent for trondhjemitic rocks. Hence, the fact that the best estimates for the initial K_2O contents of these rocks are 1.67% and 1.92% demonstrates a trondhjemitic affinity.

The trend away from the least modified strained porphyries reflects metasomatic changes, particularly introduction of K_2O. For example, sample numbers 143 and 136 contain 1.61% and 1.86% K_2O, whereas the other samples contain >2.12% K_2O and up to 3.37% K_2O.

These whole rock analyses for the strained porphyritic intrusions are similar to analyses of the Preston Porphyry in the Dome Mine area and the Eldorado Pluton in Langmuir Township (Pyke 1982). The porphyries show a less fractionated composition than other porphyritic intrusions in the Timmins area, such as the Mount Logano intrusion (Pyke 1982).

Trace Element Geochemistry

The trace element data in Table 236.2 indicate that the porphyries in the Hollinger-McIntyre area are indeed a comagmatic suite as field evidence suggests (Spooner *et al.* 1985; Burrows and Spooner, in press). TiO_2, P_2O_5, Zr, Y, Nb, Ni, V, and Cr all show relatively restricted ranges (e.g. 0.10% to 0.16% for P_2O_5; 49 ppm to 77 ppm for Cr; 98 ppm to 132 ppm for Zr). Greater variability for trace elements such as Rb (31 ppm to 71 ppm) and Sr (91 ppm to 258 ppm) probably reflects hydrothermal alteration.

ALBITITE DIKES

Petrography

The least altered sample (38-194) is a grey, slightly porphyritic rock. Plagioclase and very minor quartz are restricted to a fine (0.05 to 0.1 mm) matrix with a large amount of carbonate (up to 50%) and 2% to 5% secondary muscovite. Coarser mats of secondary chlorite (10%) and 5% altered biotite laths (up to 1.5 mm in size) give the rock a "speckled" appearance. Hence, even the apparently freshest albitite dikes are very highly altered. They exhibit a weak prolate to decussate fabric. Further recrystallization and alteration, as shown in sample number 265, result in a coarsening of the carbonate, an increase in chlorite content, and the development of clusters of randomly oriented albite grains.

Major Element Geochemistry

The high, presumable largely secondary, carbonate content is reflected in high CO_2 contents of 10.7% and 11.7%. The H_2O^+ contents are also elevated at 2.0% and 2.2%. On the other hand, S values are low (0.01% to 0.07%). Clearly, the albitite dikes have been particularly susceptible to alteration and their original igneous affinities are not clear. The major element analyses in Table 236.2 are unusual in showing low SiO_2 values of only 47.7% and 49.0%, relatively high TiO_2 values (0.55% and 0.55%), moderate Al_2O_3 values (11.6% and 11.8%), high Fe (as Fe_2O_3) contents (6.61% and 6.78%), unusually high MgO contents of 7.42% and 7.46%, high CaO contents of 7.49% and 7.98%, not very high Na_2O contents (3.55% and 3.65%), and very low K_2O contents of 0.41% and 0.58%. Even if the SiO_2 values are recalculated on a CO_2- and H_2O^+-free basis (extreme case), they are only 55.3% (number 194) and 55.8% (number 265). As will be shown in the next section, hydrothermal alteration is not accompanied by major changes in SiO_2 content.

The low SiO_2 contents and, particularly, the high TiO_2, Fe (as Fe_2O_3), MgO, and CaO contents suggest that the albitite dike magma was radically different from the earlier porphyry magma, being distinctly more primitive. Hence, there was a marked change in available magma type between intrusion of the porphyries and development of the main Au mineralization—a further item of evidence to suggest that there may have been no chemical connection between the strained porphyries and the Au mineralization (Spooner *et al.* 1985; Wood *et al.*, in press).

Trace Element Geochemistry

The relatively unfractionated nature of the albitite magma and the geochemical contrast with the porphyries are shown well by trace element contents. In particular, Cr, Ni, and V contents are relatively high, and clearly higher than values for the porphyries, e.g. 600 ppm and 601 ppm Cr >49 ppm to 77 ppm Cr, 128 ppm to 136 ppm Ni >14 ppm to 59 ppm Ni, and 169 ppm to 174 ppm V >64 ppm to 90 ppm V.

Comparison

The petrography and geochemistry of the albitite dikes appear to be most similar to those of "lamprophyre" dikes documented by Moore (1937) and Prest (1957) in the Ramore area near Matheson. Similar features include: (i) the lithologies occur as small dikes, usually only near Au deposits; (ii) considerable internal carbonate alteration and development of secondary chlorite; (iii) a relative abundance of mafic constituents; and (iv) only secondary quartz. Recent analyses of such dikes at the Canadian Arrow Au deposit near Matheson (McNeil and Kerrich 1986) confirm the validity of this comparison, since the Canadian Arrow "lamprophyres" have similarly high MgO, CaO, Fe (as Fe_2O_3), and Loss on Ignition (LOI) values, combined with high Cr, Ni, and V values. In addition, the Canadian Arrow dikes contain pebble-

TABLE 236.3. MAJOR ELEMENT GEOCHEMICAL DATA FOR PORPHYRY "PROTOLITH" AND 4 MILLERTON PORPHYRY SAMPLES WHICH EXHIBIT VARYING DEGREES OF ALTERATION.*

Sample	"Protolith"	400-312	17-109	15-43	18-28
Wt.%					
SiO_2	64.0	61.4	62.4	65.9	64.2
Al_2O_3	15.6	14.6	14.2	16.5	16.2
CaO	3.34	4.56	4.35	1.02	2.98
MgO	1.61	2.58	1.19	0.39	0.94
Na_2O	5.32	1.62	2.39	4.53	4.10
K_2O	1.74	2.72	3.04	2.77	2.86
Fe_2O_3	3.00	3.64	4.08	4.35	2.74
MnO	0.09	0.11	0.18	0.09	0.13
TiO_2	0.35	0.33	0.27	0.31	0.29
P_2O_5	0.16	0.15	0.10	0.11	0.11
CO_2	3.64	6.52	6.33	1.25	3.59
S	0.21	0.11	0.27	2.39	0.93

*Samples 15-43 and 18-28 were collected from alteration selvages proximal to quartz-carbonate veins while samples 400-312 and 17-109 were not directly associated with mineralization.

Analyst: X-Ray Assay Laboratories Ltd., Toronto. All major elements determined by standard X-ray fluorescence techniques except CO_2 which was determined by wet chemistry. Detection limits are 0.010%.

and boulder-sized inclusions of syenite which may be similar to the "granitic" inclusions ("goose eggs") in the Hollinger-McIntyre albitite dikes (e.g. Langford 1938; Spooner *et al.* 1985) (Photo 236.1b).

GEOCHEMISTRY OF HYDROTHERMAL ALTERATION

Hydrothermal alteration of wall-rocks adjacent to individual veins and vein complexes at Hollinger and McIntyre is ubiquitous and shows varying degrees of intensity. Field relationships show the close spatial association between veins and adjacent alteration selvages. This observation indicates that the fluids from which the vein minerals precipitated were also responsible for the wall-rock alteration through interaction with the host lithologies which range in composition from tholeiitic flows, carbonaceous interflow sediments, quartz-feldspar porphyries to albitite dikes. Alteration assemblages directly related to ore-bearing veins consist predominantly of carbonate (ankerite to Fe-bearing dolomite), pyrite (±chalcopyrite, ±galena, ±pyrrhotite, ±sphalerite, ±gold), sericite (muscovite), quartz, and albite. With increasing distance from the veins, alteration intensity decreases and is marked by the occurrence of increasing amounts of chlorite, calcite, and epidote. Ankerite, which comprises over 25% to 30% of the strongly altered wall-rock, decreases with increasing calcite content. The background regional greenschist facies mineral assemblage, which is unrelated to mineralization, is characterized by quartz-albite-chlorite-epidote-actinolite ± calcite.

Chemical analyses of volcanic rocks (Tisdale Group) from the Hollinger Property and the local area (Ferguson 1968; Pyke 1982) show a wide range of compositions making metasomatic chemical changes quite difficult to define. On the other hand, analyses of strained porphyry intrusions presented in this paper (discussed previously) and by other workers (Ferguson 1968), are generally quite similar in composition, and any differences appear to reflect varying degrees of alteration. Upon examining the data, and using the volatile content as an approximate indicator of alteration intensity, it was decided to use the average composition of samples 12-S136 and 12-S143 as the closest representative of the "protolith". These samples were collected to the north of the Hollinger central ore zone from relatively fresh and undeformed Northern and Miller Lake porphyries. This average composition was then compared with four samples of Millerton Porphyry (surface (400 Pit), 1550-foot (15-08-01 stope), 1700-foot, and 1800-foot (18-83-01 stope) levels). The relative chemical changes are determined by normalizing each sample relative to the "protolith" sample, the raw data for which are given in Table 236.3.

Relative enrichments and depletions are presented in Figure 236.9. Hydrothermal alteration is characterized by addition of K, Fe, and S, and depletion

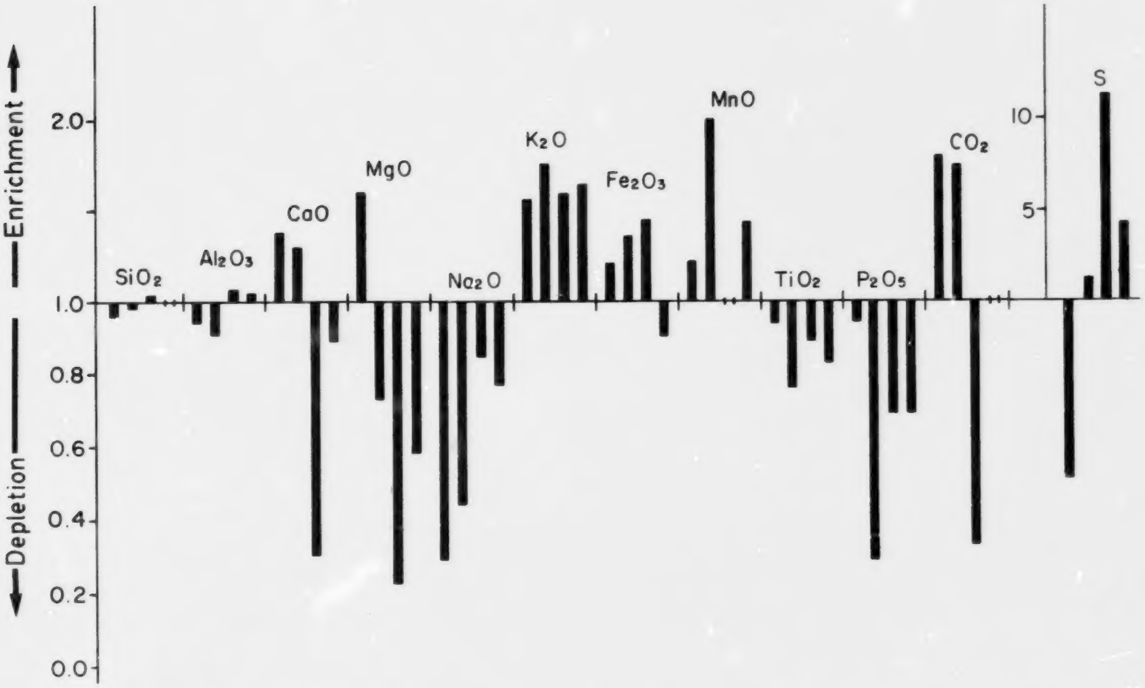

Figure 236.9. *Diagram showing enrichments and depletions in altered Millerton Porphyry samples relative to the porphyry "protolith". Samples in each major element category are plotted in the order 400-312, 17-109, 15-43, and 18-28 from left to right.*

in Mg and Na. Si and Al values are relatively constant. The CO_2 results for the altered porphyry samples collected proximal to veining are variable, ranging from 1.25% to 6.52%.

Petrographic examination of altered porphyry samples shows abundant muscovite which has completely replaced the groundmass and feldspar phenocrysts, accounting for the added K. Added Fe and S are present in pyrite, showing that formation of pyrite in altered wall-rock was *not* purely a result of sulphidation reactions. An interesting point is that pyrite alteration halos are not as strongly developed as in the altered volcanic wall-rocks. Examination during quantification of gold occurrence in altered wall-rock did not reveal any gold associated with pyrite or any other alteration minerals in altered porphyry material. It appears that the gold in porphyry stopes is located within or very close to the quartz-carbonate veins. Chip sampling across veins and wall-rock material generally reveals erratic values across veins and quite low general wall-rock values. The apparent lack of gold mineralization associated with pyrite in the altered porphyry is probably a function of its relatively low iron content compared to the Fe-tholeiites. In fact, as seen in Figure 236.8, some of the Fe was probably provided by the hydrothermal fluids which also provided the sulphur. Analysis of gold occurrence in altered volcanic wall-rocks at Hollinger indicates an intimate association between gold and pyrite (Spooner *et al.* 1985). Abundant Fe (up to approximately 10 to 15 weight percent total Fe as FeO; Ferguson 1968) in altered volcanic wall-rocks is available for formation of pyrite during sulphidation reactions (c.f. 2.33% to 6.10% Fe as Fe_2O_3 in the porphyries).

HYDROGEN AND OXYGEN ISOTOPE COMPOSITIONS AS SOURCE TRACERS

$\delta^{18}O$

The oxygen isotopic composition of the Hollinger Au fluid has been estimated from 14 vein and wall-rock carbonate, 8 vein quartz, and 2 vein scheelite samples (for measured mineral $\delta^{18}O$ values *see* Table 236.4). Fluid values were calculated using a depositional temperature estimate of 277°C derived from fluid inclusion homogenization temperatures (Wood *et al.*, in press), and appropriate mineral/H_2O oxygen isotope fractionation curves. The following fractionation curves were utilized: dolomite/H_2O—Matthews and Katz 1977 (electron microprobe analyses indicate that the Hollinger main Au stage carbonate is 40% to 80% dolomite, no fractionation data are available for the ankerite end member); quartz/H_2O—Matthews and Beckinsale 1979; scheelite/H_2O—Wesolowski and Ohmoto 1986. Isotopic equilibrium is demonstrated by a main Au stage quartz-scheelite pair giving a depositional temperature estimate of 285^{+21}_{-18}°C concordant with the fluid inclusion derived temperatures.

TABLE 236.4. MEASURED HYDROGEN AND OXYGEN ISOTOPIC COMPOSITIONS OF CARBONATE, QUARTZ, AND SCHEELITE, HOLLINGER MINE.

Sample No.	Description	Location	$\delta^{18}O$(‰)	δD(‰)
1P-S346	vein quartz	1 pit (surface)	--	-70
33P-S342	vein quartz	33 pit (surface)	+11.8	--
33P-S342	vein carb.	33 pit (surface)	+11.4	--
33P-S346	vein quartz	33 pit (surface)	--	-55
33P-S346	wallrock carb.	33 pit (surface)	+11.8	--
55P-S330	vein carb.	55 pit (surface)	+11.8	--
55-29	wallrock carb.	55 pit (surface)	+12.3	--
2-S317	vein quartz	200′ level	--	-61
4-S124	vein quartz	425′ level	+13.3	--
4-S124	vein carb.	425′ level	+12.4	--
4-S129b	vein quartz	425′ level	+11.3	--
4-S129b	scheelite	425′ level	+ 3.4	--
4-S130	wallrock carb.	425′ level	+11.3	--
8-S305	vein quartz	800′ level	--	-43
8-S310	vein quartz	800′ level	+13.3	--
8-S310	vein carb.	800′ level	+11.7	--
8-S310	wallrock carb.	800′ level	+12.2	--
12-S166	vein quartz	1250′ level	+13.2	--
12-S166	vein carb.	1250′ level	+11.8	--
15-08-01-15	vein scheelite	1550′ level	--	-74
15-08-01-35	vein scheelite	1500′ level	--	-58
15-22	wallrock carb.	1550′ level	+11.8	--
15-49	vein quartz	1550′ level	+12.5	--
15-49	scheelite	1550′ level	+ 3.4	--
17-S114	vein quartz	1700′ level	--	-47
18-16	wallrock carb.	1850′ level	+11.8	--
18-83-01	vein quartz	1850′ level	+12.8	--
18-83-01	vein carb.	1850′ level	+11.2	--
18-83-01-27	vein scheelite	1850′ level	--	-64
18-83-01-39	vein scheelite	1850′ level	--	-39
27-S155b	wallrock carb.	2750′ level	+11.1	--
27-S158	vein quartz	2750′ level	+12.1	--
27-S158	vein carb.	2750′ level	+12.0	--

•All values are quoted relative to SMOW.
•Hydrogen and Oxygen (Quartz and scheelite) analyses by Geochron Laboratories; δD determined by crushing.
•Carbonate analyses by University of Waterloo.
•Precisions determined by repeated measurements at Geochron and Waterloo Laboratories are ±0.26‰ and ±0.2‰ respectively for oxygen and ±2‰ for hydrogen.

The fluid $\delta^{18}O$ estimates are remarkably similar at +4.8±0.4‰ from carbonate, +4.5±0.8‰ from quartz, and +4.7‰ (two values) from scheelite. The histogram in Figure 236.10 shows that the Hollinger fluid $\delta^{18}O$ data are quite tightly constrained with an arithmetic mean of +4.7 ± 0.5‰ (1σ) and a narrow range of 2.2‰(+3.3‰ to +5.5‰). As Figure 236.10 also shows, this range of $\delta^{18}O$ estimates significantly overlaps the range of $\delta^{18}O$ estimates for the Mink Lake Au- and W-enriched MoS_2 fluid which has been shown to be of magmatic origin (+6.0±1.9‰, n=19; Burrows and Spooner, in preparation). More specifically, it can be seen that the Mink Lake and Hollinger estimates are similar, being in the lower part, or lower than, the general magmatic water $\delta^{18}O$ range of Taylor (1979). This similarity is consistent with a magmatic origin for the Hollinger fluids, since the Mink fluids were magmatically derived (Burrows and Spooner, in preparation). A magmatic origin is indicated more strongly by very similar fluid properties (Wood *et al.*, in press), and most strongly by statistically identical $\delta^{13}C$ values (Spooner *et al.* 1985; Burrows *et al.* 1986). However, $\delta^{18}O$ is not such a strong source indicator since it is subject to modification by water/rock interaction, and because of $\delta^{18}O$ overlap between major fields for different general fluid types (e.g. Figure 236.10).

δD

The hydrogen isotope composition of the Hollinger main stage Au mineralization has been determined by 9, to date, δD (deuterium) determinations directly on fluid inclusion H_2O in vein quartz (5 samples) and scheelite (4 samples) (Table 236.4). The reason for the high proportion of scheelite samples is that scheelite contains some of the best primary inclusion-bearing material found in Hollinger. Four of the quartz samples were selected for good primaries

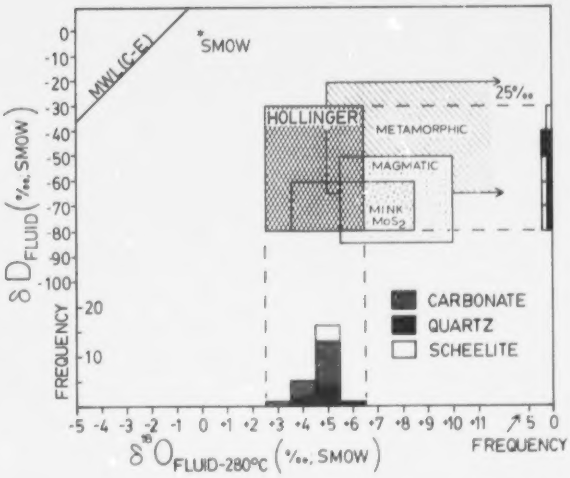

***Figure 236.10.** δD - $\delta^{18}O$ diagram showing the general metamorphic box (Taylor 1979), the general magmatic box (Taylor 1979), the specific magmatic box for the Au- and W-enriched MoS_2 mineralizaton, Mink Lake, northern Ontario, and the Hollinger Au fluid box. Histograms of measured fluid inclusion H_2O δD values and calculated fluid $\delta^{18}O$ values are also given. Note the significant overlap between the Hollinger and Mink Lake fluid boxes.*

and *one* (2-S317) because it contained a high proportion of secondaries. The latter sample was analyzed to determine the contamination effect of secondaries. Since the δD value obtained, -61‰, is indistinguishably within the range of the δD values for primary-bearing material, it appears that the effect of the secondaries is undetectable in this instance.

The δD measurements define a significant range of 35‰ from -74‰ to less negative values as high as -39‰, and an arithmetic mean of -57±12‰. Six of the nine determinations and the mean lie exactly within the general magmatic δD range of Taylor (1979), from -85‰ to -50‰ (Figure 236.10). Hence, the Hollinger values are consistent with a magmatic derivation for the main stage Au fluids suggested on the basis of the other evidence discussed above. However, three determinations are distinctly less negative at -47‰, -43‰, and -39‰. A possible explanation is related to the fact that the main stage Au fluids can contain CH_4 as indicated by gas chromatographic analysis of McIntyre fluid inclusions. Smith *et al.* (1984) detected 1 mole percent CH_4, CO, and $N_2$and trace amounts (<0.001 mole percent) of higher hydrocarbons and hydrogen in material from near graphitic interflow horizons. In Hollinger, the presence of gaseous species other than CO_2 is indicated by a slightly depressed mean CO_2 fusion temperature of -57.3±1.1°C (n=274; Wood *et al.*, in press) and individual measurements down to -63°C. CH_4 is hydrogen isotopically lighter (more negative) than H_2O at equilibrium. At 280°C, the difference is 69‰. At 25°C the difference is large at 96‰. Hence, CH_4 in the fluid inclusions will be more negative and, particularly with re-equilibration at lower temperatures during natural cooling, could drive the hydrogen isotope composition of the fluid inclusion H_2O in the opposite direction to *less* negative values such as those observed (-47‰ to -39‰). This interpretation is being tested at the present time.

PRINCIPAL CONCLUSIONS

1. Quartz-tourmaline veins which pre-date the main stage Au mineralization have been observed to crosscut, and therefore post-date, albitite dikes—a relationship which was suspected by, for example, Langford (1938) but never confirmed.
2. The prolate fabric is developed to the same degree the deformed metavolcanics and the porphyries, indicating that the porphyries were intruded before the start of development of the fabric.
3. The attitudes of the main stage Au veins are extremely variable. However, they show a principal concentration which does not correspond to the attitude of the principal foliation, and no concentrations which could reasonably correspond to extension normal to σ_3 or to Riedel shears in a shear zone.
4. The concentration of vein attitudes is interpreted to be a result of hydraulic fracturing, the concentration being normal to the σ_3 direction which existed at the time (e.g. Haimson 1981). An interpretation of the weakness of the concentration is that σ_3 was not quantitatively very different from $\sigma_1$and σ_2, so that it did not act as a very strong control.
5. An important point relevant to mineral exploration in the Timmins area, and a similarity to many examples of Au minerlization in northwestern Ontario, is that the Hollinger-McIntyre mineralization developed in a high strain shear zone (Cook and Johnstone 1929; Skavlem 1933; Furse 1953). Where veins run out of high strain zones, they feather and die.
6. The least altered porphyries are characterized by an intermediate SiO_2 content of 66.8±2.1% (1σ; n=8), a relatively high Na_2O content of 5.29% to 5.71%, and a relatively low K_2O content of 1.67% to 1.92%. On a QAP diagram (Streckeisen 1973) they plot in the quartz-monzodiorite and granodiorite fields.
7. The albitite dikes are very altered, with two analyses containing 10.7% and 11.7% CO_2. Nevertheless, they appear to be markedly different, less fractionated compositions than the porphyries, as shown by high TiO_2, Fe (as Fe_2O_3), MgO, CaO, and particularly, Cr, Ni, and V contents. SiO_2 contents, even on a completely CO_2-free basis, are only 53.9% and 54.8%.
8. Hence, there was a marked change in available magma type between intrusion of the porphyries and development of the main stage Au mineralization—a further item of evidence suggesting that there was no specific chemical connection between the porphyries and the Au mineralization (Spooner *et al.* 1985; Wood *et al.*, in press).

Grant 242 Structural Studies in the Beardmore–Geraldton Belt, Northern Ontario

Howard R. Williams

Department of Geological Sciences, Brock University, St. Catharines

ABSTRACT

Detailed structural, lithological, and metamorphic investigations in the Beardmore-Geraldton Belt concentrated on its deformation style, the presently defined Wabigoon-Quetico Subprovince boundary, and the significance of the "metasedimentary" belts of the Superior Province. The subprovince boundary is here locally redefined as the Paint Lake Fault Zone, separating the Wabigoon batholith-dominated greenstone terrain in the north, from the Quetico Subprovince by a zone of intense dextral shear. The Quetico Subprovince, now represented by all of the Beardmore-Geraldton Belt, is a linear low grade terrain consisting of repetitive units of northward-younging basaltic volcanic rocks, gabbros, and feldspathic greywacke turbidites. Predominant inhomogeneous layer-parallel shear deformation, low ambient metamorphic grades, a generally monotonous association of basic rocks and turbidites, and proximity to the batholith-dominated volcanic terrain suggest that the linear belt is an accretionary prism underplated to the southern boundary of the Wabigoon Subprovince.

INTRODUCTION

The Wabigoon-Quetico Subprovince boundary (Figure 242.1) was studied along the Beardmore-Geraldton Belt (BGB) (Figure 242.2). Within the BGB, the boundary between the Wabigoon and Quetico Subprovinces (Ayres 1963) is presently defined as the contact between two contrasting supracrustal units: a basaltic metavolcanic unit to the north and a clastic metasedimentary unit to the south (Mason and McConnell 1983; Patterson *et al.* 1985). New younging determinations, microscopic and mesoscopic structural data have been used to produce a geological sketch map (Figure 242.2) of the Beardmore-Geraldton Belt. The geology is based on the compilation of Stott (1984a, 1984b), and illustrates the contrast between the granite-greenstone terrain to the north and the relatively linear northwards-younging BGB to the south. Many east-west trending lithological units are bounded by ductile-brittle dextral shear zones (Buck and Williams 1984, 1986; Buck 1986; Williams, in preparation).

STRATIGRAPHY OF THE SUBPROVINCE BOUNDARY ZONE

Structures and lithologies on both sides of the subprovince boundary zone were mapped and compared

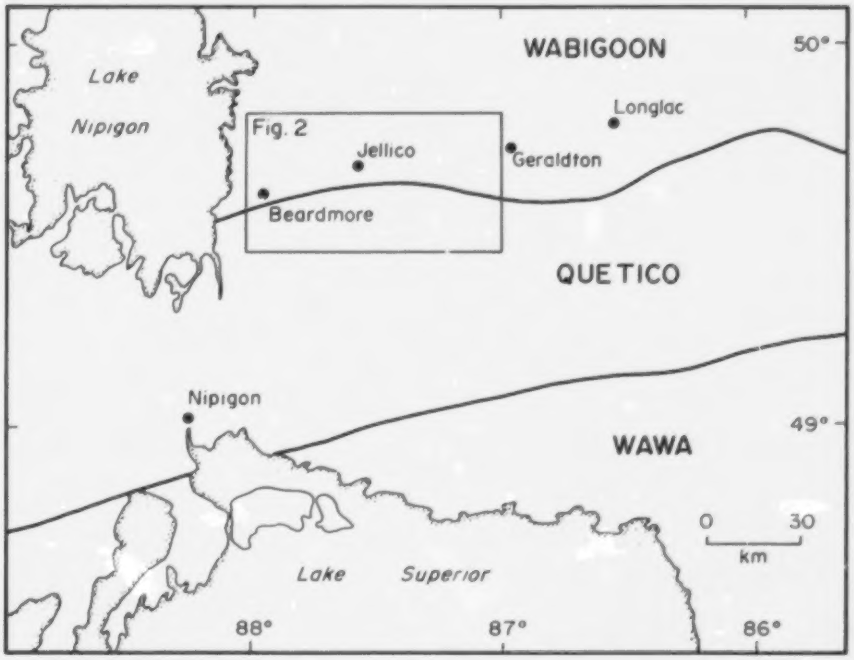

Figure 242.1. *Tectonic map of part of northern Ontario, redrawn from the Geological Highway Map published by the Ministry of Natural Resources. Subprovincial boundaries and the location of the study area, Figure 242.2, are outlined.*

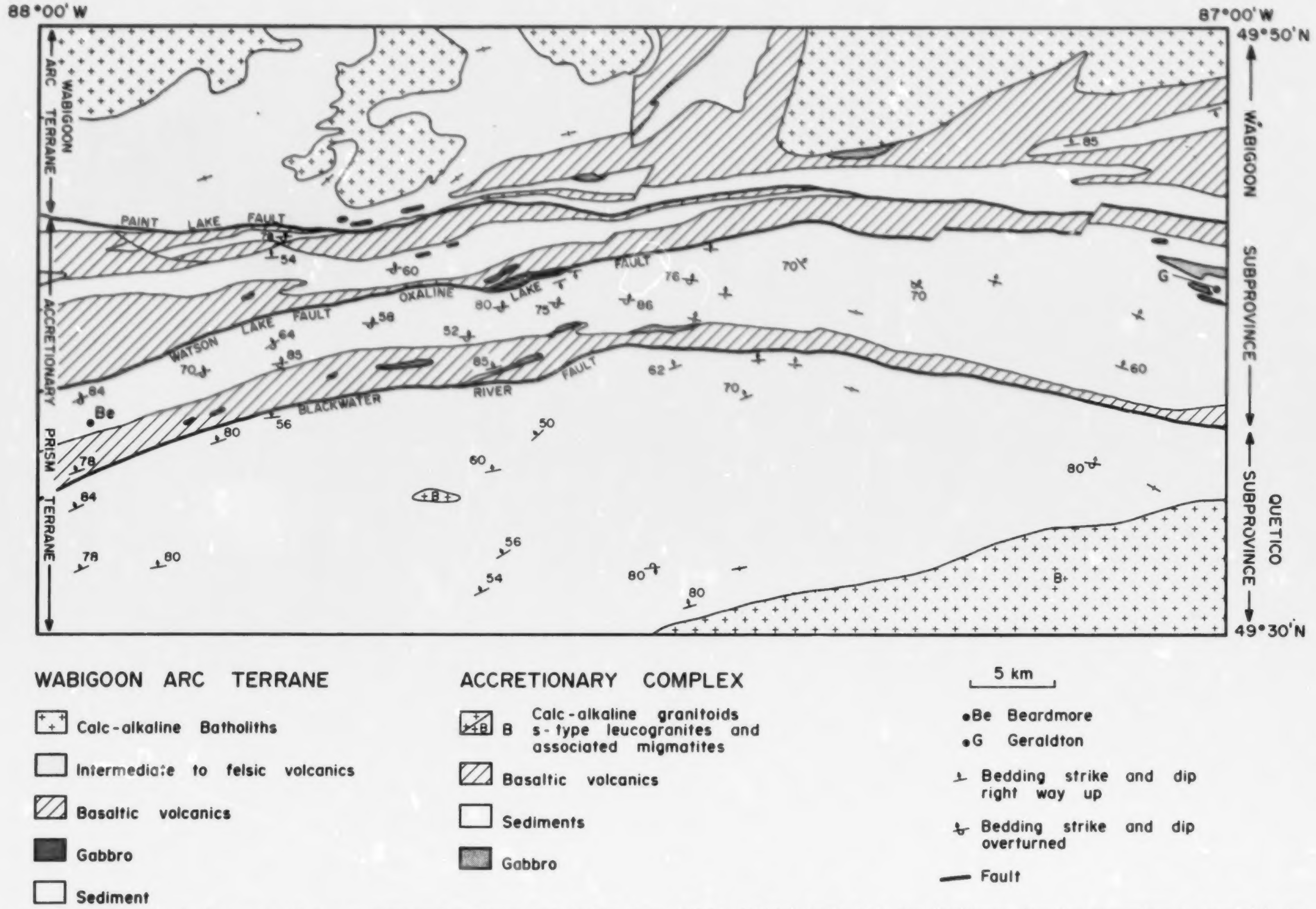
88°00'W
87°00'W
49°50'N
49°30'N
WABIGOON ARC TERRANE
ACCRETIONARY PRISM TERRANE
WABIGOON SUBPROVINCE
QUETICO SUBPROVINCE
PAINT LAKE FAULT
OXALINE LAKE FAULT
WATSON LAKE FAULT
BLACKWATER RIVER FAULT
Be
G
B
WABIGOON ARC TERRANE
Calc-alkaline Batholiths
Intermediate to felsic volcanics
Basaltic volcanics
Gabbro
Sediment
ACCRETIONARY COMPLEX
B Calc-alkaline granitoids s-type leucogranites and associated migmatites
Basaltic volcanics
Sediments
Gabbro
5 km
•Be Beardmore
•G Geraldton
Bedding strike and dip right way up
Bedding strike and dip overturned
Fault

Figure 242.2. Geological map of the Beardmore-Geraldton Belt (after Stott 1984a, 1984b). Note that the Wabigoon-Quetico boundary is placed in its defined position, which does not correspond with the suggested revised position, at the boundary of the batholith-dominated terrain with the Beardmore-Geraldton Belt.

with those found by previous workers, for example, Anglin and Franklin (1985), Mackasey (1976), and Kehlenbeck (1986). A new interpretation of the structure and geological development of the area is presented here along with many of the field relationships since their evidence is critical to the new interpretation.

Three units of basaltic metavolcanics are predominantly composed of massive and pillowed flows and minor breccia (Mackasey 1976); no volcanic rocks are reported to the south of the presently defined Wabigoon-Quetico boundary (Figure 242.2). Gabbroic bodies occur sporadically throughout the volcanic rocks but are commonly situated near or at the stratigraphic base of each unit. Gabbros and later quartz-feldspar porphyries intrude the sedimentary sequences, commonly cutting the cleavage, yet are frequently deformed by later shearing, coplanar with the cleavage.

Sedimentary units which separate the volcanic horizons are a series of dominantly "immature" grain-size-graded feldspathic wackes, rare massive arenites, three lean, thin units of banded iron formation (Anglin and Franklin 1985; Barrett and Fralick 1985; Devaney and Fralick 1985; Mackasey 1976), and the same number of thin but relatively continuous conglomeratic horizons up to 20 m thick. The massive, unbedded matrix-supported conglomerate units occur at or near the stratigraphic top of each major sedimentary package, associated with wackes and banded iron formation. The matrix to the conglomerates is frequently pelitic, not sandy. Pebbles in the conglomerate consist of basic and felsic volcanic and plutonic material. With few exceptions, the sequence of sedimentary and basaltic igneous rocks young northwards, based on grain-size grading, dewatering structures and undeformed pillow shapes. While individual beds of sedimentary rock in the wacke sequence fine and young north, sedimentary sequences within each major package coarsen northwards (Mackasey 1976; Devaney and Fralick 1985). Despite a true thickness of sediment of at least 20 km (Figure 242.3), the only regionally mappable sedimentary units are banded iron formations which, while very thin, are remarkably linear and continuous.

STRUCTURE OF THE BEARDMORE–GERALDTON BELT (BGB)

The cross section illustrated in Figure 242.3 is an interpretation of the structure derived from existing and new field data. The following points concerning the structure and metamorphism are pertinent:

1. Deformation within both volcanic rocks and sedimentary rocks is inhomogeneous, occurring predominantly at the lower contact of the basaltic sequences and at the top contact of the underlying sedimentary sequence. At these sheared contacts, both ductile and brittle deformation features such as s, c, and c′ fabrics, asymmetric mesoscopic folds, kink band swarms, and slickensided surfaces are present (Reilly and Williams 1986; Lawson 1986; Williams, in preparation). These zones of shear have been previously mapped as regional faults, such as the Paint Lake, Watson Lake, and Blackwater River Faults (Figure 242.2). Close to the basal (south) contacts of the volcanic rocks and gabbros, inhomogeneous deformation produced highly schistose rocks exhibiting an early, steeply plunging lineation of stretched amygdules, mafic, and felsic mineral clots paralleling a well developed mineral elongation lineation of hornblende and chlorite. Spatially associated with the lineation is boudinage, with axes horizontal and orthogonal to the lineation. Within the sediments, lineation development is generally restricted to a shallow easterly or westerly plunging crinkle lineation developed only in pelitic horizons. This extension lineation is developed sub-horizontally, parallel with the axes of minor asymmetric "active" z-shaped folds. Deformation within and between sedimentary bed units is demonstrated by boudinaged quartz veins and disrupted bedding. The sedimentary rocks are characteristically deformed only within narrow parallel-bedded shear zones and as a result their deformation state is highly variable. Completely undeformed, well preserved greywacke turbidite outcrop is ubiquitous yet often juxtaposed against equivalent lithologies in a highly deformed state. With increasing deformation, generally well preserved bedded wackes become sheared along the bedding, producing a slaty cleavage in pelitic horizons and a non-penetrative solution or spaced cleavage in the psammitic layers. Regionally, bedding and cleavage orientations are statistically parallel (Figure 242.4). Non-parallelism of bedding and cleavage is of local extent only. There is no compelling evidence to associate the regional cleavage with fold development. Progressive deformation by both sinistral and dextral shear along both bedding and cleavage is apparent from reorientation and displacement of quartz veins and lithological boundaries, however, dextral shear predominates. Ultimately, shear deformation causes total disruption of the bedded units along shear planes to produce lenses of psammite in a highly deformed pelitic matrix. Swarms of sub-parallel, planar quartz veins along the cleavage are characteristic of these deformed sediments, but these veins too may become deformed by further shear, into disrupted and isoclinally folded structures.

   During early stages of deformation, quartz-filled sigmoidal tension gashes formed within the psammitic units with an asymmetry that indicates a dextral sense of shear along the bedding. Further shear renders these veins highly sigmoidal and ultimately they become disrupted. The inhomogeneity of the deformation is illustrated by the presence of perfectly preserved graded bedding observed alongside structurally reworked massive to foliated rocks containing no recognizable bedding. Rocks of silty composition are characterized by lensoid layering and multitudes of isoclinally folded quartz veins.

2. Folding deformation of the original layering in the volcanics and sedimentary rocks is restricted to the upper contact of each package, where it has been tectonically juxtaposed against the overlying basaltic volcanic rocks. Folds frequently

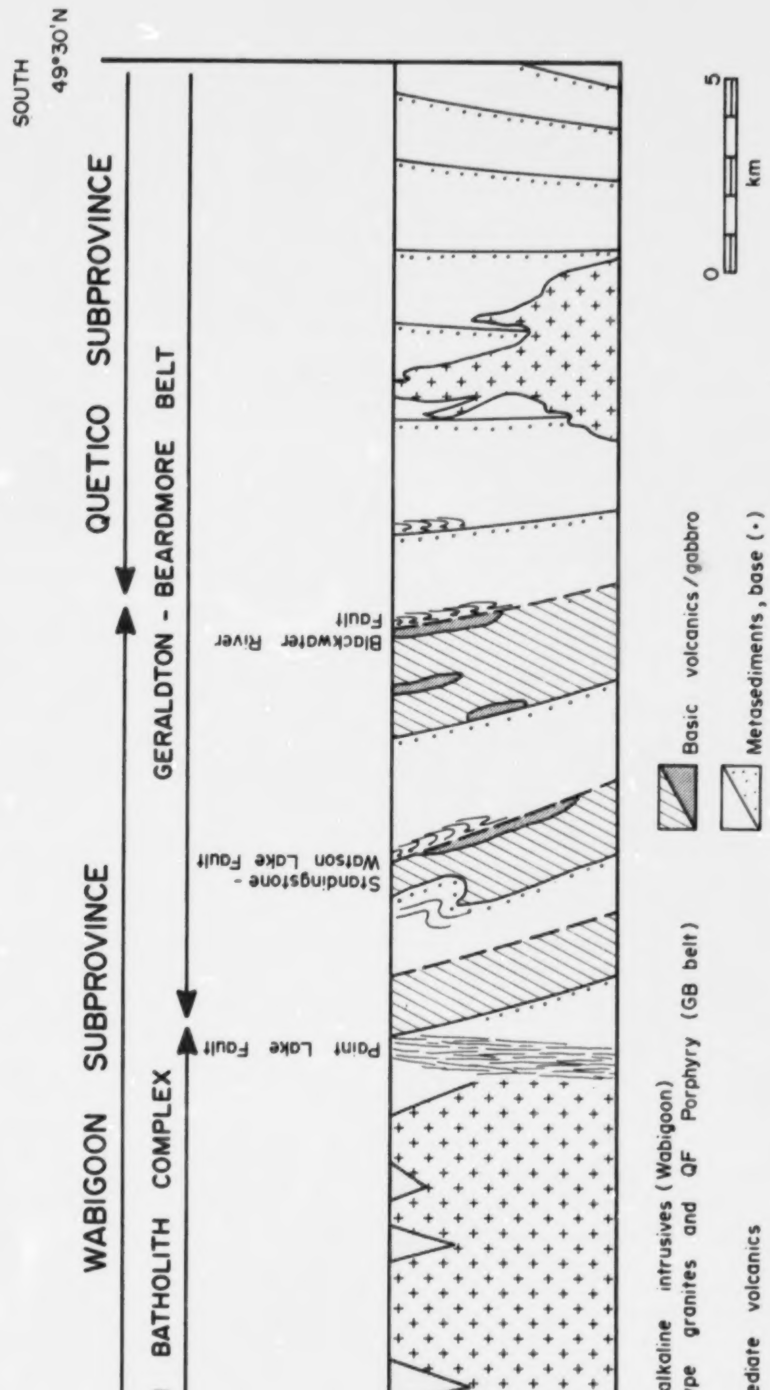
NORTH
49°50'N
SOUTH
49°30'N
WABIGOON SUBPROVINCE
QUETICO SUBPROVINCE
ONAMAN BATHOLITH COMPLEX
GERALDTON - BEARDMORE BELT
Paint Lake Fault
Standingstone - Watson Lake Fault
Blackwater River Fault
Calc - alkaline intrusives (Wabigoon)
"s" type granites and QF Porphyry (GB belt)
Intermediate volcanics
Basic volcanics / gabbro
Metasediments , base (·)
0
5
km

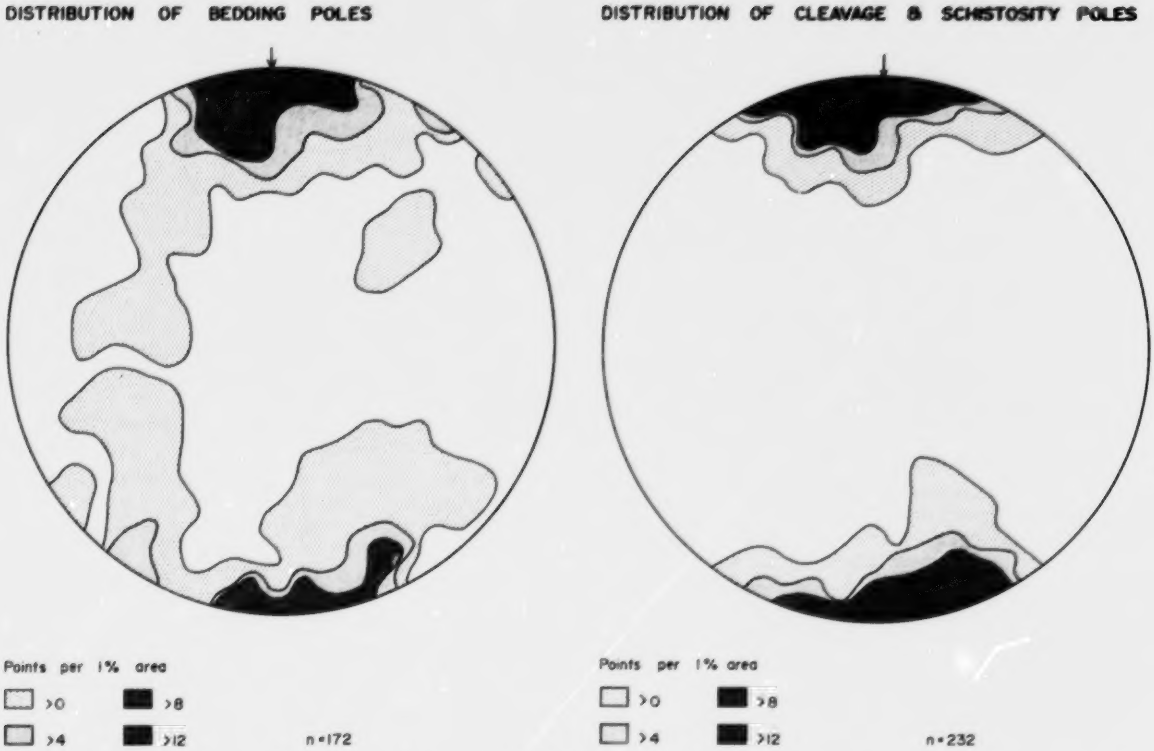

Figure 242.4. *Stereographic plots of (a) bedding and (b) cleavage poles from the Beardmore-Geraldton Belt. (Lower hemisphere, equal area plot, contours in points per 1% area.)*

occur associated with banded iron formation horizons both within pelitic wackes and basalts. Adjacent to major lithological contacts, pre-cleavage isoclinal folds are present on a mesoscopic scale. Folding in the sedimentary units has been recognized (Kehlenbeck 1986) but is only a locally important means of rock deformation. Local facing direction reversals are common, as expected in a terrain where cleavage and bedding are frequently parallel (Figure 242.4), and do not necessarily indicate the presence of regional-scale folds. Confirmation of the disrupted regional fold geometry put forward by Kehlenbeck (1986) could not be made.

3. Orientation of bedding in the sedimentary units within the belt ranges from overturned, southward dipping, in the northern part of the belt (Figure 242.3), through vertical strata for much of the belt, to steep northward dipping right-way-up strata in the south. Cleavage is ubiquitous but is strongly developed only in pelitic rocks where it has a generally steep north or south dip, trending to vertical dip, and is oriented east-west. Displacement of early-formed quartz veins indicates that the cleavage is predominantly a plane of dextral shear as well as flattening.

   Within the graded wackes are examples of hydrofracture breccia up to 0.3 m thick which form within silty to sandy layers but laterally develop into reverse slip discontinuities, concave northward. These breccia zones consist of angular, cleaved sediment fragments set in a vein quartz or silty matrix (Carson *et al.* 1982) and cut the regionally developed cleavage.

   In the northern part of the belt, where volcanic units and banded iron formation can be traced continuously as planar units for over 50 km, three paired volcanic and sedimentary units are separated by zones of strong ductile deformation. Analysis of vein systems, lineations, and foliations indicates both dextral and vertical south-side-down components of shear. The upper contact of the volcanics with the overlying sediment is frequently less deformed than the corresponding contact at the base of each volcanic unit.

   Shear related fabrics, quartz vein displacement, pebble rotation and minor z-shaped asymmetric mesoscopic and megascopic folds, mineral extension, and crinkle lineations indicate both an early south-side-down motion, associated with and succeeded by dextral shear.

METAMORPHISM

Metamorphic grade within the BGB is variable. A study by Pirie and Mackasey (1978) demonstrated an increase in grade southwards toward a group of large undeformed leucogranitic bodies around which are developed contact aureoles and metasedimentary migmatites. Field and laboratory examination clearly demonstrates that this marked southwards increase in grade is post-tectonic. These plutons post-date the deformation; recent isotopic studies indicate an age of about 2600 Ma (D. Davis, Geochronology Laboratory, Royal Ontario Museum, Toronto, personal communication, 1986). Examination of syn-tectonic mineral assemblages suggest a slight metamorphic gradient from lowermost greenschist near Oxaline Lake (Figure 242.2) to upper greenschist near the leucogranitic complexes in the south. Subtle but abrupt changes in grade seem to be lithologically controlled (Robinson 1986). Some of the basic volcanic horizons have higher grades of metamorphism than the sedimentary units with which they are interleaved, suggesting that at least some of the metamorphism reflects an early alteration of igneous assemblages. The gabbros have no metamorphic effect on either the the adjacent basic rocks or the sedimentary units which underlie them (Lawson 1986). There is no apparent metamorphic contrast across the presently defined Wabigoon-Quetico Subprovince boundary.

DISCUSSION

PREVIOUS MODELS

The tectonic relations between the Wabigoon and Quetico Subprovinces were reviewed by Blackburn (1980) who put forward a hypothesis, as did Carter (1983) and Percival and Sullivan (1986), involving large-scale folding to explain the structure of the Quetico. These models cannot be applied in the BGB because the field evidence for their support is entirely dependent on the erroneous assumption that folding in the BGB is the major rock-deforming process. The facing reversals, well displayed and recorded by Kehlenbeck (1984, 1986), Anglin and Franklin (1985), and farther west, near Thunder Bay, by Borradaile (1982), cannot be used as evidence for regional scale folds in the Beardmore-Geraldton Belt, because the cleavage frequently transects the few folds that have been recognized. Further, the low grade of metamorphism of much of the 20 km thickness of the sedimentary pile in the southern part of the area is difficult to reconcile with a tectonic regime involving crustal thickening by folding: for burial under such a mass would produce regional metamorphic mineral assemblages far higher than those actually observed away from the leucogranitic masses.

ACCRETIONARY MODEL

The data support the hypothesis that the Beardmore-Geraldton Belt is part of an accretionary prism consisting of trench and fore-arc sedimentary material interleaved with layers of basic volcanics and gabbros, cut by mildly discordant gabbros and leucogranitic major and minor intrusions.

It has been established elsewhere (Karig and Sharman 1975; Leggett 1980; Leggett *et al.* 1982; Ogawa 1985) that vast thicknesses of immature sediments with or without basaltic oceanic material may be accumulated in subduction zone complexes. Accretionary sequences of this type characteristically contain few folds, and are dominated by layer-parallel shear deformation and thrusting and strain inhomogeneity. They commonly contain sedimentary rocks rich in dewatering structures and exhibit evidence of the high pore fluid pressures necessary for hydrofracture formation. The clastic stratigraphy in accretionary prisms is frequently monotonous and rich in feldspathic debris, but contains minor quantities of chert and banded iron formation. The study of prisms (McCarthy and Scholl 1985), however, shows remarkable continuity of strata along their strike length. In the BGB, the limited occurrence of isoclinally folded zones at the stratigraphic top of each sedimentary package and the dominantly layer-parallel tectonics of thrusting and shearing, have analogues in the more recent examples of prisms studied by advanced seismic reflection techniques (McCarthy and Scholl 1985). Also in the BGB, where shearing has been identified as the major mechanism of deformation, the vertical sense of motion is generally south-side-down in association with and followed by dextral motion, as in Figure 242.5. This motion can be explained in terms of oblique subduction. The back rotation of the accretionary prism resulting from continued underplating of sedimentary and volcanic material gave rise to: the dominantly layer-parallel shears; the locally developed steeply plunging stretching lineation and sub-horizontal boudinage; a broad spectrum of bedding-discordant, northwards dipping, *en echelon* vein arrays. Oblique subduction causes a continued dextral component of shearing, even after the final consolidation of the prism (Needham and Knipe 1986). North-south trending mid- to late-Proterozoic diabase dikes are significantly displaced with the same sense, but the age of this motion is uncertain.

Prior to the intrusion of the leucogranitic complexes (B on Figure 242.2), the ambient metamorphic grade was greenschist facies (Robinson 1986), for there is local preservation of pre-metamorphic, pre-accretion igneous, and alteration assemblages in the basaltic rocks. Metamorphic assemblages in accretionary prisms are generally low (Ernst 1971; Kemp *et al.* 1985).

The southern margin of the Quetico, in contact with the Wawa Subprovince (a granite-greenstone terrain similar to the Wabigoon), is a boundary clearly containing highly strained rocks, including mylonites. A traverse across the subprovince boundary at the southern margin of the Quetico (Figure 242.1), indicates that there is some similarity of structure between the northern and southern portions of the Quetico, but there is no reason to suppose that the metasedimentary belt of the Quetico Subprovince is a symmetrical structure.

There is increasing evidence to support the inspired hypothesis of Langford and Morin (1976), that the Superior Province consists of accreted island arcs, where the Wabigoon and Wawa arc-type terrains are separated by the Quetico Subprovince.

CONCLUSIONS

1. The Beardmore-Geraldton Belt is an accretionary prism developed on the southern margin of the Onaman Plutonic Complex of greenstones and batholiths which represent a volcanic arc typical of the Wabigoon Subprovince.

(a) Archaean (c. 2770 my.)

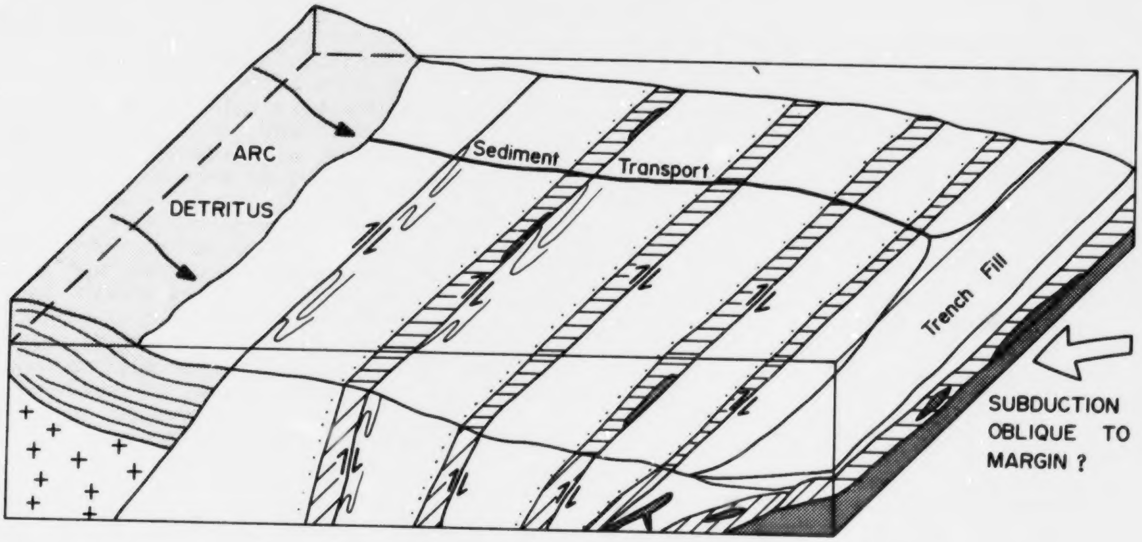
ARC
DETRITUS
Sediment Transport
Trench Fill
SUBDUCTION OBLIQUE TO MARGIN ?

(b) Post accretion (c. 2600 my.)

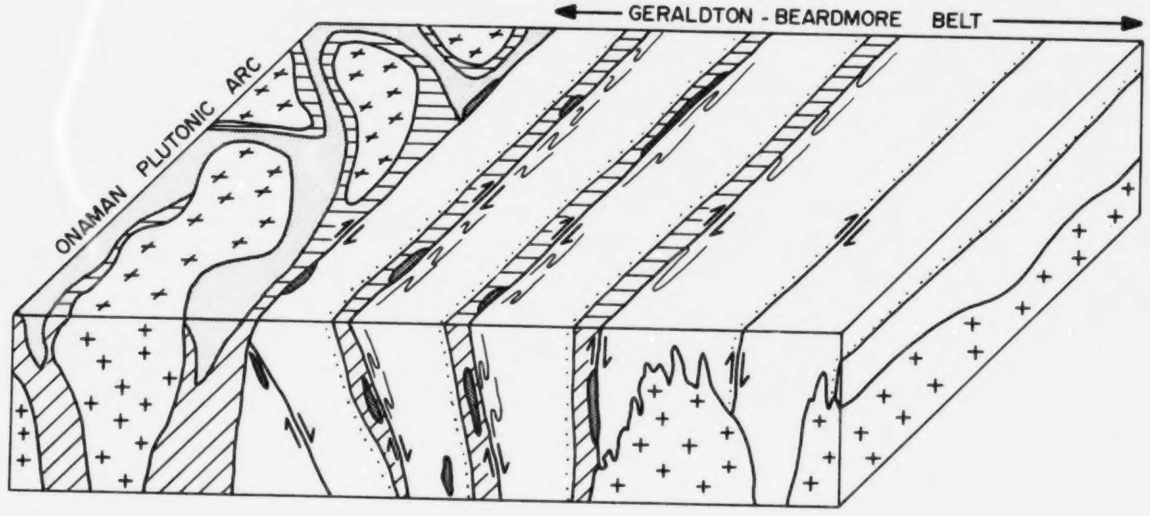
GERALDTON - BEARDMORE BELT
ONAMAN PLUTONIC ARC

Figure 242.5. Schematic diagrams of the arc-accretionary prism model during prism formation and subsequent to accretion to Wawa terrain to the south.

2. The defined boundary of the Wabigoon with the Quetico Subprovince is at present positioned within a structural domain. Relocation of the boundary to the transition between the granite-greenstone terrain to the north and the accretionary prism to the south is appropriate. This boundary is marked by a zone of ductile and brittle shear.

ACKNOWLEDGMENTS

This study has also been supported by the Natural Sciences and Engineering Research Council (NSERC). Peter Brown drew the diagrams. Earlier draughts of this manuscript benefited from two anonymous referees and discussion with K.H. Poulsen, A.C. Colvine, and other colleagues from the Ontario Geological Survey.

REFERENCES

Anglin, C.D., and Franklin, T.M.
1985: Gold Mineralisation in the Beardmore-Geraldton Area of Northern Ontario: Structural Conditions and the Role of Iron Formation; p.193-201 *in* Current Research, Part A, Geological Survey of Canada, Paper 85-1A.

Ayres, L.D.
1969: Early Precambrian Stratigraphy of Part of the Lake Superior Provincial Park, Ontario, Canada, and its Implications for the Origin of the Superior Province; Unpublished Ph.D. Thesis, University of Princeton, 399p.

Barrett, T.J., and Fralick, P.W.
1985: Sediment Redeposition in Archean Iron Formation: Examples from the Beardmore-Geraldton Greenstone Belt, Ontario; Journal of Sedimentary Petrology, Volume 55, p.205-212.

Blackburn, C.E.
1980: Towards a Mobilist Tectonic Model for Part of the Archean of Northwest Ontario; Geoscience Canada, Volume 7, p.64-72.

Borradaile, G.J.
1982: Comparison of Archean Structural Styles in Two Belts of the Canadian Superior Province; Precambrian Research, Volume 19, p.179-189.

Buck, S.
1986: Structural Studies and Gabbro Mylonitisation Within the Barton Bay Deformation Zone, Geraldton, Ontario; Unpublished M.Sc. Thesis, Brock University, Ontario, 172p.

Buck, S., and Williams, H.R.
1984: Structural Studies in the Geraldton Area; p.208-212, *in* Summary of Field Work, 1984, Ontario Geological Survey, edited by John Wood, Owen L. White, R.B. Barlow, and A.C. Colvine, Ontario Geological Survey, Miscellaneous Paper 119, 309p.
1986: Structural Analysis of a Gabbro Mylonite, Geraldton, Ontario; Geological Association of Canada Annual General Meeting Abstracts, p.50.

Carson, B., von Huene, R., Arthur, M.
1982: Small Scale Deformation Structures and Physical Properties Related to Convergence in the Japan Trench Slope Sediments; Tectonics, Volume 1, p.277-302.

Carter, M.W.
1983: McComber and Vincent Townships, District of Thunder Bay; p.32-36, *in* Summary of Field Work, 1983, Ontario Geological Survey, edited by John Wood, Owen L. White, R.B. Barlow, and A.C. Colvine, Ontario Geological Survey, Miscellaneous Paper 116, 313p.

Devaney, J.R., and Fralick, P.W.
1985: Regional Sedimentology of the Namewaminikan Group, Northern Ontario: Archaean Fluvial Fans, Braided Rivers, Deltas and an Aquabasin; p.125-132, *in* Current Research, Part B, Geological Survey of Canada, Paper 85-1B.

Ernst, W.G.
1971: Metamorphic Zonations on Presumably Subducted Lithospheric Plates from Japan, California, and the Alps; Contributions to Mineralogy and Petrology, Volume 34, p.43-59.

Karig, D., and Sharman, G.F.
1975: Subduction and Accretion in Trenches; Geological Society of America Bulletin, Volume 86, p.377-389.

Kehlenbeck, M.M.
1984: Use of Structural Facing Directions to Delineate the Geometry of Refolded Folds Near Thunder Bay, Ontario; Geoscience Canada, Volume 11, p.23-32.
1986: Folds and Folding in the Beardmore-Geraldton Fold Belt; Canadian Journal of Earth Sciences, Volume 23, p.158-171.

Kemp, A.E.S., Oliver, G.H.J., and Baldwin, J.R.
1985: Low Grade Metamorphism and Accretion Tectonics: Southern Uplands Terrain, Scotland; Mineralogical Magazine, Volume 49, p.335-344.

Langford, F.F., and Morin, J.A.
1976: The Development of the Superior Province of Northwestern Ontario by Merging Island Arcs; American Journal of Science, Volume 276, p.1023-1034.

Lawson, G.E.
1986: Geological Investigations in the Oxaline Lake Area, Near Jellico, Northern Ontario; Unpublished B.Sc. Thesis, Brock University, Ontario, 50p, Accompanied by a Map.

Leggett, J.K.
1980: The Sedimentological Evolution of a Lower Palaeozoic Accretionary Fore-Arc in the Southern Uplands of Scotland; Sedimentology, Volume 27, p.401-417.

Leggett, J.K., McKerrow, W.S., and Casey, D.M.
1982: The Anatomy of a Lower Palaeozoic Accretionary Forearc: the Southern Uplands of Scotland; p.495-520, *in* Trench-Forearc Geology: Sedimentation and Tectonics of Modern and Ancient Plate Margins, edited by J.K. Leggett, Blackwell, London, 576p.

McCarthy, J., and Scholl, D.W.
1985: Mechanisms of Subduction Accretion Along the Central Aleutian Trench; Geological Society of America Bulletin, Volume 96, p.691-701.

Mackasey, W.O.
1976: The Geology of Walters and Leduc Townships, District of Thunder Bay; Ontario Division of Mines, Geoscience Report 149, 60p.

Mason, J.K., and McConnell, C.D.
1983: Gold Mineralization in the Beardmore-Geraldton Area; p.84-97, *in* The Geology of Gold in Ontario, edited by A.C. Colvine, Ontario Geological Survey, Miscellaneous Paper 110, 278p.

Needham, D.T., and Knipe, R.J.
1986: Accretion and Collision Related Deformation in the Southern Uplands Accretionary Wedge, Southwestern Scotland; Geology, Volume 14, p.303-306.

Ogawa, Y.
1985: Variety of Subduction and Accretion Processes in Cretaceous to Recent Plate Boundaries Around Southwest and Central Japan; Tectonophysics, Volume 112, p.493-518.

Patterson, G.C., Mason, J.K., and Schneiders, B.R.
1985: Thunder Bay Resident Geologist Area, North-Central Region; p.56-133 *in* Report of Activities, 1984, Regional and Resident Geologists, edited by C.R. Kustra, Ontario Geological Survey, Miscellaneous Paper 122, 297p.

Percival, J., and Sullivan, R.W.
1986: Age Constraints on the Evolution of the Quetico Belt, Superior Province, Ontario (Abstract); p.91-93 *in* The Tectonic Evolution of Greenstone Belts, Lunar and Planetary Institute Workshop, Book of Abstracts.

Pirie, J., and Mackasey, W.O.
1978: Preliminary Examination of Regional Metamorphism in Parts of the Quetico Metasedimentary Belt, Superior Province, Ontario; p.37-48 *in* Metamorphism in the Canadian Shield, Geological Survey of Canada, Paper 78-10.

Reilly, B.A., and Williams, H.R.
1986: Structural Geology of the Paint Lake Fault System in Walters, Leduc, and Legault Townships of Northwestern Ontario; Geological Association of Canada Annual General Meeting, Abstracts, p.117.

Robinson, A.M.
1986: A study of Metamorphic Textures in the Geraldton-Beardmore Belt; Unpublished B.Sc. Thesis, Brock University, St. Catharines, Ontario, 58p. Accompanied by Maps.

Stott, G.M.
1984a: Geraldton Sheet, Thunder Bay and Cochrane Districts; Ontario Geological Survey Map 241 (revised), Compilation Series-Preliminary Map, scale 1:126 720.
1984b: Lake Nipigon Sheet, Thunder Bay District; Ontario Geological Survey, Map 257 (revised), Compilation Series-Preliminary Map, scale 1:126 720.

Williams, H.R.
In Preparation: An Archean Forearc Accretionary Prism in the Superior Province of Northern Ontario.

Grant 249 Geochemical Studies of Formation Waters from Paleozoic Strata, Southwestern Ontario

P. Dollar[1], S.K. Frape[1], R.H. McNutt[2], P. Fritz[1], and R.W. Macqueen[3]

[1]Department of Earth Sciences, University of Waterloo, Waterloo

[2]Department of Geology, McMaster University, Hamilton

[3]Institute of Sedimentary and Petroleum Geology, Geological Survey of Canada, Calgary

ABSTRACT

The groundwater of southwestern Ontario has been analyzed for: major, minor, and trace element geochemistry; stable isotope content; tritium; and strontium isotopic content. The results of these analyses indicate that most sedimentary formations contain very concentrated brines (>250 grams per litre (g/L), Total Dissolved Solids (T.D.S.), which have distinctive geochemical and isotopic signatures for individual units. However, some samples which have been collected appear to be mixtures of brines from various formations and/or mixtures of formation brines with more dilute groundwaters such as glacial meltwaters or recent meteoric waters. The mixing of various water masses would indicate that both paleo-migration and recent migration of groundwater has taken place. This, in turn, has a number of implications on the formation of economic deposits in the area and on active and proposed waste disposal schemes.

INTRODUCTION

Paleozoic strata of southwestern Ontario host valuable commodities including oil and gas deposits and sporadic uneconomic metallic sulphide occurrences. These commodities involve fluid phases in concentration, migration, and deposition. At present, the fluid-controlled processes of concentration and migration are only poorly understood.

Formation waters are commonly associated with oil and gas accumulations and metallic mineral deposits in sedimentary basins. Examination of the inorganic chemical constituents that characterize these waters is important for understanding their origin and evolution. Knowledge of the composition and variability of formation waters may be used to evaluate the importance of rock-water interactions in accounting for the composition of the waters and determining whether the present fluid distribution system is dynamic (moving at measurable rates over 10^2 to 10^3 years) or static (no apparent movement over similar time intervals). If the present fluid distribution system can be shown to be dynamic, the possibility exists of defining fluid migration routes and rates, which may have prevailed over the last few thousands of years at least. The critical question then becomes: What role might such migration routes have played in determining the known distribution of commodities in the southwestern Ontario Paleozoic section?

STRATIGRAPHIC AND STRUCTURAL CONTROLS

In order to appreciate possible hydrogeological-fluid migration aspects of the study, it is necessary to be fully acquainted with the important stratigraphic and structural features which might influence fluid movement in the area.

Southwestern Ontario is underlain by a Paleozoic sedimentary succession which ranges in age from Upper Cambrian to Lower Mississippian and consists of a variety of carbonates, shales, evaporites, and minor sandstone (Figure 249.1). The present study characterizes the inorganic chemical constitutents in brines from four hydrocarbon-bearing horizons: the Dundee Formation limestones of Devonian age, the Silurian Guelph carbonates, the Ordovician Trenton and Black River Group carbonates, and the sandstones and dolostones of Cambrian age. These essentially undisturbed Paleozoic rocks rest unconformably on Precambrian basement rocks and are overlain by Pleistocene glacial deposits.

The Algonquin and Findlay Arches, broad Precambrian highs separated by the Chatham Sag, trend northwest-southeast, dividing the Ontario Peninsula into two parts (Figure 249.2). These two structurally positive features were probably introduced during late Precambrian time, but were intermittently reactivated during the Paleozoic to form a broad platform between a more rapidly subsiding Michigan Basin on the west and the Appalachian Basin to the southeast (Sanford *et al.* 1985). The current regional dip of the Paleozoic rocks to the northwest of the

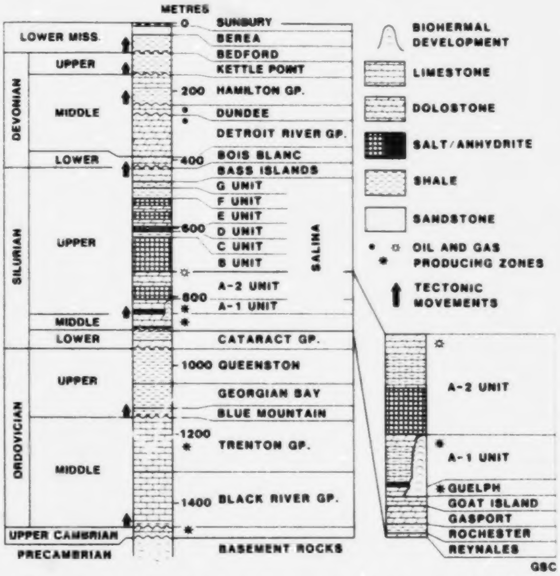
METRES
LOWER MISS.
DEVONIAN
UPPER
MIDDLE
LOWER
SILURIAN
UPPER
MIDDLE
LOWER
ORDOVICIAN
UPPER
MIDDLE
UPPER CAMBRIAN
PRECAMBRIAN
0
200
400
600
800
1000
1200
1400
SUNBURY
BEREA
BEDFORD
KETTLE POINT
HAMILTON GP.
DUNDEE
DETROIT RIVER GP.
BOIS BLANC
BASS ISLANDS
G UNIT
F UNIT
E UNIT
D UNIT
C UNIT
B UNIT
A-2 UNIT
A-1 UNIT
SALINA
CATARACT GP.
QUEENSTON
GEORGIAN BAY
BLUE MOUNTAIN
TRENTON GP.
BLACK RIVER GP.
BASEMENT ROCKS
BIOHERMAL DEVELOPMENT
LIMESTONE
DOLOSTONE
SALT/ANHYDRITE
SHALE
SANDSTONE
OIL AND GAS PRODUCING ZONES
TECTONIC MOVEMENTS
A-2 UNIT
A-1 UNIT
GUELPH
GOAT ISLAND
GASPORT
ROCHESTER
REYNALES
GSC

Figure 249.1. Composite stratigraphic succession, southwestern Ontario (after Sanford et al. 1985).

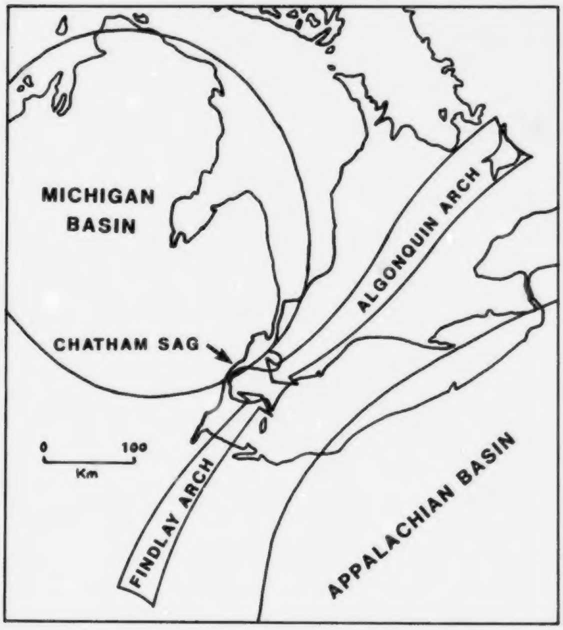

Figure 249.2. *Regional tectonic structures influencing the southwestern Ontario area.*

arches is 6 to 9 m/km into the Michigan Basin and to the southeast of the arches, the dip is 6 m/km into the Appalachian Basin (Winder and Sanford 1972). Paleozoic strata in the Chatham Sag are for the most part horizontal.

Sanford *et al.* (1985) have proposed a relatively active tectonic history for southwestern Ontario. Tectonically associated fault block readjustment has provided the structural control for the origin and development of southwestern Ontario's hydrocarbon traps. The implications of such tectonic movements on the hydrodynamic/fluid migration history are being examined.

SAMPLE COLLECTION AND ANALYSIS

The waters studied are oilfield brines from southwestern Ontario (Figure 249.3). Samples were initially collected in large polyethylene bottles from producing oil and gas wells and dry holes (no oil or natural gas encountered). Prior to geochemical analyses, samples were filtered through a hand-held Millipore filter system using 0.45 μm filters. A 500 mL aliquot for cation analyses was acidified to a pH of <2 using concentrated HCl. Analyses for cations were performed by atomic absorption spectrophotometer using standard analytical procedures. A second 500 mL aliquot was filtered and left unacidified to be used for analyses of SO_4^{2-}, Cl^-, and Br^- by a Dionex Auto Ion System 12 analyzer. All samples were treated using standard procedures, although certain special procedures as outlined by Dionex were used for Br^- analyses.

At all sites a 125 mL filtered sample was taken to be used for analyses of ^{18}O, deuterium, and tritium.

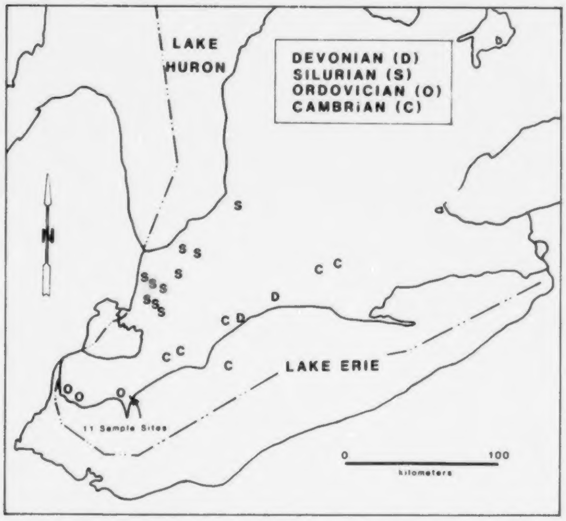

Figure 249.3. *Location of groundwater samples, southwestern Ontario.*

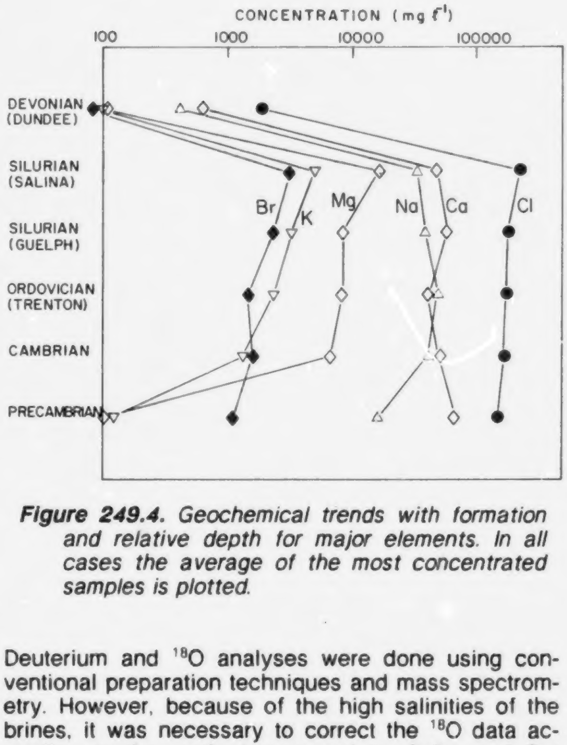

Figure 249.4. *Geochemical trends with formation and relative depth for major elements. In all cases the average of the most concentrated samples is plotted.*

Deuterium and ^{18}O analyses were done using conventional preparation techniques and mass spectrometry. However, because of the high salinities of the brines, it was necessary to correct the ^{18}O data according to the method proposed by Sofer and Gat (1972). Deuterium analyses were done on water vapour distilled from the brines. Distillations were performed at elevated temperatures to prevent formation of hydrated salts. Results are reported with respect to the Vienna-SMOW standard. Accuracy is ±0.15‰ for ^{18}O, and ±2.0‰ for deuterium.

Strontium isotopic analyses were measured on a VG 354,5-collector mass spectrometer, following separation of Sr by standard ion-exchange techniques. Elution was carried out using 2.5 M HCl. Within-run precision of a single analysis is ±0.003‰. Repeated runs of Eimer & Amend and NBS 987 standards give 0.70802 and 0.71024 respectively.

All analyses of inorganic chemical constituents and hydrogen and oxygen stable isotopes were performed at the University of Waterloo. Analyses of strontium isotopes were done at McMaster University, Hamilton, Ontario.

RESULTS AND INTERPRETATION

MAJOR ELEMENT CHEMISTRY

Almost all groundwater sampled in the present study are brines according to the classification scheme proposed by Davis (1964), since most contain >100 000 ppm total dissolved solids. Representative chemistries of the most concentrated brines from each stratigraphic horizon are presented in Table 249.1. Figure 249.4 is a plot of the major ions in these waters with increasing depth. Although general in nature, this figure shows the types of gains or losses of major elements which would be necessary in any cross-formational flow or diagenesis model. The principal ions contained in these waters are Ca^{2+}, Na^+, and Cl^- with total concentrations in excess of 300 g/L at some sites (salt units of the Silurian Salina Formation). Overall, Br^-, K^+, Mg^{2+}, Ca^{2+}, and Cl concentrations decrease with increasing depth/age, while Na^+ concentrations increase. The Precambrian waters plotted are from the Sudbury Basin (Frape and Fritz 1982).

Figure 249.5 is a normalized (molar ratios) ternary plot for calcium, sodium, and magnesium. It is readily apparent that the most concentrated brines for each age have distinctive chemistries and plot within a narrow range. More dilute waters from each formation plot outside the groupings and are often sodium rich. The more dilute nature and sodium enrichment, particularly for Silurian Guelph samples, may be due to halite dissolution and/or mixing with fresh, meteoric groundwater from shallower zones. The brines in the present study are depleted in sodium with respect to formation waters from other oil-producing basins (Collins 1975). It is interesting to note that deep saline waters from the Sudbury Basin (Frape *et al.* 1984) have similar Ca/Na ratios to the oilfield brines of southwestern Ontario, but are relatively deficient in magnesium.

HEAVY METAL CHEMISTRY

Preliminary results of trace element analyses for a number of samples representing the various stratigraphic units, indicate that some brines contain elevated concentrations of many heavy metal species.

The most concentrated brines from all formations contain about equal amounts of copper (~1.0 mg/L). More dilute waters generally have very low concentrations of all metals. Nickel concentrations were very consistent for all brine samples. Most samples had approximately 4 mg/L nickel for every 100 000 mg/L chloride. By contrast, both lead and zinc levels show considerable variation throughout the area, with the highest lead and zinc levels, 53 mg/L and 52 mg/L respectively, recorded in Cambrian brines. Other stratigraphic units usually have much lower levels (<5 mg/L) of either element. As considerable difficulty has been encountered in analyzing many of the metal species in these very concentrated brines, the authors are reluctant to speculate at any great length on the total metal composition. It is interesting that significant concentrations of some species, particularly lead and zinc, exist in the brines and much of the present study is focused on aspects relating the brine chemistry to known metal occurrences.

STABLE ISOTOPES (^{18}O and ^2H)

Oxygen and hydrogen stable isotopes are used in conjunction with geochemical compositional data to help better define the origin of water in oilfield brines of the area. Figure 249.6 shows the relationship between Oxygen-18 and Deuterium for the southern Ontario brines and other selected groundwater data from areas adjacent to the study site. For correlative purposes, brines from the Michigan Basin (Clayton *et al.* 1966), Appalachian Basin (Breen *et al.* 1985), and Precambrian Sudbury Basin (Frape and Fritz 1982) are also included.

Brines from the present study plot below the global meteoric water line. The most concentrated brine samples from the different stratigraphic units have a narrow range of composition, with Cambrian and Ordovician waters positioned nearest the global meteoric water line. The lower salinity waters of the Silurian Salina and Guelph Formations depart significantly from the line. Two low salinity samples from the Devonian age Dundee Formation are depleted in ^{18}O and ^2H, characteristic of waters recharged under cooler climatic conditions.

The brines show a large enrichment in ^{18}O but a relatively small enrichment in deuterium. Hitchon and Friedman (1969) have attributed the ^{18}O enrichment of formation waters to the exchange of oxygen isotopes between water and carbonate minerals. Although exchange of deuterium takes place between waters and hydrogen compounds in sedimentary basins, the effect is minimized by the overwhelming mass of formation water relative to hydrogen compounds (most notably H_2S, Hitchon and Friedman 1969).

Several possible mechanisms could be used to account for the observed ^{18}O - ^2H trend. The formation of clays and hydration of silicates has been shown to isotopically deplete the residual fluid in ^{18}O and enrich the fluid phase in ^2H (Fritz and Frape 1982). The end result of this process would be to move the isotopic composition of a fluid up and to the left on Figure 249.6. This is very interesting in light of the groupings and age distribution of the brines. In order to confirm this hypothesis, much more work will be required involving the identification and isotopic analyses of clay minerals in the various horizons.

Alternatively, the trends seen on Figure 249.6 could represent varying mixtures of two end members. As an example, a concentrated fossil Michigan Basin seawater, possibly similar in composition to a Canadian Shield brine. Whatever hypothesis is used

TABLE 249.1. CHEMISTRY OF TYPICAL FORMATION WATER FROM SOUTHWESTERN ONTARIO.

Formation		Cambrian	Ordovician (Black River)	Ordovician (Trenton)	Silurian (Guelph)	Silurian (Salina)	Devonian (Dundee)	Precambrian Brine (Sudbury)
Ca	mg L^{-1}	48 500	33 600	40 200	57 500	48 400	620	65 000
Na	mg L^{-1}	41 000	41 500	47 250	39 400	33 400	410	16 880
Mg	mg L^{-1}	6 700	6 100	8 300	8 800	16 600	85	12
K	mg L^{-1}	1 360	1 850	2 380	3 310	5 000	18.9	122
Sr	mg L^{-1}	1 210	670	760	1 220	1 620	11.7	1 390
Li	mg L^{-1}	1.24	9.13	12.2	12.9	-	0.22	0.77
Cl	mg L^{-1}	179 000	137 000	183 000	189 000	232 000	1 995	156 000
Br	mg L^{-1}	1 510	1 260	1 410	2 380	3 220	11.9	1 090
SO_4	mg L^{-1}	33.3	39.8	27.7	21.8	110.0	72.0	138
Si	mg L^{-1}	20.5	18.9	30.7	29.6	-	10.0	9.6

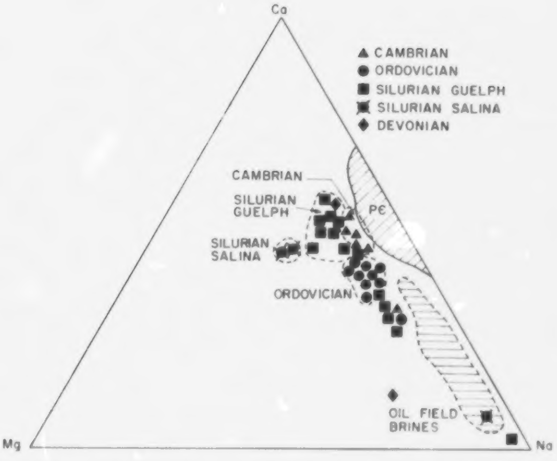

Figure 249.5. Mole percentage diagram for Ca, Na, and Mg concentrations for saline and brine samples from southwestern Ontario. Also plotted is the position of Canadian Shield Precambrian brines (Frape et al. 1984) and most oilfield brines listed for the United States by Collins (1975).

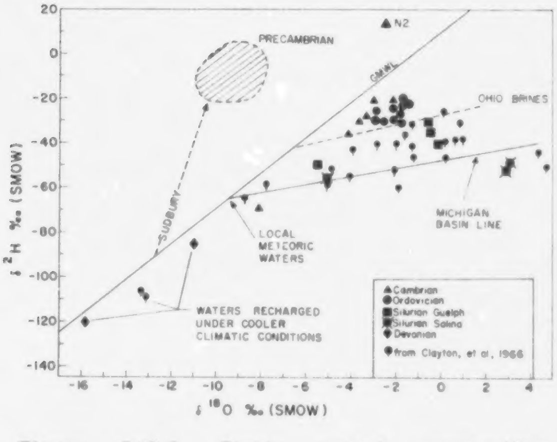

Figure 249.6. Stable isotopic composition (oxygen-18 and deuterium) for brines and saline waters from southwestern Ontario (this study), the Michigan Basin (Clayton et al. 1966), Ohio (Breen et al. 1985), and the Canadian Shield, Sudbury (Frape et al. 1984).

to account for the isotopic distributions, one must also account for the changes in chemical composition noted between formations.

STRONTIUM ISOTOPES ($^{87}Sr/^{86}Sr$ Ratios)

Strontium isotopic results are shown in Figure 249.7 as a function of the age of the host rock that contains the brine. Also shown is the curve of Burke *et al.* (1982), describing the change in the $^{87}Sr/^{86}Sr$ composition of seawater over lower Paleozoic time. Because Sr has a long residence time in the ocean, its concentration and isotopic composition is uniform throughout the world's oceans at any given time (Veizer and Compston 1974). Therefore, there is the potential for Sr to be used as a geochronological tool for marine sediments and/or as an indicator of the changes in chemistry that occur during diagenesis. It is the latter that is of interest to us in this study.

The Sr seawater curve shows a large variation over the time interval under study, varying from a high of approximately 0.7095 in the Cambrian to a low of less than 0.7080 in the late Ordovician, before increasing again in the Silurian to 0.7085 to 0.7090. If the brines measured in this study are the same age as their host rock, then they all have $^{87}Sr/^{86}Sr$ values greater than that of seawater for the time period in question, with the exception of the Silurian Salina waters and one sample from the Guelph Formation. Such elevated ratios imply that there has been water-rock interaction *in situ*. If the water is not the same age as its present host, then the interpretation is more difficult. For example, if the Guelph brines were really Cambrian in age and subsequently migrated up section, then what appears to be water-rock interaction in Guelph time may not be the case at all, i.e. there was only fluid migration with no water-rock interaction. No interaction seems a highly unlikely scenario based on our extensive experience studying the brines in rocks on the Precambrian Shield (Fritz

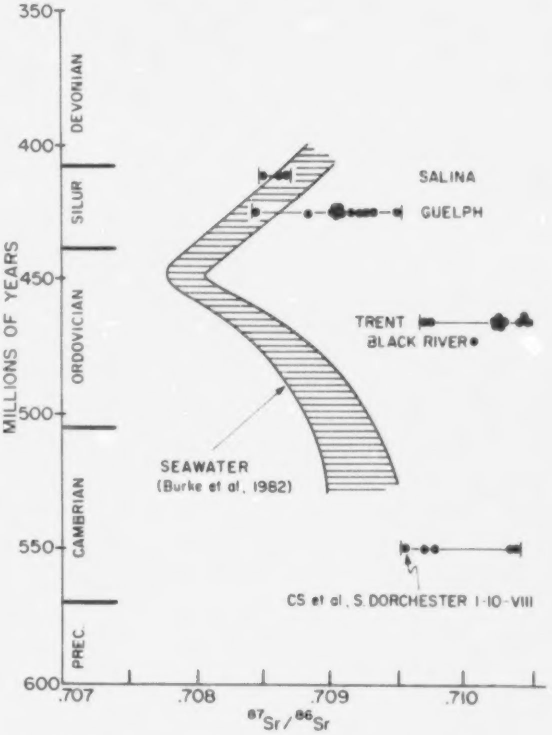

Figure 249.7. $^{87}Sr/^{86}Sr$ ratios for brine samples from southwestern Ontario compared to the seawater curve with time (after Burke et al. 1982).

TABLE 249.2. COMPARISON OF $^{87}Sr/^{86}Sr$ RATIOS FOR WHOLE ROCK, CEMENT, AND BRINE FROM A TYPICAL CAMBRIAN SAMPLE.

CS *et al.* S. Dorchester 1 - 10 - VIII
$^{87}Sr/^{86}Sr$ Study

1.	Whole rock (1069 m)	= 0.73302
2.	Calcite cement (1069 m) (leached with cold 0.5 HAc)	= 0.70964
3.	Whole rock - leachate	= 0.73895
4.	Brine (1063 - 1071 m)	= 0.70957

and Frape 1982; Frape *et al.* 1984; McNutt *et al.* 1984).

The Ordovician samples are not as ambiguous; their ratios are higher than that of seawater for all of Phanerozoic time (Burke *et al.* 1982), so some water-rock interaction is indicated. (Seawater values for the Precambrian are poorly known overall, but must be lower in value. Veizer *et al.* (1982) propose that the $^{87}Sr/^{86}Sr$ ratio of Archean time was 0.7012 to 0.7025). The same may be said for the Cambrian samples, but not with the same conviction due to the limited number of samples, and the tendency of those we do have to break into two groups (Figure 249.7). One of the samples, CS et al., Dorchester 1-10-VIII, possibly lies on the extrapolated seawater curve.

Of the samples studied to date, only the brines found in the Salina Formation have the same ratios as the seawater curve for that time. Therefore, it is possible that this brine has remained in its present host rock since Silurian time with essentially no water-rock interaction.

The drillhole CS et al., South Dorchester 1-10-VIII was studied in detail to determine if the brine's $^{87}Sr/^{86}Sr$ value relates to the host rock. Both the core samples and the brine are from the Cambrian Mount Simon Formation at a depth of 1062 to 1071 m, immediately overlying the Precambrian basement. The rock is fine- to medium-grained arkose containing a suite of diagenetic minerals including dolomite, quartz and feldspar overgrowths, clay minerals, and calcite. A detailed SEM and cathode luminoscopic study is now underway. Preliminary examination shows that the calcite cement is the last diagenetic phase to form, replacing earlier primary and secondary phases and infilling pore spaces. One sample was leached by a dilute solution of acetic acid to remove the calcite but not dissolve the other minerals. The results are given in Table 249.2 for the sample from 1069 m. The whole-rock value of 0.7330 reflects the presence of feldspar with its high Rb/Sr ratio and probable Precambrian age. The leachate, representing the dissolved calcite, has a $^{87}Sr/^{86}Sr$ value identical to the brine, i.e. 0.7096 (compare lines 2 and 4, Table 249.2). The whole-rock minus leachate fraction (line 3, Table 249.2) increases in value as expected if only the low $^{87}Sr/^{86}Sr$ phase calcite dissolves.

The Sr isotopic composition of the brine in 1-10-VIII is slightly elevated with respect to the seawater curve for Cambrian time and reflects minor water-rock interaction. Whether this occurred *in situ* or not cannot be confirmed until more studies are done. Isotopic equilibrium between calcite and brine implies that the former precipitated from the latter. Therefore, the minimum residence time for the brine in its present host rock is the age of the calcite, an unknown at present. Future work on the application of Sr isotopes in sedimentary basins has to involve the separation and analysis of all the diagenetic phases. The separation will be painstaking but the results will be rewarding in the further understanding of the origin and migration of oilfield brines.

DISCUSSION

Preliminary results and interpretation would suggest that three major groundwater types occur in the sedimentary rocks of southwestern Ontario. These would consist of (a) a distinctive formation brine which has similar geochemical and isotopic compositions throughout a particular formation; (b) meteoric groundwaters which are generally found at shallower depths across the area; and (c) a glacial meltwater which usually occurs in Devonian age sedimentary rocks. Several of the samples obtained to date appear to be mixtures of these various end members or in some cases mixtures of formation brines from different aged strata.

As an example, a plot of K/Na versus Br/Cl was prepared in order to assess similarities and differences between water types found in the area (Figure 249.8). The Br/Cl ratio has been used by a number of authors as an indicator of origin and/or evolution of brines and saline waters (Rittenhouse 1967; Carpenter 1978; Frape *et al.* 1984). Both anions are very conservative in their geochemical behaviour. Chloride is not removed from solution until halite saturation is reached and precipitation occurs; whereas bromide is usually not removed from the aqueous phase until the precipitation of the bitter salts. The K/Na ratio on the other hand, puts a relatively conservative cation Na against a very reactive cation, K. Potassium is easily weathered from many detrital silicate minerals and is a major component of several secondary clay minerals. Therefore, the use of this ratio may help to distinguish degrees of water-rock interaction, as well as distinguishing mineralogical composition (e.g. carbonates versus clastics).

Figure 249.8 shows very distinct groupings for the most concentrated brines from each site. The Precambrian brines, especially those from the Sudbury area have the lowest K/Na ratio, with ratios for other rock ages increasing with decreasing age. One particular Cambrian brine with a very high K/Na ratio (~0.094) is from a dilute water sample whose stable isotopic composition would suggest a large component of meteoric water. The $^{87}Sr/^{86}Sr$ composition (0.7089) of this sample more closely resembles Silurian Guelph brines than Cambrian brines. Other samples, such as some brines from Guelph-aged strata plot near or among the Cambrian and Ordovician brines and would appear to be mixtures of the formation water end members. In several cases, some of these samples have strontium isotopic and/or stable isotopic compositions which would support this statement. Several brine samples with

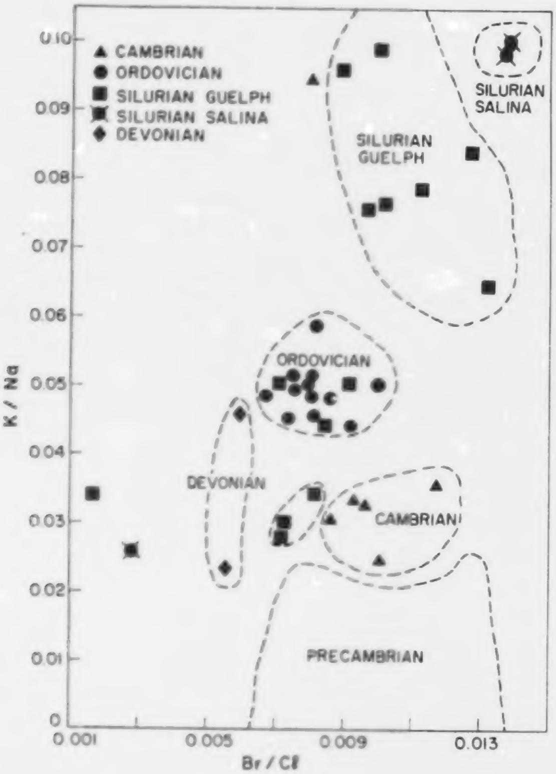

Figure 249.8. *A K/Na versus Br/Cl plot for brines and saline waters from the Paleozoic strata of southwestern Ontario. Data from the Canadian Shield is included for comparison.*

very low Br/Cl ratios found in Silurian strata have very high Na/Ca ratios (~40), which probably indicate a large salt component due to the dissolution of halite. The strontium isotopic composition of these samples appears to be identical to dilute Devonian waters which have been recharged under cooler climatic conditions (glacial meltwaters).

Many additional ratio plots can be constructed with very similar results. In all cases they show strong individual groupings of Precambrian, Cambrian, and Ordovician brines with Precambrian fluids usually resembling Cambrian fluids more closely than Ordovician fluids. Based on very preliminary results, the apparent lack of overlap between brines from these various aged rocks would argue against large-scale present-day migration and mixing between these units.

On the other hand, migration and mixing between Silurian Guelph-aged brines and most other units does appear to have occurred both in the past and more recently. Such mixing has probably been aided by the presence of solution structures and pinnacle reefs in the Silurian strata and perhaps to a more limited extent by suspected large-scale fault systems as described by Sanford *et al.* (1985).

CONCLUSIONS

Several conclusions can be drawn on the basis of the work to date.

1. Very concentrated brines (>250 g/L T.D.S.) exist in Cambrian, Ordovician, and Silurian strata of southwestern Ontario. These brines are usually Ca-Na-Cl in composition: although some variability of Ca/Na does occur.
2. Devonian-aged strata usually contain much more dilute saline waters (T.D.S. <30 g/L), whose stable isotopic signature (^{18}O and ^{2}H) would suggest they were recharged under a cooler climate, probably the last period of deglaciation.
3. The most concentrated brines and waters from each unit have similar isotopic and geochemical characteristics which are distinct from the concentrated brines of other units.
4. Although Cambrian brines come closest isotopically and geochemically to known Precambrian brines at Sudbury, Ontario, very large geochemical differences exist. All Paleozoic brines have several orders of magnitude more Mg than any Canadian Shield brine, and the stable isotope composition of the various Paleozoic brines plots, as most sedimentary brines, to the right of the Global Meteoric Water Line.
5. Many samples taken in this study appear to be mixtures of different formation fluids, recent meteoric waters, and dilute subglacial meltwaters. Such mixtures would indicate both past and present migration of fluids within the area.

Considerably more detailed sampling and supporting diagenetic work is presently underway in order to evaluate the extent and timing of fluid migration and mixing.

ACKNOWLEDGMENTS

The authors wish to thank R.A. Trevail of the Petroleum Resources Laboratory, London, for his continued interest in the project and his help in obtaining samples. We would especially like to thank all the individual and corporate petroleum producers in southwestern Ontario for allowing us access to samples. The analytical support of R. Kellerman, geochemistry and the isotope laboratory at the University of Waterloo have been of great assistance. The technical support of I. McAndrew, D. Jones, and C. Jager at McMaster University is greatly appreciated.

REFERENCES

Breen, K.J., Clifford, G.A., Masters, R.W., and Sedam, R.C.

1985: Chemical and Isotopic Characteristics of Brines from Three Oil and Gas Producing Sandstones in Eastern Ohio, with Applications to the Geochemical Tracing of Brine Sources; United States Geological Survey, Water Resources Investigations Report 84-4314, 58p.

Burke, W.H., Denison, R.E., Heatherington, E.A., Koepnick, R.B., Nelson, H.F., and Otto, J.B.

1982: Variation of Seawater $^{87}Sr/^{86}Sr$ Throughout Phanerozoic Time; Geology, Volume 10, p.516-519.

Carpenter, A.B.
1978: Origin and Chemical Evaluation of Brines in Sedimentary Basins; Oklahoma Geological Survey, Circular 79, p.60-77.

Clayton, R.N., Friedman, I., Graf, D.L., Mayeda, T.K., Meents, W.F., and Shimp, N.F.
1966: The Origin of Saline Formation Waters, 1, Isotopic Composition; Journal of Geophysical Research, Volume 71, p.3869-3882.

Collins, A.G.
1975: Geochemistry of Oilfield Brines; Elsevier Scientific Publishing Company, Amsterdam, 496p.

Davis, S.N.
1964: The Chemistry of Saline Waters by R.A. Dreiger—Discussion; Ground Water, Volume 2, Number 1, p.51.

Frape, S.K., and Fritz, P.
1982: The Chemistry and Isotopic Composition of Saline Groundwaters from the Sudbury Basin, Ontario; Canadian Journal of Earth Sciences, Volume 19, p.645-661.

Frape, S.K., Fritz, P., and McNutt, R.H.
1984: The Role of Water-Rock Interaction in the Chemical Evolution of Groundwaters from the Canadian Shield; Geochimica et Cosmochimica Acta, Volume 48, p.1617-1627.

Fritz, P., and Frape, S.K.
1982: Saline Groundwaters in the Canadian Shield—A First Overview; Chemical Geology, Volume 36, p.179-190.

Hitchon, B., and Friedman, I.
1969: Geochemistry and Origin of Formation Waters in the Western Canada Sedimentary Basin—I. Stable Isotopes of Hydrogen and Oxygen; Geochimica et Cosmochimica Acta, Volume 33, p.1321-1349.

McNutt, R.H., Frape, S.K., and Fritz, P.
1984: Strontium Isotope Composition of some Brines from the Precambrian Shield of Canada; Isotope Geoscience, Volume 2, p.205-215.

Rittenhouse, G.
1967: Bromine in Oilfield Waters and its Use in Determining Possibilities of Origin of these Waters; American Association of Petroleum Geologists Bulletin, Volume 51, p.2430-2440.

Sanford, B.V., Thomson, F.J., and McFall, G.H.
1985: Plate Tectonics—A Possible Controlling Mechanism in the Development of Hydrocarbon Traps in Southwestern Ontario; Bulletin of Canadian Petroleum Geology, Volume 33, Number 1, p.52-71.

Sofer, Z., and Gat, J.R.
1972: Activities and Concentrations of ^{18}O in Concentrated Aqueous Salt Solutions—Analytical and Geophysical Implications; Earth and Planetary Science Letters, Volume 15, p.232-238.

Veizer, J., Compston, W., Hoefs, J., and Nielsen, H.
1982: Mantle Buffering of the Early Oceans; Naturwissenschaften, Volume 69, p.173-180.

Veizer, J., and Compston, W.
1974: $^{87}Sr/^{86}Sr$ Composition of Seawater during the Phanerozoic; Geochimica et Cosmochimica Acta, Volume 38, p.1461-1484.

Winder, C.G., and Sanford, B.V.
1972: Stratigraphy and Paleontology of Paleozoic Rocks of Southern Ontario; Excursion A45-C45, Guidebook, 24th Session, International Geological Congress, Montreal, Quebec.

Grant 254 Exploration for Buried Aggregates by Remote Sensing Techniques: An Assessment

H. George[1], **M.B. Dusseault**[1], **and A.B. Kesik**[2]

[1]Department of Earth Sciences, University of Waterloo, Waterloo

[2]Department of Geography, University of Waterloo, Waterloo

ABSTRACT

The usefulness of different types of remotely sensed data, specifically airborne multispectral digital imagery and colour infrared photography, as aids in the exploration for buried near-surface aggregates near Chatham, Ontario, is currently being evaluated. The objective of the study is to identify anomalous tonal zones on the imagery that are caused by high subsurface drainage possibly associated with *shallowly* buried gravel. Some early results of the evaluation of high resolution multispectral imagery and colour infrared photography indicate that both of these media, when used in conjunction, offer considerable advantages over black-and-white panchromatic airphotos for photomorphic regionalization and detailed mapping of surficial materials and geomorphic features. In addition to the anomalous tones primarily sought in this study, improvements to the mapping of surficial deposits can lead potentially to refinements of interpretations of regional Late Quaternary deglaciation events and, subsequently, to identification of areas where processes of deglaciation were likely to concentrate coarse aggregate.

INTRODUCTION

The extreme western area of southwestern Ontario has few remaining surface sources of naturally occurring granular aggregate. Consequently, to fulfill the demands of the local construction industry, gravel is imported into the region at considerable cost from as far away as Michigan in the United States. Attempts at surficial geological mapping for aggregate exploration, using conventional airphoto interpretation of black-and-white panchromatic photographs, is difficult. This is due to a general lack of geomorphic expression in the region which is characterized mainly by fine-textured lacustrine and deltaic deposits. Furthermore, these superficial lacustrine deposits tend to mask the presence of potentially mineable subsurface gravel deposits (Sado 1980, 1981). The basic object of the research is to evaluate the use of remotely sensed data as an exploration tool for buried near-surface aggregates in an area near Chatham, southwestern Ontario (Figure 254.1). The remote sensing data that have already been acquired and are being evaluated, include two types of daytime digital multispectral imagery (MEIS-II and MSS; Till *et al.* 1983; Zwick *et al.* 1980), predawn thermal infrared imagery (TIR), and colour infrared photography (CIR) (Table 254.1). Research activities during the first year of funding were concentrated on the analysis of CIR and MEIS-II data. Selected preliminary results from these analyses only are presented in this report.

WORKING HYPOTHESIS

The working hypothesis assumed in this study is that it is possible, through comparative analysis of the tonal characteristics of different types of imagery, to distinguish anomalous tones attributable to subsurface drainage effects, possibly associated with buried gravel, from those tones due to geological variations at ground surface. Anomalous tones on imagery indicative of shallowly buried gravel can be caused by differences in the rate of downward percolation of surface water as it moves through the unsaturated zone towards the water table (Singhroy and Barnett 1984). In a region of high groundwater table, as at the study site, similar anomalous tones can arise only if the buried body of gravel can act as a drainage conduit, in a manner analogous to an agricultural drain, causing hydraulic drawdown and differential drying out of overlying material in areas immediately above the gravel zone (Figure 254.2; Goettelman *et al.* 1983). For anomalous tones to develop, a means of hydraulic exit (e.g. connection of the buried gravel zone with a free-drainage surface along a valley wall) must exist before a lateral hydraulic flux causing drawdown can be created. Preliminary numerical modeling indicates that the appearance of anomalous tones at the ground surface is strongly influenced by the hydraulic conductivity and thickness of the material which overlies the gravel zone (Skelly 1986). Generally, anomalous tonal patterns form more quickly when the hydraulic conductivity of the overlying soil is high and when its thickness is small.

Tonal patterns are often associated with differences in *surficial* materials and geomorphology (Way 1978; Mollard and Janes 1984). Thus, in order to distinguish patterns which are due to surficial geological differences from those anomalous ones attributable to subsurface drainage effects, it was necessary to prepare first a detailed photomorphic map (Townshend 1981) using the CIR transparencies for conventional stereo airphoto interpretation, followed by field checking. This map effectively delineates regions which display significant differences in surficial soil texture and associated moisture-retention characteristics. Colour infrared transparencies were selected for airphoto interpretation of the surficial materials owing to the haze-penetrating capability of CIR film leading to darker shadows and accentuation of minor relief features (Swain and Davis 1978), and the increased separability of reflectance among different bare-soil materials over the near infrared range (Sabins 1978). Analysis of *digital* imagery covering the visible to near-infrared range was useful during this mapping phase in order to enhance delineation of tonal boundaries, some of which were only partly discernible on the CIR transparencies.

Analysis of TIR imagery represents an essential stage of the current research. The imagery reflects

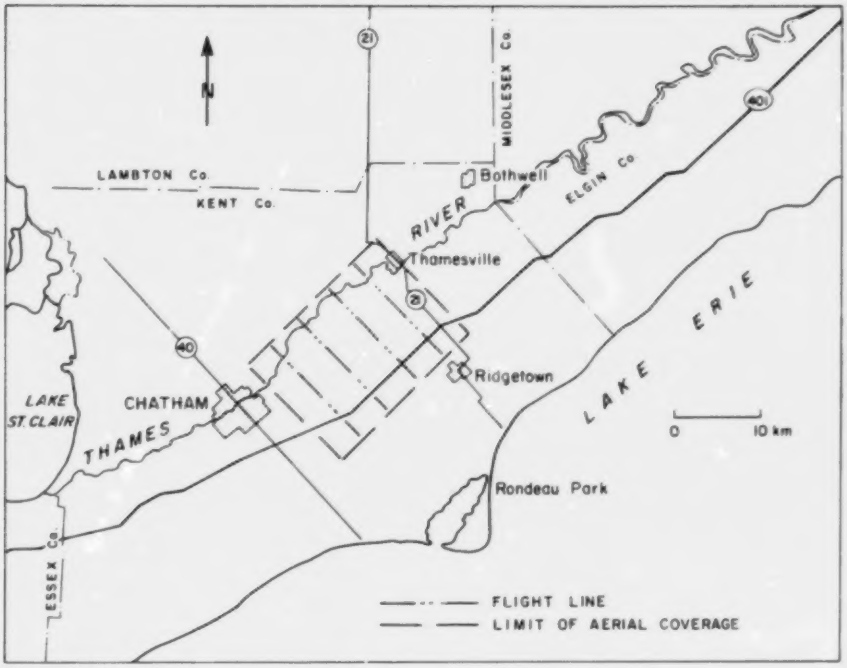

Figure 254.1. *Location map of study area near Chatham, southwestern Ontario.*

TABLE 254.1. IMAGERY SPECIFICATIONS

Photographic Data	Colour infrared transparencies; 1:26 000		
Digital Multispectral Data	**MEIS-II**		**MSS**
- spectral range, nm	CH00:522-735 CH01:793-898 CH02:626-703 CH03:508-601 CH04:542-605	CH05:456-518 CH06:751-787 CH07:613-687	CH07:625-695 CH08:680-780 CH09:765-895 CH10:865-1035 CH11:8500-14000
- ground resolution, m		2.8	8.8
Date and Time of Imagery Acquisition	May 22, 1985; 10:43-11:20 a.m. predawn on May 23.		CH11 data only acquired

variations in surface temperature (Colwell 1983) which correlate well with *both near-surface* water content (Vleck and King 1983) and *subsurface* drainage patterns (Myers and Moore 1972). Hence, by comparing tonal patterns on both CIR and TIR imagery, it is feasible to separate anomalous tonal areas which are due mainly to lower moisture levels in relatively coarse-textured soils *at surface* (readily mapped using CIR) from those attributable to lower moisture levels in soils of varied texture, caused by hydraulic drawdown in the vicinity of a buried gravel zone.

SELECTED PRELIMINARY RESULTS

The preliminary photomorphic map (Figure 254.3) shows several regions, each characterized by differing tonal uniformity and variation, and each of which appears fairly homogeneous internally (Kesik *et al.*, in press). Except for localized variations primarily associated with micromorphological features, surface-material textures within any given photomorphic region tend to be similar. This photomorphic map is providing a rational basis for an ongoing field checking program, the final objective of which is the identification of all pertinent surface-material and geomorphical characteristics at a regional level. A generalized geological map of the study site, compiled from published sources, is shown in Figure

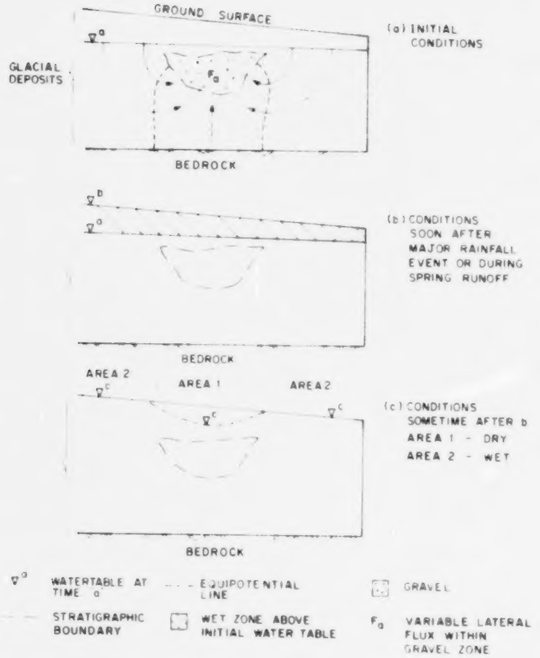

Figure 254.2. *Illustration showing how a dry area can develop above a zone of gravel in a region of high groundwater table.*

254.4 for comparison with the photomorphic map (Figure 254.3).

Digital analysis of MEIS-II imagery of a small part of the study site, known from previous studies (E.V. Sado, Geologist, Ontario Geological Survey, Toronto, personal communication, 1985; Z.L. Katona, Ministry of Transportation and Communications, Toronto, personal communication, 1986) to be underlain by gravel, indicates that only three of the eight available MEIS-II bands are needed for excellent discrimination of surficial materials using colour composites. These bands are CH05 (456-518 nm), CH00 (522-735 nm), and CH01 (793-893 nm). They carry maximum information content while simultaneously exhibiting minimum interband correlations (George *et al.* 1986). The spectral responses of these three "optimal" bands to varying surface cover within a selected photomorphic region is illustrated in Figure 254.5. Generally, the responses for all three bands are similar. For bare surfaces, the response in band CH00 tends to be higher than that of either band CH01 or CH05. As well, it shows the largest fluctuation in digital number (DN) values.

Visual analysis using band-ratio rather than individual-band images for photomorphic regionalization and subsequent geologic mapping benefits from the minimal effects that varying slope and aspect have on spectral response and from the accentuation of differences in reflectance characteristics of surface materials (Sabins 1978; Schowengerdt 1983; Siegal and Gillespie 1980). The band-ratio colour composite formed using the following ratio bands provided the best discrimination of surficial materials: CH00/CH01 (blue), CH00/CH06 (red), CH05/CH06 (green) (George and Dusseault, in press).

Detailed mapping of surficial materials in the subarea discussed above is being followed by analysis of TIR imagery of the same subarea (now in progress) in order to identify any anomalous tonal patterns which may be related to the known buried gravel deposit. Similar analyses for other subareas are planned.

OUTLINE OF FUTURE WORK

The following activities are planned for the next ten months:

1. Completion of field checking and compilation of an updated geological and geomorphological map using all available data (e.g. pedological reports, published geological maps and field notes, borehole data, bedrock structure-contour maps).
2. Continued analysis of pre-dawn TIR, MEIS-II, and MSS imagery to locate anomalous tonal zones.
3. Analysis and evaluation of C-band radar data for integration into the current investigation.

PRELIMINARY CONCLUSIONS

Colour infrared photography taken during the Spring is an excellent tool for detailed mapping of surficial materials and geomorphic features in the study area which has proved difficult to map using conventional black-and-white panchromatic airphotos. Delineation of tonal boundaries is aided considerably by selected enhancements of the digital multispectral data. Photomorphic regions, each displaying characteristic tonal texture, variation, uniformity, and soil-textural properties have been mapped. Boundaries shown on the photomorphic map are not all consistent with those of units depicted on published geological maps. The photomorphic map will be used for distinguishing anomalous tonal areas, on TIR imagery, which are attributable to subsurface drainage effects possibly related to the occurrence of buried gravel.

ACKNOWLEDGMENTS

The authors wish to express their appreciation to E.V. Sado (Ontario Geological Survey, Toronto), B. Feenstra (Ontario Ministry of Natural Resources, London), and Z.L. Katona (Ontario Ministry of Transportation and Communications, Toronto), for pertinent and useful discussion related to this study. W. Fitzgerald (Ontario Ministry of Natural Resources, Minden) kindly provided additional background detail from his Ontario Geological Survey mapping in 1979 of a part of the study area.

REFERENCES

Colwell, R.N. (Editor-in-Chief)
1983: Manual of Remote Sensing. Volume I—Theory, Instruments and Techniques. Volume II—Interpretation and Applications; American Society of Photogrammetry, Falls Church, Virgina, 2440p.

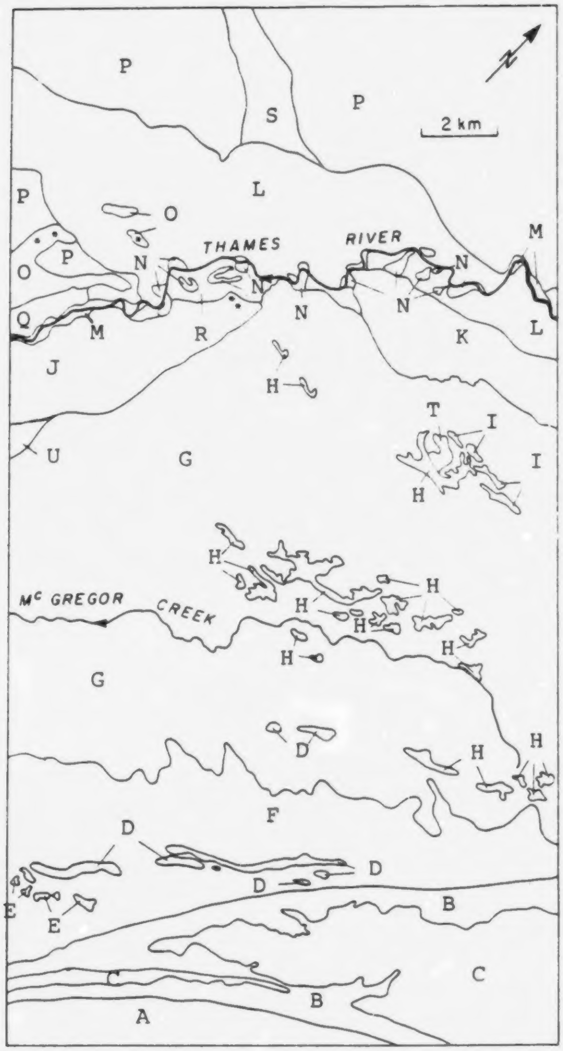
P
S
P
N
2 km
L
P
O
O
P
THAMES
RIVER
M
N
N
N
N
Q
M
R
K
L
J
H
T
I
U
G
I
H
H
H
H
Mc GREGOR
CREEK
H
H
H
G
D
H
H
F
D
D
D
E
E
B
C
C
B
A

Figure 254.3. *Photomorphic map of the study area. Each separately lettered region is characterized by a fairly homogeneous tonal texture. Boundaries may or may not coincide with those of geological units previously mapped (see Figure 254.4).*

Cooper, A.J., and Baker, C.
1978: Quaternary Geology of the Bothwell-Ridgetown Area, Southern Ontario; Ontario Geological Survey, Preliminary Map P.1973, scale 1:50 000.

Fitzgerald, W.D., and Hradsky, M.
1980: Quaternary Geology of the Wallaceburg-St. Clair Flats Area, Lambton and Kent Counties, Southern Ontario; Ontario Geological Survey, Preliminary Map P.2368, 1:50 000.

George, H., and Dusseault, M.B.
In Press: Selection of Optimum Band-Ratio Triplets Using Statistical Data of Original Single-Band Imagery; Canadian Journal of Remote Sensing.

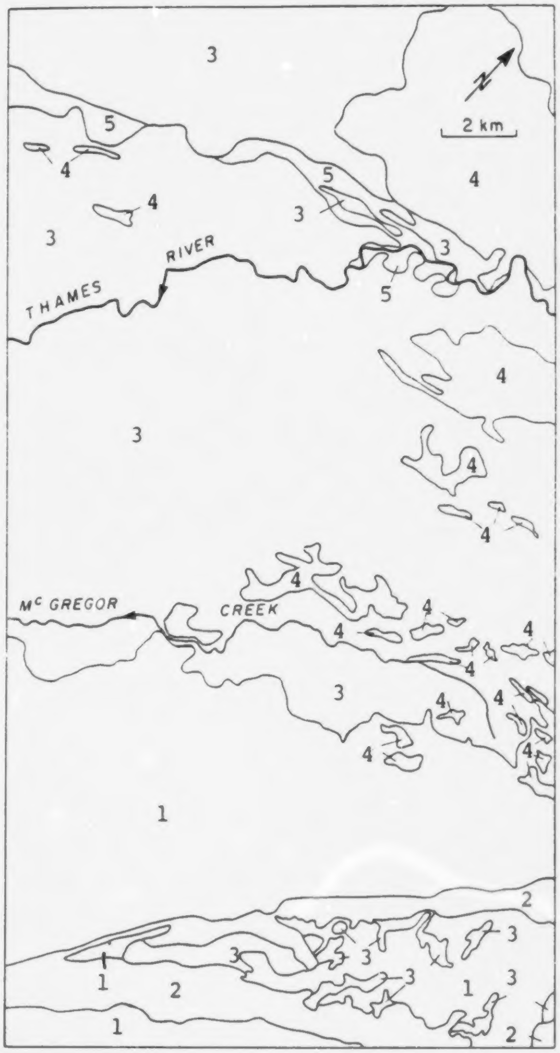
3
N
2 km
5
4
4
5
4
3
3
3
THAMES
RIVER
3
5
4
3
4
4
Mc GREGOR
CREEK
4
4
4
4
4
3
4
4
4
4
1
2
3
3
3
1
3
1
2
3
1
2

Figure 254.4. *Simplified surficial geological map of the study area compiled from Sado (in preparation); Fitzgerald and Hradsky (1980); and Cooper and Baker (1978).*

NOTE: *1 - Ground moraine: silty clay to clayey sand till; 2 - Beach deposits: sand, silt, gravel; 3 - Glaciolacustrine, lacustrine, and deltaic: silt, clay, sand; 4 - Eolian deposits: sand, silt; 5 - Alluvial deposits: sand, silt, clay.*

George, H., Dusseault, M.B., Kesik, A.B., and Sado, E.V.
1986: Evaluation of MEIS-II Multispectral Scanner Data for Quaternary Geological Mapping in the Chatham Area, Southwestern Ontario; Tenth Canadian Symposium on Remote Sensing, May 5-8, 1986, Edmonton, Alberta.

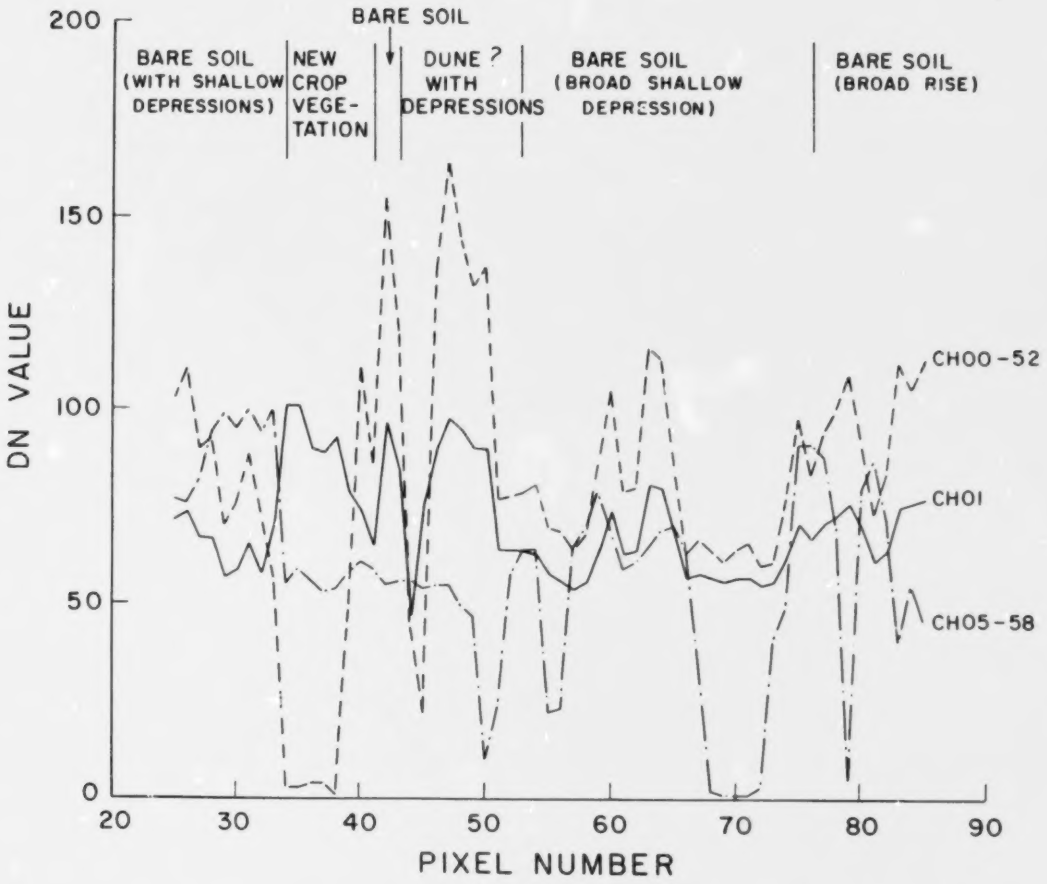

Figure 254.5. *Spectral response of bands CH00, CH01, and CH05 (adjusted for atmospheric scattering) to varying surface cover. Note: Plot is of every fifth pixel along the traverse shown as A-B in Photo 254.1.*

Goettelman, R.C., Grass, L.B., Millard, J.P., and Nixon, P.R.
1983: Comparison of Multispectral Remote-Sensing Techniques for Monitoring Subsurface Drain Conditions; NASA Technical Memorandum 84317, 16p.

Kesik, A.B., George, H., and Dusseault, M.B.
In Press: Application of Colour Infrared Photography and Multispectral Scanner Data in the Exploration for Aggregates; International Geoscience and Remote Sensing Symposium (IGARSS'86) September 8-11, 1986, Zurich, Switzerland.

Mollard, J.D., and Janes, J.R.
1984: Airphoto Interpretation and the Canadian Landscape; Canadian Government Publishing Centre, Supply and Services Canada, Hull, Quebec, 415p.

Myers, V.I., and Moore, D.G.
1972: Remote Sensing for Defining Aquifers in Glacial Drift; p.715-728 *in* Proceedings of the Eighth International Symposium on Remote Sensing in Environment, Ann Arbor, Michigan, Volume 1.

Sabins, F.
1978: Remote Sensing, Principles and Interpretation; W.H. Freeman and Company, 426p.

Sado, E.V.
1980: Glacial Stratigraphy and Sand and Gravel Prospecting (Abstract); p.17 *in* Geoscience Research Seminar, December 10-11, 1980, Abstracts, Ontario Geological Survey, 21p.
1981: Borehole and Geophysical Resistivity Methods in Unravelling the Quaternary Geology of the Chatham-Wheatley Area of Southwestern Ontario (Abstract); p.12 *in* Geoscience Research Seminar December 9-10, 1981, Abstracts, Ontario Geological Survey, 15p.
In Preparation: Quaternary Geology of the Chatham Area, Southern Ontario; Ontario Geological Survey, Preliminary Map, scale 1:50 000.

Schowengerdt, R.A.
1983: Techniques for Image Processing and Classification in Remote Sensing; Academic Press, Incorporated, 249p.

Siegal, B.S., and Gillespie, A.R.
1980: Remote Sensing in Geology; John Wiley and Sons, 702p.

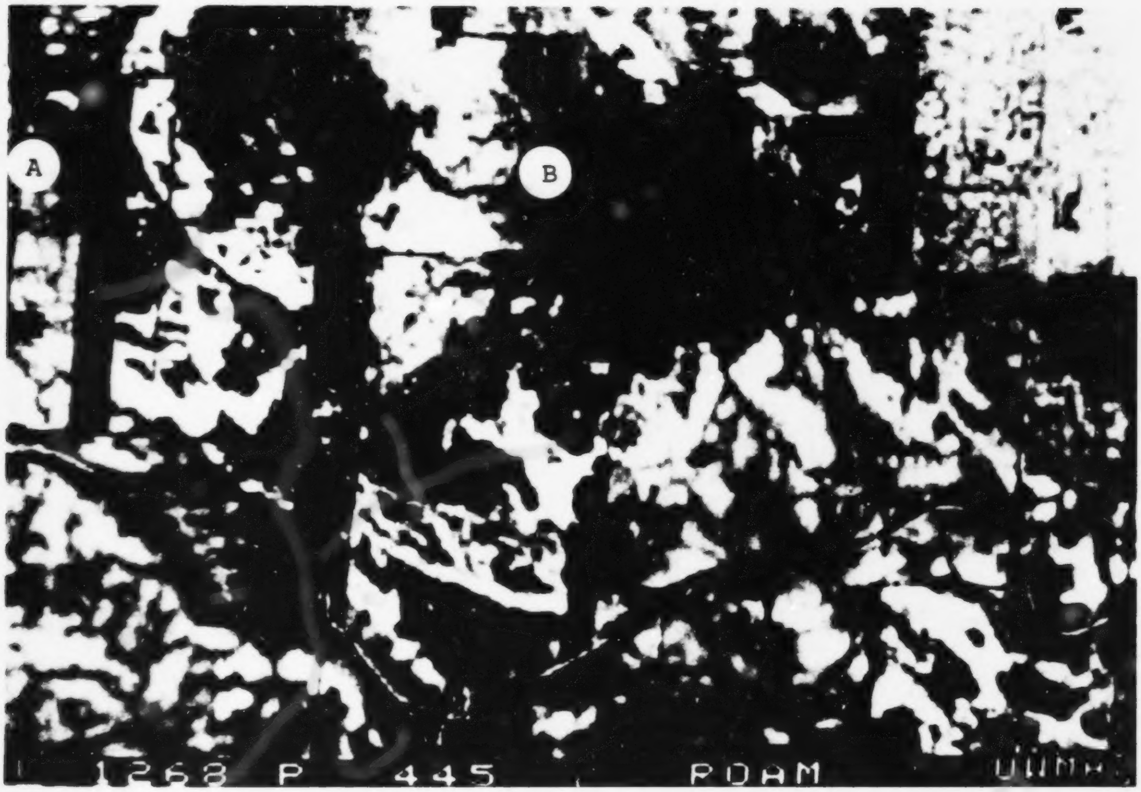

Photo 254.1. *Black and white reproduction of the colour composite formed using the three histogram-equalized contrast-stretched optimum MEIS-II bands. Filter assignments in the original colour composite were CH00-red, CH05-green, and CH01-blue.*

NOTE: *Area of photograph is outlined as box in Figure 254.3.*

Singhroy, V., and Barnett, P.J.
1984: Locating Subsurface Mineral Aggregate Deposits from Airborne Infrared Imagery (reflected and thermal): A Case Study in Southern Ontario; Paper presented at the International Symposium on Remote Sensing of Environment, Third Thematic Conference, Remote Sensing for Exploration Geology, Colorado Springs, Colorado, 19p.

Skelly, J.D.
1986: An Evaluation of Subsurface Drainage Tile Efficiency by Finite Element Analysis; Unpublished B.Sc. Thesis, Department of Earth Sciences, University of Waterloo, Waterloo, Ontario.

Swain, P.H., and Davis, S.M.
1978: Remote Sensing: The Quantitative Approach: McGraw-Hill, New York, 396p.

Till, S.M., McColl, W.D., and Nevill, R.A.
1983: Development, Field Performance and Evaluation of the MEIS-II Multi-Detector Electro-Optical Imaging Scanner. Proceedings, Seventh International Symposium on Remote Sensing of the Environment, Ann Arbor, Michigan, preprint.

Townshend, J.R.G. (Editor)
1981: Terrain Analysis and Remote Sensing; George Allan & Unwin Limited, London, 232p.

Vleck, J., and King, D.
1983: Detection of Subsurface Soil Moisture by Thermal Sensing; Results of Laboratory, Close-range and Aerial Studies; Photogrammetric Engineering and Remote Sensing, Volume 49, p.1593-1597.

Way, D.S.
1978: Terrain Analysis; McGraw-Hill Company, New York, 438p.

Zwick, H.H., McColl, W.D., and Edel, H.R.
1980: The CCRS DS1260 Airborne Multispectral Scanner (MSS); p.643-648 *in* Sixth Canadian Symposium on Remote Sensing, Halifax, Nova Scotia.

Grant 256 Cyanide in Gold Deposits

H.P. Schwarcz

Department of Geology, McMaster University, Hamilton

ABSTRACT

Fluid-inclusion-rich samples of quartz from various vein occurrences, including gold ore deposits, contain a chemical species which reacts colorimetrically like either thiocyanate or cyanide, and is present at concentrations of hundreds of ppb. It is liberated from the quartz by grinding in NaOH, and presumably occurs trapped in the fluid phase of the inclusions. This raises the possibility that the $Au(CN)_2^-$ complex may have been partly responsible for transport of gold in hydrothermal ore deposits.

INTRODUCTION

The purpose of this study was to investigate the possibility that cyanide ions (CN^-) might occur in fluid inclusions trapped in the quartz of gold ore deposits. Cyanide is known to form a very stable complex with gold, $Au(CN)_2^-$, which has a higher stability constant than that of $Au(HS)_2^-$, widely believed to be the principal ligand of gold in vein ore deposits (Seward 1983; Table 256.1). If we could demonstrate the presence of CN^- in the hydrothermal fluid, then we would consider this ion to be a likely ligand for gold.

The free CN^- ion is unstable over long time periods in the presence of water, as it hydrolyzes to ammonia and formic acid (Sanchez *et al.* 1967). If, however, cyanide ions had coexisted with sulphide or bisulphide ions in solution, then thiocyanate (SCN^-) ions would have formed, which are believed to be stable in aqueous solutions. SCN^- also complexes with gold, but with a much lower stability constant than CN^-.

Both CN^- and SCN^- have ionic radii too large to fit in lattices of any rock-forming minerals. Therefore, if they had been present in solution, we expect the only remaining traces of them would be found in the fluid inclusions, dissolved in the aqueous phase. We set about to test for the presence of these species.

TABLE 256.1. POSSIBLE COMPLEXES OF GOLD IN HYDROTHERMAL SOLUTIONS

Complex	Equilibrium Constant at 25°C (β_2)	Reference
$Au(CN)_2^-$	41.6	Seward 1983
AuS^-	39.9	Seward 1983
$Au(HS)_2^-$	37.2	Seward 1983
$Au(SO_3)_2^{3-}$	30.1	Seward 1983
$Au(S_2O_3)_2^{3-}$	29.4	Seward 1983
$Au(SO_4)_2^-$	-	Seward 1983
$Au(NH_3)_2^+$	26.5	Seward 1983
AuI_2^-	22.1	
$Au(OH)Cl^-$	19.0	Seward 1983
$AuBr_2^-$	15.6	Seward 1983
$Au(HCO_3)^-$	-	Seward 1983
$Au(SCN)_2^-$	17.0	Gamsjäger 1966

ANALYTICAL PROCEDURE

Samples were collected from several ore deposits and prospects in the Timmins gold camp (Table 256.2). Bulk vein-quartz was lightly crushed to free relatively pure lumps of quartz, which were then further crushed to millimetre-sized pieces. These were sorted to eliminate any other minerals, and then washed in hot HNO_3 and distilled water. Ten grams of pure quartz were then ground in a ceramic mortar while immersed in 10 cc NaOH, until a milky suspension was obtained. The suspension was then centrifuged and the supernatant was decanted, neutralized with acid, and tested colorimetrically for the presence of SCN/CN. The colorimetric method used was reaction of cyanogen chloride (produced by treatment of the solution with chloramine-T) with a mixture of barbituric and isonicotinic acids (Nagashima and Ozawa 1981). A blue dyestuff is produced, with an absorption peak at 600 nm. The detection limit is about 50 ppb CN or 125 ppb SCN (in quartz). There do not appear to be any naturally occurring interfering species capable of giving a false positive signal. Reagent blanks are essentially zero, and no absorption is observed in some quartz samples, showing that the sample preparation procedure does not introduce a signal.

Gold concentrations were determined on some samples by instrumental neutron activation analysis (INAA). These analyses were used to test for a relation between cyanide and gold content.

Note that the method which we are using is equally sensitive to cyanide and thiocyanate, since chloramine-T liberates CNCl from both of these species. Therefore, it is impossible to tell, on the basis of the colorimetric reaction alone, which species was present. We have shown, however, that the species which is responsible for the reaction is not oxidized by a mixture of MnO_2 and H_2O_2, which is capable of oxidizing CN^- completely. We conclude, therefore, that the main species responsible for the colorimetric signal is SCN^- ions.

ANALYTICAL RESULTS

A summary of the analytical data obtained is given in Table 256.2, for samples from Timmins, and for some "background" samples from areas where gold has not been reported. We have observed detectible amounts of SCN in extracts from almost all the quartz samples which we have analyzed, including those from presumably gold-free environments. A histogram of the SCN concentrations observed shows (Figure 256.1) that there is a large overlap in the range of SCN concentrations of gold-bearing and gold-free deposits, although the highest values are observed in gold ore deposits.

We have attempted to test, at two sites, whether there is a correlation between SCN^- and gold concentrations. At the Pamour No. 1 Mine, samples were collected from the 51 vein on the 1400-foot level. These samples show, for intermediate gold values, a positive correlation between SCN^- and Au, although

TABLE 256.2. THIOCYANATE AND GOLD CONCENTRATIONS IN ORE SAMPLES

Sample No.	SCN (ppb)	Au (ppb)
Pamour Mine No. 1		
P 16	450	55
P 17	130	17
P 18	120	620
P 20	180	20
P 21	220; 500	19
P 21, 2nd grinding	195; 304	
P 24	310	35
P 26	1460	240
P 27	890; 400	5
P 27, 2nd grinding	396; 349	
P 28	450	49
P 29	530	47
Dome Mine		
17003A	1300; 1210	35
1006C	510	-
17002	430	-
17002A	630	5.1
13008A	1140; 1220	10
13009B	1730	6.3
10007 B	1980	10
10007 C	2450	36
10007 D	1520	7400
10001 K	870	8.8
1301 B	2300	>160 000
160021 B	740	16
8010 E	360	1 400
15002 A	1160	-
8004	980	-
15003	1160	-
13010	2080	-
12008	600	-
Hollinger Mine		
H 30	360; 495	-
H 42	480; 540	-
H 46	690	-
H 50	840; 800	-
Faymar Mine		
Fa-O	710; 770	-
Fa 1	860; 510	-
Fa 3	330; 260	-
Fa-5	550; 500	-
Fa 13	250; 220	-
Fa 14	1090; 1030	-
Quartz vein, Huntsville, Ontario		
GQTZ 1	n.d.	-
GQTZ 2	380	-
GQTZ 3 (whole rock)	330	-
GQTZ 4	n.d.	-

TABLE 256.2. cont'd

Reference samples, Royal Ontario Museum

M 1891: Massey, Ont. (with chalcopyrite)	420	-
M 4298: New Rockland, P.Q.	710: 870	
M 41568: Davreuxite, Belgium	730	-
M 11117: Pylesville, Maryland	490: 840	-
E 2243: Hudson Bay, Ont. (with axinite)	340	-
unregistered: Sudbury, Ont. (with chalcopyrite)	740: 880	-

n.d. = not detected

- = not analyzed

there are two outliers at the high and low ends of the concentration range respectively (Figure 256.2). Data from the Dome Mine show a less clear correlation between these two parameters. At Pamour, the average molar ratio of SCN to Au is 32±5 (excluding the outliers), greatly in excess of the stoichiometry of the $Au(CNS)_2^-$ complex (or the corresponding CN^- complex). That is, there is a large excess of SCN^- over the amount needed to complex the Au which is present.

We have attempted to test the homogeneity of SCN distribution in a single large sample of quartz from the Dome Mine, with dimensions of about 26 by 18 by 6 cm (Table 256.3). Adjacent portions of the slab differed in SCN^- concentration by more than a factor of two (400±17 ppb versus 1050±90 ppb). These data suggest marked inhomogeneity in the thiocyanate concentration.

CONCENTRATION IN FLUID INCLUSIONS

The data given in Table 256.2 are for the bulk quartz, treated as described above. If we assume that SCN^- is entirely contained in the fluid inclusions, then the concentration in the fluid must be much higher yet. We attempted to determine the amount of trapped fluid by decrepitating the samples at 950°C for 1 hour, and then determining the weight loss. The average loss was 0.4±0.4 weight percent, implying that the average concentration in the fluid was approximately 250 times that of the bulk rock, that is, on the order of tens to hundreds of ppm. This method of determining fluid content is very crude, however, and may underestimate the total; also the SCN^- is probably concentrated in the aqueous phase of the inclusions and depleted in the CO_2-rich gas phase.

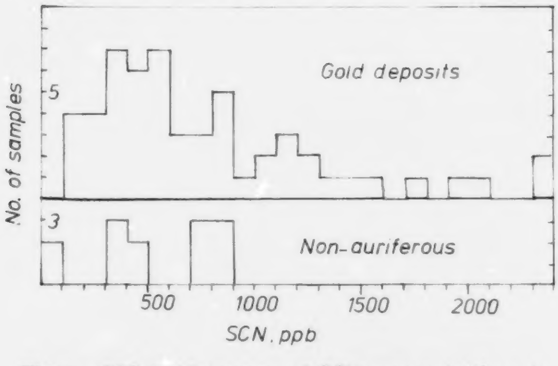

Figure 256.1. Histogram of SCN concentrations in samples from gold-bearing and non-auriferous veins.

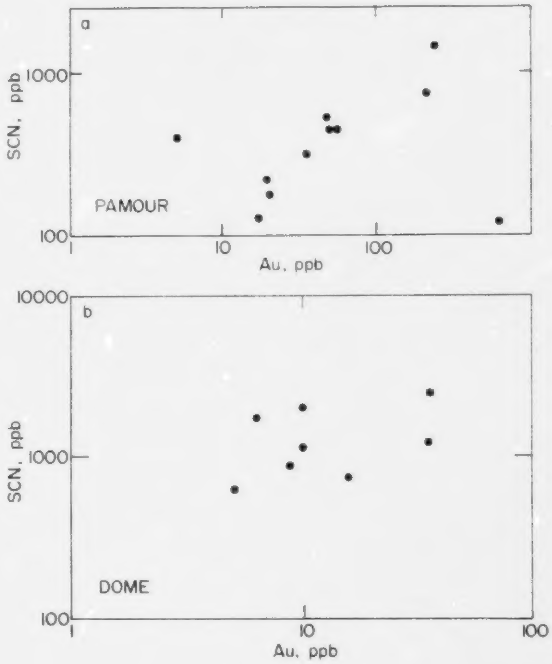

Figure 256.2. Relation between gold and thiocyanate concentrations for ore samples: a) Pamour No. 1 Mine; b) Dome Mine.

TABLE 256.3. TEST OF UNIFORMITY OF SCN CONCENTRATION SAMPLE 13001, DOME MINE.*

Section	SCN (ppb)
A	400, 370, 412; $\bar{X}$ = 397±17
B	1136, 964; $\bar{X}$ = 1050±86
A + B (1:1 mixture) (expected value: 722)	820, 739; $\bar{X}$ = 780±40
D	352

* A slab of vein quartz 26 x 18 x 6 cm was divided into 4 equal sections, each of which was homogenized and analyzed in replicate. Visible gold is present in a chlorite-rich vein cutting this sample (not included in the analyzed material).

OTHER ANALYTICAL METHODS

We attempted to confirm these results by means of a variety of other analytical methods. The most successful appeared to be gas chromatographic analysis of the CNCl formed by chloramine-T, in a hexane solution (Valentour *et al.* 1974). This method has, however, not resulted in quantitative estimates of CN (or SCN) concentration, because of its high detection limit, low sensitivity, and noisiness of the signals. It was possible, however, in some runs, to see a distinct signal corresponding to the presence of CNCl in extracts from quartz samples. Other possible methods which showed promise, but which would require further experimental development, are high-pressure liquid chromatography (HPLC) and ion chromatography, both of which are potentially sensitive enough to detect SCN at the levels reported here. Colorimetry remains, however, the most sensitive method.

REGROUND SAMPLES

The method of liberating SCN^- by wet grinding is not perfectly reproducible and we suspected that there might be some samples from which liberation of the ion was incomplete. In fact, it was found that for some samples, if we washed and dried the residue of the first grinding and then subjected this material to the same procedure, the amount of SCN^- liberated in the second grinding was almost equal to that of the first extraction. Other samples, however, give little or no yield of SCN^- on this second grinding, suggesting that this species was entirely contained in inclusions which were easily ruptured. This phenomenon was observed near the end of the work on this project, and we have not yet had the opportunity to pursue it adequately. It seems possible, at least, that some of the SCN^- is actually bound in the crystal lattice of the quartz, or in some solid inclusions in it which are only weakly soluble in NaOH.

CONCLUSIONS

Leachates of quartz ground in NaOH contain a species which behaves colorimetrically like either CN^- or SCN^-. These species, if present in the hydrothermal solution, would have acted as ligands for Au and other metals. Even if they are convincingly shown to have been present, it is not clear that these species were of deep-seated origin. Traces of graphite are found disseminated in interflow sediments in many Archean greenstone belts (Smith *et al.* 1984), and it is possible that cyanide could have formed by reaction between graphite and some nitrogen-bearing species (including N_2 gas) in the volcanic pile. Nonetheless, it is interesting to consider the possible role that cyanide complexes may have had in metal transport, and also the possible significance of the emission of CN^- or HCN vapor in emergent hydrothermal springs as possible precursors for the abiotic generation of life (Schwartz *et al.* 1984).

ACKNOWLEDGMENTS

Analytical work on this project was carried out by D. Ivanauskas. Y.K. Chau (Canada Centre for Inland Waters, Burlington) kindly assisted in the gas chromatographic analyses. A.J. Fyon (Geologist, Ontario Geological Survey, Toronto) provided most of the samples for analysis and much useful discussion. We wish to express our appreciation to the staffs at the following mines for their assistance in the collection of the samples: Pamour No. 1; Dome; Hollinger; and Faymar. We thank R.I. Gait (Royal Ontario Museum, Toronto) for providing some samples for analysis.

REFERENCES

Gamsjäger, H., Kraft, W., and Rainer, W.
1966: Löslichkeitskonstanten und Freiebildungsenthalpien von Metallsulfiden. 2. Mitteilung: Die Bestimmung von G aus Potential- und Löslichkeitsmessungen; Monatshefte für Chemie, Volume 97, p.833-845.

Nagashima, S., and Ozawa, T.
1981: Spectrophotometric Determination of Cyanide with Isonicotinic and Barbituric Acid; International Journal of Environmental Analytical Chemistry, Volume 10, p.99-106.

Sanchez, R.A., Ferris, J.P., and Orgel, L.E.
1967: Studies in Prebiotic Synthesis. II. Synthesis of Purine Precursors and Amino Acids from Aqueous Hydrogen Cyanide; Journal of Molecular Biology, Volume 30, p.223-235.

Schwartz, A.W., Voet, A.B., and Van Der Veen, M.
1984: Recent Progress in the Prebiotic Chemistry of HCN; Origins of Life, Volume 14, p.91-98.

Seward, T.M.
1983: The Transport and Deposition of Gold in Hydrothermal Systems; p.165-181 *in* Gold '82, edited by R.P. Foster, Rotterdam, Balkema.

Smith, T.J., Cloke, P.L., and Kesler, S.E.
1984: Geochemistry of Fluid Inclusions from the McIntyre-Hollinger Gold Deposit, Timmins, Ontario, Canada; Economic Geology, Volume 79, p.1265-1285.

Valentour, J.C., Aggarwal, V., and Sunshine, I.
1974: Sensitive Gas Chromatographic Determination of Cyanide; Analytical Chemistry, Volume 46, p.924-925.

Grant 259 Development of Analytical Methods for Trace Lanthanides

A.D. Westland and C. Kantipuly

Department of Chemistry, University of Ottawa, Ottawa

ABSTRACT

Novel methods for the attack and analysis of rocks and rock-forming minerals have been developed with a view to the determination of rare earths at trace levels. Two potassium-containing fluxes have been used to facilitate sample fusion and subsequent preparation. Mixed potassium superoxide-potassium hydroxide mixture is useful for weakly acidic and refractory samples such as zircon and cassiterite. Potassium orthoborate is effective for basic minerals, most notably those rich in alumina.

A phosphonic acid half-ester has been used to extract lanthanides and to separate those elements by reverse-phase chromatography. A chromatographic column was developed in which 2-ethylhexylphenylphosphonic acid was supported on phenylated Kel-F powder. The column, operated at low excess pressures, was capable of partial separation of the lanthanide group. The whole lanthanide series may be separated into two or more of the "tetrad" groups.

INTRODUCTION

The determination of relative rare earth element (REE) concentrations in rocks is of interest as an aid to the understanding of geochemical processes. This may lead to a forecast of the chemical and mineralogical nature of potential deposits. Nesbitt (1979) has discussed the matter as applied to weathering of a granodiorite.

Mapping of a geological formation in terms of lanthanide values would normally entail the determination of some half dozen of the elements in many samples. The concentrations are generally low, of the order of parts per million (ppm) or less. Consequently, the analytical challenge is great and the costs are high. Methods of determination should be element-specific and highly sensitive. Favoured methods are neutron activation analysis, mass spectrometry, and plasma-source atomic emission spectrometry. The γ-ray spectra obtained by neutron activation may be dominated by isotopes of Mn, Na, Sc, Fe, Co, etc. Moreover, the nuclide of interest may be formed by competing nuclear reactions such as (n,p), (n,α), and (n,f). Boynton (1979) and Bereznai (1971) have discussed other types of interferences. The purely instrumental use of neutron activation leaves much to be desired. Chemical isolation techniques are the most desirable.

There is a great interest in the use of inductively-coupled plasma mass spectrometry (ICP-MS). This instrument is very sensitive and offers great advantages over neutron activation. Our experience with this technique has revealed interferences due to barium oxide in the case of europium, and the interference of lighter lanthanide oxides on the heavier lanthanide signals. It may be desirable here again to isolate the lanthanides in two groups, a light and a heavy group.

Plasma source emission spectroscopy (ICP-AES or DCP-AES) is a less costly and highly specific method, but it is less sensitive than ICP-MS. Like the latter method, it relies on nebulization of a liquid sample that must not contain much dissolved salt. The salt can cause severe chemical and/or physical interferences. Our approach to sample preparation entails fusion with a flux that can be largely removed in a simple step. The fluxes used are potassium compounds, as potassium can be largely precipitated as the perchlorate without carrying down the rare earths (Westland and Kantipuly 1983).

Although ICP-AES are subject to relatively few inter-element interferences, isolation of the lanthanides as a group is mandatory. There continues to be a need for improved and rapid methods of sample treatment.

STUDY OF POTASSIUM–CONTAINING FLUXING AGENTS

The traditional strongly basic fluxes are sodium peroxide and, less effectively, sodium carbonate. The latter is ineffectual toward very weak acids like zirconium and tin oxides and corundum. The borates are effective toweard ultrabasic rock systems as well as toward acidic rock systems We have substituted potassium superoxide, KO_2, and potassium orthoborate for sodium peroxide and borax. The cooled melts dissolve readily in warm water or acid, and potassium may be separated as a crystalline precipitate by addition of perchloric acid. The $KClO_4$ is separated by filtration from an ice-cold solution.

PROCEDURE FOR FUSIONS

Mineral samples (0.5 g) were ground to -60 mesh and mixed in a crucible with 1.5 to 2.0 g of fluxing agent. The superoxide flux contained KO_2 (Alpha Ventron) and KOH in a 1:3 ratio by weight. The sample/flux mixture was heated to redness over a Meker burner in a zirconium crucible for 5 to 20 minutes. The melt was cooled and dissolved in dilute hydrochloric acid.

Potassium orthoborate fusions were carried out in a similar manner to the above, but in either a graphite or a platinum crucible.

RESULTS OF FUSION EXPERIMENTS

Unlike lithium borate melts, the potassium borate wetted the graphite crucibles which prevented the possibility of pouring out the melt. Graphite crucibles possessed no advantage therefore, and platinum crucibles were preferred. The rapidity of the lithium borate method is, therefore, not available with the potassium flux. Feldspar and quartz present no difficulties when using the familiar fluxes, such as alkali carbonate, and they responded readily to fusion with potassium superoxide or orthoborate. Difficulties are to be anticipated with some of the ferromagnesian minerals, however. A peridotite rich in olivine, pyrox-

TABLE 259.1. INTERFERENCE BY SiO_2 MATRIX

Element	λ (nm)	Concentration μg/mL	Si added μg/mL	% error
La	408.67	1.30	40	+22
			120	+22
			240	+22
		2.28	40	+23
			80	+19
Ce	418.66	0.56	83	+ 6
			166	+19
Dy	353.17	1.48	83	-47
			166	-32
Yb	328.94	0.96	83	+22
			166	+25

enes, and mica was also readily attacked by molten carbonate fusion. However, upon dissolving, a dark-coloured silica residue was obtained. The same rock, when fused with potassium borate, gave a melt that was largely soluble in water. Upon acidifying and heating, a pure white precipitate of silica was formed. The silica remains in solution as borosilicate if heat is not applied.

The above observations suggest that borate fusion is preferable whether silica is to be separated or not. Potassium may be separated as described previously (Westland and Kantipuly 1983) in order to prepare the solution for aspiration into an ICP source. We have discovered, however, that if silica is not separated, there is a serious matrix interference in lanthanide determinations by emission spectrometry (Table 259.1).

Experience has shown that certain non-acid silicates and oxides are particularly resistant to attack by hydrofluoric acid or carbonate fusion. Zircon, cassiterite, and minerals high in alumina are particularly to be mentioned. Corundum, sillimanite, mullite, and sapphirine $(Mg,Fe,Al)_8O_2[(Al,Si)_6O_{18}]$ resisted such attack almost completely. These four minerals commonly contain in excess of 60% Al_2O_3. Potassium orthoborate fusions of 20 minute duration gave complete decomposition, but decomposition with KO_2-KOH mixture or pure KO_2 was incomplete.

LANTHANIDE EXTRACTION AND GROUP SEPARATIONS

Procedures used for the isolation of the lanthanides as a group have, in most cases, been based on classical hydroxide-fluoride or hydroxide-oxalate precipitation cycles with added carrier. Several specific procedures had to be included as well as the extraction of iron and scandium with isopropyl ether in the presence of thiocyanate.

With an element-specific method of determination, it is often considered sufficient to carry out a group separation of lanthanides. A favoured scheme uses anion and cation exchange followed by ICP-AES determination (Crock and Lichte 1982). Bolton *et al.* (1982) proceeded similarly but did not include anion exchange. The latter workers opened up their samples by acid digestion rather than fusion. Our experience has been that even the Crock and Lichte method, which employs lithium metaborate fusion, seems to fail to recover quantitatively those REE with intermediate atomic numbers, when zircon, apatite, or chromite are present in the sample. We favour the vigorous fusion made possible by the use of a platinum crucible.

We have also explored the use of liquid ion exchange with 2-methylhexylphenylphosphonic acid (I), abbreviated HEHφP.

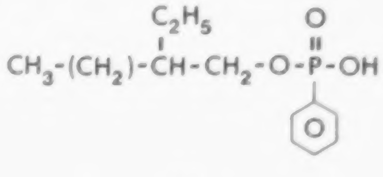

$$CH_3\text{-}(CH_2)\text{-}\overset{C_2H_5}{CH}\text{-}CH_2\text{-}O\text{-}\overset{O}{\underset{C_6H_5}{P}}\text{-}OH$$

(I)

This substance was used as an extractant in a reversed phase chromatographic mode. It is fairly specific for ions of large radius when used at moderate acidity. Preparation of I and the modified Kel-F columns upon which it was supported have been described (Kantipuly 1984).

The isolation of REE from all but the heaviest elements, i.e. the actinides and possibly barium, can be effected by collecting them on a chromatographic column of HEHφP. The experimental procedure which follows was designed to achieve either a total group separation or, if desired, a separation of the lanthanide group into its tetrads.

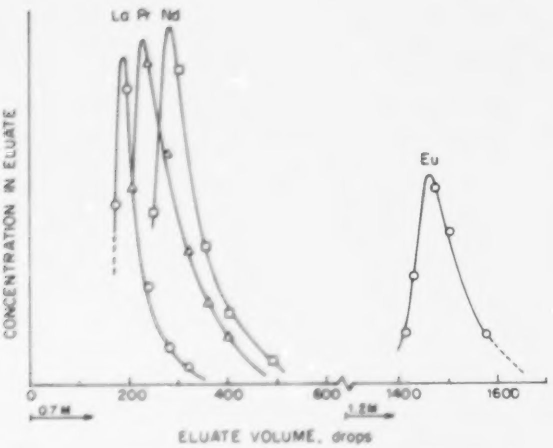

Figure 259.1. Chromatographic separation of lanthanides.

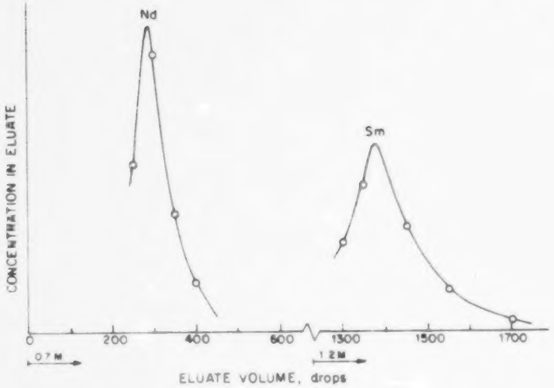

Figure 259.2. Chromatographic separation of Nd and Sm.

CHROMATOGRAPHIC SEPARATION OF THE LANTHANIDES

EXPERIMENTAL

A weighted quantity of phenylated Kel-F powder was stirred with a known amount of complexing agent (HEHφP) dissolved in o-xylene. The solvent was evaporated under a heat lamp while stirring with a glass rod. The coated polymer was acidified and hydrated by stirring in 0.1 M $HClO_4$ or 0.1 M HCl for one hour. The wet material was transferred in small portions to a glass column and pressed gently into place with a flat-ended stirring rod in order to remove voids. A plug of glass wool was placed at the bottom and on the top of the resin bed to prevent dislodging of the particles when solution was added. It also helped to prevent the top of the resin bed from drying out if the liquid on top of the column was depleted. The column was washed with several column volumes of an aqueous solution of the same type as that to be used to transfer the sample. The aqueous solutions were equilibrated in all cases with HEHφP in order to prevent depletion of the extractant phase when the column was in use.

The glass columns used were 0.6 cm I.D. by 11.5 cm long, with a reservoir 2 cm I.D. by 13 cm long at the top, and a drip tip plugged with glass wool at the bottom. The extractant percentage was 17.4 (W/W). The lanthanides were introduced on the column with the aid of an Eppendorf pipette, and they were eluted with specific volumes of acids of appropriate concentration and determined. The flow rate was about 3 drops per minute and was normally induced by gravity only. Forty drop portions of the eluate were collected in glass vials with the aid of a microfractionator. The samples were evaporated to dryness under a heat lamp and taken up in 5.0 mL of 0.1 M HNO_3. Each element was determined by DCP emission spectrometry. A blank was carried along with the samples.

Conditions for the separation of lighter lanthanides into two groups were established. Figures 259.1 and 259.2 show examples of such separations. Although separation between adjacent pairs is not quantitative, there is a remarkable gap between neodymium and samarium. Moreover, it was not possible to elute Sm and Eu with 0.7 M HCl. Therefore, we adopted a step-gradient elution technique. In the second step, we increased the acid concentration to 1.2 M.

The break in the elution curve between Nd and Sm is attributable to the "tetrad effect" described by Peppard (1969).

The heavier lanthanides are removed from the column by successively more concentrated solutions of nitric acid. Table 259.2 shows typical recoveries of REE, scandium, aluminium, and calcium.

The separation of the first and second tetrads between neodymium and samarium is quantitative. (Promethium, which does not occur naturally, was not examined, but it is expected to separate with the first tetrad. (For reasons that will not be given here, but as shown by Fidelis and Siekierski (1971), the first members of the second and fourth tetrads should separate with the members of the first and third tetrads, respectively.) Although it does not show from Table 259.2, we have established that gadolinium is separated quantitatively from the following element in the series, terbium. It is thus a simple matter to effect a sharp separation of the lighter lanthanides, including gadolinium, from the remaining heavier ones. This would enable one to avoid the interference by lighter REE oxides in the determination of the heavier REE by mass spectrometry.

We expect a separation of terbium and thulium, but the required conditions have not yet been established, as can be seen from Table 259.2. We believe that if eluate 3 were to be broken down into smaller volumes, the point at which the last tetrad would be isolated might be found.

TABLE 259.2. RECOVERY OF LANTHANIDES AND OTHER ELEMENTS
Column: 1 x 5 cm
35% w/w extractant

Element	wt. taken μg	Percents of elements recovered in portions of nitric acid				
		Effluent 100 mL 0.1M	Eluate 1 50 mL 0.7M	Eluate 2 50 mL 1.2 to 1.6M	Eluate 3 100 mL 2.5M	Eluate 4 100 mL 7.5M
Al	200.0	101.8				
Ca	540.6	104.1				
Sc	7.9	99.7				
La	20.2	-	100.0	-	-	-
Ce	30.0	-	99.6	-	-	-
Pr	26.2	-	98.5			
Sm	13.0	-	-	97.7	-	-
Eu	11.0	-	-	99.1	-	-
Gd	10.0	-	-	94.8	-	-
Dy	22.3	-	-	-	100.5	-
Er	11.5	-	-	-	102.0	-
Tm	23.2	-	-	-	93.1	4.0
Yb	36.2	-	-	-	55.5	43.9
Lu	24.8	-	-	-	-	99.6

Note: The sign (-) indicates none detected.

ANALYSIS OF STANDARD ROCK

After having established the conditions for quantitative recovery for all the lanthanides, we employed this method for the analysis of certified rock standard SY-2. One gram of sample was treated by fusion with KO_2-KOH flux. The melt was dissolved in 50 mL of 5 M HCl and the solution evaporated to dryness to dehydrate silica. The precipitate was taken up in a small volume of 5 M HCl and separated by filtering. The filtrate was again evaporated to dryness in order to render insoluble a further small amount of silicic acid. The precipitate was treated with acid as before and silica collected on a fresh filter. The two washed precipitates were combined and ignited at 850°C in a platinum crucible. The silica was volatilized by heating with a mixture of HF and $HClO_4$ in a platinum dish.

The residue was taken up in 4 molar hydrochloric acid, combined with the filtrates, and extracted twice with n-octylamine to remove elements which form anionic chlorocomplexes, including iron and uranium. The aqueous phase was evaporated to about 50 mL, and potassium from the flux was removed by precipitating as $KClO_4$. Finally, the sample was taken up in 25 mL of 0.1 M $HClO_4$. This solution was loaded on to a 5 by 1 cm column of HEHϕP. The sample was eluted with 100 mL of 0.1 M HCl and this eluate was discarded. The lanthanides were eluted with 250 mL of 7.5 M HNO_3. The solution was evaporated to near dryness, wet ashed, and taken up in 25 mL of 0.1 N HNO_3 for DCP emission spectroscopic determination. The lanthanide values obtained are shown in Table 259.3.

GENERAL DISCUSSION

New methods of determination of the rare earths in geological materials have been described above. These are designed to be applicable when either a spectrophotometric method or neutron activation analysis is to be employed at the finish. A potassium fluxing agent was developed in order to facilitate the removal of unwanted salt. The separation of the lanthanide group into subgroups is a means of reducing inter-element interferences. Crock and Lichte (1982) corrected for such interferences by a data processing procedure that they applied to atomic emission results. Data processing can be used to make corrections for oxide interferences in mass spectrometry also, but accurate raw data that does not need to be corrected is to be preferred.

Our analysis of the certified rock, employing fractionation of the lanthanides into sub-groups, gave very satisfactory agreement with the certified and literature values for that material. Although we did not fractionate the REE in carrying out those analyses, we expect that fractionation of the lanthanides will be found to be preferable when very low lanthanides values are encountered.

The separation scheme has been designed so that it can be used in NAA for the pre-irradiation separation of the lanthanides from a silicate matrix. This avoids the need for post-irradiation handling and this should make the procedure attractive to a wider number of geochemistry laboratories.

REFERENCES

Bereznai, T.
1971: Activation Analysis of Rare Earth Elements; Journal of Radioanalytical Chemistry, Volume 9, p.81-100.

TABLE 259.3. ANALYTICAL RESULTS OF CANADIAN Sy-2 (SYENITE)

Element	Literature ppm	Found, ppm Replicate 1	Found, ppm Replicate 2	Found, ppm Replicate 3
La	88	89.2	88.7	86.9
Ce	210?	205.2	203.1	206.2
Pr				
Nd	71?			
Sm	15?	13.3	14.7	13.9
Eu	2.4?	1.0	2.2	2.5
Gd				
Tb	2?			
Dy	20?	20.7	19.6	18.9
Ho				
Er	12?	10.2	11.1	10.5
Tm	2?	2.7	1.5	1.8
Yb	17	18.1	17.7	17.2
Lu	3?	2.6	2.2	2.7

Bolton, A., Hwang, J., and Vander Voet, A.
1983: The Determination of Scandium, Yttrium, and Selected Rare Earth Elements in Geological Materials by Inductively Coupled Plasma Optical Emissions Spectrometry; Spectrochimica Acta, Volume 388, p.165-173.

Boynton, W.V.
1979: Handbook on the Physics and Chemistry of Rare Earths; edited by K.A. Gschneider and L. Eyring, North Holland, New York, New York, Chapter 37F.

Crock, J.G., and Lichte, F.E.
1982: Determination of Rare Earth Elements in Geological Materials by Inductively Coupled Argon Plasma Atomic Emission Spectrometry; Analytical Chemistry, Volume 54, p.1329-1332.

Fidelis, I., and Siekierski, S.
1971: On the Regularities or Tetrad Effect in Complex Formation by f-Electron Elements. A Double-Double Effect; Journal of Inorganic and Nuclear Chemistry, Volume 33, p.3191-3194.

Kantipuly, C.
1984: Micro-separation and Determination of f-Series Elements; Unpublished Ph.D. Thesis, University of Ottawa, Ottawa.

Nesbitt, H.W.
1979: Mobility and Fractionation of Rare Earth Elements During Weathering of a Granodiorite; Nature, Volume 270, p.206-210.

Peppard, D.F., Mason, G.W., and Lewey, S.
1969: A Tetrad Effect in the Liquid-Liquid Extraction Ordering of Lanthanides; Journal of Inorganic and Nuclear Chemistry, Volume 31, p.2271-2272.

Westland, A.D., and Kantipuly, C.
1983: Potassium Superoxide as a Flux in Ore and Rock Analysis; Analytica Chimica Acta, Volume 154, p.355-358.

Grant 260 Magnetotelluric Mapping of the Destor–Porcupine Fault

J.D. Redman[1], **S.K. Zhao**[1], **and D.W. Strangway**[2]

[1]Department of Geology, University of Toronto, Toronto

[2]Office of the President, University of British Columbia, Vancouver

ABSTRACT

An Audio-Frequency Magnetotelluric (AMT) survey was carried out in Stock Township on two lines that cross the Destor-Porcupine Fault (DPF) in an area covered by 20 to 50 m of conductive overburden. The purpose of this survey was to determine the location and structural features of any conductive zone associated with the DPF. There were 64 stations located on the two lines which were each approximately 2 km in length. Apparent resistivities were measured for two orthogonal directions of the electric field dipoles at 83 Hz and 8.6 kHz. The interpretation of these profiles shows that on one of the lines there is a relatively wide, conductive, and anisotropic zone in the basement. This zone is centred on the previously mapped (Pyke *et al.* 1973) location of the DPF. On the other line, we did not find a distinctive conductive zone that could be attributed to the fault zone. Tensor AMT measurements at two stations show that the strike of the most conductive axis is east-west at low frequencies indicating the principal direction of fractures or an intrinsic anisotropy in the metasediments. The Destor-Porcupine Fault appears to be a good electrical conductor on one line and on this line AMT can detect its presence below a significant thickness of overburden.

INTRODUCTION

The results and interpretation of an AMT (Audio-Frequency Magnetotelluric) survey across the Destor-Porcupine Fault (DPF) will be presented in this paper. The purpose of the survey was to determine the location and nature of any conductive zone associated with the fault in an area where a significant thickness of overburden makes other methods difficult to apply.

The Destor-Porcupine Fault is a major east-west fault zone that extends from west of Timmins in Ontario to the Noranda area in Quebec. It is thought to represent a fundamental fracture in the Early Precambrian crust (Pyke 1982). The location and nature of this fault are important to mineral exploration because gold deposits in the Abitibi Belt are associated spatially with the major fault zones, such as the DPF. This spatial association reflects "an important symbiotic relationship between the volcano-tectonic environment, hydrothermal activity, and ore genesis" (Fyon and Crocket 1983).

Direct observation of the fault over much of its length is not possible because of overburden. In our study area (Figure 260.1), the cover has a typical thickness of 30 to 50 m (Baker *et al.* 1984). Thus, the location of the fault must be inferred from magnetic, gravity, or electrical surveys and from surface lineaments.

Magnetic methods are able to locate the fault in some regions, if there are differences in the susceptibility for adjacent units along the fault, if the fault zone itself has a different magnetic susceptibility, or if there are offsets in the magnetic features that can be traced across the fault.

Middleton (1976) has used gravity surveys to locate the contact between the metasediments and the metavolcanics which is the assumed location of the DPF. Since there is a significant contrast in density (200 kg/m^3) between the metasediments and the metavolcanics, gravity surveys have been useful in locating the boundary between the two units. However, the resolution of the technique is somewhat limited. For the profile along Highway 577, Middleton gives the location of this contact zone to within 400 m.

A difficulty with both the gravity and magnetic methods is that they do not, in most cases, directly detect a fault zone but instead map the contact between adjacent units. The fault zone and the observed contact may not be at the same location. Electrical methods, by contrast, can detect the fault zone itself and can determine the conductivity of the individual units in the basement. The direct detection of the fault zone depends on the fractures being open and thus conductive due to the presence of water. Clay or graphite within the fault zone may also enhance the conductivity of the fault relative to the surrounding rocks.

The airborne AFMAG method measures the tilt angle of the natural magnetic field at 150 and 510 Hz. Only lateral changes in the resistivity structure can be detected using this technique. This method has been used successfully by Sutherland (1967) to map the location of the DPF in Quebec. The technique is no longer in use. Labson *et al.* (1985) have reported on a tensor ground-based AFMAG technique that overcomes a number of limitations in the original AFMAG technique and may prove to be useful for these applications in the future.

The VLF technique can also be used for mapping faults, however this technique cannot be used where there is significant conductive overburden or in areas where the strike of the fault results in poor coupling with the source fields. Also because the frequency dependence of the response is not measured, the interpretation is limited to simple models.

The AMT method is a good technique for mapping earth resistivities both laterally and with depth. Because of the high lateral resolution and the ability to see through conductive overburden, it is an excellent technique for mapping the location of fault zones. The technique has proven to be useful in locating faults for the Nuclear Fuel Waste Management Program at test sites near Atikokan (Redman *et al.* 1980) and East Bull Lake, Ontario (Kurtz and Niblett 1984). The AMT method also measures over a wide frequency range (10 Hz to 10 kHz) which allows one to determine more details of the resistivity structure than is possible with single frequency techniques.

AMT METHOD

SCALAR AMT

The scalar AMT method was described previously by Strangway *et al.* (1973). In this technique, the apparent resistivity is computed from simultaneous measurements of the horizontal orthogonal components of the electric and magnetic fields, at frequencies between 10 Hz and 10 kHz, according to:

$$\rho_a = \frac{1.3 \times 10^5}{f} \left| \frac{E}{H} \right|^2$$

f - frequency (Hz)
E - Magnitude of the electric field (volt/m)
H - Magnitude of the magnetic field (amp/m)

The functional dependence of apparent resistivity with frequency and with station location can be interpreted to determine the local resistivity structure of the earth.

For this study, the emphasis was on profiling, with a high station density along the line, since the purpose of the survey was to determine lateral changes in resistivity. To obtain the higher station density, it was necessary to restrict the measurement frequencies to 8 kHz and 83 Hz. Full soundings, at 11 frequencies between 12 Hz and 8 kHz, were also completed at a number of stations and these were used as an aid in the two-dimensional modeling process. An induction coil was used to measure the magnetic field and an electric dipole with a length of 50 m was used to measure the electric field. On line 1 there were 25 stations which, in general, were spaced every 100 m with detail stations 50 m apart in some areas. On line 2, there were 39 stations spaced 50 m apart. The apparent resistivity was measured at each station for two orthogonal directions of the electric and magnetic field sensors. The measurement directions were chosen to be roughly parallel and perpendicular to the known structural directions (i.e. east-west and north-south). The differences in apparent resistivity for these two directions gave a measure of the two-dimensionality of the earth.

TENSOR AMT

Tensor AMT measurements can provide apparent resistivity data of higher quality than is possible with the scalar technique. However, tensor AMT measurements are considerably more difficult and time consuming than scalar AMT measurements and for this reason only two tensor stations were completed. Most of the tensor measurements in the past have been restricted to frequencies less than 500 Hz. The tensor AMT equipment developed at the University of Toronto can measure in the frequency range of 1 Hz to 10 kHz but useful measurements were only obtained in a more restricted range because of the weak source fields

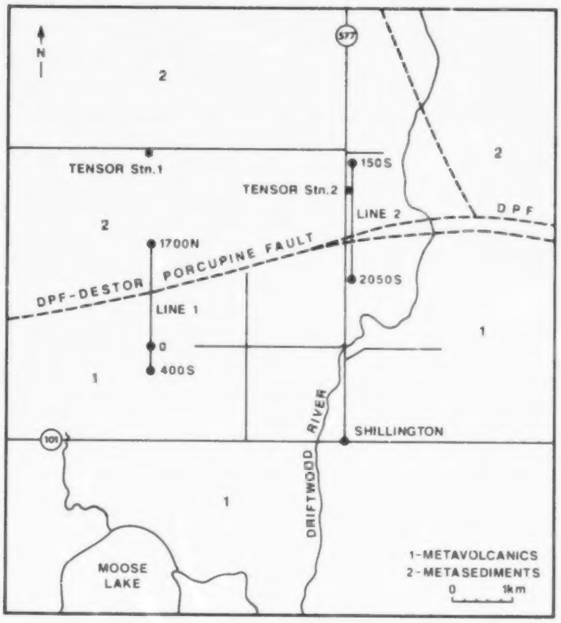

Figure 260.1. *Location map for AMT lines and tensor stations. The faults shown are taken from Map 2205 (Pyke et al. 1973).*

Three components of the magnetic field, (two horizontal and one vertical) and two horizontal electric field components were digitized and recorded simultaneously. The elements of the impedance tensor Z_{ij} and associated apparent resistivity ρ_{ij} were calculated from the relationship between the digitized horizontal components of the electric and magnetic fields, as described in Vozoff (1972, p.103):

$$E_x = Z_{xx}H_x + Z_{xy}H_y \qquad \text{where} \left[\begin{array}{l} |\rho_{ij}| = \dfrac{|\,Z_{ij}\,|^2}{\omega\mu} \\[2ex] \angle\rho_{ij} = \angle Z_{ij} \end{array} \right.$$

$$E_y = Z_{yx}H_x + Z_{yy}H_y$$

The tensor data were collected in four bands: band 1: 1 to 40 Hz; band 2: 40 to 400 Hz; band 3: 400 to 4000 Hz; and band 4: 4000 to 10000 Hz. In band 4, data were digitized on 6 channels every 25 μsec. Within each band, a digitized data set (time series) of 512 points in length were collected. A data set was only accepted for analysis if the signal level was above a preset threshold level. Since the tensor field work was carried out in November when the signal levels are quite low, only a small percentage of the data sets had sufficient amplitude to be saved on floppy disk for later analysis.

A typical data set recorded on band 4, of a lightning strike event, is shown in Figure 260.2. These kinds of plots of captured events are seen on the video monitor in the field and allow one to accept or reject the data set for further analysis. The vertical scales have been normalized on the plot to the maxi-

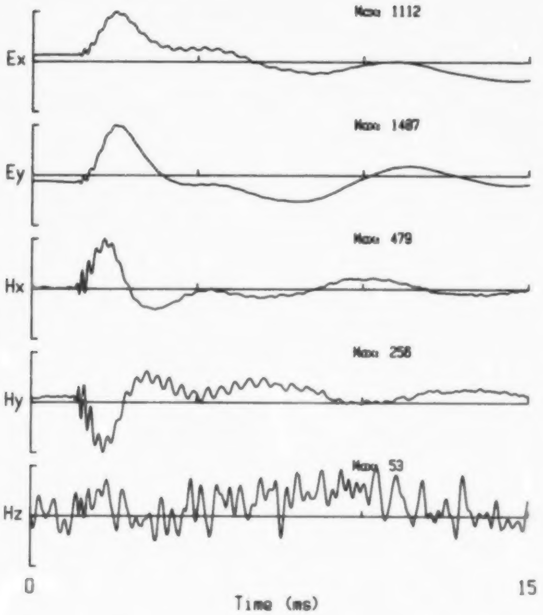

Figure 260.2. *Typical time series for band 3 (4 kHz low-pass filtered). The fields are sampled at 29 μsec intervals and 512 samples are collected on each channel. The "max" values shown are the full scale for each plot.*

mum value in each data set. The units on the vertical scale are simply the uncalibrated A/D converter outputs. The vertical magnetic field is quite small compared with the horizontal components as one would usually expect and is dominated by noise.

The crosspower and autopower spectra were averaged for approximately 20 time series in each band and these spectra were used to compute the impedance tensor elements and the associated apparent resistivities. The amplifier gains and induction coil sensitivities are measured at each station in the field at the completion of the natural signal measurements as part of the calibration procedure.

One of the advantages of the tensor technique is that one can obtain a measure of data quality by computing the coherence between the measured electric fields and the predicted electric fields based on the computed impedance elements and measured magnetic fields. A coherency greater than .95 was considered to be acceptable for these data sets.

RESULTS AND DISCUSSION

SCALAR AMT PROFILING

Two profiles near Shillington (Figure 260.1) were measured over the fault zone that is indicated on geology maps. The geology maps indicate that the fault structures around line 2 are more complex than around line 1 and that there is a change in the character of the fault zone where line 1 crosses the fault. Since this region encompassing lines 1 and 2 is buried under 20 to 50 m of overburden, there is no direct evidence to locate the fault and the strength of the evidence for mapping the faults in the location shown on geology maps is uncertain. In fact, the location and configuration of the faults in this region are probably not known with accuracy.

The profiles for lines 1 and 2 are shown in Figures 260.3a and 260.4. In general, at 83 Hz, the apparent resistivities reflect the variation in the bedrock resistivity and at 8570 Hz they are mainly influenced by variations in the overburden resistivity or thickness. On both of these lines, conductive zones in the bedrock are indicated by the anisotropy (differences in resistivity for the two measurement directions) shown in Figure 260.5. The apparent resistivities at 83 Hz, in the east-west direction are, in general, lower, indicating that there are conductive structures with relatively long strike length in this direction.

For line 1, the presence of a conductive zone is quite evident by simply examining the 83 Hz profile. The high frequency profile is quite uniform indicating that the overburden resistivity is relatively constant and that the overburden thickness does not decrease to any great extent along the line.

The differences in the profiles for the two measurement directions are characteristic of two-dimensional structures. The computed response for the two-dimensional model of the resistivity structure for line 1, shown in Figure 260.3b, fits our field data quite well for both measurement orientations. The model response was computed using the finite element technique (Zhao and Xu 1983; Xu and Zhao 1985). A trial and error technique was used to arrive at the optimum model shown.

In the modeling process, an attempt was made to keep the model as simple as possible while still providing a reasonable fit with the data. There is likely some topography on the bedrock surface but the uniformity of the 8 kHz data implies that the thickness of the overburden is relatively uniform.

The main conductive feature in the bedrock observed on line 1 between 675N and 1175N has been modeled by a zone in which the resistivity is anisotropic. The east-west resistivity is 170 ohm-m compared to 2200 ohm-m in the north-south direction. This observed anisotropy is probably a macroscopic anisotropy caused by the principal direction of fracturing. This zone of apparent anisotropic resistivity in the basement could also be modeled with a region of vertical dike-like conductive structures embedded in a resistive background medium. A zone of vertical fractures striking east-west would be an example of this kind of structure. We were also able to fit our apparent resistivity profiles with this kind of model. But, in practice, information about the specific fractures in this zone can not be obtained since there are many models of this kind that would fit our data. Thus, this zone is treated simply as a zone in which the resistivity is anisotropic. The 45° dip to the south of this conductive zone produces an asymmetry in the profile that provides a better fit to our data than could be obtained with a vertical structure. The zone south of the major conductive zone is also an-

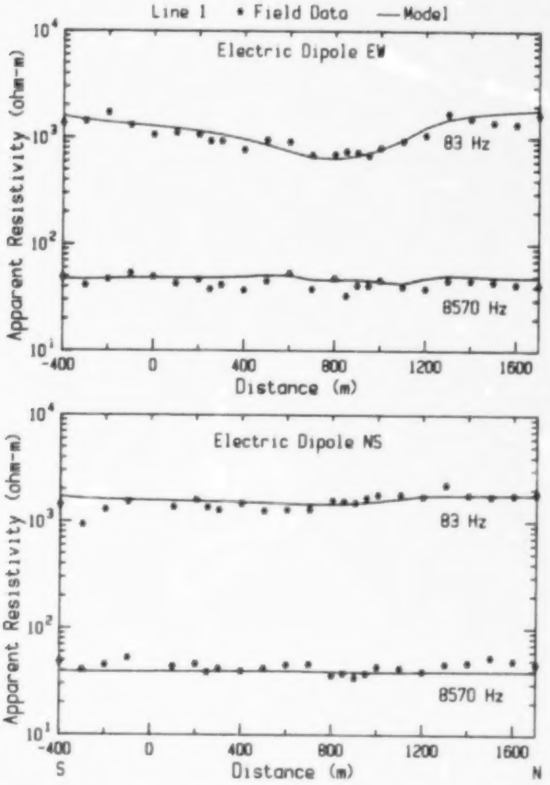

Figure 260.3a. AMT profiling results for line 1. The computed resistivities for the two-dimensional model and the field data for the two measurement orientations are shown.

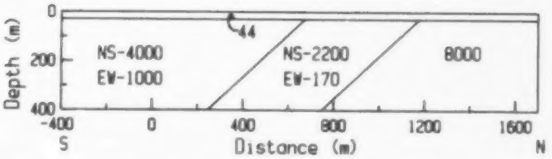

Figure 260.3b. Two-dimensional resistivity model (vertical cross section in the north-south direction) used to fit field data for line 1. The numbers shown in each region are resistivities in ohm-m. The model has infinite extent in the east-west direction.

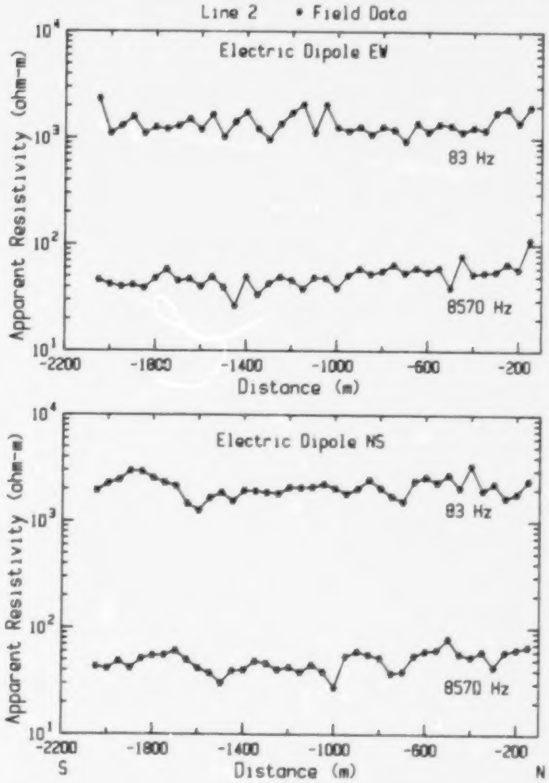

Figure 260.4. AMT profiling results for line 2. Field data for the two measurement orientations are shown.

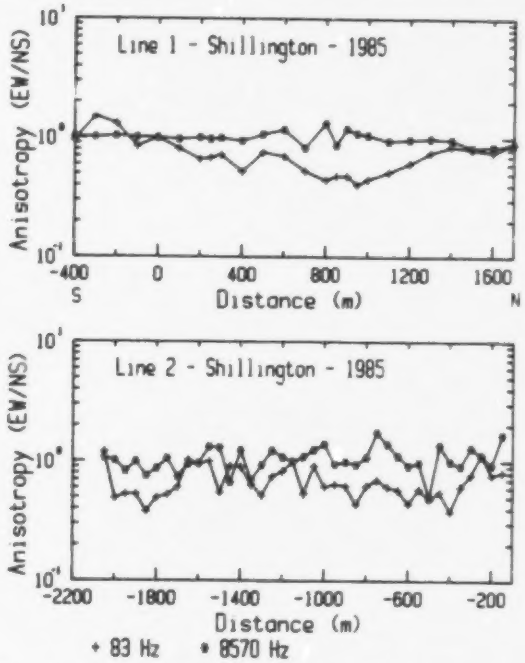

Figure 260.5. Anisotropy observed in the apparent resistivities for lines 1 and 2.

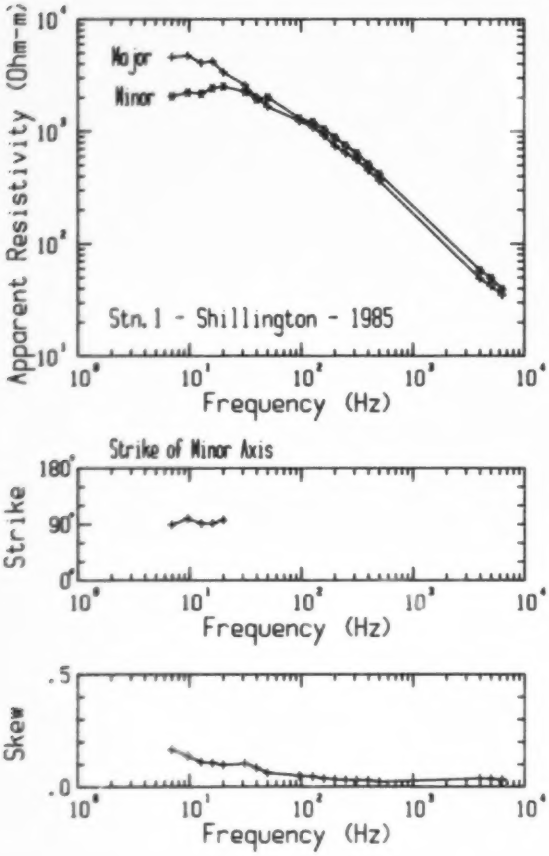

Figure 260.6a. *Tensor AMT results for station 1. The strike of the minor axis is only given for frequencies at which the resistivity structure is clearly two-dimensional. Only data for which the coherency was greater than 0.95 have been plotted.*

isotropic reflecting possibly less extensive fracturing in the east-west direction.

The profiles for line 2 are more complicated than line 1, and as seen on the anisotropy plots for the 83 Hz data, the east-west direction is also more conductive. The 8570 Hz profile is more variable showing that the overburden conductivity or thickness is less uniform. There are conductive zones centred at 1600S and 700S on this line. We have attempted to fit a two-dimensional model to this data as well, but we were unable to get a good fit to the apparent resistivity profile. This profile is much more complicated than for line 1 and does not show the same distinctive conductive zone. The overburden thickness and/or resistivity are more variable on this line and this effect obscures the response of the basement structure.

On line 1, the DPF appears to be an anisotropic conductive zone 500 m wide, centred about 900N. This is consistent with a wide fracture zone with fractures that strike in the east-west direction. The geology map for this area places the DPF at approximately 900N. The DPF has been observed in the subsurface, 5 km to the west at the St. Andrew Goldfields deposit, as a system of chlorite and talc-chlorite shear zones with a width of approximately 150 m (Malczak 1985). This is consistent with the kind of structure suggested by our interpretation. A similar conductive zone was not observed on line 2. If the main conductive zone on line 1 is the DPF, then the profile for line 2 indicates that the DPF is clearly not as conductive on line 2. In fact, there is no feature seen in the profile that we can clearly attribute to the DPF.

TENSOR AMT STATIONS

Tensor AMT data were collected at two stations. Station 1 is at the north end of line 1 and is situated well within the metasedimentary zone. Station 2 is at 600S on line 2. The station locations were limited to areas in which we could obtain access with a vehicle since our equipment is mounted in a truck.

The results of these measurements are summarized in Figures 260.6a and 260.6b. The impedance tensor has been rotated into its principal directions to give the major and minor apparent resistivity curves and the strike of the more conductive direction or minor axis. The strike is only plotted for frequencies at which the resistivity structure is clearly two-dimensional. A high skew indicates that the structure is three-dimensional. The skews observed for these stations indicate that the structure is one or two-dimensional.

Both stations show that at high frequencies (above 200 Hz), the structure is effectively one-dimensional. That is, the overburden is a simple layered structure. At the lower frequencies, there is increasing anisotropy indicating that the structure is two-dimensional. For both stations the most conductive direction, at low frequencies, is east-west. For station 2, this is probably reflecting a conductive zone that is also indicated on the profiles. For station 1, the effect may be the result of an intrinsic anisotropy, possibly on a large physical scale, similar to what we have observed for metasediments in Moody Township (Strangway 1983).

A one-dimensional or layered earth model has been fitted to the average of the logarithm of the apparent resistivity of the major and minor axes. For both stations, a simple two-layer model, of conductive overburden over resistive basement, was used to fit the dependence of apparent resistivity on frequency. For station 1, the upper layer is 29 m thick with a resistivity of 41 ohm-m and the lower layer has a resistivity of 7000 ohm-m. For station 2, the upper layer is 31 m thick with a resistivity of 50 ohm-m overlying a 8500 ohm-m section. These one-dimensional fits are used as input for the two-dimensional modeling process.

CONCLUSIONS

The interpretation of the apparent resistivity profile for line 1 clearly indicates the presence of a wide, conductive, and anisotropic zone centred at 900N that is attributed to the Destor-Porcupine Fault zone.

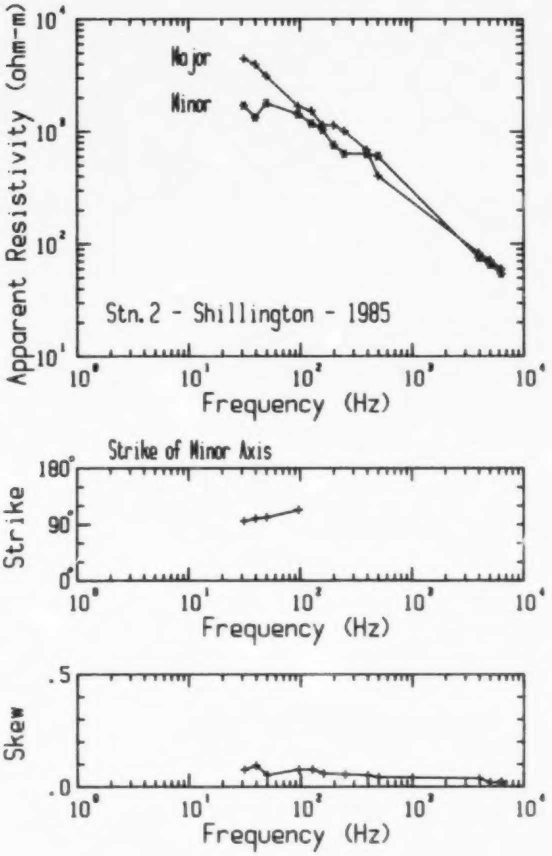

Figure 260.6b. *Tensor AMT results for station 2. The strike of the minor axis is only given for frequencies at which the resistivity structure is clearly two-dimensional. Only data for which the coherency was greater than 0.95 have been plotted.*

This kind of structure is also consistent with direct observations of the fault zone in this area. A conductive zone associated with the presumed location of the DPF on line 2 was not seen on our profile. Although the interpretation for line 2 is more difficult, there is clearly not a significant conductive zone in the basement similar to that seen on line 1. The DPF must be much less conductive than on line 1. The tensor data for station 1 show that the strike of the most conductive axis is east-west at low frequencies indicating either the principal direction of fractures or an intrinsic anisotropy in the metasediments.

This survey has shown that the DPF is a good electrical conductor in one region and that in this region AMT can detect its presence below a significant thickness of overburden.

REFERENCES

Baker, C.L., Steele, K.G., Mclenaghan, M.B., and Fortescue, J.A.C.
1984: Location of Gold Grains in Sonic Drill Core Samples, Matheson Area, Cochrane District; Ontario Geological Survey, Map P.2736, Geophysical/Geochemical Series-Preliminary Map, scale 1:100 000. Geology 1984.

Fyon, J.A., and Crocket, J.H.
1983: Gold Exploration in the Timmins Area: Using Field and Lithological Characteristics of Carbonate Alteration Zones; Ontario Geological Survey, Study 26, 56p.

Kurtz, R.D., and Niblett, E.R.
1984: A Magnetotelluric Survey Over the East Bull Lake Gabbro-Anorthosite Complex. TR-236, Scientific Document Distribution Office, Atomic Energy of Canada Limited, Research Company, Chalk River, Ontario.

Labson, V.F., Becker, A., Morrison, H.F., and Conti, U.
1985: Geophysical Exploration with Audiofrequency Natural Magnetic Fields; Geophysics, Volume 50, p.656-664.

Malczak, J.
1985: Preliminary Report on the St. Andrew Goldfields and Maude Lake Gold Deposits, District of Cochrane; p.316-319 *in* Summary of Field Work and Other Activities 1985, Ontario Geological Survey, edited by John Wood, Owen L. White, R.B. Barlow, and A.C. Colvine, Ontario Geological Survey, Miscellaneous Paper 126, 351p.

Middleton, R.S.
1976: Gravity Survey of Geological Structures in the Timmins and Matheson Area, Districts of Cochrane, Timiskaming, and Sudbury; Ontario Geological Survey, Report 135, 45p.

Pyke, D.R.
1982: Geology of the Timmins Area, District of Cochrane; Ontario Geological Survey, Report 219, 141p.

Pyke, D.R., Ayres, L.D., and Innes, D.G.
1973: Timmins-Kirkland Lake Sheet, Cochrane, Sudbury, and Timiskaming District: Ontario Geological Survey, Geological Compilation Series, Map 2205.

Redman, J.D., Hsu, D., and Strangway, D.W.
1980: Audio-Frequency Magnetotelluric Measurements on the Eye-Dashwa Lakes Pluton, Atikokan, Ontario: Unpublished Report, Geology Department, University of Toronto, Toronto.

Strangway, D.W., Swift, C.M., and Holmer, R.C.
1973: The Application of Audio-Frequency Magnetotellurics (AMT) to Mineral Exploration; Geophysics, Volume 37, p.98-141.

Strangway, D.W., Ilkisik, O.M., and Redman, J.D.
1983: Surface Electromagnetic Mapping in Selected Positions of Northern Ontario, 1982-1983. Ontario Geological Survey, Miscellaneous Paper 113, p.159-173.

Sutherland, D.B.
1967: AFMAG for Electromagnetic Mapping, Mining and Groundwater Geophysics/1967; Geological Survey of Canada, Economic Geology Report Number 26, p.228-237.

Vozoff, K.
1972: The Magnetotelluric Method in the Exploration of Sedimentary Basins; Geophysics, Volume 37, p.98-141.

Xu, Shizhe, and Zhao, Shengkai.
1985: Solution of Magnetotelluric Field Equations for a Two-dimensional, Anisotropic Geoelectric Section by the Finite Element Method; Acta Seismologica Sinica, Volume 7, p.80-90.

Zhao, Shengkai, and Xu, Shizhe.
1983: Two-dimensional Magnetotelluric Modelling by Finite Element Method; Computing Techniques for Geophysical and Geochemical Exploration, Number 1, p.14-21.

Grant 262 Lithological Features and Economic Significance of Reduced Carbonaceous Rocks in Gold Deposits

Graham C. Wilson and John C. Rucklidge

IsoTrace Laboratory, University of Toronto, Toronto

ABSTRACT

The widespread occurrence of carbonaceous rocks in a subset of North American gold deposits is being examined. A detailed overview is being prepared. This paper concentrates on the Owl Creek and Hoyle Pond Mines, located on the east side of the Timmins mining camp, northern Ontario. Transmitted and reflected light petrographic observations are combined with electron microprobe results in order to describe aspects of gold mineralization from these Ontario mines and from selected analogous sites elsewhere. A number of other localities, with outcrop of Archean-Proterozoic lithologies which are carbonaceous but not strongly enriched in gold, are also included in this survey for comparison with mine site suites. Although no mine generates carbonaceous ores alone, the proportion of such ores varies widely from mine to mine, camp to camp. Some critical questions remain, particularly with regard to the chemical behaviour of the reduced carbon, but two common factors of prime economic relevance are established. These are the importance of: (a) fluid focusing through incompetent carbonaceous units during tectonism; and (b) localization of high (commonly visible) gold values on vein-wallrock contacts.

INTRODUCTION AND RESUME

An ongoing study into the characteristics of carbonaceous precious-metal ores, begun in 1984, has encompassed suites of material from deposits across Ontario, Nevada (Windfall, Alligator Ridge, and Jerritt Canyon), Montana (Red Pine), and California (Mother Lode district). Simple mineral names are employed so as not to anticipate the results of forthcoming analyses (a relevant caveat is the variable composition of gold-related "muscovite", described within).

This report is based on microscopic examination of prepared slices of 72 samples. Many of the samples are polished mounts and thin sections suitable for *in situ* analysis, both by electron microprobe and by techniques developed in our microchemical project on the carbon itself. This upcoming ion beam analysis will use our microprobe stage (Wilson *et al.* 1984); preliminary results on "graphites" have been presented elsewhere (Wilson and Rucklidge 1984; Rucklidge *et al.* 1985).

A significant economic development related to carbonaceous ores is located east of Timmins, north of Highway 101 in Hoyle Township, along the general trend of the Destor-Porcupine Fault zone in the Archean Abitibi greenstone belt (Ludden *et al.* 1986). A number of deposits are being developed in this area (The Northern Miner, December 23, 1985, p.B5). Two deposits featured in this work are (references in brackets are to "The Northern Miner"):

1. Owl Creek Mine, a Kidd Creek Mines project, with estimated minable reserves of 0.725 MT grading 4.5 g/T (0.13 ounce per ton). This value includes 0.09 MT of siliceous graphitic ore which presents the refining problems common to carbonaceous ores. Kidd Creek Mines determined that this material could be accepted in the nearby copper smelter as fluxing ore (August 22, 1985, p.1.6 and December 23, 1985, p.B5). Much material for this project was collected on levels 2, 3, and 4 of the open pit operation. Work has concentrated on the east side of the open pit, where a thick zone of vein quartz and deformed country rock (the "quartz dike") is located along the (roughly east-west) contact between basic metavolcanics to the north and argillic (greywacke) sediments to the south (Brisbin 1984; Paul R. Coad, Kidd Creek Mines, Timmins, personal communication, 1986).
2. Hoyle Pond (Downes *et al.* 1984), another Kidd Creek Mines development, with reserves of 0.405 MT at 13.9 g/T (0.45 ounce per ton). Expected 1986 production is about 40 000 ounces Au (December 23, 1985, p.B5). Reserves seem likely to be extended by exploration of the optioned Schumacher Property to the west. Underground sampling on levels 2 and 3 provided the material described below.

In the Abitibi greenstone belt, visibly "sooty" units have been named for their regional setting as "interflow sediments"; for their relationship to major faults ("graphite faults" and "breaks"); or for their macroscopic appearance ("carbonaceous tuffs"). The mineralogy of the carbonaceous rocks (Wilson 1986) depends to a certain extent on the primary lithology, but variable quartz, carbonate, phyllosilicate, and sulphide assemblages predominate, with minor reduced carbon (whose crystallinity is thought to correlate to first order with metamorphic grade), plus one or more of tourmaline, native gold (<20 weight percent Ag), sulphosalts, and other phases. Fine-grained muscovitic mica is common, and with quartz it is commonly a major constituent of highly sheared zones. Carbonate may be of either ankeritic or rather pure calcitic composition. The dominant sulphide is generally pyrite, which may in outcrop scale display any of three habits, described in the next section. In the suites examined so far, the porous or fluffy habit is associated with gold mineralization. Further efforts are being made to characterize both the carbon and its associated paragenesis. Protolith recognition and microstructural interpretation, standard problems in gold deposits and in Archean geology (Lowe and Byerly 1986), are dealt with in turn. Since macroscopic pyrite is usually the most prominent mineral in otherwise black, fine-grained rocks from the carbonaceous zones of all the localities involved, the opaque phases are described first.

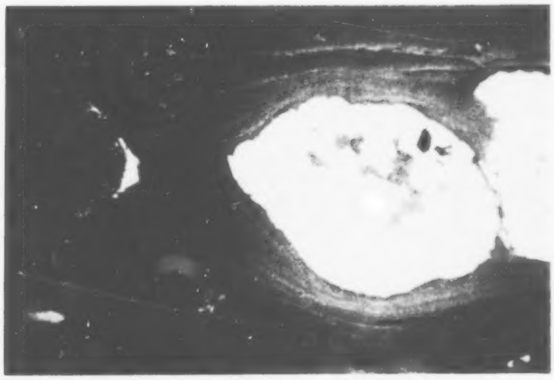

Photo 262.1a. *Nodular sedimentary pyrite, from Owl Creek. Photo width is ≅10 mm.*

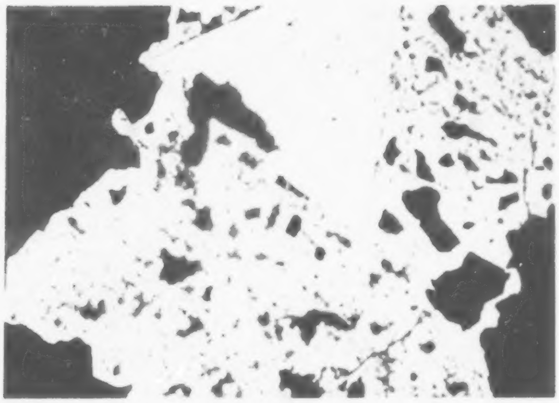

Photo 262.1b. *"Fluffy" pyrite overgrowth on fine-grained euhedral pyrite from the ore zone (Owl Creek). High but erratic arsenic signal seen on electron microprobe in the most porous areas. Photo width is ≅1 mm.*

PYRITE AND OTHER ORE MINERALS

The lack of spectacular habit variations in the carbon itself, compared with the coarse graphite of the Pt-rich association (Volborth and Housley 1984), is partly compensated by the variable forms of the pyrite which comprises the bulk of the opaque phases in most of the samples examined.

The Owl Creek ore zone material, in particular, shows clear contrast between solid and porous forms of pyrite, which blend into each other across the width of a single pyrite mass. These habits constitute the second of three generations of pyrite which are, in general, macroscopically distinct:

1. Nodular pyrite, entrained by the predominant foliation in the metasedimentary host rock (Photo 262.1a)—apparently diagenetic in origin.
2. The "fluffy" or "porous" pyrite and associated fine euhedral pyrite. The porous material is commonly concentrated in marginal parts of grains, or forms a mantle on small euhedra (Photo 262.1b). In form it resembles the "'dusty' intermediate pyrite" of Frater (1985), a form ascribed by that author to imply growth of secondary pyrite via a marcasite stage.
3. Coarse, late, euhedral and porphyroblastic pyrite, sometimes containing unrotated inclusions of foliated matrix, still clearly aligned with the bulk rock foliation (Photo 262.1c), it overgrows primary depositional features (lamination, fining-upward sequences) in the relatively undeformed sediments south of the ore zone at Owl Creek (Photo 262.1d).

The pyrite habits in the second "generation", which is typical of many ore-grade samples, may be crudely divided between fine euhedral pyrite and porous pyrite (often gradational with the former). The so-called "fluffy" or "snowflake" pyrite occurs as separate smaller aggregates of the porous material. The latter show passing resemblance to the much smaller (typically <10 μm), ramboidal pyrite derived by diagenesis of sediments (Love and Amstutz 1966), but is clearly of a different origin. Apparent anisotropy occasionally seen in the pyrite is probably due to "depolarisations . . . owing to the marked relief of the grains" (Ramdohr 1969, p.780), a reference to the difficulties often encountered in polishing pyrite, particularly in the soft, fine-grained matrices commonly found in carbonaceous ores.

The chemistry of the pyrite and associated phases has been examined by energy-dispersive electron microprobe analysis. Minor (<1 weight percent) Co, Ni, Zn contents detected by the microprobe are not out of the ordinary, according to the pioneering spectrographic study of Auger (1941). While the Timmins camp does not show the locally spectacular anomalies in "indicator elements" that characterize the disseminated, low-grade, carbonaceous gold deposits of Nevada, some elements appear consistently in mineralized areas. Perhaps the best case is that of arsenic. Whitehead *et al.* (1981) chose As >10 ppm (whole rock) as one of several criteria of mineralization for whole-rock analysis in the area. This correlation between As and Au was confirmed for the Hollinger-McIntyre Deposit by Smith and Kesler

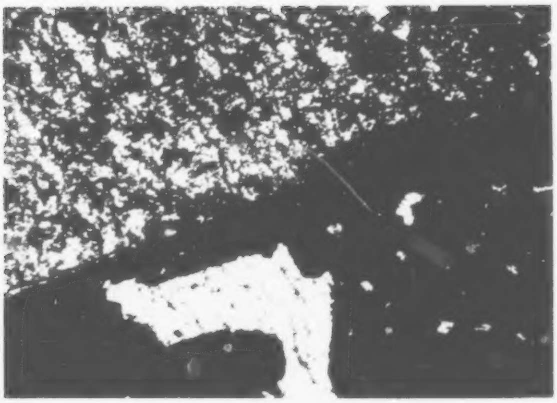

Photo 262.1c. Porphyroblastic pyrite enclosing unrotated mass of host rock, displaying early metamorphic foliation (from Owl Creek). Crossed polars. Photo width is ≅3 mm.

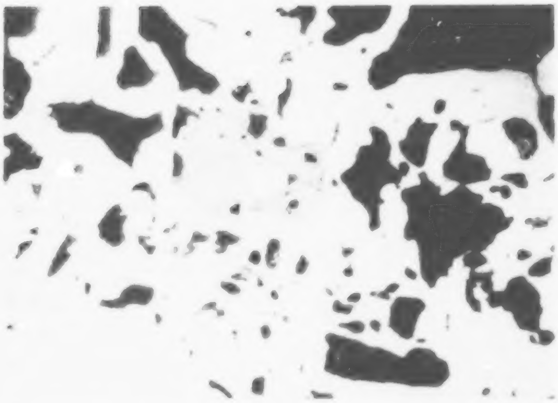

Photo 262.1e. Native gold in porous pyrite. Photo width is ≅0.4 mm. Same sample as Photo 262.1b

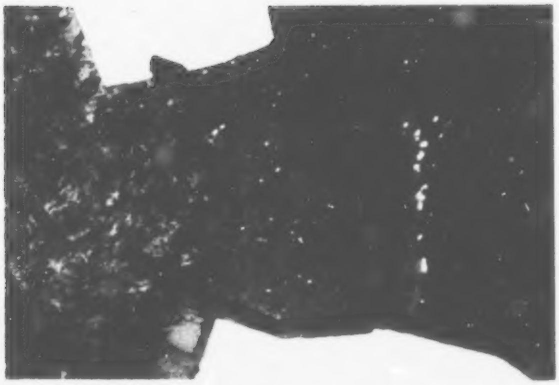

Photo 262.1d. Porphyroblastic pyrite cubes with thin pressure shadows cutting across sedimentary layering in wacke. Photo width is ≅3 mm. Same sample as Photo 262.1c.

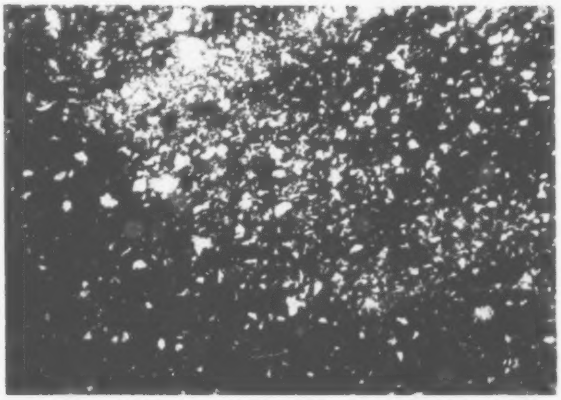

Photo 262.1f. Very fine grained Upper Paleozoic sediment (Pilot Shale) broadly typical of the rocks hosting disseminated gold deposits in the southwestern U.S.A. This example is a decalcified silicified siltstone from Alligator Ridge, Nevada. Photo width is ≅3 mm.

(1985), who found values of up to 50 ppm As associated with pervasive carbonate alteration. Microprobe analyses from Owl Creek and from Nevadan mines confirm the arsenical nature of some of the ores. While this is a cryptic phenomenon at Owl Creek (erratic As values in the gold-related pyrite: highest value to date 1.7 weight percent in one point of a small euhedron containing a native gold inclusion), some of the Nevadan ore comprises a siliceous matrix containing major amounts of a pure realgar, as well as pyrite containing up to 3.0 weight percent or more As. The Au-As association is of course well established; a good example is Carlin, where mineralized rocks have a mean arsenic content of 0.06% and a range from <0.02% to 0.7% (Akright *et al.* 1969). Arsenical pyrite with As >5 weight percent has been reported from Nevada (Wells and Mullens 1973).

The mineralogical site of the arsenic has not been conclusively demonstrated for the Ontario suite; electron microscopy may provide the answer. Three possibilities are: (1) thin films of arsenical phases (native As?) on pores or grain boundaries (perhaps adsorbed on exposed surfaces during crystal growth); (2) submicroscopic (<2 μm) inclusions of sulphides; or (3) solid solution of As in pyrite. At Carlin, Au and Hg commonly form very thin (micron scale) coats on pyrite; As and Sb do this to some extent, but also occur as late sulphides (Radtke 1985, p.76). The high As results of Wells and Mullens (1973) were for very fine-grained (<5 μm) grains, and for rims on larger grains; arsenic in the cores of larger grains fell below the detection limit of the electron microprobe. These findings are compatible with thin arsenical coatings on larger grains a location of arsenic also suspected by Rytuba (1985, p.32) for Getchell. We are not aware of definitive work on the solubility of arsenic within the pyrite lattice. However, it seems likely to be of the order of 0.5% or less (Clark 1960). Small pyrrhotite inclusions might carry As in associated ultra fine-grained arsenopyrite, but were not recognized in our arsenical pyrites. Pyrrhotite and native arsenic are not compatible under greenschist-amphibolite conditions (Barton 1969). We will investigate the possibility that hypothesis (1) outlines the bulk of the As observed.

It has been suggested that high concentrations of gold on sulphide surfaces may accrue at p-n semiconductor junctions in pyrite, inferred to form from hydrothermal fluids under rapidly variable conditions (*see* Colvine *et al.* 1984, p.53-54; Springer 1983, 1984a, 1984b). Such variation may be consistent with the noted variation in pyrite habit. Minor amounts of chalcopyrite, pyrrhotite, sphalerite, and native gold occur in the ore. The sulphides may occur as overgrowths, as small inclusions in pyrite, and as discrete grains. Gold at Owl Creek and Hoyle Pond may be found in hand specimens, generally along contacts between milky white vein quartz and dark carbonaceous wallrock, often associated with pale greenish, silky "hydromuscovite". Gold samples from all deposits in the study also exhibit the familiar late paragenesis of native gold grains within and adjacent to (quartz-carbonate) fractures in pyrite. Pyrite-trapped gold constitutes a second setting for gold grains at Owl and Hoyle (Photo 262.1e). In Nevadan deposits realgar (orpiment) and stibnite are locally abundant. Cinnabar may also be present, as at Getchell (Joralemon 1951), where Sb and As have also been detected in the composite sulphide getchellite (Weissberg 1965). Fe-Ti oxides are commonly present as accessory phases in the wallrocks of carbonaceous deposits, often as fine-grained TiO$_2$ (rutile or anatase).

In some deposits a different sulphide/sulphosalt mineralogy may be found: chalcopyrite, enargite-luzonite, tetrahedrite-tennantite, and covellite. Samples from the Red Pine Mine, Montana, are being examined. This material currently constitutes our only sampling of Cu-Fe-As-S sulphide assemblages (McKinstry 1963) in a carbonaceous setting.

Other ore minerals have been observed in restricted occurrence from Hoyle Pond but have not been identified in our suite: arsenopyrite, galena, native silver, a Ag-Bi telluride, electrum, molybdenite, marcasite, and scheelite (J.D. Scott, Kidd Creek Mines, Timmins, personal communication, 1985).

THE FINE–GRAINED MATRIX OF THE CARBONACEOUS ROCKS

1. Quartz, carbonate, white micas, and chlorite are the dominant minerals. The combination of opacity and minute grain size is typical of the black argillites examined (Photo 262.1f).
2. The carbon, which appears as ill-defined opaque clumps, typically 20 microns or less in size, aligns readily with the dominant cleavages, and is apparently remobilized during deformation. Both outcrop and microscopic-scale observations support movement of carbon along and near late faults and fractures, as does the minor occurrence of reduced carbon in deformed and altered lavas. This mobility can obscure the provenance of such carbon, although the field evidence of abundant sedimentary carbon in the Archean and Proterozoic of Ontario is convincing. Such carbon is thought to be largely of biogenic origin. Little of the Ontario gold mine carbon may be very well ordered graphite, although it is locally concentrated into coarser flakes on fractures, and may appear quite massive and pure; such material occurs at the Kerr Addison, Hollinger, McIntyre, and other major mines.

At Carlin, slight enrichment over the unaltered country rocks (from 0.2-0.3 to 0.5-0.6 weight percent) in organic carbon is seen in the most common form of unoxidized ore (Radtke 1985, p.52). Up to 6 weight percent organic carbon occurs in the carbonaceous ore (Radtke 1985, p.57). Such values are not that unusual in black shales. Mesozoic siltstones from the eastern United States may contain up to 30% total organic carbon (Olsen 1985). Maturation of organic matter near gold mineralization has been noted by Ilchik *et al.* (1986) in carbonaceous sediment at the Alligator Ridge Deposit.

MAJOR GANGUE PHASES ASSOCIATED WITH GOLD

1. Vein quartz is commonly crowded with dark specks of carbonaceous matter. It is commonly

deformed and carries a range of fluid inclusions. Chalcedonic silica has been observed in Red Pine ore, but is uncommon.

2. Sheet silicates are intimately associated with the most spectacular native gold occurrences seen in this work. The results of 40 electron microprobe analyses of grains in a single sample ("700A") from Hoyle Pond are summarized, as they are relevant to the chemistry of the ore fluid and its evolution. Two views of this sample are presented (Photos 262.1g, 262.1h); note the mineralogical similarity to the "stylolite" described in the next section. The chlorite has optical properties consistent with homogeneous ripidolite, an oxidized chlorite. This is confirmed. However, microprobe analysis within and between chlorite laths from wallrock to quartz margin reveals strong zoning, with the most iron-rich compositions within a few tens of microns of gold grains (Figure 262.1).

   The white mica also shows wide inter- and intragrain variation, although no spatial-chemical correlation is immediately obvious. Microprobe data (Figure 262.2) indicate a wide range of sodic compositions, some approaching pure paragonite. Some of the coarser mica is a sodic hydromuscovite or brammallite (Brammall *et al.* 1937, and Figure 262.2), corresponding to an earlier analysis of a mica separate from Hoyle Pond (J.D. Scott, Kidd Creek Mines, Timmins, personal communication, 1985).

3. Tourmaline is locally abundant, with yellow-brown body colour in thin section and a dravitic (magnesian) composition.

4. Plagioclase (a nearly pure albite) is not common in our suite, although it occurs along a quartz(-tourmaline) vein margin in one Hoyle Pond sample.

5. Carbonates. The pale grey carbonate in samples carrying the quartz-hydro-muscovite-(chlorite-pyrite-gold) association at Hoyle Pond is a ferroan dolomite, locally overgrown by dolomite. Siderite has also been identified (J.D. Scott, Kidd Creek Mines, Timmins, personal communication, 1985). Preliminary data on the carbonates suggest coexistence of near-pure calcite with ankerite of a composition compatible with the work of Rosenberg (1967). Late barren calcitic veining appears to be a common feature in a number of deposits.

MICROSTRUCTURAL GEOLOGY OF CARBONACEOUS LITHOLOGIES

Examination of microstructures reinforces the view that the major tectonic significance of these rocks derives from their weak, incompetent nature. Carbonaceous units (whether formed as shales, siltstones, or tuffaceous sediments) serve as high strain-rate loci during deformation. Pervasive "C" fabrics and near-ubiquitous development of pressure shadows around sulphides attest to the role that such units play as foci for shear zones. Fringes of blocky quartz and plate-like overgrowths of phyllosilicates

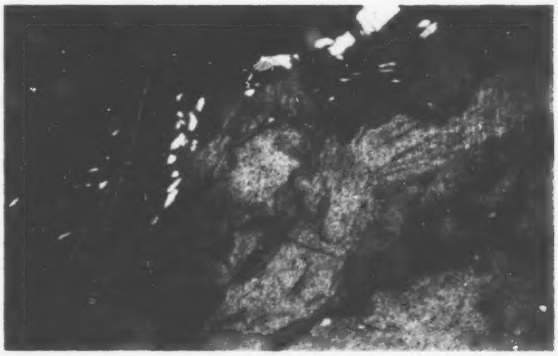

Photo 262.1g. *Chlorite and white micas in selvage between wallrock (upper left) and vein quartz (lower right). Many analyses of sheet silicates (Figures 262.1, 262.2) were made across selvage on right hand side of photograph. Sample is from Hoyle Pond. Photo width is ≅1.5 mm.*

Photo 262.1h. *Same sample as Photo 262.1g. Some gold is located in fractures at base of curved tourmaline (T) lath growing from sheet silicate selvage (SSS) between wallrock (WR) and quartz vein (vein quartz (VQ) at lower right). Photo width is ≅1.5 mm.*

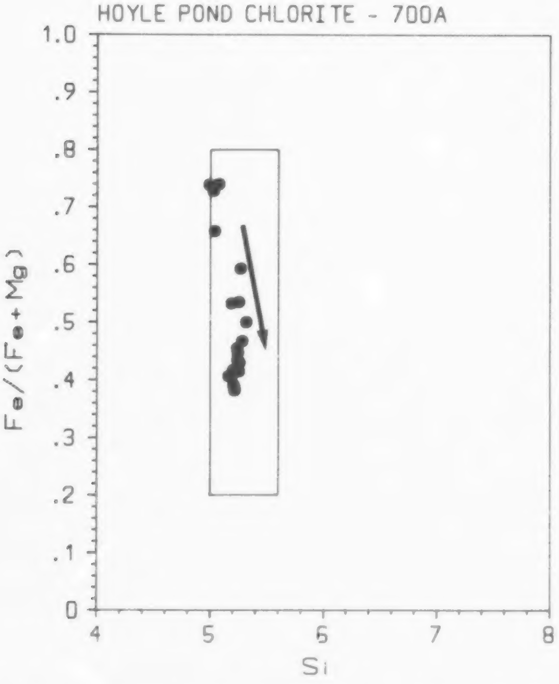

Figure 262.1. *Electron microprobe analyses of chlorite in sheet silicate, carbon tourmaline selvage showing extreme enrichment in native gold. The gold is almost entirely within the thin selvage separating micaceous wallrock from barren vein quartz. It is often concentrated on either side of the selvage, commonly near the wallrock margin, in close association with the chlorite and mica. Chlorite adjacent to the gold is Fe-rich; the general compositional variation with increasing distance from gold grains (and, overall, from wallrock to interior vein quartz) is shown by the arrow in Figure 262.1. Nineteen out of twenty analyses plot in the ripidolite field, indicated by the box (after Deer et al. 1966). All Fe determined as FeII. On this basis, total Fe (FeO) variation is from 20 to 35 weight percent.*

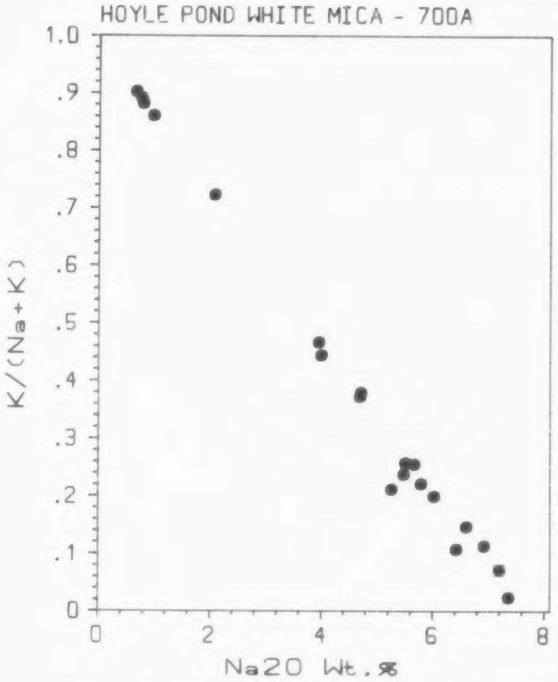

Figure 262.2. *Electron microprobe data for white micas coexisting with the chlorite of Figure 262.1. A plot highlighting the variation in alkali content. Sodic hydromuscovite (some of the coarser mica in the selvage) plots at the top left; five analyses of one large grain showing significant inhomogeneity. The remaining fifteen analyses indicate relatively sodic micas, widely variable from near end-member paragonite to an intermediate composition; the gap in the 2 to 4 weight percent Na_2O range corresponds to the miscibility gap between muscovite and paragonite noted by Deer et al. (1962, p.31-34, p.218-219). Thirteen of these analyses are from finer, curving flakes of mica in the selvage; the other two are from two of the larger mica laths in the adjacent wallrock.*

are phenomena related to well developed pressure shadows of fibrous quartz.

The following phenomena are observed in carbonaceous metasediments sheared in "the ductile to semi-brittle" regime, under greenschist facies metamorphism (definitions of McClay 1984, p.138; Rutter 1986):

- development of crenulation cleavage
- fracturing and remobilization of fine-grained carbonaceous matter
- prominent pressure shadows

These features can be interpreted in terms of progressive simple shear. While late Mesozoic to Tertiary-age examples (southwestern United States) are often extremely fine grained, the Archean analogues (Abitibi belt) are mineralogically more tractable. In the latter, greenshist assemblages predominate, and there is evidence of complementary brittle behaviour (such as subhorizontal quartz sheets north of the "quartz dike" sheared ore zone at Owl Creek). Pyrite is commonly fractured, c.f. the ductile behaviour possible at higher temperature-pressure (Cox *et al.* 1981). Small open fractures constitute a late development at Owl Creek, cutting carbonaceous fractures in vein quartz, without necessarily displacing the carbon within.

A large grab sample from the dumps at the old Kenilworth (Naybob) Mine, Timmins, provides a good example of the contrast between a carbonaceous sediment and a competent porphyry which intrudes it (Photo 262.2). Comparison of porphyry and siltstone suggests that the former has the potential to record and preserve a set of fabrics of progressive deforma-

Photo 262.2. *Felsic porphyry within carbonaceous pyritic siltstone, from the old Kenilworth Mine, Ogden Township, Timmins area.*

tion, whereas a hand specimen of the fine-grained, incompetent rock may display traces of only (the latest) one or two events. Brecciation is not usually prominent in the most carbonaceous zones, probably because the strongly-laminated host sediments appear to spall off into intruding quartz veins, and are rapidly disaggregated. The best example of a carbonaceous breccia yet examined in this study is an anthraxolite from the Sudbury Basin, which is a Proterozoic vein-hosted occurrence within highly C-rich metasediments, unrelated to gold mineralization. This can be ascribed to the coarser structure and higher ordering (inferred from moderately high reflectivity and physical coherence) displayed by the carbonaceous component (Photo 262.3a). Given the nature of the host sediments (Arengi 1977), an origin by remobilization and concentration of organic carbon seems plausible.

A transect from relatively undisturbed country rock into a shear zone can reveal some or all of the following features, all displayed in the east wall at Owl Creek:

1. Original (S_0) lamination, sometimes truncated by coarse, euhedral, porphyroblastic pyrite, with variable development of primary (S_1) and secondary (S_2, crenulation) cleavages. S_1 may be preserved in inclusions within porphyroblastic pyrite.
2. Within the shear zone, there may be a ubiquitous development of pressure shadows around rigid "shelters", commonly pyrite crystals (Photo 262.3b). Fibrous quartz in such shadows locally achieves rock-forming proportions (>5%) in the sediments immediately south of the Owl Creek ore zone.
3. Transposition of the S-fabric into a progressively more shear-aligned C-fabric. Evidence of recrystallization of the coarser crystals, especially quartz. As mentioned earlier, the ease with which fine-grained carbonaceous rocks respond to deformation is such that more brittle materials, including massive vein quartz, broaden the spectrum of preserved structures.

Crenulation cleavage is locally well developed. It can develop from initial buckling instabilities by pressure solution or mineral migration. Sometimes the crenulation is subordinate to microfaulting developed parallel to the axial planes of the crenulation folding (Hobbs *et al.* 1976, p.218-221). Such fractures, when developed in carbonaceous rocks, appear to fill up with remobilized fine carbon. Carbonaceous fractures may be planes of movement which truncate earlier structures (Photo 262.3c). This is reminiscent of descriptions of stylolites (Heald 1959), a term adopted in the present context (pressure solution in sediments tends to localize along partings rich in clay or in carbonaceous material). Solution cleavage may redistribute carbon along the newly-formed surfaces (Beutner 1978, p.20). Photo 262.3c illustrates a pro-

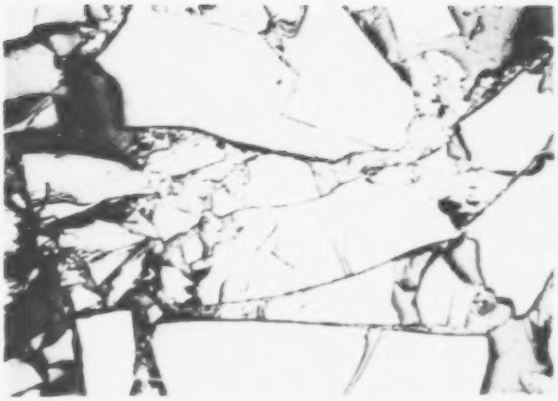

Photo 262.3a. *Anthraxolite hydrocarbon breccia with quartz matrix (from Balfour Township, western Sudbury Basin). Photo width is ≅3 mm.*

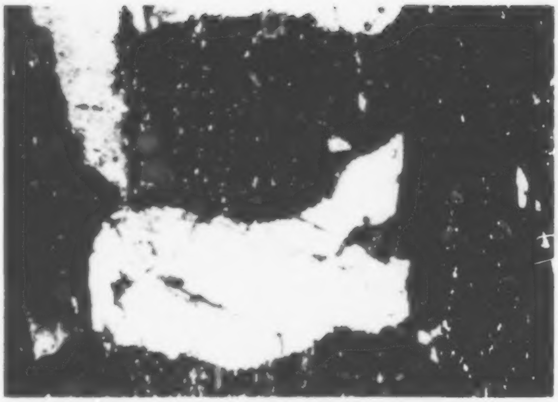

Photo 262.3c. *Deformed carbonaceous metasediment, carbonate veining truncated by slip on carbonaceous microshear (from Hoyle Pond). Photo width is ≅5 mm. Crossed polars.*

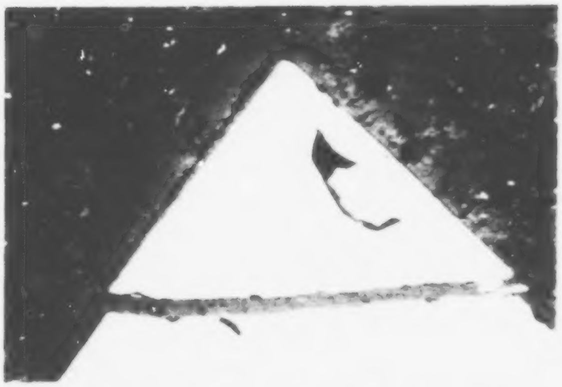

Photo 262.3b. *Quartz pressure shadow on fractured pyrite (from Owl Creek). Photo width is ≅1 mm.*

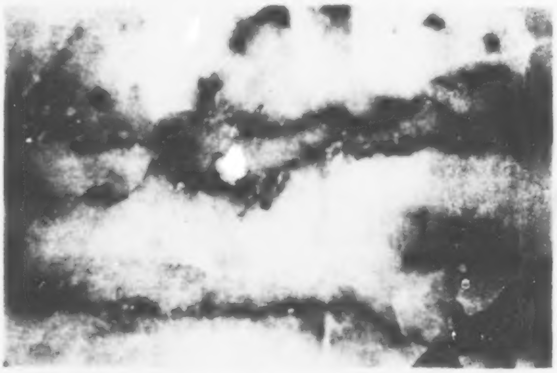

Photo 262.3d. *Stylolitic fractures with native gold, fine-grained carbon, tourmaline and hydromicas (from Hoyle Pond). Photo width is ≅50 mm.*

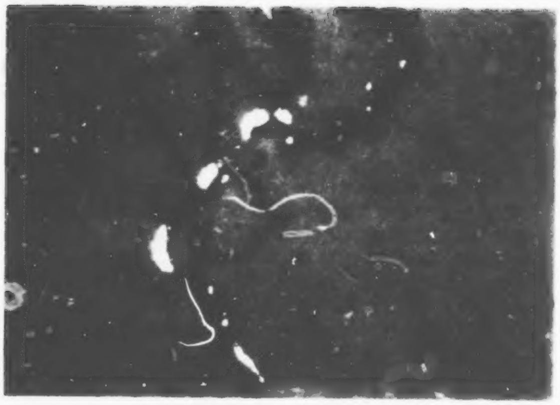

Photo 262.3e. Photomicrograph of same sample as Photo 262.3d; note restriction of gold to immediate proximity of the fracture. Photo width is ≅0.2 mm).

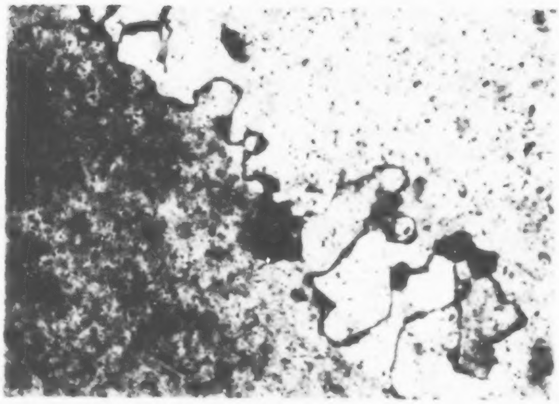

Photo 262.3g. Subgrain development on quartz crystal margins within altered and deformed metavolcanics for a sample from Kerr Addison Mine (compare these sutured boundaries with the carbonaceous gold-bearing fractures illustrated in Photos 262.3d, and 262.3e). Photo width is ≅ 1.0 mm. Crossed polars.

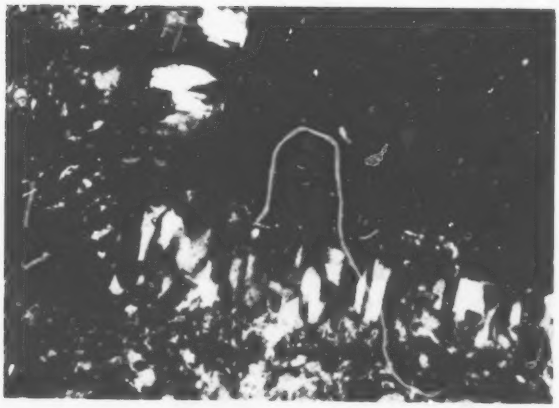

Photo 262.3f. Large pressure shadows of quartz with subsidiary carbonate on pyrite in wacke. Same sample as Photos 262.1c, 262.1d, and 262.3b. Photo width is ≅ 1 mm. Crossed polars.

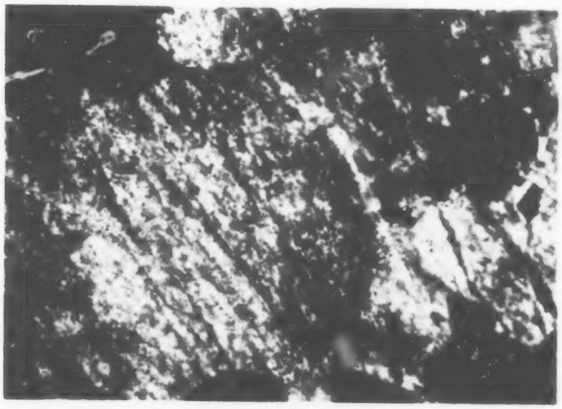

Photo 262.3h. Vein quartz crowded with carbonaceous specks and fluid inclusions, from Owl Creek. Photo width is ≅0.5 mm). Crossed polars.

cess which may result in a highly-deformed rock where the early features of the protolith are obliterated by strong metamorphic segregation (Robin 1979). Such a lithology, from the Uchi Lake Belt, marked by intense penetrative fabric high carbon contents, strong grain size reduction, and anomalous values of "invisible gold" (F.T. Manns, Orofino Resources Limited, Toronto, personal communication, 1986) is currently under investigation. Pressure solution cleavage is very common in such zones. The dark fracture-fills ("seams") are thought to be insoluble material left after dissolution of quartz, carbonate, or other, more mobile, phases. Such solution can lead to local volume reduction, although the large amounts of nearby quartz veining in some localities suggests rapid redeposition. Tectonic stylolites "are probably initiated perpendicular to the maximum compressive tectonic stress" (Ramsay and Huber 1983, p.52). Hence they may cut and displace related veins whose substance has been fed by the very material exiting along the stylolite channelways (Ramsay and Huber 1983 and Photo 262.3c). An example of a stylolitic fracture set (Hoyle Pond Mine, Timmins) carrying abundant gold within vein quartz is shown in Photos 262.3d and 262.3e.

Pressure shadows may achieve large relative and absolute dimensions, exceptional cases having quartz fibres (oriented in the direction of minimum compressive stress) several times longer than the width of the central pyrite, and with the "wings" around the nucleus up to 2 cm total width (seen at Owl Creek, in the ore zone). They mostly occur surrounding brittle pyrite euhedra. Pressure shadows are filled by those phases remobilized under the prevailing conditions. They may be simple (usually quartz, of variable fibrous to equant habit) or composite with layers of carbonate or chlorite in addition to quartz. Variations in composition and/or fibre orientation during growth attest to the changing conditions at their formation (Photo 262.3f). These features may also contain minor fine-grained (comminuted?) pyrite and sometimes chalcopyrite (Melling *et al* 1985, p.142). Such shadows are well known. Particularly good examples of fibrous shadows around coarse (~100 μm) framboidal pyrite grains have been documented in the Ordovician slates of New Jersey (Beutner and Diegel 1985).

Shear zone fabrics may be prominently displayed in relatively competent lithologies, such as intrusive felsic porphyries (Photo 262.2). Progressive recrystallization is recorded in "mortar" textures, i.e. by subgrain development visible along intricately sutured grain boundaries in vein quartz (Photo 262.3g). Such structures may develop along zones rich in fluid inclusions (Photo 262.3h), an illustration of the hydrolytic weakening effect of Griggs and others (Griggs 1967; Blacic 1975).

CONCLUSIONS

We have demonstrated that, in the case of the sites examined, reduced carbonaceous lithologies play both a structural and a chemical role in the deposits concerned. Among the main findings are the following:

1. The rocks which contain reduced carbon as a prominent macroscopic component carry less carbon ("graphite") than their appearance would suggest—commonly from <1 to 10 (estimated modal or analyzed weight) percent.
2. Field and microstructural relations are compatible with a remobilized sedimentary origin for the bulk of the carbon.
3. Carbonaceous rocks serve as foci for shearing during episodes of deformation; they are favourable sites for high fluid flow. It has been demonstrated that shear zones are critical features in Archean gold deposits in Ontario (Hugon and Schwerdtner 1984).
4. On a microscopic scale carbonaceous matter provides a suitable environment for deposition of gold.
5. Carbonaceous zones are rich in volatiles, as attested by the occurrence of two or more of carbonaceous matter, chlorite, hydromicas, and tourmaline, and by the apparent elevation of Cl levels within the carbon (Wilson and Rucklidge 1984). Further mineralogical clues to the nature of the vein fluids and to the prevailing conditions at the time of gold deposition are the Fe-rich nature of the chlorite, the sodic compositions of the micas, and the relative scarcity of secondary albite.
6. High levels of arsenic commonly accompany gold-related carbonaceous lithologies. Sometimes phases such as realgar, enargite, or tetrahedrite contain the As, but lower levels are accommodated (in a manner as yet undetermined) into pyrite.

In the concluding phase of this study we will:

1. Further characterize the gold-related mineralogy, principally by electron microprobe work.
2. Search in appropriate samples for micron-scale gold and try to determine the situation of arsenic in pyrite (by electron microscopy).
3. Obtain geochemical data on small-scale (by accelerator mass spectrometry) and larger (by neutron activation) samples, possibly incorporating a study of separates, with emphasis on the chemistry of the carbon itself. The constraints offered by fluid inclusion work will become valuable at this point, because we have, so far, no firm data concerning possible sources and transportation mechanisms for the gold, although the fluid from which the gold was deposited was probably quite rich in As, Fe, and a mixture of volatiles in unknown proportions.
4. Make a concentrated synthesis of our data on the two mines in Hoyle Township, update an earlier review (Wilson 1985), and relate the findings to an overview of carbonaceous gold deposits. Sites in Ontario sampled for this study are located on the sketch map (Figure 262.3).

ACKNOWLEDGMENTS

Generous assistance with sample collection, and many subsequent discussions on the general geology and on the results of this study were provided by the

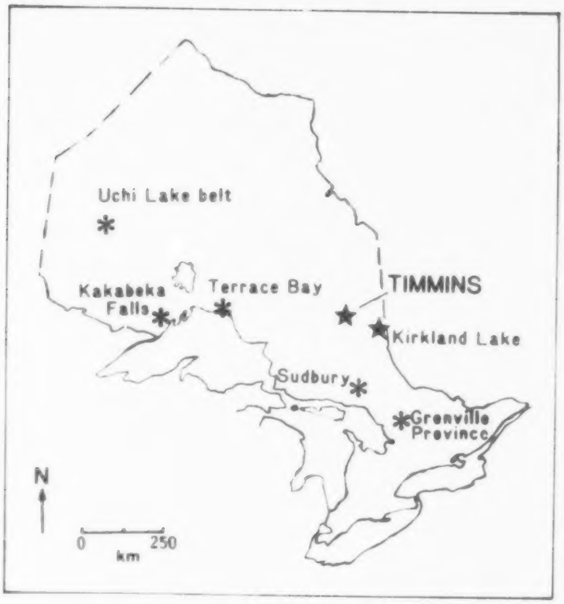

Figure 262.3. *Sketch map indicating provenance of material examined in this study. The localities are of two types. ★ denotes variable content of carbonaceous ore and/or other carbonaceous rocks in gold producers past and present. In the Timmins area, besides Owl Creek and Hoyle Pond, these include the Hollinger and McIntyre Mines (now the Timmins and Schumacher Properties), and the Kenilworth (Naybob) Mine. "Graphite" has also been reported (and samples examined) from the Kerr Addison Mine in Virginiatown, the Macassa and Lake Shore Mines in Kirkland Lake, and the Omega Property in the Larder Lake area. ✱ denotes carbonaceous sediments in other locations. Only the Uchi Lake Belt site has significantly anomalous gold; as far as is known, the rest are below 200 ppb, the majority probably at "normal" (ppb) levels. These include shales and "carbonaceous iron formation" from Kakabeka Falls and Terrace Bay areas, and Proterozoic sediments from the west side of the Sudbury Basin.*

Kidd Creek Mines staff, particularly by mineralogist J.D. Scott. Other suppliers of samples, including T. Kinley (Montana State University, Bozeman; Red Pine suite) have helped provide a wider perspective on the subject. Thanks are also due to other mining firms and individuals, too numerous to mention here, who provided material and/or permission for site visits. The technical staff of the Geology Department (University of Toronto) and Geoplastech Incorporated (Toronto) prepared many thin and polished sections. C. Cermignani (University of Toronto) ably assisted with electron microprobe work. Photographic facilities made available by the Ontario Geological Survey and the Royal Ontario Museum are appreciated. Finally, discussions and practical assistance from A. James Macdonald, Janet S. Springer, and others (Mineral Deposits Section, Ontario Geological Survey, Toronto) and W.D. Hicks (Geoscience Laboratories, Ontario Geological Survey, Toronto) are gratefully acknowledged.

REFERENCES

Akright, R.L., Radtke, A.S., and Grimes, D.J.
1969: Minor Elements as Guides to Gold in the Roberts Mountains Formation, Carlin Gold Mine, Eureka County, Nevada; Quarterly of the Colorado School of Mines, Volume 64, Number 1, p.49-66.

Arengi, J.T.
1977: Sedimentary Evolution of the Sudbury Basin, Ontario; Unpublished M.Sc. Thesis, University of Toronto, 141p.

Auger, P.E.
1941: Zoning and District Variations of the Minor Elements in Pyrite of Canadian Gold Deposits; Economic Geology, Volume 36, p.401-423.

Barton, P.B.
1969: Thermochemical Study of the System Fe-As-S; Geochimica et Cosmochimica Acta, Volume 33, p.841-857.

Beutner, E.C.
1978: Slaty Cleavage and Related Strain in Martinsburg Slate, Delaware Water Gap, New Jersey; American Journal of Science, Volume 278, p.1-23.

Beutner, E.C., and Diegel, F.A.
1985: Determination of Fold Kinematics from Syntectonic Fibers in Pressure Shadows, Martinsburg Slate, New Jersey; American Journal of Science, Volume 285, p.16-50.

Blacic, J.D.
1975: Plastic-Deformation Mechanisms in Quartz: the Effect of Water; Tectonophysics, Volume 27, p.271-294.

Brammall, A., Leech, J.G.C., and Bannister, F.A.
1937: The Paragenesis of Cookeite and Hydromuscovite Associated with Gold at Ogofau, Carmarthenshire; Mineralogical Magazine, Volume 24, p.507-520.

Brisbin, D.I.
1984: The Owl Creek Mine, p.108-111 *in* Geological Association of Canada-Mineralogical Association of Canada, Field Trip Guidebook 14, edited by H.L. Gibson, S.D. Walker, and P.R. Coad.

Clark, L.A.
1960: The Fe-As-S System: Phase Relations and Applications; Economic Geology, Volume 55, p.1345-1381.

Colvine, A.C., Andrews, A.J., Cherry, M.E., Durocher, M.E., Fyon, A.J., Lavigne, M.J., Macdonald, A.J., Marmont, S., Poulsen, K.H., Springer, J.S., and Troop, D.G.
1984: An Integrated Model for the Origin of Archean Lode Gold Deposits; Ontario Geological Survey, Open File Report 5524, 98p.

Cox, S.F., Etheridge, M.A., and Hobbs, B.E.
1981: The Experimental Ductile Deformation of Polycrystalline and Single Crystal Pyrite; Economic Geology, Volume 76, p.2105-2117.

Deer, W.A., Howie, R.A., and Zussman, J.
1962: Rock-Forming Minerals, Volume 3, Sheet Silicates; Longman, London, 270p.
1966: An Introduction to the Rock-Forming Minerals; Longman, London, 528p.

Downes, M.J., Hodges, D.J., and Derweduwen, J.
1984: A Free Carbon- and Carbonate-Bearing Alteration Zone Associated with the Hoyle Pond Gold Occurrence, Ontario, Canada; p.435-448 *in* Gold '82: The Geology, Geochemistry and Genesis of Gold Deposits, edited by R.P. Foster, A.A. Balkema, Rotterdam.

Frater, K.M.
1985: Mineralization at the Golden Grove Cu-Zn Deposit, Western Australia. I: Premetamorphic Textures of the Opaque Minerals; Canadian Journal of Earth Sciences, Volume 22, p.1-14.

Griggs, D.
1967: Hydrolytic Weakening of Quartz and Other Silicates; Geophysical Journal of the Royal Astronomical Society, Volume 14, p.19-31.

Heald, M.T.
1959: Significance of Stylolites in Permeable Sandstones; Journal of Sedimentary Petrology, Volume 29, p.251-253.

Hobbs, B.E., Means, W.D., and Williams, P.F.
1976: An Outline of Structural Geology; Wiley, 571p.

Hugon, H., and Schwerdtner, W.M.
1984: Structural Signature and Tectonic History of Deformed Gold-Bearing Rocks in Northwestern Ontario; Grant 149, p.164-176 *in* Geoscience Research Grant Program, Summary of Research 1983-1984, edited by V.G. Milne, Ontario Geological Survey, Miscellaneous Paper 121, 252p.

Ilchik, R.P., Brimhall, G.H., and Schull, H.W.
1986: Hydrothermal Maturation of Indigenous Organic Matter at the Alligator Ridge Gold Deposits, Nevada; Economic Geology, Volume 81, p.113-130.

Joralemon, P.
1951: The Occurrence of Gold at the Getchell Mine, Nevada; Economic Geology, Volume 46, p.267-310.

Love, L.G., and Amstutz, G.C.
1966: Review of Microscopic Pyrite; Fortschritte der Mineralogie, Volume 43, p.273-309.

Lowe, D.R., and Byerly, G.R.
1986: The Rock Components and Structures of Archean Greenstone Belts: an Overview; p.9-13 *in* Workshop on the Tectonic Evolution of Greenstone Belts, Lunar and Planetary Institute, Houston, Contribution 584, Supplement.

Ludden, J., Hubert, C., and Gariepy, C.
1986: The Tectonic Evolution of the Abitibi Greenstone Belt of Canada; Geological Magazine, Volume 123, p.153-166.

McClay, K.R.
1984: Mapping Geological Structures; Geological Association of Canada-Mineralogical Association of Canada, Short Course 2, Part 1, 215p.

McKinstry, H.
1963: Mineral Assemblages in Sulfide Ores: the System Cu-Fe-As-S; Economic Geology, Volume 58, p.483-505.

Melling, D.R., Watkinson, D.H., Poulsen, K.H., and Chorlton, L.B.
1985: The Geological Setting and Genesis of the Cameron Lake Gold Deposit; Grant 193, p.136-150 *in* Geoscience Research Grant Program, Summary of Research 1984-1985, edited by V.G. Milne, Ontario Geological Survey, Miscellaneous Paper 127, 246p.

Olsen, P.E.
1985: Distribution of Organic-Matter-Rich Lacustrine Rocks in the Early Mesozoic Newark Supergroup; p.61-64 *in* Proceedings of the 2nd United States Geological Survey Workshop on the Early Mesozoic Basins of the Eastern United States, edited by G.R. Robinson and A.J. Froelich, United States Geological Survey, Circular 946, 147p.

Radtke, A.S.
1985: Geology of the Carlin Gold Deposit, Nevada; United States Geological Survey, Professional Paper 1267, 124p. Plus map folder.

Ramdohr, P.
1969: The Ore Minerals and Their Intergrowths; English Translation of Third Edition, Pergamon Press, 1174p.

Ramsay, J.G., and Huber, M.I.
1983: The Techniques of Modern Structural Geology, Volume 1: Strain Analysis; Academic Press, 307p.

Robin, P.Y.F.
1979: Theory of Metamorphic Segregation and Related Processes; Geochimica et Cosmochimica Acta, Volume 43, p.1587-1600.

Rosenberg, P.E.
1967: Subsolidus Relations in the System $CaCO_3$-$MgCO_3$-$FeCO_3$ between 350C and 550C; American Mineralogist, Volume 52, p.787-796.

Rucklidge, J.C., Wilson, G.C., Stumpfl, E.F., and Ballhaus, C.G.
1985: Analysis of Pt-Associated Graphite by Accelerator Mass Spectrometry; Canadian Mineralogist, Volume 23, p.313-314.

Rutter, E.H.
1986: On the Nomenclature of Mode of Failure Transitions in Rocks; Tectonophysics, Volume 122, p.381-387.

Rytuba, J.J.
1985: Geochemistry of Hydrothermal Transport and Deposition of Gold and Sulfide Minerals in Carlin-Type Gold Deposits; p.27-34 *in* Geologic Characteristics of Sediment- and Volcanic-Hosted Disseminated Gold Deposits—Search for an Occurrence Model, edited by E.W. Tooker, United States Geological Survey, Bulletin 1646, 150p.

Smith, T.J., and Kesler, S.E.
1985: Relation of Fluid Inclusion Geochemistry to Wallrock Alteration and Lithogeochemical Zonation at the Hollinger-McIntyre Gold Deposit, Timmins, Ontario, Canada; Canadian Institution of Mining and Metallurgy, Bulletin, Volume 78, Number 876, p.35-46.

Springer, J.S.

1983: Invisible Gold: p.240-250 *in* The Geology of Gold in Ontario, edited by A.C. Colvine, Ontario Geological Survey, Miscellaneous Paper 110, 278p.

1984a: Active Carbon in Archean Rocks and its Effect on Gold Concentration, Geological Association of Canada/Mineralogical Association of Canada, Program with Abstracts, Volume 9, 107p.

1984b: Enrichment of Gold by Sulphides and Carbon in Archean Gold Ores of Ontario: Geological Society of America, Abstracts with Programs, Volume 16, 665p.

Volborth, A., and Housley, R.M.

1984: A Preliminary Description of Complex Graphite, Sulfide, Arsenide, and Platinum-Group Element Mineralization in a Pegmatoid Pyroxenite of the Stillwater Complex, Montana, USA: Tschermaks Mineralogische und Petrologische Mitteilungen, Volume 33, p.213-230.

Weissberg, B.G.

1965: Getchellite, $AsSbS_3$, a new Mineral from Humboldt County, Nevada; American Mineralogist, Volume 50, p.1817-1826.

Wells, J.D. and Mullens, T.E.

1973: Gold-Bearing Arsenian Pyrite Determined by Microprobe Analysis, Cortez and Carlin Gold Mines, Nevada: Economic Geology, Volume 68, p.187-201.

Whitehead, R.E.S., Davies, J.F., Cameron, R.A., and Duff, D.

1981: Carbonate, Alkali, and Arsenic Anomalies Associated with Gold Mineralization, Timmins Area: Grant 30, p.318-333 *in* Geoscience Research Grant Program, Summary of Research 1980-1981, edited by E.G. Pye, Ontario Geological Survey, Miscellaneous Paper 98, 340p.

Wilson, G.C.

1985: The Role of Free Carbon in Metallic Mineral Deposits; University of Toronto IsoTrace Laboratory, Report 1985-1, 58p.

1986: A Petrographic Study of Carbonaceous Rocks in Gold Deposits; Geological Association of Canada/Mineralogical Association of Canada, Program with Abstracts, Volume 11, 145p.

Wilson, G.C., and Rucklidge, J.C.

1984: Mass Spectrometric Studies of Carbonaceous Materials from Archean Gold Deposits: Geological Society of America, Abstracts with Programs, Volume 16, 696p.

Wilson, G.C., Rucklidge, J.C., Kieser, W.E., and Beukens, R.P.

1984: Development of an Ion Microprobe Stage for Accelerator Mass Spectrometry; Nuclear Instruments and Methods, Volume B5, p.200-203.

Grant 265 Metal Uptake By Microorganisms: Retardation of Toxic Heavy Metal Dispersion From Tailing Environments, Elliot Lake, Timmins, and Sudbury

H. Mann[1], F.G. Ferris[1], T.J. Beveridge[2], W.S. Fyfe[1], R. Humphrey[2], and K. Tazaki[1]

[1]Department of Geology. University of Western Ontario. London

[2]Department of Microbiology. Guelph University. Guelph

ABSTRACT

The contribution of microoganisms to the retardation of heavy metal dispersion from mine tailing environments at Elliot Lake, Timmins, and Onaping has been examined. Algae samples from tailing drainage at Elliot Lake typically contained $\sim$20 ppm U. and up to a maximum of 0.13% U by weight. Other metals. which include Al, Ti, Pb, Zn, Ba, Cu, Ni, Mo, Th, Be, and Zr, were also concentrated by algae. In sediment cores taken from the Stanrock tailing impoundment at Elliot Lake, there was a high degree of coincidence between metal abundance and organic-rich layers. Examination of the organic material by analytical electron microscopy revealed heavily mineralized remains of bacteria and algae. Filamentous algae from Gilles Lake near Timmins were also analyzed for metal content. These algae, like their counterparts at Elliot Lake, contained significant quantities of metals with concentrations 10^4 to 10^6 times that of the lake water. At Onaping, in the Sudbury area, samples of a finely dispersed, black, anoxic sediment were obtained from the bottom of Lower Moose Lake, downstream from tailings impoundments. When examined by analytical electron microscopy, bacteria and their remains were prominent as templates for the formation of metal sulphides and silicates. Similar accumulations of metals by bacteria in geothermal sediments are described.

INTRODUCTION

Bacteria are widespread in nature and live in an unparalleled variety of habitats, many of which are devoid of or inimical to higher organisms. They have, for example, been isolated from concentrated brines of salt lakes, acidic mine tailings drainage, and boiling hot springs (Brock 1974, 1978). Indeed, bacteria are recognized as the most abundant and versatile of all living organisms (Ferris and Beveridge 1985).

Although all forms of life possess properties that make them of critical importance biogeochemically, bacteria are especially significant (Trudinger and Swaine 1979; Beveridge and Fyfe 1985). This uniqueness arises not only from the great diversity of environments populated by bacteria, but also because they perform many biochemical transformations relevant to geochemistry that are carried out poorly or not at all by other organisms or which are kinetically inhabited for nonbiogenic reactions. These span an entire spectrum of reactions which include the oxidation of elemental sulphur or sulphide minerals to sulphuric acid, and the reduction of sulphate to hydrogen sulphide (Trudinger and Swaine 1979). In addition, bacterial cell surfaces are typically anionic and exhibit a profound ability to bind substantial quantities of dissolved metallic ions (Beveridge and Fyfe 1985). Recent descriptions of bioconcentration of uranium by algae in tailing areas of the Elliot Lake mining district (Mann 1984) and studies of metal fixation by bacteria (Beveridge and Fyfe 1985) have prompted a further investigation of *in situ* interactions between microoganisms and metals. This association between metals and bacteria is of particular interest with regard to research on the formation of sedimentary ore deposits, the development of economically favourable secondary metal recovery methods, and environmental problems arising from heavy metal pollution.

Beveridge *et al.* (1983) have studied low temperature (circa 100°C) diagenesis of organic-rich sediments in the laboratory by mixing metal-loaded bacteria into a synthetic sediment of quartz and calcite. The sediment mixtures were monitored during the experiment by electron microscopy, selected area electron diffraction, and energy dispersive X-ray spectroscopy. The metals were initially associated with the surface of the bacteria and, as the cells aged, elements from the synthetic sediment combined with the bound metal. In this way, the bacterial cells served as discrete nucleation sites for the formation of authigenic mineral phases which are sometimes found in sedimentary ore deposits.

The discovery and description of spectacular growths of algal mats in tailings areas of the Elliot Lake uranium mining district (Mann 1984; Mann and Fyfe 1985) prompted further investigation of the interaction of microorganisms with heavy metal charged effluent from tailings environments. Acid seepage waters at Elliot Lake containing high concentrations of dissolved uranium, along with other heavy metals, provides the opportunity to examine the response of microorganisms to those elevated levels of toxic metals in a quasi-natural habitat.

We report here that bacteria and algae growing in drainage arising from mine tailing areas at Elliot Lake, Timmins, and Onaping, not only concentrate a wide range of metals but also promote the formation of distinct authigenic mineral phases during early sediment diagenesis. Similar accumulation of metals by bacteria in geothermal sediment, which are also continuallly exposed to waters containing elevated levels of dissolved metals, is described.

ELLIOT LAKE

SETTING

The Elliot Lake district is located in Ontario, approximately 40 km north of Lake Huron's north shore and 130 km due west of Sudbury (Figure 265.1). The region has an annual precipitation of 800 mm; precipitation is fairly evenly distributed throughout the year. From November to late April, or even May, the area is snow covered. Summer temperature varies from 10°C to 30°C.

Uranium mining and milling started in the Elliot Lake area in 1954. Since then a total of 12 mines and 10 mills have been in operation, producing approximately 100 million tonnes of tailings. There are currently 3 mills operating at Elliot Lake.

The uranium ore is milled and extracted using an acid leach process. The sand-size and silt-size tailings, along with process water from the milling operations are discharged hydraulically into surface impoundments as a slurry consisting of 30% to 40% solids. The acid process water from the mill is currently neutralized with lime to a pH of 9 to 11 before discharge to the tailings impoundments. In the 1950s and 1960s, the process water was only neutralized to a pH of 6 to 7. The tailings and process water from the mills at Elliot Lake have been deposited in a variety of impoundments, most of which are presently inactive (Feenstra *et al.* 1981).

Suspended solids in slurry discharged to the tailings impoundments contain 3% to 7% pyrite (FeS_2). When the discharge of tailings and neutralized process water ceases, and the tailings are exposed to the atmosphere, pyrite oxidation can occur close to the surface, generally within 1 m. Pyrite oxidation, according to the following reaction:

$$2FeS_2 + 7O_2 + 2H_2O \longrightarrow 2Fe^{2+} + 4SO_4^{2-} + 4H^+$$

produces low pH conditions with correspondingly high concentrations of iron and sulphate in the tailing porewater (Cherry *et al.* 1980). The low pH conditions and high concentrations of iron plus sulphate also result in the release of abundant dissolved heavy metals, together with the radionuclides U, Th, Ra, and other daughter elements from the tailings solids, into tailing porewater.

This porewater moves out of the tailings impoundments either via surface water runoff or by groundwater seepage, and the aqueous toxic species could collectively have a potentially unacceptable effect on the surrounding environment (Cherry *et al.* 1980). At the present time in the Elliot Lake area, the effect of tailings impoundments on the surrounding environment is managed by collection and treatment of contaminated surface water runoff and localized groundwater seepage from the tailings impoundments (Cherry *et al.* 1980).

DISSOLVED URANIUM IN WATERS OF ELLIOT LAKE REGION

Natural Draining Upstream of Tailings

The uranium solute concentration for river, lake, and tailings waters of the Elliot Lake region is summarized from a reconnaissance study in Figure 265.1 and Table 265.1. Upstream from the Nordic tailings, natural drainage waters of Pardee and Stintson Lakes, along with their interconnecting streams, average 0.18 ppb, 0.36 ppb ± (0.25 1σ), and 0.14 ppb (± 0.17 1σ) for three sampling periods. The first figure excludes one data point of 7.0 ppb from a stream (station d) located only 200 m east of the Nordic Main tailings impoundment. This anomalous uranium value is omitted because the author suspects it may be due to groundwater contamination from tailings seepage.

Natural drainage waters of the Serpent River upstream from the Quirke tailings impoundment average 0.2 ppb (Figure 265.1). This figure is closely comparable to the data recorded for Pardee and Stintson Lakes. The grand average for dissolved uranium, taken over all natural drainage sampling stations and seasons, is 0.23 ppb (±0.19 1σ). This figure is in accord with the dissolved uranium content of rivers draining the Canadian Shield (Wenrich-Verbeek 1976, Thomson 1977), but about a factor of three less than the global average riverine aqueous uranium abundance of 0.6 ppb as estimated by Bloch (1976).

Dissolved Uranium in Tailings Waters

Uranium abundances measured in surface drainage waters carrying the seepage effluent from tailings impoundments to discharge treatment points is reported in Table 265.1. Tailings discharge waters arise both from the slow dewatering of tailings slurry, as well as from through-flow of precipitation landing on the tailings surface (Moffett and Tellier 1978; Cherry *et al.* 1980).

Levels of dissolved uranium in tailings drainage ditch waters exhibit extreme variations, but all are high, as might be expected, when compared to background in natural waters, as discussed above. Values of 56 ppb (±3.5 1σ) to 155 ppb (+7 1σ) were recorded for effluent of the Nordic Main tailings at sampling stations E through F (Mann 1984; Figure 265.1). The drainage ditch water values are 240 and 670 times the background aqueous uranium of 0.23 ppb.

For the Westarm tailings seepage waters, uranium levels of 63 (station J) to 580 ppb (station K) were recorded. Corresponding figures for the Stanrock tailings of the Denison Mine are 80 (station P) to 660 ppb (Station R). The grand averages of dissolved uranium in tailings discharge waters, taken over all sampling stations and seasons are 85 ppb (±62 1σ) [Nordic Main], 230 ppb (±230 1σ) [Westarm], and 273 ppb (±215 1σ) [Stanrock].

The uranium levels in the tailings drainage waters located 300 m southeast of the Stanrock impoundment, and receiving the Stanrock discharge, is only 16.5 ppb. This pronounced decrease from 660 ppb in Stanrock discharge is attributable to the efficacy of the intervening treatment plant (Mann 1984; Figure 265.1).

Levels of dissolved uranium in tailings effluent, as reported above, are fully commensurate with the results of Moffett and Tellier (1978). These authors quoted average uranium solute concentrations of 247, 8840, and 270 ppb U for low acid class, high acid class, and surface effluent waters, respectively.

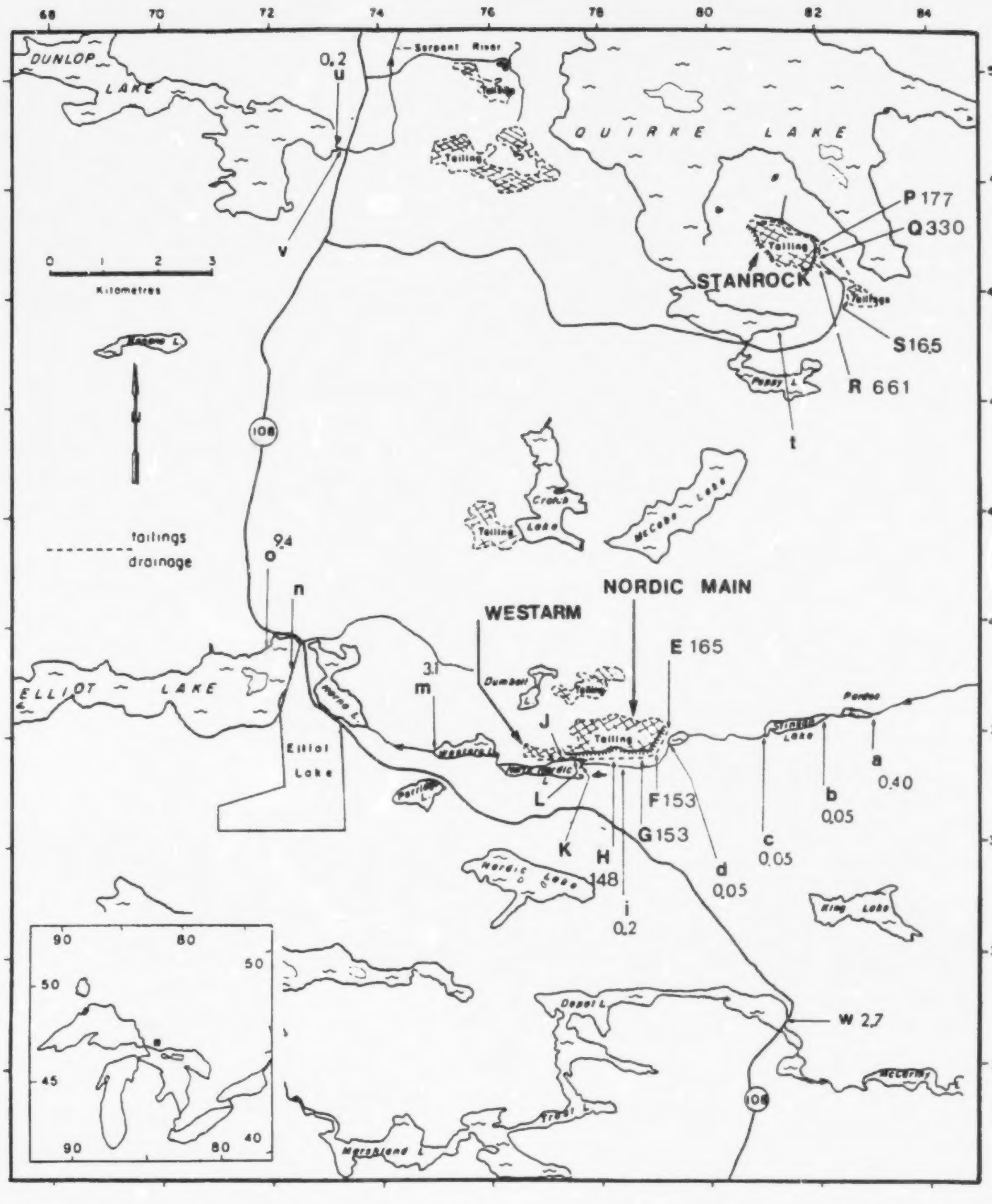
68
70
72
74
76
78
80
82
84
50
48
46
44
42
40
38
36
34
32
DUNLOP LAKE
0.2
u
Serpent River
Tailings
Tailing
QUIRKE LAKE
P 177
Q330
STANROCK
Tailing
Tailings
S16.5
R 661
Pecors L.
t
v
0 1 2 3
Kilometres
108
Crotch Lake
Tailing
McCabe Lake
tailings
drainage
9.4
o
n
NORDIC MAIN
WESTARM
E 165
3.1
m
Dunlop
Tailing
ELLIOT LAKE
Horne L.
Elliot Lake
Westarm L.
J
Tailing
Nordic L.
L
K
H
148
i
0.2
F153
G153
d
0.05
c
0.05
b
0.05
a
0.40
Pardee
Lake
Nordic Lake
King Lake
W 2.7
Depot L.
Marshland L.
Trout L.
McCarthy
106
90
80
50
45
40

Figure 265.1. Uranium solute concentration of river, lake, and tailings waters of the Elliot Lake district, with sample localities indicated. Light numerals are representative data for U in natural waters, bold face for tailings waters (U in ng/g = ppb).

TABLE 265.1. SOLUTE ABUNDANCES OF ELEMENTS IN WORLD RIVER WATER, TOGETHER WITH REPRESENTATIVE DATA FOR THE NORDIC AND STANROCK TAILINGS DISCHARGE. RESULTS FOR ALGAE REFERENCED TO DRY WEIGHT (ALL FIGURES IN ng/g).

	World River Water	Nordic tailings	Stanrock tailings	Euglena I	Euglena II	Euglena III
Ca	21 000	101 000	94 000	712 000	861 000	16 440 000
Si	9 000	3 970	60	104 000	148 000	1 790 000
Na	9 000	10 900	11 300	92 800	148 000	2 853 000
Mg	5 000	13 900	20 100	1 109 000	1 473 000	11 300 000
K	1 400	4 220	3 070	712 000	811 000	9 100 000
Fe	483	12 860	350 000	5 000 000	65 000 000	66 000 000
Al	332	4 180	25 530	2 080 000	1 930 000	18 000 000
Sr	62	150	90	3 990	4 070	63 000
Ba	27	70	10	14 800	12 200	134 000
Zn	21	220	2 470	150 000	48 700	210 600
P	19.5	30	440	903 000	3 170 000	4 198 000
Mn	13	300	2 060	36 300	45 000	414 000
B	11.5	420	216	20	30	540
Cd	7	0.5	0.5	260	87	1 360
Ti	5.8	40	220	35 900	82 500	1 135 000
Ni	5.1	100	199	43 600	6 540	55 700
Cu	4.9	287	447	11 200	22 600	96 600
Pb	3.6	146	131	30 900	35 000	366 000
Cr	2.7	14	111	4 950	4 098	50 270
As	1.8					16 000
Sb	1.5					500
V	1.0	21	23	5 211	5 145	42 500
Mo	0.83	75	457	13 400	12 200	81 500
U	0.6	2 010	688	4 500	4 900	13 000
Ag	0.23	2.5	0.5	25	43	670
Se	0.2					2 700
Co	0.14	182	563	2 270	2 000	10 800
Be	0.1	0.27	2.43	50	50	400
Th	0.098	464	734	10 680	10 800	39 400
Zr	0.03	24	98	4 700	6 200	46 200
Cs	0.02					
Hf	0.008					900
W	0.004					1 000
Sc	0.004					2 600
Ta	0.0025					800
Au	0.002					88
La	0.051					55 000
Ce	0.088					80 000
Nd	0.0438					25 000
Sm	0.0355					5 900
Eu	0.0034					420
Tb	0.008					1 100
Dy	0.05					3 800
Yb	0.05					1 400
Lu	0.008					370

- Elements arranged in order of decreasing abundance in average world river water (Holland 1978), except for the rare earth elements which are in sequence of increasing atomic number.
-Note considerable uncertainties exist in published values of elements at low solute concentrations such as Hf, Ta and Lu.

TABLE 265.2. COMPILATION OF THE PRINCIPAL SUSPENDED MICROORGANISMS IDENTIFIED TO DATE IN NATURAL AND TAILINGS DRAINAGE WATERS, ELLIOT LAKE REGION.

Types of Algae

Ulothrix sp.
Spirogyra sp.
Zygnenematales sp.
Phaeaster sp.
Euglena elastica sp.
Klebsormidium sp.
Zygnema sp.
Oedogonium sp.
Tabellaria sp.
Vaucheria sp.
Rhizoclonium sp.
Cladophora sp.

Dispersion of Uranium

The downstream dispersion of anomalous uranium induced by seepage waters from tailings impoundments is mapped out for the Elliot Lake region in Mann (1984). Uranium levels of up to 115 ppb and 5609 ppb in drainage ditch water of the Nordic Main and Westarm tailings respectively, diminish to 29 ppb in North Nordic Lake, to 5 ppb in Westner Lake, and 2.4 to 9 ppb in Elliot Lake, the last one being a distance of about 6 km downstream from the tailings impoundments. In Elliot Lake (stations n, o), the mean recorded uranium level over three periods is 4.9 ppb (±3.9 1σ), and several tens of kilometres downstream from Elliot Lake, waters of the Marshland River carry 1.5 to 2.7 ppb U, still a factor of 6 to 12 times above background (Figure 265.1; Mann 1984).

The dispersion of anomalous uranium from Elliot Lake over a much wider geographical area is reported in Mann (1984). Some 50 km downstream of the tailings dams, close to where the Serpent River debouches into Lake Huron, its waters carry 1.2 to 1.9 ppb dissolved uranium. Elsewhere in the Georgian Bay-Lake Huron area, natural waters were found to possess a remarkably uniform dissolved uranium content of 0.6 ppb.

Presumably, the progressively diminishing levels of aqueous uranium in the Serpent River downstream from Elliot Lake reflect dilution of the artificial contamination spike by the addition of waters from tributaries which carry normal background levels of uranium. However, the observed trend to lower values, especially in tailings drainage ditches where algae thrive, may also result from microbiological activity, and this factor is explored in the ensuing section.

Although at its mouth the Serpent River carries twice the dissolved uranium content of Lake Huron and Georgian Bay waters, and seven times the uranium of its headwaters, this may largely be due to the fact that the bedrock of its drainage basin is intrinsically uraniferous, as well as due to the tailings water contamination. Furthermore, uranium in the Huronian sediments occurs principally as the soluble mineral uraninite, whereas uranium in granitic rocks of the Grenville Province to the east, drained by the French River, etc., is not only at a lower absolute level, but is largely hosted in relatively insoluble minerals such as allanite, monazite, and zircon.

THE METAL COMPLEMENT OF MICROORGANISMS, ELLIOT LAKE

A prominent feature of tailings waters at Elliot Lake is the presence of extensive communities of the unicellular green algae, *Euglena* sp. These algal growths are especially prolific at the immediate base of tailings dams, where the discharged seepage is most acidic, with a pH in the range 1.8 to 4.

Unlike filamentous algae in natural stagnant waters, *Euglena* was observed in relatively still waters as well as in fast flowing discharge. Communities of microorganisms dominated by *Euglena* developed either as mats carpeting the base of drainage ditches (stations F, G, J, L, P, O, Figure 265.1) or as suspensions in quieter waters such as at station H (Figure 265.1). *Euglena* communities were sampled and separated from the sandy bottom material they were attached to, for analysis of their uranium content, as described in "Analytical Methods". A complete list of microorganisms identified to date is given in Table 265.2.

Uranium concentrations in individual communities of *Euglena* ranged up to 42 300 ppb (±36 000 1σ) to 1 127 000 ppb (±1 191 000 1σ), the second figure corresponding to 0.127% U by dry weight. Average figures are reported in Table 265.1. Given such high levels of uranium, these *Euglena* presented an interesting possibility for microanalysis of uranium siting in the cells.

MULTI-ELEMENT ANALYSES OF WATERS AND MICROORGANISMS

Comprehensive chemical analyses of waters, specifically of tailings discharge, were conducted in the Elliot Lake region, with the principal objective of monitoring dissolved contaminants and their dispersion (Moffett and Tellier 1978; Cherry *et al.* 1980; Blair *et al.* 1980). However, little attention has been directed to the interaction of the biological domain with such heavy-metal-rich waters, except for the immediate problem of tailings surface restoration (Murray and Moffett 1977).

Given the magnitude of uranium uptake from tailings waters by *Euglena*, as described previously, a selected number of multi-element analyses were performed on both natural and tailing waters, as well as the microorganisms of these two aquatic environments. If *Euglena* accepted up to 0.13% uranium by weight (Mann and Fyfe 1985a, 1985b), what other dissolved chemical elements were also present in the algal cells, or what natural inorganic elements were displaced? For the tailings environment, discharge waters from the Nordic and Stanrock impoundments (station p, Figure 265.1), along with *Euglena* from Stanrock were analyzed.

Tailings drainage waters are profoundly more concentrated solutions, with respect to nearly all chemical elements, as anticipated from their low pH which supports elevated concentrations of dissolved solids in solution. Tailings waters are dominated by Fe, Ca, Si, Na, Mg, and K, presumably from hydrolysis of feldspar and ferromagnesian minerals, along with the oxidation of pyrite. The above listed elements are present at a concentration of 1 to 5 times their average world riverine abundances, excepting iron, which is 100-fold enriched. Even the relatively insoluble element aluminum is present at 36 ppm, about 100 times the world average riverine figure (Table 265.1).

Of the trace elements in solution, all are present at about 100 times their dissolved levels in typical river water, with Co, Th, and of course uranium about 1000-fold greater (Table 265.1). Measured solute abundances in the effluent are comparable to, or slightly greater than, data reported by Blair *et al.* (1980) for groundwater recovered from standpipe piezometers in the tailings vicinity.

Communities of *Euglena* thriving in tailings waters at Stanrock are compositionally dominated by Ca, K, Mg, and P, among the essential chemical components of cellular structure (Figure 265.2). In addition, the algae are characterized by systematically enhanced levels of a wide array of transition metals, and trace elements include Al (18 000), Ti (1100), Pb (370), Zn (210), Ba (134), Cu (97), Ni (56), Mo (81), Th (39), Be (400), and Zr (46) in ppm. Such elements are present at levels far in excess of their known physiological function. Even the extremely rare and/or insoluble elements such as Sc, Hf, Ta, Au, and the rare earth elements (REE) are present at significant levels of 10 to 8 x 10^5 ng/g in the algae. Although no data for REE solute concentrations in tailings waters were obtained in this study, levels considerably in excess of world average river water are anticipated in view both of the low pH and presence of REE-bearing minerals in the ore.

On a plot of concentration factor, the algae are characterized by systematic enrichments of Fe, Al, Zn, P, Ti, Pb, As, Mo, U, Se, Hf, W, Sc, Ta, and the REE at 10^4 to 10^6 times aqueous solute abundances (Figure 265.3). Systematic "lows" are recorded for Si, Sr, Cd, Ag, and Be. The largest single cause of variation in measured element concentrations is believed to be the admixture of "silt size" material. Algae were separated from their sandy substrate by means of screening through a 400 mesh sieve, but some of the fine mineral particulates inevitably pass through with the algae. We note, however, that the highest measured element concentrations in algae correspond to those samples with the smallest mineral component as determined optically and by X-ray diffraction (XRD), (Table 265.1, Euglena III), such that the inorganic fraction of 5% acts only as a dilutant to trace elements associated with the algae.

The spectacular extent of biosorption of certain aqueous toxic heavy metals by algae raises questions as to the fate of both the organic components and its associated metals in the water-sediment system. In order to explore this question, a 0.3 m depth sediment core was taken from the Stanrock tailings area, at the site where *Euglena* thrive (Figure 265.1, Photo 265.1). A prominent feature of the core is the sporadic layers of dark, organic-rich material, composed both of decayed leaves and microorganisms.

Trends in the abundance of selected elements through the 30 cm core are graphically depicted in Figure 265.4. It is clear that significant concentrations of "transition and trace" elements such as Cr, Ni, Co, Pb, and Th are incorporated into the sediment and may be specifically associated with the organic fraction.

Scanning and transmission electron microscopy (STEM) showed populations of bacteria (Photos 265.2, 265.3, 265.5) and algae (Photo 265.4) in the organic-rich layers, with heavily mineralized cell walls. EDAX analysis combined with SAED identified those as iron-rich phases, including γ-lepidocrocite, magnetite, and amorphous Fe-oxyhydroxides. Such cell wall iron concentrations are commensurate with the enhanced iron contents of algal populations as measured by bulk chemical analysis (Table 265.1). The predominance of iron associated with communities of microorganisms, as revealed both by bulk analysis of samples and EDAX analysis, makes identification of the cellular siting of the less abundant elements less tractable. This is the subject of ongoing studies.

It is clear that communities of microorganisms thriving in tailings discharge are partly responsible for biosorption of toxic heavy metals from the effluent and their incorporation into sediments, thereby retarding the dispersion of such toxic species into the natural environment.

TIMMINS

Timmins is the most important gold mining district in Canada, with more than 15 past- and present-producing mines. Continuous dewatering of the mines involves pumping several tens of millions of litres daily. Discharge waters from the Hollinger-McIntyre Mine system are debouched into Gilles Lake: prolific growths of filamentous green algae thrive in these warm ($\sim 20^{\circ}$C), mildly acidic (pH 5 to 6) waters throughout the year.

In a reconnaissance study of the metal inventory of the algae, several kilogram samples of algal communities were collected and analyzed for an array of elements as described in the section "Analytical Methods". The data are graphically portrayed in Figure 265.5 as concentration factors, referenced to both world average river waters (A) and water from Gilles Lake (B).

The algal communities were characterized by systematically enhanced concentration factors, in the range of 10^3 to 10^6, for K, Fe, Al, Ba, Zn, P, Ti, Cu, Pb, Cr, Mo, Co, Th, and Zr. Gold was concentrated by 10^4 to 10^5 over ambient levels in Gilles Lake waters, and may approach abundances of 0.9 mg/g (≅ppm) in the algae, by dry body weight. As discussed for the case of *Eugiena* at Elliot Lake, relatively high contents of K and P are anticipated, these being essential chemical components of the cellular structure. However, the absolute abundances of transition and other "trace" elements such as Co, Th, Zr, and Au itself, are far in excess of that required for known physiological function. Low concentration factors are recorded for Si, Na, Sr, B, V, Ag, and Be; this pattern appears to be common to several varieties of microorganisms, from both acidic and natural habitats (Mann 1984).

Given the observed enrichment of gold by up to 10^6 times its aqueous solute level, the potential arises for microorganism ion exchange extraction of

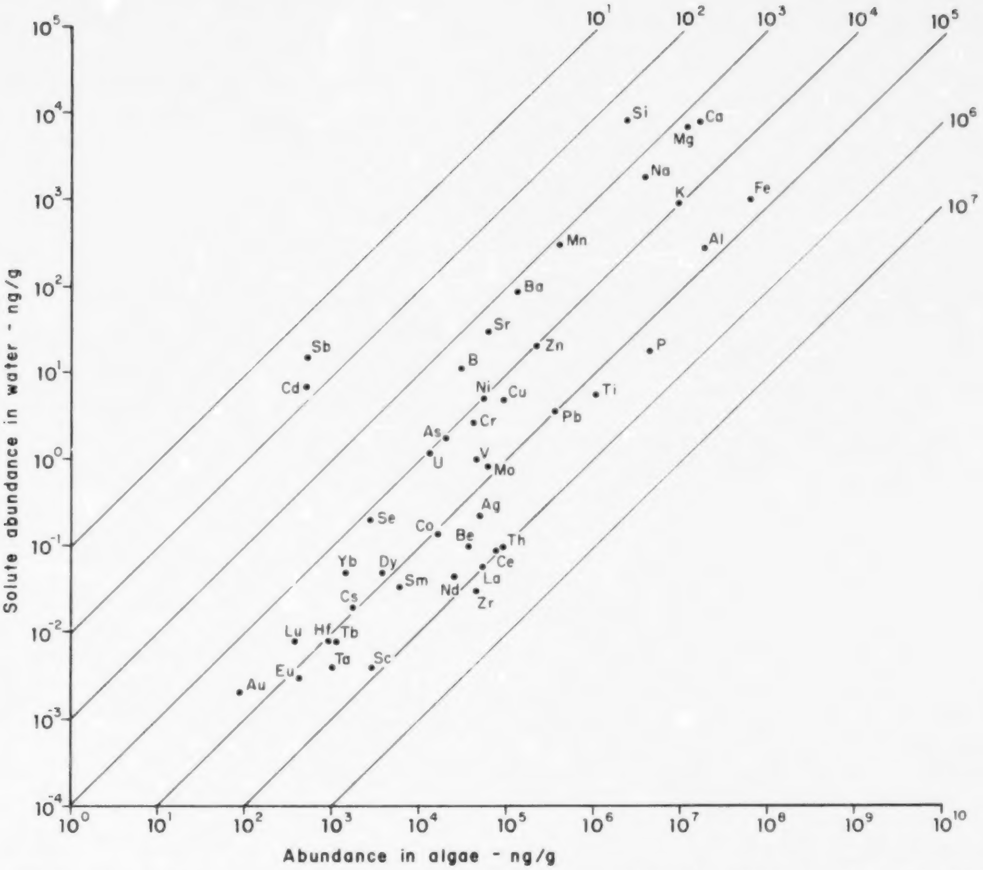

Figure 265.2. *Abundance of specified elements in Euglena sp. from the Stanrock tailings environment referenced to metal solute abundance in world average river water (see Table 265.1). The family of diagonal lines represent concentration factors. All metal abundances in ng/g.*

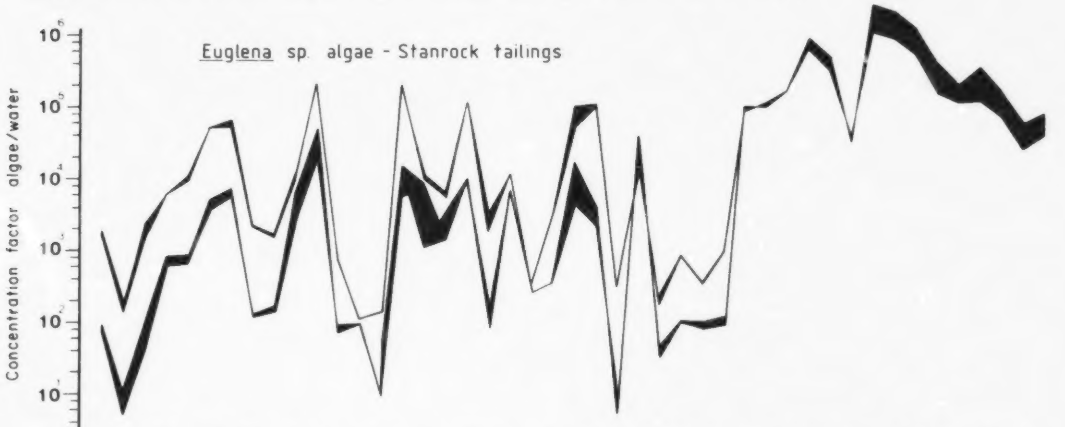

Figure 265.3. *Concentration factors for specified elements in Euglena sp. from the Stanrock tailings environment. Lower envelope referenced to solute abundances in Stanrock tailings discharge, upper envelope to world average river water (see Table 265.1).*

precious metals from process or other waters, when metal concentrations are otherwise too low for recovery by conventional methods.

LOWER MOOSE LAKE, ONAPING

To extend the evaluation of these processes in natural settings, we obtained sediment samples from Lower Moose Lake near Onaping, Ontario, and several hot springs in Yellowstone National Park, Wyoming. Immediately after the sediment samples were collected, they were placed into 5 mL metal-free plastic tubes containing 1 mL of 1% (v/v) aqueous glutaraldehyde, a fixative for electron microscopy. After the samples were returned to the laboratory, they were prepared for thin-sectioning by dehydration through an ethanol-propylene oxide series, and embedding in epoxy resin (Epon 812). Sections, approximately 150 mm in thickness, were cut using a Reichert Ultra-Cut E ultramicrotome. The thin sections were then mounted on Formvar-carbon coated copper or aluminum grids. Electron microscopy was done using a Philips EM 400T TEM/STEM which is equipped with a goniometer stage and an EDAX energy dispersive X-ray spectrometer. The electron microscope was operated at 100 KeV with a liquid nitrogen cooled anticontamination device in place at all times. Electron beam spot sizes of 100 nm or less were used for energy dispersive X-ray spectroscopy, and counts were collected for 100 seconds (live-time). Spacings in selected area electron diffraction (SAED) patterns were determined using evaporated aluminum as a standard.

The water flowing into Lower Moose Lake is acidic, and a crushed limestone slurry is used to raise the pH to near neutrality. Dissolved metals arising from the drainage of two mill tailings ponds, one of which is still active, are precipitated by the elevated pH. Consequently, metal loading in the lake sediment is high.

Our samples were obtained in areas where the water was approximately 6.0 m deep. At these sites, the sediment occurred as a finely dispersed black mud with a gritty texture and an average surficial pH of 7.3. A hydrogen sulphide odour was detected in all samples, indicating slightly reducing conditions. Although the sediment showed signs of oxidation if left exposed to air for prolonged periods of time, it remained black throughout the entire embedding procedure for electron microscopy.

In thin-sectioned material, membrane fragments derived from bacteria and the cells themselves were prominent as nucleation sites for iron and nickel sulphides. Trace amounts of copper and zinc were also detected. Although the metal sulphide accumulates usually occurred together, areas of discrete single mineral phases could be found. Typically, the metal sulphides were observed as small electron-dense aggregates which ranged from 10 to 50 nm in diameter. A thin-section profile and energy dispersive X-ray spectrum are shown in Photo 265.6.

Metal to sulphur weight ratios determined from energy dispersive X-ray point analysis indicated that metastable mackinawite (FeS_{1-x}) was the principal iron sulphate species present. These deposits did not exhibit an obvious crystal habit, and their amorphous or near amorphous state was confirmed by SAED. Neither pyrite nor its precursor, greigite, were detected (Berner 1970). In contrast, nickel sulphide phases frequently exhibited a crystalline structure (Photo 265.7). The hexagonal symmetry of the nickel sulphide microcrystals is characteristic of millerite.

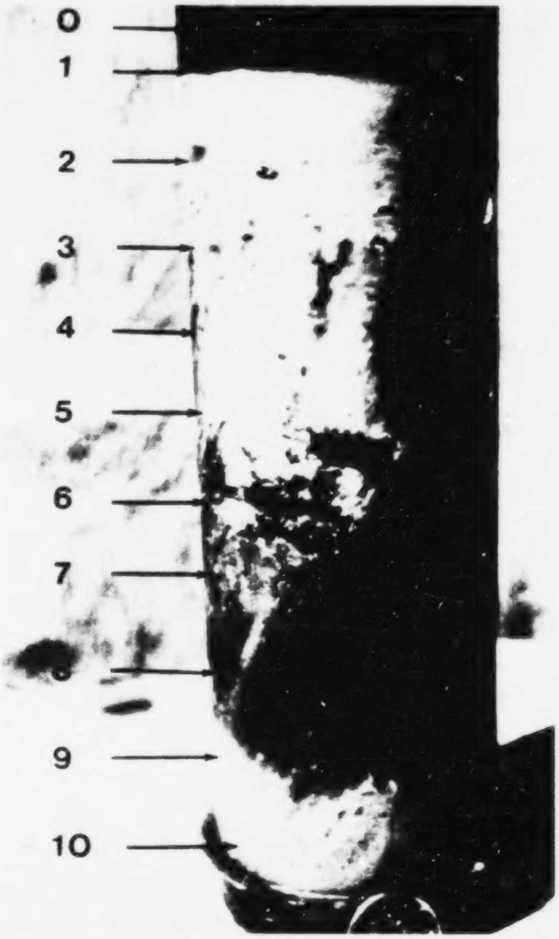

Photo 265.1. *Photograph of sediment core from the Stanrock tailings area, Elliot Lake. Height, 0.3 m. Numerals signify sampling points. Note dark organic-rich layers.*

The most common mineral phase observed in the Lower Moose sediment was an iron-aluminum silicate. At least two different structural varieties were identified, and both were ubiquitously associated with the surfaces of intact bacterial cells. The first variety had a fine granular appearance, whereas the second exhibited a more crystalline morphology (compare Photo 265.8a and Photo 265.8b). However, no difference in the elemental composition between the two structural forms could be detected by energy dispersive X-ray spectroscopy (Photo 265.9).

The amount of iron, aluminum, and silicon in the silicate surrounding the bacteria was quite variable, but compared favourably to that of chamosite, an

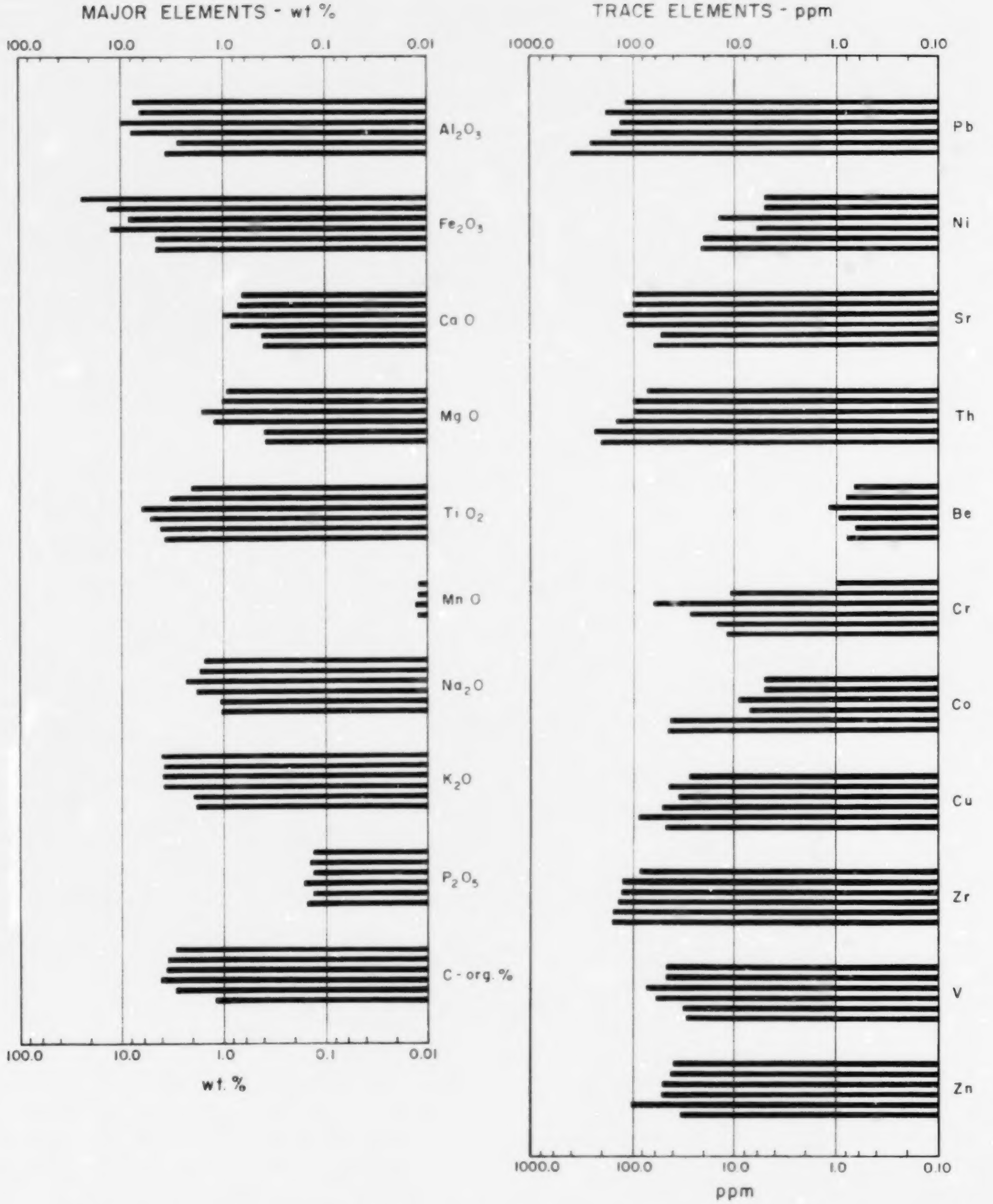

Figure 265.4. *Abundances of selected major element oxides and trace elements as a function of depth for the core illustrated in Photo 265.1. Note the consistently high levels of organic carbon.*

Photo 265.2. *Whole mounts of sediments from uranium tailings showing "live" bacteria, with no sign of any deposition of metals. Magnification 90 000 x. Sample position 6.*

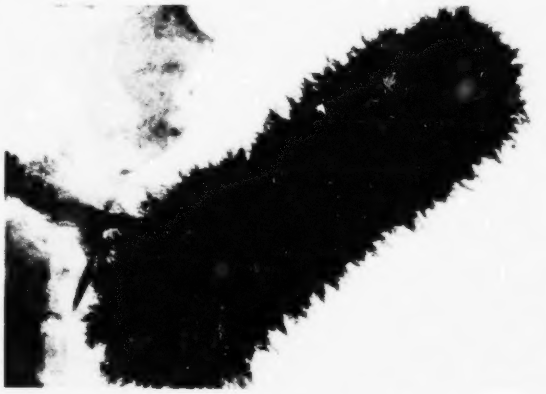

Photo 265.3. *Whole mounts of sediment from uranium tailings showing precipitation of crystalline iron on the cell wall. Magnification 90 000 x. EDAX analysis of this "dead" bacteria revealed the presence of an Fe-compound containing Fe (85%), S (6%), P (3%), Al (2%), and Si (1%). Sample position 6.*

iron-chlorite. However, SAED patterns obtained from whole mounts and thin sections did not reveal the intense 7.0 angstrom d-spacing that is characteristic of chamosite (Bayliss *et al.* 1980). Perhaps the silicate in our samples is actually a complex mixed mineral assemblage, or alternatively, a type of primitive hydrous precursor to a more mature interstratified clay, such as chamosite.

YELLOWSTONE NATIONAL PARK

In view of the general interest in Canada of precipitation in hydrothermal systems, some observations from Yellowstone are included here. Accumulations of iron and silica were observed on bacteria in sediment samples from Cyanidium Creek in Yellowstone National Park (Photo 265.10a) (Ferris *et al.* 1986). The water that flows into the creek, which is situated in the south central portion of the Norris Geyser Basin, has a pH of 3.1 and contains high levels of dissolved metals (Brock 1978).

Most of the organic matter in the sediment of this acidic stream is of microbial origin, derived from the eukaryotic algae *Cyanidium caldarium* (the only thermophilic photoautotroph of acidic hot springs), and thermoacidophilic bacteria (Brock 1978; Castenholz 1984).

The fine structure of the iron-silica accumulates around the bacteria is more easily discerned in the cell shown at a higher magnification in Photo 265.10b. The entire cell is encrusted by an electron opaque matrix consisting of granular and spheroidal crystallites. Presumably the cells promoted the deposition of dissolved silica by serving as sites for crystallite nucleation, whereas the iron was probably bound by the bacteria as a soluble cationic species. Similar results, where bacterial cells were aged in dilute silica solutions at 70°C, have been obtained in the laboratory (Photo 265.11).

Microbial mats that grow in the effluent channels of many hot springs are considered to be organo-sedimentary structures (Smith 1986). The structures of these mats is similar in geothermal areas around the world, and all form by accretion from the top (Castenholz 1984; Ward *et al.* 1984). In the present study, samples were obtained from a mat at Terrace Spring, a thermal feature located 2 km north of the confluence of the Gibbon and Firehole Rivers in Yellowstone National Park. The water overlying the mat at the collection site had a depth of 10 mm, a pH of 7.1, and a temperature of 48°C.

Electron microscopy and energy dispersive X-ray spectroscopy of thin-sectioned material from the Terrace Spring mat revealed a variety of bacterial forms encrusted by a manganese-bearing mineral (Photo 265.12) (Ferris *et al.* 1986). The bulk manganese concentration increased with depth in the mat, and oxidation state determinations using a modified Winkler iodemetric titration revealed O/Mn ratios of 1.7 to 1.9 (Kalhorn and Emerson 1984). A 10 angstrom lattice fringe image prominent in the precipitates and a 2.44 angstrom d-spacing in the corresponding pseudohexagonal SAED patterns, indicated that todorokite was the predominant manganese-oxide polymorph formed within the mat (Photo 265.13) (Turner and Buseck 1981; Chukhrov *et al.* 1979).

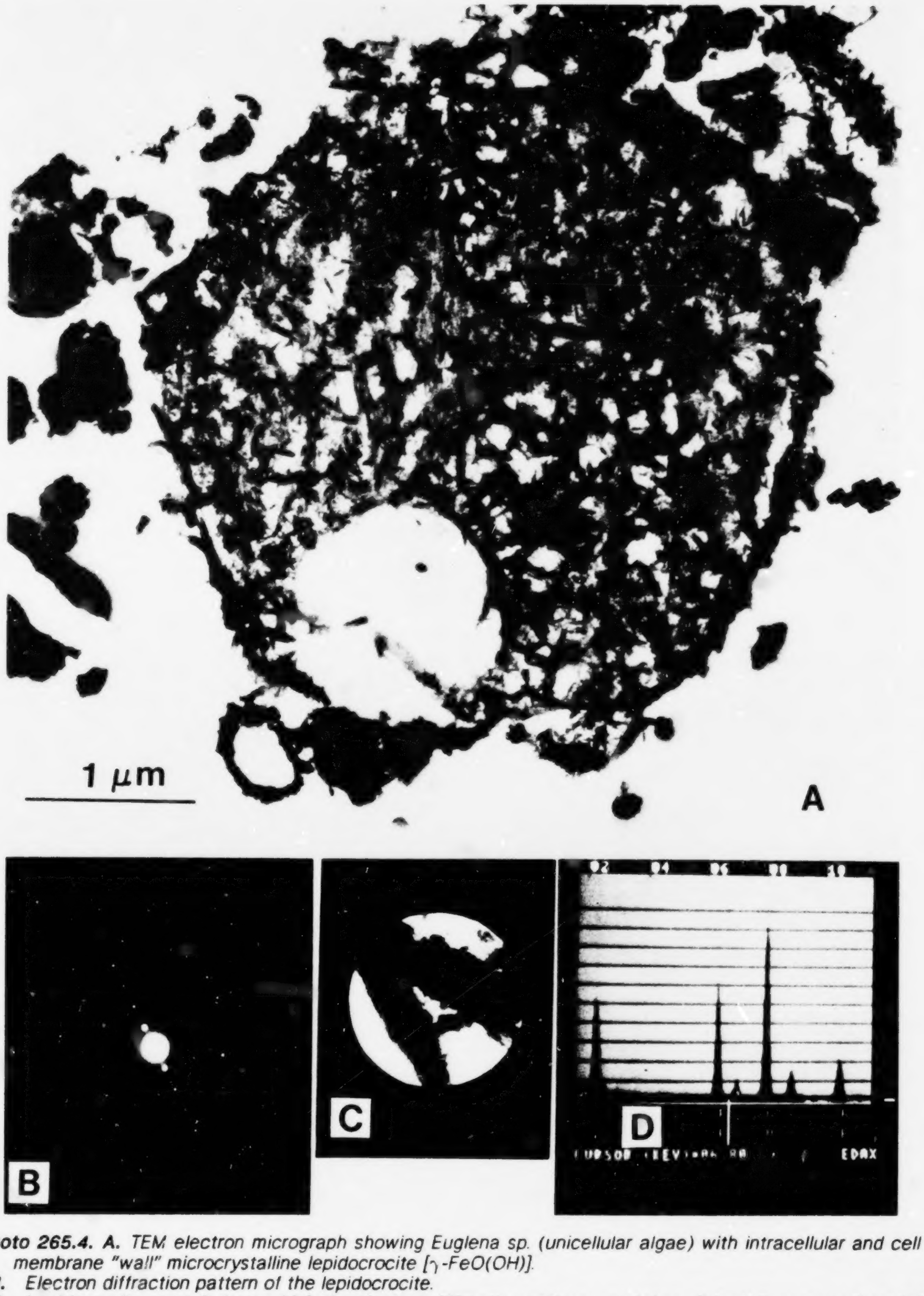

***Photo 265.4.* A.** *TEM electron micrograph showing Euglena sp. (unicellular algae) with intracellular and cell membrane "wall" microcrystalline lepidocrocite [γ-FeO(OH)].*

- ***B.*** *Electron diffraction pattern of the lepidocrocite.*
- ***C.*** *Lepidocrocite crystals from which the electron diffraction pattern was taken. Orientations come from left crystallite as in B.*
- ***D.*** *Energy dispersive X-ray analysis of crystals.*

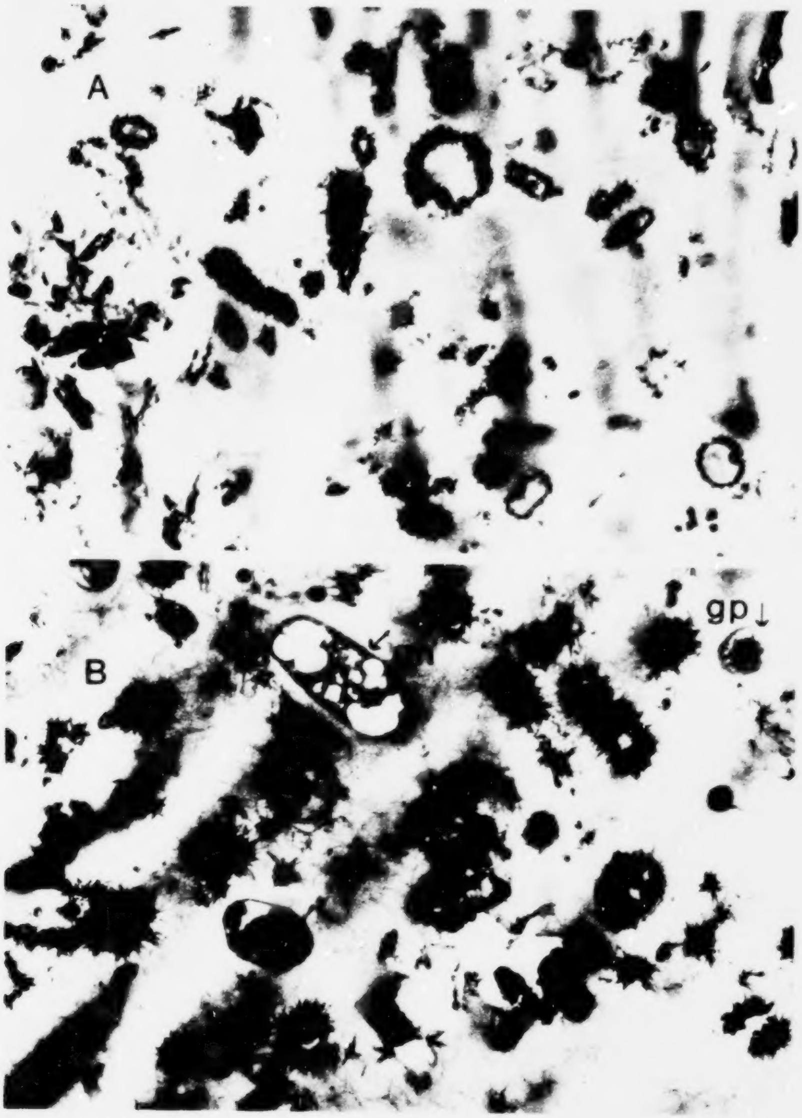

Photo 265.5. A. *Thin section photomicrograph of bacterial population, depicting variable intensities of Fe-rich cell wall mineralization. Fe-rich phase principally crystalline magnetite. Sample level 6. Magnification 10 000 x.* ***B.*** *Thin section photomicrograph of bacterial population stained to reveal both gram - positive (gp) and gram - negative (gn) varieties. Sample level 6. Magnification 19 000 x.*

Although the oxidation of manganese by bacteria has been studied in laboratory experiments, the mechanisms leading to manganese-oxide accumulation by bacterial cells in nature are not yet known. Current hypotheses suggest that at least a three-step deposition process is involved with the formation of such manganates (Ghiorse 1984). First, soluble manganese is believed to bind to aniomic groups at the surface of the cell. Then the bound metal could be oxidized by enzymes or some other factors excreted by the bacterium. Once inititated, deposition of the manganese-oxide could be further accelerated by surface catalysis reactions.

CONCLUSIONS

Significant quantities of dissolved metals are immobilized by microorganisms growing in mine tailing discharge and other natural environments. In some cases, concentration factors approaching 10^6 are realized and in such situations real possibilities exist for the secondary recovery of the metals. Microbial bioconcentration of metals also appears to be at least partly responsible for the partitioning of metals into sediments. Moreover, metals are often tenaciously bound during early diagenesis by some microoganisms which serve as nucleation sites for authigenic mineral formation. All of these processes may play important roles in the retardation of toxic heavy metal dispersion from tailing environments, and the formation of sedimentary ore deposits.

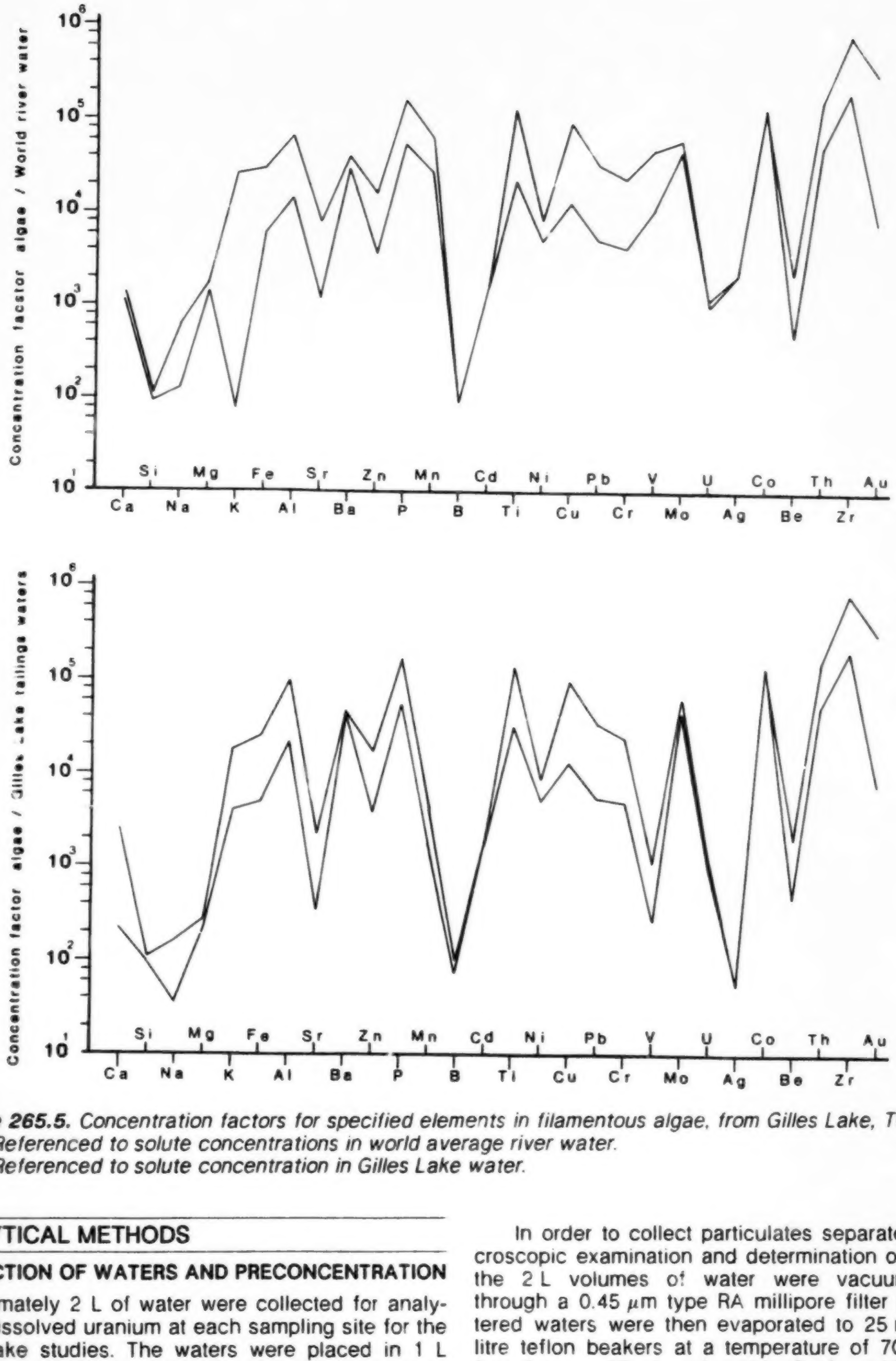

Figure 265.5. *Concentration factors for specified elements in filamentous algae, from Gilles Lake, Timmins.*
A. *Referenced to solute concentrations in world average river water.*
B. *Referenced to solute concentration in Gilles Lake water.*

ANALYTICAL METHODS

COLLECTION OF WATERS AND PRECONCENTRATION

Approximately 2 L of water were collected for analysis of dissolved uranium at each sampling site for the Elliot Lake studies. The waters were placed in 1 L polypropylene bottles which had been precleaned with 50% HNO_3 and distilled deionized water (DDW) and then acidified on site with premeasured aliquots of 10 mL reagent grade HNO_3.

In order to collect particulates separately for microscopic examination and determination of uranium, the 2 L volumes of water were vacuum filtered through a 0.45 μm type RA millipore filter paper. Filtered waters were then evaporated to 25 mL in one litre teflon beakers at a temperature of 70°C, transferred to a 25 mL volumetric flask, acidified with 5 mL HNO_3 and taken to volume, giving a preconcentration of about 80.

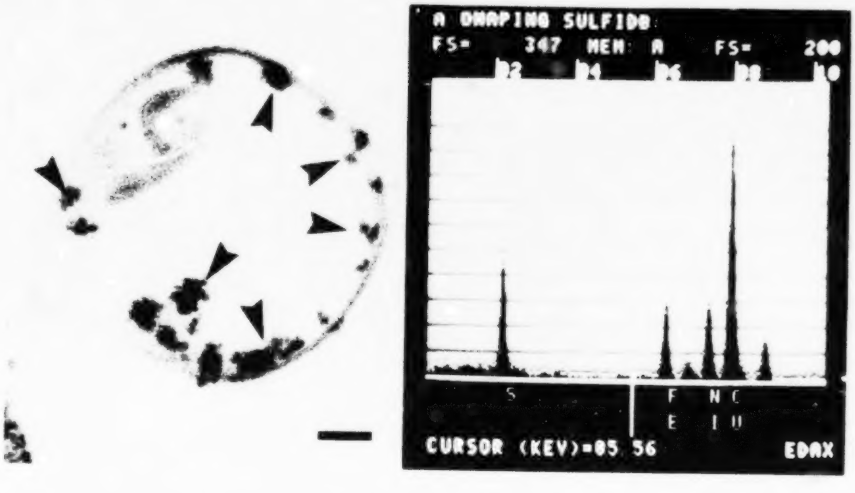

Photo 265.6. *Thin-section electron micrograph of metal sulphide accumulates (arrow heads) on a membranous ghost of a bacterium in the Lower Moose Lake sediment (scale bar, 100 mm), and the corresponding energy dispersive X-ray spectrum. Iron (K_α and K_β), Ni, and S peaks are from the sample; Cu (K_α and K_β) peaks are from the supporting grid.*

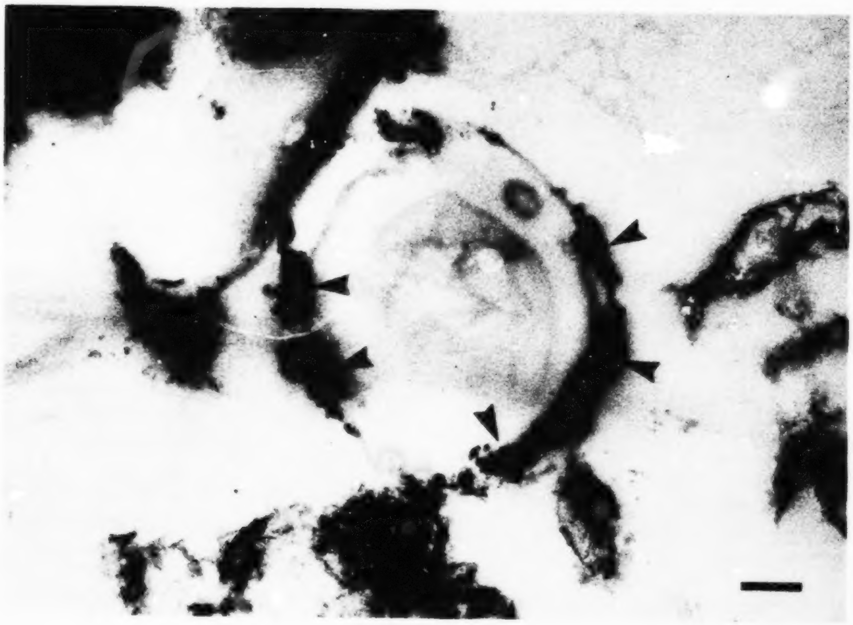

Photo 265.7. *Electron micrograph of nickel sulphide microcrystals (arrow heads) associated with a bacterium in a thin section from Lower Moose Lake (scale bar, 100 nm).*

For those samples in which U was analyzed by both fluorimetry and delayed neutron counting, the waters were preconcentrated to 100 mL, then split to 25 and 75 mL aliquots, the former for fluorimetry and the latter for delayed neutron counting. All glassware and teflon beakers were cleaned with 50% HNO_3 followed by DDW.

DIGESTION OF ALGAE

Large populations of filamentous algae weighing 0.5 to 2.0 kg were gathered by hand in the field using surgical gloves to avoid possible contamination. The algae were washed in clean natural river water to remove attached particulates, placed in a polythene bag, and drained of excess water.

In the laboratory, the algae were transferred to a preweighed litre teflon beaker and dried to constant weight at a temperature of 65°C, prior to final weighing.

Ashing of organic matter as a preconcentration process prior to analysis of metals is notorious for loss of the metals to the volatiles. Consequently, all preconcentration of the algae was performed by wet chemical digestion. Dry algae were initially digested in boiling nitric acid in a covered beaker, and finally in a mixture of boiling nitric and perchloric acids for three hours. The digestates were diluted with DDW and taken to appropriate volumes. For some samples containing larger quantities of algae, a 100 mL volume was split into 25 and 75 mL aliquots for analysis by fluorimetry and delayed neutron counting respectively.

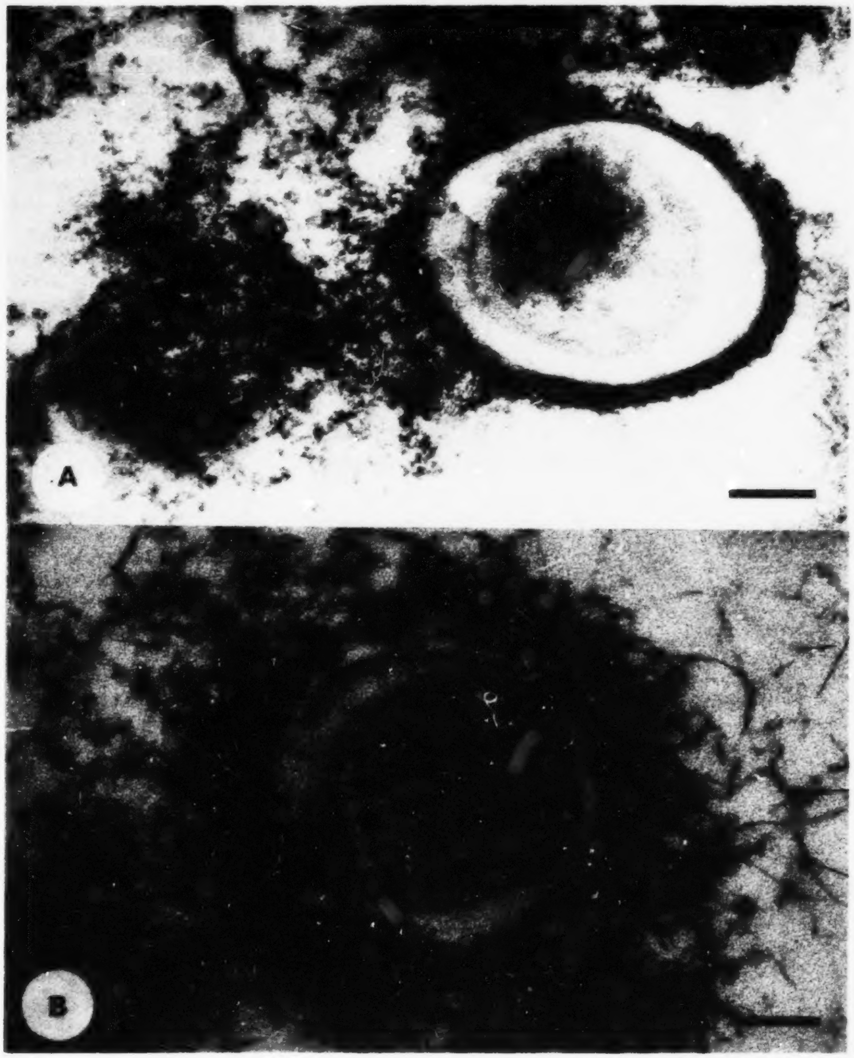

Photo 265.8.
Thin-section profiles from a Lower Moose Lake sediment sample showing bacteria encrusted by: (A) a granular form of an iron-aluminum silicate (scale bar, 200 nm); and (B) a microcrystalline form of an iron-aluminum silicate (scale bar, 200 nm). The section was stained with uranyl acetate and lead citrate to enhance the contrast of the cells before imaging in the electron microscope.

URANIUM ANALYSIS BY NEUTRON ACTIVATION DELAYED NEUTRON COUNTING

Uranium analysis by neutron activation delayed neutron counting has been extensively examined by several groups of researchers whose work indicates that the method is a rapid, accurate, and precise analytical procedure for samples with 40 to 40 x 10^5 ng U. A number of the fission products produced by thermal neutron induced fission of ^{235}U themselves emit neutrons in their subsequent decay to stable nuclides. The mean number of delayed neutrons emitted following thermal fission of ^{235}U is 0.016 neutrons per ^{235}U fission. The half-lives of the delayed neutron emitters are short (virtually all less than one minute), so that approximately 40% of the delayed neutrons are emitted within one minute of the completion of the irradiation. The system at the McMaster reactor centre is calibrated using IAEA reference low grade uranium ores.

The method is subject to very few interferences when used to analyze natural materials. Certain nuclides such as ^{10}B, ^{113}Cd, ^{157}Gd, and indeed U itself, having large thermal neutron capture cross-sections, can introduce errors due to flux depression. The effect from U is minimized by using appropriate standards; Cd and Gd are not abundant in either most natural waters or biological materials.

Seventy-five millilitre aliquots, split from 100 mL volumes of aqueous solutions of algae or preconcentrated waters, were placed into a polythene bag liner in a 100 mL polypropylene beaker. The beakers were loaded into a vacuum oven operating at 70°C, until the solutions were entirely evaporated. Then the polythene bags were rolled up and inserted into a standard 3 mL polyethylene irradiation capsule. In this way, as much as 2000 mL river water or 500 g algae could be concentrated into a 3 mL volume.

Four sets of University of Western Ontario (UWO) standards made up from stock solution to give aque-

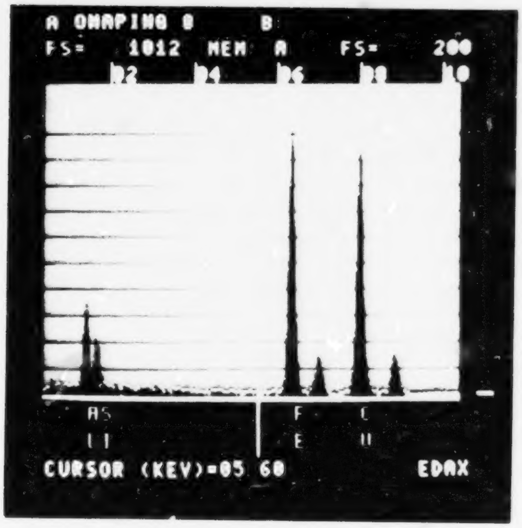

Photo 265.9. *An energy dispersive X-ray spectrum generated by the iron-aluminum silicate matrix surrounding a bacterium in the Lower Moose Lake sediment. Iron (K_α and K_β), Al, and Si peaks are from the sample; Cu K_β) peaks are from the supporting grid.*

ous uranium concentrations of 0.5, 5, 10, 100, 1000, and 10 000 ng/g were dried in the same manner as the other samples, and forwarded together with unknowns for analysis. These gave a near perfect one to one correlation for four orders of magnitude in concentration (Figure 265.6). In addition, 10 L of laboratory DDW and 100 mL HNO_3 were separately preconcentrated and dried, to test for possible uranium contamination from reagents; results were below the limits of detection.

MULTI-ELEMENT ANALYSIS

Multi-element analysis of waters and algae were made on preconcentrated solutions and aqueous digestates respectively. Analysates were split, one portion being analyzed by inductively coupled plasma emission spectroscopy by Barringer Magnenta Limited, and the second by neutron activation (INAA) at the McMaster Reactor Centre, following vacuum evaporation of the solution in a polythene liner. Samples for INAA were prescreened for <100 ppm U, in order to circumvent significant production of U fission nuclides.

ANALYTICAL ELECTRON MICROSCOPY

Immediately after algal and sediment samples were collected, small specimens were placed in 5 mL metal-free plastic tubes containing 1 mL of 1% (v/v) aqueous glutaraldehyde, a fixative for electron microscopy. After the samples were returned to the laboratory, they were prepared for thin-sectioning by dehydration through an ethanol-propylene oxide series, and embedding in epoxy resin (Epon 812). Sections, approximately 150 nm in thickness, were cut using a Reichert Ultra-Cut E ultramicrotome. The thin sections were then mounted on Formvar-carbon coated copper or aluminum grids. Electron microscopy was done using a Philips EM 400T TEM/STEM which is equipped with a goniometer stage and and EDAX energy dispersive X-ray spectrometer. The electron microscope was operated at 100 KeV with a liquid nitrogen-cooled anticontamination device in place at all times. Electron beam spot sizes of 100 nm or less were used for energy dispersive X-ray spectroscopy, and counts were collected for 100 seconds (live-time). Spacings in selected area electron diffraction (SAED) patterns were determined using evaporated aluminum as a standard.

ACKNOWLEDGMENTS

The authors thank Rio Algom Limited and Denison Mines Limited for permission to collect materials in the Elliot Lake district. We are grateful to Al Vivyurka (Rio Algom) and Bill Zelvenak (Denison) for invaluable guidance during collecting. Algae were obtained from the Timmins area courtesy of Pamour Porcupine Mines Limited, and with the assistance of Ed Van-Hees.

We also thank the staff and management of Falconbridge Limited, especially Mark Wiseman, for their assistance and permission to do field work at Onaping. The Philips electron microscope 400T was purchased with funds from Natural Sciences and Engineering Research Council (NSERC), and is maintained by funds from the University of Guelph and user fees. We also acknowledge support from NSERC to W.S. Fyfe for expenses involved in sampling at Yellowstone National Park.

REFERENCES

Bayliss, P., Berry, L.G., Mrose, M.E., and Smith, D.K.
1980: Mineral Powder Diffraction File Data Book; JCPDS International Centre for Diffraction Data, Swarthmore, Pennsylvania, 1168p.

Berner, R.A.
1970: Sedimentary Pyrite Formation; American Journal of Science, Volume 268, p.1-23.

Beveridge, T.J., and Fyfe, W.S.
1985: Metal Fixation by Bacterial Cell Walls; Canadian Journal of Earth Sciences, Volume 22, p.1883-1898.

Beveridge, T.J., Meloche, J.D., Fyfe, W.S., and Murray, R.G.E.
1983: Diagenesis of Metals Chemically Complexed to Bacteria: Laboratory Formation of Metal Phosphates, Sulphides, and Organic Condensates in Artificial Sediments; Applied and Environmental Microbiology, Volume 45, p.1094-1108.

Blair, R.D., Cherry, J.A., Lim, T.P., and Vivyurka, A.J.
1980: Groundwater Monitoring and Contaminant Occurrence at an Abandoned Tailings Area, Elliot Lake, Ontario: Conference on Uranium Mine Waste Disposal, Vancouver, May 12 to 21. Society of Mining Engineers of AIME, Proceeding, Volume C, edited by Brawner.

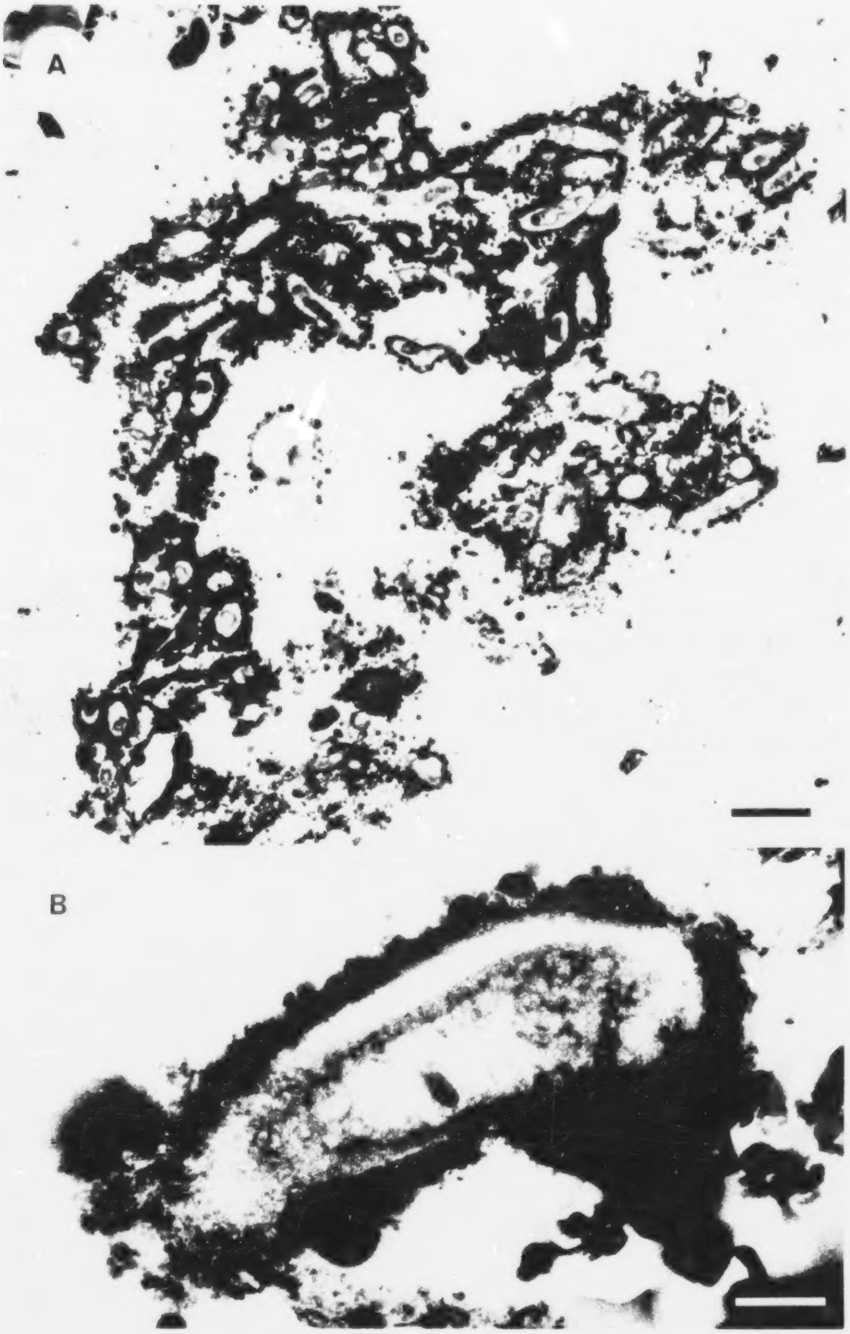

Photo 265.10. *Thin-sectioned electron micrographs showing bacteria seen in a sediment sample collected from Cyanidium Creek, Yellowstone National Park, Wyoming. The section was stained with uranyl acetate and lead citrate to increase the electron contrast of the cells.*

A. *An electron-opaque matrix of granular and spheroidal iron-silica crystallites has formed on the surfaces of the bacterial cell (scale bar, 1.0 μm).*

B. *At this higher magnification, the fine structure of the matrix is more easily discerned (scale bar, 200 nm).*

Bloch, S.
1976: Some Factors Controlling the Concentration of Uranium in the World Ocean; Geochimica et Cosmochimica Acta, Volume 44, p.373-377.

Brock, T.D.
1974. Biology of Microorganisms, Second Edition; Prentice Hall, Englewood Cliffs, New Jersey, 852p.
1978: Thermophilic Microorganisms and Life at High Temperatures; Springer Verlag, New York, 465p.

Castenholz, R.W.
1984: Composition of Hot Spring Microbial Mats: A Summary; p.101-119 *in* Microbial Mats: Stromatolites, edited by Y. Cohen, R.W. Castenholz, and H.O. Halvorson, Alan R. Liss Publishing, New York, 498p.

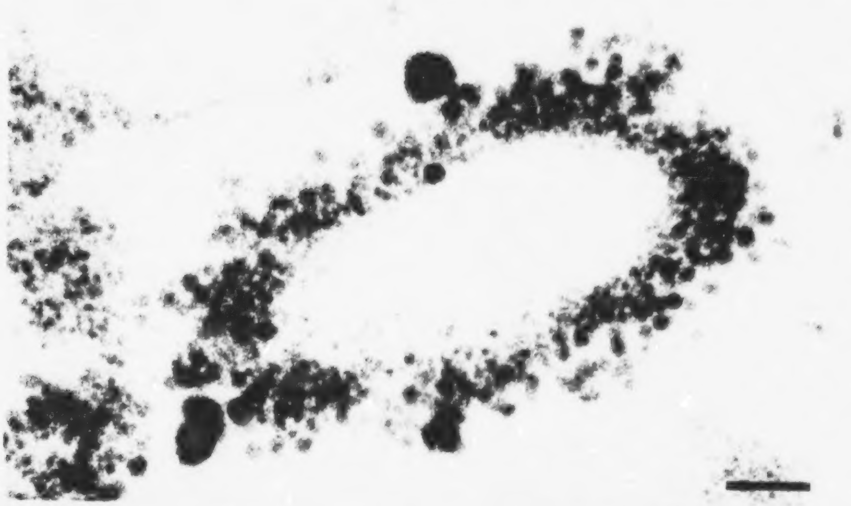

Photo 265.11. *An unstained thin section profile of Bacillus subtilis, a rod shaped gram-positive bacterium, aged in the laboratory for 6[illegible] days at 70° C in a dilute silica solution. Small silica particles have formed on, and completely cover, the surface of the cell (scale bar, 200 nm).*

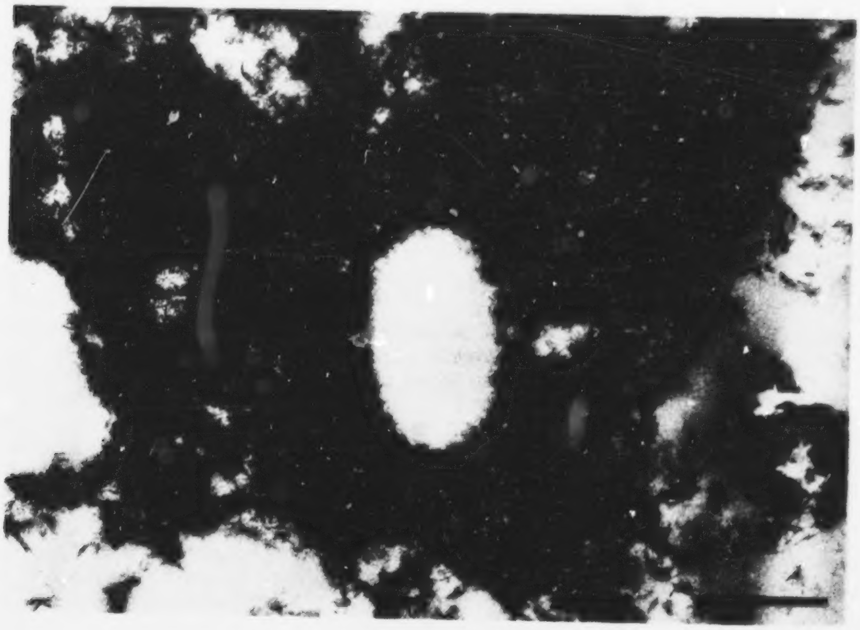

Photo 265.12. *Electron micrograph of a manganese-oxide encrusted bacterium in an unstained thin section of material from the microbial mat at Terrace Spring, Yellowstone National Park, Wyoming (scale bar, 500 nm).*

Cherry, J.A., Blackport, R.J., Dubrovsky, V., Gillham, R.W., Lim, T.P., Murray, D., Reardon, E.J., and Smyth, D.J.A.

1980: Subsurface Hydrology and Geochemical Evolution, Inactive Pyritic Tailings in the Elliot Lake Uranium District, Canada; Proceedings, Third Symposium on Uranium Tailings Management, Colorado State University, Fort Collins, Colorado, Session 5.

Chukhrov, F.V., Gorshkov, A.I., Sivtsov, A.V., and Beresovskaya, V.V.

1979: New Data on Natural Todorokites; Nature, Volume 278, p.631-632.

Feenstra, S., Blair, R.D., Cherry, J.A., Chakravatti, J.L., and LaRocque, E.

1981: Hydrogeochemical Investigations of Two Inactive Tailing Areas in the Elliot Lake Uranium District, Ontario, Canada; p.367-389 *in* Proceedings of the Fourth Symposium on Uranium Mill Tailings Management.

Ferris, F.G., and Beveridge, T.J.

1985: Functions of Bacterial Cell Surface Structures; BioScience, Volume 35, p.172-177.

Ferris, F.G., Beveridge, T.J., and Fyfe, W.S.

1986: Iron-Silica Crystallite Nucleation by Bacteria in a Geothermal Sediment; Nature, Volume 320, p.609-611.

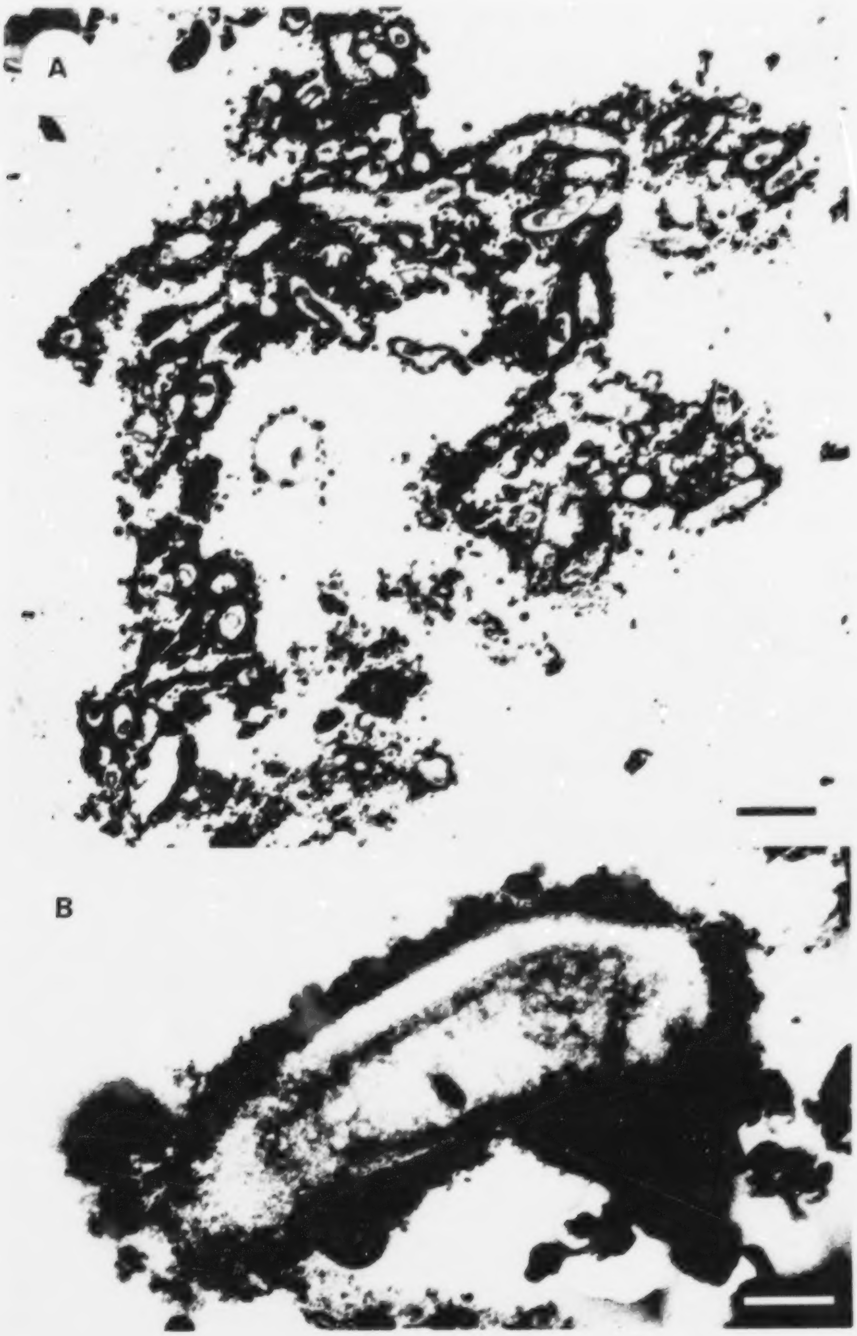

Photo 265.10. *Thin-sectioned electron micrographs showing bacteria seen in a sediment sample collected from Cyanidium Creek, Yellowstone National Park, Wyoming. The section was stained with uranyl acetate and lead citrate to increase the electron contrast of the cells.*
A. *An electron-opaque matrix of granular and spheroidal iron-silica crystallites has formed on the surfaces of the bacterial cell (scale bar, 1.0 μm).*
B. *At this higher magnification, the fine structure of the matrix is more easily discerned (scale bar, 200 nm).*

Bloch, S.
1976: Some Factors Controlling the Concentration of Uranium in the World Ocean; Geochimica et Cosmochimica Acta, Volume 44, p.373-377.

Brock, T.D.
1974: Biology of Microorganisms, Second Edition; Prentice Hall, Englewood Cliffs, New Jersey, 852p.
1978: Thermophilic Microorganisms and Life at High Temperatures; Springer Verlag, New York, 465p.

Castenholz, R.W.
1984: Composition of Hot Spring Microbial Mats: A Summary; p.101-119 *in* Microbial Mats: Stromatolites, edited by Y. Cohen, R.W. Castenholz, and H.O. Halvorson, Alan R. Liss Publishing, New York, 498p.

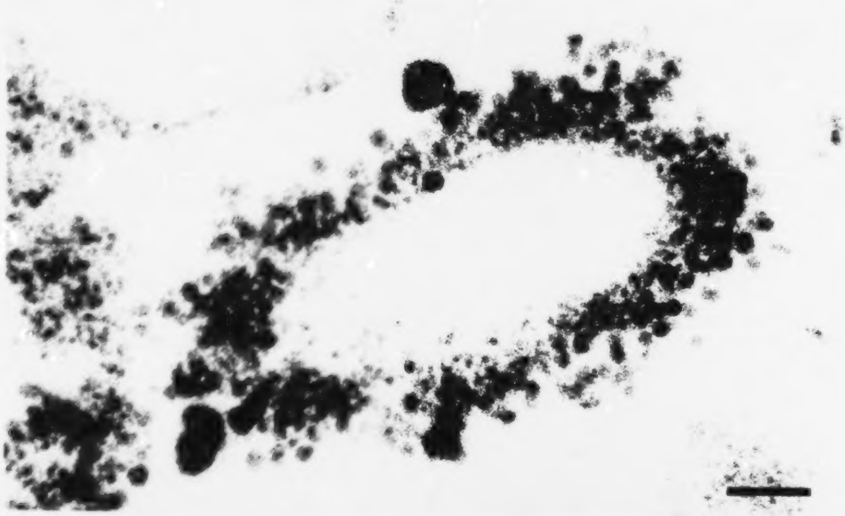

Photo 265.11. *An unstained thin section profile of Bacillus subtilis, a rod shaped gram-positive bacterium, aged in the laboratory for 60 days at 70°C in a dilute silica solution. Small silica particles have formed on, and completely cover, the surface of the cell (scale bar, 200 nm).*

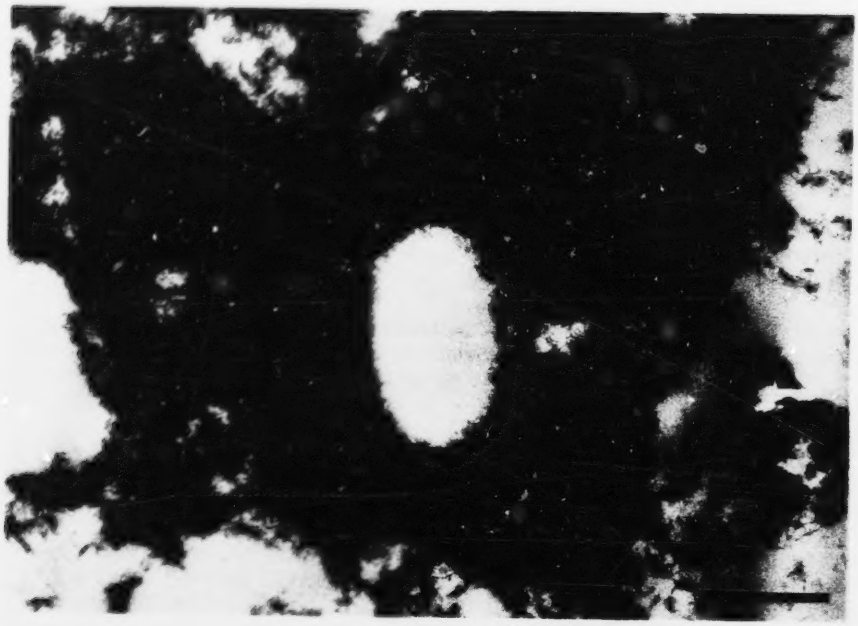

Photo 265.12. *Electron micrograph of a manganese-oxide encrusted bacterium in an unstained thin section of material from the microbial mat at Terrace Spring, Yellowstone National Park, Wyoming (scale bar, 500 nm).*

Cherry, J.A., Blackport, R.J., Dubrovsky, V., Gillham, R.W., Lim, T.P., Murray, D., Reardon, E.J., and Smyth, D.J.A.
1980: Subsurface Hydrology and Geochemical Evolution, Inactive Pyritic Tailings in the Elliot Lake Uranium District, Canada; Proceedings, Third Symposium on Uranium Tailings Management, Colorado State University, Fort Collins, Colorado, Session 5.

Chukhrov, F.V., Gorshkov, A.I., Sivtsov, A.V., and Beresovskaya, V.V.
1979: New Data on Natural Todorokites; Nature, Volume 278, p.631-632.

Feenstra, S., Blair, R.D., Cherry, J.A., Chakravatti, J.L., and LaRocque, E.
1981: Hydrogeochemical Investigations of Two Inactive Tailing Areas in the Elliot Lake Uranium District, Ontario, Canada; p.367-389 *in* Proceedings of the Fourth Symposium on Uranium Mill Tailings Management.

Ferris, F.G., and Beveridge, T.J.
1985: Functions of Bacterial Cell Surface Structures; BioScience, Volume 35, p.172-177.

Ferris, F.G., Beveridge, T.J., and Fyfe, W.S.
1986: Iron-Silica Crystallite Nucleation by Bacteria in a Geothermal Sediment; Nature, Volume 320, p.609-611.

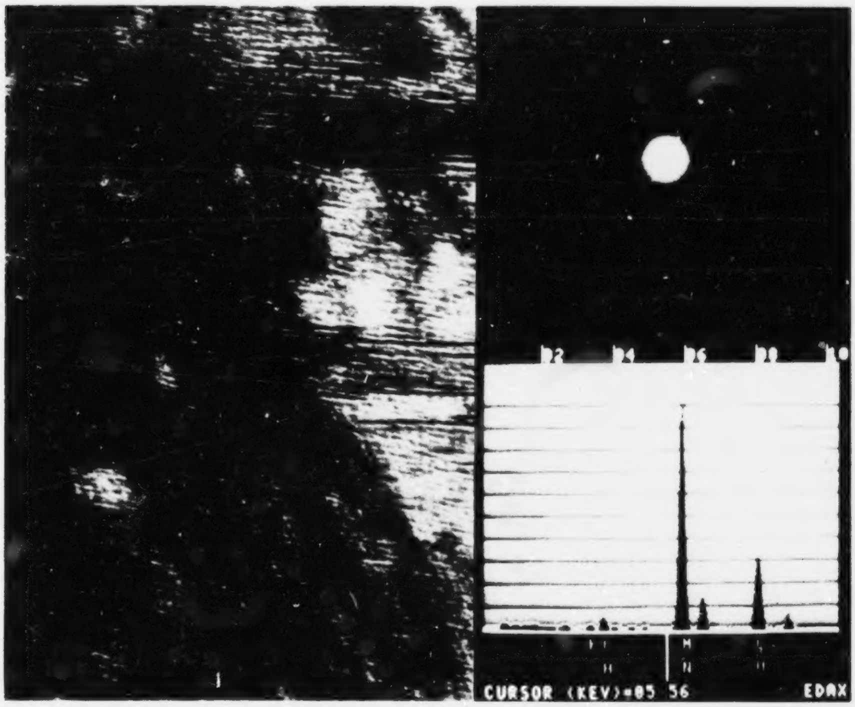

Photo 265.13. *High resolution electron micrograph of a thin manganese oxide crystal showing the 10 angstrom lattice and twinning of fibers oriented at 120° angles that are characteristic of todorokite (scale bar, 10 nm). Insets show the corresponding selected area electron diffraction pattern (the first strong reflections have a 2.44 angstrom d-spacing), and energy dispersive X-ray spectrum for the todorokite. Manganese (K_α and K_β), potassium, and calcium peaks are from the sample; copper (K_α and K_β) peaks are from the supporting grid.*

Ghiorse, W.C.

1984: Biology of Iron- and Manganese-Depositing Bacteria; Annual Review of Microbiology, Volume 38, p.515-550.

Holland, H.D.

1978: The Chemistry of the Atmosphere and Oceans; Wiley, New York, p.351.

Kalhorn, S., and Emerson, S.

1984: The Oxidation State of Manganese in Surface Sediments of the Deep Sea; Geochimica et Cosmochimica Acta, Volume 48, p.897-902.

Mann, H.

1984: Algal Uptake of U, Ba, Co, Ni and V, Studies of Natural and Experimental Systems, Unpublished Ph.D. Thesis, Geology Department, University of Western Ontario, London, Ontario.

Mann, H., and Fyfe, W.S.

1985a: Algal Uptake of U and Some Other Metals: Implications for Global Geochemical Cycling; Precambrian Research, Volume 30, p.337-349.

1985b: Uranium Uptake by Algae: Experimental and Natural Environments; Canadian Journal of Earth Sciences, Volume 22, Number 12, p.1899-1903.

Moffett, D., and Tellier, M.

1978: Radiological Investigations of an Abandoned Uranium Tailings Area; Journal of Environmental Quality, Volume 7, Number 3, p.310-314.

Murray, D., and Moffett, D.

1977: Vegetating the Uranium Mine Tailings at Elliot Lake, Ontario; Journal of Soil and Water Conservation, Volume 32, Number 4, p.121-132.

Smith, P.J.

1986: Growing Stromalites; Nature, Volume 320, p.396.

Thomson, I.

1977: A Selected Bibliography of the Applied Geochemistry of Uranium; Internal Report for United Sisco Mines Ltd., P.O. Box 306l, Toronto Dominion Centre, Suite 1806l, Commercial Union Tower, Toronto, Ontario, M5K 1K2.

Trudinger, P.A., and Swaine, D.J.

1979: Biogeochemical Cycling of Mineral Forming Elements; Elsevier, Amsterdam, 612p.

Turner, S., and Buseck, P.R.

1981: Todorokites: A New Family of Naturally Occurring Manganese Oxides; Science, Volume 212, p.1024-1027.

Ward, D.M., Beck, E., Revsbech, N.P., Sandbeck, K.A., and Winfrey, M.R.

1984: Decomposition of Hot Spring Microbial Mats; p.191-214 *in* Microbial Mats: Stromatolites, edited by Y. Cohen, R.W. Castenholz, and H.O. Halvorson, Alan R. Liss Publishing, New York, 498p.

Wenrich-Verbeek, K.J.

1976: Water and Stream Sediment Sampling Techniques for Use in Uranium Exploration; United States Geological Survey Open File Report, Number 76-77, 30p.

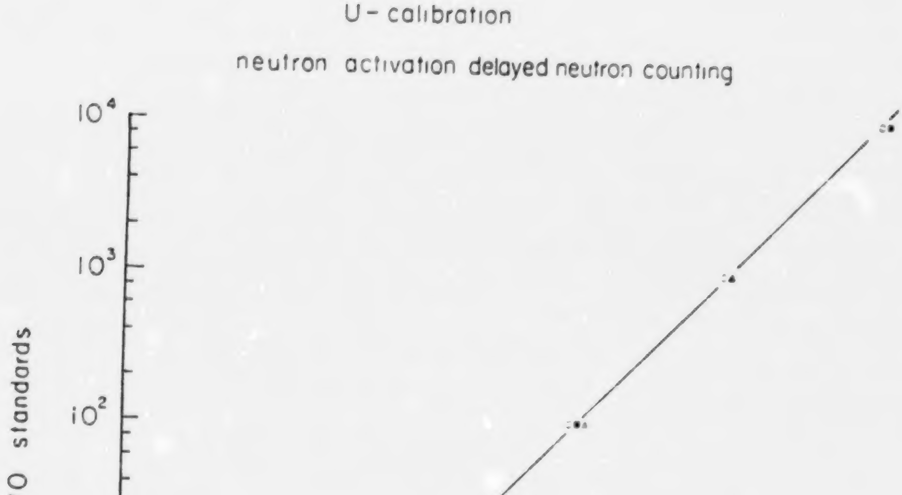

Figure 265.6. *Calibration graph of 100 mL uranium aqueous standards made up at University of Western Ontario, and preconcentrated by evaporation to dryness, versus their analytically determined values by means of neutron activation delayed neutron counting. Analysis conducted at the McMaster Nuclear Reactor Centre, Hamilton. Different symbols represent individual sets of aqueous standards: where symbols overlap, only the extreme values are depicted.*

Grant 266 Carbonate Till on the Canadian Shield: Economic and Environmental Implications in the Hemlo Area, Ontario.

Stephen R. Hicock

Department of Geology, University of Western Ontario, London

ABSTRACT

Calcareous tills from the Canadian Shield are examined in order to determine how they were glacially transported and deposited, and how their occurrence near Hemlo could affect gold exploration, aggregate quality, and acid rain susceptibility.

Three calcareous tills deposited by lodgment and subglacial meltout are underlain by a basal noncalcareous till and overlain by a noncalcareous supraglacial meltout till. The entire till sequence can be explained by deposition during a single glacial advance over uplands. The model involves simultaneous stoss side upshearing to eventually produce supraglacial till, and lee side downshearing of englacial debris to produce subglacial tills, followed by stagnation.

Supraglacial till comprises coarse local Precambrian materials and is richest in metals. Carbonate tills are finer textured, are dominated by Paleozoic materials, and contain less metals. The supraglacial and the basal noncarbonate tills are the most likely to contain well defined ore dispersal trains that may be traced upglacier to source (probably within 20 km). The carbonate tills are too far-travelled to contain distinct and traceable trains; however, they should make excellent buffers against acid precipitation, as well as dam cores for acidic mine tailings ponds. Little chert occurs in the tills so that aggregate quality should be generally high.

INTRODUCTION

Many authors have documented the advantages of applying drift prospecting techniques to mineral exploration projects in glaciated shield areas of the northern hemisphere (*see* Shilts 1984 and his references). They recommended studying lodgment till (as opposed to other genetic types) because it is dominated by local clasts and should reflect nearby sources of till materials (Goldthwait 1971; Shilts 1975, 1984).

The carbonate till of this study occurs in an area where gold exploration has recently been extremely active. Thus, the genesis of the till has important implications for the usefulness of drift prospecting in the Hemlo area in finding other gold sources.

This study was initiated in order to assess the influence of the carbonate till on: 1) mineral exploration using drift prospecting; 2) the buffering of acid precipitation; 3) aggregate quality (cherts); and finally, 4) the determinion of till genesis and propose a depositional model for the area. These objectives will be accomplished by analyzing the till character and stratigraphy in order to interpret its mode of formation, occurrence, and provenance.

Field work during three weeks in July, 1985, concentrated on seven key exposures which were studied in detail for stratigraphic and structural relations of sediment units (Figure 266.1). In the laboratory, granulometric analyses were performed by the hydrometer-sieve method of the American Society for Testing and Materials (1972), using 0.002 mm and 0.063 mm as the clay-silt and silt-sand boundaries, respectively. Carbonate analyses were done on the -0.063 mm fraction after the method of Dreimanis (1962) and geochemical analyses were completed by Barringer Magenta Limited of Toronto, using atomic absorption techniques on total digests of the minus 0.002 mm fraction of till matrices.

Till criteria and terminology used in this paper follow the system of the International Quaternary Association's Commission on Lithology and Genesis of Glacial Deposits as summarized by Dreimanis (1982).

PHYSICAL SETTING AND PREVIOUS WORK

In the Hemlo area, uplands dominate the northern part, and low-lying areas containing abundant lakes dominate the southern, with a combined relief up to 220 m (Figure 266.1). The area is underlain by a structurally complex sequence of Precambrian lithologies including metavolcanic, metasedimentary, and granitoid plutonic and gneissic rocks (Muir 1982a, 1982b; Siragusa 1984a, 1984b, 1985a, 1985b). Diabase dikes have intruded other lithologies and rare patches of iron formation and ultramafic rocks (mainly peridotite) occur on the bedrock surface.

Recent Quaternary studies north of Lake Superior have concentrated on surficial mapping and glacial lake studies (Farrand 1962; Zoltai 1965a, 1965b, 1967; Boissonneau 1966); Zoltai and Boissonneau recognized the carbonate-rich till. Coker and Shilts (1979) generally described the till in a lake geochemistry study, and Fortescue and Geddes (1983), Geddes (1984a, 1984b, 1984c, 1985a, 1985b), Geddes and Bajc (1985a, 1985b), Geddes *et al.* (1985), and Woods (1985) have described it with more detailed mapping and case studies. Gartner and McQuay (1979, 1980) provided engineering and terrain studies of the area, and Cowan (1976) an aggregate inventory.

TILL STRATIGRAPHY AND GENESIS

Five tills are recognized in the Hemlo area: three are calcareous and are sandwiched by noncalcareous tills. The oldest is a locally derived basal till observed in mine excavations by Geddes (1984a, 1984b, 1984c) and Geddes *et al.* (1985); it was not encountered in the sections studied by the author.

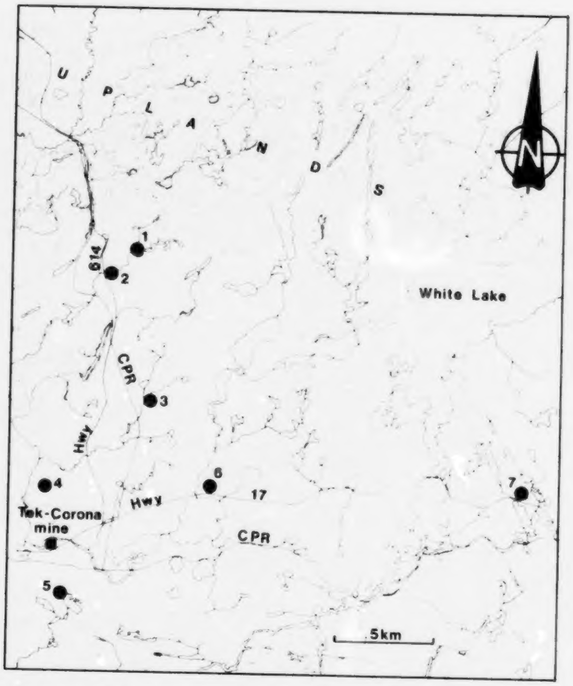

Figure 266.1. *Topographic map of the study area with site localities. Contour interval is 76 m.*

LOWER LODGMENT TILL

The overlying unit occurs in three sections and comprises dark grey, compact, calcareous diamicton. It is fissile, stony, and contains striated, faceted, and bullet-nosed stones, as well as clasts of sand at sites 2 and 7. Till matrix (-2.00 mm) comprises about 35% sand, 55% silt, 10% clay, and 35% to 40% total carbonates (calcite and dolomite; Table 266.1).

Stones are generally subrounded to subangular and dominated by Paleozoic lithologies, indicating distal glacial transport. Parallel and transverse alignment of stones in the till, extension fractures, and till wedges within the unit are consistently oriented with striae on the stones.

These characteristics indicate that this compact diamicton was deposited subglacially by lodgment (in the meaning of Dreimanis 1976, 1982; Shaw 1985).

MELTOUT TILL

The compact calcareous till is overlain by a light grey, noncompacted, coarser textured diamicton. This middle calcareous till was observed at least at six sites and is the most abundant one in the study area.

It commonly contains interlayered and lenticular silt, sand, gravel, and diamicton strata, as well as percussion and splash structures around boulders and sediment diapirs. Bedding is commonly truncated by dropstones or draped over them. Weakly striated and faceted stones, as well as angular, faulted clasts of sorted sediment and compact till are abundant. Till matrices contain 50% to 65% sand, 35% to 50% silt, under 5% clay, and 20% to 35% carbonate (Table 266.1).

Stones are generally subrounded to subangular and the Paleozoic content is commonly similar to the Precambrian content. Alignment of stones is better developed than in the underlying lodgment till and is parallel to striae on stones within the till.

These data indicate that this unit was deposited subglacially, mainly by meltout (in the meaning of Dreimanis 1976, 1982; Shaw 1982, 1983, 1985) but with subglacial stream and subglacial debris flow forming some of the gravelly and diamictic strata.

UPPER LODGMENT TILL

Another fissile carbonate diamicton overlies the meltout till at sites 1, 5, and 6. It is dark grey, fissile, compacted, and stony with matrix compositions approximating 50% sand and silt, with less than 5% clay, and 30% to 35% carbonate (Table 266.1). These are values which may reflect reworking of underlying meltout till.

Pebbles are striated, faceted, and bullet nosed, generally subrounded to subangular, and include clasts of calcareous sand at site 6. Paleozoic clasts dominate over Precambrian in this unit. Pebble alignment is weakly developed but generally agrees with the orientations of shear planes, fissility, till wedges, and striae on stones in the till.

The above data indicate that this unit was also deposited subglacially by lodgment.

SUPRAGLACIAL TILL

Capping the carbonate till package is a generally rusty, noncompacted, coarse-textured diamicton dominated by subangular to angular Precambrian clasts. It is commonly bouldery and the matrix sample analyzed yielded 86% sand and 14% silt but no clay or carbonate (Table 266.1). Stone alignment in this unit is very weak and ambiguous.

It was most likely deposited by supraglacial meltout and commonly covers the ground surface in upland areas (Geddes *et al.* 1985). Younger glaciofluvial and glaciolacustrine sediments were studied by Geddes and Bajc (1985a, 1985b) and Geddes *et al.* (1985).

GLACIER MOVEMENT AND CLASTIC DISPERSAL

An accurate knowledge of glacier movement directions in the area is essential for developing a strategy for mineral exploration by drift prospecting, as well as constructing a depositional model for the tills and determining their source areas. Geddes and Bajc (1985a, 1985b) determined that general ice advance was towards the south-southwest.

LOWER LODGMENT TILL

Some fabric orientations (pebble long axes) in the lower lodgment till display both parallel and transverse clast alignment, indicating that glacier advance was towards the south-southwest. This agrees with the dips of extension fractures and till wedges, as well as striae on stones within the till. Distal Paleozoic lithologies dominate the stones (Table 266.1) but local rocks have been incorporated, including serpen-

TABLE 266.1. TILL MATRIX AND PEBBLE DATA

Till Unit	Site on Figure 1	Matrix Grain Size (-2.0 mm fraction)			Matrix Carbonate (-0.063 mm fraction)		Pebble Data (1-10 cm fraction)	
		%sand	%silt	%clay	%carb	cal/dol	roundness	Paleoz/Prec
supraglacial	7	86	14	0	0	0	sa-a	<0.1
upper lodgment	1	52	44	04	36	0.9	sr	4.3
	5	46	52	02	34	0.9	sr-sa	3.0
	6	58	39	03	30	1.0	sr-sa	0.9
middle meltout	1	64	34	02	32	0.8	sr	1.0
	2	61	37	02	32	0.9	sr-sa	1.5
	3	57	43	0	28	0.6	sa-sr	1.3
	4 upper	57	41	02	22	0.8	sr-sa	<0.1
	4 middle	55	43	02	24	0.8	sr-sa	0.1
	4 lower	66	32	02	23	0.8	sr-sa	0.1
	5 upper	48	50	02	32	0.8	sr-sa	1.1
	5 lower	50	50	0	33	0.8	sr-sa	1.1
	7	62	38	0	27	0.5	sr-sa	0.4
lower lodgment	2	32	59	09	37	1.3	sr-sa	2.5
	5 top	32	58	10	37	1.3	sr-sa	1.3
	5 upper	33	56	11	38	1.3	sr-sa	--
	5 middle	34	55	11	37	1.4	sr-sa	1.3
	5 lower	31	56	13	38	1.4	sr-sa	--
	5 bottom	32	56	12	37	1.4	sr-sa	1.4
	7	36	55	09	26	0.9	sr-sa	0.8

cal=calcite, dol=dolomite, carb=total calcite and dolomite

Paleoz=Paleozoic lithologies, Prec=Precambrian lithologies

a=angular, sa=subangular, sr=subrounded

tinized peridotite originating from the northeast of Hemlo.

MELTOUT TILL

Fabric orientations in the meltout till suggest that glacial advance was to the south-southwest, which is supported by striae on stones in the unit. Paleozoic clasts are commonly the most abundant, but stones of local to intermediate provenance (including peridotite) were also upsheared into the ice when it was actively advancing prior to meltout deposition.

UPPER LODGMENT TILL

In the upper lodgment till, fabric orientations, shear structures, till wedges, and striae on stones indicate that glacial advance was to the south and west. Pebbles are clearly dominated by Paleozoic clasts but do contain some local lithologies as well.

SUPRAGLACIAL TILL

A very weak (random?) fabric was detected in the supraglacial till which is clearly dominated by angular, local clasts derived from granitoid and metavolcanic rocks to the northeast.

SUMMARY

The glaciotectonic and fabric data agree with the ice movement data of Geddes and Bajc (1984a, 1984b) and clearly indicate southwestward advance. Paleozoic, peridotite, and iron formation clasts confirm this since they originated from bedrock sources to the northeast. The Paleozoic pebbles were derived from the James Bay Lowlands, at least 150 km distant. Pebble assemblages indicate that ice advanced southwestward across lithologic contacts rather than parallel to them.

TABLE 266.2. GEOCHEMICAL ANALYSES OF HEMLO TILL SAMPLES (-0.002 mm fraction)

Site	Till Facies	Cu ppm	Ni ppm	Ca %	Pb ppm	Ag ppm	Mo ppm	As ppm	Sb ppm	Ba ppm	Au ppb
1	upper lodgment	38	34	19.3	7	.6	6	2.3	<.2	418	2.9
1	meltout	50	36	19.1	9	.8	4	2.5	<.2	421	9.6
2	meltout	74	61	11.2	12	.4	3	4.0	<.2	701	6.1
2	lower lodgment	39	44	9.89	11	.4	2	3.7	<.2	570	1.7
3	meltout	65	68	4.58	23	.4	2	5.3	<.2	734	24.8
4	meltout (upper)	120	100	9.06	9	.6	6	2.3	<.2	742	9.4
4	meltout (middle)	110	91	11.5	9	.4	6	2.3	<.2	693	7.2
4	meltout (lower)	105	80	12.1	11	.6	6	2.7	<.2	681	5.9
5	upper lodgment	48	46	14.8	13	.8	6	4.3	<.2	481	4.4
5	meltout	41	45	15.6	12	.4	5	3.7	<.2	465	11.2
5	meltout	50	48	13.0	16	.4	3	5.0	<.2	467	8.0
5	lower lodgment (top)	25	46	12.2	10	.4	5	1.2	<.2	574	1.6
5	lower lodgment (upper)	25	44	12.1	8	.4	6	1.8	<.2	558	1.7
5	lower lodgment (middle)	10	20	13.1	3	.4	2	1.9	<.2	558	2.2
5	lower lodgment (lower)	10	20	12.9	4	.6	3	1.8	<.2	540	1.4
5	lower lodgment (bottom)	10	20	12.6	3	.6	2	1.9	<.2	560	2.4
6	upper lodgment	62	43	18.1	8	.6	2	2.5	<.2	473	2.3
7	supraglacial	200	130	.86	40	.4	3	5.2	<.2	669	57.3
7	meltout	220	93	2.21	25	.4	3	5.2	<.2	724	17.1
7	lower lodgment	85	65	3.82	13	.4	5	3.7	<.2	625	3.2

GEOCHEMICAL GLACIAL DISPERSAL

Atomic absorption analyses of the -0.002 mm fraction in till matrices for nine metals and arsenic are presented in Table 266.2. This size fraction was chosen because it most accurately reflects pre-weathering proportions of metals in the till matrix (Shilts 1975, 1984).

The supraglacial meltout till is generally richest in metals, especially gold, whereas the calcareous tills contain lesser amounts of metals, with the exception of calcium. Meltout till is generally richer in metals than the lodgment facies, but has lesser matrix carbonate. The relationship between metal content and matrix carbonate is demonstrated in Figure 266.2 for four significant metals; in general, as matrix carbonate increases, metal content decreases. This trend reflects relative dilution of metals of local to intermediate provenance by distal carbonate matrix during glacial transport and deposition. Supraglacial till has little or no carbonate matrix and better reflects the local bedrock geochemistry.

DEPOSITIONAL MODEL AND GLACIAL HISTORY

The entire till sequence in the Hemlo area can be explained by one glacial advance over uplands to the northeast. The carbonate tills are probably the result of glacial deposition in the lee sides of the uplands (Figure 266.1) resulting in deposition of englacial debris that was downsheared to the basal zone as the glacier temporarily experienced extending flow, and later, stagnation.

The depositional model depicted in Figure 266.3 bears similarities to that proposed by Gillberg (1965) in Sweden, although Shilts (1973) has also reported on upland lee side glacial deposition in Quebec. A hypothesis of ice behaviour and till deposition is presented below (Figure 266.3).

Glacier ice advancing from the north-northeast met the stoss side of the upland and experienced local compressional flow which was diverted around it, as well as inducing upshearing of glacial debris.

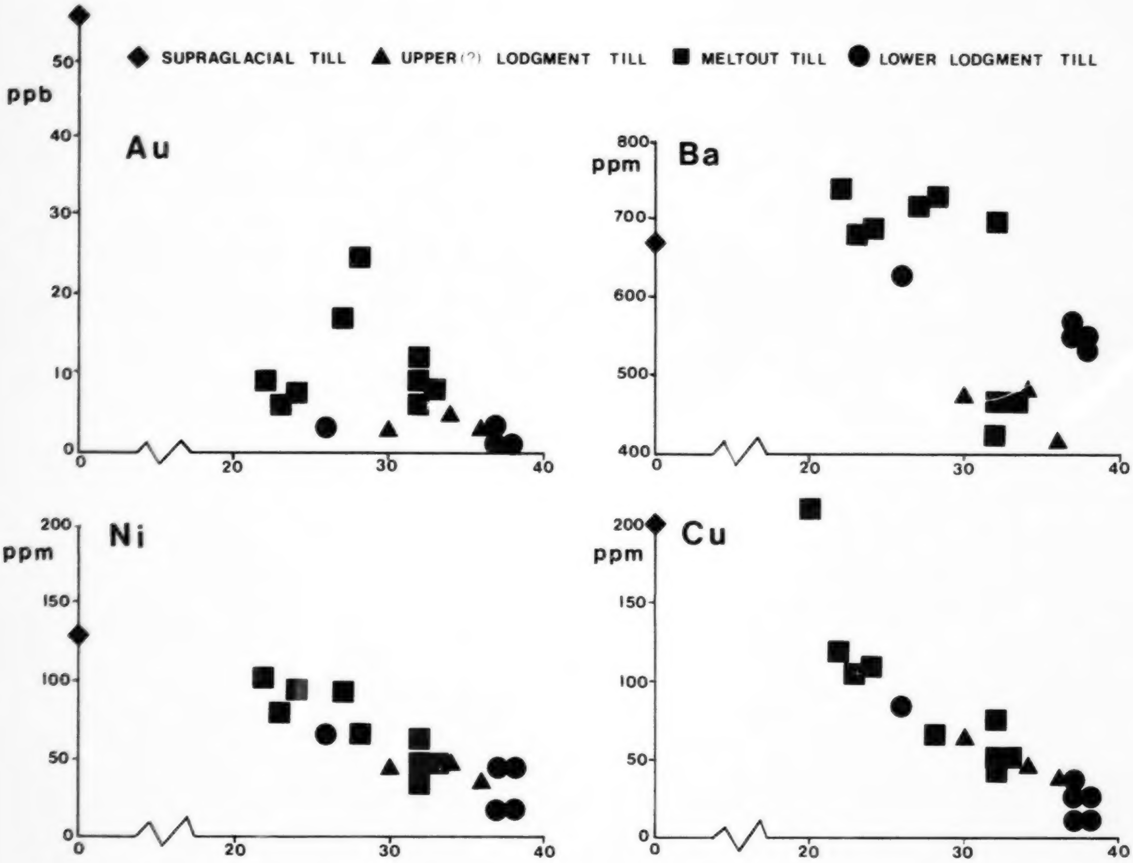

Figure 266.2. *Geochemical comparison of significant metals in Hemlo till matrices (-0.002 mm fraction) with matrix carbonate (-0.063 mm fraction).*

and eroding the local bedrock and depositing Geddes' (1984a, 1984b, 1984c), Geddes and Bajc's (1985a, 1985b), and Geddes' *et al.* (1985) basal noncarbonate till. The englacial zone overrode the retarded basal ice and continued the stoss side upshearing of local debris to the supraglacial position (above englacially transported distal debris; Figure 266.3). It then advanced over the upland while experiencing downshearing of its debris during extending flow. This resulted in lodgment of englacial debris on top of the basal noncarbonate till, on the lee side of the upland.

After the glacier reached its maximum extent, it probably stagnated in the Hemlo area where the bulk of the glacial debris was deposited by subglacial meltout. This is supported by the various late glacial ice disintegration features in the area (Geddes and Bajc 1984a, 1984b). The upper till probably represents a late reactivation of the glacier during general downwasting, and further deposition of englacial debris as lodgment till.

Finally, upland stoss side debris that was upsheared to the supraglacial position was lowered to the surfaces of the underlying calcareous meltout and lodgment tills by supraglacial meltout.

ECONOMIC AND ENVIRONMENTAL ASPECTS

The above results and interpretations indicate that an understanding of till genesis, stratigraphy, and ice movements are important for mineral exploration strategies and environmental considerations. Some recommendations are presented below for the Hemlo area.

DRIFT PROSPECTING

The supraglacial meltout till, and probably Geddes' basal noncarbonate till, are best to sample in overburden drilling programs.

They comprise material that has been transported for relatively short distances (mainly derived from uplands less than 20 km upglacier; Figure 266.1) and are, therefore, most likely to contain well defined dispersal fans of ore anomalies which may be traced back to source (c.f. Shilts 1976, 1984). This is exemplified by the relatively high gold value in the supraglacial till, which occurs within an active gold mining area.

The calcareous tills, however, are detrimental to drift prospecting because they contain mainly distally transported materials (some from at least 150 km

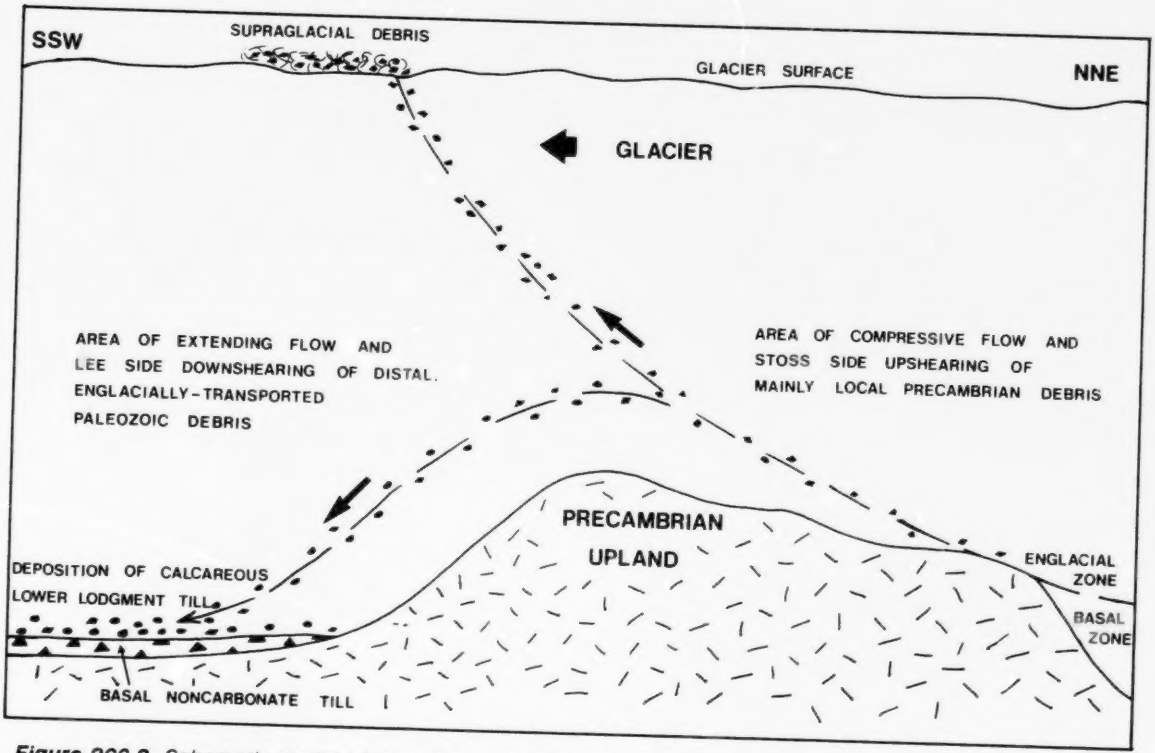
SSW
SUPRAGLACIAL DEBRIS
GLACIER SURFACE
NNE
GLACIER
AREA OF EXTENDING FLOW AND LEE SIDE DOWNSHEARING OF DISTAL, ENGLACIALLY-TRANSPORTED PALEOZOIC DEBRIS
AREA OF COMPRESSIVE FLOW AND STOSS SIDE UPSHEARING OF MAINLY LOCAL PRECAMBRIAN DEBRIS
PRECAMBRIAN UPLAND
ENGLACIAL ZONE
BASAL ZONE
DEPOSITION OF CALCAREOUS LOWER LODGMENT TILL
BASAL NONCARBONATE TILL

Figure 266.3. Schematic model of the glacier advancing over an upland northeast of Hemlo. Not to scale.

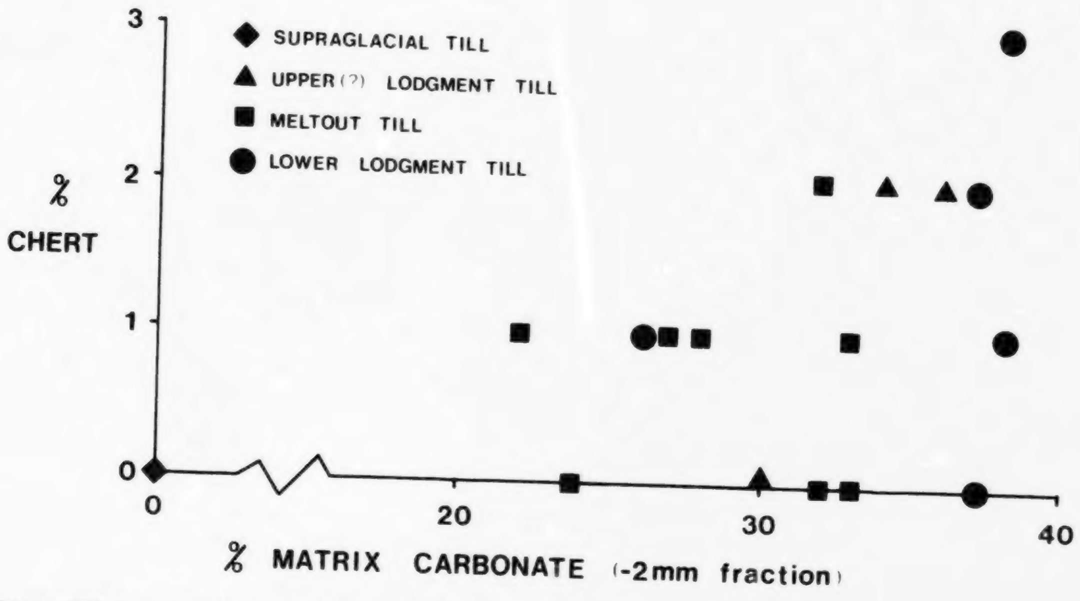

Figure 266.4. Comparison of chert pebble content in Hemlo tills with till matrix carbonate (-0.063 mm fraction).

away) which mask glacially dispersed ore of local to intermediate provenance. Any disperal fans within the calcareous tills will probably be too diffuse to recognize, or to successfully trace anomalies back to source, because ore values are near background levels this far downglacier from distal ore sources.

AGGREGATE QUALITY

Gravel in the Hemlo area should be good for construction purposes. The highest chert content (which can cause hydration and cracking problems in southern Ontario concrete) was only 3% in the till samples collected, and generally increases with matrix carbonate (Figure 266.4). Several samples contained no chert. Associated outwash deposits should also contain low amounts of chert as they were probably derived from the same glacier.

However, rotted amphibolite, granitoid, and gneissic stones are relatively abundant in a few places and may be problematic for aggregate usage.

ACID RAIN

The calcareous tills should be excellent buffers. They are almost as calcareous as those overlying carbonate bedrock in southern Ontario where till matrix carbonate would attain a maximum.

Map unit 3b of Geddes and Bajc (1984a, 1984b) is the least susceptible to acid rain, although some glaciolacustrine deposits are also calcareous. Thus a map of acid rain susceptibility could be constructed based on the matrix carbonate of the various sediment units in the area, such as that attempted by Woods (1985, p.45).

Lakes within areas of calcareous glacial drift are more alkaline than those without and also serve as buffers (Woods 1985; Coker and Shilts 1979).

TAILINGS DAM CORES

The calcareous lodgment tills serve well as low-permeability cores with high capacity for buffering acidic mine tailings. Lac Minerals used the lower lodgment till for this purpose, the excavation of which provided the exposure at site 5.

ACKNOWLEDGMENTS

R.S. Geddes (Engineering and Terrain Geology Section, Ontario Geological Survey) provided invaluable logistical and scientific support throughout the course of this study. E.V. Sado (Engineering and Terrain Geology Section, Ontario Geological Survey) suggested the project and was generous with advice and support. G.O. and S.L. Brown (Department of Geology, University of Western Ontario) ably performed field and laboratory duties. S.L. Brown and J.-A. Potter (Department of Geology, University of Western Ontario) assisted in drafting the diagrams. Research was funded by the Ontario Geoscience Research Grant Program.

REFERENCES

American Society for Testing and Materials
1972: Standard Method for Particle-size Analysis of Soils. Annual Book of Standards D422-63; p.112-122. Philadelphia, Pennsylvania.

Boissoneau, A.N.
1966: Glacial History of Northeastern Ontario: 1. The Cochrane-Hearst Area; Canadian Journal of Earth Sciences, Volume 3, Number 5, p.559-578.

Coker, W.B., and Shilts, W.W.
1979: Lacustrine Geochemistry Around the North Shore of Lake Superior: Implications for Evaluation of the Effects of Acid Precipitation; Geological Survey of Canada, Paper 79-1C, p.1-15.

Cowan, W.R.
1976: Evaluation of Selected Granular Aggregate Deposits, North Shores of Lakes Huron and Superior; Ontario Division of Mines, Miscellaneous Paper 67, p.137-138.

Dreimanis, A.
1962: Quantitative Gasometric Determination of Calcite and Dolomite by Using Chittick Apparatus; Journal of Sedimentary Petrology, Volume 32, p.520-529.
1976: Tills: Their Origin and Properties; p.11-49 *in* Glacial Till, edited by R.F. Legget, Royal Society of Canada, Special Publication 12.
1982: Genetic Classification of Tills and Criteria for Their Differentiation; p.12-31 *in* International Quaternary Association, Commission on Genesis and Lithology of Quaternary Deposits, Report of Activities 1977-1982, edited by C. Schlüchter, Honggerberg, Zurich, Switerzerland.

Farrand, W.R.
1962: Postglacial Uplift in North America; American Journal of Science, Volume 260, p.181.

Fortescue, J.A.C., and Geddes, R.S.
1983: A Small Scale Geochemistry/Quaternary Geology Study in the Hemlo Camp, District of Thunder Bay; p.159-160 *in* Summary of Field Work, 1983, by the Ontario Geological Survey, edited by John Wood, Owen L. White, R.B. Barlow, and A.C. Colvine, Ontario Geological Survey, Miscellaneous Paper 116, 313p.

Gartner, J.F., and McQuay, D.F.
1979: Heron Bay Area, District of Thunder Bay; Ontario Geological Survey, Northern Ontario Engineering Geology Terrain Study 60, 15p. Accompanied by Map 5093, scale 1:100 000.
1980: White River Area, Districts of Thunder Bay and Algoma; Ontario Geological Survey, Northern Ontario Engineering Geology Terrain Study 61, 18p. Accompannied by Map 5098, scale 1:100 000.

Geddes, R.S.
1984a: An Exotic Till in the Hemlo Area, Northern Ontario; Geological Association of Canada, Annual Meeting Program with Abstracts, Volume 9, p.66.
1984b: Long Distance Glacial Dispersion and Mineral Exploration; Till Tomorrow '84 Symposium Abstracts, p.35, Held at Kirkland Lake, Ontario May 8-12, 1984, Sponsored by Canadian Institute of Mining and Metallurgy and the Ontario Geological Survey.

1984c: Quaternary Geology of the Hemlo Area; p.97-103 *in* Summary of Field Work, 1984, by the Ontario Geological Survey, edited by John Wood, Owen L. White, R.B. Barlow, and A.C. Colvine, Ontario Geological Survey, Miscellaneous Paper 119, 309p.

Geddes, R.S., and Bajc, A.F.

1985a: Quaternary Geology of the White Lake Area, District of Thunder Bay; Ontario Geological Survey, Map P.2849, scale 1:50 000.

1985b: Quaternary Geology of the Cedar Lake Area, District of Thunder Bay; Ontario Geological Survey, Map P.2850, scale 1:50 000.

Geddes, R.S., Bajc, A.F., and Kristjansson, F.J.

1985: Quaternary Geology of the Hemlo Region, District of Thunder Bay; p.151-154 *in* Summary of Field Work and Other Activities, 1985, by the Ontario Geological Survey, edited by John Wood, Owen L. White, R.B. Barlow, and A.C. Colvine, Ontario Geological Survey, Miscellaneous Paper 126, 351p.

Gillberg, G.

1965: Till Distribution and Ice Movements on the Northern Slopes of the South Swedish Highlands; Geologiska Foreningens i Stockholm Forhandlingar, Volume 86, p.433-484.

Goldthwait, R.P.

1971: Introduction to Till, Today; p.3-26 *in* Till: A Symposium, edited by R.P. Goldthwait, Ohio State University Press, Columbus, Ohio.

Muir, T.W.

1982a: Geology of the Heron Bay Area, District of Thunder Bay; Ontario Geological Survey, Report 218, 89p.

1982b: Geology of the Hemlo Area, District of Thunder Bay; Ontario Geological Survey, Report 217, 65p.

Shaw, J.

1982: Melt-out Till in the Edmonton Area, Alberta, Canada; Canadian Journal of Earth Sciences, Volume 19, p.1548-1569.

1983: Forms Associated with Boulders in Melt-out Till; p.3-12 *in* Tills and Related Deposits, edited by E.B. Evenson, C. Schlüchter, and J. Rabassa, A.A. Balkema Publishers, Rotterdam, Netherlands.

1985: Subglacial and Ice Marginal Environments; p.7-84 *in* Glacial Sedimentary Environments, edited by G.M. Ashley, J. Shaw, and N.D. Smith, Society of Economic Mineralogists and Paleontologists, Short Course 16.

Shilts, W.W.

1973: Glacial Dispersal of Rocks, Minerals, and Trace Elements in Wisconsinan Till, Southeastern Quebec, Canada; p.189-219 *in* The Wisconsinan Stage, edited by R.F. Black, R.P. Goldthwait, and H.B. Willman, Geological Society of America, Memoir 136.

1975: Principles of Geochemical Exploration for Sulphide Deposits Using Shallow Samples of Glacial Drift; Canadian Institute of Mining and Metallurgy Bulletin, May 1985, p.73-80.

1976: Glacial Till and Mineral Exploration; p.205-224 *in* Glacial Till, edited by R.F. Legget, Royal Society of Canada, Special Publication 12.

1984: Till Geochemistry in Finland and Canada; Journal of Geochemical Exploration, Volume 21, p.95-117.

Siragusa, G.M.

1984a: Precambrian Geology of the White Lake Area, Eastern Part, Thunder Bay District; Ontario Geological Survey, Map P.2702, scale 1:15 840.

1984b: Precambrian Geology of the White Lake Area, Western Part, Thunder Bay District; Ontario Geological Survey, Map P.2701, 1:15 840.

1985a: Precambrian Geology of the White Lake Area, Animons Lake Section, District of Thunder Bay; Ontario Geological Survey, Map P.2739, scale 1:15 840.

1985b: Precambrian Geology of the White Lake Area, District of Thunder Bay; Ontario Geological Survey, Map P.2738, scale 1:15 840.

Woods, E.A.

1985: The Relationship Between the Surficial Geology and Lake Water Alkalinity in the Hemlo-Manitouwadge Area, Ontario; Unpublished B.Sc. Thesis, University of Western Ontario, London, Ontario.

Zoltai, S.C.

1965a: Glacial Features of the Quetico-Nipigon Area, Ontario; Canadian Journal of Earth Sciences, Volume 2, p.247-269.

1965b: Surficial Geology of the Thunder Bay Map Area; Ontario Department of Lands and Forests, Map S265.

1967: Glacial features of the North-Central Lake Superior Region, Ontario; Canadian Journal of Earth Sciences, Volume 4, p.515-528.

Grant 269 Compositional Characteristics of Pyrite in Barren and Gold Mineralized Veins

N.D. MacRae and H.W. Nesbitt

Department of Geology, University of Western Ontario, London

ABSTRACT

Based on the assumption that trace elements incorporated in quartz vein pyrite grains reflect the character of solution at the time of their growth, an attempt has been made to thus separate vein systems into genetic types: gold bearing and gold barren. Samples from two such clearly distinguishable vein types were obtained from the Canadian Arrow Mine near Matheson, Ontario. *In situ* secondary ion mass spectrometry was employed since trace element contents were too low for other techniques. As-Ag variation pairs show some potential for genetic separation, but other variation pairs, such as Co-Ni, suggest pyrite from both vein systems are closely related, but unrelated to gold content of the veins. The trends differ for localities.

INTRODUCTION

This research study is an examination of some trace elements of pyrite contained in and adjacent to quartz veins for the purpose of determining if these elements are useful in quantifying gold contents of the vein-forming solutions. Samples from two intersecting sets of quartz veins, one bearing gold and one barren, were obtained from the Canadian Arrow Mine near Matheson, Ontario. Field relations, petrography, and geochemistry of the rock units are already well documented (McNeil 1983; Cherry 1982; Prest 1957).

It has been demonstrated (Seward 1973; Helgeson and Garrels 1968; Henley 1973) that the chemical properties of solutions control transportation and deposition of gold. For some factors, such as pH, the favourable range for transportation is narrow (Seward 1973). Similarly in these environments, transition metal contents of minerals are largely controlled by the characteristics of solutions (Barnes 1979). The premise of this study is, therefore, that pyrite, which is ubiquitous in these hydrothermal systems, should reflect transition metal contents of the formative fluids. This, in turn, could permit separation of the vein systems into genetic groups, some of which are suited to gold deposition and others which are not.

FIELD AREA

The Canadian Arrow Mine, last worked in early 1982, is an abandoned open pit development located in the southwest portion of Hislop Township near Matheson, Ontario. It was based upon hydrothermal quartz veins carrying low gold contents which developed in an Archean trondhjemitic stock. The following pertinent geologic details are summarized from a study of the mine area by McNeil (1983).

Two prominent vein-fracture systems, each distinguished by characteristic orientation and petrography, appear in wall rocks of the open pit. The earlier set has a general northeast-trending dip, and contains coarse quartz and calcite commonly in a vuggy texture, with disseminated pyrite, galena, and occasional chalcopyrite. They range in thickness from 0.5 to 1.0 cm and are spaced roughly 2 m apart. The later set cleanly cuts the first, is oriented with a general northwest-trending dip, and consists largely of coarse quartz grains with an elongation parallel to the vein walls. The groundmass consists of much smaller and equant quartz with rare calcite. A few pyrite cubes (approximately 0.5 mm) commonly appear at the vein walls. This vein set ranges in thickness from 1 mm to 5 cm but is much less regularly distributed than the early set.

Most diagnostic of the later set of veins are brick-red 0.3 cm thick selvages paralleling both contacts, indicative of intense hematization and K-feldspar enrichment of the adjacent trondhjemite. These selvages show a 1400% enrichment in Au over the parent igneous rock. No similar alteration and no similar Au enrichment are associated with the earlier quartz veins.

Based upon considerable geochemistry, including oxygen isotope data, McNeil (1983) concludes that the early quartz veins fill hydraulic fractures developed at a discharge site of convecting low temperature (200° to 300°C) ocean brines. The later gold-bearing fluids were hydrothermal, near neutral pH, oxidizing fluids of 300° to 370°C, but their origin is speculative.

ANALYTICAL TECHNIQUE

Excluding iron, the transition metals may be present only at ppm levels, and those contents may change dramatically from grain to grain or even within grain zones. Because of these possible variations, an *in situ* analytical method was deemed essential.

In situ analyses of geological materials by electron microprobe have been routine for many years. However, determinations in the ppm range, certainly below 100 ppm, have been generally unsuccessful by electron probe because of the background noise inherent in any X-ray technique. Secondary Ion Mass Spectrometry (SIMS) is also an *in situ* analytical technique, but with the obvious advantage of no inherent background noise. It is a destructive technique, however, in which secondary ions are sputtered from a small volume of sample, extracted from the sample area, and analyzed by a mass spectrometer for virtually any isotope or ratio of isotopes.

While the SIMS technique offers great promise to geochemical studies, the presence of molecular ions and multiple charged ions in the analyzed spectra, together with enhancement and/or suppression effects due to matrix variations, have greatly limited its application.

Interferences can be reduced by using a very high mass resolution or by filtering molecular and complex ion energies from atomic ion energies (Shimizu and Hart 1982; Ray and Hart 1982). Both methods, unfortunately, result in considerable signal loss, thus limiting the ultimate sensitivity. A variation of energy filtering, called the "specimen isolation" (SI) mode, developed at Surface Science Western (Metson *et al.* 1983, 1984), retains more signal and more effectively filters complex ions, but employs a primary beam of approximately 50 μm diameter (i.e. 10 to 20 times larger than for most conventional methods), thus requiring larger target grain sizes. The SI method has previously been used successfully to measure, for example, rare earth element contents in silicates to about 20 ppb (MacRae and Metson 1985). Until the present study, nearly all SI method analyses have been of silicate minerals and glasses or oxides.

Mainly because of the conductive nature of pyrite, initial analytical sessions concentrated on a conventional energy filtering technique, using a finely focused $^{16}O^-$ primary beam on gold-coated samples. The plethora of combinations of Fe, S, and O complexes necessitated abandoning the method. Only in the SI mode of operation, with a primary beam of $^{16}O^-$ on uncoated samples, could a "clean" spectrum at the desired level of sensitivity be obtained. The reader is referred to MacRae and Metson (1985) and publications noted therein for additional details of the SI mode of analysis.

The problem of matrix composition variations influencing isotope yields is not applicable to this problem since, in terms of major elements, all material being analyzed is the same—pyrite.

TRACE ELEMENT ANALYSIS

Preliminary analyses examined a number of pyrite grains rapidly for every isotope from 1 to 250. From these spectra a number of masses were chosen (Table 269.1) as representative of the various categories of potentially useful elements. Also, the masses were selected on the basis of higher abundances and least possible interferences for the elements. To minimize variations in instrument conditions from one operating session to the next, ^{57}Fe was also analyzed for and each of the trace isotopes in ratio to it. The trace isotopes were divided into two batches, with a counting time per mass of 20 seconds for the more abundant elements (Co, Ni, Cu, Zn, Ga, Ge, and As) and 40 seconds per mass for the less abundant ones (Ag, Cd, In, Te, Ir, Au, Tl, and Bi). The analytical data presented in Table 269.1 are average ratios of electron multiplier counts of {trace element mass/^{57}Fe} for, normally, three complete repetitions of all the masses per analytical spot.

A typical pyrite grain and SIMS crater are shown in Photo 269.1. The photo illustrates the major problem with the technique: a very large beam, possibly because of the conducting target isolated in silicate, and small pyrite grains.

Samples prefixed 23, 25, 28, and 31a (Table 269.1) are of pyrite from the quartz veins and selvages which represent the gold-enriched system; samples 2 and 34 are of pyrite from the gold-barren veins of the Canadian Arrow Deposit. Also from quartz veins but from completely unrelated deposits are analyses for sample MD4 (highly gold enriched system) and for samples PC and RICCO (gold barren systems).

SULPHUR ISOTOPE ANALYSIS

SIMS permits *in situ* analysis of virtually any isotope, thus the possibility of determining $^{34}S/^{32}S$ ratios had to be tested. In fact, while the isotope distribution could be readily graphed and quantified, precision was sufficiently poor that this aspect of the study was not persued. The variability may have been due to true isotope zoning in the sputtered volume of natural sample, to isotope fractionation after sputter-

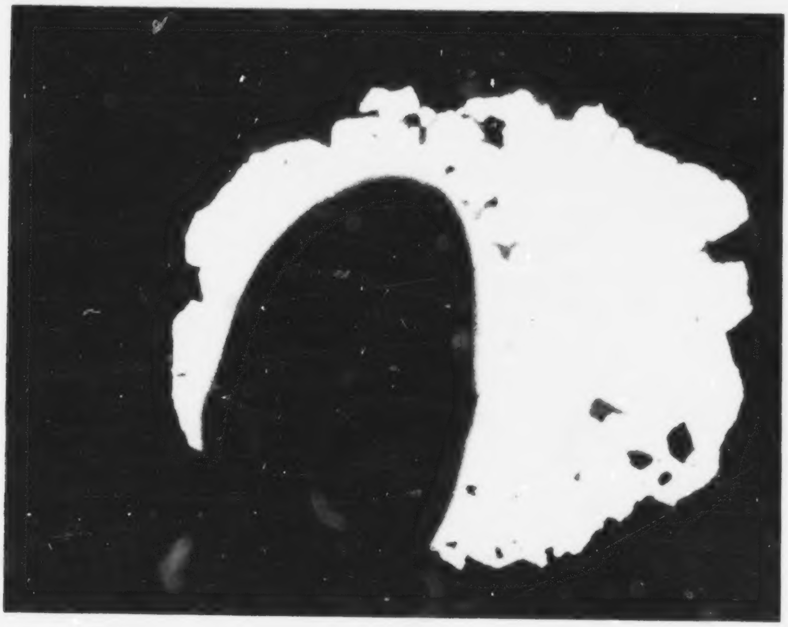

Photo 269.1.
Photomicrograph of typical pyrite grain and SIMS SI-mode crater. Bar is 0.2 mm.

TABLE 269.1. RELATIVE MASS ABUNDANCE RATIOS OF TRACE ELEMENTS IN PYRITE GRAINS. (page 1 of 3)

	25-1	25-2	25-3	RICCO-1	34-1	PC-1	PC-2
Co 59/Fe 57	3.82×10^{-3}	1.00×10^{-2}	1.31×10^{-3}	4.98×10^{-4}	1.57×10^{-2}	8.37×10^{-1}	1.20×10^{0}
Ni 60/Fe 57	1.40×10^{-3}	1.29×10^{-3}	6.06×10^{-4}	5.34×10^{-5}	1.90×10^{-4}	8.00×10^{-4}	1.02×10^{-3}
Cu 63/Fe 57	1.92×10^{-3}	1.29×10^{-3}	1.27×10^{-3}	1.10×10^{-4}	7.89×10^{-5}	1.63×10^{-5}	3.39×10^{-5}
Zn 66/Fe 57	6.35×10^{-5}	1.18×10^{-3}	2.47×10^{-5}	1.24×10^{-5}	1.33×10^{-5}	1.26×10^{-5}	8.71×10^{-6}
Ga 69/Fe 57	8.41×10^{-6}	1.62×10^{-3}	1.66×10^{-6}	2.43×10^{-6}	1.74×10^{-5}	0	0
Ge 70/Fe 57	1.38×10^{-4}	2.03×10^{-4}	1.05×10^{-4}	3.27×10^{-5}	2.36×10^{-5}	4.87×10^{-5}	6.32×10^{-5}
As 75/Fe 57	1.46×10^{-4}	8.81×10^{-5}	2.12×10^{-5}	1.86×10^{-5}	0	3.23×10^{-4}	4.92×10^{-4}
Ag 107/Fe 57	1.02×10^{-4}		2.04×10^{-4}	1.95×10^{-6}	3.87×10^{-5}		1.33×10^{-6}
Cd 111/Fe 57	3.88×10^{-6}		1.45×10^{6}	5.49×10^{-6}	0		0
Te 130/Fe 57	8.47×10^{-6}		5.27×10^{-6}	1.02×10^{-5}	5.96×10^{-5}		0
Ir 193/Fe 57	1.32×10^{-6}		0	1.71×10^{-6}	3.93×10^{-6}		0
Au 197/Fe 57	0		5.88×10^{-7}	0	0		0
Tl 205/Fe 57	1.18×10^{-6}		4.08×10^{-7}	0	7.86×10^{-6}		1.33×10^{-6}
Bi 209/Fe 57	3.58×10^{-6}		0	9.38×10^{-6}	8.95×10^{-5}		1.33×10^{-6}
	PC-3	**34-2**	**23-2**	**23.1**	**31A.3**	**31A.1**	**31A.2**
Co 59/Fe 57	4.58×10^{-2}	2.43×10^{-3}	5.36×10^{-3}	1.78×10^{-2}	3.87×10^{-3}	1.33×10^{-2}	3.13×10^{-2}
Ni 60/Fe 57	2.12×10^{-3}	5.24×10^{-5}	3.83×10^{-4}	4.44×10^{-3}	9.87×10^{-4}	2.24×10^{-3}	6.10×10^{-3}
Cu 63/Fe 57	1.52×10^{-5}	2.00×10^{-4}	1.50×10^{-3}	1.31×10^{-4}	5.27×10^{-4}	1.70×10^{-4}	8.41×10^{-4}
Zn 66/Fe 57	1.15×10^{-5}	1.70×10^{-5}	5.11×10^{-4}	5.94×10^{-5}	2.50×10^{-5}	2.72×10^{-5}	3.38×10^{-5}
Ga 69/Fe 57	0	1.32×10^{-5}	8.80×10^{-6}	3.43×10^{-5}	2.31×10^{-6}	1.96×10^{-5}	5.72×10^{-6}
Ge 70/Fe 57	6.12×10^{-5}	8.08×10^{-5}	7.30×10^{-5}	1.07×10^{-4}	1.09×10^{-4}	9.82×10^{-5}	1.09×10^{-4}
As 75/Fe 57	3.70×10^{-5}	6.60×10^{-6}	9.55×10^{-7}	8.67×10^{-6}	1.31×10^{-5}	3.74×10^{-6}	6.00×10^{-6}
Ag 107/Fe 57			3.03×10^{-6}		8.64×10^{-5}	1.12×10^{-5}	1.65×10^{-5}
Cd 111/Fe 57			0.97×10^{-7}		2.26×10^{-6}	2.22×10^{-6}	2.06×10^{-6}
Te 130/Fe 57			6.18×10^{-7}		9.09×10^{-6}	6.44×10^{-7}	4.21×10^{-6}
Ir 193/Fe 57			0		0	3.34×10^{-7}	0
Au 197/Fe 57			0		1.85×10^{-6}	9.06×10^{-7}	2.50×10^{-7}
Tl 205/Fe 57			3.44×10^{-7}		1.66×10^{-7}	0	0
Bi 209/Fe 57			7.99×10^{-5}		4.72×10^{-5}	4.48×10^{-5}	3.14×10^{-4}

Table 269.1. (page 2 of 3)

	MD4-1	MD4-2	PC-3	PC-4
Co 59/Fe 57	6.39×10^{-1}	5.47×10^{-1}	6.88×10^{-3}	2.46×10^{0}
Ni 60/Fe 57	1.17×10^{-3}	4.75×10^{-4}	1.89×10^{-2}	2.29×10^{-3}
Cu 63/Fe 57	4.77×10^{-5}	2.50×10^{-5}	2.53×10^{-5}	2.21×10^{-6}
Zn 66/Fe 57	1.15×10^{-5}	1.12×10^{-5}	1.36×10^{-5}	7.86×10^{-6}
Ga 69/Fe 57	3.46×10^{-5}	7.84×10^{-6}	4.61×10^{-5}	8.70×10^{-7}
Ge 70/Fe 57	2.42×10^{-5}	5.51×10^{-5}	8.17×10^{-5}	3.89×10^{-5}
As 75/Fe 57	4.82×10^{-3}	6.02×10^{-3}	8.43×10^{-5}	1.73×10^{-3}
Ag107/Fe 57	3.05×10^{-6}	4.08×10^{-6}	1.69×10^{-6}	1.01×10^{-6}
Cd 111/Fe 57	4.42×10^{-7}	9.63×10^{-7}	2.07×10^{-6}	6.33×10^{-7}
Te 130/Fe 57	0	6.12×10^{-7}	1.96×10^{-7}	0
Ir 193/Fe 57	4.30×10^{-7}	0	0	0
Au 197/Fe 57	8.84×10^{-7}	1.34×10^{-7}	2.68×10^{-7}	7.91×10^{-8}
Tl 205/Fe 57	4.42×10^{-7}	1.34×10^{-7}	1.17×10^{-7}	1.58×10^{-7}
Bi 209/Fe 57	1.08×10^{-6}	2.18×10^{-6}	2.46×10^{-7}	7.37×10^{-7}

TABLE 269.1. (page 3 of 3)

	28-2-1	28-2-5	28-2-3	28-2-4	28-1-2	28-1-1	28-1-3
Co 59/Fe 57	2.16×10^{-2}	1.07×10^{-2}	5.95×10^{-3}	5.20×10^{-2}	5.23×10^{-3}	2.60×10^{-3}	3.28×10^{-2}
Ni 60/Fe 57	3.98×10^{-3}	3.03×10^{-3}	2.40×10^{-3}	8.85×10^{-3}	8.81×10^{-4}	5.54×10^{-4}	4.98×10^{-3}
Cu 63/Fe 57	2.14×10^{-3}	2.75×10^{-3}	2.44×10^{-3}	3.85×10^{-3}	5.64×10^{-3}	7.22×10^{-3}	7.59×10^{-2}
Zn 66/Fe 57	7.48×10^{-4}	1.93×10^{-3}	6.27×10^{-4}	6.70×10^{-4}	8.60×10^{-4}	5.11×10^{-3}	9.45×10^{-4}
Ga 69/Fe 57	8.15×10^{-5}	4.51×10^{-5}	1.77×10^{-4}	1.03×10^{-4}	1.40×10^{-4}	1.67×10^{-4}	2.63×10^{-4}
Ge 73/Fe 57	7.58×10^{-3}	4.45×10^{-3}	8.57×10^{-3}	6.67×10^{-3}	8.85×10^{-3}	9.39×10^{-3}	7.81×10^{-3}
Ag 107/Fe 57	3.10×10^{-5}	1.58×10^{-5}	2.55×10^{-5}	6.89×10^{-5}	4.45×10^{-5}	1.26×10^{-4}	6.54×10^{-5}
Cd 111/Fe 57	2.84×10^{-4}	2.05×10^{-4}	1.10×10^{-4}	2.21×10^{-4}	3.37×10^{-4}	4.20×10^{-4}	2.82×10^{-4}
In 113/Fe 57	5.22×10^{-3}	4.03×10^{-3}	1.78×10^{-3}	4.33×10^{-3}	6.01×10^{-3}	6.42×10^{-3}	4.91×10^{-3}

	25-1-1	25-3-1	25-2-2	25-2-1	25-1-3	2-1-1	2-1-2
Co 59/Fe 57	5.17×10^{-3}	5.10×10^{-3}	7.89×10^{-3}	5.62×10^{-3}	2.01×10^{-2}	7.88×10^{-3}	8.56×10^{-3}
Ni 60/Fe 57	1.41×10^{-3}	4.92×10^{-4}	1.94×10^{-3}	1.13×10^{-3}	5.74×10^{-3}	4.25×10^{-5}	4.25×10^{-5}
Cu 63/Fe 57	4.48×10^{-3}	4.53×10^{-3}	1.13×10^{-2}	5.27×10^{-3}	1.06×10^{-3}	2.55×10^{-3}	2.62×10^{-3}
Zn 66/Fe 57	1.26×10^{-3}	6.85×10^{-4}	1.18×10^{-3}	1.93×10^{-3}	7.91×10^{-4}	4.66×10^{-4}	5.04×10^{-4}
Ga 69/Fe 57	2.11×10^{-4}	1.15×10^{-4}	1.02×10^{-4}	6.59×10^{-5}	1.62×10^{-4}	6.27×10^{-5}	5.41×10^{-5}
Ge 73/Fe 57	1.25×10^{-2}	1.49×10^{-2}	1.50×10^{-2}	7.75×10^{-3}	1.05×10^{-2}	4.48×10^{-3}	2.92×10^{-3}
Ag 107/Fe 57	1.49×10^{-4}	4.66×10^{-5}	1.95×10^{-4}	2.15×10^{-5}	2.06×10^{-5}	1.10×10^{-5}	4.41×10^{-6}
Cd 111/Fe 57	4.40×10^{-4}	3.71×10^{-4}	4.66×10^{-4}	3.17×10^{-4}	2.87×10^{-4}	1.84×10^{-4}	1.80×10^{-4}
In 113/Fe 57	6.05×10^{-3}	6.03×10^{-3}	6.79×10^{-3}	4.94×10^{-3}	5.44×10^{-3}	3.71×10^{-3}	3.36×10^{-3}

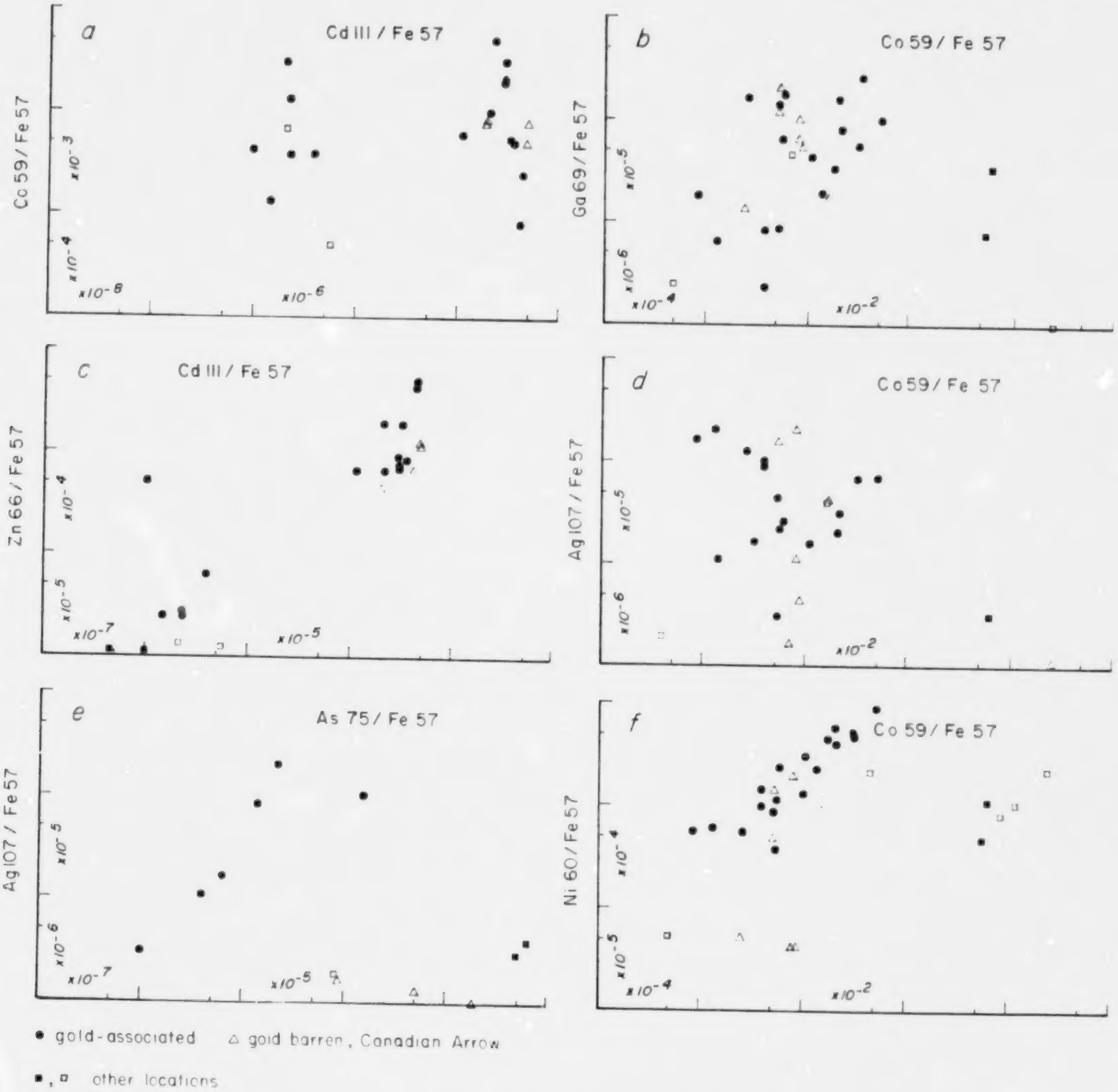

Figure 269.1. *Variation diagrams of isotope pairs for analyzed pyrite grains.*

ing, or simply to limited resolution from the relatively short flight path of the Cameca IMs-3f instrument.

RESULTS AND DISCUSSION

Six pairs of the isotope ratios recorded in Table 269.1 are illustrated in Figure 269.1. With the exception of the ^{107}Ag/^{57}Fe versus ^{75}As/^{57}Fe plot (for which the data are too few to be potentially meaningful), the diagrams do not indicate a separation of pyrite for the Canadian Arrow samples into gold association categories.

A major drawback to the analytical technique was the necessity to abandon the conventional mode of SIMS operation because of the abundance of Fe, S, and O interferences even with energy filtering. The large beam size contrasted with small grain size of SI mode of operation undoubtably is reflected in the quality of data recovered. Some of the apparent correlations of elements, for example Cd-Co or Cd-Zn, are actually due to incorporation in the sputtered volume of small inclusions such as sphalerite.

The As-Ag relationship should be further examined, as should the Co-Ni relationship. The latter shows a significantly high correlation of all samples from the Canadian Arrow deposit as distinct from samples of any other locality. The implication is that the pyrite grains of the one locality are related in some chemical properties, but not related to gold distribution.

ACKNOWLEDGMENTS

M.E. Cherry (Geologist, Ontario Geological Survey, Toronto) contributed nearly all samples of the Canadian Arrow deposit, as well as his time and thoughts in discussion of the pertinent geology. A.M. McNeil (Graduate Student, Department of Geology, University of Western Ontario, London) supplied sample 34, and contributed invaluable information from his B.Sc. thesis. Other samples were available from within the student/faculty collections of the Department of Geology, University of Western Ontario, London.

REFERENCES

Barnes, H.L.
1979: Solubilities of Ore Solutions; *in* Geochemistry of Hydrothermal Ore Deposits, Second Edition; John Wiley, New York.

Cherry, M.E.
1982: Felsic Intrusion Associated Lode Gold Deposits in the Matheson Area, Cochrane District; p.176-179 *in* Summary of Field Work, 1982, by the Ontario Geological Survey, edited by John Wood, Owen L. White, R.B. Barlow, and A.C. Colvine, Miscellaneous Paper 106, 235p.

Helgeson, H.C., and Garrels, R.M.
1968: Hydrothermal Transport and Deposition of Gold; Economic Geology, Volume 63, 622p.

Henley, R.
1973: Solubility of Gold in Hydrothermal Chloride Solutions; Chemical Geology, Volume 11, p.73-87.

MacRae, N.D., and Metson, J.B.
1985: *In-Situ* Rare-Earth Element Analysis of Coexisting Pyroxene and Plagioclase by Secondary Ion Mass Spectrometry; Chemical Geology, Volume 53, p.325-333.

McNeil, A.M.
1983: Petrology and Geochemistry of Lithologies and Alteration Regimes within the Canadian Arrow Gold Mine, Matheson, Ontario; Unpublished B.Sc. Thesis, University of Western Ontario, London.

Metson, J.B., Bancroft, G.M., McIntyre, N.S., and Chauvin, W.J.
1983: Suppression of Molecular Ions in the Secondary Ion Mass Spectra of Minerals; Surface and Interface Analysis, Volume 5, p.181-185.

Metson, J.B., Bancroft, G.M., Nesbitt, H.W., and Johasson, R.G.
1984: Analysis for Rare Earth Elements in Accessory Minerals by Specimen Isolated Secondary Ion Mass Spectrometry; Nature, Volume 307, p.347-349.

Prest, V.K.
1957: Geology of Hislop Township, Cochrane District, Ontario; Ontario Department of Mines, Annual Report for 1956, Volume 65, Part 5, 51p. Accompanied by Map 1955-5, scale 1:12 000 or inch to 1000 feet.

Ray, G., and Hart, S.R.
1982: Quantitative Analysis of Silicates by Ion Microprobe; International Journal of Mass Spectrometry and Ion Physics, Volume 44, p.231-255.

Seward, T.M.
1973: Thio Complexes of Gold and the Transport of Gold in Hydrothermal Solutions; Geochimica et Cosmochimica Acta, Volume 37, p.379-399.

Shimizu, N., and Hart, S.R.
1982: Applications of the Ion Microprobe to Geochemistry and Cosmochemistry; Annual Review of Earth and Planetary Science, Volume 10, p.483-526.

Grant 271 Petrographic and Chemical Properties Affecting Calcining of High Purity Carbonates

Peter P. Hudec

Department of Geology, University of Windsor, Windsor

ABSTRACT

High purity limestone and dolostone are used for various industrial purposes which involve "calcining" or roasting the stone. The behaviour of the carbonates during calcining was found to depend on the grain size, the MgO content, and the insoluble residue content of the rock. Larger grain size increased the abrasion potential of the calcined product which results in increased "dust" content of the stack gasses. Larger grain size also increases the compressive strength of the calcined stone, important in steel production.

The increase in the insoluble residue content of dolostones increases their strength and abrasion resistance. The MgO content in the limestones is related to the insoluble residue; increase in the residue decreases the strength of the calcined limestone.

The Amabel dolomite was found to have the fastest calcining rates; the slowest rates were found in the Detroit River limestones. The calcining rate of both limestones and dolostone increases with the insoluble residue content.

INTRODUCTION

The calcining of carbonates takes place for various purposes: reduction of iron, production of cement, production of lime, and production of industrial chemicals, to mention a few (Harben and Bates 1984). Determining the properties of carbonates that affect the calcining process can aid in selecting the most suitable ones, or adjusting the process to the available sources.

Carbonates used as flux in the steel industry do not behave in similar fashion even though their bulk chemical composition is the same. This observation was made when the author was asked to compare two United States sources of flux stone (Drummond Island and Cedarville) against a Canadian source (Manitoulin Dolomite). Although all three quarries operate in the same formational unit (Amabel Dolomite), have the same bulk chemistry, and are located in the same geographic area, the Canadian source stone was reported to have "dusting" and "low strength" problems when used as flux stone in steel making.

The strength and dusting are probably interrelated and caused by the same property of the stone. In the absence of other variables, it was thought that the grain size was the rock property causing the difference.

In carbonate rocks of different bulk chemistry, the rate of calcining and the calcined strength and abrasion of the clinker vary. The rate and temperature of calcining are important from energy and economic points of view. The strength of the clinker determines the amount of dust that is produced during calcining. Dust is objectionable more because it is annoying rather than from ecologic or health points of view; nevertheless, steel, lime, and cement plants must control it, adding significantly to their capital and operating costs.

CALCINING OF CARBONATES

The calcining (burning) of carbonate rocks ranges from 545° to 1500°C (Bowen *et al.* 1973), depending on the minerals involved and the bulk composition of the rock. In most instances, CO_2 begins to be driven off from limestone at about 725°C.

For most carbonate minerals, the greatest CO_2 production occurs within a definite temperature range. For relatively pure limestones, this is between 900° to 1000°C. Kiln temperature of about 1200°C is maintained to insure complete dissociation. The time required to convert limestone to lime depends on the particle size and the type of kiln used.

The dissociation range for pure dolostone has been found to lie between 825° to 945°C. The maximum evolution of CO_2 takes place at 945°C. The properties of the calcined product vary with the intensity and rate of calcination. The calcination of dolostone is, therefore, more complex than that of limestone.

The particle size of the carbonate being calcined varies, depending on the purpose and kiln type. Dolostone and limestone used as flux in steel making is crushed to a relatively coarse size. Limestone used as source of cement is ground and mixed with other ingredients which fuse to produce a clinker.

The research described below attempted to determine the effect of some of the main chemical, physical, and petrographic properties of the carbonate rocks on the calcining rates, and more importantly, on their resistance to abrasion (dusting). The rock used, the method of experiments, and the results are given in the following sections.

DESCRIPTION OF TESTS

SAMPLE COLLECTION AND PREPARATION

Samples were collected from quarries that currently produce stone which is subjected to calcining (Hewitt 1972, Hewitt and Vos 1972). Three formational units in southwestern Ontario are mined for this purpose: Lockport dolomite, Detroit River limestone, and Black River limestone. The latter unit is mined as source of cement.

Two quarries operating in each of the above units were sampled. Eight to twelve large blocks from different beds within the formation were sampled at each quarry, for a total of 67 samples. The sampling was governed by the grain size and the texture of the stone. All distinctly different units within each quarry were sampled. The formational units, the quarries, and their location are given in Table 271.1. Figure 271.1 is an index map showing the location of the quarries.

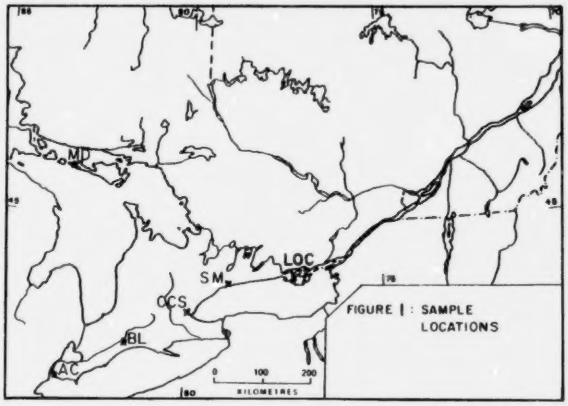

Figure 271.1. Sample locations.

The blocks were cored in the laboratory to provide sized pieces for calcining and strength testing. Three sizes of core were obtained: 19.05 mm (3/4 inch) diameter, 25.4 mm (1 inch) diameter, and 63.5 mm (2.5 inches) diameter. The largest cores were cut exactly in half down the axis of the core. The cores were trimmed to standard size for strength testing and calcining.

A thin section for each sample was prepared from one of the 19 mm cores. The thin sections were used for texture and grain size determinations. Another 19 mm core from each block was crushed and pulverized for chemical analysis for CaO, MgO, and insoluble residue determination.

CALCINING EXPERIMENTS

A Thermolyne Type 10500 oven was used for calcining experiments. The temperature control of the oven was checked by thermocouples, and found to be within 15°C of the dial setting. Once set for a given temperature, the dial setting was not changed, assuring comparable temperatures for all the tests.

Pilot calcining experiments were run to determine the average calcining times for each size core at two temperatures: 900° and 1000°C. It was found that the 19 mm and 25.4 mm cores calcined fully in 180 minutes, regardless of composition. The 63.5 mm half cores fully calcined in 210 minutes.

The rate of calcining was determined by weighing the 19 mm and 25.4 mm cores at 5, 10, 30, 60, 90, and 180 minute cumulative calcining time intervals. Similarly, the weighing of the largest cores was done at 10, 30, 60, 90, 120, and 210 cumulative time intervals.

Two calcining tests were done at 1000°C, and one at 900°C on each core size.

STRENGTH TESTING

The three sizes of cores from each block were squared off and tested on a uniaxial compression machine prior to calcining. Following calcining, the 19 mm and 25.4 mm cores were again tested for strength. Since the strength of the calcined rock is very low, a calibrated load cell was used to measure the uniaxial strength of the sample.

ABRASION TESTING

The sample broken in the load cell test was placed in a low intensity abrasion machine. The machine is essentially a modified shale slaking apparatus. The apparatus consists of four steel-mesh drums with 1.68 mm (#12 mesh) size openings through which abraded material falls. The drums are 14 cm in diameter, and 10 cm in length. A shelf in the drum lifts the sample during each revolution and throws it, along with three steel balls, to the bottom of the drum. The apparatus is in effect a miniature Los Angeles Abrasion machine used for aggregate testing. The equipment provides a gentle abrasive action for uncal-

TABLE 271.1. DESCRIPTION AND LOCATION OF SAMPLES.

Code	Quarry	Location	Geologic Unit & Description
CCS	Canada Crushed Stone Co.	Clappison Corners	Gasport Dolomite Member Lockport Dolomite Medium-grained dolomite
MD	Manitoulin Dolomite	Meldrum Bay Manitoulin	Amabel Dolomite Member Lockport Dolomite Medium- to coarse-grained
LOC	Lake Ontario Cement	Picton	Black River Formation Lime Mudstone
SM	St. Mary's Cement	Bowmanville	Black River Formation Lime mudstone
BL	Beachville Limestone	Beachville	Detroit River Group Wackestone
AC	Allied Chemical	McGregor	Detroit River Group

cined rocks; however, because of the greatly reduced strength of the calcined carbonates, the abrasion was severe. The drum was revolved at 20 rpm for 10 minutes (200 revolutions). The sample remaining in the drum was weighed, and the difference between the original and abraded sample mass expressed as percent loss.

CHEMICAL ANALYSIS

Crushed 19 mm core was pulverized and prepared for X-ray fluorescence spectrometer analysis. CaO and MgO contents of each sample were determined. The remainder of the pulverized sample was used to determine the insoluble residue content. Loss on ignition was determined during the course of calcining experiments.

GRAIN SIZE DETERMINATION

Thin sections were prepared from the 19 mm diameter cores. The relative grain sizes were determined by counting the number of grain boundaries intercepted by the vertical and horizontal cross hairs of the petrographic microscope. Initially, 25 random locations were selected within the area of the thin section for counting. However, statistical comparison of 25 locations with 15 locations, in 40 thin sections analyzed, showed no statistical difference in the results, and 15 locations were then used for the remainder of the grain size analysis.

Only well defined crystals within the sections were counted. The fine-grained groundmass was considered as matrix, and its proportion estimated at each of the 15 locations within each section.

Depending on the grain size of the rock, two magnifications, 35 x and 60 x were used, and a relationship between them was determined statistically, so that in the final results, all grain boundary intercepts were reported in the dominant magnification used, 3 x.

EXPERIMENTAL RESULTS

EXPERIMENTAL CONDITIONS

Two sets each of the 19 mm and 25.4 mm cores were calcined at 1000°C, and one set each at 900°C. The results of the two sets were averaged. The 63.5 mm cores were cut length-wise in half, and the half calcined at 1000°C.

The calcining of the 19 mm and the 25.4 mm cores was done in lots of four to six samples. The calcining of the 25.4 mm cores was done in lots of four samples. Two 63.5 mm half cores were calcined at one time. The cores were taken out of the furnace individually, weighed, and returned to the furnace. Because the high heat obliterated core markings, the cores were identified by their position in the furnace.

The temperature of the furnace was maintained by a built-in calibrated rheostat. The accuracy of the temperature settings was independently checked, and found to be within 20° of the setting. The opening of the furnace for the weight measurements resulted in slight cooling; however, the design temperature was re-established within a few minutes following the completion of measurements at each time interval. Since all cores were treated equally, the results are thus directly comparable.

At the completion of the run, the calcined cores were placed in a desiccator over silica gel, and allowed to cool sufficiently to allow them to be handled. Compressive strength was then determined on the warm samples. The failed samples were placed directly in the abrasion drums, and their abrasion determined.

PRESENTATION OF DATA

The results of the calcining tests, the mechanical properties (compressive strength and abrasion), the chemical analyses, and the grain size analyses on the 25.4 mm cores at 1000°C are presented in Tables 271.2 through 271.4. The calcining and mechanical data represent the average of two runs; the chemical and grain size data is constant for all size cores and temperatures. The results are representative and similar to those obtained for other size cores and temperatures; space restrictions do not permit the listing of the other test results.

Each table contains the data from two quarries in the same formational units. Quarry averages (means) and their standard deviation have been calculated for each measured property. The means also appear in the summary tables (Tables 271.5 and 271.6).

Based on the data in the above tables, a series of figures have been prepared. The relationships between the various measured properties are presented in scatter diagrams. Figures 271.2 through 271.9 show the difference between dolostones in Table 271.1 and limestones in Tables 271.2 and 271.3; Figures 271.10 through 271.13 show the significant relationships from Tables 271.4 and 271.5. Figure 271.14 gives the summary of calcining rates.

DISCUSSION OF RESULTS

CALCINING RATES AND ROCK TYPE

Dolostones calcine more readily than do limestones. Figures 271.2 and 271.3 compare the calcining loss measured after 5 minutes and after 15 minutes calcining at 1000°C for limestones and dolostones respectively. For dolostone, there is a five-fold increase in mass loss at 15 minutes compared to 5 minutes, on the average. The rocks showing high early mass loss show proportionately lower loss later; the mass loss curves for individual samples all show linear trends with time in early stages, and exponential trends after about 20% of the initial mass has been lost.

Similar trends hold for limestones, except that the mass loss in early stages is significantly lower, followed by a more rapid mass loss in later stages. Limestones typically exhibit an "S" curve for the time versus mass loss relationship.

The insoluble residue content (mostly clay) has an effect on the calcining properties of carbonates. When individual formational units are considered, a scattergraph of calcined loss at either 5, 15, or 30 minute times and insoluble residue show diffuse positive trends (i.e. as the insoluble residue increases, so does the mass loss on calcining). These

TABLE 271.2. TEST RESULTS: LOCKPORT DOLOMITE FORMATION.

							25.4mm Core Test Results							
	Calcining Tests, % mass loss						Mechanical Tests				Chemical & Mineralogical Tests			
Sample	0min	5min	15min	30min	90min	180min	AbrLoss %	Str*100 kg/cm^2	CaO %	MgO %	Insol. %	GrSz/100 mm	Matrix %	Porosity %
XMD.9	78.25	3.90	23.74	32.81	44.62	48.20	55.41	11.40	27.59	20.45	7.90	3.88	.0	.00
XMD.8	76.90	2.44	11.60	21.16	45.06	46.86	44.41	5.85	28.90	20.99	4.37	5.76	.1	.00
XMD.7	78.65	1.73	13.21	23.41	42.52	47.51	54.26	14.15	29.35	21.10	3.37	8.45	.0	.00
XMD.6	79.65	8.82	24.33	31.96	45.31	46.76	41.95	11.25	30.53	20.19	3.66	8.14	.0	.00
XMD.5	77.27	6.57	26.89	33.51	44.02	46.55	64.03	9.55	30.19	21.25	2.30	10.78	.0	.00
XMD.4	78.71	2.86	14.63	23.57	47.29	48.00	44.27	4.15	29.72	21.75	1.74	9.24	5.0	.00
XMD.3	77.79	3.37	14.58	22.76	42.20	48.33	37.94	9.60	28.90	21.52	4.06	8.96	.3	.10
XMD.2	67.33	1.80	11.29	19.15	35.53	36.09	54.38	8.55	27.37	21.41	5.81	9.41	1.6	.60
XMD.12	79.74	2.08	8.40	20.84	43.11	48.21	67.51	17.20	29.82	20.83	2.26	9.23	.0	.00
XMD.11	77.74	8.41	21.63	26.04	44.84	47.62	38.89	9.00	29.72	21.00	2.99	8.45	.0	.00
XMD.10	77.52	3.79	17.34	23.92	45.32	47.53	75.44	15.05	29.79	20.68	4.75	8.57	.0	.00
XMD.1	78.98	9.67	21.87	26.63	45.36	46.97	33.49	2.90	28.85	21.45	3.77	6.44	.0	1.20
Average	77.38	4.62	17.46	25.48	43.77	46.55	51.00	9.89	29.23	21.05	3.92	8.11	.58	.16
St.Dev.	3.29	2.93	6.04	4.86	2.95	3.35	13.06	4.30	.97	.46	1.70	1.88	1.46	.37
N	12.00	12.00	12.00	12.00	12.00	12.00	12.00	12.00	12.00	12.00	12.00	12.00	12.00	12.00
XCCS.9	73.18	.72	2.90	12.84	43.40	47.24	68.86	9.35	30.82	20.54	2.07	6.24	.8	6.40
XCCS.8	73.34	1.63	6.96	17.51	45.83	47.74	63.31	15.45	30.54	20.98	1.41	5.22	2.4	12.30
XCCS.7	72.74	.37	1.56	6.09	39.59	46.79	71.33	16.90	30.72	20.66	2.55	7.83	.3	3.80
XCCS.6	74.50	1.30	7.85	20.24	46.88	47.64	70.51	20.55	30.67	20.89	1.60	7.11	.3	2.90
XCCS.5b	69.75	2.05	5.61	13.86	43.81	47.50	79.83	6.95	30.34	21.03	2.09	5.77	2.5	6.60
XCCS.5a	70.83	6.30	11.71	20.20	45.08	47.48	55.67	8.70	30.34	21.03	2.09	5.77	2.5	6.60
XCCS.4	70.10	2.92	7.06	21.75	44.70	46.61	51.04	7.55	29.82	20.85	2.69	4.92	2.2	4.70
XCCS.3	68.18	2.57	12.06	22.54	44.15	47.36	69.22	10.05	30.22	20.54	3.38	5.75	3.6	3.50
XCCS.2	70.24	.67	3.49	11.67	46.23	48.32	53.27	19.70	30.67	21.00	1.54	5.43	4.9	10.80
XCCS.11	72.35	1.04	5.20	15.78	44.29	49.06	55.28	2.60	30.83	20.65	1.05	5.79	.1	1.20
XCCS.10	71.25	1.71	15.65	27.00	45.52	47.54	57.68	9.30	30.49	21.11	1.41	5.86	2.0	3.00
XCCS.1	74.66	.48	1.42	7.31	42.86	47.32	63.23	25.65	30.14	21.42	1.42	6.76	1.1	5.00
Average	71.76	1.81	6.79	16.40	44.36	47.55	63.27	12.73	30.47	20.89	1.94	6.04	1.89	5.57
St.Dev.	2.02	1.63	4.45	6.33	1.91	.64	8.85	6.82	.31	.26	.67	.83	1.45	3.26
N	12.00	12.00	12.00	12.00	12.00	12.00	12.00	12.00	12.00	12.00	12.00	12.00	12.00	12.00

TABLE 271.3. TEST RESULTS: BLACK RIVER FORMATION LIMESTONES.

Sample	Calcining Tests, % mass loss						25.4mm Core Test Results Mechanical Tests		Chemical & Mineralogical Tests					
	0min	5min	15min	30min	90min	180min	AbrLoss %	Str*100 kg/cm²	CaO %	MgO %	Insol. %	GrSz/100 mm	Matrix %	Porosity %
BL.9	75.48	.30	6.54	14.98	31.12	42.78	44.24	16.75	54.50	.21	2.25	3.53	55.7	.00
BL.8	68.84	.46	1.63	6.01	28.68	43.61	40.02	10.15	54.84	.18	2.09	6.87	.0	1.10
BL.7	68.23	.43	.81	3.60	30.16	43.61	72.04	11.60	55.52	.21	1.10	10.02	22.3	.40
BL.6	80.03	.39	6.00	14.02	25.63	41.66	49.85	16.10	54.87	.06	2.22	4.91	30.4	.00
BL.5	74.68	.14	.38	1.45	22.13	41.57	36.30	11.25	54.34	.28	1.89	5.64	28.1	.20
BL.4	74.61	.31	.72	1.68	27.82	42.49	63.32	8.15	54.84	.08	1.96	2.11	88.5	.00
BL.3	73.25	.29	.77	3.27	27.21	42.29	46.28	9.85	54.82	.19	1.46	3.72	47.2	.00
BL.2	75.54	.30	1.09	12.72	33.59	43.88	25.38	2.25	54.73	.02	2.05	3.51	68.8	.20
BL.12	75.09	.23	.69	8.52	31.43	48.55	31.73	.00	54.41	.03	2.49	3.07	72.6	.40
BL.11	73.88	.21	1.39	4.51	31.31	42.36	31.21	16.85	52.97	.11	4.48	4.40	35.3	.60
BL.10	73.53	.33	5.08	13.08	30.18	43.34	64.12	12.35	54.74	.14	1.50	9.66	43.9	.90
BL.1	73.65	.47	2.57	6.82	34.08	44.45	46.22	5.85	54.97	.26	1.88	4.38	46.2	.70
Average	73.90	.32	2.31	7.55	29.45	43.38	45.89	10.10	54.63	.15	2.11	5.15	44.92	.38
St.Dev.	3.07	.10	2.25	4.98	3.39	1.85	14.47	5.39	.60	.09	.84	2.51	24.26	.38
N	12.00	12.00	12.00	12.00	12.00	12.00	12.00	12.00	12.00	12.00	12.00	12.00	12.00	12.00
AC.9	77.59	.34	.86	2.46	31.39	42.95	21.39	7.00	54.04	.24	2.89	1.97	87.1	.00
AC.7	73.55	.58	8.91	19.33	36.19	44.48	47.50	3.65	53.77	.59	2.67	3.63	55.3	.20
AC.6	73.72	.39	.69	1.63	28.04	42.59	21.80	10.75	54.93	.11	2.08	3.76	74.3	.10
AC.5	74.07	.33	2.70	9.31	32.12	43.74	45.88	2.45	53.66	.29	3.81	3.82	69.8	3.00
AC.4	73.90	1.20	7.63	17.57	31.76	32.21	71.39	8.55	39.27	.08	30.10	5.60	73.8	.00
AC.2	72.08	.40	2.29	7.77	35.03	43.88	34.47	.00	54.48	.29	1.52	3.41	41.8	1.80
AC.11	72.34	.30	2.24	8.94	29.71	42.70	32.75	8.85	53.70	.23	3.69	3.97	55.5	.50
AC.10	74.89	.73	2.99	8.85	33.13	43.88	14.51	5.20	52.40	.55	4.89	2.33	81.6	.30
AC.1	70.81	.50	1.53	6.36	34.26	43.44	20.30	.00	54.94	.25	1.14	3.50	47.1	.40
Average	73.66	.53	3.31	9.13	32.40	42.21	34.44	5.16	52.35	.29	5.87	3.55	65.14	.70
St.Dev.	1.92	.29	2.93	5.97	2.57	3.80	18.02	3.92	4.97	.17	9.16	1.03	15.79	1.02
N	9.00	9.00	9.00	9.00	9.00	9.00	9.00	9.00	9.00	9.00	9.00	9.00	9.00	9.00

TABLE 271.4. TEST RESULTS: DETROIT RIVER GROUP LIMESTONES

	Calcining Tests, % mass loss						25.4mm Core Test Results Mechanical Tests				Chemical & Mineralogical Tests			
Sample	0min	5min	15min	30min	90min	180min	AbrLoss %	Str*100 kg/cm^2	CaO %	MgO %	Insol. %	GrSz/100 mm	Matrix %	Porosity %
SM.2.4	75.37	1.80	18.91	31.81	38.63	39.15	60.64		47.63	.83	13.04	2.07	89.4	.00
SM.2.3	65.23	1.78	14.53	25.85	38.26	39.95	20.33	4.55	42.09	1.96	20.39	3.83	68.7	.00
SM.2.2	75.54	2.03	3.99	9.50	36.93	40.37	11.52	14.55	46.31	1.25	14.80	2.83	90.2	.00
SM.2.1	72.38	1.02	6.96	16.39	35.29	39.81	12.20	7.70	46.08	1.64	14.85	2.03	88.4	.00
SM.1.4	79.56	.87	3.21	7.69	32.46	41.83	8.62	3.05	49.74	1.27	8.93	3.42	80.6	.00
SM.1.3	73.71	1.52	5.92	11.67	31.38	41.96	13.39		38.81	1.94	25.99	2.45	86.0	.00
SM.1.2	74.62	1.39	3.73	8.13	33.24	40.64	36.39	6.55	51.92	.85	5.25	4.75	23.2	.00
SM.1.1	74.78	2.45	12.68	25.71	40.28	41.40	12.93	5.40	48.64	1.32	11.60	2.99	79.9	.00
Average	73.90	1.61	8.74	17.09	35.81	40.64	22.00	6.97	46.40	1.38	14.36	3.05	75.80	.00
St.Dev.	4.06	.52	5.88	9.44	3.23	1.01	17.91	4.05	4.22	.44	6.48	.93	22.40	.00
N	8.00	8.00	8.00	8.00	8.00	8.00	8.00	6.00	8.00	8.00	8.00	8.00	8.00	8.00
LOC.4.3	73.87	.50	3.45	8.71	33.58	37.77	31.94	13.10	53.50	.22	3.42	3.53	37.2	.00
LOC.4.2	76.39	.56	3.88	10.53	32.53	42.85	75.27	10.50	50.93	.87	8.78	12.70	7.8	.00
LOC.4.1	69.15	1.10	7.74	13.86	32.86	41.45	27.91	7.00	42.17	1.67	21.11	3.60	16.2	.00
LOC.3.3	75.79	.42	.86	3.70	29.00	42.83	60.49	19.70	53.26	.22	4.18	16.08	.0	.00
LOC.3.2	69.93	.53	2.33	3.90	30.91	41.32	29.49	7.45	50.93	.52	5.52	8.95	8.5	.00
LOC.3.1	73.25	.63	1.03	3.32	26.92	43.03	31.73	16.40	53.18	.53	3.22	7.45	11.4	.00
LOC.2.2	73.21	.44	1.72	5.44	32.56	41.91	67.43	11.55	52.66	.51	4.55	16.28	17.6	.00
LOC.2.1	78.25	1.80	9.54	21.54	37.54	41.08	47.42	15.85	52.13	.69	5.51	5.47	26.2	.00
LOC.1.3	68.26	1.04	3.22	8.83	33.91	40.10	23.96	16.35	46.58	1.35	14.15	3.95	26.9	.00
LOC.1.2	69.81	2.39	5.22	10.01	33.56	41.55	25.91	9.45	48.15	1.17	11.25	7.07	36.0	.00
LOC.1.1	68.68	2.26	4.65	10.45	33.95	40.68	28.09	8.15	53.76	.31	2.99	23.34	.0	.00
Average	72.41	1.06	3.97	9.12	32.48	41.33	40.87	12.32	50.66	.73	7.70	9.86	17.07	.00
St.Dev.	3.46	.75	2.72	5.34	2.79	1.50	18.57	4.27	3.63	.48	5.72	6.46	13.11	.00
N	11.00	11.00	11.00	11.00	11.00	11.00	11.00	11.00	11.00	11.00	11.00	11.00	11.00	11.00

TABLE 271.5. SUMMARY OF CALCINING PROPERTIES
25.4mm CORE, CALCINING @ 1000°C (average of two runs)

Location		Mass g	Calcining Rates Percent Calcined					Mechanical Properties	
		0min	5min	15min	30min	90min	180min	Abras. %	Strength (kg/cm^2) x 100
XMD	Average	77.38	4.62	17.46	25.48	43.77	46.55	51.00	9.89
	St.Dev.	3.29	2.93	6.04	4.86	2.95	3.35	13.06	4.30
	N	12.00	12.00	12.00	12.00	12.00	12.00	12.00	12.00
XCCS	Average	71.76	1.81	6.79	16.40	44.36	47.55	63.27	12.73
	St.Dev.	2.02	1.63	4.45	6.33	1.91	.64	8.85	6.82
	N	12.00	12.00	12.00	12.00	12.00	12.00	12.00	12.00
SM	Average	73.90	1.61	8.74	17.09	35.81	40.64	22.00	6.97
	St.Dev.	4.06	.52	5.88	9.44	3.23	1.01	17.91	4.05
	N	8.00	8.00	8.00	8.00	8.00	8.00	8.00	6.00
LOC	Average	72.41	1.06	3.97	9.12	32.48	41.33	40.87	12.32
	St.Dev.	3.46	.75	2.72	5.34	2.79	1.50	18.57	4.27
	N	11.00	11.00	11.00	11.00	11.00	11.00	11.00	11.00
BL	Average	73.90	.32	2.31	7.55	29.45	43.38	45.89	10.10
	St.Dev.	3.07	.10	2.25	4.98	3.39	1.85	14.47	5.39
	N	12.00	12.00	12.00	12.00	12.00	12.00	12.00	12.00
AC	Average	73.66	.53	3.31	9.13	32.40	42.21	34.44	5.16
	St.Dev.	1.92	.29	2.93	5.97	2.57	3.80	18.02	3.92
	N	9.00	9.00	9.00	9.00	9.00	9.00	9.00	9.00

TABLE 271.6. CHEMICAL AND MINERALOGICAL PROPERTIES.

Location		CaO %	MgO %	Insol. %	GrainSz mm/100	Matrix %	Porosity %
XMD	Average	29.23	21.05	3.92	8.11	.58	.16
	St.Dev.	.97	.46	1.70	1.88	1.46	.37
	N	12.00	12.00	12.00	12.00	12.00	12.00
XCCS	Average	30.47	20.89	1.94	6.04	1.89	5.57
	St.Dev.	.31	.26	.67	.83	1.45	3.26
	N	12.00	12.00	12.00	12.00	12.00	12.00
SM	Average	46.40	1.38	14.36	3.05	75.80	.00
	St.Dev.	4.22	.44	6.48	.93	22.40	.00
	N	8.00	8.00	8.00	8.00	8.00	8.00
LOC	Average	50.66	.73	7.70	9.86	17.07	.00
	St.Dev.	3.63	.48	5.72	6.46	13.11	.00
	N	11.00	11.00	11.00	11.00	11.00	11.00
BL	Average	54.63	.15	2.11	5.15	44.92	.38
	St.Dev.	.60	.09	.84	2.51	24.26	.38
	N	12.00	12.00	12.00	12.00	12.00	12.00
AC	Average	52.35	.29	5.87	3.55	65.14	.70
	St.Dev.	4.97	.17	9.16	1.03	15.79	1.02
	N	9.00	9.00	9.00	9.00	9.00	9.00

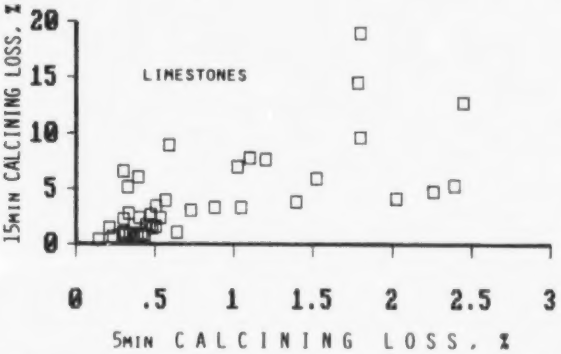

Figure 271.2. Caicining mass loss at 5 and 15 minute interval, limestones.

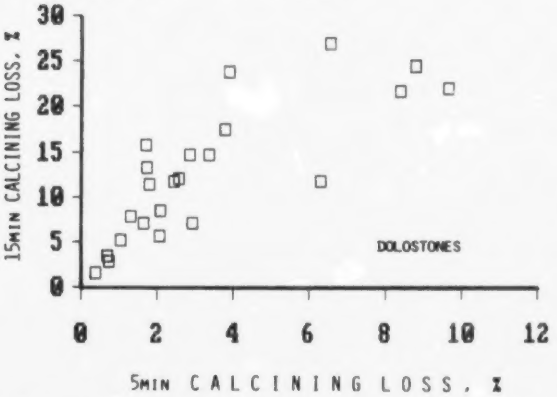

Figure 271.3. Calcining mass loss at 5 and 15 minute interval, dolostones.

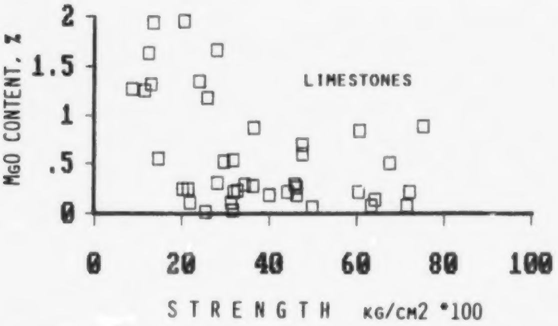

Figure 271.4. Calcined strength versus MgO content in limestones.

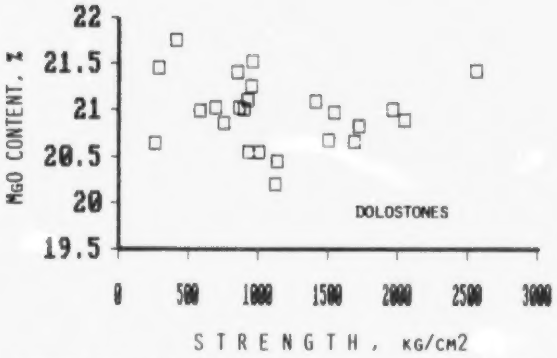

Figure 271.5. Calcined strength versus MgO content in dolostones.

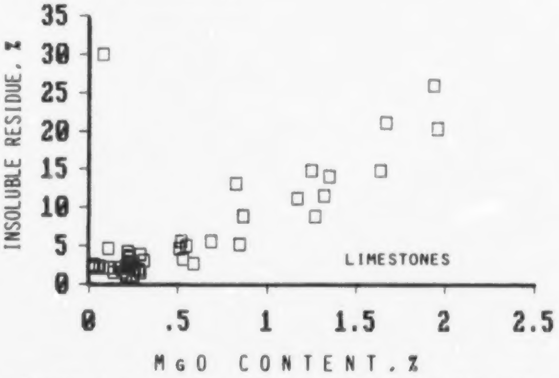

Figure 271.6. MgO versus insoluble residue content in limestones.

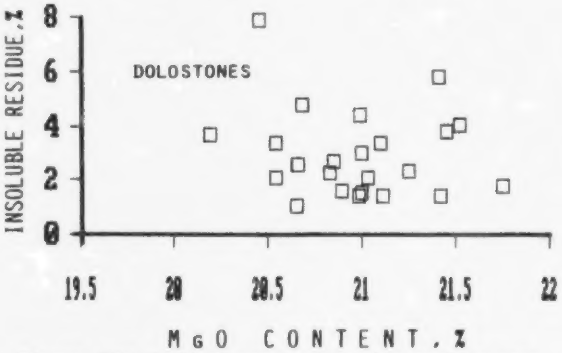

Figure 271.7. MgO versus insoluble residue content in dolostones.

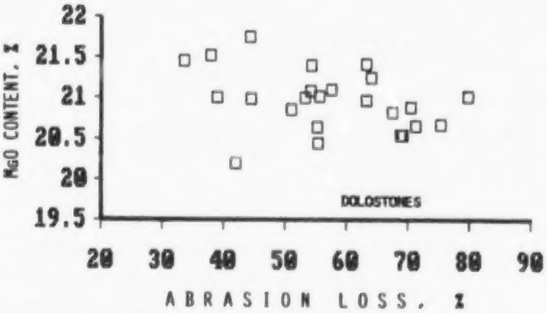

Figure 271.8. *Abrasion loss versus MgO content in dolostones.*

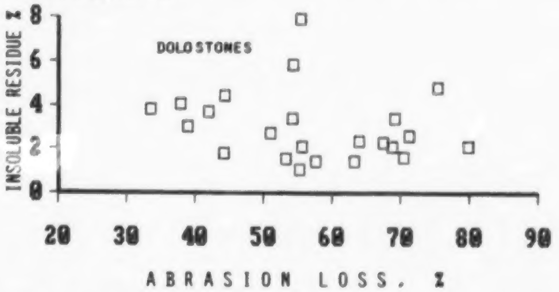

Figure 271.9. *Abrasion loss versus insoluble residue in dolostones.*

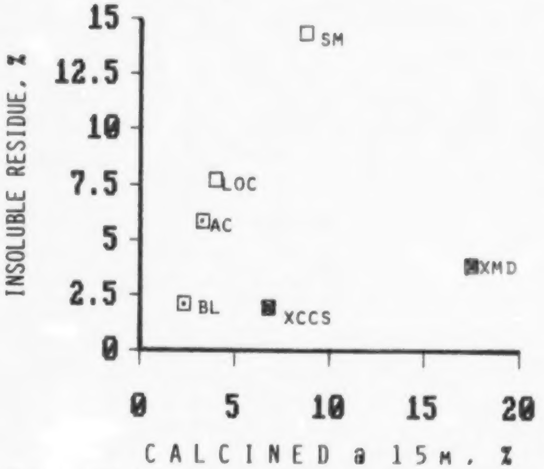

Figure 271.10. *Calcined mass loss at 15 minutes versus insoluble residue. Averages for each quarry. Lockport Formation indicated by "x"; Detroit River Group "."; Black River Formation blank.*

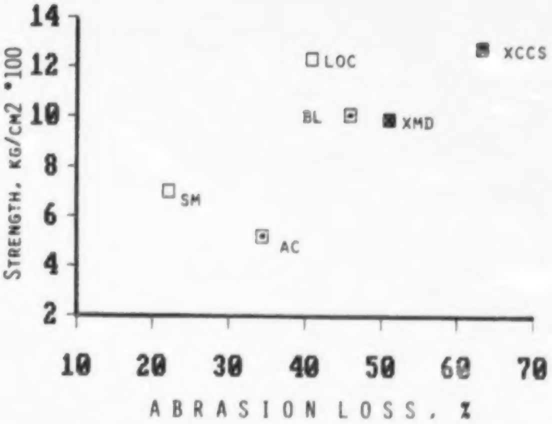

Figure 271.11. *Abrasion loss versus calcined strength. averages for each quarry. Lockport Formation indicated by "x"; Detroit River Group "."; Black River Formation blank.*

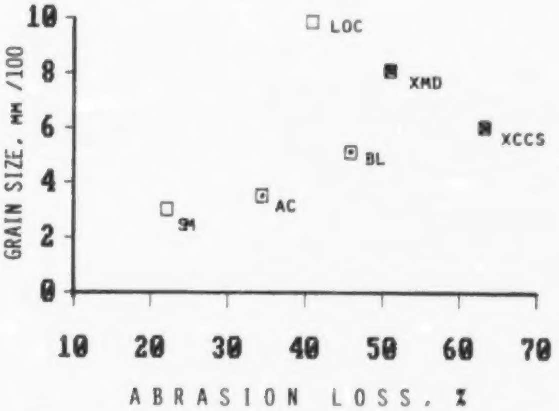

Figure 271.12. *Abrasion loss versus grain size. Averages for each quarry. Lockport Formation indicated by "x"; Detroit River Group "."; Black River Formation blank.*

trends are better defined when means of samples for each quarry site for the insoluble residue and calcined loss are plotted, as Figure 271.10 shows. The limestones and dolostones follow a different pattern, but both show that as the insoluble content increases, so does the percent calcined for a given time period.

CHEMICAL AND MINERALOGICAL RELATIONSHIPS

One of the more interesting relationships observed was that between insoluble residue and the MgO content (Figure 271.6). Limestones showed a very significant, positive relationship: an increase in MgO content correlated well with the increase of the insoluble residue content. It would appear that the MgO is carried by the clay fraction rather than in the calcite.

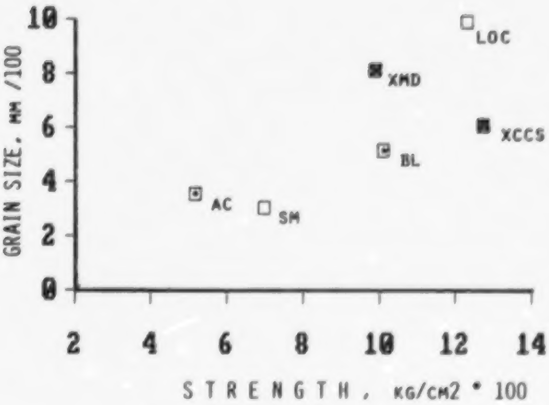

Figure 271.13. Calcined strength versus grain size. Averages for each quarry. Lockport Formation indicated by "x"; Detroit River Group "."; Black River Formation blank.

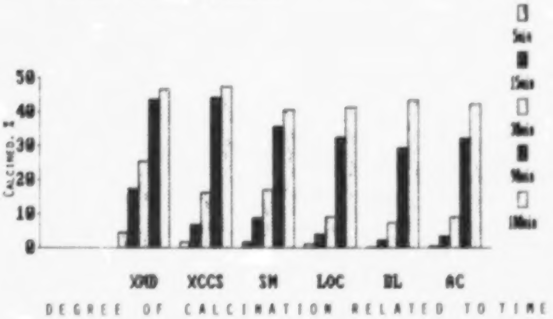

Figure 271.14. Bar graph summary of calcining rates of each deposit at different times.

Dolostones (Figure 271.7) showed a much less defined, inverse relationship. As the insoluble content increased, the MgO content decreased. The minerals accounting for the insoluble residue simply displaced the dolomite in the sample.

FACTORS AFFECTING MECHANICAL PROPERTIES OF CALCINED CARBONATES

Dusting of the rock during calcination and during iron ore reduction is both an economic and an environmental problem. Dusting is a function of abradability of the calcining product which, in turn, is a function of the strength of the product.

Strength and Grain Size

When compared on individual deposit basis, the strength of the calcined product increases as the grain size increases in the Lockport dolostones, and in the Detroit River limestones. The limestones of the Black River Formation show an inverse relationship: decrease of strength with increasing grain size. The latter tend to be lime mudstones, whereas the former are wackestones. It would thus seem that where the rock has been recrystallized, the larger the grain size, the greater the strength.

When deposit means of strength and grain size are plotted (Figure 271.13), the general relationship shows that the strength increases as the grain size.

Abrasion and Grain Size

On an individual deposit comparison of abrasion loss to grain size, each deposit shows that as the grain size increases, the abrasion loss increases. However, when all dolostones and all limestones are plotted together, no such relationship emerges.

When the means of abrasion loss and grain size for each deposit are plotted (Figure 271.12), the same relationship is found. The lime mudstones and wackestones show separate positive trends; however, the dolostones show a negative trend. Although each of trends is based on two means, the differences in the means are statistically significant.

Strength and Abrasion

Figure 271.11 shows the plotted means of calcined strength and abrasion. A positive relationship emerges, showing that as the strength of the calcined sample increases, so does the abrasion. However, the three distinct rock groups follow their own independent trends.

On an individual quarry basis, only the dolostones show a strong positive relationship between strength and abrasion loss, particularly the Manitoulin Dolomite samples. The limestones show no relationship.

The results are somewhat unexpected. Normally, the increased strength of the rock implies higher abrasion resistance; however in the case of calcined dolostones, the reverse is true, the increased strength correlates with increased abrasion.

MgO Content Effect on Strength and Abrasion

On an individual deposit basis, there is a broad inverse trend of strength and the MgO content for both the dolostones and limestones. A similar relationship is seen when all limestones and dolostones are grouped (Figures 271.4 and 271.5). The trend in limestones may simply indicate the effect of clay content on strength: the higher the clay content, the lower the strength. In the dolostones, the opposite seems to be indicated: the purer the dolomite, the lower its strength. However, both of these relationships are too diffuse to draw definite conclusions.

The effect of MgO content on abrasion is similar (Figure 271.8) for dolostones, i.e. increased MgO decreases abrasion loss; however, no relationship is seen for limestones.

Summary and Conclusions

The effect of mineralogic, chemical, and textural variables on the calcining properties of the carbonates can be summed up as follows:

CALCINING RATES OF DOLOSTONES AND LIMESTONES

Dolostones calcine faster at any given temperature than do limestones.

There are significant variations in the calcining rates within both the dolostone and the limestone groups. The Amabel unit of the Lockport Formation on Manitoulin Island showed the fastest calcining rate of all quarries tested. In the early stages of calcining, the Amabel unit samples calcined almost three times faster than the dolomite from the Gasport unit of the Lockport.

The Black River limestones gave intermediate calcining rates. Within this group, the samples collected from the St. Mary's Cement quarry at Bowmanville calcined approximately twice as fast as did equivalent samples from the Lake Ontario Cement quarry at Picton.

The slowest calcining rates were determined for the Detroit River Group rocks. Statistically there was little difference between the results from the McGregor quarry and the Beachville quarry.

The calcining rates seem to be governed most by the insoluble mineral (clay) content of the rocks, but differently so for the dolostones and limestones. Increase in the insoluble content increases the calcining rate.

STRENGTH AND ABRASION OF CALCINED CARBONATES

The strength and abrasion loss of calcined carbonates are directly correlatable: as the strength increases, so does the abrasion loss. This unexpected relationship holds for dolostones, but not for limestones, when individual deposits are considered. Limestones show no relationship.

These findings present a problem when dolostone is considered for use as flux stone, since both a high strength and a low abrasion are the desirable properties of the stone. Some beds within the quarry may have a high strength, but also a high abrasion loss, whereas others have low strength and low abrasion loss.

EFFECT OF GRAIN SIZE

The grain size has a significant effect on the abrasion, but lesser effect on the strength of the calcined product. In all cases, increase in grain size increases the abrasion of the product. Thus, the coarser grained stone will cause increased dusting; if a choice can be made, then the finer grained stone is preferable.

Grain size also affects the strength of dolostones and recrystallized limestones; the larger grain size stones increase the strength of the calcined clinker. Thus, increase in grain size increases strength, but decreases the abrasion resistance.

EFFECT OF MgO AND INSOLUBLE (CLAY) CONTENT

The MgO content in the limestones is related to the insoluble residue content; both the MgO and the insoluble residue content are inversely related to the strength of the limestone clinker. The loss of strength is probably due to the presence of clay; however, how the clay, which at this stage is in some ceramic form, affects the strength is not known.

The dolostones, on the other hand, increase both in strength and in abrasion resistance with increase in the insoluble residue content.

RECOMMENDATIONS

The quarries sampled in this report supply stone that is calcined and used for a variety of purposes, such as cement raw material, chemical stone, and flux stone. In each of these applications, the stone is fired and calcined in kilns. Dust from the kilns is an environmental problem, controlled by expensive collectors. Thus, for all of these purposes, a stone that is low in dusting potential is desirable. Dusting and abrasion loss are related. Thus a low abrasion stone is desired.

The ideal stone would be fine grained, or lacking that, containing some minor insoluble residue content (clay).

The cement industry requires only high purity limestones; the common impurity found is clay. The clay provides part of the alumina and silica required for cement. However, the clay was shown to carry most of the magnesium present in the stone. Thus, for the most desirable low magnesium and low alkali cements a relatively clay-free rock is preferable. The required alumina obtained from other sources may contain lower magnesium content than that present in the limestones.

Dolostones are preferable as flux stones. They contain a higher proportion of carbonate and calcine quicker, saving energy. An intermediate-grained dolostone, with minor insoluble residue content, would be the best choice to provide strength, abrasion resistance, and rapid calcining.

REFERENCES

Bowen, O.E., Clifton, H.G., James, R.E.
1973: The Mineral Economics of Carbonate Rocks; Bulletin, California Division of Mines and Geology, 33p.

Harben, P.W., and Bates, R.L.
1984: Geology of the Nonmetallics; Metal Bulletin Incorporated, New York, p.159-160.

Hewitt, D.F.
1972: Paleozoic Geology of Southern Ontario; Ontario Division of Mines, Geological Report 105, 18p. Accompanied by Map 2254, scale 1 inch to 16 miles.

Hewitt, D.F., and Vos, M.A.
1972: Limestone Industries of Ontario; Ontario Division of Mines, Industrial Mineral Report 39, 79p. Accompanied by Map 2264, scale 1 inch to 16 miles.